Intelligent Reflecting Surfaces for Wireless Communications: Low-Complexity Techniques and Performance Analysis

A Thesis

Submitted for the Degree of

Doctor of Philosophy

in the **Faculty of Engineering**

by

Yashvanth L.

under the Guidance of

Chandra R. Murthy

Electrical Communication Engineering
Indian Institute of Science, Bangalore
Bangalore – 560 012 (INDIA)

September 2025

Acknowledgments

I owe the successful completion of my Ph.D. to the unfailing support of my advisor, *Prof. Chandra R. Murthy*. His insightful guidance, patience, and encouragement have been instrumental at every stage of my journey. Under his mentorship, I honed many essential skills, ranging from writing good technical papers and delivering effective presentations to critically examining technical ideas and managing multiple tasks efficiently. His support also helped me secure competitive fellowships and build collaborations with top academic and industrial groups worldwide, by which I learnt the art of teamwork and the power of collective expertise. What I admire the most about him is his rare blend of humility, empathy, and integrity. He treats everyone with kindness and respect and is always willing to offer thoughtful support to everyone around him. I consider it a privilege to have been guided by him and will count myself fortunate if I can imbibe at least a few of his qualities in my own life. I thank him for shaping both my professional and personal growth.

I am deeply grateful to *Prof. Bhaskar D. Rao* from UCSD for the brainstorming discussions and fruitful collaborations we shared during my Ph.D. His perspective on developing elegant and simple solutions to complex problems has profoundly influenced my approach to research. I feel privileged to have co-authored a few papers with him. I also extend my sincere thanks to my fellow student collaborators: *Souradeep, Siddhartha, Kanchan,* and *Deepak* for broadening the scope of my research.

I would like to thank my teachers: *Prof. Neelesh B. Mehta, Prof. B. Sundar Rajan, Prof. K. V. S. Hari, Prof. Parimal Parag,* and *Prof. Sundeep P. Chepuri*, for imparting strong foundational knowledge through their courses that has helped in formulating and solving sound research problems during my Ph.D. I am also grateful to my doctoral committee members: *Prof. Sudhan Majhi, Prof. Kunal Narayan Chaudhury,* and *Prof. Chandramani Singh*, for thoroughly reviewing my research progress and offering constructive feedback that influenced the direction and depth of my work. I thank the ECE office members, especially *Mr. Srinivasa Murthy* and *Ms. Rajani*, for their administrative support. Further, I would like to place my thanks on record to the funding agencies: the Ministry of

Education, Qualcomm, IISc, and IEEE for generously supporting my research through the PMRF, QInF, GARP, and IEEE ComSoc travel grants. This financial support provided the stability necessary to focus wholeheartedly on my work. In this regard, I thank *Prof. Aditya K. Jagannatham* from IIT Kanpur and *Dr. Sanjeev Gurugopinath* from PSEIT, for offering me multiple teaching opportunities at NPTEL and DSU to help me fulfill my PMRF teaching requirements. I am also thankful to *Dr. Kapil Bhattad, Dr. Tanummay Datta, Mr. Pranav Viswanathan,* and all other reviewers for their continued support and efforts in the renewal process of these fellowships.

I have been truly fortunate to be surrounded by peers and friends who supported me during the most challenging moments of my Ph.D. journey. My academic home was the *Signal Processing for Communications* (SPC) lab, and I am grateful to all its members I had the privilege of interacting with: *Bharath, Ranjitha, Sanjeev, Geethu, Sai Thoota, Arun, Chirag, Anubhab, Sameera, Kanchan, Sangeeta Bhattacharjee, Niladri, Praveen, Prabhat, Shankadheep, Akeelah, Sanu, Aniket, Sangeeta Bind, Swetha, Shivani Aggrawal, Sunny, Souradeep, Abhishek, Aastha, Sai Mahesh, Harit, Guna Sai, Monika, Preethi, Adrija, Rupam, Abhinav* and *Sahil*, each of whom influenced my Ph.D. journey in their own meaningful way. The countless coffee breaks and candid conversations with members of the SPC and Next-Gen Wireless labs were quite rejuvenating. In this regard, I fondly thank *Anubhab, Niladri, Sruthy, Shivani Dhok, Arthi, and Sandeep* for the cherished memories we created together. A special word of thanks goes to *Anubhab*, who was far more than a lab-mate – he was a wonderful friend, mentor, well-wisher, and an integral part of my daily life during my Ph.D. I am sincerely grateful for his unwavering companionship and support, which I will always treasure. I am also fortunate to have spent time with many wonderful friends whose encouragement contributed to maintaining a sound and productive mind. I especially enjoyed the many delightful outings with *Anubhab, Chirag, Krishnan* and *Elizabath* to explore and enjoy local cuisines, and I am thankful to *Sruthy* for accompanying me on several visits to temples. I also appreciate the engaging conversations with *Prasobh, Robin, Anjana, Arvind, Sai Pradeep, Vineetha, Satwika, Swati, Kavya, Nagabhushan, Venkat,* and *Safwan*, each of whom added joy to my journey.

Finally, I owe my deepest gratitude to my parents, grandparents, uncle, and aunt, and all my close family members for their constant encouragement and care throughout this journey. In particular, my parents and uncle have provided exceptional support to ensure I could pursue my Ph.D. with peace of mind. Above all, I am grateful to the Almighty for blessing me with wisdom, favorable circumstances, and the presence of kind and supportive individuals who have enriched my life.

Abstract

Intelligent reflecting surface (IRS), also referred to as reconfigurable intelligent surface (RIS), is an emerging technology aimed at dynamically controlling the propagation environment of next-generation wireless systems. An IRS comprises a large array of passive phase shifters whose configurations can be adaptively adjusted to co-phase the reflected signals at the receiver, thereby mitigating the channel impairments such as fading and shadowing. Despite its promising benefits, the practical deployment of IRS entails several signal processing challenges that require careful investigation. This thesis addresses three fundamental problems in this context, with an emphasis on low-complexity solutions and rigorous performance analysis of IRS-assisted wireless systems.

The first part of this thesis focuses on developing a low-complexity approach to harness the full potential of IRS-aided systems. Conventionally, optimizing the IRS phase configuration involves a three-stage procedure: (i) estimating the channels of all the links, (ii) computing the optimal phase shifts, and (iii) transporting the phase angles from the base station (BS) to the IRS, resulting in a *three-fold* overhead. To circumvent this, we develop an alternative scheme wherein, in every time slot, the IRS phases are randomly sampled, and a user equipment (UE) is scheduled opportunistically for data transmission. The central idea is that, with a sufficiently large number of UEs, a randomly chosen IRS configuration is likely to be near-optimal (i.e., beamforming-aligned) for at least one UE. Scheduling such a UE, for e.g., using a proportional-fair (PF) scheduler, for data transmission allows us to obtain most of the IRS gains without explicitly optimizing the IRS, thereby eliminating the associated overheads. Moreover, it is easy to find the UE that experiences the highest SNR (or PF metric) for a given randomly chosen phase configuration using one of several splitting or timer-based methods. We perform an in-depth analysis of this scheme under various channel models and frequency bands. For example, we show that the number of UEs required to attain a spectral efficiency (SE) close to the beamforming SE grows exponentially with the rank of the IRS spatial covariance matrix. We also propose alternative strategies that improve this scaling. Furthermore, we extend the scheme to frequency-selective channels using orthogonal frequency-division multiplexing

(OFDM) and characterize the resulting performance tradeoffs.

The second part of this thesis explores the impact of IRS deployment in a multi-operator wireless system, where each operator serves its UEs over non-overlapping frequency bands. Given that IRSs are inherently passive and lack active RF components such as band-pass filters, they cannot selectively reflect signals confined to specific frequency bands. This raises a key question: if an IRS is deployed and controlled by one operator, how does it affect the performance of out-of-band (OOB) operators operating in adjacent frequency bands? To address this, we first analyze a two-operator scenario where one operator controls a single IRS. Our findings reveal that, although the IRS introduces random phase shifts to the OOB signals, the IRS elements collectively enhance the OOB UE performance, albeit with lower gains than those experienced by the controlling operator. Specifically, in sub-6 GHz bands, the IRS induces rich scattering for the OOB UEs, while in mmWave bands, it increases the likelihood of virtual line-of-sight (LoS) paths. We further show that deploying multiple IRSs amplifies these benefits for OOB users due to spatial diversity. Further, for ease of implementing a multiple-IRS setup, we propose a low-complexity channel estimation technique tailored for distributed IRS deployments, which notably maintains constant pilot overhead when the number of IRSs does not exceed a threshold. Lastly, we generalize our analysis to multi-operator networks where each operator controls its own IRS, and investigate the limits of inter-operator cooperation gains in realistic wireless environments.

The final part of this thesis investigates the performance of wideband beamforming with IRS, where the IRS configuration is designed to beamform wideband signals. A fundamental challenge in this case arises due to the frequency-flat nature of phase shifters, which limits their ability to focus energy uniformly across a wide frequency band. This results in a spatial-wideband effect at the UE, leading to the beam-squint or beam-split (B-SP) effect in the frequency domain, causing a degradation of the array gain and the achievable throughput. To address this issue, we propose two low-complexity mitigation strategies. First, we introduce a distributed IRS architecture in which multiple smaller IRSs are strategically deployed. This architecture reduces the severity of the spatial-wideband effect by parallelizing the spatial delay spread and exploiting the angle diversity. However, it may introduce temporal delay spread (TDS) unless signals from different sub-IRSs arrive within the same sampling bin. In this view, we formulate and solve an optimization problem to determine the optimal placement of IRSs that minimizes TDS over a set of all possible UE locations. In the second approach, we leverage the law of energy conservation to show that, under the B-SP effect, the IRS must inherently form different

beams across different frequency components. Exploiting this insight, we propose an opportunistic OFDMA framework that assigns different subbands to different UEs, enabling the system to harness full array gain across the entire bandwidth through multi-user diversity. Lastly, we observe that in sub-6 GHz bands, frequency selectivity is dominated by rich multipath effects rather than the B-SP phenomenon. Accordingly, we develop a joint IRS phase optimization strategy using a majorization-minimization framework tailored for OFDM systems that maximizes the overall sum-rate at a given UE.

In summary, this thesis explores three core aspects of IRS-aided wireless systems: opportunistic user scheduling, performance of IRS-aided multi-operator systems, and wideband beamforming strategies. *It demonstrates how even a randomly configured IRS can extract most of its benefits and improve the performance of wireless communication systems.* The major takeaways are as follows:

- We develop novel opportunistic scheduling schemes that employ randomly selected IRS phase configurations and leverage multi-user diversity. These *schemes deliver near-optimal IRS gains without explicit optimization of the IRS phase configurations or incurring the associated signaling overheads.*

- We analyze the impact of the IRS in multi-operator environments, particularly on the OOB users. A key finding is that *IRSs, despite being controlled by one operator, can enhance the performance of OOB operators by improving their effective channels.*

- Finally, we develop low-complexity techniques to enable wideband beamforming using phase-shifter-based IRSs. In particular, we show that *a distributed IRS architecture inherently mitigates the B-SP effect, while an opportunistic OFDMA strategy exploits it to enhance system throughput* under a randomly configured IRS phase.

By benchmarking the proposed techniques in this thesis against other existing methods, we show that our solutions can achieve superior performance while maintaining low time and computational complexities.

Glossary

Acronym	Definition
3GPP	Third Generation Partnership Project
5G NR	Fifth Generation New Radio
AWGN	Additive White Gaussian Noise
BS	Base Station
B-SP	Beam-Split
B-SQ	Beam-Squint
BF	Beamforming
BW	Bandwidth
CCDF	Complementary Cumulative Distribution Function
CDF	Cumulative Distribution Function
CLT	Central Limit Theorem
CP	Cyclic Prefix
CS	Cauchy-Scwartz
CSI	Channel State Information
DFT	Discrete Fourier Transform
DL	Downlink
DoA	Direction of Arrival
DoD	Direction of Departure
EE	Energy Efficiency
EMBB	Enhanced Mobile Broadband
ESPRIT	Estimation of Signal Parameters via Rotational Invariance Technique
ETSI	European Telecommunications Standards Institute
EWMA	Exponentially Weighted Moving Average
FDD	Frequency Division Duplex

FR	Frequency Range
HPBW	Half-Power Beam Width
I.I.D.	Independent and Identically Distributed
IRS	Intelligent Reflecting Surface
ISI	Inter-Symbol Interference
IoT	Internet of Things
KPI	Key Performance Indicator
LMMSE	Linear Minimum Mean Squared Error
LS	Least Square
LoS	Line-of-Sight
MCSI	Modulation and Coding Scheme Index
MIMO	Multiple-Input Multiple-Output
ML	Maximum Likelihood
mmWave	Milli-meter Waves
mMIMO	Massive Multiple-Input Multiple-Output
MM	Majorization - Minimization
MMSE	Minimum Mean Squared Error
MMTC	Massive Machine Type Communications
MMV	Multiple Measurement Vector
MO	Mobile Operator
MR	Max-Rate
MRC	Maximal Ratio Combining
MRT	Maximal Ratio Transmission
MSE	Mean Squared Error
MUSIC	Multiple Signal Classification
NLoS	Non Line-of-Sight
NMSE	Normalized Mean Squared Error
OC	Opportunistic Communications
OFDM	Orthogonal Frequency Division Multiplexing
OFDMA	Orthogonal Frequency Division Multiple Access
OOB	Out-of-Band
PF	Proportional Fairness
QoS	Quality of Service

RF	Radio Frequency
RIS	Reconfigurable Intelligent Surface
RR	Round Robin
SC	Sub-carrier
SE	Spectral Efficiency
SI	Self-Intereference
SINR	Signal-to-Interference-plus-Noise Ratio
SISO	Single-Input Single-Output
SNR	Signal-to-Noise Ratio
SOMP	Simultaneous Orthogonal Matching Pursuit
SSB	Synchronization Signal Block
SU-OFDM	Single-User OFDM
SW	Spatial-Wideband
TDD	Time Division Duplex
TDMA	Time Division Multiple Access
TDS	Temporal Delay Spread
THz	Tera Hertz
TTD	True-Time Delay
UE	User-Equipment
UL	Uplink
ULA	Uniform Linear Array
UPA	Uniform Planar Array
URLLC	Ultra Reliable and Low Latency Communications
ZF	Zero Forcing

General Mathematical Notation

Vectors and matrices are denoted by boldface small and capital letters, respectively. Sets are denoted by calligraphy letters. The rest of the notation is listed below.

Field

$\mathbb{R}, \mathbb{R}^+$	:	Field of real numbers, positive real numbers
$\mathbb{C}$	:	Field of complex numbers

Set

$[N]$	:	Set of truncated natural numbers: $\{1, 2, \ldots, N\}$
$\lvert\mathcal{A}\rvert$	:	Cardinality of the set $\mathcal{A}$
$\mathcal{A} \cup \mathcal{B}$	:	Union of the set $\mathcal{A}$ and $\mathcal{B}$
$\mathcal{A} \cap \mathcal{B}$	:	Intersection of the set $\mathcal{A}$ and $\mathcal{B}$
$\mathcal{A} \backslash \mathcal{B}$	:	Set difference: set of elements in $\mathcal{A}$ that are not in $\mathcal{B}$
$\mathcal{A}^c$	:	Complement of the set $\mathcal{A}$
$\mathcal{A} \subseteq \mathcal{B}$	:	$\mathcal{A}$ is subset of $\mathcal{B}$

Vectors

$[\mathbf{a}]_i$	:	ith element of vector $\mathbf{a}$
$\langle \mathbf{a}, \mathbf{b} \rangle$	:	Inner product between two vectors $\mathbf{a}$ and $\mathbf{b}$
$\lVert\mathbf{a}\rVert_p$	:	l_p norm of a vctor $\mathbf{a}$: $\left(\sum_{n=1}^{N} \lvert[\mathbf{a}]_n\rvert^p\right)^{1/p}$
$\mathbf{e}_i$	:	ith column of identity matrix
$\mathbf{0}_N$	:	All zero vector of length N
$\mathbf{1}_N$	:	All one vector of length N
$\mathrm{diag}(\mathbf{a})$	:	Diagonal matrix with entries of $\mathbf{a}$ along its diagonal
$\mathrm{supp}(\mathbf{a})$	:	Support of the vector $\mathbf{a}$

Matrices

$\mathbf{I}_N$	:	Identity matrix of dimension $N \times N$
$\mathbf{0}_{M\times N}$	:	All zero matrix of dimension $M \times N$
$\mathbf{A} = [\mathbf{a}_1, \ldots, \mathbf{a}_N]$	:	A matrix $\mathbf{A}$ whose columns are $\mathbf{a}_1, \ldots, \mathbf{a}_N$
$[\mathbf{A}]_{m,n}$	:	(m,n)th entry of $\mathbf{A}$
$[\mathbf{A}]_{:,n}$	:	nth column of $\mathbf{A}$
$[\mathbf{A}]_{m,:}$	:	mth row of $\mathbf{A}$
$\mathbf{A}^T$	:	Transpose of a matrix $\mathbf{A}$
$\mathbf{A}^{-1}$	:	Inverse of a matrix $\mathbf{A}$
$\mathbf{A}^\dagger$	:	Pseudo-inverse of a matrix $\mathbf{A}$
$\mathbf{A}^*$	:	Conjugation of a matrix $\mathbf{A}$
$\mathbf{A}^H$	:	Conjugate transpose (Hermitian) of a matrix $\mathbf{A}$
$\mathbf{A} \otimes \mathbf{B}$	:	Kronecker product of matrices $\mathbf{A}$ and $\mathbf{B}$
$\mathbf{A} \diamond \mathbf{B}$	:	Khatri-Rao product of matrices $\mathbf{A}$ and $\mathbf{B}$
$\mathbf{A} \odot \mathbf{B}$	:	Hadamard product of matrices $\mathbf{A}$ and $\mathbf{B}$
$\mathbf{A} \oslash \mathbf{B}$	:	Element-wise division of matrices $\mathbf{A}$ and $\mathbf{B}$
$\mathrm{diag}(\mathbf{A})$	:	Vector containing the diagonal entries of the matrix $\mathbf{A}$
$\mathrm{vec}(\mathbf{A})$	:	Column-wise vectorized version of matrix $\mathbf{A}$
$\|\mathbf{A}\|_F$	:	Frobenius norm of matrix $\mathbf{A}$
$\mathbf{A} \succeq \mathbf{B}$	:	$\mathbf{A} - \mathbf{B}$ is a positive semi-definite matrix

Standard Symbols

$\mathbb{R}^{N\times M}$	:	The set of real-valued $N \times M$ matrices
$\mathbb{C}^{N\times M}$	:	The set of complex-valued $N \times M$ matrices
$\|x\|$, x^*	:	Absolute value/complex conjugate of a complex scalar/vector $x/\mathbf{x}$
$\angle x$, $\arg(x)$	:	Phase of a complex scalar/vector $x/\mathbf{x}$
$\mathcal{O}(\cdot), \Omega(\cdot), o(\cdot)$	:	Landau's Big-O, Omega, Small-O notations
$*, \circledast$	:	Linear convolution operator
$x!$	:	Factorial of x
$\forall x$	:	The statement holds for all x (in the set that x belongs to)
$\Re(x), \Im(x)$	:	Real part and imaginary part of x
$\mathbf{F}(\mathbf{F}^H)$	:	DFT (IDFT) matrix (unless otherwise mentioned.)

Functions

$\Upsilon_2^{(L)}(\cdot\,;\cdot\,;)$	:	Confluent Lauricella function
$F_N(x)$	:	Nth order Fejér Kernel evaluated at x
$\Gamma(x)$	:	Gamma function
$\Gamma(\alpha, x; b)$	:	Generalized upper incomplete Gamma function
$\Gamma(\alpha, x)$	:	Upper incomplete Gamma function
$K_n(x)$	:	nth order modified Bessel function of second kind
$sgn(x)$	:	sign of x
$\mathbb{1}_{\{\cdot\}}$	:	Indicator function
$\lceil\cdot\rceil, \lfloor\cdot\rfloor$	:	Ceil and floor functions
$\delta(x)$	:	Dirac-delta function
$\delta_{\{x,y\}}$	:	Kronecker delta function
$W(\cdot)$	:	Lambert-W function
$\bigtriangledown, \bigtriangledown^2$	:	Gradient and Hessian operators
$\mathbf{a}(\phi)$	:	Array steering response vector at angle ϕ

Probability

$\mathsf{Pr}(\cdot)$	:	Probability measure of an event
$\mathbb{E}[\cdot]$	:	Expectation of a random variable/vector
$\mathrm{var}(\cdot)$	:	Variance of a random variable/vector
$\mathcal{CN}(\boldsymbol{\mu}, \boldsymbol{\Sigma})$	:	Circularly symmetric complex normal distribution with mean $\boldsymbol{\mu}$, covariance $\boldsymbol{\Sigma}$
$\mathcal{N}(\boldsymbol{\mu}, \boldsymbol{\Sigma})$	:	Real normal distribution with mean $\boldsymbol{\mu}$, covariance $\boldsymbol{\Sigma}$
$\mathcal{U}[\phi_0, \phi_1]$	:	Uniform distribution over support $[\phi_0, \phi_1]$
$\exp(\lambda)$	:	Exponential distribution with parameter λ
$\mathrm{Ber}(p)$	:	Bernoulli distribution with parameter p
$\mathrm{Bin}(n, p)$	:	Binomial distribution with parameters n, p
i.i.d.	:	independent and identically distributed
$\xrightarrow{d}$	:	Convergence in distribution
$\xrightarrow{a.s}$	:	Convergence in almost sure sense
$X >_{st} Y$	:	Random variable X stochastically dominates the variable Y
$X \overset{d}{=} Y$	:	Random variables X and Y are equal in distribution
$F_X(x)$	:	Cumulative distribution function (CDF) of random variable X
$f_X(x)$	:	Probability density function (PDF) of random variable X
$\Phi(x)$	:	CDF of a real standard normal Gaussian variable
$Q(x)$	:	The regular Q-function obtained as $1 - \Phi(x)$

Contents

List of Figures

List of Tables

1 Intelligent Reflecting Surfaces: A Game Changer for 5G & Beyond

With the rapid advancement of communication technologies, the wireless industry is increasingly prioritizing the delivery of high-speed, highly reliable, and ubiquitous connectivity services. Wireless cellular communication began in the 1980s with the first generation (1G), and since then, a new generation of cellular technology has emerged approximately every decade, leading to the current deployment of fifth-generation (5G) networks, known as "5G-New Radio" (5G NR). Looking ahead, next-generation wireless systems are expected to support an even broader range of applications across various sectors, including enhanced broadband, the Internet of Things (IoT), healthcare, and smart vehicles. 5G is envisaged to cater to three key use cases [1]: 1) enhanced mobile broadband (eMBB), 2) massive machine-type communications (MMTC), and 3) ultra-reliable and low-latency communications (URLLC). The success of 5G networks in meeting the requirements of these use-cases is quantified using a diverse range of key performance indicators (KPIs.) However, meeting these growing demands necessitates a fundamental shift in how wireless systems are designed. A key breakthrough in this evolution has been the introduction of multiple-antenna array systems, which have significantly enhanced performance (such as higher data rates) without consuming additional scarce resources like time, bandwidth, and energy. We next briefly outline the fundamental contributions of antenna array signal processing to wireless communication, laying the groundwork for the necessity of intelligent reflecting surfaces (IRSs) for next-generation wireless systems, which is the central focus of this thesis.

1.1 Array Signal Processing for Wireless Communications: Benefits and Limitations

With the integration of antenna arrays at both the base station (BS) and user equipment (UE), significant performance improvements have been achieved on several fronts. The key advantages of using antenna arrays include:

1. Beamforming (or) array gain,
2. Spatial diversity gain,
3. Spatial multiplexing gain.

Beamforming gain: It is the ability of multiple antennas to collectively form a beam, concentrating the transmitted signal's energy towards the receiver. This technique enhances the signal-to-noise ratio (SNR) at a UE, which significantly improves the communication rate. At its core, beamforming is a form of *spatial filtering*, where multiple antennas sample the signal in the spatial domain and selectively transmit/receive signals within a specific range of spatial frequencies, corresponding to a specific physical direction or angle. Since beamforming relies on antenna arrays, it is also known as array gain. Depending on the application, different beamforming techniques can be employed, including maximal ratio transmission (MRT), zero-forcing (ZF) precoding, and minimum mean-square error (MMSE) precoding, each offering unique trade-offs in performance and complexity.

Spatial diversity gain: Wireless channels are prone to fading, which can lead to deep fade events, which are periods when the signal strength drops significantly. These events can increase packet error rates at the receiver, making reliable communication challenging. In this context, diversity serves as a fundamental technique to mitigate the effects of fading by enabling signals to propagate through multiple independent wireless paths. The core principle is that while some channels may undergo deep fades, others are likely to remain strong, thereby preserving the overall link reliability. When multiple antennas are deployed, the channel independence across these antennas introduces *spatial diversity*, which significantly improves robustness and minimizes the detrimental effects of fading.

Spatial multiplexing gain: In a multiple-input multiple-output (MIMO) system, we can leverage the additional *spatial degrees of freedom* to transmit multiple data streams simultaneously over independent channels without requiring additional bandwidth or time resources. This enables us to efficiently use the spectrum, leading to higher throughput and network performance.

Although antenna array systems provide significant advantages, fully harnessing their potential requires the implementation of advanced and efficient array signal processing algorithms. As a result, these systems also come with many challenges and overheads, like

1. Higher energy consumption due to multiple antennas, radio-frequency (RF) chains, and amplifiers
2. Larger time complexity incurred for channel estimation and beamforming
3. Pilot contamination and need for more robust interference mitigation hardware
4. Higher cost of implementation/larger form factors of the antenna array
5. Sophisticated data decoding procedures, costly feedback/control overheads, etc.

Therefore, unless *low-complexity and efficient array signal processing techniques* are deployed, the overheads mentioned above can easily undermine the advantages of using antenna arrays in a system. Moreover, a fundamental characteristic of multiple-antenna systems is that they enhance data transmission by *adapting* the transmitted signal to the propagation environment, rather than directly *controlling* the wireless channel itself. This limitation, along with the need for low-complexity solutions, serves as the motivation for the development of intelligent reflecting surfaces (IRSs).

Unlike traditional antenna arrays, IRSs provide a means to *shape and control* the wireless channel while remaining nearly passive. Thus, integrating IRS technology enables next-generation antenna array systems to jointly control and adapt to the wireless channel. We next explore the innovative IRS technology in detail and subsequently remark on how IRS

further enhances the beamforming, spatial diversity, and spatial multiplexing capabilities, which helps to place the contributions of this thesis in context.

1.2 Intelligent Reflecting Surfaces: Working Principle and State-of-the-Art

Intelligent reflecting surface, also referred to as reconfigurable intelligent surface (RIS), consists of an array of passive elements capable of manipulating an incident electromagnetic wave to steer its reflection in a required direction. A prominent technique to implement an IRS involves the use of metamaterials, which are artificially engineered structures with reconfigurable electromagnetic properties [2]. These materials allow the effective refractive index of each element to be dynamically adjusted, thereby enabling precise control of the reflection coefficient at the point of incidence. Consequently, by tuning the IRS elements to induce specific phase shifts and amplitude responses, it becomes feasible to reconfigure the wireless environment as per our requirement. In particular, this capability facilitates the intelligent control of the wireless channels between any pair of transceivers in the network, opening new avenues for enhancing spectral efficiency (SE), reliable communication, mitigating interference, etc.

To make the discussion more concrete, a simplified schematic of an IRS-assisted wireless communication system is illustrated in Fig. 1.1. This example considers a single BS and a single UE, each equipped with a single antenna. An IRS consisting of N passive reflecting elements is deployed at an appropriate location within the environment, and as described above, the reflection coefficient of each element of the IRS is independently programmable. As a consequence, the overall channel at a UE, say, indexed by k, can be expressed as

$$h_k = \sqrt{\beta_{r,k}}\mathbf{h}_{2,k}^T \boldsymbol{\Theta} \mathbf{h}_1 + \sqrt{\beta_{d,k}} h_{d,k}, \tag{1.1}$$

where $h_{d,k}$ is the small-scale fading channel from BS to UE-k in the direct link, $\mathbf{h}_1, \mathbf{h}_{2,k} \in \mathbb{C}^N$ are the small-scale fading channels from BS to IRS, and IRS to UE-k respectively, and $\beta_{d,k}, \beta_{r,k}$ denote the large-scale path loss of direct and cascaded channels via the IRS at

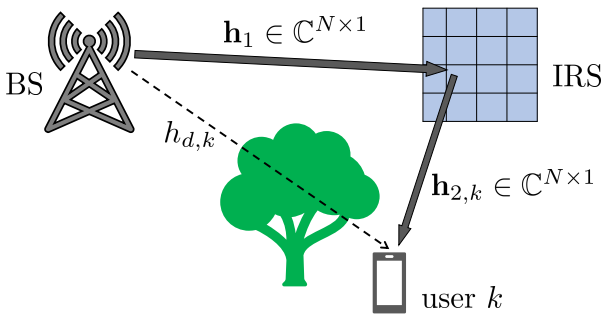

Figure 1.1: An IRS-assisted wireless system.

UE-k. Further, $\mathbf{\Theta} \in \mathbb{C}^{N\times N}$ is a diagonal matrix that contains the reconfigurable reflection coefficients of the IRS elements and is modeled as $\mathbf{\Theta} = \text{diag}\left(\left[\zeta_1 e^{j\phi_1}, \zeta_2 e^{j\phi_2}, \ldots, \zeta_N e^{j\phi_N}\right]^T\right)$, where $\zeta_n \in [0,1]$ and $\phi_m \in [0, 2\pi)$ denote the amplitude and phase of the reflection coefficient at nth IRS element. If we design our IRS circuit elements such that the reflection coefficients have equal magnitude, then, we can set $\zeta_n = 1$ for all $n \in [N] \triangleq \{1, 2, \ldots, N\}$ without loss of generality, and the IRS reflection coefficient matrix, $\mathbf{\Theta}$ becomes a phase shift matrix: $\mathbf{\Theta} = \text{diag}\left(\left[e^{j\phi_1}, e^{j\phi_2}, \ldots, e^{j\phi_N}\right]^T\right)$.

It is evident from (1.1) that the overall wireless channel can be effectively manipulated using the phase-shift array at the IRS, even when both the BS and the UE are equipped with just a single antenna. Extending this idea further, when multiple active antennas are employed at the BS and/or UE in conjunction with a large array of passive reflecting elements at the IRS, the system acquires substantial flexibility. Specifically, the IRS enables us to shape the channel, and the transmitter array at the BS adapts the transmission to channel conditions, thereby allowing for fine-tuned optimization of the end-to-end wireless link in accordance with specific performance objectives.

1.2.a Integrating IRSs into Next-Generation Wireless Systems

We now shift our focus toward understanding the different protocols involved in integrating IRSs into next-generation wireless communication systems. As previously discussed, the IRS modifies the channel by imparting a carefully designed phase shift at each of its elements. However, to apply the desired configuration at the IRS, it is essential to implement a structured *three-phase protocol*, as described below:

1. *Channel estimation*: The first step involves acquiring knowledge of the underlying channel coefficients, also called channel state information (CSI), between the BS and the UE. Specifically, from (1.1), it can be observed that in the presence of an IRS comprising N elements, the total number of channel coefficients is $2N + 1$, including the direct BS–UE path, BS–IRS link, and IRS–UE link. However, since the knowledge of the *cascaded channel*, denoted as $\mathbf{h}_{r,k} \triangleq \mathbf{h}_{2,k} \odot \mathbf{h}_1$, where $\odot$ represents the element-wise (Hadamard) product, is sufficient for optimizing the IRS phase shifts [2], we need to estimate $N + 1$ coefficients, which in turn requires the use of at least $N + 1$ known pilot signals, unless these parameters are significantly correlated.

2. *Channel feedback & phase optimization*:

   (a) The goal of the channel feedback step is to enable the BS to acquire the CSI estimated in the previous step. In the case of frequency division duplexing (FDD), the estimated CSI is fed back to the BS via a dedicated feedback link, after the UE performs channel estimation in the downlink. However, in time-division duplexing (TDD) systems, by leveraging channel reciprocity, the BS can directly estimate the uplink channel and infer the corresponding downlink CSI from it. This, in turn, enables efficient signaling strategies that eliminate the need for explicit CSI feedback from UE to BS, thereby reducing the signaling overheads.

   (b) In the phase optimization step, the BS computes the optimal IRS phase configuration based on the acquired CSI. This typically involves formulating and solving an optimization problem aimed at enhancing a specific performance metric, such as received signal power, spectral efficiency, or signal-to-interference-plus-noise ratio, while satisfying the unit-modulus constraint imposed by the IRS phase shifts.

3. *IRS phase transportation:* This is the final step in configuring an IRS. Owing to the passive nature of the IRS, the BS is responsible for performing the phase optimization process. Once the optimal phase shifts are determined, these phase angles are transported from the BS to the IRS controller through a dedicated control link. The IRS controller then programs each reflecting element with its respective phase shift, thereby

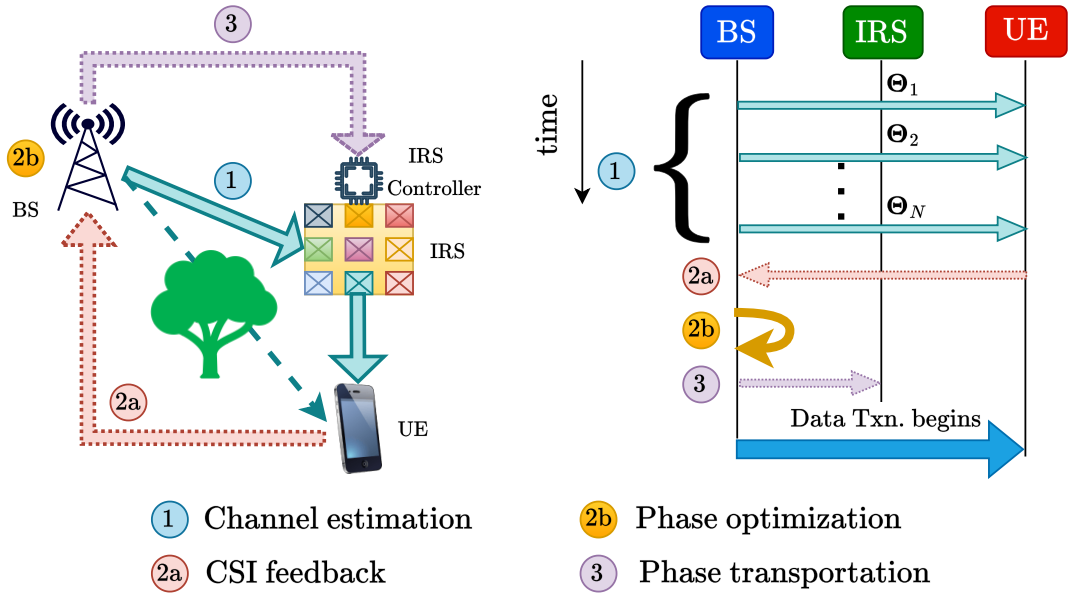

Figure 1.2: Control signaling steps in configuring an IRS. The left-hand figure shows the exchange of information among different nodes, and its timing diagram is shown on the right.

realizing the intended manipulation of the wireless channel.

Figure 1.2 provides a schematic illustration of the complete procedure for configuring an IRS and integrating it into a wireless communication system.

1.2.b Use-cases and Deployment Scenarios: The State-of-the-Art

Integrating an IRS into a wireless system enables overall channel optimization and can enhance system performance in multiple ways [3–8]. Below, we briefly summarize several approaches proposed in the literature for configuring the IRS and harnessing its benefits:

In [9], the authors demonstrate that an IRS can create a virtual line-of-sight (LoS) path between the BS and UEs, leading to improved SNR and spectral efficiency (SE). Similarly, [10] shows that optimizing IRS phase shifts for a given channel increases the received SNR quadratically with the number of IRS elements. In [11], the authors focus on maximizing the energy efficiency, while works in [12–14] propose joint active and passive beamforming algorithms that underscore the adaptability and controllability of IRS-enabled systems, as discussed in Sec. 1.1. Moreover, IRS phase optimization in MIMO and orthogonal frequency division multiplexing (OFDM) systems has been addressed in [15–20].

However, realizing the benefits of an IRS requires accurate CSI; accordingly, several works have investigated channel estimation with various guarantees and complexities [21–35]. Coverage enhancement via IRS is explored in [5, 36], the effect of IRSs on inter-BS interference in [37], and IRS-based interference nulling in [38]. Additionally, physical layer security improvements using IRSs are discussed in [39], and the role of IRS in integrated sensing and communications is demonstrated in [40].

A few studies have also investigated randomly configured IRSs. Blind beamforming and diversity analysis with random IRS phases are reported in [41–44], although these methods incur high time complexity. Also, [45] employs randomized IRSs to protect against wireless jammers. For wideband systems, methods for channel estimation and beam training accounting for spatial wideband effects have been developed in [46–48], Localization of UEs is addressed in [49], while [50, 51] leverage wideband phenomena to enhance cell coverage and the performance of OFDM-based multiple access. Finally, several works [52–55] use true time-delay (TTD) units at the IRS to enable coherent beamforming over the entire operational bandwidth.

Regarding deployment scenarios, IRS technology is envisioned for indoor environments, where it can enhance throughput and coverage for IoT applications [56], as well as for outdoor scenarios, as discussed in the previous paragraph.

Beyond academic research, several industrial bodies are also actively advancing through the IRS technology. The European Telecommunications Standards Institute (ETSI) has dedicated study items on IRS [57], the Telecommunications Standards Development Society (TSDSI), an standards development organization of India has proposed interface design options and implementation methods for IRS-aided systems [58, 59], and industry leaders such as Qualcomm and ZTE routinely host workshops, underscoring the growing interest in practical IRS implementation.

Despite these advances, the key challenges remain. Incorporating an IRS into a wireless system introduces substantial overheads. Without the development of low-complexity, high-performance schemes, the real-time deployability of IRS becomes a challenge. Also, the fundamental performance limits of many IRS use cases are still not well understood.

Addressing these issues is crucial for fully realizing the benefits of IRSs in practical systems.

1.3 Scope of this Thesis

This thesis primarily investigates two key aspects of IRS-aided wireless systems:

1. Design of IRS-aided wireless systems with particular emphasis on *low-complexity*,
2. Performance analysis of IRS-aided systems under practical deployment constraints.

Accordingly, the thesis is organized into three main parts, each addressing a distinct, yet interconnected class of problems. In the following, we provide an overview of the research questions tackled in each part and discuss the key contributions of this thesis.

1.3.a PART - 1: Low-Complexity Methods for Optimal Benefits

The first part of this thesis delves into the fundamental principles governing the operation of the IRS, as outlined in Section 1.2.a. We first recognize that incorporating an IRS into a wireless communication system leads to incurring the following **three-fold overheads**:

1. **CSI estimation overheads**: As detailed in Section 1.2.a, the first step involves estimating the CSI of all the links. Notably, the required pilot overhead scales linearly with the number of reflecting elements at the IRS. Even when advanced estimation techniques are employed to reduce this complexity, the system still suffers from channel estimation errors, which again scale with the number of IRS elements [60].
2. **Optimization overheads**: To determine the optimal phase angles, the BS must first acquire the CSI estimated in the first step. In scenarios where CSI is obtained via feedback, this process introduces its own overheads [61]. Once the CSI is acquired at the BS, it solves an optimization problem to jointly determine the IRS phase configuration along with other relevant system parameters. In general, this optimization problem is inherently non-convex, making it computationally intractable to solve optimally. As a result, significant computational resources must be allocated to obtain a near-optimal IRS phase configuration, particularly when the system dimensions are large.

3. **Transportation overheads**: Finally, since the phase information of every element has to be transported from BS to IRS (see the phase transportation step in Sec. 1.2.a), this overhead also potentially scales linearly in the number of IRS elements, N. For e.g., if the resolution of the phase shifter at an IRS element is d, then $N \log_2(d)$ bits have to be conveyed to the IRS every time the IRS is reconfigured.

Clearly, when compared to a system without an IRS, an IRS-aided system can incur a significant amount of additional time and computational complexity. These added complexities reduce the time and power available for data transmission, thereby undermining the professed benefits of incorporating an IRS. This observation raises a crucial question, which forms the central focus of PART 1 of this thesis.

Problem for PART - 1

How can we obtain optimal IRS benefits **without optimizing the IRS** and **without incurring the three-fold overheads**?

We provide an affirmative answer to this question using the following idea:

Solution for the problem of PART - 1

Configure the **IRS phases randomly** and adopt **opportunistic scheduling**!

The core concept underlying an opportunistic communication (OC) framework is to allocate system resources to those UEs that experience the most favorable channel conditions within a given resource element. For instance, in a time-division multiple access (TDMA) system employing single-carrier transmission, the BS schedules, in each time slot, the UE witnessing the strongest instantaneous channel conditions for data transmission. Within this context, the central premise of our approach is as follows:

Premise of the idea in PART - 1: Random IRS becomes optimal IRS

With multiple UEs, a random IRS phase is **near-optimal to at least one UE**; **opportunistically scheduling** that UE reaps optimal gain without optimization!

While the effectiveness of this approach is inherently tied to scenarios involving a large

number of UEs, such conditions are generally anticipated in next-generation wireless networks to support dense user populations [62]. Consequently, the proposed strategy is well-aligned with the characteristics and requirements of advanced wireless systems.

Within the scope of this framework, PART 1 of the thesis addresses the following key research questions:

Q1: What performance guarantees can be established for different opportunistic scheduling policies when the IRS configurations are randomly selected?

Q2: What is the appropriate sampling distribution from which random IRS phase configurations should be drawn to achieve (near-)optimal system performance?

Q3: What is the minimum number of UEs required to attain a specified opportunistic scheduling gain from the IRS?

Q4: How does the proposed scheme perform under various channel models, including sub-6 GHz and mmWave propagation environments?

Q5: Finally, how does system performance vary between narrowband and wideband channel conditions?

In Sec. 1.4.a (and in Sec. 1.4.c.ii for mmWave bands), we summarize the answers to the above questions and outline the key contributions of this part of the thesis. Our main finding is that an opportunistic scheduling framework can achieve near-optimal IRS performance without relying on complex optimization procedures while maintaining low time and computational overheads, and even when there are only a moderate number of UEs in the system.

1.3.b PART - 2: Does an IRS Degrade Out-of-Band Performance?

This part of the thesis investigates a critical concern associated with the deployment of IRSs in practical wireless systems. In real-world network environments, it is common for multiple wireless service providers (or mobile operators) to offer services within the same geographical region. Each operator is typically allocated a distinct yet closely spaced

frequency band for serving its subscribers. In such a setting, consider a scenario where one operator (called the in-band operator) deploys and controls an IRS to optimize service for its own users. Then, a natural question is: How does the deployment of this IRS impact the channel characteristics and performance of users served by a different operator, referred to as the out-of-band (OOB) operator that operates in a nearby but non-overlapping band?

This question is of practical relevance due to the passive and frequency-agnostic nature of IRSs, as discussed in Section 1.2. Unlike active devices, IRSs are not equipped with band-pass filters capable of selectively reflecting signals of the operator who deployed the IRS. As a result, an IRS reflects all incident electromagnetic signals, thereby unintentionally altering the wireless propagation environment for OOB users as well. For instance, consider the n78 band in 5G New Radio (NR), which spans the frequency range of 3300–3800 MHz, corresponding to a total bandwidth of 500 MHz. Since the maximum carrier bandwidth permitted in 5G NR is 100 MHz, this band can simultaneously accommodate five different operators even if the full 100 MHz is allotted to each operator. In such a deployment scenario, although each operator transmits within a non-overlapping portion of the spectrum, the IRS will reflect signals from all operators with comparable efficiency, given that they operate within the same frequency range. This creates the possibility of unintended channel modifications for OOB users.

Thus, PART 2 of the thesis is dedicated to rigorously addressing the pivotal question:

Problem for PART - 2

How does an IRS deployed by a mobile operator affect the performance of an OOB operator providing services in the same geographical area?

We find that the answer to this question is as follows:

Solution for the problem of PART - 2

The OOB **channel gain improves due to the presence of an uncontrolled IRS**. In sub-6 GHz bands, the gain improves monotonically ($\mathcal{O}(N)$) with the number of IRS elements, N. In mmWave bands, the gain dramatically improves ($\mathcal{O}(N^2)$) with a probability whose value decreases as $\mathcal{O}(1/N)$.

To arrive at the above conclusion, we consider a wireless system comprising two operators, wherein only one of them deploys and controls an IRS. Through this setup, we aim to systematically answer the following key research questions:

Q1: How does the ergodic spectral efficiency scale for both the in-band and OOB operators in the presence of an IRS controlled only by the in-band operator?

Q2: What is the behavior of the outage probability of UEs associated with both the in-band and OOB operators?

Q3: How does performance vary for sub-6 GHz and mmWave propagation environments?[1]

Q4: How do the performance trends differ between single-IRS and multiple-IRS deployments for both operators?

Q5: How can we design efficient CSI estimation algorithms for multi-IRS setups that incur minimal pilot overhead at the in-band operator?

Q6: To what extent does the OOB performance depend on the choice of scheduling algorithms employed by the OOB operator?

Q7: Finally, focusing specifically on the mmWave regime, if each operator independently deploys and controls its own IRS, what are the individual performance gains or losses arising from the presence of OOB IRSs, and what additional benefit, if any, can be realized through inter-operator cooperation?

The answers to these questions are summarized in Section 1.4.b. Our finding reveals that each mobile operator can independently deploy and manage its own IRS infrastructure without significant cooperation with other operators, thereby maintaining network autonomy while benefiting from the advantages of IRS technology.

[1] We consider scenarios where both operators operate in the same frequency regime—either sub-6 GHz or mmWave; but exclude cases where one operator uses sub-6 GHz and the other mmWave bands.

1.3.c PART - 3: IRS-aided Wideband Beamforming

In this final part of the thesis, we turn our focus to a critical and largely open challenge: enabling IRSs to effectively beamform wideband signals, and we propose viable solutions to address this issue. This study encompasses both sub-6 GHz and mmWave communication bands. The core challenge arises from the fundamental limitations of using phase shifters at the IRS for beamforming. Specifically, wideband signals generally experience frequency-selective fading, where the channel response differs across frequency components. In contrast, IRS phase shifters exhibit a frequency-flat response over the entire bandwidth, limiting their ability to adapt to the frequency-dependent variations of the channel. Consequently, the IRS cannot perfectly align its reflection phases with the desired channel across all frequency subbands, thereby degrading its beamforming efficiency in wideband settings. This issue can be better understood in the context of classical array signal processing theory [63], where the canonical structure for wideband beamforming is the *delay-and-sum architecture* using true-time delay (TTD) units. Under the narrowband assumption, this architecture simplifies to a phase shift-and-sum beamformer, which mirrors the operational design of typical IRS implementations. However, incorporating TTD units at the IRS is impractical due to their bulkiness, power consumption, and complexity, which defeat the low-cost and passive design philosophy of IRSs. Motivated by this gap, we explore and develop low-complexity, hardware-friendly techniques to enable wideband beamforming of IRSs, which constitutes the central focus of this part of the thesis.

mmWave bands: In this frequency range, the frequency selectivity of the channel is attributed to the spatial-wideband effect—a phenomenon where the signal propagation delay across the aperture of a large IRS becomes comparable to, or even exceeds, the sampling duration. This leads to the so-called beam-split (B-SP) effect, wherein the IRS focuses its reflected energy toward a given UE only over a portion of the operating bandwidth. As a result, both the array gain and throughput degrade significantly in wideband scenarios.

Motivated by the above considerations, we aim to address the following core problem:

Problem for PART - 3

How to **handle/control beam-split effects** using low-complexity techniques?

To tackle this challenge, we pursue two complementary approaches:

- In the first approach, the B-SP effect is treated as an impairment. Accordingly, we develop a low-complexity **mitigation strategy** to suppress its adverse impact on the achievable array gain and throughput at a UE.
- In the second approach, we take a different perspective wherein the B-SP effect can be **exploited** to enhance system throughput from a network-level viewpoint.

Then, the key ideas behind these approaches are outlined as follows.

Premise of the idea in PART - 3

1. **Partitioning a large IRS into multiple smaller, distributed IRSs** allows for effective control and mitigation of the B-SP effect at a given UE.
2. Adopting an **opportunistic OFDMA** approach exploits the B-SP effect to yield the full array gain across the entire bandwidth from a network perspective.

In particular, we address the following specific questions:

Mitigating beam-split effect

Q1: What is the maximum permissible number of IRS elements required to effectively control the B-SP effect?

Q2: How does the delay spread introduced by distributed sub-IRSs impact the achievable data rate at a given UE?

Q3: What is the optimal choice of locations of the sub-IRSs?

Q4: Can multiple IRSs offer diversity benefits to further mitigate the B-SP effect?

Q5: How does the complexity of the proposed approach compare with existing methods?

We address these questions in Sec. 1.4.c.i and summarize the key contributions related to mitigating the B-SP effect.

Exploiting beam-split effect

Q1: What is the precise nature of the frequency selectivity induced by the B-SP effect?

Q2: What is the rationale behind employing an opportunistic OFDMA strategy with multiple UEs to achieve full beamforming gain over the bandwidth?

Q3: What is the success rate of the scheme for achieving a target SNR across the BW?

Q4: How many UEs are necessary to achieve a target success rate with high probability?

Q5: What is the achievable throughput of the system using the proposed opportunistic OFDMA strategy?

In Sec. 1.4.c.ii, we briefly answer these questions and highlight the key contributions concerning the exploitation of the B-SP effect.

Sub-6 GHz bands: Here, the channel frequency selectivity primarily arises due to the rich scattering induced by multipath propagation through the IRS. As a result, in multi-carrier communication systems such as OFDM, each subcarrier experiences a distinct channel gain. This variation poses a fundamental challenge to IRS-based beamforming in wideband systems, where the phase configuration of the IRS cannot be simultaneously optimal across all subcarriers.

Motivated by this observation, we pose the following research question:

Q1: What is the optimal IRS phase configuration that maximizes the OFDM system's sum-rate while maintaining low complexity and high performance?

In the next section, we summarize the key contributions of this thesis, addressing the key questions and challenges discussed above.

1.4 Outline and Contributions of this thesis

As mentioned earlier, this thesis is organized in three parts. We outline the contributions of these parts in the following subsections.

1.4.a PART - 1: IRS-assisted Opportunistic Communications

Part-1 comprises Chapters 2 and 3 and deals with IRS-assisted opportunistic communications, where the key objective is to obtain SNR-optimal performance without explicitly optimizing the IRS or incurring the associated overheads. In particular, when the number of UEs gets large, a randomly chosen IRS configuration will be near-optimal to at least one UE in the system with high probability; this is the benefit of *multi-user* diversity. Then, it can be shown that, for a randomly chosen IRS configuration, opportunistic scheduling of UEs using a proportional-fair (PF) scheduler leads to a network sum throughput that, in the limit of a large number of UEs, converges to the rate achieved by a round-robin (RR) scheduler with the IRS phase configurations optimized for the scheduled UE's channel. In this context, our specific contributions are as follows:

1. We show that, when the phase angles of the IRS are sampled using a uniform distribution and a PF scheduler is employed, the number of UEs required to obtain near-optimal benefits in independently and identically distributed (i.i.d.) channels scales exponentially in the number of IRS elements.

2. We analyze the throughput of a few other promising IRS-assisted OC schemes for i.i.d. narrowband wireless channels. Specifically, we exploit the fast switching time of IRS phase configurations to obtain reflection diversity from the IRS and show that this helps to reduce the number of users required to obtain near-optimal throughput.

3. Next, we exploit the directional nature of the channels in the IRS-aided system and design channel model-aware randomly configured OC schemes that converge to the coherent beamforming rate without requiring the users to scale exponentially with the number of IRS elements. Further, using max-rate scheduling, we show that not only

does this scheme achieve the quadratic scaling of the SNR with the number of IRS elements, but its throughput can even surpass that of the scheme that involves IRS optimization techniques due to the lack of multi-user diversity gain in the latter. We also discuss how this scheme can be applied to narrowband channels in the mmWave frequencies, which bear a similar structure.

4. We extend our results to a generic spatial correlation model at the IRS, and provide the following contributions:

   (a) We pose and solve a variational functional problem to obtain the optimal sampling distribution for the random IRS phases, as a function of the distribution of the channels. We show how the distribution should match the channel statistics.

   (b) Next, we show that when the above spatial-correlation-aware distribution is used to sample the IRS configuration, it is sufficient for the number of UEs to scale exponentially in the *rank of the channel covariance matrix* to obtain near-optimal SNR in every time slot.

   (c) In the process, we derive the tail probability of the Rayleigh quotient of a heteroscedastic complex Gaussian vector, a result that may be of independent interest.

5. We extend the OC schemes to IRS-aided systems with wideband wireless channels in the sub-6 GHz frequency bands. Specifically, we consider an OFDM system and discuss two OC schemes, namely, single-user OFDM, where we schedule a single user across all subcarriers, and OFDMA, where multiple users are potentially scheduled across the subcarriers. We derive the sum throughput scaling laws for the two schemes and provide interesting insights about these systems.[2]

In a nutshell, we show that even a randomly configured IRS, along with opportunistic scheduling of UEs, can procure optimal benefits without incurring overheads that scale

[2]We provide a detailed list of contributions in the context of IRS-assisted opportunistic communications in wideband scenarios in the mmWave frequency bands in Sec. 1.4.c.ii.

with the number of IRS elements. The next part of the thesis explores another aspect of IRS-aided communication systems where random phase configurations will prove to be beneficial.

1.4.b PART - 2: Impact of IRS on Out-of-Band Performance

This part comprises Chapters 4, 5, 6, and 7, where we consider a system with two network operators, X and Y, providing service in different frequency bands in the same geographical area. The IRS is deployed by and optimized to serve the UEs subscribed to the *in-band* operator X, and we are interested in analyzing the achievable SE and outage probability witnessed by the UEs subscribed to the *OOB* operator Y, which does not control the IRS. Specifically, we (separately) evaluate the IRS-assisted performance in both sub-6 GHz and the mmWave bands, which are provisioned as the FR1 and FR2 bands in 5G, respectively [64]. Further, in the mmWave bands, inspired by [65], we study two scenarios: (a) LoS (line-of-sight) and (b) (L+)NLoS (LoS and Non-LoS.) In the LoS scenario, the IRS is optimized or aligned to the dominant cascaded path (called the *virtual* LoS path) of the in-band UE's channel. This is also considered in [9, 66], where the in-band UEs' channels are approximated by the dominant LoS path to reduce the signaling overhead required for the BS to program the IRS: the phase of the second IRS element relative to the first element determines the entire phase configuration. Contrarily, in the (L+)NLoS case, the IRS optimally combines all the spatial paths to maximize the SNR at the receiver, for which the overhead scales linearly with the number of IRS elements. Using tools from high-dimensional statistics, stochastic-dominance theory, and array processing theory, we make the following contributions.

1.4.b.i OOB Performance in sub-6 GHz Bands

Here, the operators serve their UEs over the sub-6 GHz frequency bands where the channels are rich-scattering. In this context, our key findings are as follows.

1. We derive the ergodic sum-SEs of the two operators as a function of the system parameters, under round-robin (RR) scheduling of the UEs served by both operators. We

show that the sum-SE scales log-quadratically and log-linearly with the number of IRS elements for the in-band and OOB networks, respectively. Thus, the OOB operator benefits from the IRS, even though the IRS is not controlled by the OOB operator.

2. We show that the outage probability at an arbitrary OOB UE decreases monotonically with the number of IRS elements. Further, via the complementary cumulative distribution function (CCDF) of the difference in the OOB channel gain with and without the IRS, we prove that the OOB channel gain with an IRS *stochastically dominates* the gain without the IRS, with the difference increasing with the number of IRS elements. Thus, an OOB UE gets instantaneous benefits that monotonically increase with the number of IRS elements.

1.4.b.ii OOB Performance in mmWave Bands

In the mmWave bands, the channels are directional, with only a few propagation paths. In this context, using novel probabilistic approaches based on the resolvable criteria of the mmWave spatial beams, our key findings are as follows.

1. In LoS scenarios, where the IRS is optimized to match the dominant path of the in-band UE's channel, we derive the ergodic sum-SEs of the two operators under RR scheduling of the UEs. The SE at the in-band UE scales log-quadratically in the number of IRS elements, whereas the SE gain at an OOB UE depends on the number of spatial paths in the OOB UE's channel. If there are sufficiently many paths in the cascaded channel, the SE improvement due to the IRS scales log-linearly in the number of IRS elements. Otherwise, the OOB UE's SE improves only marginally compared to that in the absence of the IRS.

2. We evaluate the outage probability and CCDF of an OOB UE's channel gain with-/without an IRS in LoS scenarios and prove that the channel gain in the presence of IRS *stochastically dominates* the gain in its absence. Thus, even in mmWave bands, the IRS provides positive instantaneous gains to all the OOB UEs.

3. We next consider the (L+)NLoS scenario where the IRS is jointly optimized considering

all the spatial paths. We first evaluate the directional energy response of the IRS and show that it exhibits peaks only at the channel angles to which the IRS is optimized. To the best of our knowledge, this is a novel and fundamental characterization of the IRS response under multi-path alignment in mmWave systems, which has not been studied in the existing literature on IRS-aided communications.

4. We derive the ergodic sum-SE of both operators in (L+)NLoS scenarios. We find that the OOB performance is even better than the LoS scenario (and hence better than the system without an IRS). This is because the odds that an OOB UE benefits improve when the IRS has a nonzero response in multiple directions. Thus, the OOB performance in mmWave bands does not degrade even when the OOB operator serves its UEs while remaining oblivious to the presence of the IRS.

5. We then consider a system with multiple smaller distributed IRSs obtained by partitioning a single large IRS. Then, in LoS scenarios, our findings are the following:

   (a) Under RR scheduling, we derive the ergodic sum-SEs of the mobile operators (MOs). If N is the total number of IRS elements, we show that the SE of MO-X grows as $\mathcal{O}(2\log_2(N))$, and the SE of MO-Y scales as $\mathcal{O}(\tau\log_2(N))$, where the pre-log factor $\tau \in [0, 1]$ increases with the ratio of the number of OOB paths through the IRS to the number of elements at an IRS.

   (b) We design a distributed IRS system and specify the minimum number of IRSs for MO-Y to *almost surely* achieve the maximum SE (i.e., for $\tau = 1$.)

   (c) Finally, we show that the outage probability at an arbitrary OOB UE decreases exponentially as the number of IRSs deployed by MO-X increases.

   Thus, we demonstrate that multiple IRSs help the OOB MOs better than a single IRS, both on average and in an instantaneous sense.

6. Next, since multiple IRSs also increase the CSI estimation overheads at the in-band MO, we develop a low-complexity CSI estimator (for a general setting with multiple antennas at both the BS and UE), and make the following contributions:

(a) We formulate the cascaded CSI estimation problem as a direction of arrival (DoA) and direction of departure (DoD) estimation problem. We develop a cascaded CSI estimation algorithm at the BS (in the uplink mode) for distributed IRS-aided massive MIMO systems by exploiting the subspace properties of the mmWave channels based on a combination of direction-finding algorithms in the array processing literature. In particular, since the channel model has both DoAs and DoDs coupled, we develop a novel *joint ESPRIT-MUSIC* algorithm that jointly estimates the DoA at the BS and DoD from the UE, with the estimation being performed at the BS. The DoA is estimated first and is passed as an input to the DoD estimator using an appropriately chosen MUSIC-based cost function. Then, the path gain coefficients are estimated using a low complexity least-squares (LS) method.

(b) We show that our approach yields accurate channel estimates with a dramatically reduced pilot overhead compared to conventional approaches. This is made possible by the aforementioned reformulation, which reduces the number of parameters to be estimated to depend only on the total number of paths in the system, i.e., on the number of IRSs and the number of antennas at the UE and *not* on the total number of IRS elements and the number of BS antennas, which are generally very large in mmWave massive MIMO systems.

(c) We compare our method against that in [33], where the sparsity in the angular domain of the mmWave channel is exploited to formulate the problem as a multiple measurement vector (MMV) based sparse recovery problem, which is then solved using simultaneous orthogonal matching pursuit (SOMP). We numerically show that our method outperforms SOMP, with the performance gap increasing as the number of IRSs increases.

7. Finally, we deal with the case where each MO deploys and controls its own IRS, and in this case, we make the following contributions for the LoS scenarios:

(a) Considering that 2 MOs, X and Y, control an IRS each, we derive the ergodic sum SE of the MOs when an overall phase at each IRS is configured as per the

following implementation schemes:

i. *Optimization with Time-sharing*: In each time slot, while an MO serves its own UE, the overall phases at the IRSs are optimized for a UE served by either MO-X or MO-Y.

ii. *Joint-optimization with MO cooperation*: The overall IRS phases are jointly tuned to maximize the weighted sum-SE of UEs served by the MOs in every time slot.

iii. *No MO cooperation*: In this scheme, each MO focuses exclusively on optimizing its IRSs to ensure coherent signal reception at only its own UEs.

(b) We show that the IRS controlled by one MO does not degrade the SE of the other MO. We quantify the gain in the sum-SE of the MOs obtained with/without OOB IRS, and with/without cooperation (for time-sharing/joint optimization) as a function of the number of OOB IRS elements.

(c) We extend our results to a system where more than 2 MOs co-exist, which deploy and control an IRS each. In particular, we derive the ergodic-sum-SE of the MOs for the above-mentioned three schemes.

(d) Finally, even with more than 2 MOs, we show that the OOB IRSs do not degrade the in-band performance. Further, although joint optimization/time sharing with MO cooperation still offers marginal gains relative to sum-SE when the MOs do not cooperate, the gain increases at least linearly with the number of OOB MOs.

1.4.b.iii Opportunistic Enhancement of OOB Performance

Having shown that an IRS positively benefits OOB UEs, we next suggest ways to exploit the uncontrolled IRS to enhance the performance of OOB operators further. In particular, by using opportunistic selection techniques, we leverage multi-user diversity and show that a significant boost in the OOB performance can be obtained compared to RR scheduling. Specifically, we demonstrate the following.

1. By using a proportional-fair scheduler over a large number of OOB UEs, the sum-SE

of the OOB operator Y converges to the so-called *beamforming SE*, which is the SE obtained when the IRS is optimized for an OOB UE in every time slot.

2. By using a max-rate scheduler, the ergodic sum-SE of operator Y monotonically increases with both the number of IRS elements and OOB UEs in the system.

This marks the conclusion of PART-2 of the thesis.

1.4.c PART-3: Wideband Beamforming with Phased Arrays at IRS

This final part comprises Chapters 8, 9, and 10, where the key focus is to enable the low-complexity promoting IRS phase shifters to perform wideband beamforming over a frequency-selective wideband channel. In particular, we address the key questions listed in Sec. 1.3.c and make the following key contributions.

1.4.c.i Mitigating beam-split effects in mmWaves using distributed IRSs

1. *SW effect reduction:* We mathematically show that a distributed IRS design naturally parallelizes the spatial delays and mitigates the SW effect.

2. *Number of IRS elements*: We determine the maximum number of elements at each IRS so that the loss in the array gain due to B-SP is within acceptable limits while retaining the achievable peak gain.

3. *Sum-rate and array gain:* Next, we analyze the impact of the *temporal delay spread* (TDS) caused by multiple paths arriving at the UE through different IRSs. We show that the achievable rate on every subcarrier (SC) scales log-quadratically in the number of elements at each IRS and at least log-linearly in the number of IRSs, thus effectively mitigating deep nulls in the channel response due to the B-SP effect. When the TDS is zero, the sum-rate across all the SCs in the bandwidth (BW) grows log-quadratically in the total number of IRS elements, and yields the full array gain over the BW.

4. *Optimizing the IRS locations:* Having noted that the value of TDS is crucial in determining the achievable peak channel gain, we next focus on optimizing the IRS locations:

(a) Single UE: To minimize the TDS at a single UE, we show that it is optimal to position the IRSs on an ellipse with the locations of BS and UE as its foci. The TDS then becomes zero, allowing the effect of B-SP to be maximally mitigated.

(b) Multiple UEs: With multiple UEs located within a hotspot, we position the IRSs over an ellipse whose foci are given by the location of the BS and the centroid of the distribution of the UE locations. We derive the achievable TDS at an arbitrary location and subsequently characterize a lower bound on the achievable sum-rate.

5. *Angle diversity gain:* Finally, we reveal that multiple IRSs additionally introduce angle diversity gain due to multiple independent paths seen by the UE. In particular, we show that the probability that the array gain equals the worst-case acceptable value (due to the residual beam squint) decreases exponentially with the number of IRSs. On the other hand, the outage probability of a centralized IRS for a target SNR close to the peak array gain is bounded away from zero as the number of IRS elements increases.

1.4.c.ii Exploiting beam-split effects in mmWaves using OFDMA

1. Using a max-rate scheduler in OFDMA, and when the IRS configurations are randomly sampled from an appropriate distribution, we show that, on every SC, the probability that at least one UE will achieve nearly full beamforming gain from the IRS increases as the number of UEs increases.

2. We derive the achievable system throughput and show that a peak data rate that scales log-quadratically in the total number of IRS elements can be obtained on all SCs in addition to the multi-user diversity benefits, with a large number of UEs.

Next, we consider the problem of IRS-aided wideband beamforming in the context of sub-6 GHz bands. We recall from Sec. 1.3.c that the key issue in this case arises due to the multi-path propagation in a rich-scattering setting.

1.4.c.iii Optimizing the IRS in sub-6 GHz wide bands

1. We first develop a low pilot overhead CSI estimation algorithm by leveraging the sparsity in the OFDM channel induced by the IRS. To elaborate, the cascaded BS-IRS and

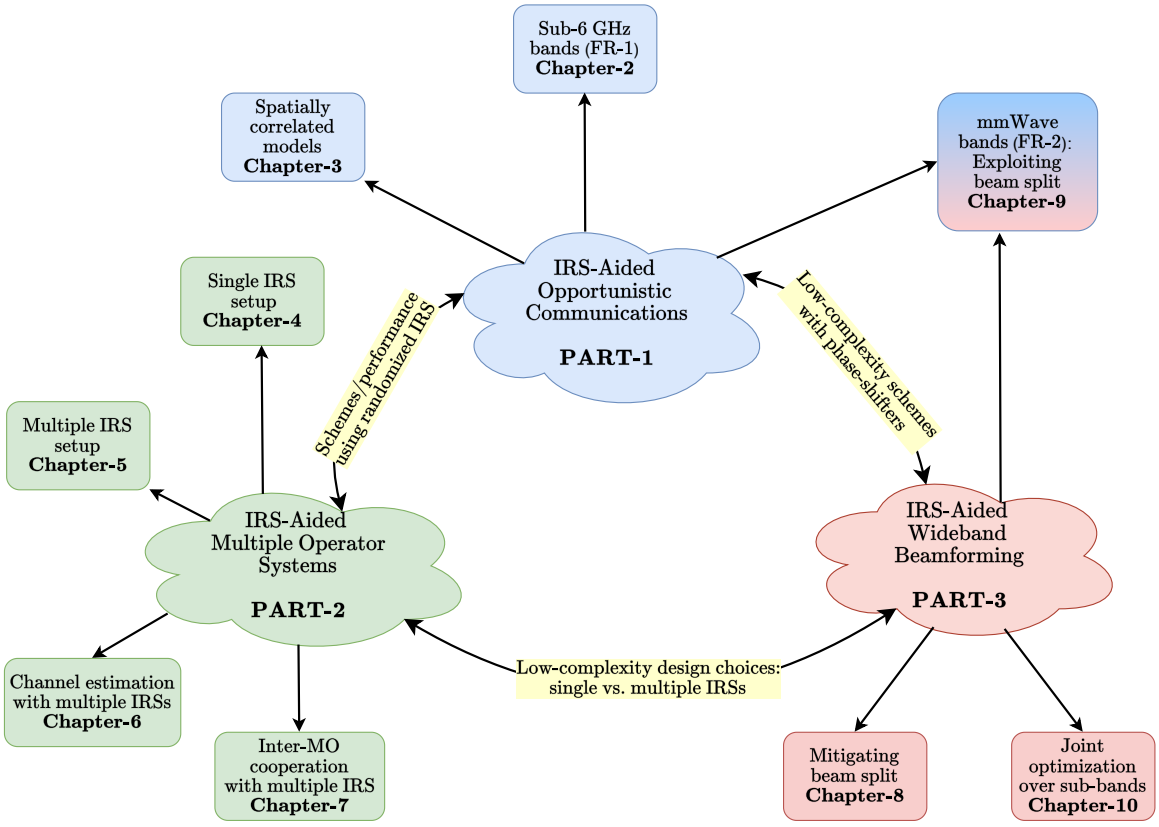

Figure 1.3: Summarizing the scope and contribution of the thesis with connections between parts.

IRS-UE channel is sparse in the angular domain and exhibits joint row sparsity across the OFDM subcarriers. We exploit this to estimate the CSI using the SOMP algorithm.

2. We propose a computationally efficient binary phase optimization solver for IRS-aided OFDM using the majorization-minimization (MM) theory [67] to optimize the sum rate. The key novelty of our MM-based approach is in finding tractable lower bounds on the non-convex sum rate that are tight at the current iterate and amenable to optimization via closed-form solutions. We develop such bounds via a series of matrix inequalities and eventually provide closed-form solutions to the inner optimization problems.

In Fig 1.3, we pictorially illustrate how different parts of the thesis are interconnected in terms of the system models and proposed schemes.

1.5 Key Takeaways from the Thesis

Based on the contributions outlined in Sec. 1.4, we have the following key takeaways:

1. **Achieving Beamforming Gain with Low Complexity**: The adoption of an opportunistic communication framework significantly reduces IRS-related overheads. Specifically, it eliminates the three-fold costs associated with channel estimation, phase optimization, and configuration signaling, without compromising on the performance and thereby enabling seamless integration of IRSs into future wireless systems.

2. **Practical Requirements on the Number of UEs**: The OC framework leverages multi-user diversity to bypass signaling overheads, shifting the trade-off towards the minimum number of UEs required to realize IRS gains. We demonstrate that to attain a target fraction of the IRS beamforming gain, the required number of UEs scales exponentially with the rank of the channel covariance matrix at the IRS.

3. **IRS Benefits Extend to All Operators**: An IRS, even when deployed by a single operator, does not degrade the performance of other (OOB) operators. In fact, in sub-6 GHz bands, it enhances multipath richness, while in mmWave bands, it improves the likelihood of establishing virtual LoS links for OOB users.

4. **IRS Provides Spatial Diversity**: The deployment of multiple IRSs provides additional channel degrees of freedom and hence provides spatial diversity, offering considerable performance improvements for OOB operators compared to a single IRS setup.

5. **IRS Facilitates Spatial Multiplexing**: A distributed deployment of many IRSs allows mmWave systems to perform spatial multiplexing even in LoS propagation conditions. This is because multiple IRSs improve the rank of an mmWave channel, thereby enhancing the spatial multiplexing capabilities of mmWave MIMO systems.

6. **Large IRSs Break the Narrowband Condition**: In wideband systems, especially in mmWave bands, large IRSs induce propagation delays that cannot be approximated as phase shifts. This gives rise to the spatial-wideband effect and results in a beam-split effect, leading to degradation in array gain and throughput.

7. **Mitigating B-SP via Multiple IRSs**: Partitioning a large IRS into multiple smaller, distributed IRSs mitigates B-SP through angle diversity and reduced propagation delays, thereby restoring full array gain from a user-centric perspective.

8. **Exploiting B-SP with OFDMA**: An opportunistic OFDMA-based strategy leverages the B-SP effect by scheduling multiple UEs across sub-bands, enabling the system to achieve the full array gain from the viewpoint of the network.

In general, this thesis provides evidence of how even a randomly sampled set of IRS phase configurations, when combined with low-complexity and appropriately designed signal processing techniques, can deliver significant performance gains in next-generation wireless communication systems.

1.6 List of Publications from this Thesis

Journal Articles

J1: **L. Yashvanth**, and Chandra R. Murthy, "Performance Analysis of Intelligent Reflecting Surface Assisted Opportunistic Communications," *IEEE Transactions on Signal Processing*, vol. 71, pp. 2056-2070, Mar. 2023. (**See Chapter 2.**)

J2: **L. Yashvanth**, and Chandra R. Murthy, "On the Impact of an IRS on the Out-of-Band Performance in Sub-6 GHz and mmWave Frequencies," *IEEE Transactions on Communications*, vol. 72, no. 12, pp. 7417-7434, Dec. 2024. (**See Chapter 4.**)

J3: **L. Yashvanth**, and Chandra R. Murthy, "Distributed IRSs Always Benefit Every Mobile Operator," *IEEE Wireless Communications Letters*, vol. 13, no. 11, pp. 2975-2979, Nov. 2024. (**See Chapter 5.**)

J4: S. Ghosh[3], **L. Yashvanth**[3], and Chandra R. Murthy, "Performance Analysis of Multi-IRS Aided Multiple Operator Systems at mmWave Frequencies," Accepted to *IEEE Transactions on Communications*, Jun. 2025 (**See Chapter 7.**)

J5: **L. Yashvanth**, Chandra R. Murthy, and Bhaskar D. Rao, "Spatial Correlation-Aware Opportunistic Beamforming in IRS-aided Multi-User Systems," Accepted to *IEEE Wireless Communications Letters*, Jul. 2025 (**See Chapter 3.**)

J6: **L. Yashvanth**, Chandra R. Murthy, and Bhaskar D. Rao, "Mitigating Spatial-Wideband and Beam-Split Effects Via Distributed IRSs: Design and Analysis," in *IEEE Transactions on Signal Processing*, vol. 73, pp. 3286-3301, Jul. 2025. (**See Chapter 8.**)

J7: **L. Yashvanth**, and Chandra R. Murthy, "Exploiting Beam-Split Effect in IRS-Aided Systems via Opportunistic OFDMA: Design and Analysis," under review at *IEEE Transactions on Signal Processing*, Jul. 2025. (**See Chapter 9.**)

[3]S. Ghosh and L. Yashvanth have contributed equally to this paper.

Conference Proceedings

C1: **L. Yashvanth**, Chandra R. Murthy and Deepak Battu, "Binary Intelligent Reflecting Surfaces Assisted OFDM Systems," in *Proc. IEEE International Conference on Signal Processing and Communications (SPCOM)*, July 2022, Bangalore, India. pp. 1-5. (**See Chapter 10.**)

C2: **L. Yashvanth**, and Chandra R. Murthy, "Cascaded Channel Estimation for Distributed IRS Aided mmWave Massive MIMO Systems," in *Proc. IEEE Global Communications Conference (GLOBECOM)*, Rio de Janeiro, Brazil, December 2022, pp. 717-723. (**See Chapter 6.**)

C3: **L. Yashvanth**, and Chandra R. Murthy, "Comparative Study of IRS Assisted Opportunistic Communications over I.I.D. and LoS Channels," in *Proc. IEEE International Conference on Acoustics, Speech and Signal Processing (ICASSP)*, Rhodes Island, Greece, June 2023, pp. 1-5. (**See Chapter 2.**)

C4: **L. Yashvanth** and Chandra R. Murthy, "Does an IRS Degrade Out-of-Band Performance?," in *Proc. IEEE 24th International Workshop on Signal Processing Advances in Wireless Communications (SPAWC)*, Shanghai, China, September 2023, pp. 216-220. (**See Chapter 4.**)

C5: **L. Yashvanth**, Chandra R. Murthy, and Bhaskar D. Rao, "Distributed IRSs Mitigate Spatial Wideband & Beam Split Effects," in *Proc. IEEE International Conference on Acoustics, Speech and Signal Processing (ICASSP)*, Hyderabad, India, Apr. 2025. (**See Chapter 8.**)

C6: P. Siddhartha[4], **L. Yashvanth**[4], and Chandra R. Murthy, "Exploiting Beam-Split in IRS-aided Systems via OFDMA," in *Proc. IEEE International Conference on Acoustics, Speech and Signal Processing (ICASSP)*, Hyderabad, India, Apr. 2025. (**See Chapter 9.**)

[4]P. Siddhartha and L. Yashvanth have contributed equally to this paper.

Part I

IRS-Assisted Opportunistic Communications: Schemes and Performance Analysis

2 Opportunistic Scheduling in IRS-aided Sub-6 GHz Systems

Chapter Highlights

Intelligent reflecting surfaces (IRSs) are a promising technology for enhancing coverage and spectral efficiency for next-generation wireless systems. Existing approaches to leverage the benefits of the IRS involve the use of a resource-intensive channel estimation step followed by a computationally expensive algorithm to optimize the reflection coefficients at the IRS.

In this chapter, focusing on the sub-6 GHz band of communications, we present and analyze several alternative schemes, where the phase configuration of the IRS is randomized and multi-user diversity is exploited to opportunistically select the best user at each point in time for data transmission. We show that the throughput of an IRS-assisted opportunistic communication (OC) system asymptotically converges to the optimal beamforming-based throughput under a fair allocation of resources as the number of users gets large. We also introduce schemes that enhance the rate of convergence of the OC rate to the beamforming rate with the number of users. For all the proposed schemes, we provide the distribution for sampling the IRS phase angles and subsequently derive the scaling law of the throughput in terms of the system parameters as the number of users gets large. Following this, we extend the setup to wideband channels via an orthogonal frequency division multiplexing (OFDM) system and discuss two OC schemes in an IRS-assisted setting: 1) Single-user OFDM (SU-OFDM): motivated by the fact the IRS bears a frequency flat response, in this scheme, we opportunistically schedule a single UE over the entire BW, and 2) orthogonal frequency division multiple access (OFDMA), where we multiplex different UEs on different sub-carriers following an opportunistic scheduling scheme. The numerical results clearly elucidate the superior performance that IRS-aided OC systems can offer over conventional systems at very low implementation cost and complexity.

2.1 Introduction

Intelligent Reflecting Surfaces (IRSs) have become a topic of active research for enhancing the performance of next-generation wireless communication systems both in the sub-6 GHz and in the millimeter wave (mmWave) bands. An IRS consists of passive elements made out of meta-materials that can be tuned to offer a wide range of load impedances using a PIN diode. Using this, each element of the IRS can be tuned to have a different reflection coefficient, thereby enabling the IRS to reflect the incoming signals in any desired direction [2, 68–70]. However, realizing these benefits entails high overheads in terms of resource-intensive channel estimation followed by solving a computationally heavy optimization problem to determine the phase configuration at the IRS. In this work, we consider an alternative approach, where the phase configuration of the IRS is set randomly in each slot, yet extracts the benefits from the IRS in terms of enhancing the system throughput. This approach only requires a short training signal for estimating the received signal power at the users, followed by feedback-based selection of the best user in each slot for subsequent data transmission. Multi-user diversity ensures that at least one user will see a good channel in the randomly chosen phase configuration [71].

Despite its short history, significant work has gone into the design and optimization of IRS-aided communication systems. Here, we briefly summarize the existing literature, in order to place the contributions of this chapter in context. In [9], the authors show that an IRS can create a virtual line-of-sight (LoS) path between the base station (BS) and the user, leading to improved coverage and SNR in mmWave systems. In [10], it is shown that the received SNR increases quadratically with the number of IRS elements, provided the phase configuration of the IRS is optimized to ensure coherent combining of the signal at the receiver location. Also, since the IRS is passive in nature, it boosts the spectral efficiency without compromising on the energy efficiency [11]. In [12], the authors propose joint active and passive beamforming algorithms at the BS and IRS, respectively, to maximize the weighted sum rate of an IRS-aided system. IRS phase optimization in the context of multiple-input multiple-output (MIMO) and orthogonal frequency division multiplexing (OFDM) systems has been studied in [15–19], and the list

of potential applications of IRS continues to grow [3, 69, 72].

All of the above-mentioned works describe and solve complex phase optimization problems, which are computationally intensive and difficult to implement in real-time systems. Further, this optimization becomes even more complicated in the context of OFDM systems, as it requires one to optimize the IRS jointly across all the OFDM subcarriers. More importantly, these phase optimization algorithms work on the premise of the availability of accurate channel state information (CSI) of the links between the BS and the user through every IRS element. Elegant methods for channel estimation in IRS-aided systems are described in [21, 22], but in all these schemes, the channel estimation overhead scales linearly with the number of IRS elements. The time, energy, and resource utilization for channel estimation can quickly erase much of the benefits offered by the IRS. One approach to mitigate this loss is to exploit structure in the channel model to estimate the channel with lower overhead [23–25], but these approaches trade off the reduction in overhead with more complex channel estimation algorithms, thereby substantially increasing the computational cost. In addition, the complexity of the overall algorithm increases with the resolution with which phase shifts are configured [73]. Furthermore, since the IRS is passive, these optimization algorithms have to run at the BS, and a dedicated control link from the BS to the IRS is needed to communicate the phase configuration information to the IRS. As the number of IRS elements increases, this becomes an additional bottleneck, as the control link overhead also scales with the number of IRS elements [69].

In the context of the above, an interesting alternative approach is to configure the IRS with random phases and make the communications opportunistic in nature. In opportunistic communications (OC), at every point in time, the BS serves the user who witnesses the best instantaneous channel condition. When there are a large number of users in the system,[1] with high probability, deep fades are avoided at any given user, enhancing the average system throughput without incurring the overheads mentioned above [71, 78, 79]. In particular, opportunistic scheduling is pertinent when the goal is to maximize the system

[1] In sub-6 GHz band communication system, the consideration of large number of users is realistic [71, 74–76], especially in the context of massive machine-type communications (mMTC) for 5G communications [77].

average throughput, i.e., the average sum-rate across the users over a long time horizon. Such an approach is suitable in delay-tolerant networks, where users can afford to wait before being scheduled for transmission.

Initial work along these lines was reported in [76], where the phase angles of the reflection coefficients at the IRS elements are drawn uniformly and independently from the interval $[0, 2\pi)$. As we show in the sequel, a drawback of this approach is that the number of users needed to achieve a performance comparable to coherent beamforming increases exponentially with the number of IRS elements, making it unattractive for practical implementation. Moreover, the average effective SNR scales linearly, not quadratically, in the number of IRS elements (as achieved by coherent beamforming.) In this work, we develop novel, alternative schemes that overcome these drawbacks. Although we focus on communications over the sub 6-GHz bands (FR-1 band in the 5G NR specifications [64]) assisted by an IRS, we also briefly discuss how one of the proposed schemes is relevant in mmWave bands.[2] For all the schemes, we analyze the system throughput as a function of the number of users. We show that, by exploiting the structure in the channel, we can significantly improve the convergence rate of opportunistic throughput to the beamforming throughput and also achieve the quadratic scaling of the SNR with the number of IRS elements. This, in turn, allows us to achieve near-optimal beamforming performance and obtain an additional gain from opportunistic user selection without requiring a very large number of users in the system.

The specific contributions of this chapter are as follows:

- We analyze the throughput of several proposed IRS-assisted OC schemes for independent and identically distributed narrowband wireless channels. We exploit the fast switching time of IRS phase configurations to obtain additional reflection diversity from the IRS, and show that this helps to reduce the number of users required to obtain near-optimal throughput. We also analytically characterize the throughput

[2] An IRS can boost the performance in both mmWave and sub-6 GHz bands. In mmWave bands, they help in improving coverage by establishing a virtual line-of-sight channel. In sub-6 GHz bands, they boost the received SNR by making the environment more rich-scattering [80]. This work primarily focuses on the performance in sub-6 GHz bands.

achievable by this scheme. (See Theorem 2.1 and Sec. 2.3.b.)

- Next, we consider directional channels in the IRS-aided system and design channel model-aware randomly configured OC schemes that converge to the coherent beamforming rate without requiring the users to scale exponentially with the number of IRS elements. In Theorem 2.2, we show that not only does this scheme achieve the quadratic scaling of the SNR with the number of IRS elements, its throughput can even surpass that of the scheme that involves IRS optimization techniques, due to the lack of multi-user diversity gain in the latter. We also discuss how this scheme can be applied to mmWave channels, which also bear a similar structure. (See Sec. 2.3.c.)

- We extend the OC schemes to IRS-aided systems with wideband wireless channels. Specifically, we consider an OFDM system and discuss two OC schemes: single-user OFDM, where we schedule a single user across all subcarriers, and orthogonal frequency division multiple access (OFDMA), where multiple users are potentially scheduled across the subcarriers. We derive the sum throughput scaling laws in Theorems 2.3 and 2.4 for the two schemes, and provide interesting insights about these systems. (See Sec. 2.4.)

The results (in Sec. 2.5) show that the presence of an IRS can significantly enhance the throughput of conventional BS-assisted OC schemes [71]. Specifically, the throughput of IRS-aided OC grows with the number of IRS elements N, whereas such growth is not possible in BS-assisted OC as the number of antennas at the BS is increased. This is due to the power constraint at the transmitter, which eventually limits the maximum achievable throughput. Secondly, the numerical results elucidate the significant reduction in the number of users to achieve the optimal throughput compared to existing schemes such as in [76]. For example, in an 8-element IRS system, the approach in [76] has a gap of 175% from the optimal rate; this gap reduces to 60% by using the proposed reflection diversity enhanced scheme. Further, the offset from the coherent beamforming throughput reduces to 11% in the proposed channel model-aware IRS-assisted OC scheme. Also, the channel model aware OC scheme is within a small offset (18%) with a modest number of users

Variable	Definition	Variable	Definition
N	Number of IRS elements	$R_k(t)$	Acheivable rate of UE-k at time t
K	Number of UEs	$T_k(t)$	Average rate of UE-k till time t
Q	Number of IRS reflection patterns	h_k or $\mathbf{h}_k$	Overall channel at UE-k
M	Number of subcarriers in the OFDM	$\mathbf{h}_1$	Channel from BS to IRS
L	Number of taps in the channel	$\mathbf{h}_{2,k}$ or $\mathbf{H}_{2,k}$	Channel from IRS to UE-k
P/σ^2	Ratio of transmit power at the BS to noise variance at UE	$\boldsymbol{\theta}$ or $\boldsymbol{\Theta}$	IRS configuration vector/matrix
ζ	Fraction of slots for pilot txn.	$h_{d,k}$	Direct channel from BS to UE-k
d/λ	Ratio of inter-elemental spacing to the signal wavelength	$\beta_{d,k}$, $\beta_{r,k}$	Path loss in the direct link / cascaded link via the IRS
θ_A	Angle of arrival at the IRS from BS	$\theta_{D,k}$	Angle of departure at the IRS to UE-k
$\mathbf{a}$	Power delay profile of the multi-tap channel	$R^{(K)}$	Acheivable system throughput under opportunistic scheduling
τ	Design parameter of PF scheduler	R_k^{BF}	Beamforming rate at UE-k

Table 2.1: Commonly encountered variables/notations in chapter 2.

(≈ 50), even when the number of IRS elements is as large as 1024. Thus, IRS-aided OC is a promising approach for exploiting the benefits of IRS-aided systems without incurring the cost of training, phase angle optimization, and communication to the IRS.

Notation: For general notations used in this chapter, see the section on "General Mathematical Notations" on page ix. For the notations/variables specific to this chapter, please refer to Table 2.1.

2.2 Preliminaries of Opportunistic Scheduling

Opportunistic communication schemes exploit the variation of the fading channels across users in order to improve the throughput of a multi-user system. For example, in max-rate scheduling [79], the BS sends a common pilot signal to all the users in the system, and the users measure the received SNR. The BS then collects feedback from the user who

witnesses the highest SNR,[3] and schedules data to that user in the rest of the slot. That is, in a K user system, the BS serves user k^* at time t, where $k^* = \arg\max_{k\in[K]} |h_k(t)|^2$, with $h_k(t)$ denoting the channel seen by user k at time t. However, this scheme is unfair to users located far from the BS due to their higher path loss. An alternative is to consider proportional fair (PF) scheduling, which provides a trade-off between fairness and throughput [71]. The PF scheduler serves user k^* such that

$$k^* = \arg\max_{k\in[K]} \frac{R_k(t)}{T_k(t)}, \tag{2.1}$$

where $R_k(t) = \log_2\left(1 + \frac{P|h_k(t)|^2}{\sigma^2}\right)$ is the achievable rate[4] of user k at time t, P is the transmit power at the BS, σ^2 is the noise variance at the user, and $T_k(t)$ captures the long-term average throughput of user k. We will refer to the term $\frac{R_k(t)}{T_k(t)}$ as the PF metric in this chapter. Now, $T_k(t)$ is updated as

$$T_k(t+1) = \begin{cases} \left(1-\frac{1}{\tau}\right) T_k(t) + \frac{1}{\tau} R_k(t), & k = k^*, \\ \left(1-\frac{1}{\tau}\right) T_k(t), & k \neq k^*. \end{cases} \tag{2.2}$$

Here, the variable τ represents the length of a window that captures the tolerable latency of the application and dictates the trade-off between fairness and throughput. Going forward, we will refer to the term $\frac{R_k(t)}{T_k(t)}$ as the PF metric.

A simple illustration of exploiting multi-user diversity through opportunistic scheduling based on the PF scheduler is shown in Fig. 2.1 for various values of τ. We consider a time-varying channel across time slots modeled as a Gauss-Markov process, i.e., the channel at user k varies as

$$h_k(t) = \alpha h_k(t-1) + \sqrt{1-\alpha^2} v_k(t), \tag{2.3}$$

where α dictates the correlation of channel coefficients across time slots and $v_k(t) \sim \mathcal{CN}(0,1)$ is an innovation process.

Further, the performance of the OC scheme is compared with that of a non-opportunistic

[3] We note that various timer-based and splitting-based schemes can be used to identify the best user with low overhead [81, 82].

[4] In this work, we use the terms rate and throughput interchangeably.

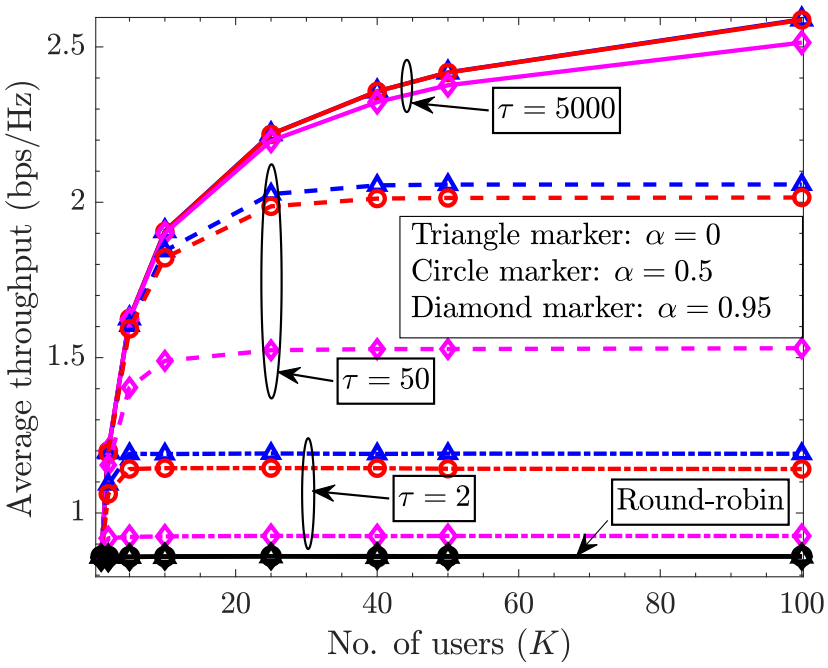

Figure 2.1: Throughput achieved via PF scheduling.

scheduling scheme, namely, round-robin time division multiple access (TDMA).

As can be seen from the figure, the average throughput of the system at higher τ grows substantially with the number of users. This marks the rate-constrained regime, where the instantaneous rate is the primary factor determining which user gets scheduled (the system still offers fairness, but only over very large time scales). Thus, for large τ, the PF scheduler is approximately the same as a max-rate scheduler, and the throughput achieved by the PF scheduler approaches that achieved by the max-rate scheduler as τ goes to infinity. On the other hand, at lower τ, the average throughput has negligible improvement after a few users, indicating that this is a fairness-constrained regime where users are selected in a near round-robin fashion to ensure short-term fairness. On the other hand, for a given choice of τ, opportunistic scheduling performs better for lower values of α (representing a fast-fading scenario) compared to higher values (representing slow-fading scenarios). This is because, in fast-fading environments, the rate of channel fluctuations is enhanced, which improves the performance of opportunistic scheduling schemes.

We note that such an enhancement of the rate of channel fluctuations can be obtained by choosing different, random phase configurations at an IRS. This has the additional

advantage that the fluctuations induced by the IRS increase with the number of elements. This motivates us to take a fresh look at the opportunistic scheduling schemes in IRS-assisted scenarios. Specifically, we analyze the achievable throughput in IRS-assisted OC schemes. We show that one can obtain the benefits of using an IRS over conventional systems with low overhead and complexity by obviating the need for CSI acquisition, IRS phase optimization, and feedback between the BS and the IRS.

2.3 Single IRS Assisted Opportunistic User Scheduling for Narrowband Channels

In this section, we present three OC schemes for narrowband channels in a single IRS-assisted setting. We consider a single cell containing a BS equipped with one antenna serving K single antenna users. An IRS equipped with N reflecting elements is deployed at a suitable location in the radio propagation environment, as shown in Fig. 2.2.

2.3.a IRS-Enhanced Multi-user Diversity

2.3.a.i Channel Model

The signal transmitted by the BS reaches each user via a direct path as well as via the IRS. Thus, the effective downlink channel seen by user k (at time slot t), denoted by h_k (we omit the dependence on t for notational brevity), is given by

$$h_k = \sqrt{\beta_{r,k}}\mathbf{h}_{2,k}^T\mathbf{\Theta}\mathbf{h}_1 + \sqrt{\beta_{d,k}}h_{d,k}, \tag{2.4}$$

where $\mathbf{h}_{2,k}$ and $\mathbf{h}_1 \in \mathbb{C}^{N\times 1}$ represent the channels between the IRS and user k, and between the BS and IRS, respectively, and $h_{d,k}$ denotes the direct non-IRS channel between the BS and user k. We model $\mathbf{h}_1 \sim \mathcal{CN}(\mathbf{0}, \mathbf{I})$, $\mathbf{h}_{2,k} \overset{\text{i.i.d.}}{\sim} \mathcal{CN}(\mathbf{0}, \mathbf{I})$ and $h_{d,k} \overset{\text{i.i.d.}}{\sim} \mathcal{CN}(0, 1)$ across all users. Further, $\beta_{r,k}$ and $\beta_{d,k}$ represent the path loss between the BS and user k through the IRS and direct paths, respectively. The diagonal matrix $\mathbf{\Theta} \in \mathbb{C}^{N\times N}$ contains the reflection coefficients programmed at the IRS, with each diagonal element being of the form $e^{j\theta_i}$, where $\theta_i \in [0, 2\pi)$ is the phase angle of the reflection coefficient at the ith IRS

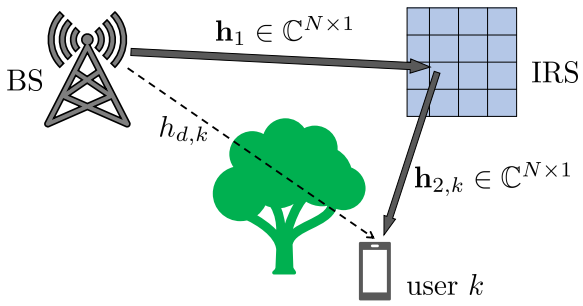

Figure 2.2: A single IRS-assisted wireless system.

element. The signal received at every user is corrupted by AWGN $\overset{\text{i.i.d.}}{\sim} \mathcal{CN}(0, \sigma^2)$.

2.3.a.ii Scheme for IRS-Enhanced Multi-user Diversity

In every time slot, the IRS sets a random phase configuration. Consequently, the effective channels seen by the users change in every slot. The BS transmits a pilot signal in the downlink at the start of the slot. The users measure the SNR from the pilot signal and compute their respective PF metrics. The user with the highest PF metric feeds back its identity to the BS, which schedules that user for data transmission for the rest of the slot.

Feedback Mechanism: We consider timer or splitting based schemes [81,82] for identifying the best user at the BS. These are low-overhead *distributed* user selection schemes, where only the best user transmits its identity to the BS, based on their channel-utility metric (e.g., using a timer that expires after a time interval that is inversely proportional to the SNR or the PF metric). It is known that, with these schemes, the BS can identify the best user within 2 or 3 (mini-)slots on average even as $K \to \infty$ [81, 82]. Since the average overhead of a timer-based feedback scheme is small compared to the time slot duration, we ignore its effect in this work.

In the above scheme, as the number of users in the system grows, the randomly chosen IRS configuration is likely to be close to the beamforming (BF) configuration for at least one of the users in the system [71]. Note that, in this scheme, there is no communication from the BS to the IRS, making it attractive from an implementation perspective. Thus, the benefits of an optimized IRS can be readily obtained without requiring careful optimization of the IRS, provided there is a large number of users in the system, and the multi-user

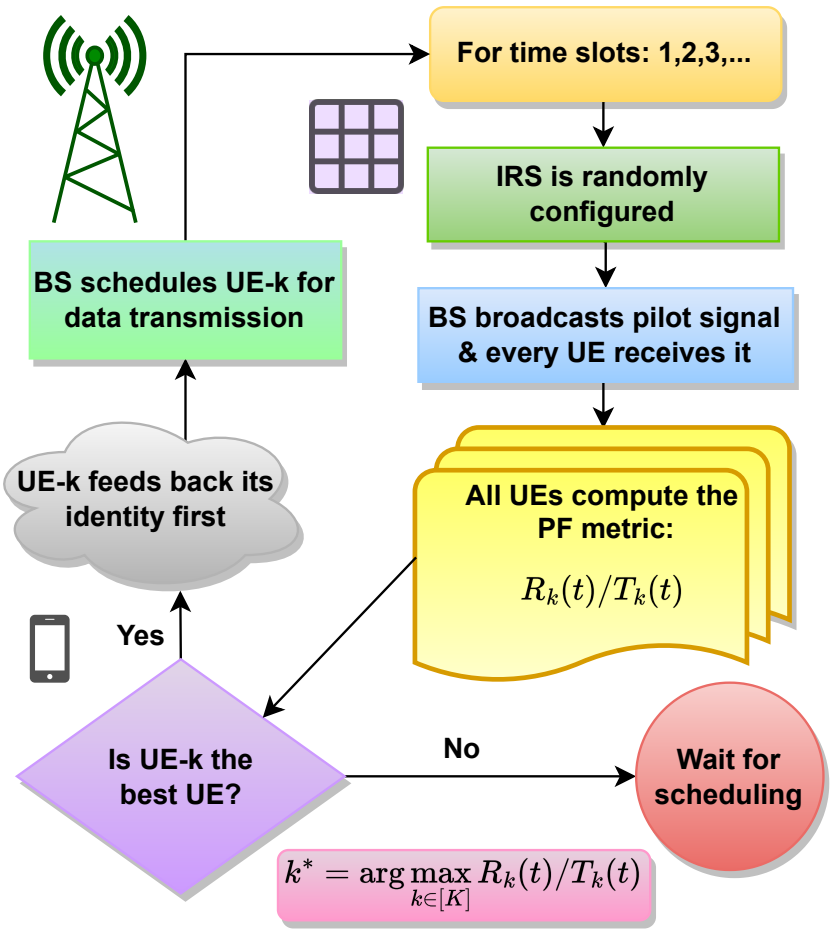

Figure 2.3: IRS-aided opportunistic communication scheme: A pictorial representation.

diversity gain is exploited. The scheme is illustrated pictorially in Fig. 2.3, and the slot structure of the scheme is illustrated in Fig. 2.4. In particular, the time scale of UE scheduling and reconfiguring the IRS with a random phase are assumed to be of the same order, and these are shorter than the time scale of channel variations (channel coherence time) at the UEs.

We begin our discussion with the following lemma on the performance of an IRS that adopts a beamforming configuration for a given user, which will serve as a benchmark for evaluating the OC-based schemes.

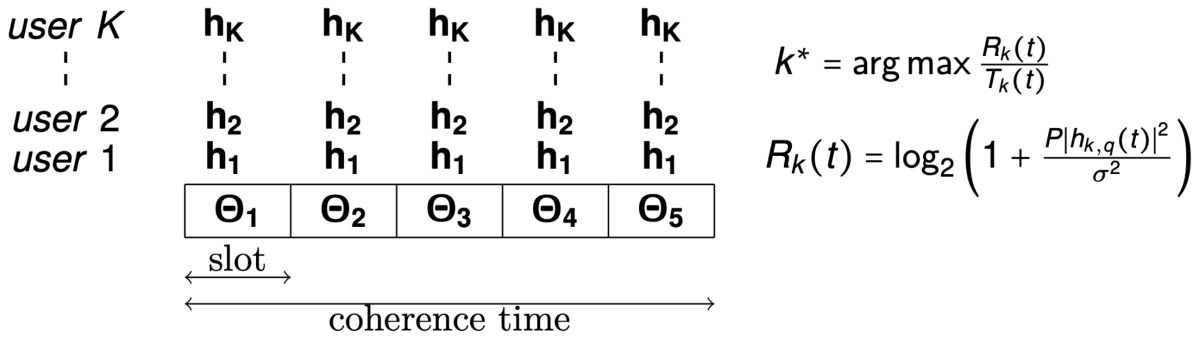

Figure 2.4: Slot structure of the opportunistic communication scheme.

Lemma 2.1 ([76]). *The rate achieved by user k in an IRS aided system under the* beamforming configuration *is*

$$R_k^{BF} = \log_2 \left(1 + \frac{P}{\sigma^2} \left| \sqrt{\beta_{r,k}} \sum_{n=1}^{N} |h_{1,n} h_{2,k,n}| + \sqrt{\beta_{d,k}} |h_{d,k}| \right|^2 \right), \tag{2.5}$$

with the beamforming configuration at the IRS given by

$$\theta_{n,k}^* = \angle h_{d,k} - \angle (h_{1,n} \times h_{2,k,n}), \quad n = 1, \ldots, N. \tag{2.6}$$

The above lemma quantifies the gain that an IRS can offer compared to a system without an IRS. However, achieving the rate in (2.5) requires the knowledge of the CSI through every IRS element, whose complexity scales linearly with the number of elements, as stated earlier.

Next, consider the system where the phase of every IRS element is selected uniformly at random from $[0, 2\pi)$ in each slot, and the user with the best PF metric is selected for transmission. We define the average rate achieved by the randomly configured IRS assisted system to be $R^{(K)} = \mathbb{E}\left[\log_2\left(1 + P|h_{k^*}|^2/\sigma^2\right)\right]$, where k^* is the user selected in time slot t, and the expectation is taken over the randomness in the phase configuration. Then, under PF scheduling, as $\tau \to \infty$, it is known that the average rate of the randomly configured IRS-assisted system almost surely converges to the average rate achievable in

the beamforming configuration under fair resource allocation across users, i.e., [76]

$$\lim_{K\to\infty}\left(R^{(K)}-\frac{1}{K}\sum_{k=1}^{K}R_k^{BF}\right)=0. \tag{2.7}$$

Note that, in (2.7), the factor $\frac{1}{K}$ in the second term on left hand side accounts for the fairness ensured by the system.

Remark 2.1 (On the convergence rate)**.** *Let us compute the scaling of the number of users K with the number of IRS elements N, such that, with a given (fixed) probability, a randomly selected phase configuration $\boldsymbol{\theta}$ at the IRS is nearly in beamforming configuration for at least one user. Consider an arbitrary user, and define the event $\mathcal{E}_i \triangleq \{\theta_i \in [\theta_i^* - \epsilon, \theta_i^* + \epsilon]\}$, where θ_i^* is the phase angle required for the ith element of the IRS to be in beamforming configuration for that user. Since the phase angles at the IRS are chosen as $\theta_i \overset{i.i.d.}{\sim} \mathcal{U}[0, 2\pi)$, if we define $\mathcal{E} \triangleq \cap_{i=1}^{N}\mathcal{E}_i$, we have $Pr(\mathcal{E}) = (\epsilon/\pi)^N$. Then, the probability that at least one user in a K-user system sees an IRS phase configuration that is within ϵ distance of its beamforming configuration is $P_{succ} = 1 - \left(1 - (\epsilon/\pi)^N\right)^K$. Hence, in order to have a fixed probability of success via i.i.d. randomly selected phase configurations, when $\epsilon/\pi \ll 1$, the number of users must scale with N as*

$$K \geq (-\log(1 - P_{succ}))\,(\pi/\epsilon)^N. \tag{2.8}$$

Thus, in the i.i.d. phase configuration scheme, the number of users must grow exponentially in the number of IRS elements to achieve near beamforming configuration. Contrariwise, this scheme constrains the number of IRS elements that can be deployed when the number of users is limited. [5] *In the next subsections, we present and analyze schemes that improve the rate of convergence of $R^{(K)}$ to $\frac{1}{K}\sum_{k=1}^{K}R_k^{BF}$.*

[5] Note that the rate obtainable in an IRS-assisted OC system always increases with N. However, if N is increased keeping K fixed, the gap between the rate achieved by OC and the rate achievable under the beamforming configuration with fair resource allocation across users also increases, because the probability that no user is close to the beamforming configuration increases. In fact, for a large but fixed K with i.i.d. channels, the average rate in a randomly configured IRS grows as $\mathcal{O}(\log_2 N)$ (see (2.10)), whereas, in the beamforming configuration, it grows as $\mathcal{O}(\log_2 N^2)$ (see (2.5)).

2.3.b IRS-Aided Multi-user Diversity with Reflection Diversity

In this subsection, we study an enhancement of the foregoing scheme by offering additional *reflection* diversity gain. In this scheme, the IRS is configured using random and independent reflection coefficients during multiple consecutive pilot symbols transmitted at the beginning of each time slot. Note that, in this scheme, there is a one-to-one mapping between the pilot symbol index and the phase configuration used at the IRS. Hence, the effective channel between the BS and the kth user during the qth pilot transmission in a given time slot, denoted by $h_{k,q}$, is different for each of the pilot symbols because the phase configuration of the IRS is different for each value of q.

2.3.b.i Channel Model

We model the effective downlink channel $h_{k,q}$ using (2.4), with the phase configuration $\mathbf{\Theta}$ replaced with $\mathbf{\Theta}_q$ for the qth pilot interval.

2.3.b.ii Scheme for IRS-Enhanced Multi-user Diversity Aided with Reflection Diversity

Inspired by the fast switching time of IRS phase configurations [83, 84] compared to the time slot (e.g., 10 ms frame duration in 5G NR [85]), we can obtain additional reflection diversity on top of the multi-user diversity by configuring the IRS with several random and independent reflection coefficients (phase configurations) during the pilot symbols transmitted at the beginning of each time slot. Every user chooses the best configuration among all the IRS phase configurations in every time slot, computes its PF metric, and the best user feeds back the corresponding phase configuration index and SNR to the BS.[6] The BS then sets the IRS with the phase configuration index received from the user selected for transmission, for the rest of the slot.

Let Q be the number of randomly chosen IRS phase configurations within a time slot, which is the same as the number of pilot transmissions. In the rest of this section, for

[6] In slowly varying channels, one can maintain the history of the phase configurations used in the previous time slots and the corresponding SNRs reported by the users, and avoid multiple pilot transmissions in each slot.

analytical tractability, and similar to [75], we consider the path loss coefficients to be equal across all links and users: $\beta_{r,k} \approx \beta_{d,k} = \beta$.[7] We then have the following proposition.

Proposition 2.1. *The effective channels, $h_{k,q}$, are i.i.d. across users and pilots for reasonably large N, and $Q \ll K, N$,[8] and further they follow the distribution $\mathcal{CN}(0, \beta(N+1))$.*

Proof. See Appendix 2.A. ■

We can also observe numerically (See Fig. 2.7, Sec. 2.5) that this proposition holds even for moderate values of N.[9] We now note that, as Q increases, the time remaining for data transmission in each frame decreases. Thus, the average throughput of a system adopting this scheme is

$$R^{(K,Q)} = (1 - \zeta Q)\, \mathbb{E}\left[\log_2\left(1 + \max_{\substack{q\in[Q],\\ k\in[K]}} \frac{P|h_{k,q}|^2}{\sigma^2}\right)\right], \tag{2.9}$$

where $(1 - \zeta Q)$ is the pre-log factor accounting for the loss in the throughput due to transmitting Q pilot symbols in each slot, ζ is the fraction of the time slot expended in a single pilot transmission, and the expectation is taken with respect to the random IRS phase configurations and fading channels. Note that we account for the $(1 - \zeta Q)$ factor only in this subsection, since multiple pilot symbols are used. In the rest of the chapter, since only a single pilot transmission occurs, we ignore its effect on the throughput. The following theorem characterizes the scaling of the average system throughput of IRS enhanced multi-user diversity aided with reflection diversity as a function of the system parameters.

[7] The first approximation is realistic as long as the IRS path is not much longer than the non-IRS path. Also, due to the second equality, the PF scheduler approximates the max-rate scheduler for large τ [71].

[8] More precisely, this approximation would be accurate as long as Q is smaller than the number of IRS elements, where the Q projections result in independent random variables.

[9] Note that, if the BS and IRS are deployed at fixed and high locations, the channel between the BS and IRS will remain static for several time slots and have a strong LoS component. One can then model this channel using a deterministic array steering response vector [76]. Since the distribution of a circularly symmetric Gaussian random variable is unchanged under rotation by a deterministic phase angle, $h_{k,q} \sim \mathcal{CN}(\cdot)$ still holds true for any N.

Theorem 2.1. *Consider an N-element IRS-aided system with K users and Q pilot transmissions, as described above. Under Proposition 2.1, the average system throughput scales as*

$$\lim_{K\to\infty}\left(R^{(K,Q)}-(1-\zeta Q)\log_2\left(1+\frac{\beta P}{\sigma^2}(N+1)\ln(QK)\right)\right)=0. \tag{2.10}$$

Proof. See Appendix 2.B. ■

In (2.10), the pre-log factor decreases with Q, while the logarithmic factor increases with Q, making $R^{(K,Q)}$ an unimodal function of Q. The following lemma provides the Q for which (2.10) is maximized as the solution of an implicit equation, which can be solved using fixed-point iteration methods. In particular, we state this when ζ is a small positive number and under a high SNR scenario. We skip the proof as it is straightforward.

Lemma 2.2. *The number of pilots Q that maximizes $R^{(K,Q)}$ in (2.10) for a given K and N, denoted by $\hat{Q}$, satisfies the fixed point equation $\ln(QK)=e^{W\left(\left(\zeta^{-1}Q^{-1}-1\right)\beta(N+1)\right)}/\beta(N+1)$, where $W(\cdot)$ is the Lambert W function. Then, the optimal integer valued Q is $Q^*=\underset{\lceil\hat{Q}\rceil,\lfloor\hat{Q}\rfloor}{\arg\max}\, R^{(K,Q)}$.*

We note that solving the fixed-point equation in Lemma 2.2 is not straightforward. Nevertheless, we can deduce the following trends in the variation of optimal Q^*:

(a) With all other parameters fixed, the optimal Q^* is a non-increasing function of ζ. This is because an increase in ζ raises the overhead per pilot transmission, making a smaller Q^* preferable. This behavior is also evident from the expression in (2.10), where, under fixed system parameters, the pre-log factor decreases as ζ increases, thereby driving the optimal solution toward a smaller Q^*.

(b) When N or K increases, again with all other parameters fixed, Q^* decreases. The reason is that the logarithmic term provides limiting returns with increasing N or K, so further increases in Q yield negligible improvement in the log term. Consequently, the dominant influence on performance comes from the pre-log factor, so the optimal Q^* becomes small.

Remark 2.2 (On the feedback requirement)**.** *The feedback requirement in this scheme is slightly higher than in the previous scheme. In addition to feeding back the best overall SNR, each user also sends an additional* $\log_2 Q$ *bits to indicate the index of the IRS phase configuration that yielded this best SNR at the user. Furthermore, after scheduling the user by the BS, the BS has to inform the IRS to configure the phase configuration that gives the best SNR to the scheduled user. However, this additional signaling is still substantially lower than the signaling required by conventional IRS phase optimization schemes.*

Remark 2.3 (On the convergence rate)**.** *Continuing with Remark 2.1, in order to ensure that with probability at least* P_{succ}*, there is a user for which the IRS configuration used in one of the* Q *pilots is within an* ϵ *ball of its optimal configuration, we need*

$$K \geq \frac{1}{Q}\left(-\log(1-P_{succ})\right)(\pi/\epsilon)^N, \tag{2.11}$$

when $\epsilon/\pi \ll 1$*. Thus, employing* Q *random phase configurations at the IRS during the pilot transmissions is equivalent to having* KQ *users in the system. Hence, a performance close to that achieved by optimal configuration at the IRS is possible with fewer users compared to the scheme in Sec. 2.3.a.ii.*

2.3.c IRS Channel Model Aware Multi-user Diversity

In the preceding section, a method to improve the performance of the basic scheme in Sec. 2.3.a was proposed by introducing multiple pilot transmissions. However, as we will see in Sec. 2.5, for both the schemes, the gap between the optimal rate and opportunistic rate increases with the number of IRS elements, especially in the large user regime. We now describe a method to overcome this limitation by accounting for the channel structure in IRS-aided systems, namely, that the IRS is deployed so that the BS-IRS and IRS-user channels exhibit strong LoS paths. On the other hand, the direct link between the BS and the user may be non-LoS and experience high path loss/shadowing effects. Thus, in this section, we ignore the contribution of the direct link, as in [86].

2.3.c.i Channel Model

We represent $\mathbf{h}_1$ and $\mathbf{h}_{2,k}$ as LoS channels using array steering vectors. Considering an N-element uniform linear array (ULA) based IRS, the LoS channels in the sub-6 GHz bands can be modeled as [86]

$$\mathbf{h}_1 = \left[1, e^{-j\frac{2\pi d}{\lambda}\sin(\theta_A)}, e^{-j\frac{4\pi d}{\lambda}\sin(\theta_A)}, \ldots, e^{-j\frac{2\pi(N-1)d}{\lambda}\sin(\theta_A)}\right]^T, \tag{2.12}$$

$$\mathbf{h}_{2,k} = h'_k \left[1, e^{-j\frac{2\pi d}{\lambda}\sin(\theta_{D,k})}, e^{-j\frac{4\pi d}{\lambda}\sin(\theta_{D,k})}, \ldots, e^{-j\frac{2\pi(N-1)d}{\lambda}\sin(\theta_{D,k})}\right]^T, \tag{2.13}$$

where θ_A and $\theta_{D,k}$ are the direction of arrival (DoA) and direction of departure (DoD) of the kth user at the IRS, d and λ are the inter-IRS element distance and signal wavelength, and h'_k is the Rayleigh distributed channel for the kth user. The other parameters are as in Sec. 2.3.a.i except for the absence of the non-IRS path. For the analysis, the total path loss is considered to be equal to β for all users as in [75].

2.3.c.ii Scheme for IRS Channel Model Aware Multi-user Diversity

Under the above channel model, with $\theta'_k \triangleq \frac{2\pi d}{\lambda}(\sin(\theta_A) + \sin(\theta_{D,k}))$, the channel at user k for the IRS configuration $\mathbf{\Theta}$ is given by

$$h_k = \sqrt{\beta}\mathbf{h}_{2,k}^T \mathbf{\Theta} \mathbf{h}_1 = \sqrt{\beta} h'_k \sum_{n=1}^{N} e^{-j\left((n-1)\theta'_k\right)+j\theta_n}. \tag{2.14}$$

Clearly, due to the Cauchy-Schwarz inequality, $|h_k|$ is maximized iff $\theta_i = \frac{2\pi(i-1)d}{\lambda}(\sin(\theta_A) + \sin(\theta_{D,k}))$ for all i, and this is also the beamforming configuration of the IRS.

Recall that the DoA at the IRS from the BS is θ_A, and let the DoDs from the IRS to the users be independent and uniformly distributed over $[\phi_0, \phi_1]$. Then, in each time slot, the phase configuration θ_i of the ith IRS element is set as

$$\theta_i = \frac{2\pi(i-1)d}{\lambda}(\sin(\theta_A) + \sin(\phi)), \tag{2.15}$$

where $\phi \sim \mathcal{U}[\phi_0, \phi_1]$ is a random phase. Note that this assumes that the value of θ_A is known. This is reasonable because the IRS and BS are typically installed at pre-fixed

locations with a direct LoS between them.[10] Additionally, if $[\phi_0, \phi_1] = [0, 2\pi]$, knowledge of θ_A is not required. The rest of the scheme proceeds as in Sec. 2.3.a.ii, with the BS scheduling the user with the highest PF metric for data transmission.

To investigate the performance of this scheme, first, using (2.14), it is clear that

$$|h_k|^2 = \beta \left| \sum_{n=1}^{N} e^{-j\left((n-1)\theta'_k - \theta_n\right)} \right|^2 \cdot |h'_k|^2. \tag{2.16}$$

The maximum value of the first term in (2.16) is βN^2 which is achieved by the beamforming configuration. Thus, when K is large, for every $\eta \in (0, 1)$, there exists a $\delta > 0$ such that, for a subset of ηK users, almost surely, we have [71, Sec.III.B]

$$\beta \left| \sum_{n=1}^{N} e^{-j\left((n-1)\theta'_k - \theta_n\right)} \right|^2 > \beta N^2 - \delta. \tag{2.17}$$

Thus, when K is large, for any randomly chosen IRS phase configuration as per (2.15), there will almost surely exist a set of users whose overall channel experiences a near-optimal beamforming configuration. The second term in (2.16) denotes the square of the channel gains, which are i.i.d. across users. We characterize the behavior of this term using extreme value theory. In particular, using Lemma 2.3 given in Appendix 2.B at the end of this chapter, it can be shown that $\max_k |h'_k|^2$ grows as $\ln K$. Hence, among the ηK users, the maximum of $|h_k|^2$ grows with K at least as fast as

$$(\beta N^2 - \delta) \ln(\eta K) = (\beta N^2 - \delta) \ln(K) + \mathcal{O}(1), \tag{2.18}$$

as $K \to \infty$. Clearly, the case with $\delta = 0$, which happens when at least one user is in beamforming configuration, serves as an upper bound on the rate of growth of the $|h_k|^2$ in (2.18). As a consequence, we have the following theorem.

Theorem 2.2. *For the IRS channel model-aware multi-user diversity scheme, the average*

[10] For example, in [23], the authors consider a receiver near the IRS, whose channel to the BS is similar to the BS-IRS channel, which helps in estimating θ_A.

system throughput scales as

$$\lim_{K\to\infty}\left(R^{(K)}-\mathcal{O}\left(\log_2\left(1+\frac{\beta P}{\sigma^2}N^2\ln K\right)\right)\right)=0. \tag{2.19}$$

The term N^2 in (2.19) shows that this scheme attains the maximum possible array gain from the IRS by exploiting the presence of strong LoS paths, while the $\log K$ term is due to multi-user diversity. This scheme thus even outperforms the scheme where optimization methods are used in IRS-aided systems without multi-user diversity (e.g., see (2.5)). Also, the SNR scaling under i.i.d. channels is $\mathcal{O}(N)$, whereas it is $\mathcal{O}(N^2)$ under strong LoS channels. This is because, under i.i.d. channels, the variance of the effective channel scales as N (see Proposition 2.1), while in the latter case it scales as N^2, at least for the subset of users satisfying (2.17). In turn, when the scheduler selects the best user for data transmission, the SNR scales as $\mathcal{O}(N^2)$ as per (2.19). A similar observation is made in [71] in the non-IRS context, when comparing the performance of i.i.d. fast fading channels and correlated channels.

Remark 2.4 (On the convergence rate)**.** *Similar to Remark 2.1, under the channel model in (2.12), (2.13), we have* $Pr(\mathcal{E})=1-\left(1-\left(\frac{\epsilon}{\pi}\right)\right)^K$ *when the IRS phases are sampled as in (2.15). Thus, the* K *required for near-optimal beamforming does* not *grow with* N*, and the opportunistic rate converges much faster to the beamforming-based rate compared to the scheme in Sec. 2.3.a. This is illustrated in Figs. 2.8 and 2.9 in the sequel.*

Remark 2.5 (mmWave bands)**.** *The channel model in (2.12), (2.13) is a special case of mmWave channels [87] with the number of paths set to* 1*. Since, by exploiting the knowledge of the channel statistics to design the distribution from which the random phase configurations are drawn, we can obtain significant multi-user diversity gains even with a relatively small number of users, randomly configured IRS-aided OC can also obtain significant benefits in mmWave scenarios.*

Remark 2.6 (Comparison with SSBs in 5G NR)**.** *In the context of 5G NR, the proposed scheme can significantly improve the performance by deploying an IRS with negligible overheads. We note that the scheme using the synchronization signal blocks (SSBs) as per NR*

specifications is user-centric*, wherein the BS sweeps through several beams across many time slots [88]. Thus, a given user measures the beam quality on every beam, and in the end, it reports to the BS the index of the beam which procured the best channel quality. This procedure focuses on obtaining the best beam for a given user and expends as many time resources as the number of beams the BS sweeps. As a consequence, the time complexity scales linearly with the number of beams used for sweeping. In contrast, the proposed scheme is* IRS centric *where the random phase configuration selected at the IRS in a given time slot can be considered to be the generation of a beam in a random (spatial) direction. The scheme then tries to locate the user who finds this random beam to yield the best beam quality. Thus, the proposed scheme does not need more than one time resource for scheduling, i.e., it entails lower overhead.*

2.4 Single IRS Assisted Opportunistic User Scheduling for Wideband Channels

This section investigates IRS-assisted OC over an L tap wideband channel. We consider a multiuser OFDM system where all users are served over a given total bandwidth. Since the IRS operates over the entire bandwidth (i.e., it is not possible to apply different phase configurations for different sub-bands),[11] we first analyze the performance of an IRS-assisted OFDM system where all the subcarriers are allocated to a single user with the best channel condition collectively among the subcarriers. In the second scheme, we configure OFDM-based multiple access (OFDMA) and study the performance improvement offered

[11] This assumes that the IRS elements are not frequency selective, similar to past work in the area [15, 89]. In fact, by appropriately designing the tuning parameters of the IRS circuit elements, it is possible to achieve non-frequency selectivity of the IRS elements even in wideband systems [90]. Having said that, as we will see in Chapter 8, as the number of IRS elements increases, so does the aperture of the IRS, and the propagation delay across the aperture can make the overall channel frequency selective. This is because the reflections from the different IRS elements contribute to a delay spread in the channel. This frequency selectivity is ignored in this chapter, and it is a good approximation as long as the aperture of the IRS and/or the bandwidth of the signal are not too large; this is precisely characterized in Chapter 8. However, the response of the individual phase shifters in the IRS is indeed frequency flat.

by the multiplexing gain and multi-user diversity. We refer to the former scheme as single-user OFDM (SU-OFDM) and the latter scheme as OFDMA. As before, for the analysis, we assume that all users experience similar large-scale propagation effects with path loss coefficient β, and hence we model the channels across the users in an i.i.d. fashion.

2.4.a IRS Enhanced Multi-user Diversity in a Single-user OFDM (SU-OFDM) System

2.4.a.i Channel Model

Consider a time domain channel seen by the kth user in an N-element IRS setting. Let $\mathbf{h}_{d,k} \in \mathbb{C}^{L\times 1}$ be the L-tap channel between the BS and user k through the direct (non-IRS) path. Let $\mathbf{H}_{2,k} \in \mathbb{C}^{N\times L}$ denote the L-tap channel between IRS and user k across all IRS elements. Note that, without loss of generality, we assume that the number of taps in the direct channel and the IRS-user channel to be the same. This can be done by letting L denote the larger of the numbers of taps in the two channels. Since the channel between the BS and IRS is typically LoS, it can be modeled as a single-tap channel between the BS and each of the N elements of the IRS, denoted by $\mathbf{h}_1 \in \mathbb{C}^{N\times 1}$ (see [16].) Furthermore, due to the strong LoS component, $\mathbf{h}_1$ can be modelled as an array steering response vector when the IRS is configured as a ULA (see (2.12)). We assume that channels between the IRS and the users across all the L taps are independent of each other [76, 91]. The exact statistics of the channels are provided below. The composite channel of user k can then be compactly written as

$$\mathbf{h}_k = \mathbf{h}_{d,k} + \mathbf{H}_{2,k}^T \mathbf{\Theta} \mathbf{h}_1 \in \mathbb{C}^{L\times 1}. \tag{2.20}$$

In this work, we use an exponentially decaying power delay profile (PDP) in the lag domain. Let $\breve{h}_{k,l,n} \triangleq h_{1,n} h_{2,k,l,n}$ denote the gain of the lth tap of the fading channel between the BS and the kth user through the nth IRS element. Then, the PDP of the link is given by

$$a_l \triangleq \mathbb{E}[|\breve{h}_{k,l,n}|^2] = ce^{-\nu l/L},\ \forall k \in [K], n \in [N], \tag{2.21}$$

where c is chosen such that $\sum_l \mathbb{E}[|\breve{h}_{k,l,n}|^2] = 1$, and ν captures the decay rate of the channel tap power with l. Hence, we have, $\|\mathbf{a}\|_1 = 1$, where $\mathbf{a} \triangleq [a_1, a_2, \ldots, a_L]^T$ represents the

power in each of the L taps. Therefore, the lth component of the channel in (2.20) can be written as $h_{k,l} = h_{d,k,l} + \sum_{i=1}^{N} e^{j\theta_i} \breve{h}_{k,l,i}$. If $h_{d,k,l}, h_{2,k,l,i} \sim \mathcal{CN}(0, a_l)$ across the IRS elements and since $|h_{1,n}|^2 = 1$ for all $n \in [N]$, it is easy to show that $h_{k,l} \sim \mathcal{CN}(0, (N+1)a_l)$ and independent across the users and L taps. Equivalently, in the OFDM system with M subcarriers, if we let $\tilde{\mathbf{h}}_k \in \mathbb{C}^{M\times 1}$ denote the frequency-domain channel vector for user k, we have $\tilde{\mathbf{h}}_k = \mathbf{F}_{M,L}\mathbf{h}_k$ where $\mathbf{F}_{M,L}$ is the matrix containing the first L columns of the $M \times M$ DFT matrix.[12] Thus, the channel at subcarrier m for user k follows $\tilde{h}_k[m] \sim \mathcal{CN}(0, N+1)$, and we also have the Parseval's relation $\mathbb{E}[\|\tilde{\mathbf{h}}_k\|_2^2] = M\,\mathbb{E}[\|\mathbf{h}_k\|_2^2]$.

2.4.a.ii Scheme for IRS-Enhanced Multi-user Diversity in SU-OFDM Systems

As before, we randomly set the phase configuration at the IRS at every time slot. The BS then applies equal power to all the subcarriers and broadcasts pilot symbols to all the users. In this section, for simplicity and analytical tractability, we assume that the BS uses equal power allocation across subcarriers during data transmission; note that this is near-optimal in the high SNR regime. The users estimate the channels, compute the sum rate obtainable across all subcarriers, and compute their respective PF metrics. The user with the highest PF metric sends its identity back to the BS, and is scheduled for transmission using all the subcarriers by the BS. Note that, with a slightly higher feedback overhead, the scheme easily extends to the case where the BS uses optimal water-filling-based power allocation. Here, after estimating the channels across the subcarriers, the user computes the sum rate achievable by it with water-filling power allocation, and uses this to calculate its PF metric. In this case, instead of feeding back just the user identity and the SNR, the user with the highest PF metric will also need to include the power allocation vector, which is of size $\approx 4M$ bits (assuming 16-levels of power control in each subcarrier.)

Under equal power allocation, in a K user system, the maximum average sum rate

[12] In this work, we compute the discrete Fourier transform (DFT) as $X[m] = \sum_{l=0}^{M-1} x[l]e^{-j\frac{2\pi ml}{M}}$ for all $m \in \{0, 1, \ldots, M-1\}$.

obtainable across subcarriers with a total power constraint P and noise variance σ^2 is

$$R_{\text{SU-OFDM}}^{(K)} = \max_{1\leq k\leq K} \sum_{m=0}^{M-1} \log_2\left(1+\frac{\beta P}{M\sigma^2}|\tilde{h}_k[m]|^2\right). \tag{2.22}$$

From (2.22), it is clear that we need to characterize the maxima of the sum of random variables. However, since the expression is not easily tractable, we upper-bound the term by invoking Jensen's inequality. From Parseval's theorem, $\sum_{m=0}^{M-1}|\tilde{h}_k[m]|^2 = M\sum_{l=0}^{L-1}|h_{k,l}|^2$. Using the monotonicity of $\log(\cdot)$, we get

$$R_{\text{SU-OFDM}}^{(K)} \leq \log_2\left(1+\frac{\beta P}{\sigma^2}\left\{\max_{1\leq k\leq K}\sum_{l=0}^{L-1}|h_{k,l}|^2\right\}\right). \tag{2.23}$$

We illustrate the tightness of the above upper bound in the numerical results section. Recall that $|h_{k,l}|^2 \sim \exp(\frac{1}{(N+1)a_l})$ and these form a set of independent and non-identically distributed (i.n.d.) random variables across L taps. First, we characterize the distribution of the sum-term in (2.23). We can show from [92] that if $\{X_i\}_{i=1}^{L}$ are a set of L i.n.d. exponential random variables with mean μ_i, then the cumulative distribution function (cdf) of $Y \triangleq \sum_{i=1}^{L} X_i$ is given by

$$F_Y(y) = \frac{y^L}{\Gamma(1+L)\prod_{i=1}^{i=L}\mu_i^{-2}} \times \Upsilon_2^{(L)}\left(1,\ldots,1;1+L;-\mu_1 y,\ldots,-\mu_L y\right), \tag{2.24}$$

where $\Upsilon_2^{(L)}(\cdot)$ is the confluent Lauricella function [93]. Thus, setting $\mu_i = (N+1)a_i$ in (2.24) will give the distribution of the sum-term in (2.23) and call it $\tilde{F}(\cdot)$. In what follows, we characterize the maximum of such i.i.d. sum-terms. To that end, we can show that the cdf in (2.24) satisfies the Von Mises' condition (see Lemma 2.5 in Appendix 2.C) [92]. Thus,

$$\max_{1\leq k\leq K}\sum_{l=0}^{L-1}|h_{k,l}|^2 \xrightarrow{K\to\infty} \tilde{F}\left(1-\frac{1}{K}\right), \tag{2.25}$$

where, by $X_K \xrightarrow{K\to\infty} c$, we mean $\lim_{K\to\infty} X_K - c \xrightarrow{d} Y$, and Y is a degenerate random variable. In other words, the sum-term in (2.23) can be replaced with the right-hand side of (2.25) when K is large. However, the resultant expression, although accurate, has two demerits: 1) It does not provide any explicit and useful insight on how the sum-rate scales

with the total number of users, 2) the characterization is not tractable for comparison and analyzing the performance.

Hence, we seek approximations by considering large L (In Remark 2.7, we discuss how large L needs to be.) In Sec. 2.5, we numerically show that this approximation works well even when L is as small as 5. Then, in view of (2.23), we have the following theorem for reasonably large L.

Theorem 2.3. *Consider an N-element IRS-assisted SU-OFDM system with M subcarriers and L time-domain taps with power delay profile $\mathbf{a}$, a total power constraint P, and noise variance σ^2. Then, for large L, the average sum rate of IRS enhanced multi-user diversity in an SU-OFDM system under equal power allocation, $R^{(K)}_{SU\text{-}OFDM}$, scales as*

$$\lim_{K\to\infty}\left(R^{(K)}_{SU\text{-}OFDM}-\mathcal{O}\left(\log_2\left\{1+\frac{\beta P}{\sigma^2}(N+1)\times\left[1+\|\mathbf{a}\|_2\Phi^{-1}\left(1-\frac{1}{K}\right)\right]\right\}\right)\right)=0, \tag{2.26}$$

where $\Phi^{-1}(\cdot)$ is the inverse cdf of a standard Gaussian random variable.

Proof. See Appendix 2.C. ■

In the above result, since the argument of $\Phi^{-1}(\cdot)$ is close to 1 for large K, we can use $\Phi(x)\approx\frac{1}{2}\left(1+\sqrt{1-e^{-\frac{2}{\pi}x^2}}\right)$ [94]. Consequently, from (2.26), we can explicitly determine the dependence of the sum rate on K as in the following corollary.

Corollary 2.1. *For the setup in Theorem 2.3, we have*

$$\lim_{K\to\infty}\left(R^{(K)}_{SU\text{-}OFDM}-\mathcal{O}\left(\log_2\left\{1+\frac{\beta P}{\sigma^2}(N+1)\left[1+\|\mathbf{a}\|_2\sqrt{\frac{\pi}{2}\ln K}\right]\right\}\right)\right)\approx 0. \tag{2.27}$$

Comparing the SU-OFDM performance given by the above equation with the performance in narrowband channels (see (2.10), with $Q=1$), the main difference in the multi-carrier case is the presence of $\|\mathbf{a}\|_2$ and the dependence on the number of users as $\sqrt{\ln K}$ instead of $\ln K$. The $\sqrt{\ln K}$ dependence is a consequence of the upper-bounding technique used to obtain (2.27); and apart from the $\|\mathbf{a}\|_2$ factor, the performances are similar in the two cases.

Remark 2.7. *To quantify how large L should be in order for Theorem 3 to hold, we use the Berry–Esseen theorem [95] which describes the error bound in approximating the normalized sum of random variables with a normal random variable through the CLT. We can show that the worst case absolute error, i.e.,* $\sup_{x\in\mathbb{R}} |F_n(x) - \Phi(x)| \lesssim C_1 \cdot a_1/\|\mathbf{a}\|_2$, *where $F_n(x)$ and $\Phi(x)$ denote the cdf of the normalized sum-random variable and standard normal random variable, for some constant $C_1 > 0$. Thus, for a given L, this bound becomes tighter when the PDP is slowly decaying, with the power in the dominant tap being comparable to other taps (which occurs when ν is small), and in this case, the convergence in CLT occurs faster.*

2.4.b IRS Enhanced Multi-user Diversity in OFDMA Systems

We now consider an OFDMA system, where, instead of allotting all the subcarriers to one of the users, each subcarrier is allotted to a single, possibly different user. On the other hand, a given user can be allotted one or more subcarriers. We consider the same channel model as in Sec. 2.4.a.i.

2.4.b.i Scheme for IRS-Enhanced Multi-user Diversity in OFDMA Systems

The scheme is similar to the single-user OFDM system in Sec. 2.4.a, except that the user scheduling is done on a per-subcarrier basis instead of allotting all the subcarriers to the user with the best sum rate across subcarriers. Recall that the channel coefficient of the mth subcarrier of user k is denoted by $\tilde{h}_k[m]$. Then, the average sum rate under equal power allocation in the IRS enhanced OFDMA-based multi-user diversity scheme is given by

$$R^{(K)}_{\text{OFDMA}} = \sum_{m=0}^{M-1} \log_2 \left\{ 1 + \frac{\beta P}{M\sigma^2} \max_{1\le k\le K} |\tilde{h}_k[m]|^2 \right\}. \tag{2.28}$$

Thus, we have the following theorem that characterizes the average sum rate of an OFDMA system.

Theorem 2.4. *Consider an N-element IRS assisted OFDMA system with M subcarriers, a total power constraint P, and noise variance σ^2. Then, the average sum rate exploiting*

multi-user diversity under equal power allocation, $R_{OFDMA}^{(K)}$, scales as

$$\lim_{K\to\infty}\left\{R_{OFDMA}^{(K)} - M\log_2\left(1+\frac{\beta P}{M\sigma^2}(N+1)\ln K\right)\right\} = 0. \tag{2.29}$$

Proof. The key step is to characterize the random variable $\max_{1\le k\le K}|\tilde{h}_k[m]|^2$ for large K. Since $|\tilde{h}_k[m]|^2 \overset{\text{i.i.d.}}{\sim} \exp(1/(N+1))$, we can apply Lemma 2.3 to obtain the scaling law in (2.29) in the same way as derived in Appendix 2.B. ■

Remark 2.8 (On the performance of OFDMA and SU-OFDM)**.** *The IRS-assisted OFDMA scheme outperforms the SU-OFDM scheme for two reasons: 1) Since there are M parallel channels in the OFDMA scheme, this offers additional selection/frequency diversity gain over an SU-OFDM system. 2) While a given user may see different channel coefficients on different subcarriers, the IRS configuration is common across all subcarriers. Thus, even in the asymptotic number of users, no user can be in beamforming configuration on all the subcarriers in an SU-OFDM scheme. On the other hand, in the OFDMA scheme, since the setup boils down to the availability of M parallel channels, and when K is large, the IRS can be close to the beamforming configuration with high probability on all subcarriers, by scheduling different users on different subcarriers. However, the feedback overhead in the OFDMA scheme is M times that of SU-OFDM, since the BS needs to find the best user on each of the M subcarriers. Note that, with OFDMA, one can still use a low feedback overhead timer- or splitting-based scheme [81, 82] for identifying the best user to schedule for data transmission, but on a subcarrier-by-subcarrier basis.*

2.5 Numerical Results

In this section, we validate the derived analytical results and quantify the relative performance of the schemes proposed in the previous sections through Monte Carlo simulations. A single antenna BS is located at $(0, 0)$ (in metres), the IRS is at $(0, 250)$, and single antenna users are uniformly distributed in the rectangular region with diagonally opposite corners $(100, 500)$ and $(500, 1000)$. The path losses are computed as $\beta = 1/d^\alpha$ where d is the distance and α is the path loss exponent. We use $\alpha = 2, 2.8$ and 3.6 in the BS-IRS,

IRS-user and BS-user (direct) links, respectively [76]. Further, we consider a BS transmitting with power $P = -10$ dBm and noise variance at the receiver $\sigma^2 = -117.83$ dBm, corresponding to a signal bandwidth of 400 kHz at a temperature of 300 K. Then, in the absence of the IRS, a user at the point closest to the BS experiences an average SNR of about 10.3 dB, while the farthest user experiences an average SNR of -1.9 dB. The fading channels are randomly generated as per the distributions discussed in the previous sections.

We first evaluate the performance of the scheme described in Sec. 2.3.a. In Fig. 2.5, we plot the average throughput offered by a randomly configured IRS-assisted OC scheme operated using a proportional fair scheduler with $\tau = 5000$. We compare the performance of the OC scheme against that of the beamforming-optimal scheme, given by (2.7). The throughput of the OC system improves with the number of IRS elements and users in the system. On the other hand, the gap between the throughput of the OC scheme and that of the optimally configured IRS-based scheme also increases with the number of IRS elements, in line with our discussion in Remark 2.1. We also see that the IRS assisted system significantly outperforms opportunistic scheduling in the absence of the IRS, when the BS is equipped with N antennas [71, Sec. III.A] (i.e., the same as the number of IRS elements used.)[13] This is because the BS is constrained by the total radiated power. Hence, increasing the number of antennas reduces the transmit power per antenna, resulting in a throughput that improves only marginally with the number of antennas at the BS. On the other hand, since the IRS uses passive reflective elements, the total received power at the user increases quadratically with the number of IRS elements under the optimal beamforming configuration (see, e.g., Theorem 2.2 or [10]).

Next, in Figs. 2.6 and 2.7, we evaluate the scheme in Sec. 2.3.b. In this experiment, we use $\zeta = 0.01$ in (2.10).[14] Hence, the rate goes to zero when $Q = 100$, since no symbols are left for data transmission. In Fig. 2.6, we plot the throughput as a function

[13] The BS uses weights $\alpha_n(t)$ and phase $\theta_n(t)$ at the nth antenna at time t, leading to $h_k(t) = \sum_{n=1}^{N} \sqrt{\alpha_n(t)}\, e^{j\theta_n(t)} h_{nk}(t)$ as the effective channel gain. At each t, $\alpha_n(t)$ and $\theta_n(t)$ are set randomly.

[14] We note that ζ depends on the coherence time of the channel. It has been shown in [96] that an optimal ζ is around 0.01 for channels with moderate fading rate operating at moderate SNR, in single antenna systems.

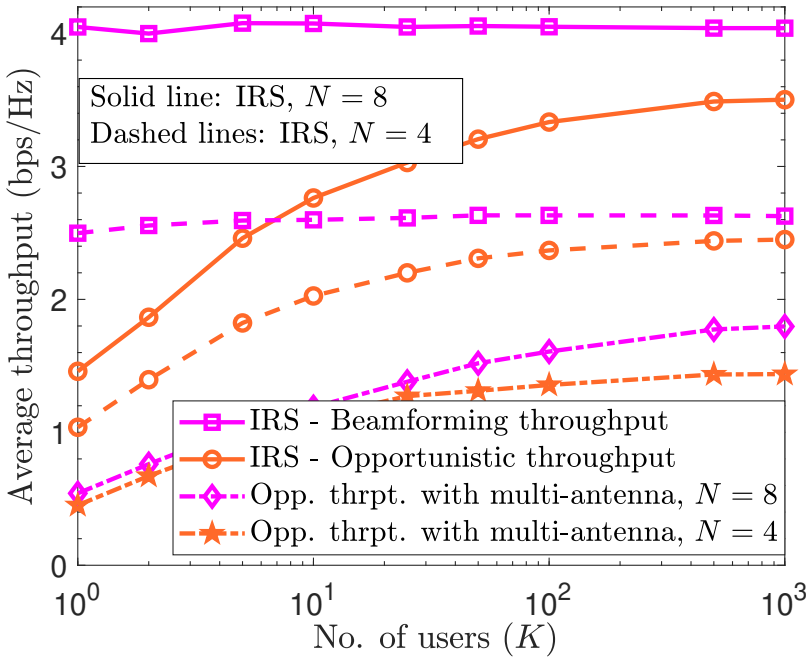

Figure 2.5: Average throughput vs. the number of users compared with the opportunistic scheme using multiple antenna BS used in [71, Sec.III.A].

of Q, the number of pilot transmissions. The optimal Q^* that yields the best trade-off between the pilot overhead and reflection diversity gain, given by Lemma 2.2, agrees with the integer Q at which the throughput achieves its maximum. In Fig. 2.7, we compare the performance in terms of the achievable system throughput obtained using $Q = 1$ ("Opportunistic throughput, $Q = 1$") against that obtained by using $Q = Q^*$ pilot transmissions ("Opportunistic throughput, $Q = Q^*$".) The figure shows the additional gain due to the reflection diversity, particularly when the number of users is small. The gain is marginal when K is large, partly because the throughput depends weakly on Q since it scales as $\log(\ln(QK))$, and partly because Q^* itself reduces with K. In the same figure, we also plot the performance of the IRS assisted opportunistic system under equal path loss across users, and see that the simulations ("Equal path loss - opp. throughput, $Q = Q^*$") match with the theoretical result in Theorem 2.1 ("Theorem 1, $Q = Q^*$".)

In Fig. 2.8, we study the performance of the channel model aware OC scheme as in Sec. 2.3.c and the IRS draws phase angles randomly as per (2.15), with users' DoDs (at the IRS) being randomly and independently sampled from a uniform distribution in

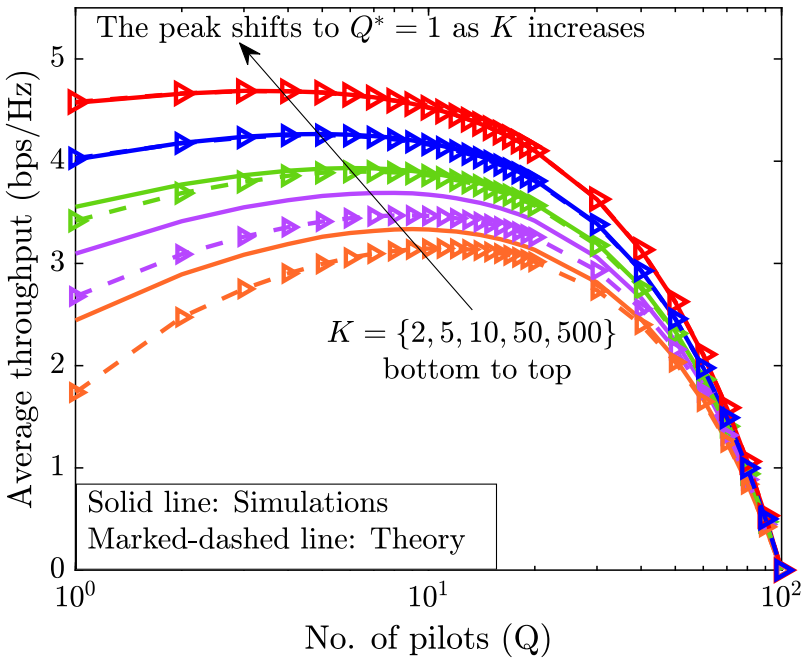

Figure 2.6: Average throughput as a function of the number of pilot transmissions, for $N = 8$.

$[-40°, 40°]$ with $\theta_A = 20°$. Further, the users are located in the region as mentioned in paragraph 1 of this section. We also use the uniform distribution to independently draw the phase angles at all the IRS elements, and show its performance in the same figure. We see that the performance of the OC system improves dramatically when the channel model and DoD statistics at the IRS are used in selecting the phase configurations. In Fig. 2.9, we investigate the performance gap between the randomly configured IRS-based OC and the rate obtained from the beamforming configuration, as a function of the number of IRS elements with and without the knowledge of DoD statistics at the IRS. The different curves correspond to the system having a varying number of users. We see that, for a given number of users, the performance of the system with the IRS phase angles drawn exploiting the knowledge of the DoD statistics is very close to the performance of an optimized IRS, even if the number of IRS elements is as large as 1024. Furthermore, in this regime, even when the number of users in the system is as small as 50, the OC performance is still close to the coherent beamforming rate. On the other hand, the performance of an IRS-assisted OC scheme with the phase angles drawn independently from the uniform distribution becomes increasingly worse relative to the beamforming rate as the number

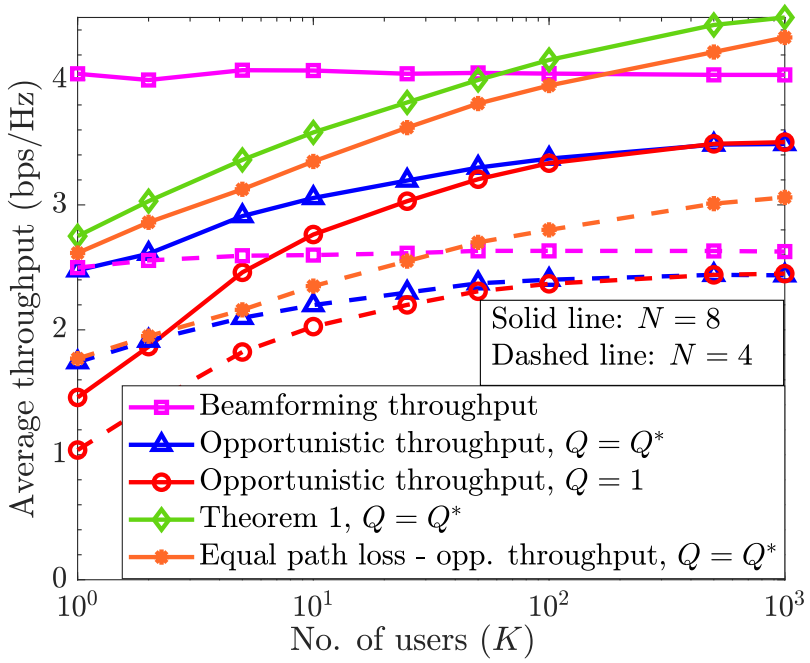

Figure 2.7: Average throughput as a function of the number of users, with Q^* pilot transmissions.

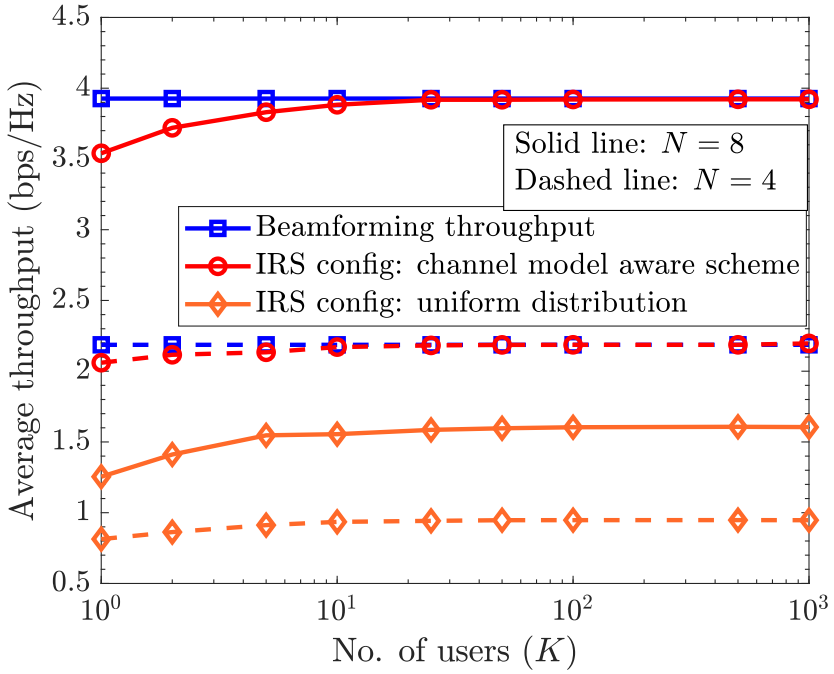

Figure 2.8: Average throughput as a function of the number of users, for channel model aware scheme.

of IRS elements increases. Moreover, the effect of multi-user diversity is hardly evident in the latter case, when the number of IRS elements is large. In a nutshell, for a given

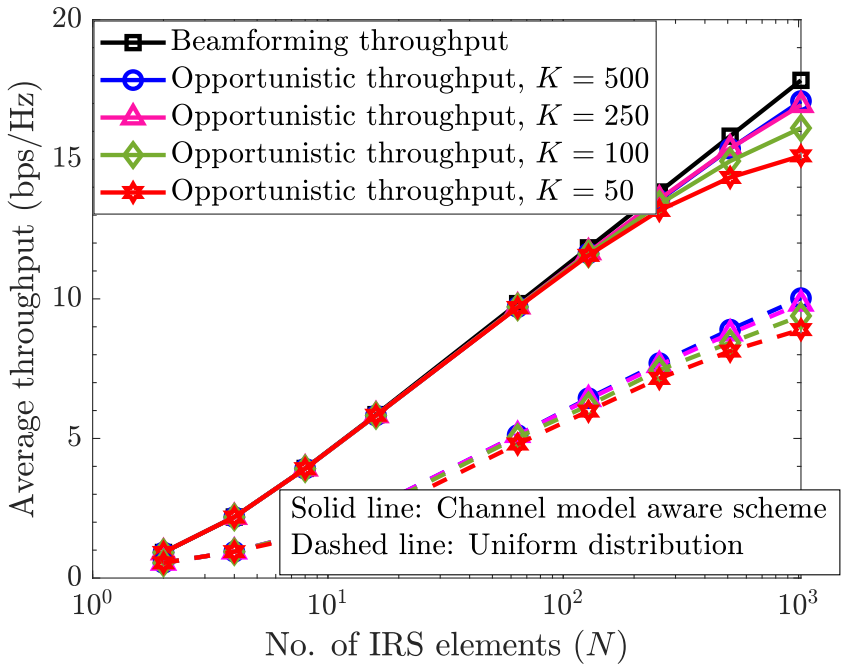

Figure 2.9: Average throughput as a function of N, for different number of users.

number of users, the channel model aware scheme offers two benefits: 1) The rate of the OC system remains close to the optimal beamforming rate even with a large number of IRS elements; 2) The effect of multi-user diversity is well captured, even with a small number of users.

We next illustrate the average SNR scaling of both schemes under opportunistic scheduling in Fig. 2.10. We plot the variation of the average SNR (the average of the maximum of the squared effective channel magnitudes across users) as a function of the number of IRS elements for a large number of users ($K = 10,000$) in the system. In the top part of the figure, the channels across all users are taken to be i.i.d. as per Sec. 2.3.a, with $\beta = 1$. Clearly, the average SNR scales as $\mathcal{O}(N)$, in line with Theorem 2.1. In the bottom part, we plot the effective SNR in the channel model aware scheme with IRS phase angles sampled from (2.15), and the channels taken as per Sec. 2.3.c. In this case, opportunistic scheduling significantly boosts the performance over the i.i.d. case and gives an SNR scaling of $\mathcal{O}(N^2)$, in line with Theorem 2.2. This is again because, for every random IRS configuration, the effective channel corresponds to a strong LoS channel to a fraction of users, and the scheduler picks the best among them.

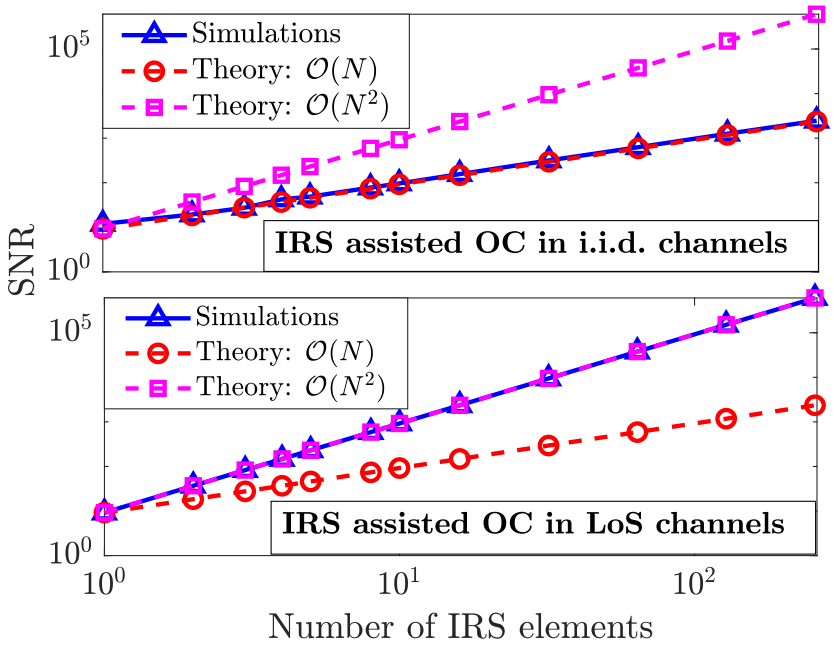

Figure 2.10: Scaling of the SNR in i.i.d. vs. LoS channels.

As the last experiment in this section, we consider the performance of IRS-aided OC over wideband channels as discussed in Sec. 2.4. We fix the number of time domain channel taps to two different values: $L = 25$ [97] and 5 with $\nu = 1$, in (2.21), and perform communication through an OFDM system with $M = 1024$ subcarriers and subcarrier spacing of 30 kHz. As a result, the total system bandwidth is 30.72 MHz, which corresponds to a total noise variance $\sigma^2 = -98.95$ dBm at 300 K. We choose a total power budget $P = 24$ dBm at the BS, and as a consequence, the nearest user experiences an average per-subcarrier SNR of 11 dB and the farthest user -1.2 dB, respectively. The channels are generated in an i.i.d. fashion across the users by setting the path loss coefficient to be equal for all users, such that the average SNR is 4.3 dB, and the BS power is allotted equally across all the subcarriers. Before we look at the numerical performance of the schemes, we first ascertain the applicability of the analytical rate scaling law in (2.26) for the choice of $L = 25$ at $\nu = 1$ in SU-OFDM systems. To characterize the Gaussianity of the sum-term in the left-hand side of (2.50), we compute its excess kurtosis, which measures how close a given distribution is to the Gaussian distribution [98]. The excess kurtosis, κ, of a random

Table 2.2: Excess kurtosis κ as a function of the number of taps.

L	1	2	5	10	20	**25**	50	100
κ	5.96	3.52	1.5	0.76	0.35	**0.28**	0.13	0.07

variable X with mean μ is defined as

$$\kappa = \frac{\mathbb{E}[|X-\mu|^4]}{\left(\mathbb{E}[|X-\mu|^2)\right)^2} - 3. \tag{2.30}$$

For a Gaussian random variable, $\kappa = 0$. In Table 2.2, we list the excess kurtosis of the L-sum-term in (2.50) as a function of L. We see that, for $L = 25$, we obtain an excess kurtosis of approximately 0.28, which is within 4% of the distance between a Gaussian and exponential random variable (corresponding to $L = 1$) and closer to the Gaussian random variable. Thus, it is reasonable to consider that this sum term is nearly Gaussian distributed, making the scaling law in (2.26) valid for $L = 25$. Subsequently, we relax the requirement on large values for L and study the validity of the scaling law for smaller L (particularly at $L = 5$.)

We present the OC throughput of SU-OFDM and OFDMA for $L = 25$ and 5, respectively, in Figs. 2.11a and 2.11b. We set the constant in the upper bound in (2.26) to 1 for plotting the theoretical result. The throughput offered by the IRS-assisted OFDMA is superior to that of SU-OFDM, in line with Remark 2.8. We also see that the performance of both OFDMA and SU-OFDM increases with N. However, while the simulated and theoretical performance of OFDMA given in Theorem 2.4 (marked as "OFDMA, Theorem 4" in the figures) match well as K increases, there is a gap between the two in the case of SU-OFDM (the theory is marked as "SU-OFDM, Theorem 3 on the plot".) This is partly because the throughput analysis of SU-OFDM is an upper bound (see (2.23)), and partly because the channels across the subcarriers become more disparate as the number of IRS elements increases, making the upper bound looser as N increases. We also observe that although the scaling law in Theorem 2.3 was derived assuming a large L, the expression captures the rate scaling performance even for moderate values of L such as 5 (in Fig. 2.11b). Nonetheless, the plot shows that one can obtain a performance boost by deploying an

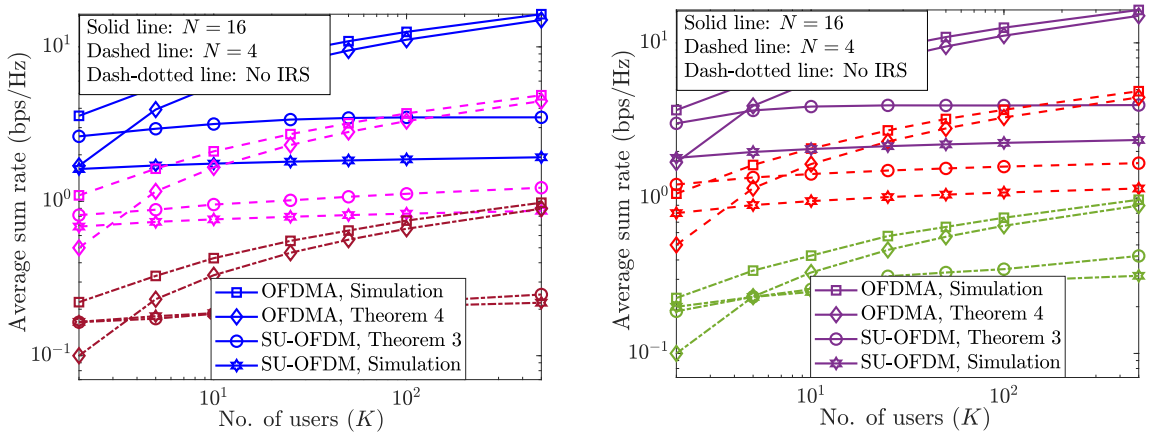

(a) $L = 25$. (b) $L = 5$.

Figure 2.11: Average sum rate as a function of number of users, for an OFDM-based communication system with $M = 1024$ subcarriers.

IRS, even without using complex optimization algorithms, by merely obtaining multi-user diversity gains over randomly configured IRSs.

2.6 Conclusions

In this chapter, we presented several opportunistic schemes in a single IRS-aided setting for exploiting and enhancing the multi-user diversity gains, both in narrowband and wideband channels. The schemes completely avoid the need for CSI estimation and computationally expensive phase optimization, and require little or no communication from the BS to the IRS. First, we saw that, in narrowband channels, a basic multi-user diversity scheme using a randomly configured IRS provides a performance boost over conventional systems as the number of users, K, gets large. In order to improve the rate of convergence of the opportunistic rate to the optimal rate (in terms of the number of users), we presented two alternative approaches and analyzed their performances: one where we obtained additional reflection diversity, and the other where we exploited the channel structure in IRS assisted systems. Both these schemes improve the rate of convergence of the throughput from the OC schemes with the number of users. In particular, exploiting the channel structure allows us to significantly increase the number of IRS elements

(and also achieve the coherent beamforming throughput) without requiring an exponentially large number of users to achieve significant multi-user diversity gains. Finally, we considered IRS-aided OC over a wideband channel in an OFDM system, and analyzed the performance of two different schemes, namely, SU-OFDM and OFDMA. Overall, IRS-assisted OC schemes offer significant performance improvement over conventional schemes, while incurring very low system overheads. Potential future research directions include extending the IRS-aided opportunistic communication framework to more general mmWave systems, multiuser MIMO-OFDM settings, and its integration with other transmission protocols within the broader class of multiple-antenna systems, such as spatial multiplexing. Another important direction is to adapt opportunistic UE selection schemes for delay-sensitive applications.

Appendix 2.A Proof of Proposition 2.1: Statistics of $h_{k,q}$

2.A.a Independent and Identically Distributed nature of $h_{k,q}$

We recognize that $h_{k,q}$ (ignoring the direct path) at any time can be decomposed as

$$h_{k,q} = \sum_{i=1}^{N} \sqrt{\beta} h_{1,n} h_{2,k,n} e^{j\theta_{q,n}}. \tag{2.31}$$

That the distributions of $h_{k,q}$ are identical is clear due to $\beta_{r,k} \approx \beta_{d,k} = \beta$. In the sequel, we first prove that the channels are uncorrelated and then argue their independence under random and independent IRS phase configurations.

Since the analysis holds true for any user, we consider the channels at a single user with normalization of path losses, and subsequently extend the analysis across other users. Hence, we drop the subscript k going forward, and let $f_n \triangleq h_{1,n}$, and $g_n \triangleq h_{2,k,n}$ for the sake of brevity. We then have from (2.31)

$$h_{k,q}/\beta \triangleq h_q = \sum_{i=1}^{N} f_n g_n e^{j\theta_{q,n}}. \tag{2.32}$$

We define the correlation coefficient as

$$\rho_{q,r} \triangleq \frac{\mathbb{E}[(h_q - \mathbb{E}[h_q])(h_r - \mathbb{E}[h_r])^*]}{\sqrt{\underbrace{\left(\mathbb{E}[|h_q|^2] - |\mathbb{E}[h_q]|^2\right)}_{\mathrm{Var}(h_q)} \underbrace{\left(\mathbb{E}[|h_r|^2] - |\mathbb{E}[h_r]|^2\right)}_{\mathrm{Var}(h_r)}}}. \tag{2.33}$$

We also decompose these complex random variables into their constituent real and imaginary parts as: $f_n = \Re(f_n) + j\Im(f_n)$, $g_n = \Re(g_n) + j\Im(g_n)$, and $e^{j\theta_{q,n}} = \cos(\theta_{q,n}) + j\sin(\theta_{q,n})$, so that $\Re(f_n), \Im(f_n), \Re(g_n), \Im(g_n) \overset{\text{i.i.d.}}{\sim} \mathcal{N}(0, \frac{1}{2})$, where $\Re(\cdot)$ and $\Im(\cdot)$ are the real and imaginary parts of a complex number. Then, h_q in (2.32) can be written as $h_q = X_q + jY_q$, with

$$X_q \triangleq \sum_{n=1}^{N} \{ \overbrace{(\Re(f_n)\Re(g_n) - \Im(f_n)\Im(g_n))}^{\triangleq a_n} \cos(\theta_{q,n}) - \underbrace{(\Re(f_n)\Im(g_n) + \Im(f_n)\Re(g_n))}_{\triangleq b_n} \sin(\theta_{q,n}) \}, \tag{2.34}$$

$$Y_q \triangleq \sum_{n=1}^{N} a_n \sin(\theta_{q,n}) + b_n \cos(\theta_{q,n}). \tag{2.35}$$

Computation of $\mathbb{E}[h_q]$: Since $\theta_{q,n}$'s are sampled from the uniform distribution in $[0, 2\pi]$, $\mathbb{E}[\cos(\theta_{q,n})] = \mathbb{E}[\sin(\theta_{q,n})] = 0 \ \forall q, n$. Since $\theta_{q,n}$ is independent of f and g, $\mathbb{E}[X_q] = \mathbb{E}[Y_q] = 0$ by linearity of expectation over finite sums, and hence $\mathbb{E}[h_q] = \mathbb{E}[h_r] = 0$. Hence, (2.33) becomes

$$\rho_{q,r} = \frac{\mathbb{E}[h_q h_r^*]}{\sqrt{\mathrm{Var}(h_q)\mathrm{Var}(h_r)}}. \tag{2.36}$$

Computation of $\mathbb{E}[h_q h_r^*]$: It is again clear that

$$\mathbb{E}[h_q h_r^*] = \mathbb{E}[X_q X_r] + \mathbb{E}[Y_q Y_r] + j\left(\mathbb{E}[X_r Y_q] - \mathbb{E}[X_q Y_r]\right). \tag{2.37}$$

Expanding the first term in the RHS of (2.37) using (2.34), we have $\mathbb{E}[X_q X_r] =$

$$\mathbb{E}\left\{ \sum_{n=1}^{N}\sum_{m=1}^{N} a_n a_m \cos(\theta_{q,n})\cos(\theta_{r,m}) - \sum_{n=1}^{N}\sum_{m=1}^{N} a_n b_m \cos(\theta_{q,n})\sin(\theta_{r,m}) - \sum_{n=1}^{N}\sum_{m=1}^{N} a_m b_n \cos(\theta_{r,m})\sin(\theta_{q,n}) + \sum_{n=1}^{N}\sum_{m=1}^{N} b_m b_n \sin(\theta_{r,m})\sin(\theta_{q,n}) \right\}. \tag{2.38}$$

Focusing on the first term in RHS of (2.38), we have by linearity of expectation over finite sums and by independence of IRS phase angles and channel fading coefficients, $\forall n, m$,

$$\mathbb{E}\left\{\sum_{n=1}^{N}\sum_{m=1}^{N} a_n a_m \cos(\theta_{q,n})\cos(\theta_{r,m})\right\} = \sum_{n=1}^{N}\sum_{m=1}^{N} \mathbb{E}[a_n a_m]\mathbb{E}[\cos(\theta_{q,n})\cos(\theta_{r,m})]. \tag{2.39}$$

But, from the properties of trigonometric functions, we have

$$\cos(\theta_{q,n})\cos(\theta_{r,m}) = \frac{1}{2}\left(\cos(\theta_{q,n}+\theta_{r,m}) + \cos(\theta_{q,n}-\theta_{r,m})\right). \tag{2.40}$$

Also, we have

$$\mathbb{E}[\cos(\theta_{q,n} \pm \theta_{r,m})] \overset{(a)}{=} \frac{1}{4\pi^2}\int_0^{2\pi}\int_0^{2\pi} \cos(\omega \pm \phi) d\omega d\phi, \tag{2.41}$$

since the IRS phase configurations are independent across IRS elements and pilots. Computing the above integral, we have, $\forall n, m$, $\mathbb{E}[\cos(\theta_{q,n} \pm \theta_{r,m})] = 0$. Therefore, the expectation in (2.39) is 0, and so is the first term in (2.38). We can similarly show that all the other terms in (2.38) equal 0, in turn making the first term in (2.37) equal to 0. Similarly, we can show that all terms in (2.37) are also 0, i.e., $\mathbb{E}[h_q h_r^*] = 0$. It is also straightforward show that $\mathrm{Var}(h_q) = \mathrm{Var}(h_r) > 0$ (see Appendix 2.A.b.) Hence, from (2.36), $\rho_{q,r} = 0$. Extending the argument across all users, we have that $h_{k,q}$ forms a set of uncorrelated random variables. Now, under the joint Gaussianity assumption [43] (see Appendix 2.A.b), these uncorrelated random variables are also independent. Finally, adding the direct path in the scenario does not change the result because the direct paths are independent across users, and using the fact that functions of independent random variables are independent, the result follows.

2.A.b On the distribution of $h_{k,q}$

Recall that the cascaded channel ignoring path loss at a given user is given by (2.32). From the real and imaginary parts in (2.34), (2.35), X_q and Y_q are a sum of N zero-mean random variables. Then, for large N, by the central limit theorem (CLT), we have that X_q and Y_q are normal random variables. What remains is to compute their variances.

Computation of Var(X_q): $\mathrm{Var}(X_q) = \mathbb{E}[X_q^2]$, with

$$X_q^2 = \sum_{n=1}^{N} \left(a_n \cos(\theta_{q,n}) - b_n \sin(\theta_{q,n})\right)^2 + \sum_{\substack{n,m=1 \\ n \neq m}}^{N} \left\{\left[a_n \cos(\theta_{q,n}) - b_n \sin(\theta_{q,n})\right]\left[a_m \cos(\theta_{q,m}) - b_m \sin(\theta_{q,m})\right]\right\}. \quad (2.42)$$

We simplify the first term in (2.42) as

$$\sum_{n=1}^{N} \left(a_n^2 \cos^2(\theta_{q,n}) + b_n^2 \sin^2(\theta_{q,n}) - 2a_n b_n \cos(\theta_{q,n}) \sin(\theta_{q,n})\right). \quad (2.43)$$

It is also straightforward to compute the following values.

1. $\mathbb{E}[\cos(\theta_{q,n})] = \mathbb{E}[\sin(\theta_{q,n})] = 0$,
2. $\mathbb{E}[\cos^2(\theta_{q,n})] = \mathbb{E}\left[\frac{1+\cos(2\theta_{q,n})}{2}\right] = \frac{1}{2}$,
3. $\mathbb{E}[\sin^2(\theta_{q,n})] = \mathbb{E}\left[\frac{1-\cos(2\theta_{q,n})}{2}\right] = \frac{1}{2}$, and
4. $\mathbb{E}[a_n^2] = \mathbb{E}[b_n^2] = \frac{1}{2}$.

Taking expectations on both sides of (2.42), we can show that $\mathbb{E}[X_q^2] = \frac{N}{2}$. Similarly, $\mathrm{Var}(Y_q) = \mathbb{E}[Y_q^2] = \frac{N}{2}$. Thus, by CLT, $X_q \sim \mathcal{N}(0, \frac{N}{2})$, and $Y_q \sim \mathcal{N}(0, \frac{N}{2})$. Further, we can verify that X_q and Y_q are uncorrelated. Since they are jointly Gaussian (see Appendix 2.A.a), they are i.i.d. as well. Therefore, $h_q \sim \mathcal{CN}(0, N)$. Finally, adding the contributions from path loss and the direct path, $h_{k,q} \sim \mathcal{CN}(0, \beta(N+1))$.

Appendix 2.B Proof of the Theorem 2.1

The proof of the theorem uses the following lemma on the extreme values of i.i.d. random variables.

Lemma 2.3. *([71]). Let $z_1, \ldots, z_K$ be i.i.d. random variables with a common cumulative distribution function (cdf) $F(\cdot)$ and probability density function (pdf) $f(\cdot)$ that satisfy*

$F(z) < 1$ and are twice differentiable for all z. Let the corresponding hazard function, $\Omega(z) \triangleq \left[\frac{f(z)}{1-F(z)}\right]$ be such that

$$\lim_{z\to\psi} \frac{1}{\Omega(z)} = c > 0, \tag{2.44}$$

for $\psi \triangleq \sup\{z : F(z) < 1\}$ and some constant c. Then, $\max_{1\le k\le K} z_k - l_K$ converges in distribution to a Gumbel random variable with cdf $e^{(-e^{-x/c})}$, where $F(l_K) = 1 - \frac{1}{K}$.

In words, the lemma states that, asymptotically, the maximum of K i.i.d. random variables grows like l_K. From Theorem 2.1, $|h_{k,q}|^2 \sim \exp\left(\frac{1}{\beta(N+1)}\right)$ for all $k \in [K]$ and $q \in [Q]$. Further, since the phase angles are independently generated at the IRS during each pilot transmission, we have that $\grave{h}_{k,q} \triangleq |h_{k,q}|^2$ form a set of QK i.i.d. exponential random variables with mean $\beta(N+1)$. Thus, we have the pdf, $f_{\grave{h}_{k,q}}(h) = \frac{1}{\beta(N+1)} e^{-\frac{h}{\beta(N+1)}}$ for $h \ge 0$ and hence the cdf, $F_{\grave{h}_{k,q}}(h) = 1 - e^{-\frac{h}{\beta(N+1)}}$ for $h \ge 0$ and 0 otherwise. Also, here $\psi = \infty$. Thus, we have,

$$\lim_{h\to\infty} \frac{1}{\Omega(h)} = \lim_{h\to\infty} \left(\frac{e^{-\frac{h}{\beta(N+1)}}}{\frac{1}{\beta(N+1)} e^{-\frac{h}{\beta(N+1)}}} \right)^{-1} = \frac{1}{\beta(N+1)} > 0. \tag{2.45}$$

Hence, by virtue of the above lemma, we have $l_{QK} = F^{-1}\left(1 - \frac{1}{QK}\right)$ and solving, we get $l_{QK} = \beta(N+1)\ln(QK)$, and applying the lemma to (2.9), we get the desired result.

Appendix 2.C Proof of the Theorem 2.3

We use the fact that L is large and invoke the following version of the central limit theorem (CLT) [99]:

Lemma 2.4 (Lyapounov's Central Limit Theorem)**.** *Suppose that $X_1, X_2, \ldots, X_n$ form a sequence of independent random variables such that $\forall i \in [n]$, $\mathbb{E}[X_i] \triangleq \mu_i$, $\sigma_i^2 \triangleq \mathbb{E}[|X_i|^2]$ and $s_n^2 \triangleq \sum_{i=1}^n \sigma_i^2$. If, for some $\delta > 0$,*

$$\mathcal{L} \triangleq \lim_{n\to\infty} \sum_{i=1}^{n} \frac{1}{s_n^{2+\delta}} \mathbb{E}\left[|X_i - \mu_i|^{2+\delta}\right] = 0, \tag{2.46}$$

then

$$\frac{1}{s_n}\sum_{i=1}^{n}(X_i-\mu_i)\xrightarrow[n\to\infty]{d}\mathcal{CN}(0,1), \tag{2.47}$$

where $\xrightarrow[n\to\infty]{d}$ *stands for convergence in distribution.*

To check whether the random variables $\{|h_{k,l}|^2\}_l$ satisfy (2.46), let $\delta=1$. Then $\mathbb{E}\left[|X_i-\mu_i|^3\right]=2\left((N+1)a_l\right)^3$. Further, $s_n^2=\sum_{i=1}^{n}a_l^2(N+1)^2$, hence $s_n^3=\left(\|\mathbf{a}\|_2(N+1)\right)^3$. Thus, $\mathcal{L}=\lim_{n\to\infty}2\frac{\|\mathbf{a}\|_3^3}{\|\mathbf{a}\|_2^3}$. We can lower and upper bound the ratio on the right-hand side as follows:

$$2\frac{n\min\limits_{i\in[n]}a_i^3}{n^{3/2}\max\limits_{i\in[n]}a_i^3}\le 2\frac{\|\mathbf{a}\|_3^3}{\|\mathbf{a}\|_2^3}\le 2\frac{n\max\limits_{i\in[n]}a_i^3}{n^{3/2}\min\limits_{i\in[n]}a_i^3}. \tag{2.48}$$

Hence, when $n\longrightarrow\infty$ and $\|\mathbf{a}\|<\infty$, both lower and upper bounds go to zero, and by the sandwich theorem, $\mathcal{L}=0$. Thus, the given exponential random variables satisfy the condition in the lemma. Therefore, we have,

$$\frac{1}{(N+1)\|\mathbf{a}\|_2}\sum_{l=1}^{L}\left(|h_{k,l}|^2-(N+1)a_l\right)\xrightarrow[L\to\infty]{d}\mathcal{CN}(0,1), \tag{2.49}$$

which implies

$$\sum_{l=1}^{L}|h_{k,l}|^2\xrightarrow[L\to\infty]{d}(N+1)\left\{1+\|\mathbf{a}\|_2\bar{h}_k\right\}, \tag{2.50}$$

where $\bar{h}_k\sim\mathcal{CN}(0,1)$. Thus, (2.23) can be rewritten as,

$$R_{\text{SU-OFDM}}^{(K)}\le\log_2\left(1+\frac{\beta P}{\sigma^2}(N+1)\ \times\left[1+\|\mathbf{a}\|_2\left\{\max_{1\le k\le K}\bar{h}_k\right\}\right]\right). \tag{2.51}$$

To characterize the extreme value of K i.i.d. Gaussian random variables, we note that Lemma 2.3 cannot be used as (2.44) is not satisfied by Gaussian random variables. Instead, we use another lemma to characterize the extreme values of i.i.d. Gaussian random variables from [100].

Lemma 2.5 (Von Mises' sufficient condition for weak convergence of extreme values)**.** *Let* $X_1,X_2,\ldots,X_K$ *be i.i.d. random variables each having an absolutely continuous cdf* $F(x)$ *and pdf* $f(x)$*. Let* $M_K\triangleq\max\{X_1,X_2,\ldots,X_K\}$*,* $\Omega(x)\triangleq\left[\frac{f(x)}{1-F(x)}\right]$ *and* $\psi\triangleq\sup\{x:F(x)<$

1}. *If*

$$\lim_{x\to\psi} \frac{d}{dx}\left(\frac{1}{\Omega(x)}\right) = 0, \tag{2.52}$$

then

$$M_K - l_K \xrightarrow[K\to\infty]{d} G, \tag{2.53}$$

where G is a Gumbel random variable with cdf, $e^{(-e^{-x/c})}$ and l_K is given by $F(l_K) = 1 - \frac{1}{K}$ for some constant $c > 0$.

As before, the result shows that the extreme value of K i.i.d. random variables satisfying (2.52) grows like l_K, asymptotically. In what follows, we check the applicability of the lemma to K i.i.d. Gaussian random variables. Clearly, $\psi = \infty$. Let $\Phi(x)$ and $f(x)$ be the cdf and pdf of a standard complex normal random variable. We then have,

$$\frac{\mathrm{d}}{\mathrm{d}x}\left(\frac{1-\Phi(x)}{f(x)}\right) = \frac{(1-\Phi(x))x}{f(x)} - 1 = \sqrt{2}x\frac{Q(x)}{f(x)} - 1, \tag{2.54}$$

where $Q(x)$ is the standard Q function. But we know that,

$$\frac{1}{\sqrt{2\pi}x}e^{-\frac{x^2}{2}}\left(1-\frac{1}{x^2}\right) \leq Q(x) \leq \frac{1}{\sqrt{2\pi}x}e^{-\frac{x^2}{2}}. \tag{2.55}$$

Using (2.55) to lower and upper bound (2.54) and taking the limit x to ∞ and applying the sandwich theorem, it is straightforward to show that (2.52) is satisfied by Gaussian random variables. Thus, $l_K = \Phi^{-1}\left(1-\frac{1}{K}\right)$. Substituting it in (2.51) yields the desired result in (2.26).

3 Spatial Correlation Aware Oppotunistic Beamforming in IRS-Aided Communications

Chapter Highlights

This chapter addresses the question of how to exploit the inherent spatial correlation in the channels through the different intelligent reflecting surface (IRS) elements to reduce the overheads in IRS-aided wireless communications. We propose a novel approach that randomly samples the IRS phase configurations from a carefully designed distribution and opportunistically schedules the user equipments (UEs) for data transmission. The key idea is that when the IRS configuration is randomly chosen from a channel statistics-aware distribution, it will be near-optimal for at least one UE, and upon opportunistically scheduling that UE, we can obtain nearly all the benefits from the IRS without explicitly optimizing it. We formulate and solve a variational functional problem to derive the optimal phase sampling distribution. Interestingly, we find that, with the IRS phase configuration drawn from the optimized distribution, it is sufficient if the number of UEs scales exponentially with the *rank* of the channel covariance matrix, not with the number of IRS elements, to achieve a given target signal-to-noise ratio (SNR) with high probability. Our numerical studies reveal that even with a moderate number of UEs, the opportunistic scheme achieves near-optimal performance without incurring the conventional IRS-related signaling overheads and complexities.

3.1 Introduction

An intelligent reflecting surface (IRS) comprises multiple passive elements that can be independently configured to reflect signals in required directions [68]. This enables one to control the wireless channel between any two nodes and thereby improve the spectral efficiency (SE) of next-generation wireless systems. However, optimally configuring every IRS element entails *three-fold* control overheads: 1) acquisition of channel state information (CSI), 2) optimization of IRS phase angles, and 3) phase transportation from the base station (BS) to the IRS via control links. These overheads can easily undermine the professed benefits of an IRS when the number of IRS elements is large. This chapter overcomes this bottleneck by leveraging a spatial correlation-aware opportunistic beamforming (BF) framework that obtains the optimal IRS gains without optimization/three-fold overheads as described above.

In the pursuit of reducing the complexity while maximizing the IRS-aided performance, [101] leverages correlation among different user equipments (UEs) to minimize the pilot overheads, and [102] proposed to use only the partial CSI of the channel. In [41], a blind beamforming approach is proposed, which does not need CSI estimation; however, it suffers from high time complexity. In this context, [76] and our previous work [103] utilize opportunistic scheduling techniques in IRS-aided systems to mitigate both time and computational complexity. However, they consider independent fading channels and consequently need a very large number of UEs to achieve optimal gains.

In this chapter, we progress upon this problem by exploiting the inherent spatial correlation at the IRS and show that the performance of the opportunistic scheme can be significantly improved even with a small number of UEs at very low time and computational complexities. Our key contributions are:

1. We pose and solve a variational functional problem to obtain the optimal sampling distribution for the random IRS phases, as a function of the channel statistics. (Sec. 3.4.c.)

2. We show that when the above spatial-correlation-aware distribution is used to sample the IRS configuration, it is sufficient for the number of UEs to scale exponentially in

Variable	Definition	Variable	Definition
N	Number of IRS elements	$R_k(t)$	Achievable rate of UE-k at time t
K	Number of UEs	$T_k(t)$	Average rate of UE-k till time t
$\mathbf{\Sigma}$	Covariance matrix at IRS	h_k	Overall channel at UE-k
M	Rank of $\mathbf{\Sigma}$	$\mathbf{h}_1$	Channel from BS to IRS
$\mathbf{U}$	Eigenvector matrix of $\mathbf{\Sigma}$	$\mathbf{h}_{2,k}$	Channel from IRS to UE-k
$\mathbf{\Lambda}$	Eigen value matrix of $\mathbf{\Sigma}$	$\boldsymbol{\theta}$	Effective IRS phase vector
P/σ^2	Ratio of transmit power at BS to the noise variance at UE	$h_{d,k}$	Direct channel from BS to UE-k
R_K^{opp}	Acheivable system SE using opportunistic beamforming	$\mathbf{h}_{r,k}$	Cascaded channel from BS to UE-k
R_K^{opt}	Acheivable system SE using IRS optimization under RR scheduling	$\mathbf{h}_{f,k}$	Composite fading ch.: BS to UE-k
P_{succ}	Success probability of the scheme	$\beta_{d,k}$, $\beta_{r,k}$	Path loss in the direct link / cascaded link via the IRS

Table 3.1: Commonly encountered variables/notations in chapter 3.

the *rank* of the channel covariance matrix to obtain near-optimal SNR in every time slot. (Sec. 3.5.)

3. In the process, we derive the tail probability of the Rayleigh quotient of a heteroscedastic complex Gaussian random vector, which may be of independent interest. (Lemma 3.3.)

We empirically verify our findings and show the efficacy of the opportunistic scheme even with a moderate number of UEs in the system. For e.g., when the number of IRS elements is $N = 32$, even with as few as $K = 25$ UEs, the sum-SE is just 0.7 bps/Hz away from the SE obtained by IRS optimization.

Notation: For general notations used in this chapter, see the section on "General Mathematical Notations" on page ix. For the notations/variables specific to this chapter, please refer to Table 3.1.

3.2 System Model and Problem Description

We consider an N-element IRS-aided downlink scenario where a BS serves K UEs in a time-division multiple-access fashion. Let the small-scale channel from the BS to IRS be $\mathbf{h}_1 \in \mathbb{C}^N$, and from IRS to UE-$k$ be $\mathbf{h}_{2,k} \in \mathbb{C}^N$. Since the BS and IRS are envisioned to be deployed at fixed positions, we model $\mathbf{h}_1$ as a deterministic vector, with entries given by [75]

$$[\mathbf{h}_1]_n = \exp\left(j2\pi d_n/\lambda\right), \; n = 1, 2, \ldots N, \tag{3.1}$$

where d_n is the distance between the BS antenna and the nth IRS element. The channel from IRS to UE can be random; so, we model $\mathbf{h}_{2,k} \sim \mathcal{CN}(\mathbf{0}, \mathbf{\Sigma}_k)$, where $\mathbf{\Sigma}_k$ is the spatial correlation matrix at the IRS for UE-k. The overall channel at UE-k is

$$h_k = \sqrt{\beta_{d,k}} h_{d,k} + \sqrt{\beta_{r,k}} \mathbf{h}_{2,k}^T \tilde{\mathbf{\Theta}} \mathbf{h}_1,$$

where $h_{d,k} \sim \mathcal{CN}(0, 1)$ is the direct channel from BS to UE-k, $\tilde{\mathbf{\Theta}} \in \mathbb{C}^{N \times N}$ is a diagonal matrix containing the IRS phase shifts, and $\beta_{d,k}$, $\beta_{r,k}$ denote the path loss of the direct path and cascaded path via the IRS, respectively. We now write

$$h_k = \sqrt{\beta_{d,k}} h_{d,k} + \sqrt{\beta_{r,k}} \; \tilde{\boldsymbol{\theta}}^T (\mathbf{h}_{2,k} \odot \mathbf{h}_1) \triangleq \boldsymbol{\theta}^H \mathbf{h}_{f,k}, \tag{3.2}$$

where $\odot$ is the Hadamard product, $\boldsymbol{\theta} \triangleq \left[1, \tilde{\boldsymbol{\theta}}^{*T}\right]^T \in \mathbb{C}^{N+1}$ is called as the effective IRS vector with $\tilde{\boldsymbol{\theta}} \in \mathbb{C}^N$ comprising of the diagonal elements of $\tilde{\mathbf{\Theta}}$, and $\mathbf{h}_{f,k} \triangleq [\sqrt{\beta_{d,k}} h_{d,k}, \sqrt{\beta_{r,k}} \mathbf{h}_{r,k}^T]^T$ is the fading vector with $\mathbf{h}_{r,k} \triangleq \mathbf{h}_{2,k} \odot \mathbf{h}_1$. The system is illustrated in Fig. 3.1.

Let P and σ^2 denote the transmit power and noise variance, respectively. The overheads incurred when the BS schedules UE-k and configures the IRS with the SE-optimal phase vector

$$\boldsymbol{\theta}^{\text{opt}} = \arg\max_{\boldsymbol{\theta}} \; \log_2\left(1 + |\boldsymbol{\theta}^H \mathbf{h}_{f,k}|^2 P/\sigma^2\right), \tag{P1}$$

$$\text{s.t. } [\boldsymbol{\theta}]_1 = 1, \quad |[\boldsymbol{\theta}]_n| = 1, \; n = 2, \ldots, N+1, \tag{C1-1}$$

are computationally expensive (explained in Sec. 3.3.) We then address the following

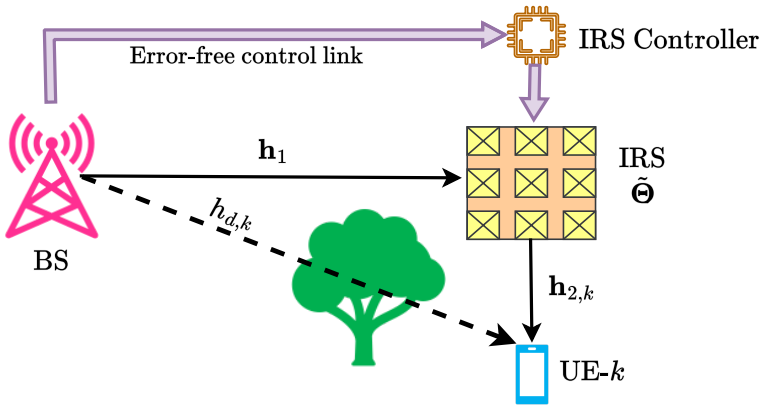

Figure 3.1: System model for one UE.

questions:

1. Leveraging the spatial correlation, how can we randomly configure the IRS phase vector $\boldsymbol{\theta}$ (i.e., without determining $\boldsymbol{\theta}^{\text{opt}}$), and still obtain near-optimal benefits from the IRS?

2. For the above scheme, what is the probability that a random IRS phase procures a target near-optimal SE as in (P1)?

To this end, we first analyze the benchmark SE obtained under IRS optimization with round-robin (RR) scheduling of UEs.

3.3 The Benchmark Sum-SE Via IRS Optimization

Under RR scheduling, the BS sequentially schedules UEs using a pre-defined ordering. Considering that the IRS is configured as per (P1) in every time slot, the achievable beamforming (BF) sum-SE is characterized in the following [103].

Lemma 3.1. *With K-UEs, under RR scheduling, the BF sum-SE obtained when the BS optimizes the IRS to the channel of the scheduled UE in every time slot is given by* $R_K^{\text{opt}} =$

$$\frac{1}{K}\sum_{k=1}^{K}\log_2\left(1+\left|\sqrt{\beta_{d,k}}\,|h_{d,k}|+\sqrt{\beta_{r,k}}\sum_{n=1}^{N}|[\mathbf{h}_{r,k}]_n|\right|^2\frac{P}{\sigma^2}\right),$$

and is achieved with the optimal IRS configurations given by

$$[\boldsymbol{\theta}^{\text{opt}}]_n = \exp\Big\{ j \left(\angle [\mathbf{h}_{r,k}]_{n-1} - \angle h_{d,k} \right) \Big\}, \; n = 2, \ldots, N+1. \tag{3.3}$$

Remark 3.1. *Achieving* R_K^{opt} *as in Lemma 3.1 incurs computationally expensive* three-fold *overheads in every time slot:*

1. *Channel estimation: The BS acquires the CSI of all the links; this potentially requires* $\mathcal{O}(N)$ *pilot transmissions.*

2. *Phase optimization: The BS employs solvers to optimize the IRS for achieving the best SE during data transmission.*

3. *Phase transportation: The BS transports the optimal phase of each IRS element to the IRS controller via an error-free control link; its overhead scales as* $\mathcal{O}(N)$*.*

3.4 Spatial correlation-aware Opportunistic BF

3.4.a The Proportional-fair Scheduler

In every slot, the PF scheduler selects a UE that achieves the highest SE relative to the average SE of the UE till that time for data transmission [71]. In this way, the system opportunistically enhances the throughput while ensuring fairness in UE scheduling, thereby exploiting multi-user diversity. Let $R_k(t) \triangleq \log_2(1 + |h_k(t)|^2 P/\sigma^2)$ be the achievable SE of UE-k at time t. The PF scheduler selects the $k^*(t)$th UE, where

$$k^*(t) = \underset{k \in \{1,\ldots,K\}}{\arg\max} \frac{R_k(t)}{T_k(t)},$$

where $T_k(t)$ is the exponentially weighted moving average (EWMA) SE seen by UE-k till time t, which is parameterized by the EWMA factor τ [71]. Smaller (larger) values of τ favor short-term (long-term) fairness in UE scheduling.

We will refer to $R_k(t)/T_k(t)$ as the *PF metric* of UE-k at time t.

3.4.b Opportunistic Communication using an IRS

The proposed opportunistic communication (OC) scheme has two steps per slot: 1) the IRS configuration is randomly chosen from an *appropriate* sampling distribution, and 2) the BS opportunistically selects a UE using the PF scheduler. Then, if there are many UEs, the random IRS configuration will be near-optimal for at least one UE. In this view, we have the following lemma, proved similar to [71].

Lemma 3.2. *In a K-UE system, which uses a PF scheduler with $\tau \to \infty$, when the IRS configurations are randomly sampled from a spatial correlation-aware distribution, the sum-SE of the IRS-aided OC scheme, denoted by R_K^{opp}, obeys*

$$\lim_{K\to\infty} \left(R_K^{\text{opp}} - R_K^{\text{opt}}\right) = 0,$$

where R_K^{opt} is the optimal sum-SE as given in Lemma 3.1.

From Lemma 3.2, we deduce that with a large number of UEs, the PF scheduler selects the UE for which the random IRS phase is close to its BF configuration, and procures the BF benefits without actually optimizing the IRS [71]. This is called *opportunistic beamforming*. We next characterize the IRS phase sampling distribution that satisfies Lemma 3.2 from a variational perspective, which is one of our key contributions.

3.4.c Optimal Distribution for Sampling the Random IRS Phases

We observe that the optimal IRS vector in (3.3) is obtained as the deterministic map $\mathcal{F} : \mathbb{C}^{N+1} \longrightarrow \{1\} \times \mathbb{U}^N$, given by

$$\mathcal{F} : \mathbf{h}_{f,k} \longmapsto \left[1, \left(\exp\left\{j\left(\angle \mathbf{h}_{r,k} - \angle h_{d,k}\right)\right\}\right)^T\right]^T, \tag{3.4}$$

where $\mathbb{U}^N \triangleq \left\{\mathbf{z} \in \mathbb{C}^N \middle| |\mathbf{z}_i| = 1, i = 1, \ldots, N\right\}$. As a consequence, the design of the random distribution is also tightly connected to the statistics of the channels to the UEs. We can write the small-scale channel between the IRS and UE-k as

$$\mathbf{h}_{2,k} = \mathbf{\Sigma}_k^{1/2}\widetilde{\mathbf{h}_{2,k}} \overset{(a)}{\approx} \mathbf{\Sigma}^{1/2}\widetilde{\mathbf{h}_{2,k}}, \tag{3.5}$$

where $\widetilde{\mathbf{h}_{2,k}} \sim \mathcal{CN}(\mathbf{0}, \mathbf{I}_M)$, $M = \text{rank}(\mathbf{\Sigma})$, $\mathbf{\Sigma}_k^{1/2}$ contains the first M columns of a square root of $\mathbf{\Sigma}_k$, and in (a), we used $\mathbf{\Sigma}_k = \mathbf{\Sigma}$, $\forall k$. This corresponds to a Kronecker channel model where the correlation is induced by local spatial scattering at the IRS elements, or a scenario where many UEs are located in a hotspot area [76, 104].[1] Since $\mathcal{R}(\mathbf{\Sigma}^{1/2}) = \mathcal{R}(\mathbf{\Sigma})$, where $\mathcal{R}(\mathbf{A})$ is the range space of $\mathbf{A}$, from (3.5), we get $\mathbf{h}_{2,k} \in \mathcal{R}(\mathbf{\Sigma})$. Thus, $\mathbf{h}_{2,k}$ lies in an M-dimensional subspace of $\mathbb{C}^N$. Let $\mathbf{\Sigma} = \mathbf{U}\mathbf{\Lambda}\mathbf{U}^H$ be the spectral decomposition of $\mathbf{\Sigma}$ and $\mathbf{\Lambda}$ contains the non-zero eigenvalues of $\mathbf{\Sigma}$. Then, for every $\mathbf{h}_{2,k} \in \mathcal{R}(\mathbf{\Sigma})$, by the Karhunen–Loève Theorem, there exists $\{\alpha_{k,i}\}_{i=1}^M$ such that

$$\mathbf{h}_{2,k} = \sum_{i=1}^{M} \alpha_{k,i}\mathbf{u}_i, \text{and } \alpha_{k,i} = \langle \mathbf{h}_{2,k}, \mathbf{u}_i \rangle, \tag{3.6}$$

with $\mathbf{u}_i$ being the ith orthonormal eigenvector of $\mathbf{\Sigma}$. Hence, the channel at each UE is uniquely determined by the UE-specific coefficients $\{\alpha_{k,i}\}_{i=1}^M$ along with the basis vectors $\{\mathbf{u}_i\}_{i=1}^M$.

Conversely, with a large number of UEs, for any given $\{\alpha_{k,i} \in \mathbb{C}\}_{i=1}^M$, there exists a UE whose channel corresponds to the chosen coefficients via (3.6). Since $\mathbf{h}_{2,k}$ is a Gaussian vector, $\alpha_{k,i} \sim \mathcal{CN}(0, [\mathbf{\Sigma}_\alpha]_{i,i})$, with $[\mathbf{\Sigma}_\alpha]_{i,i} = \mathbb{E}\left[\left|\mathbf{u}_i^H \mathbf{h}_{2,k}\right|^2\right] = \mathbf{u}_i^H \mathbf{\Sigma} \mathbf{u}_i$, i.e., $\mathbf{\Sigma}_\alpha = \mathbf{U}^H \mathbf{\Sigma} \mathbf{U} = \mathbf{\Lambda}$. We have the following result.

Theorem 3.1. *The probability density function for drawing the random samples of the IRS vector in every time slot to ensure that a PF scheduler achieves the BF-SE as in Lemma 3.2 is*

$$f_{\boldsymbol{\theta}}^{\text{opt}}(\boldsymbol{\theta}') = \int_{\mathcal{F}^{-1}(\boldsymbol{\theta}')} \delta\left(\mathbf{h} - \mathcal{F}^{-1}(\boldsymbol{\theta}')\right) p_{\mathbf{h}_f}(\mathbf{h}) \mathrm{d}\mathbf{h},$$

where $\mathcal{F}^{-1}(\boldsymbol{\theta}')$ denotes the set-inverse under the $\mathcal{F}(\cdot)$ mapping, i.e., $\mathcal{F}^{-1}(\boldsymbol{\theta}') \triangleq \{\mathbf{h} \in \mathbb{C}^{N+1} : \mathcal{F}(\mathbf{h}) = \boldsymbol{\theta}'\}$, and $p_{\mathbf{h}_f}(\mathbf{h})$ is the probability density function of $\mathbf{h}_f = \left[h_d, (\mathbf{h}_1 \odot \mathbf{h}_2)^T\right]^T$ with $h_d \sim \mathcal{CN}(0,1)$, $\mathbf{h}_1$ as given in (3.1), and $\mathbf{h}_2 \sim \mathcal{CN}(\mathbf{0}, \mathbf{\Sigma})$.

Proof. See Appendix 3.A. ■

[1] To serve UEs with different covariance matrices at the IRS, we first cluster UEs sharing similar covariance matrices as in [105]. Then, we select a cluster in an RR manner, and within the slots alloted for the selected cluster, a UE is served via the opportunistic BF scheme proposed in this chapter.

Algorithm 3.1: Spatial correlation-aware Opportunistic BF

Input: Correlation values: $\mathbf{U}$, $\boldsymbol{\Sigma}_\alpha$; BS-IRS link: $\mathbf{h}_1$.

for *time slot* $t = 1, 2, 3, \ldots$ **do**

`/* Random sampling of IRS configurations */`

Sample the random vector $\boldsymbol{\beta} \sim \mathcal{CN}(\mathbf{0}, \boldsymbol{\Sigma}_\alpha)$.

Set $\boldsymbol{\theta}_{\text{rand}} = \mathcal{F}\left(\left[1, (\mathbf{h}_1 \odot \mathbf{U}\boldsymbol{\beta})^T\right]^T\right)$, as per (3.4).

`/* Towards identifying the best UE */`

BS broadcasts a common pilot signal to every UE.

All UEs compute their PF metrics & feedback their identities to BS using *timer* schemes [82].

`/* Proportional-fair scheduling of UEs */`

Identity of the *best* UE-$k^*(t)$ arrives BS first, with

$$k^*(t) = \underset{k=1,\ldots,K}{\arg\max}\, R_k(t)/T_k(t).$$

The BS schedules UE-$k^*(t)$ for data transmission.

Remark 3.2. *The IRS-aided OC scheme achieves the BF-SE* without *incurring the overheads discussed in Remark 3.1:*

1. *CSI acquisition with single pilot only: In the OC scheme, only one pilot is needed to estimate the composite channel.*

2. *No phase optimization: The phase optimization procedure is absent since the IRS phases are randomly chosen.*

3. *No phase transportation: The IRS picks a random phase on its own in every slot, so phase transportation is obviated.*

Further, to help the BS identify the best UE that yields the highest PF metric, efficient and low-complexity feedback schemes like timer/splitting-based methods can be used [82].

Using Theorem 3.1, we present the overall protocol of spatial-correlation-aware OC in

Algorithm 3.1 of this chapter.[2]

3.5 How many Users are Sufficient in Practice?

We now consider the success rate of Algorithm 3.1 for a practical system with a finite number of UEs. Let $\mathcal{E}_k^\delta$ denote the $(1-\delta)N^2$-*success event* that the channel gain at UE-k is at least a $(1-\delta)$ factor of the BF gain obtained via the IRS, i.e.,

$$\mathcal{E}_k^\delta \triangleq \left\{ |\boldsymbol{\theta}^H \mathbf{h}_{f,k}|^2 \geq (1-\delta) \left\| \mathbf{h}_{f,k} \right\|_1^2 \right\}, \ \delta \in (0,1). \tag{3.7}$$

In the sequel, we evaluate the probability of $\mathcal{E}_k^\delta$. To that end, we require a characterization of the Rayleigh quotient of heteroscedastic Gaussian random vectors, discussed next.

Lemma 3.3. *Let $\mathbf{A} \in \mathbb{C}^{L\times L}$ be a hermitian rank-1 matrix, and $\alpha \in \mathbb{R}$ be such that $0 < \alpha < \|\mathbf{A}\|_F$. If $\mathbf{x} \in \mathbb{C}^L \sim \mathcal{CN}(\mathbf{0}, \mathbf{R})$ and $\mathbf{R}$ has full rank, the Rayleigh quotient of $\mathbf{A}$ w.r.t. $\mathbf{x}$ obeys*

$$\mathsf{Pr}\left(\frac{\mathbf{x}^H \mathbf{A} \mathbf{x}}{\mathbf{x}^H \mathbf{x}} \geq \alpha \right) \geq \prod_{l=1}^{L} \left(1 \Big/ \left\{ 1 + \frac{\alpha}{(\|\mathbf{A}\|_F - \alpha)} \cdot \frac{\lambda_{\mathbf{x},l}}{\lambda_{\mathbf{x},L}} \right\} \right),$$

where $\lambda_{\mathbf{x},1} \geq \ldots \geq \lambda_{\mathbf{x},L}$ are the ordered eigenvalues of $\mathbf{R}$.

Proof. See Appendix 3.B. ■

We are now ready to state the main theorem of this section.

Theorem 3.2. *The probability of the $(1-\delta)N^2$-success event at a scheduled UE (as defined in (3.7)) using a PF scheduler over K UEs, denoted by P_{succ}, with the spatial correlation-aware random IRS configuration as in Theorem 3.1 is bounded as*

$$P_{succ} \geq 1 - \left(1 - \prod_{m=1}^{M} \frac{1}{1 + \frac{1-\delta}{\delta} \cdot \frac{\lambda_m}{\lambda_M}} \right)^K, \tag{3.8}$$

[2]We absorb the overall phase in the $\mathcal{F}$-mapped channel vectors due to the angle of the direct channel into the randomness in the angle of the cascaded channel. So, the 1st entry in the input to $\mathcal{F}$-map in line 3 equals 1. We also assume that the spatial correlation matrix $\boldsymbol{\Sigma}$ is known, which can be estimated using works whose focus is to estimate the channel covariance matrices.

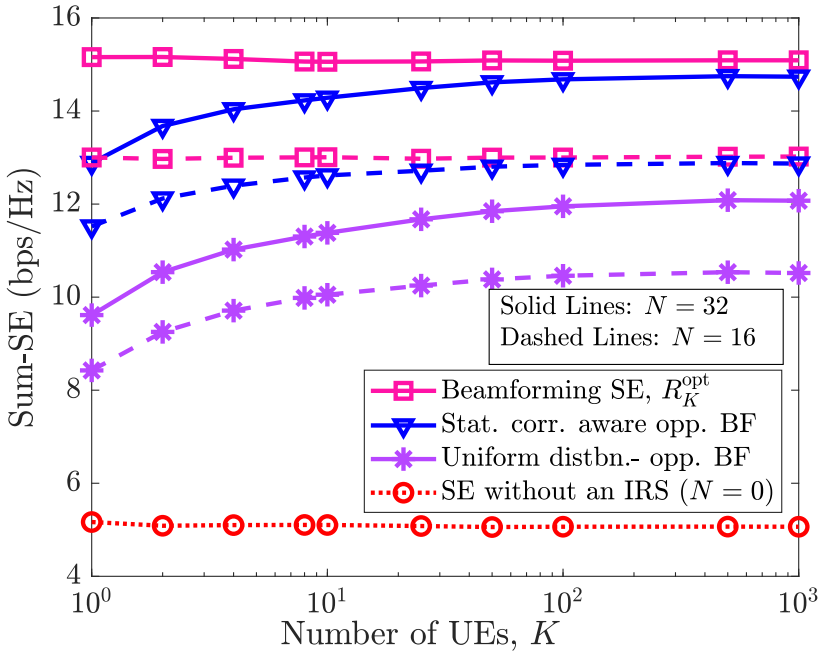

Figure 3.2: Sum-SE vs. K for different N, $\rho = 0.9$. Compared with [76, 103] using unif. distbn.

where $M = \mathit{rank}(\mathbf{\Sigma})$ *and* $\lambda_1 \geq \ldots \geq \lambda_M$ *are the ordered non-zero eigenvalues of the channel covariance matrix,* $\mathbf{\Sigma}$.

Proof. See Appendix 3.C. ■

As a consequence, we have the following result.

Corollary 3.1. *Let* $\delta \in (0, 1)$. *With Scheme 3.1, if* K *is at least*

$$K^* \triangleq -\log\left(1 - P_{succ}\right) \prod_{m=1}^{M} 1 + \left[\left((1-\delta)\Big/\delta\right)\left(\lambda_m \Big/ \lambda_M\right)\right]$$
$$\sim \mathcal{O}\left(-[\log\left(1 - P_{succ}\right)]/\delta^M\right), \tag{3.9}$$

then, with probability P_{succ}, *the channel gain using a randomly configured IRS exhibits a* $(1-\delta)N^2$ *success in every time slot.*

Proof. The first step is obtained by rearranging the probability expression derived in (3.8) as

$$K \geq \log\left(1 - P_{\text{succ}}\right) \Big/ \log\left(1 - \prod_{m=1}^{M-1} \frac{1}{1 + \frac{1-\delta}{\delta} \cdot \frac{\lambda_m}{\lambda_M}}\right). \tag{3.10}$$

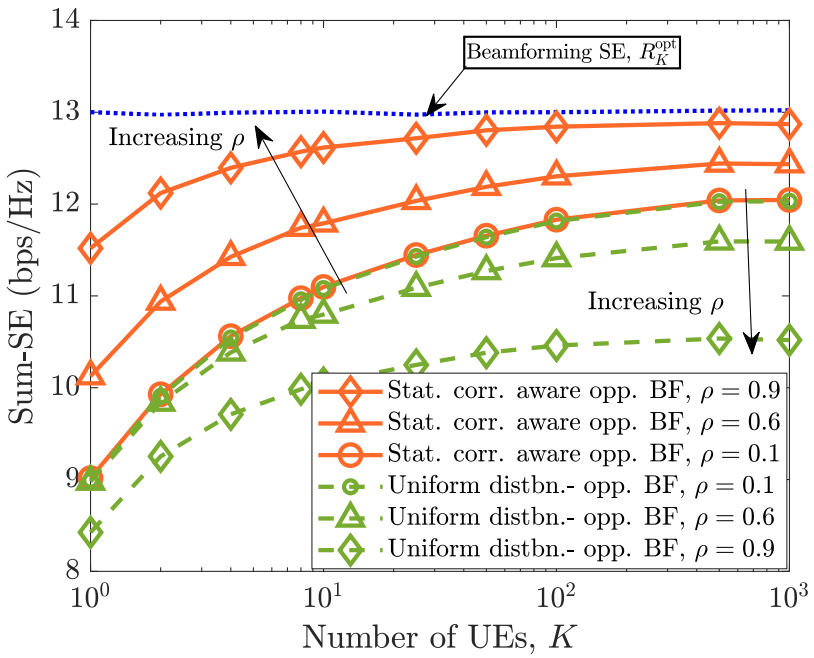

Figure 3.3: Sum-SE vs. K for different ρ at $N = 16$.

Then, using the fact that for small x, $\log(1-x) \approx x$ in the above, when δ is very small, the proof follows. ■

Corollary 3.1 shows that a sufficient number of the UEs for $(1-\delta)N^2$-success grows exponentially with the *rank* of the channel covariance matrix, and not with the number of IRS elements. Thus, if the UE's channel lies in a fixed-dimensional subspace, the number of UEs needed to reap the benefits from the IRS is fixed even if the number of IRS elements grows. We note that the number of UEs given in Corollary 3.1 generalizes the results for i.i.d. and LoS scenarios discussed in Remarks 2.1 and Remark 2.4, respectively.

3.6 Numerical Results

We now illustrate our results numerically via Monte Carlo simulations. We consider a setup where the BS is located at $(0, 0)$ (measured in meters) and up to $K = 1000$ UEs are located in a square region described by $[900, 1100] \times [900, 1100]$, and an IRS positioned at $(1000, 1000)$. The path loss is modeled as $\beta = C_0(d/d_0)^{\kappa}$, where κ is the path-loss exponent, set to $2, 2, 4$ in the BS-IRS, IRS-UE and BS-UE links, respectively [106]. We run the PF

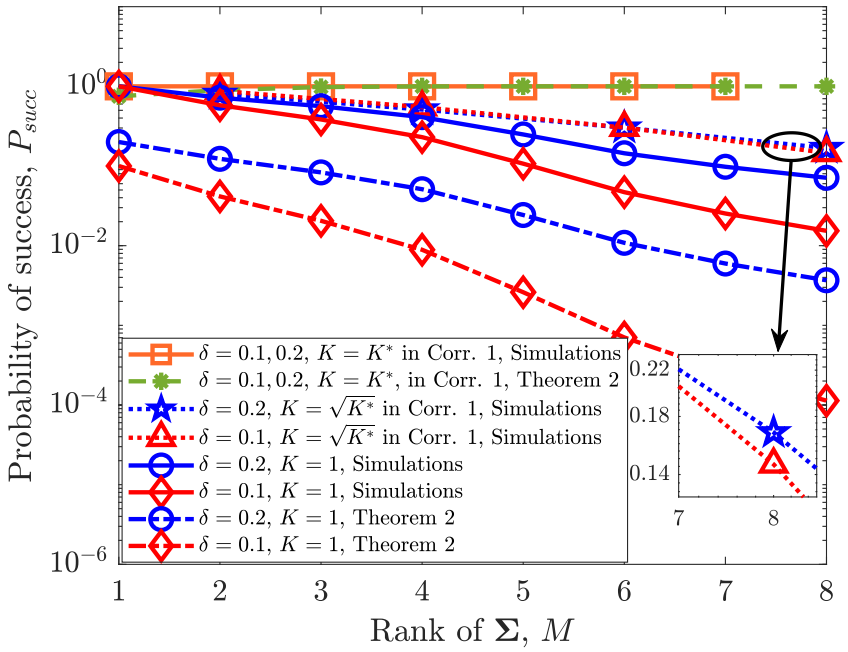

Figure 3.4: Success probability vs. M.

scheduler with $\tau = 5000$ over $50,000$ time slots. The channel covariance matrix at the IRS is $\mathbf{\Sigma} = \mathsf{Toeplitz}\left(\left[1, \rho, \rho^2, \ldots, \rho^{N-1}\right]\right)$, where $\mathsf{Toeplitz}(\mathbf{x})$ returns a hermitian Toeplitz matrix with $\mathbf{x}$ as the first row, and ρ is the correlation coefficient between two nearby IRS elements. Since $\mathbf{\Sigma}$ as above is full-rank when $\rho \neq 1$, we use the effective rank [107] for Algorithm 3.1.

In Fig. 3.2, we plot the sum-SE vs. the number of UEs, K, for $N = 16$ and 32, at $\rho = 0.9$. For both values of N, the sum-SE with the *spatial-correlation-aware OC scheme* grows with K and approaches the SE obtained by optimizing the IRSs in every time slot using an RR scheduler. Thus, we can leverage multi-user diversity and achieve the BF sum-SE in Lemma 3.1 without incurring the overheads associated with optimizing the IRS. We also compare the sum-SE with the OC in [76] that uses the i.i.d. uniform distribution to sample the IRS phases. In this case, although the SE grows with K, the gap with respect to the BF-SE is large, which underscores the importance of choosing the random IRS configuration based on the channel statistics. Our scheme also outperforms a system without an IRS.

In Fig. 3.3, we plot the sum-SE versus K for $N = 16$ and different correlation values

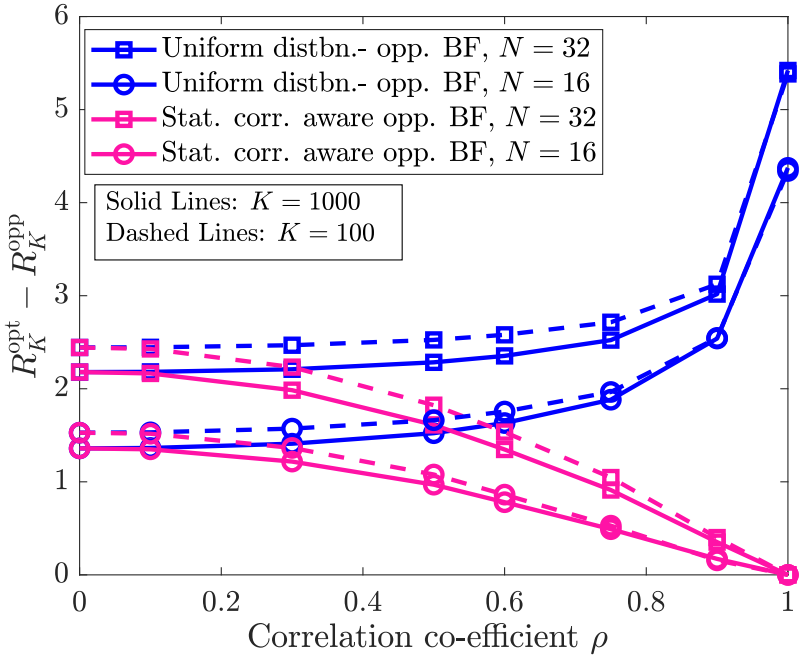

Figure 3.5: Difference between OC-SE and BF-SE vs. ρ.

ρ. For a fixed K, the gap between the BF-SE and OC-SE decreases as ρ increases. This happens because the effective rank of the channel decreases with ρ, making it easier for the IRS to achieve a near-BF configuration even with a moderate number of UEs, as shown in Corollary 3.1. Conversely, when the IRS phases are sampled from a uniform distribution, the gap between the SEs is large because the IRS configuration is uniformly distributed over the full N-dimensional space, whereas the channels lie in a lower M-dimensional subspace. So, as ρ increases, the mismatch between the IRS phase sampling distribution and channel phase distribution increases, worsening the performance gaps.

In Fig. 3.4, we plot the success probability, P_{succ} (see (3.7)) vs. $M = \text{rank}(\mathbf{\Sigma})$. For fixed K, P_{succ} decreases with M because the effective dimension grows with M. Also, Theorem 3.2 (marked "Theorem 2" on the plot) is a valid lower bound and succinctly captures the scaling with M. Finally, we verify that $P_{\text{succ}} = 1$ for any M, δ if $K = K^*$ (see Corollary 3.1 (marked as "Corr. 1")), and $P_{\text{succ}} < 1$ when $K = \sqrt{K^*} < K^*$, validating that the scaling we derived is tight.

Finally, in Fig. 3.5, we plot the gap between the BF-SE and OC-SE, i.e., $R_K^{\text{opt}} - R_K^{\text{opp}}$ versus ρ for different values of K and N. For the spatial-correlation-aware OC, as ρ

increases, the difference goes to 0 for any N, even for moderate values of K, in line with Fig. 3.3. However, for the OC scheme using a uniform distribution, the difference increases with ρ because the probability that a random configuration matches the channel decreases as the sub-space dimension, M, reduces. This further exacerbates as N increases, as the difference in the dimensional mismatch between the IRS search space and the channel space becomes more pronounced.

3.7 Conclusions

We developed a low-complexity spatial-correlation-aware opportunistic beamforming scheme for IRS-aided wireless systems. By leveraging the multi-user diversity, we showed that randomly drawing the IRS phase angles from an appropriate distribution procures near-optimal benefits from the IRS. For the SE to be arbitrarily close to the BF-SE, the number of UEs needs to grow exponentially only with the rank of the spatial covariance matrix, and not with the number of IRS elements.

Appendix 3.A Proof of Theorem 3.1

Suppose the IRS-UEs channel state process is jointly stationary and ergodic. With PF scheduling, the optimal sampling distribution at the IRS, so that a scheduled UE achieves the BF-SE as $K \to \infty$, is the solution to the variational functional problem:

$$\arg\max_{f_{\boldsymbol{\theta}}(\boldsymbol{\theta}')} \bar{R} \triangleq \mathbb{E}_{\boldsymbol{\theta},\mathbf{h}_{f,k}}\left[\log_2\left(1+|\boldsymbol{\theta}'^H\mathbf{h}_{f,k}|^2P/\sigma^2\right)\right], \tag{P2}$$

$$\text{s.t.} \int_{\boldsymbol{\theta}'\in\mathbb{U}^N\bigcup\{1\}} f_{\boldsymbol{\theta}}(\boldsymbol{\theta}')\mathrm{d}\boldsymbol{\theta}' = 1, \tag{C2-1}$$

$$\text{and} \int_{[\boldsymbol{\theta}']_2}\dots\int_{[\boldsymbol{\theta}']_{N+1}} f_{\boldsymbol{\theta}}(\boldsymbol{\theta}')\mathrm{d}\boldsymbol{\theta}' = \delta([\boldsymbol{\theta}']_1-1), \tag{C2-2}$$

where in (P2), we seek to maximize the achievable throughput, and (C2-1), (C2-2) account for the constraints of a density function and the structure of $\boldsymbol{\theta}'$ as per (3.2), respectively. Also, in (P2), the expectation is taken over the joint distribution of the UEs' channels. We first solve the unconstrained version of (P2) and analyze the feasibility of its solution

in the constrained case. Thus, the variational problem becomes

$$\max_{f_{\boldsymbol{\theta}}(\boldsymbol{\theta}')} \mathbb{E}_{\mathbf{h}_{f,k}}\left[\mathbb{E}_{\boldsymbol{\theta}|\mathbf{h}_{f,k}}\left[\log_2\left(1+\left|\boldsymbol{\theta}'^{H}\mathbf{h}_{f,k}\right|^2\frac{P}{\sigma^2}\right)\Big|\mathbf{h}_{f,k}\right]\right]$$
$$\overset{(a)}{=}\max_{g_{\boldsymbol{\theta}}(\boldsymbol{\theta}')}\int_{\mathbf{h}}\left(\int_{\boldsymbol{\theta}'}\log_2\left(1+\left|\boldsymbol{\theta}'^{H}\mathbf{h}_{f,k}\right|^2\frac{P}{\sigma^2}\right)g_{\boldsymbol{\theta}}(\boldsymbol{\theta}')\mathrm{d}\boldsymbol{\theta}'\right)p_{\mathbf{h}_f}(\mathbf{h})\mathrm{d}\mathbf{h},$$

where in (a), $g_{\boldsymbol{\theta}}(\boldsymbol{\theta}') \equiv g_{\boldsymbol{\theta}|\mathbf{h}_f}(\boldsymbol{\theta}')$ is the conditional density function of the IRS configurations given the channel realization. It is related to $f_{\boldsymbol{\theta}}(\boldsymbol{\theta}')$ via the law of total probability:

$$f_{\boldsymbol{\theta}}(\boldsymbol{\theta}') = \int_{\mathbf{h}} g_{\boldsymbol{\theta}}(\boldsymbol{\theta}')p_{\mathbf{h}_f}(\mathbf{h})\mathrm{d}\mathbf{h}. \tag{3.11}$$

Then, an equivalent functional optimization problem is

$$\mathcal{I} \triangleq \max_{g_{\boldsymbol{\theta}}(\boldsymbol{\theta}')}\int_{\boldsymbol{\theta}'}\log_2\left(1+|\boldsymbol{\theta}'^{H}\mathbf{h}_{f,k}|^2P/\sigma^2\right)g_{\boldsymbol{\theta}}(\boldsymbol{\theta}')\mathrm{d}\boldsymbol{\theta}'. \tag{3.12}$$

Using the Hölder's inequality: $|\boldsymbol{\theta}'^{H}\mathbf{h}_{f,k}| \leq \|\mathbf{h}_{f,k}\|_1 \|\boldsymbol{\theta}'\|_\infty$ along with the fact that $\|\boldsymbol{\theta}'\|_\infty = 1$ due to the unit-modulus nature of the IRS phase configurations, we upper bound (3.12) as

$$\mathcal{I} \leq \mathcal{I}_{\mathrm{U}} \triangleq \log_2\left(1+\|\mathbf{h}_{f,k}\|_1^2P/\sigma^2\right)\max_{g_{\boldsymbol{\theta}}(\boldsymbol{\theta}')}\underbrace{\int_{\boldsymbol{\theta}'}g_{\boldsymbol{\theta}}(\boldsymbol{\theta}')\mathrm{d}\boldsymbol{\theta}'}_{=1}.$$

From Lemma 3.2, since the PF scheduler achieves the BF-SE, $g_{\boldsymbol{\theta}}(\boldsymbol{\theta}')$ must satisfy the following lower bound:

$$\mathcal{I} \geq \mathcal{I}_{\mathrm{L}} \triangleq \max_{g_{\boldsymbol{\theta}}(\boldsymbol{\theta}')}\int_{\boldsymbol{\theta}'}\log_2\left(1+\left\{\|\mathbf{h}_{f,k}\|_1^2+o(K)\right\}\frac{P}{\sigma^2}\right)g_{\boldsymbol{\theta}}(\boldsymbol{\theta}')\mathrm{d}\boldsymbol{\theta}'.$$

Now, letting $K \to \infty$ and using the sandwich theorem, $\lim_{K\to\infty}\mathcal{I} = \mathcal{I}_{\mathrm{L}} = \mathcal{I}_{\mathrm{U}}$, which can be achieved if and only if $\boldsymbol{\theta}' = \mathcal{F}(\mathbf{h}_{f,k})$. So, the optimal conditional density for a given channel at scheduled UE-k is

$$g_{\boldsymbol{\theta}}^{\mathrm{opt}}(\boldsymbol{\theta}') = \delta\left(\boldsymbol{\theta}' - \mathcal{F}(\mathbf{h}_{f,k})\right). \tag{3.13}$$

Substituting (3.13) in (3.11), we get

$$f_{\boldsymbol{\theta}}^{\mathrm{opt}}(\boldsymbol{\theta}') \overset{(b)}{=} \int_{\mathbf{h}}\delta\left(\boldsymbol{\theta}' - \mathcal{F}(\mathbf{h})\right)p_{\mathbf{h}_f}(\mathbf{h})\mathrm{d}\mathbf{h}$$

$$\overset{(c)}{=} \int_{\mathcal{F}^{-1}(\boldsymbol{\theta}')} \delta\left(\mathbf{h} - \mathcal{F}^{-1}(\boldsymbol{\theta}')\right) p_{\mathbf{h}_f}(\mathbf{h}) \mathrm{d}\mathbf{h}, \tag{3.14}$$

where, in (b), we dropped the index k from (3.13) as $\mathcal{F}(\mathbf{h}_{f,k})$ are i.i.d. across $k \in [K] \triangleq \{1, \ldots, K\}$; and in (c), we used the definition $\mathcal{F}^{-1}(\cdot)$ and the sifting property of the Dirac-delta function. By construction, since $f_{\boldsymbol{\theta}}^{\text{opt}}(\cdot)$ in (3.14) is a valid probability density function obtained via the $\mathcal{F}(\cdot)$ mapping, (C2-1) and (C2-2) are trivially satisfied. This completes the proof.

Appendix 3.B Proof of Lemma 3.3

We note that the required probability can be written as

$$P_\alpha \triangleq \mathsf{Pr}\left(\mathbf{x}^H \mathbf{A} \mathbf{x} \geq \alpha \mathbf{x}^H \mathbf{x}\right) = \mathsf{Pr}\left(\mathbf{x}^H \left(\mathbf{A} - \alpha \mathbf{I}_L\right) \mathbf{x} \geq 0\right).$$

Let $\mathbf{B} \triangleq \mathbf{A} - \alpha \mathbf{I}_L$. Now $\mathbf{B}$ is a full-rank, hermitian matrix; so its spectral decomposition is written as $\mathbf{B} = \mathbf{V} \boldsymbol{\Gamma} \mathbf{V}^H$. Then

$$P_\alpha \overset{(a)}{=} \mathsf{Pr}\left(\tilde{\mathbf{x}}^H \boldsymbol{\Gamma} \tilde{\mathbf{x}} \geq 0\right) \overset{(b)}{=} \mathsf{Pr}\left(\sum_{l=1}^{L} \gamma_l \left|[\tilde{\mathbf{x}}]_l\right|^2 \geq 0\right),$$

where in (a), $\tilde{\mathbf{x}} \triangleq \mathbf{V}^H \mathbf{x} \sim \mathcal{CN}(\mathbf{0}, \mathbf{V}^H \mathbf{R} \mathbf{V})$; in (b), γ_l is the lth largest eigenvalue of $\mathbf{B}$. Since $\mathbf{A}$ is hermitian, $\mathbf{A} = \mathbf{a}\mathbf{a}^H$ for some $\mathbf{a} \in \mathbb{C}^L$. Then, the eigenvalues of $\mathbf{B}$ are $\gamma_1 = \|\mathbf{a}\|_2^2 - \alpha > 0$, and $\gamma_2 = \gamma_3 \ldots = \gamma_L = -\alpha < 0$. Using this, we have

$$\begin{aligned} P_\alpha &= \mathsf{Pr}\left(\left|[\tilde{\mathbf{x}}]_1\right|^2 \geq \frac{\alpha}{\|\mathbf{a}\|_2^2 - \alpha} \sum_{l=2}^{L} \left|[\tilde{\mathbf{x}}]_l\right|^2\right) \\ &= \mathbb{E}_{\{[\tilde{\mathbf{x}}]_l\}_{l=2}^L}\left[\mathsf{Pr}\left(\left|[\tilde{\mathbf{x}}]_1\right|^2 \geq \frac{\alpha}{\|\mathbf{a}\|_2^2 - \alpha} \sum_{l=2}^{L} \left|[\tilde{\mathbf{x}}]_l\right|^2 \middle| [\tilde{\mathbf{x}}]_2, \ldots, [\tilde{\mathbf{x}}]_L\right)\right]. \end{aligned}$$

Now, we decompose $\mathbf{x} = \mathbf{R}^{1/2} \mathbf{x}'$, where $\mathbf{R}^{1/2} \in \mathbb{C}^{L \times L}$ is a square root of $\mathbf{R}$, and $\mathbf{x}' \sim \mathcal{CN}(\mathbf{0}, \mathbf{I}_L)$. In particular, we can write $\mathbf{R}^{1/2} = \mathbf{U}_{\mathbf{x}} \boldsymbol{\Lambda}_{\mathbf{x}}^{1/2}$ so that $\tilde{\mathbf{x}} = \mathbf{W}^H \boldsymbol{\Lambda}_{\mathbf{x}}^{1/2} \mathbf{x}'$, where $\mathbf{W} \triangleq \mathbf{U}_{\mathbf{x}}^H \mathbf{V} = [\mathbf{w}_1, \ldots, \mathbf{w}_L] \in \mathbb{C}^{L \times L}$ is a unitary matrix. We then have $[\tilde{\mathbf{x}}]_1 \sim \mathcal{CN}(0, \sum_{l=1}^{L} \lambda_{\mathbf{x},l} |[\mathbf{w}_1]_l|^2)$.

Since $\|\mathbf{A}\|_F = \|\mathbf{a}\|_2^2$, and $\sum_{l=1}^{L} \lambda_{\mathbf{x},l}|[\mathbf{w}_1]_l|^2 \geq \lambda_{\mathbf{x},L}$, we can lower bound P_α as

$$P_\alpha \geq \mathbb{E}_{[\tilde{\mathbf{x}}]_2,\ldots,[\tilde{\mathbf{x}}]_L}\left[e^{-\left(\alpha/\left((\|\mathbf{A}\|_F-\alpha)\lambda_{\mathbf{x},L}\right)\right)\sum_{l=2}^{L}|[\tilde{\mathbf{x}}]_l|^2}\right]. \tag{3.15}$$

Define $\tilde{\mathbf{x}}_{(1)} \triangleq [[\tilde{\mathbf{x}}]_2, \ldots, [\tilde{\mathbf{x}}]_L]^T$, $\mathbf{W}_{(1)} \triangleq [\mathbf{w}_2, \ldots, \mathbf{w}_L]$. Then,

$$\sum_{l=2}^{L}|[\tilde{\mathbf{x}}]_l|^2 = \left\|\tilde{\mathbf{x}}_{(1)}\right\|_2^2 = \mathbf{x}'^H\mathbf{\Lambda}_{\mathbf{x}}^{1/2}\mathbf{W}_{(1)}\mathbf{W}_{(1)}^H\mathbf{\Lambda}_{\mathbf{x}}^{1/2}\mathbf{x}' \overset{(c)}{\leq} \left\|\mathbf{\Lambda}_{\mathbf{x}}^{1/2}\mathbf{x}'\right\|_2^2,$$

where in (c), we first noted that $\mathbf{W}_{(1)}\mathbf{W}_{(1)}^H$ is an orthogonal projector and that its eigenvalues are either 0 or 1; then used the Rayleigh-Ritz Theorem. So, we further bound (3.15) as

$$\begin{aligned}
P_\alpha &\geq \mathbb{E}_{[\mathbf{x}']_2,\ldots,[\mathbf{x}']_L}\left[e^{-\left(\alpha/\left((\|\mathbf{A}\|_F-\alpha)\lambda_{\mathbf{x},L}\right)\right)\sum_{l=2}^{L}\lambda_{\mathbf{x},l}|[\mathbf{x}']_l|^2}\right] \\
&\overset{(d)}{=} \prod_{l=1}^{L}\mathbb{E}_{[\mathbf{x}']_l}\left[e^{-\left(\alpha/\left((\|\mathbf{A}\|_F-\alpha)\lambda_{\mathbf{x},L}\right)\right)\lambda_{\mathbf{x},l}|[\mathbf{x}']_l|^2}\right] \\
&\overset{(e)}{=} \prod_{l=1}^{L}\left(1\Big/\left\{1+\frac{\alpha}{(\|\mathbf{A}\|_F-\alpha)}\cdot\frac{\lambda_{\mathbf{x},l}}{\lambda_{\mathbf{x},L}}\right\}\right),
\end{aligned}$$

where in (d), we used the independence of $\{[\mathbf{x}']_l\}_{l=1}^{L}$; in (e), we used the expression for the moment generating function of the exponential random variables $|[\mathbf{x}']_l|^2, l \in [L]$. This completes the proof of the lemma.

Appendix 3.C Proof of Theorem 3.2

With a PF scheduler used over K UEs, the probability of at least one UE witnessing the $(1-\delta)N^2$-success event is

$$P_{succ} = \mathsf{Pr}\left(\bigcup_{k=1}^{K}\mathcal{E}_k^\delta\right) \overset{(a)}{=} 1 - \prod_{k=1}^{K}\left(1-\mathsf{Pr}\left(\mathcal{E}_k^\delta\right)\right), \tag{3.16}$$

where (a) follows by the independence of channels across the K UEs. Let $\mathbf{f}' \triangleq \mathbf{h}_1 \odot \mathbf{f}$, where $\mathbf{f} = \mathbf{U}\mathbf{\Lambda}^{1/2}\tilde{\mathbf{f}}$ with $\tilde{\mathbf{f}} \sim \mathcal{CN}(\mathbf{0}, \mathbf{I}_M)$. So, $\boldsymbol{\theta} = [1, e^{j\angle[\mathbf{f}']_1}, \ldots, e^{j\angle[\mathbf{f}']_N}]$ is a candidate random IRS phase vector as stated in Theorem 3.1. For simplicity of exposition, we ignore the

direct path from the BS to UE, which can be easily included in the analysis. Then, in (3.7), $\boldsymbol{\theta} = [e^{j\angle[\mathbf{f}']_1}, \ldots, e^{j\angle[\mathbf{f}']_N}]$, and the channel vector is $\mathbf{h}_{f,k} = \sqrt{\beta_{r,k}}[[\mathbf{h}_{r,k}]_1, \ldots, [\mathbf{h}_{r,k}]_N]^T$. Now, we have $\mathsf{Pr}\left(\mathcal{E}_k^{\delta}\right) =$

$$\mathsf{Pr}\left(\left|\sum_{n=1}^{N} e^{-j\angle[\mathbf{f}']_n}[\mathbf{h}_{r,k}]_n\right|^2 \geq (1-\delta)\left|\sum_{n=1}^{N}|[\mathbf{h}_{r,k}]_n|\right|^2\right)$$
$$= \mathsf{Pr}\left(\left|\sum_{n=1}^{N} e^{-j\angle[\mathbf{f}]_n}[\mathbf{h}_{2,k}]_n\right|^2 \geq (1-\delta)\left\|\mathbf{h}_{2,k}\right\|_1^2\right),$$

where we used the form of $\mathbf{f}'$ and $|[\mathbf{h}_1]_n| = 1$. From the decomposition $\mathbf{h}_{2,k} = \mathbf{U}\boldsymbol{\Lambda}^{1/2}\tilde{\mathbf{h}}_{2,k}$, $\mathbf{f} = \mathbf{U}\boldsymbol{\Lambda}^{1/2}\tilde{\mathbf{f}}$, since the channel and IRS vectors are generated using the same basis $\mathbf{U}$, and their distributions are invariant to left multiplication by a unitary matrix, we let $\mathbf{U} = [\mathbf{e}_1, \ldots, \mathbf{e}_M]$ without loss in generality, where $\mathbf{e}_m$ is mth column of $\mathbf{I}_N$. Thus, $\mathsf{Pr}\left(\mathcal{E}_k^{\delta}\right) =$

$$\mathsf{Pr}\left(\left|\sum_{m=1}^{M} e^{-j\angle[\tilde{\mathbf{f}}]_m}\sqrt{\lambda_m}[\tilde{\mathbf{h}}_{2,k}]_m\right|^2 \geq (1-\delta)\left\|\boldsymbol{\Lambda}^{1/2}\tilde{\mathbf{h}}_{2,k}\right\|_1^2\right)$$
$$\geq \mathsf{Pr}\left(\left|\sum_{m=1}^{M}\sqrt{\lambda_m}[\tilde{\mathbf{h}}_{2,k}]_m\right|^2 \geq (1-\delta)M\left\|\boldsymbol{\Lambda}^{1/2}\tilde{\mathbf{h}}_{2,k}\right\|_2^2\right)$$

where we dropped $e^{-j\angle[\tilde{\mathbf{f}}]_m}$ because $\angle[\tilde{\mathbf{f}}]_m$ is uniformly distributed in $[0, 2\pi)$ and independent of $\angle[\tilde{\mathbf{h}}]_m$, which does not alter the distribution of $[\tilde{\mathbf{h}}]_m$. Also, the right-hand side does not depend on $\angle[\tilde{\mathbf{h}}]_m$, and we used the property: $\|\mathbf{x}\|_1 \leq \sqrt{M}\|\mathbf{x}\|_2$. Now, the above probability can be rewritten as

$$\mathsf{Pr}\left(\mathcal{E}_k^{\delta}\right) \geq \mathsf{Pr}\left(\hat{\mathbf{h}}_k^H\mathbf{E}\hat{\mathbf{h}}_k \Big/ (\hat{\mathbf{h}}_k^H\hat{\mathbf{h}}_k) \geq (1-\delta)M\right),$$

where $\hat{\mathbf{h}}_k \triangleq \boldsymbol{\Lambda}^{1/2}\tilde{\mathbf{h}}_{2,k}$, and $\mathbf{E} \triangleq \mathbf{1}_M\mathbf{1}_M^H$ with $\mathbf{1}_M$ being an M-length all one vector. Note that $\|\mathbf{E}\|_F = M > (1-\delta)M > 0$, and that $\mathbb{E}[\hat{\mathbf{h}}_k\hat{\mathbf{h}}_k^H] = \boldsymbol{\Lambda}$ has full-rank. Then, using Lemma 3.3,

$$\mathsf{Pr}\left(\mathcal{E}_k^{\delta}\right) \geq \prod_{m=1}^{M}\left(1 \Big/ \left\{1 + \frac{1-\delta}{\delta}\cdot\frac{\lambda_m}{\lambda_M}\right\}\right). \tag{3.17}$$

Substituting (3.17) in (3.16), we get (3.8) as desired.

Part II

IRS-Aided Multiple Operator Wireless Systems: Does an IRS Degrade Out-of-Band Performance?

4 Performance of IRS-Aided Wireless Communications with Multiple Operators

Chapter Highlights

From a network service provider's viewpoint, a concern with the use of an IRS is its effect on out-of-band (OOB) quality of service. Specifically, if two operators, say X and Y, provide services in a given geographical area using non-overlapping frequency bands, and if operator X uses an IRS to enhance the spectral efficiency (SE) of its users (UEs), does it degrade the performance of UEs served by operator Y?

We answer this by analyzing the average and instantaneous performances of the OOB operator considering both sub-6 GHz and mmWave bands. Specifically, we derive the ergodic sum-SE achieved by the operators under round-robin scheduling. We also derive the outage probability and analyze the change in the SNR caused by the IRS at an OOB UE, using stochastic dominance theory.

Surprisingly, even though the IRS is randomly configured from operator Y's point of view, the OOB operator still benefits from the presence of the IRS, witnessing a performance enhancement *for free* in both sub-6 GHz and mmWave bands. This is because the IRS introduces additional paths between the transmitter and receiver, increasing the overall signal power arriving at the UE and providing diversity benefits. Specifically, in the sub-6 GHz bands, the OOB sum-SE increases log-linearly in the number of IRS elements, and in mmWaves, the sum-SE exhibits a unimodal behavior as a function of the number of IRS elements. Finally, we show that the use of opportunistic scheduling schemes can further enhance the benefit of the uncontrolled IRS at OOB UEs.

We numerically illustrate our findings and conclude that an IRS is always beneficial to every operator, even when the IRS is deployed and controlled by only one operator.

4.1 Introduction

Intelligent reflecting surfaces (IRSs) have been extensively studied to enhance the performance of beyond 5G and 6G communications [2,3]. They are passive reflecting surfaces with many elements that can introduce carefully optimized phase shifts while reflecting an incoming radio-frequency (RF) signal, thereby steering the signal towards a desired user equipment (UE). Although a recent topic of research, several use-cases elucidating the benefits of IRS-aided communications have already been investigated [3–8]. All these studies implicitly assume that only *one operator* deploys and controls single or multiple IRS(s) to provide wireless services to their subscribed UEs. However, in practice, multiple wireless network operators simultaneously exist in a given geographical area, each operating in non-overlapping frequency bands. Then, if an IRS is deployed and optimized by one of the operators to cater to its subscribed UEs' needs, it is unclear whether the IRS will boost or degrade the performance of the UEs served by the other operators. This point is pertinent because the IRS elements are passive and have no band-pass filters. They reflect all the RF signals that impinge upon them across a wide range of frequency bands, including signals from *out-of-band (OOB)* operators intended to be received by OOB UEs. Thus, this chapter focuses on understanding how an IRS controlled by one operator affects the performance of other OOB operators.

4.1.a Related Literature and Novelty of This Work

The benefits of using an optimized IRS have been illustrated in several use-cases, see [3–8]. For e.g., in [4], outage analysis with randomly distributed IRSs is investigated. In [5, 36], coverage enhancement due to an IRS is studied, and in [37], the effect of IRSs on inter base station (BS) interferences is explored. Contrary to this, a few works also use randomly configured IRSs and obtain benefits from them. For instance, [75, 76, 103] use opportunistic communications using randomly configured IRSs. Similarly, blind beam forming approaches and diversity order analysis are reported in [41], and [42–44], respectively. Also, in [45], random IRSs are used to protect against wireless jammers. However, none of these works consider the scenario where multiple network operators coexist in an area. Very

few studies have considered using an IRS in multi-band, multi-operator systems. In [108], the effect of pilot contamination on channel estimation in a multiple-operator setting is reported. In [109, 110], the authors jointly optimize the IRS configurations across multiple frequency bands via coordination among the BSs, which is impractical and incurs high signal processing overhead.[1] Further, the solutions and analyses provided therein are not scalable with the number of operators (or frequency bands). More fundamentally, none of these works consider the effect on the OOB performance, even in the scenario of two operators providing services in non-overlapping bands when the IRS is optimized for only one operator. In this work, we investigate whether an IRS degrades the performance of other OOB operators. If not, can the mere presence of an IRS in the vicinity provide *free gains* to OOB operators? Below, we explain our contributions in this context.

4.1.b Contributions

We consider a system with two network operators, X and Y, providing service in different frequency bands in the same geographical area. The IRS is optimized to serve the UEs subscribed to the *in-band* operator X, and we are interested in analyzing the spectral efficiency (SE) achieved and outage probability witnessed by the UEs subscribed to the *OOB* operator Y who does not control the IRS. Specifically, we (separately) evaluate the IRS-assisted performance in both sub-6 GHz and the mmWave bands, which are provisioned as the FR1 and FR2 bands in 5G, respectively [64]. Further, in the mmWave bands, inspired by [65], we study two scenarios: (a) LoS (line-of-sight) and (b) (L+)NLoS (LoS and Non-LoS.) In the LoS scenario, the IRS is optimized or aligned to the dominant cascaded path (called the *virtual* LoS path) of the in-band UE's channel. This is also considered in [9, 66], where the in-band UEs' channels are approximated by the dominant LoS path to reduce the signaling overhead required for the base station (BS) to program the IRS: the phase of the second IRS element relative to the first element determines the entire phase configuration. Contrarily, in the (L+)NLoS case, the IRS optimally combines all

[1] The works that assume inter-BS coordination to optimize the IRS configuration jointly consider a single operator deploying many BSs. Coordination among BSs may be feasible in this scenario. However, it is impractical for the BSs owned by two different operators to coordinate with each other.

the spatial paths to maximize the signal-to-noise ratio (SNR) at the receiver, for which the overhead scales linearly with the number of IRS elements. Using tools from high-dimensional statistics, stochastic-dominance theory, and array processing theory, we make the following contributions.

4.1.b.i OOB Performance in sub-6 GHz Bands (See Section 4.3)

Here, the operators serve their UEs over the sub-6 GHz frequency band where the channels are rich-scattering. In this context, our key findings are as follows.

1-a) We derive the ergodic sum-SEs of the two operators as a function of the system parameters, under round-robin (RR) scheduling of the UEs served by both operators. We show that the sum-SE scales log-quadratically and log-linearly with the number of IRS elements for the in-band and OOB networks, respectively, even though the OOB operator does not control the IRS (see Theorem 4.1.)

1-b) We show that the outage probability at an arbitrary OOB UE decreases monotonically with the number of IRS elements. Further, via the complementary cumulative distribution function (CCDF) of the difference in the OOB channel gain with and without the IRS, we prove that the OOB channel gain with an IRS *stochastically dominates* the gain without the IRS, with the difference increasing with the number of IRS elements. Thus, an OOB UE gets instantaneous benefits that monotonically increase with the number of IRS elements (see Theorem 4.2 and Proposition 4.1.)

4.1.b.ii OOB Performance in mmWave Bands (See Section 4.4)

In the mmWave bands, the channels are directional, with only a few propagation paths. In this context, using novel probabilistic approaches based on the resolvable criteria of the mmWave spatial beams, our key findings are as follows.

2-a) In LoS scenarios, where the IRS is optimized to match the dominant path of the in-band UE's channel, we derive the ergodic sum-SEs of the two operators under RR scheduling of the UEs. The SE at the in-band UE scales log-quadratically in the number of IRS elements, whereas the SE gain at an OOB UE depends on the

number of spatial paths in the OOB UE's channel. If there are sufficient paths in the cascaded channel, the SE improvement due to the IRS scales log-linearly in the number of IRS elements. Otherwise, the OOB UE's SE improves only marginally compared to that in the absence of the IRS (see Theorem 4.3.)

2-b) We evaluate the outage probability and CCDF of an OOB UE's channel gain with-/without an IRS in LoS scenarios and prove that the channel gain in the presence of IRS *stochastically dominates* the gain in its absence. Thus, even in mmWave bands, the IRS provides positive instantaneous gains to all the OOB UEs (see Theorem 4.4.)

2-c) We next consider the (L+)NLoS scenario where the IRS is jointly optimized considering all the spatial paths. We first evaluate the directional energy response of the IRS and show that it exhibits peaks only at the channel angles to which the IRS is optimized. This is a fundamental and new characterization of the IRS response when it is aligned to multiple paths in an mmWave system. (see Lemma 4.1.)

2-d) We derive the ergodic sum-SE of both operators in (L+)NLoS scenarios. We find that the OOB performance is even better than the LoS scenario (and hence better than the system without an IRS.) This is because the odds that an OOB UE benefits improve when the IRS has a nonzero response in multiple directions. Thus, the OOB performance in mmWave bands does not degrade even when the OOB operator serves its UEs while remaining oblivious to the presence of the IRS (see Theorem 4.5.)

4.1.b.iii Opportunistic Enhancement of OOB Performance (See Section 4.5)

Having shown that an IRS positively benefits OOB UEs, we next suggest ways to exploit the uncontrolled IRS to enhance the performance of OOB operators further. In particular, by using opportunistic selection techniques, we leverage multi-user diversity and show that a significant boost in the OOB performance can be obtained compared to RR scheduling. Specifically, we demonstrate the following.

3-a) By using a proportional-fair scheduler over a large number of OOB UEs, the sum-SE of operator Y converges to the so-called *beamforming SE*, which is the SE obtained

when the IRS is optimized for an OOB UE in every time slot (see Lemma 4.2.)

3-b) By using a max-rate scheduler, the ergodic sum-SE of operator Y monotonically increases with both the number of IRS elements and OOB UEs in the system (see Lemma 4.3.)

Next, we highlight the practical utility of our results.

4.1.c Practical Implications and Useful Insights

Our results offer several interesting insights into the performance of IRS-aided wireless systems where one operator deploys and controls an IRS. First, in all the scenarios mentioned in Sec. 4.1.b, we present novel, compact, and insightful analytical expressions that uncover the dependence of the performance on system parameters such as the number of IRS elements, SNR, number of channel paths, etc. As shown both analytically and through simulations, an IRS is beneficial to OOB users even though the IRS phase configuration is chosen randomly from the OOB operator's viewpoint, and this holds both in terms of the average and instantaneous SE. In particular, in rich scattering environments, the average SE at any OOB UE scales log-linearly in the number of IRS elements. On the other hand, in mmWave channels, the average SE improvement at the OOB UE due to the IRS is an increasing function of the number of spatial paths in the OOB UE's channel. Thus, deploying an IRS enriches the overall wireless channels (in both sub-6 GHz and mmWave bands) and can only benefit all wireless operators in the area. Our study also reveals that there exists an interesting trade-off between reducing the signaling overhead to program the IRS at the in-band operator (as in LoS scenarios) versus boosting the gain at the OOB operators (as in (L+)NLoS scenarios) in the mmWave bands. Finally, our results and insights derived for 2 operators directly extend to any number of OOB operators and other settings like a planar array IRS.

Notation: For general notations used in this chapter, see the section on "General Mathematical Notations" on page ix. For the notations/variables specific to this chapter, please refer to Table 4.1.

Variable	Definition	Variable	Definition
N	Number of IRS elements	$\gamma_{i,p}^{(1)}$	Gain of ith path from BS-p to IRS
K	Number of UEs served by BS-X	$\gamma_{j,\ell}^{(2)}$	Gain of jth path from IRS to UE-ℓ
Q	Number of UEs served by BS-Y	$h_{d,k}$	Direct channel from BS-X to UE-k
$L_{1,p}$	Number of paths from BS-p to IRS	$h_{d,q}$	Direct channel from BS-Y to UE-q
$L_{2,\ell}$	Number of paths from IRS to UE-ℓ	$\mathbf{g}_k/\mathbf{g}_q$	Channel from IRS to UE-k/q
L	Number of cascaded paths ($L = L_1L_2$)	$\mathbf{f}^X/\mathbf{f}^Y$	Channel from BS-X/Y to IRS
P	Transmit power at the BS	$\boldsymbol{\theta}$ or $\boldsymbol{\Theta}$	IRS configuration vector/matrix
σ^2	Noise variance at the UE	β_x	Path loss in link-x
$\omega_{X,k}^1$	Dominant cascaded normalized angle from BS-X to UE-k via the IRS	$\omega_{Y,q}^l$	Cascaded normalized angle from BS-Y to UE-q in the lth path
d/λ	Ratio of inter-elemental spacing to the signal wavelength	R_k^{BF}	Achievable beamforming SE at UE-k
$\mathcal{A}$	Resolvable beam book: set of resolvable array steering vectors	$\bar{R}^{(X)}/$ $\bar{S}_1^{(X)}/$ $\bar{S}_L^{(X)}$	Acheivable ergodic sum-SE of op. X in sub-6 GHz/ mmWave scenarios
$\boldsymbol{\Phi}$	Resolvable angle book: set of resolvable normalized angles	$\bar{R}^{(Y)}/$ $\bar{S}_1^{(Y)}/$ $\bar{S}_L^{(Y)}$	Acheivable ergodic sum-SE of op. Y in sub-6 GHz/ mmWave scenarios
$\bar{R}_{\text{PF}}^{(Y)}$	Acheivable sum-SE of op. Y under PF scheduling	$\bar{R}_{\text{MR}}^{(Y)}$	Acheivable ergodic sum-SE of op. Y under max-rate scheduling

Table 4.1: Commonly encountered variables/notations in chapter 4.

4.2 System Model

We consider a single-cell system with two mobile network operators, X and Y, who provide service to K and Q UEs, respectively, on different frequency bands and in the same geographical area. The BSs of operators X and Y (referred to as BS-X and BS-Y, respectively) and UEs are equipped with a single antenna, and all the channels undergo frequency-flat fading [111].[2] An N-element IRS is deployed by operator X to enhance the SNR at the UEs it serves. So, operator X configures the IRS with the SNR-optimal phase configuration for a UE scheduled by BS-X in every time slot. On the other hand, operator Y does not deploy any IRS and is oblivious to the presence of operator X's IRS. Then,

[2]For simplicity of exposition and to focus on the *effect of the IRS on OOB users*, we consider single antennas at the BSs and UEs, similar to [6–8, 112, 113]. The extension to the multiple antenna case does not change our broad conclusions, but we relegate this to future work.

the downlink signal received at the kth UE served by BS-X is

$$y_k = \left(h_{d,k} + \mathbf{g}_k^T \mathbf{\Theta} \mathbf{f}^X\right) x_k + n_k, \tag{4.1}$$

where $\mathbf{g}_k \in \mathbb{C}^{N\times 1}$ is the channel from IRS to the kth UE, $\mathbf{f}^X \in \mathbb{C}^{N\times 1}$ is the channel from BS-X to the IRS, $\mathbf{\Theta} \in \mathbb{C}^{N\times N}$ is a diagonal matrix containing the IRS reflection coefficients of the form $e^{j\theta}$, and $h_{d,k}$ is the direct (non-IRS) path from BS to the UE-k. Also, x_k is the data symbol for UE-k with average power $\mathbb{E}[|x_k|^2] = P$, and n_k is the additive noise $\sim \mathcal{CN}(0, \sigma^2)$ at UE-k. Similarly, at UE-q served by BS-Y, we have

$$y_q = \left(h_{d,q} + \mathbf{g}_q^T \mathbf{\Theta} \mathbf{f}^Y\right) x_q + n_q. \tag{4.2}$$

In Figure 4.1, we pictorially illustrate the considered network.

4.2.a Channel Model in sub-6 GHz Frequency Bands

Similar to [111], in the sub-6 GHz band, we consider that all the fading channels are statistically independent[3] and identically distributed (i.i.d.) following the Rayleigh distribution.[4] Specifically, $h_{d,k} = \sqrt{\beta_{d,k}}\tilde{h}_{d,k}, h_{d,q} = \sqrt{\beta_{d,q}}\tilde{h}_{d,q}; \tilde{h}_{d,k}, \tilde{h}_{d,q} \overset{\text{i.i.d.}}{\sim} \mathcal{CN}(0,1)$; $\mathbf{g}_k = \sqrt{\beta_{\mathbf{g},k}}\tilde{\mathbf{g}}_k, \mathbf{g}_q = \sqrt{\beta_{\mathbf{g},q}}\tilde{\mathbf{g}}_q; \tilde{\mathbf{g}}_k, \tilde{\mathbf{g}}_q \overset{\text{i.i.d.}}{\sim} \mathcal{CN}(\mathbf{0}, \mathbf{I}_N)$; $\mathbf{f}^X = \sqrt{\beta_{\mathbf{f}^X}}\tilde{\mathbf{f}}^X, \mathbf{f}^Y = \sqrt{\beta_{\mathbf{f}^Y}}\tilde{\mathbf{f}}^Y; \tilde{\mathbf{f}}^X, \tilde{\mathbf{f}}^Y \overset{\text{i.i.d.}}{\sim} \mathcal{CN}(\mathbf{0}, \mathbf{I}_N)$. All terms of the form β_x represent the path losses.

4.2.b Channel Model in mmWave Frequency Bands

In the mmWave band, we consider a Saleh-Valenzuela type model for all the channels [114]. At UE-ℓ, the channels are

$$\mathbf{f}^p = \sqrt{\frac{N}{L_{1,p}}} \sum_{i=1}^{L_{1,p}} \gamma_{i,p}^{(1)} \mathbf{a}_N^*(\phi_{i,p}); \ \mathbf{g}_\ell = \sqrt{\frac{N}{L_{2,\ell}}} \sum_{j=1}^{L_{2,\ell}} \gamma_{j,\ell}^{(2)} \mathbf{a}_N^*(\psi_{j,\ell}), \tag{4.3}$$

[3] We consider that IRS elements are placed sufficiently far apart that the spatial correlation in the channels to/from the IRS is negligible.

[4] Our results can be easily extended to other sub-6 GHz channel fading models also. From the approach used to show the results here, it is easy to see that the scaling law of the SE as a function of the IRS parameters will remain the same, although the scaling constants depend on the fading model. Thus, the conclusions on the impact of the IRS on OOB performance reported in this chapter will continue to hold.

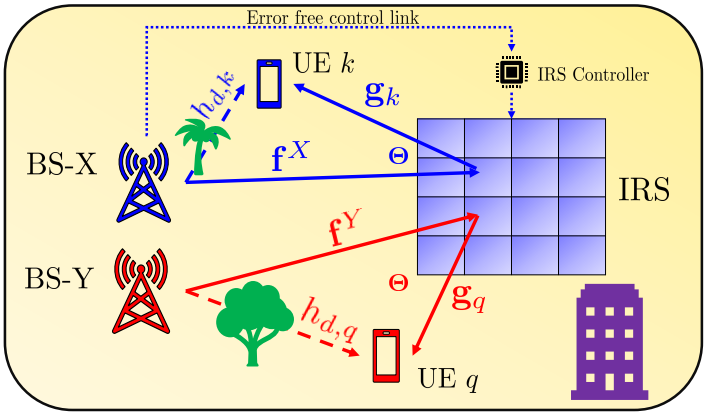

Figure 4.1: Network scenario of an IRS-aided two-operator system.

where $p \in \{X, Y\}$, $L_{1,p}$ and $L_{2,\ell}$ are the number of spatial paths in the BS-p to IRS, and IRS to UE-ℓ links, respectively. Since the in-band and OOB BSs/UEs are distributed arbitrarily with respect to the IRS, for notational simplicity, we let $L_{1,X} = L_{1,Y} \triangleq L_1$, and $L_{2,\ell} = L_2 \ \forall \ell$ (including in-band and OOB UEs.) Also, $\phi_{i,p}$ and $\psi_{j,\ell}$ denote the sine of the angle of arrival of the signal from BS-p to the IRS via the ith path, and the sine of the angle of departure from the IRS to the ℓth UE via the jth path, where sine of an angle (ϕ_x) is related to the physical spatial angle (χ) by[5] $\phi_x = (2d/\lambda)\sin(\chi)$, with d, λ being the inter-elemental distance and signal wavelength, respectively. The sine terms are sampled from a distribution $\mathcal{U}_{\mathcal{A}}$, which depends on the beam resolution capability of the IRS (elaborated next.) The fading coefficients, $\gamma_{i,p}^{(1)}$ and $\gamma_{j,\ell}^{(2)}$, are independently sampled from $\mathcal{CN}(0, \beta_{\mathbf{f}^p})$, and $\mathcal{CN}(0, \beta_{\mathbf{g},\ell})$, respectively. Finally, $\mathbf{a}_N(\phi)$ is an array steering vector of a uniform linear array (ULA)[6] based IRS oriented at the angle ϕ, given by

$$\mathbf{a}_N(\phi) = \frac{1}{\sqrt{N}}[1, e^{-j\pi\phi}, \ldots, e^{-j(N-1)\pi\phi}]^T. \tag{4.4}$$

4.2.b.i Beam Resolution Capability of the IRS

We now describe the beam resolution capability of an IRS, which is important to account for when the array contains a finite number of elements. Beam resolution measures the

[5] In the sequel, the term "angle" will denote the sine of a physical angle.

[6] All our main conclusions remain unchanged even if other array geometries (e.g., a uniform planar array) are used at the IRS, similar to [33, 115–117].

degree to which two closely located beams are distinguishable (or resolvable.) Spatial paths in (4.3) will become non-resolvable if the angles associated with the paths are spaced less than the beam resolution and can be modeled as being clustered into a single path with an appropriate channel gain. To measure the beam resolution of the ULA-based IRS model [33, 115–117], we enumerate all possible D beams as

$$\mathbf{A} = [\mathbf{a}_N(\phi_1), \mathbf{a}_N(\phi_2), \ldots, \mathbf{a}_N(\phi_D)] \in \mathbb{C}^{N \times D}. \tag{4.5}$$

We can verify that $\mathbf{A}$ is a Vandermonde matrix and hence its column vectors $\{\mathbf{a}_N(\phi_i)\}_{i=1}^{D}$ are linearly independent when $D \leq N$ provided $\{\phi_i\}_{i=1}^{D}$ are distinct [118, Pg. 185]. On the other hand, when $D > N$, the vectors are always linearly dependent and hence are non-resolvable. So, the total number of independent (or resolvable) beams that can be formed by an N-element IRS is at most N. This fact has been observed in the literature [114, 119, 120], and also in the current works on IRS-aided mmWave wireless systems [65, 121]. Thus, the complete set of resolvable beams $\mathcal{A}$ (called the *resolvable beambook*) at the IRS is[7]

$$\mathcal{A} \triangleq \{\mathbf{a}_N(\phi), \phi \in \mathbf{\Phi}\}; \mathbf{\Phi} \triangleq \left\{ \left(-1 + \frac{2i}{N} \right) \middle| i = 0, \ldots, N-1 \right\}. \tag{4.6}$$

Here $\mathbf{\Phi}$ is the *resolvable anglebook* of the IRS, and, without loss in generality, we model its distribution $\mathcal{U}_{\mathcal{A}}$ by

$$\mathcal{U}_{\mathcal{A}}(\phi) = \frac{1}{|\mathbf{\Phi}|} \mathbb{1}_{\{\phi \in \mathbf{\Phi}\}} = \frac{1}{N} \mathbb{1}_{\{\phi \in \mathbf{\Phi}\}}. \tag{4.7}$$

Also, for large N, $\mathcal{A}$ constitutes a set of orthonormal vectors:

$$\mathbf{a}_N^H(\phi_1)\mathbf{a}_N(\phi_2) \to \delta_{\{\phi_1, \phi_2\}} \forall \mathbf{a}_N(\phi_1), \mathbf{a}_N(\phi_2) \in \mathcal{A}, \tag{4.8}$$

where $\delta_{\{x,y\}}$ is the usual dirac-delta function.

[7] For analytical tractability, we consider a *flat-top* RF directivity pattern of the IRS [122, Eq. 5]. This is a good approximation to practical array systems and becomes accurate as N gets large [114, 122].

4.2.c Problem Statement

We are now ready to state the problem mathematically. Suppose BS-X tunes the IRS with the SNR-optimal vector $\boldsymbol{\theta}^{\text{opt}} \triangleq \text{diag}(\boldsymbol{\Theta}^{\text{opt}})$ to serve UE-k by solving the problem:

$$\boldsymbol{\Theta}^{\text{opt}} = \underset{\boldsymbol{\Theta} \in \mathbb{C}^{N \times N}}{\arg\max} \quad \left| h_{d,k} + \mathbf{g}_k^T \boldsymbol{\Theta} \mathbf{f}^X \right|^2, \tag{4.9}$$

subject to $\boldsymbol{\Theta}$ being a diagonal matrix with unit-magnitude diagonal entries. Then, we wish to characterize the impact of the IRS on the channel gain, $\left| h_{d,q} + \mathbf{g}_q^T \boldsymbol{\Theta}^{\text{opt}} \mathbf{f}^Y \right|^2$, of OOB UE-$q$ scheduled by BS-Y. In particular, we wish to answer:

1. Does the IRS degrade OOB performance? That is, when or how often will $\left| h_{d,q} + \mathbf{g}_q^T \boldsymbol{\Theta}^{\text{opt}} \mathbf{f}^Y \right|^2 < |h_{d,q}|^2$ hold?
2. How does the OOB channel gain $\left| h_{d,q} + \mathbf{g}_q^T \boldsymbol{\Theta}^{\text{opt}} \mathbf{f}^Y \right|^2$ depend on N?

Clearly, these aspects of an IRS are fundamental to understanding the overall impact of an IRS in practical systems when many operators exist together. In the sequel, we answer these by analyzing the ergodic and instantaneous characteristics of the OOB UE's channel in both sub-6 GHz and mmWave bands in the presence of an IRS controlled by a different operator.

Remark 4.1. *The next two sections focus on cases where both operators provide services in the sub-6 GHz band (Sec. 4.3) or both provide services in the mmWave band (Sec. 4.4), using non-overlapping frequency allocations. We do not consider the case where one operator uses the sub-6 GHz band while the other uses the mmWave band, as it is unclear whether an IRS can efficiently reflect signals in both these frequency bands.*

4.3 OOB Performance: sub-6 GHz bands

Suppose an operator X deploys and controls an IRS to enhance the SE of the UEs being served by it in a sub-6 GHz band. We wish to characterize the effect of the IRS on operator Y, which is operating in a different sub-6 GHz frequency band with no control over the

IRS. Thus, to serve the kth UE, BS-X configures the IRS with the SNR/SE-optimal phases [2, 3, 103]

$$\theta_{n,k}^{\text{opt}} = e^{j\left(\angle h_{d,k} - \left(\angle f_n^X + \angle g_{k,n}\right)\right)}, n = 1, \ldots, N, \tag{4.10}$$

which results in the coherent addition of the signals along the direct and IRS paths, leading to the maximum possible received SNR. Then, the SE achieved by the kth UE is

$$R_k^{BF} = \log_2\left(1 + \frac{P}{\sigma^2}\left|\left|h_{d,k}\right| + \sum_{n=1}^{N}\left|f_n^X g_{k,n}\right|\right|^2\right). \tag{4.11}$$

Due to the independence of the channels of the UEs served by operators X and Y, the IRS phase configuration used by operator X to serve its own UEs appears as a *random* phase configuration of the IRS for any UE served by operator Y.

We consider RR scheduling of UEs at both BS-X and BS-Y.[8] Since the BSs are equipped with a single antenna, one UE from each network is scheduled at every time slot. A summary of the protocol is given in Fig. 4.2.

We characterize the average OOB performance by deriving the ergodic sum-SE of both networks and then infer the degree of degradation/enhancement of the OOB performance caused by the IRS. The ergodic SE at UE-k is

$$\langle R_k^{(X)} \rangle = \mathbb{E}\left[\log_2\left(1 + \left|\sum_{n=1}^{N}\left|f_n^X g_{k,n}\right| + \left|h_{d,k}\right|\right|^2 \frac{P}{\sigma^2}\right)\right], \tag{4.12}$$

since the IRS is configured with the optimal phase configuration for (scheduled) UE-k. On the other hand, the ergodic SE for (scheduled) UE-q of operator Y is

$$\langle R_q^{(Y)} \rangle = \mathbb{E}\left[\log_2\left(1 + \left|\sum_{n=1}^{N} f_n^Y g_{q,n} + h_{d,q}\right|^2 \frac{P}{\sigma^2}\right)\right], \tag{4.13}$$

where we used the fact that the channels are circularly symmetric random variables, i.e., $f_n^Y g_{q,n} e^{j\theta} \overset{d}{=} f_n^Y g_{q,n}$ for any θ. Here, the expectations are taken with respect to the distribution of the channels to the respective UEs. With RR scheduling, the ergodic sum-SEs

[8] The extension of our results to the proportional fair and max-rate scheduling schemes is provided in Sec. 4.5.

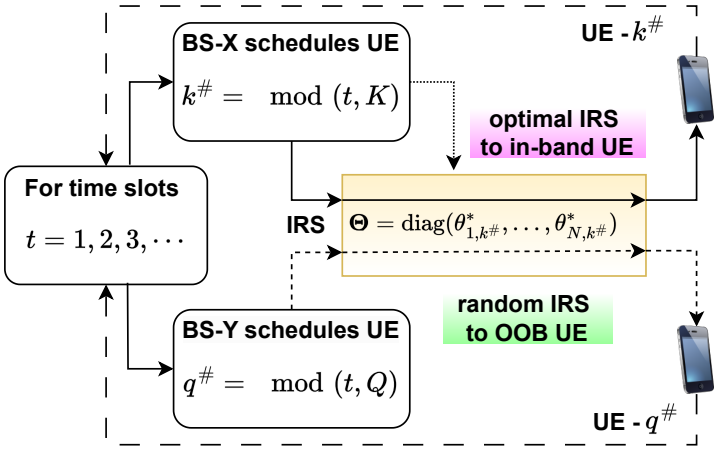

Figure 4.2: Flowchart of the round-robin scheduling-based protocol.

of two operators are given by

$$\bar{R}^{(X)} \triangleq \frac{1}{K}\sum_{k=1}^{K}\langle R_k^{(X)}\rangle, \text{ and } \bar{R}^{(Y)} \triangleq \frac{1}{Q}\sum_{q=1}^{Q}\langle R_q^{(Y)}\rangle. \tag{4.14}$$

We note that closed-form expressions for the ergodic sum-SE are difficult to obtain due to the complicated distribution of the SNR and SE terms (e.g., in (4.12) and (4.13).) Although we can use the approach in [123] to obtain the exact ergodic sum-SE in terms of standard integrals, the resulting expressions do not provide insights into how the sum-SE scales with the system parameters. Instead, we rely on applying tight approximations to obtain insightful results. However, we note that it is important to choose approximations such that the analysis across different scenarios can be unified in a single framework and the corresponding results are comparable. To that end, we apply Jensen's inequality, and after careful simplification, we arrive at elegant and interpretable expressions for the ergodic sum-SEs in all scenarios. In this view, we have the following theorem for the sub-6 GHz band of communication.

Theorem 4.1. *Under independent Rayleigh fading channels in the sub-6 GHz bands, with RR scheduling, and when the IRS is optimized to serve the UEs of operator X, the ergodic*

sum-SEs of operators X and Y scale as

$$\bar{R}^{(X)} \approx \frac{1}{K}\sum_{k=1}^{K}\log_2\left(1+\left[N^2\left(\frac{\pi^2}{16}\beta_{r,k}\right)+N\left(\beta_{r,k}-\frac{\pi^2}{16}\beta_{r,k}+\frac{\pi^{3/2}}{4}\sqrt{\beta_{d,k}\beta_{r,k}}\right)+\beta_{d,k}\right]\frac{P}{\sigma^2}\right), \tag{4.15}$$

where $\beta_{r,k} \triangleq \beta_{\mathbf{f}^X}\beta_{\mathbf{g},k}$, *and*

$$\bar{R}^{(Y)} \approx \frac{1}{Q}\sum_{q=1}^{Q}\log_2\left(1+\left[N\beta_{r,q}+\beta_{d,q}\right]\frac{P}{\sigma^2}\right), \tag{4.16}$$

where $\beta_{r,q} \triangleq \beta_{\mathbf{f}^Y}\beta_{\mathbf{g},q}$.

Proof. See Appendix 4.A. ■

From the above theorem, we infer the following:

- The IRS enhances the average received SNR by a factor of N^2 at any scheduled (in-band) UE of operator X when BS-X optimizes the IRS. This is the benefit that operator X obtains by using an optimized N-element IRS.
- Operator Y, who does not control the IRS, also witnesses an enhancement of average SNR by a factor of N for free, i.e., without any coordination with the IRS. This happens because the IRS makes the wireless environment more rich-scattering on average, and facilitates the reception of multiple copies of the signals at the (OOB) UEs.

Next, we prove that even the instantaneous characteristics of the OOB channel are favorable due to the IRS. We recognize that the instantaneous channel at an OOB UE-q is given by $|h_q|^2$, where $h_q \triangleq \sum_{n=1}^{N} f_n^Y g_{q,n} + h_{d,q}$. In the sequel, we provide two kinds of results: first, we compute the outage probability experienced by UE-q, and then provide stronger results on the OOB channels via stochastic dominance theory.

The outage probability of UE-q is given by

$$P_{q,\text{out}}^{\rho} = \mathsf{Pr}(|h_q|^2 < \rho), \tag{4.17}$$

where ρ is a constant that depends on the receiver sensitivity threshold. Although works like [43] provide closed-form expressions for the outage probabilities of randomly configured IRSs, these expressions do not provide insight into the system performance. So, using [103, Proposition 1], we approximate $h_q \sim \mathcal{CN}(0, N\beta_{r,q} + \beta_{d,q})$ which becomes accurate as N gets large.[9] Hence, $|h_q|^2$ is a exponential random variable with mean $N\beta_{r,q} + \beta_{d,q}$, and the outage probability in (4.17) can be easily obtained as shown in Theorem 4.2 below.

Next, we characterize the stochastic behavior of the channel gains witnessed by UE-q with/without an IRS. In this view, define the following random variables.

$$|h_{1,q}|^2 \triangleq \left| \sum_{n=1}^{N} f_n^Y g_{q,n} + h_{d,q} \right|^2 ; |h_{2,q}|^2 \triangleq |h_{d,q}|^2 . \tag{4.18}$$

Note that $|h_{1,q}|^2$ and $|h_{2,q}|^2$ represent the channel power gain of UE-q in the presence and absence of the IRS, respectively. We now characterize the *change* in the channel gain at UE-q served by BS-Y in the presence and absence of the IRS:

$$Z_N^{(Y)} \triangleq |h_{1,q}|^2 - |h_{2,q}|^2 \, \mathbb{1}_{\{N \neq 0\}}. \tag{4.19}$$

The event $\{Z_N^{(Y)} < 0\}$ indicates an SNR degradation at the OOB UE due to the IRS. In the following theorem, we show that, almost surely, $Z_N^{(Y)}$ is non-negative by deriving the CCDF of $Z_N^{(Y)}$, $\bar{F}_{Z_N^{(Y)}}(z) \triangleq \mathsf{Pr}(Z_N^{(Y)} \geq z)$.

Theorem 4.2. *The probability of outage at UE-q served by an (OOB) operator Y in the sub-6 GHz band, when an IRS is optimized to serve the UEs of operator X, is given by*

$$P_{q,out}^{\rho} = 1 - e^{-\frac{\rho}{N\beta_{r,q} + \beta_{d,q}}}. \tag{4.20}$$

[9] This approximation works well even with $N = 8$ [103].

Further, for reasonably large N,[10] *the CCDF $\bar{F}_{Z_N^{(Y)}}(z)$ of $Z_N^{(Y)}$ is given by*

$$\bar{F}_{Z_N^{(Y)}}(z) = \begin{cases} 1 - \dfrac{1}{N\tilde{\beta}+2} \times e^{\left(\dfrac{z}{\beta_{d,q}}\right)}, & \text{if } z < 0, \\ \left(\dfrac{N\tilde{\beta}+1}{N\tilde{\beta}+2}\right) \times e^{-\left(\dfrac{z}{\beta_{d,q}\left(1+N\tilde{\beta}\right)}\right)}, & \text{if } z \geq 0. \end{cases} \tag{4.21}$$

where $\tilde{\beta} \triangleq \beta_{r,q}/\beta_{d,q}$.

Proof. We can obtain $P_{q,\text{out}}^{\rho}$ using the CCDF of an exponential random variable. For (4.21), see Appendix 4.B. ■

Theorem 4.2 shows that the outage probability is strictly monotonically decreasing with N, which shows that the IRS only improves the OOB performance. In fact, from a first-order Taylor series approximation, we can show that $P_{q,\text{out}}^{\rho} \approx \rho/(N\beta_{r,q} + \beta_{d,q})$, i.e., the outage probability decreases linearly in N. Further, since $\bar{F}_{Z_N^{(Y)}}(0) = 1 - 1/\left(2 + N\tilde{\beta}\right)$, for a given $\tilde{\beta}$, the probability that the SNR/gain offset in (4.19) is negative decays as $\mathcal{O}(1/N)$. Also, $\bar{F}_{Z_{N'}^{(Y)}}(z) \geq \bar{F}_{Z_{N''}^{(Y)}}(z)$ for all z and $N' > N''$. Consequently, we have the following proposition.

Proposition 4.1. *For any $M, N \in \mathbb{N}$ with $M > N$, the random variable $Z_M^{(Y)}$* stochastically dominates[11] *$Z_N^{(Y)}$. In particular, the channel gain in the presence of the IRS stochastically dominates the channel gain in its absence.*

The above proposition states that the random variables $\left\{Z_n^{(Y)}\right\}_{n\in\mathbb{N}}$ form a sequence of *stochastically larger* random variables as a function of the number of IRS elements, where $\mathbb{N}$ is the set of natural numbers. Thus, the SNR offset increases with the number of

[10] We will later numerically show that the result holds even for $N \geq 4$.

[11] A real-valued random variable X is stochastically larger than, or dominates, the real-valued random variable Y, written $X >_{st} Y$, if

$$\mathsf{Pr}(X > a) \geq \mathsf{Pr}(Y > a), \text{for all } a. \tag{4.22}$$

Note that, if the random variables X and Y have CCDFs $\bar{F}$ and $\bar{G}$, respectively, then $X >_{st} Y \iff \bar{F}(a) \geq \bar{G}(a)\ \forall\ a \in \mathbb{R}$ [124].

IRS elements even at an OOB UE, i.e., the IRS only enhances the channel quality at an OOB UE at any point in time, with high probability. Therefore, the performance of OOB operators *does not degrade* even when the operator is entirely oblivious to the presence of the IRS. Note that this holds true for any operator in the area; hence, no operator will be at a disadvantage due to the presence of an IRS being controlled by only one operator.

Remark 4.2. *The outage probability and the CCDF of the SNR offset as in Theorem 4.2 at the in-band UE (for whom the IRS is optimized) decay to zero as $\mathcal{O}(e^{-N})$ (see Appendix 4.C.) This improvement in decay is the benefit of using an optimized IRS.*

Having asserted that IRS can only benefit every OOB operator in the sub-6 GHz bands, we next move on to understand the effect of IRS on the OOB performance in the mmWave bands of communications, where the IRSs can significantly boost the in-band operators' performance in establishing link connectivity, improving coverage, etc.

4.4 OOB Performance: mmWave bands

In this section, we evaluate the in-band and OOB performance of an IRS-aided mmWave system under RR scheduling of the UEs. The wireless channels in the mmWave bands are typically spatially sparse and directional, with a few propagation paths, as against the rich-scattering sub-6 GHz channels. Consequently, the analysis in the sub-6 GHz bands does not extend to mmWave bands, and it is necessary to evaluate the OOB performance in the mmWave bands independently. We consider two different scenarios inspired by [65], namely, the LoS and (L+)NLoS scenarios, as explained in Sec. 4.1.b. In both cases, we assume that the channel (see (4.3)) to the OOB UEs is a mixture of LoS and NLoS paths.

4.4.a IRS Optimized for LoS Scenarios

The dominant LoS channel of the in-band UE is [9, 66]

$$h_k = N\gamma_{1,X}^{(1)}\gamma_{1,k}^{(2)}\mathbf{a}_N^H(\psi_{1,k})\boldsymbol{\Theta}\mathbf{a}_N^*(\phi_{1,X}) + h_{d,k} \tag{4.23}$$

$$\overset{(a)}{=} N\left(\gamma_{1,X}^{(1)}\gamma_{1,k}^{(2)}\left(\mathbf{a}_N^H(\phi_{1,X}) \odot \mathbf{a}_N^H(\psi_{1,k})\right)\right)\boldsymbol{\theta} + h_{d,k}, \tag{4.24}$$

where $\boldsymbol{\theta} = \text{diag}(\boldsymbol{\Theta}) \in \mathbb{C}^N$, and (a) is obtained using the properties of the Hadamard product. Since the Hadamard product of two array response vectors is also an array vector but aligned in a different direction [33], we simplify (4.24) as

$$h_k = N\gamma_{X,k}\dot{\mathbf{a}}_N^H(\omega_{X,k}^1)\boldsymbol{\theta} + h_{d,k}, \tag{4.25}$$

where $\omega_{X,k}^1 \triangleq \sin_{(p)}^{-1}(\sin(\phi_{1,X}) + \sin(\psi_{1,k}))$,[12] and $\gamma_{X,k} \triangleq \gamma_{1,X}^{(1)}\gamma_{1,k}^{(2)}$. Here, $\dot{\mathbf{a}}_N$ is an array vector that is normalized by N instead of $\sqrt{N}$ (see (4.4)), and so $\dot{\mathbf{a}}_N(\cdot) = \frac{1}{\sqrt{N}}\mathbf{a}_N(\cdot)$. Then by the Cauchy-Schwarz (CS) inequality, the nth entry of the optimal IRS configuration vector $\boldsymbol{\theta}^{\text{opt}}$ which maximizes the channel gain $|h_k|^2$ is $\theta_n = e^{j\left(\angle h_{d,k} - \pi(n-1)\omega_{X,k}^1 - \angle\gamma_{X,k}\right)}$, and hence the optimal IRS vector is

$$\boldsymbol{\theta}^{\text{opt}} = \frac{h_{d,k}\gamma_{X,k}^*}{|h_{d,k}\gamma_{X,k}|} \times N\dot{\mathbf{a}}_N(\omega_{X,k}^1). \tag{4.27}$$

From (4.27), it is clear that the IRS vector is *directional*; it is aligned in the direction of the in-band UE's channel. To illustrate this, we plot the correlation function $\mathbb{E}\left[\left|\dot{\mathbf{a}}^H(\nu)\boldsymbol{\theta}^{\text{opt}}\right|^2\right]$ versus $\nu \in \boldsymbol{\Phi}$ in Fig. 4.3, where $\boldsymbol{\theta}$ is set to align with an arbitrary in-band UE with $\omega_{X,k}^1 = 0.52$. The expectation is with respect to the channel fading coefficients. Clearly, when $\nu = 0.52 = \omega_{X,k}^1$, the function takes its maximum value of 1. This confirms that the IRS aligns with the in-band channel to which it is optimized. Contrariwise, the IRS phase shift as optimized by BS-X will be aligned at a *random* direction from any OOB UE's view with the distribution given by $\mathcal{U}_{\mathcal{A}}$ in (4.7). We now characterize the ergodic sum-SEs of both operators.

Theorem 4.3. *Under the Saleh-Valenzuela LoS model in the mmWave channels, with RR scheduling, and when the IRS is optimized to serve the UEs of operator X, the ergodic*

[12] We define $\sin_{(p)}^{-1}(x)$ so that x is in the principal argument $[-1, 1)$ as

$$\sin_{(p)}^{-1}(x) = \begin{cases} \sin^{-1}(x-2), & \text{if } x \geq 1, \\ \sin^{-1}(x), & \text{if } x \in [-1, 1), \\ \sin^{-1}(x+2), & \text{if } x < -1. \end{cases} \tag{4.26}$$

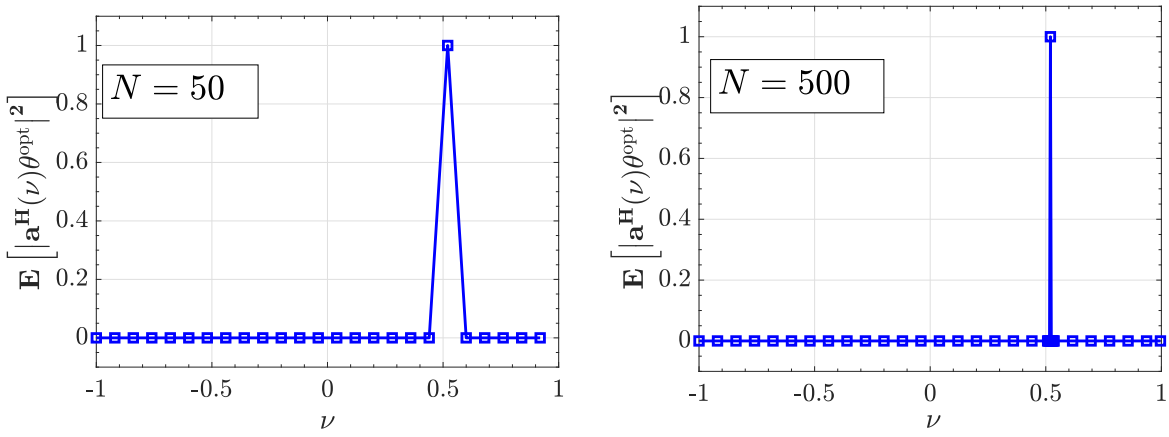

Figure 4.3: Correlation response of the IRS vector and array steering vectors pointing at different spatial angles, ν, for (a) $N = 50$ and (b) $N = 500$. When $\nu = \omega^1_{X,k}$, the response attains its maximum value of 1.

sum-SEs of operators X and Y scale as

$$\bar{S}_1^{(X)} \approx \frac{1}{K}\sum_{k=1}^{K}\log_2\left(1+\left[N^2\beta_{r,k}+N\left(\frac{\pi^{3/2}}{4}\sqrt{\beta_{d,k}\beta_{r,k}}\right)+\beta_{d,k}\right]\frac{P}{\sigma^2}\right), \tag{4.28}$$

and

$$\bar{S}_1^{(Y)} \approx \frac{1}{Q}\sum_{q=1}^{Q}\left(\frac{\bar{L}}{N}\log_2\left(1+\left[\frac{N^2}{\bar{L}}\beta_{r,q}+\beta_{d,q}\right]\frac{P}{\sigma^2}\right)+\left(1-\frac{\bar{L}}{N}\right)\log_2\left(1+\beta_{d,q}\frac{P}{\sigma^2}\right)\right), \tag{4.29}$$

respectively, where $\bar{L} \triangleq \min\{L, N\}$, *and* $L \triangleq L_1 L_2$.

Proof. See Appendix 4.D. ■

From the above theorem, it is clear that an IRS can never degrade the OOB performance in LoS scenarios of the mmWave bands. Even when L is small and N is large, the second term in (4.29) remains, which is the achievable SE in the absence of IRS. Thus, almost surely, the IRS results in an OOB-SE that is at least as high as the SE seen in its absence.

Remark 4.3 (OOB performance as a function of L for large N)**.** *From* (4.29)*, we can show that when* $N \to \infty$ *for a fixed and finite* L*, the SE is a unimodal function of* N*. Hence, there exists an* $N = N_0$ *which provides the maximum gain and distinguishes the* favorable

region ($N \leq N_0$) *from the* non-favorable *region* ($N \geq N_0$).[13] *Here,* N_0 *itself increases with* L *because the probability of establishing connectivity via the IRS, i.e.,* $\mathsf{Pr}(\mathcal{E}_1)$ *increases.*

Remark 4.4 (Distributed IRSs always benefit)**.** *As noted in Remark 4.3, the OOB UEs benefit more if the number of channel paths at these UEs is large. A natural way to obtain more paths is to deploy multiple distributed IRSs so that each IRS can provide an additional path to the UEs. This, in turn, increases the overall probability of benefiting the OOB UEs. We refer the reader to our follow-up work in Chapter 5 and [125] for more details.*

Similar to Theorem 4.2, the outage probability and CCDF of an OOB UE with/without IRS in mmWave bands is analyzed next.

Theorem 4.4. *The probability of outage at UE-q served by an OOB operator Y in the mmWave bands, when an IRS is optimized to serve the UEs of operator X, is*

$$F_{|h_q|^2}(\rho) \triangleq \mathsf{Pr}(|h_q|^2 < \rho) = 1 - e^{-\rho/\beta_{d,q}} - \frac{\bar{L}}{N}\left(\frac{\bar{L}e^{\frac{\bar{L}\beta_{d,q}}{N^2\beta_{r,q}}}}{N^2\beta_{r,q}}\mathcal{I}_0\left(\rho; \beta_{d,q}, \frac{N^2}{\bar{L}}\beta_{r,q}\right) - e^{-\rho/\beta_{d,q}}\right), \tag{4.30}$$

where $\bar{L} \triangleq \min\{L, N\}$*, and* $\mathcal{I}_0(x; c_1, c_2) \triangleq \int_{c_1}^{\infty} e^{-\left(\frac{x}{t}+\frac{t}{c_2}\right)} \mathrm{d}t$*. Further, define the random variables* $G_1 = |h_q|^2$*, and* $G_0 = |h_{d,q}|^2$ *(the channel gain in the* presence *and* absence *of the IRS, respectively.) Then,*

$$\mathsf{Pr}(G_1 > \rho) \geq \mathsf{Pr}(G_0 > \rho), \quad \forall \rho \in \mathbb{R}^+, \tag{4.31}$$

i.e., the channel gain of the OOB-UE in the presence of an IRS stochastically dominates *the channel gain in its absence.*

Proof. See Appendix 4.E. ■

The above theorem characterizes the instantaneous behavior of the OOB UEs' channels in the LoS scenarios and shows that the IRS never degrades the performance of OOB UEs.

[13] By non-favorable, we mean that the SE does not grow linearly with N beyond $N = N_0$. However, the SE never drops below the achievable SE in the absence of the IRS.

4.4.b IRS Optimized for (L+)NLoS Scenarios

In the previous section, we studied the OOB performance when the IRS is only optimized to the dominant path in the cascaded channels of the scheduled in-band UEs and concluded that the OOB performance does not degrade due to the IRS. However, when the IRS is programmed to align jointly along all the in-band UE's channel paths, it remains unclear whether an IRS can still benefit an OOB operator due to the unit-modulus preserving property of IRS coefficients. In fact, the directional response of the IRS is not easy to characterize since the IRS does not align completely along a single channel direction. To that end, we first determine the directional response of the IRS when it is optimized to a channel comprising multiple paths. We can write the channel to the in-band UE-k with L resolvable spatial paths as in the following equation.[14]

$$h_k = h_{d,k} + \frac{N}{\sqrt{L}} \sum_{l=1}^{L} \gamma_{l,X}^{(1)} \gamma_{l,k}^{(2)} \dot{\mathbf{a}}_N^H(\omega_{X,k}^l) \boldsymbol{\theta}. \tag{4.32}$$

Then, we can show that nth element of the optimal IRS configuration $\boldsymbol{\theta}^{\text{opt}}$ is given by (using CS inequality)

$$\theta_n^{\text{opt}} = e^{j\angle h_{d,k}} \frac{\sum_{l=1}^{L} \gamma_{l,X}^{(1)*} \gamma_{l,k}^{(2)*} e^{-j(n-1)\pi\omega_{X,k}^l}}{\left| \sum_{l=1}^{L} \gamma_{l,X}^{(1)*} \gamma_{l,k}^{(2)*} e^{-j(n-1)\pi\omega_{X,k}^l} \right|}. \tag{4.33}$$

Hence, the optimal IRS vector $\boldsymbol{\theta}^{\text{opt}}$ is

$$\frac{h_{d,k}}{|h_{d,k}|} \left(\sum_{l=1}^{L} \gamma_{l,X}^{(1)*} \gamma_{l,k}^{(2)*} \dot{\mathbf{a}}_N(\omega_{X,k}^l) \right) \odot \frac{1}{\left| \sum_{l=1}^{L} \gamma_{l,X}^{(1)} \gamma_{l,k}^{(2)} \dot{\mathbf{a}}_N(\omega_{X,k}^l) \right|}, \tag{4.34}$$

where $|\mathbf{x}|$ is the vector containing the magnitudes of the entries of $\mathbf{x}$ and $1/|\mathbf{x}|$ is an entry-wise inverse.

[14] For the sake of exposition, we consider that all cascaded paths through the IRS have the same average energy, similar to [126]. However, our results can be directly extended to scenarios where the paths have unequal energies.

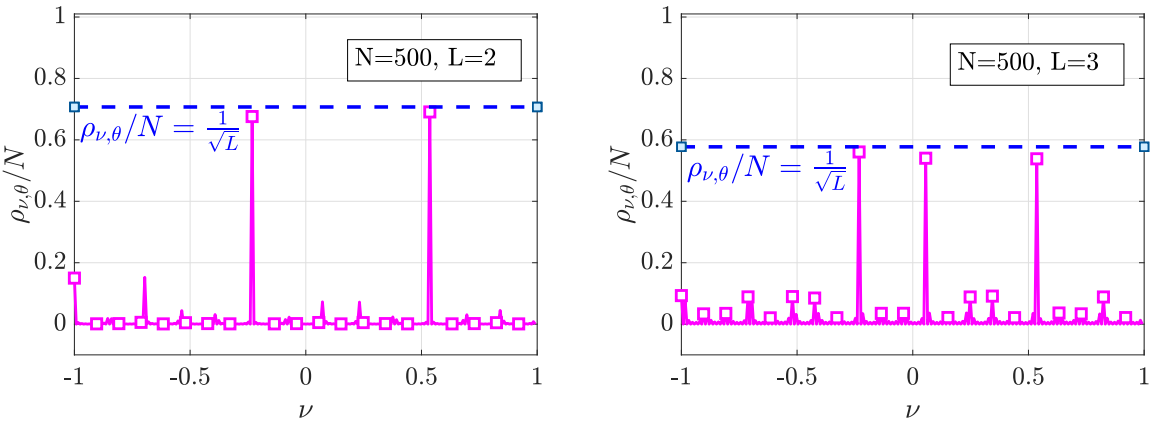

(a) $L = 2$. (b) $L = 3$.

Figure 4.4: Normalized Correlation response of the IRS (in (L+)NLoS scenarios) and array vectors at different ν for $N = 500$ with (a) $L = 2$, and (b) $L = 3$. When $\nu \in \mathcal{L}_2$ (or) $\mathcal{L}_3$, the response, $\rho_{\nu,\theta}/N$ peaks and $\approx 1/\sqrt{L}$.

Directional Response of the IRS: To determine the directional response of an IRS optimized for (L+)NLoS scenarios, similar to Sec. 4.4.a, we evaluate the correlation function: $\rho_{\nu,\theta} \triangleq N\mathbb{E}\left[\left|\dot{\mathbf{a}}^H(\nu)\boldsymbol{\theta}^{\text{opt}}\right|\right]$ at various angles of ν. We then focus on the values of ν that match the channel angles of UE-k and ascertain the distribution of the IRS-reflected energy along these directions. We have the following lemma.

Lemma 4.1. *The optimal IRS configuration as in* (4.34) *has the following spatial amplitude response* $\rho_{\nu,\theta}$ *as defined above:*

$$\rho_{\nu,\theta} = \begin{cases} \Omega\left(\frac{N}{\sqrt{L}}\right) + o(N), \text{if } \nu \in \left\{\omega_{X,k}^1, \ldots, \omega_{X,k}^L\right\}, \\ o(N), \qquad \text{if } \nu \in \boldsymbol{\Phi} \setminus \left\{\omega_{X,k}^1, \ldots, \omega_{X,k}^L\right\}. \end{cases} \tag{4.35}$$

Proof. See Appendix 4.F. ■

The above Lemma shows that when the IRS is optimized to align jointly along L directions, it has a spatial energy response of $1/L$ in each of these L directions and a negligible response in other directions. We perform a similar experiment as in the LoS scenario to numerically verify Lemma 4.1. In Fig. 4.4, we plot the normalized correlation response $\rho_{\nu,\theta}/N$ as function of $\nu \in \boldsymbol{\Phi}$, for $L = 2$ and $L = 3$. We consider that the IRS is optimized to an in-band UE whose equal-gain paths have channel angles drawn from $\mathcal{L}_2 = \{-0.23, 0.54\}$,

and $\mathcal{L}_3 = \{-0.23, 0.06, 0.54\}$, for $L = 2$, and $L = 3$, respectively. We see that whenever $\nu \in \mathcal{L}_2$ for $L = 2$ ($\mathcal{L}_3$ for $L = 3$), the response is maximum, and is nearly $1/\sqrt{L}$, and is 0, otherwise. We now provide the ergodic sum-SEs of the system when the IRS is optimized for (L+)NLoS scenarios.

Theorem 4.5. *Under the Saleh-Valenzuela (L+)NLoS model in the mmWave channels, with RR scheduling, and when the IRS is optimized to serve the UEs of operator X, the ergodic sum-SEs of operators X and Y scale as*

$$\bar{S}_L^{(X)} \approx \frac{1}{K} \sum_{k=1}^{K} \log_2 \left(1 + \left(N^2 \beta_{r,k} + N \sqrt{\pi \beta_{d,k} \beta_{r,k}} + \beta_{d,k} \right) \frac{P}{\sigma^2} \right), \tag{4.36}$$

and

$$\bar{S}_L^{(Y)} \approx \begin{cases} \dfrac{1}{Q} \displaystyle\sum_{q=1}^{Q} \sum_{i=i_0}^{L} \dfrac{\binom{L}{i}\binom{N-L}{L-i}}{\binom{N}{L}} \times \log_2 \left(1 + \left(\beta_{d,q} + i \dfrac{N^2}{L^2} \beta_{r,q} \right) \dfrac{P}{\sigma^2} \right), & \text{if} \quad L < N, \\ \dfrac{1}{Q} \displaystyle\sum_{q=1}^{Q} \log_2 \left(1 + (\beta_{d,q} + N \beta_{r,q}) \dfrac{P}{\sigma^2} \right), & \text{if} \quad L \geq N, \end{cases} \tag{4.37}$$

respectively, where $i_0 \triangleq \max\{0, 2L - N\}$.

Proof. See Appendix 4.G. ■

Theorem 4.5 shows that the IRS provides an $\mathcal{O}(\log_2(N))$ scaling of the SE at OOB UEs when $L \geq N$. In fact, in Sec. 4.6, we numerically show that this bound can be improved to $L \geq \sqrt{N}$ while preserving the $\mathcal{O}(\log_2(N))$ growth of SE. In that case, for $L < \sqrt{N}$, the OOB-SE is shown to be log-sub-linear in N, which is still better than the SE in the absence of IRS.[15] Subsequently, we show that the OOB sum-SE in (L+)NLoS scenarios is at least as good as in LoS scenarios and present further insights on the OOB performance in the presence of an uncontrolled IRS.

[15] We reiterate that we need $L \geq \sqrt{N}$ only for $\mathcal{O}(\log_2(N))$ scaling of SE. More generally, the OOB-SE in mmWave bands scales as $\mathcal{O}(\log_2(N^\delta)), \delta > 0$. Thus, an IRS strictly benefits the OOB system under all conditions.

4.5 Enhancement of OOB Performance Using Opportunistic Scheduling

In the previous sections, we saw that an IRS that is optimally configured to serve the UEs of operator X also benefits operator Y, but to a lesser extent than the benefit to the UEs of operator X. In this section, we show that the benefit of the uncontrolled IRS to the UEs of operator Y can be further enhanced using opportunistic user selection. Specifically, since the IRS is *randomly* configured from an OOB UE's view, if there are sufficiently many OOB UEs, at least one of the UEs will experience an SNR that is close to the SNR when the IRS is optimized for that UE (i.e., when the IRS is in *beamforming configuration* for that UE), as explained in Chapters 2 and 3. Then, opportunistically scheduling the UE for which the IRS is in beamforming configuration in every slot extracts multi-user diversity in the system and enhances the OOB performance better than RR-based UE scheduling [71]. We now analyze the OOB performance for two such opportunistic schedulers: the proportional-fair (PF) and max-rate (MR) schedulers.

4.5.a Multi-user Diversity for Operator Y using PF Scheduler

The PF scheduler serves UE-q^* at time t, where [71]

$$q^*(t) = \underset{q\in\{1,2,\ldots,Q\}}{\arg\max} \frac{\log_2\left(1+|h_q(t)|^2P/\sigma^2\right)}{T_q(t)} \triangleq \frac{R_q(t)}{T_q(t)}, \tag{4.38}$$

where $T_q(t)$ is the exponential moving average SE seen by UE-q till time t which is updated as

$$T_q(t+1) = \begin{cases} \left(1-\frac{1}{\tau}\right)T_q(t) + \frac{1}{\tau}R_q(t), & \text{if } \; q = q^*(t), \\ \left(1-\frac{1}{\tau}\right)T_q(t), & \text{if } \; q \neq q^*(t). \end{cases} \tag{4.39}$$

Here, the parameter τ controls the trade-off between fairness and throughput [103, Sec.II]. The following Lemma shows the achievable sum-SE of operator Y under PF scheduling.

Lemma 4.2. *([76, 103]) Under independent Rayleigh fading channels in the sub-6 GHz bands, when the IRS is optimized to serve the UEs of operator X, and operator Y uses the*

PF scheduler, the sum-SE of operator Y, $R_{\mathrm{PF}}^{(Y)}$, obeys

$$R_{\mathrm{PF}}^{(Y)} - \frac{1}{Q}\sum_{q=1}^{Q}\log_2\left(1+\left|\sum_{n=1}^{N}|f_n^Y g_{q,n}|+|h_{d,q}|\right|^2\frac{P}{\sigma^2}\right)\longrightarrow 0, \tag{4.40}$$

as $Q,\tau\longrightarrow\infty$.

From (4.40) and (4.11), we see that UE-q achieves the optimal SNR from the IRS even though the IRS is not explicitly programmed to be in beamforming configuration for this UE. Thus, operator Y also experiences $\mathcal{O}(N^2)$ gain in the SNR, free of cost, provided the number of UEs it serves is very large. However, one drawback of using the PF scheduler with large τ is that the latency in UE scheduling also becomes large [71]. Thus, an OOB operator has to judiciously choose τ to balance the achievable sum rate with the latency in UE scheduling.

4.5.b Multi-user Diversity for Operator Y using MR Scheduler

The MR scheduler serves UE-q^* at time t, where

$$q^*(t) = \underset{q\in\{1,2,\ldots,Q\}}{\arg\max}\ \log_2\left(1+|h_q(t)|^2\frac{P}{\sigma^2}\right). \tag{4.41}$$

Unlike the PF scheduler, an MR scheduler maximizes the overall system throughput, disregarding fairness across the UEs. As a result, the achievable benefit from the IRS when using an MR scheduler has a different flavor than the PF scheduler. Specifically, the random IRS configurations are used to enhance the dynamic range of fluctuations in the SNR at OOB UEs. Then, the ergodic sum-SE of the operator Y is

$$\bar{R}_{\mathrm{MR}}^{(Y)} = \mathbb{E}\left[\log_2\left(1+\max_{q\in\{1,\ldots,Q\}}|h_q|^2\frac{P}{\sigma^2}\right)\right]. \tag{4.42}$$

A closed-form characterization of (4.42) is given below under a special case where $\{h_q\}_q$ form a set of i.i.d. random variables.

Lemma 4.3. *(Theorem 1, [127]) Under i.i.d. Rayleigh fading channels in the sub-6 GHz bands, when the IRS is optimized to serve the UEs of operator X, and operator Y uses the*

MR scheduler, the ergodic sum-SE of operator Y, $\bar{R}_{\mathrm{MR}}^{(Y)}$, scales as

$$\bar{R}_{\mathrm{MR}}^{(Y)} \xrightarrow{Q\to\infty} \log_2\left(1+\log_e(Q)\left(N\beta_r+\beta_d\right)\frac{P}{\sigma^2}\right), \tag{4.43}$$

where β_r, β_d are the common direct and cascaded path losses.

Thus, the MR scheduler leverages multi-user diversity to obtain a $\log_e(Q)$-fold improvement in SNR and focuses less on achieving the beamforming SE at the selected OOB UE.

We note that practical aspects, such as the number of UEs required to achieve a target multi-user diversity, efficient feedback schemes to identify the best UE for scheduling, etc., are not discussed here for brevity, and we refer the reader to previous chapters, and also to [127, Sec. II] and [103, Sec. III-A] for more details.

The results in Lemmas 4.2, 4.3 pertain to the sub-6 GHz bands. Similar results can also be derived for operator Y in mmWave bands using PF and MR schedulers, e.g., using the opportunistic scheme presented in [103, Sec.III-C] and [127, Sec. III].

4.6 Numerical Results and Discussion

In this section, we demonstrate all our results via Monte Carlo simulations. Let BS-X and BS-Y be located at $(0, 50)$, and $(50, 0)$ (in meters), the IRS is at $(1025, 1025)$, and the UEs are randomly and uniformly located in a rectangular region with diagonally opposite corners $(950, 950)$ and $(1100, 1100)$. The path loss in each link is modeled as $\beta = C_0\,(d_0/d)^{\alpha}$, where C_0 is the path loss at the reference distance d_0, d is the distance of the link, and α is the path loss exponent. We let $d_0 = 1$ meter, $C_0 = -30$ dB and -60 dB for sub-6 GHz and mmWave bands, respectively. We use $\alpha = 2, 2$, and 4.5 in the BS X/Y-IRS, IRS-UE, and BS X/Y-UE (direct) links, respectively. Finally, we consider $K = Q = 10$ UEs served over 5000 time slots.

4.6.a OOB Performance in sub-6 GHz Bands using RR Scheduler

In Fig. 4.5, we plot the empirical ergodic sum-SE vs. the transmit SNR $\left(\gamma \triangleq P/\sigma^2\right)$ for both the operators as a function of N, the number of IRS elements, and in the sub-6 GHz

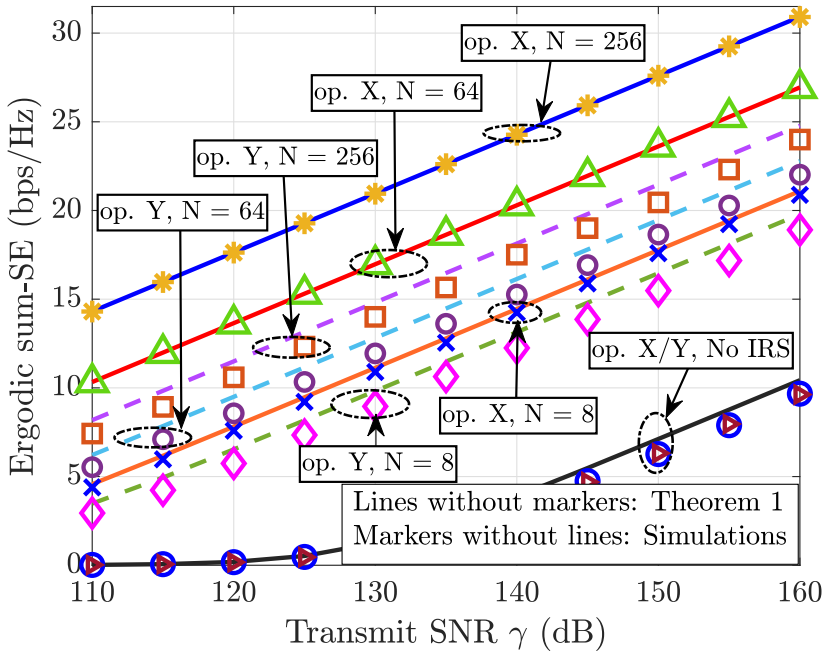

Figure 4.5: Ergodic sum-SE vs. transmit SNR.

frequency band.[16] We also plot the sum-SE obtained from the analytical expressions in Theorem 4.1 (marked as "Theorem 1" in the plot.) We see that the IRS enhances the sum-SEs of both operators, although operator X benefits more from the IRS. We also see that the improvement in SE with N is log-quadratic for operator X, while it is log-linear for operator Y, as expected. For example, the gap between the $N = 64$ and $N = 256$ curves for operator X is about 4 bits ($\approx \log_2(4^2) = 4$), the gap is about 2 bits ($\approx \log_2(4)$) for operator Y. Also, the analytical expressions tightly match the simulated values, i.e., the approximation error introduced using Jensen's inequality is very small.

Next, in Fig. 4.6, we examine the effect of the number of IRS elements, N, by plotting the ergodic sum-SE vs. $\log_2(N)$ for transmit SNRs of 130 dB and 150 dB to validate the scaling of the received SNR as a function of N. On the plot, we mark the slope of the different curves, and as expected from Theorem 4.1, it is clear that while the received SNR for a UE served by operator X scales as N^2, it also scales as N for a UE served by operator Y.

[16] We set the range of γ in $110 - 160$ dB for sub-6 GHz bands. For e.g., when $N = 8$ and $\gamma = 160$ dB, the *received* SNR is $\approx 5, -10$ dB with and without an IRS, respectively, at an OOB UE at $(1000, 1000)$.

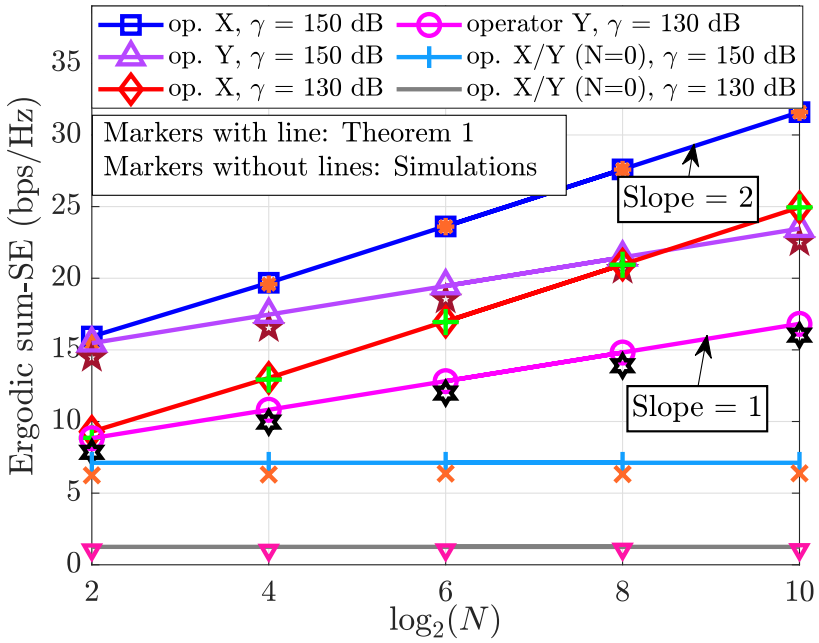

Figure 4.6: Ergodic sum-SE vs. $\log_2(N)$.

Next, we study the effect of the IRS on the OOB operator Y by considering the behavior of the random variable $Z_N^{(Y)}$ (see (4.19)), which represents the difference in the SNR/channel gain at a UE q served by BS-Y (which does not control the IRS) with and without the IRS in the environment. In Fig. 4.7, we plot the empirical and theoretical CCDF of $Z_N^{(Y)}$ (at $\gamma = 130$ dB.) The analytical expression derived in Theorem 4.2 (marked as "Theorem 2") matches well with the simulations. Also, almost surely, $Z_N^{(Y)}$ is a non-negative random variable for any $N > 0$, which confirms that the channel gain at an OOB UE *with* an IRS is at least as good as the channel gain at the same UE *without* an IRS with probability 1. The CCDF shifts to the right as the N is increased, as expected. The left-most curve in the figure is the CCDF of received SNR in the absence of the IRS, which shows that the probability that an operator benefits from the presence of a randomly configured IRS increases with N for operators who do not control the IRS. Thus, the instantaneous SNRs witnessed at an arbitrary UE of an OOB operator stochastically dominate the SNR seen by the same UE in the absence of the IRS, in line with Proposition 4.1.

Finally, we compare the outage probabilities of the in-band and OOB UEs in Fig. 4.8a as a function of N. While the probability decreases as $\mathcal{O}(e^{-N})$ at the in-band UEs (in-line

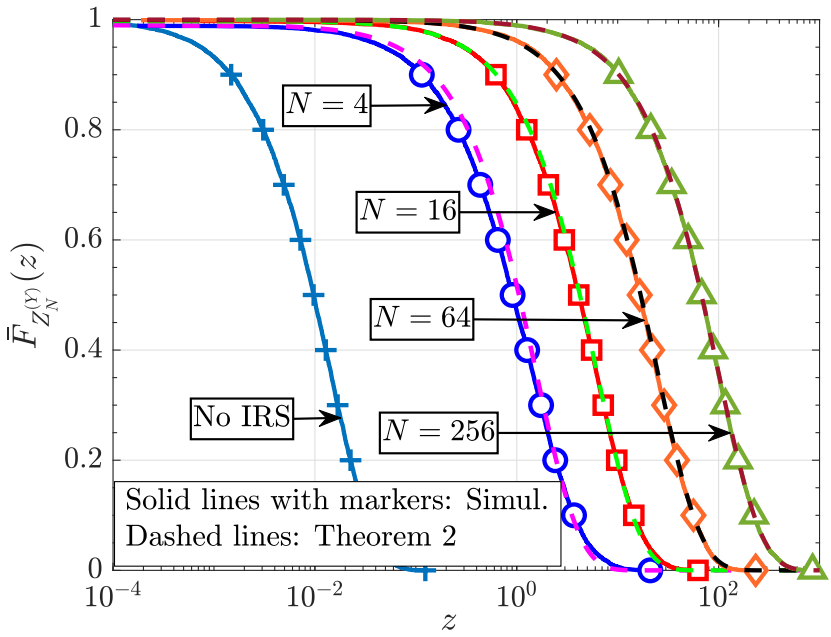

Figure 4.7: CCDF of $Z_N^{(Y)}$ as a function of N.

with Remark 4.2), it also uniformly decreases at OOB UEs, but at the rate of $\mathcal{O}(1/N)$ as per Theorem 4.2. Thus, the outage probability of the OOB UEs monotonically decreases with the IRS elements *free of cost*. For completeness, in Fig. 4.8b, we also validate that the CCDF of the SNR offset as in Remark 4.2 for the in-band UEs grows to 1 at the rate of $1 - \mathcal{O}(e^{-N})$.

4.6.b OOB Performance in mmWave Bands using RR Scheduler

We now numerically illustrate our findings in the mmWave band. First, we focus on the OOB performance when the IRS is optimized for in-band UEs in the LoS scenarios. In Figs. 4.9 and 4.10, we plot the ergodic sum-SEs vs. N, of both operators, at low and high (received) SNRs, respectively. At low SNR, we observe that 1) The ergodic sum-SE scales linearly with N, and 2) The OOB performance is insensitive to L. This can be explained by analyzing the behavior of the SE in (4.29) at low SNRs. Namely $\log(c\gamma) \approx c\gamma$ for small $c\gamma$. Thus, an OOB UE witnesses an SE which scales as N^2/L for an L/N fraction of time, leading to an effective scaling of SE as $\mathcal{O}(N)$. Thus, if the OOB system is designed to operate at low SNRs, then even an OOB UE obtains benefits from the IRS

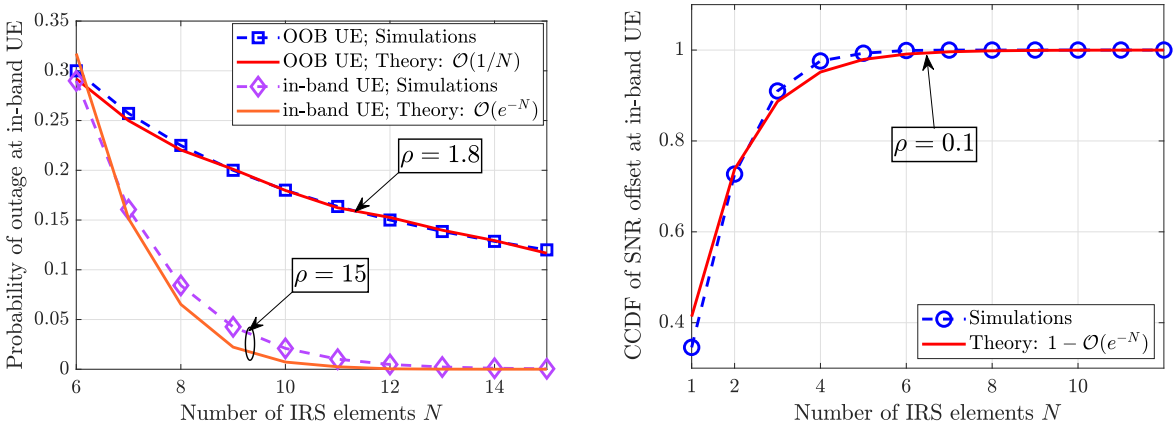

(a) Outage probability at in-band UEs vs. OOB UEs. (b) CCDF of the SNR offset at in-band UEs.

Figure 4.8: Instantaneous channel quality of the in-band/OOB UEs in the sub-6 GHz bands.

that monotonically increase with N. On the other hand, at high SNRs, for any given L, the SE is an unimodal function of N, as described in Remark 4.3. As long as $L \geq N$, i.e., the number of paths is sufficiently large (at least as many as the number of resolvable beams the IRS can form), almost surely, the IRS aligns with one of the OOB UE's channel angles and provides benefits which linearly increases with N. However, when $L < N$, the IRS beam does not always align with the OOB UE; hence, the performance starts to decline as N grows, with the peak SE obtained when $L = N$. In any case, the OOB SE is higher than the SE obtained without the IRS. This confirms that the IRS *never* degrades the average OOB performance even in mmWave bands. Also, the simulations and analytical expressions match very well, which validates the correctness of Theorem 4.3. Finally, we note that the SNR of the in-band operator monotonically grows as N^2, as expected.

Next, we validate the instantaneous OOB performance by plotting the CCDFs of the channel gains of an arbitrary OOB UE in Figs. 4.11, 4.12, and 4.13, for $L = 5$, 20, and 50, respectively. Clearly, the effective channel in the presence of the IRS stochastically dominates the effective channel in its absence, as found in Theorem 4.4. Further, with high probability, the channel gains of the OOB UEs achieve their maximum value when $N = L$, which is in line with our previous observations.

Next, we focus on when the IRS is optimized for (L+)NLoS mmWave scenarios. Specifically, we study the operators' ergodic sum-SE behavior in a high SNR regime. In Fig. 4.14,

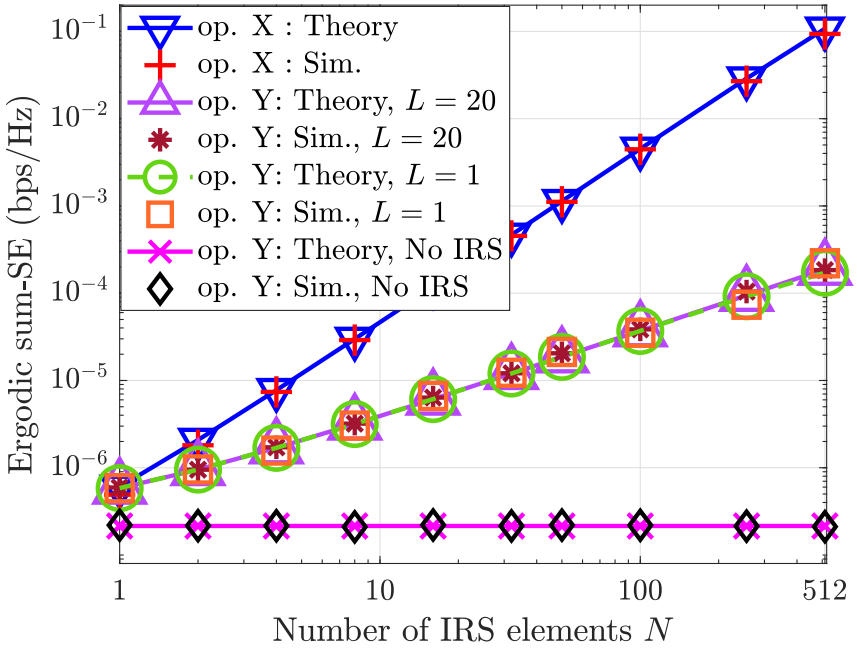

Figure 4.9: Ergodic sum-SE vs. N in LoS scenarios at $C_0\gamma = 90$ dB.

we plot the ergodic sum-SE vs. N when the IRS is optimized for (L+)NLoS scenarios. The OOB performance in this case is very similar to the LoS scenarios, where the enhancement in the OOB SE due to the IRS is contingent on the number of spatial paths available in the OOB UEs' channel. However, the main difference lies in the number of paths needed in the OOB UE's channel to obtain performance enhancement by the IRS. While the LoS scenarios require L to scale with N, it is sufficient for L to scale with $\sqrt{N}$ in the (L+)NLoS scenarios to obtain an OOB performance boost which is monotonic in N. Intuitively, this is because, in addition to the probability that one of the L paths of the OOB channel aligns with the IRS (which scales as L/N), the IRS provides an additional opportunity for alignment by having a directional response in L directions. This leads to the probability of alignment improving to L^2/N in the OOB system. We confirm this in Fig. 4.14: the peak performance is attained roughly at $N = L^2$ for every L. Recall that the probability that i of the IRS beams align with the OOB channel is given by (4.89). Consider the scenario $L \ll N$. Using Stirling's approximation $\binom{n}{i} \approx \frac{n^i}{i!}$ we can simplify (4.89) as $\mathsf{Pr}(Y = i) \approx \frac{1}{i!}\left(\frac{L^2}{N}\right)^i$. Then, letting $i = 1$ (to compare against the

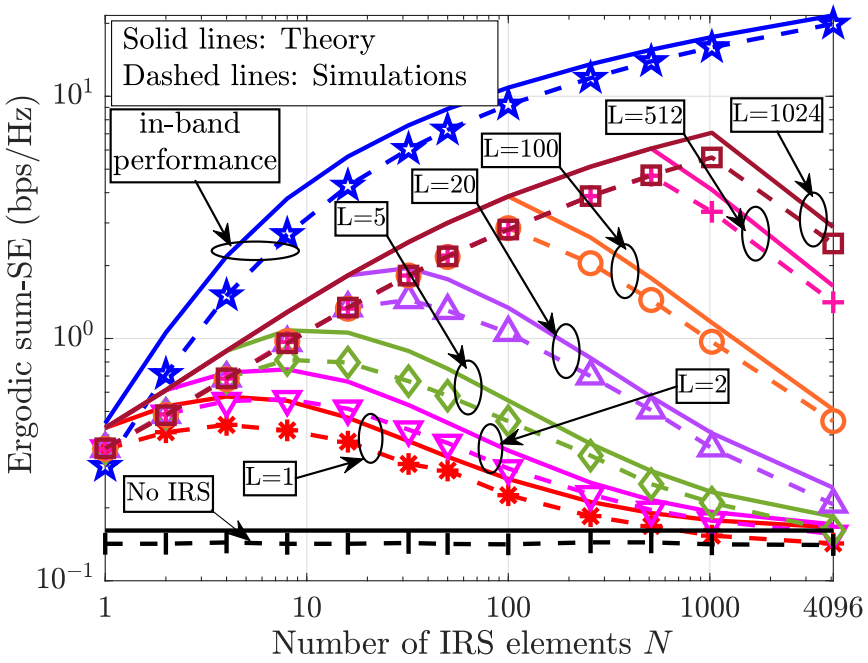

Figure 4.10: Ergodic sum-SE vs. N in LoS scenarios at $C_0\gamma = 150$ dB.

LoS scenario), the probability is L^2/N, supporting the fact that $\sqrt{N}$ paths are sufficient to obtain an OOB SE that log-linearly grows with the IRS elements. Finally, Fig. 4.15 compares the OOB performance in LoS and (L+)NLoS scenarios. For a fixed N, L, the performance is enhanced much faster in (L+)NLoS than in LoS scenarios, which is in line with our discussions.

4.6.c OOB performance with PF and MR schedulers

We now numerically illustrate the OOB performance enhancement that can be obtained using the PF and MR schedulers described in Sec. 4.5. We plot the OOB SE versus the number of OOB UEs Q in Fig. 4.16. Here, we compare the SE for RR, PF, and MR schedulers for different N. Using an MR scheduler, the OOB SE increases monotonically as $\mathcal{O}(\log(\log(Q)))$, in line with Lemma 4.3. Next, we consider the OOB SE using a PF scheduler. For $N = 4$, the SE increases with Q, and it converges to the SE that is achievable as though the IRS is also optimal to the OOB UEs under RR scheduling, in line with Lemma 4.2. Thus, for large Q, OOB UEs enjoy optimal beamforming IRS benefits without explicitly optimizing the IRS to them when the OOB operator uses a PF

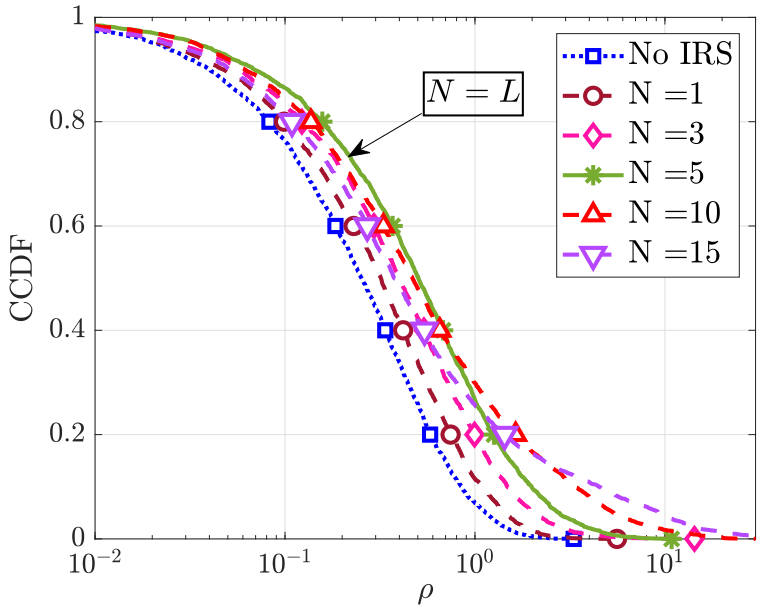

Figure 4.11: CCDF of OOB UE's channel gain $|h_q|^2$ as a function of N in LoS scenarios of the mmWave bands at $C_0\gamma = 150$ dB and $L = 5$.

scheduler. Even with $N = 16$ using a PF scheduler, a similar trend as in $N = 4$ is observed, except that the convergence rate to the optimal SE is now reduced. We observe this from the unequal gaps between the optimal SE and SE obtained by PF schedulers for $N = 4$ and 16, namely: $\Delta_{16} > \Delta_4$. This is because the degree of randomness increases with N, which requires the number of UEs to scale with N. We refer the reader to [127, Prop. 1] for more details on the required number of UEs for a target gap in the SE. Finally, the OOB SE using the RR scheduler is invariant to Q because it does not leverage multi-user diversity in the system.

In the final study of this section, we plot the OOB SE as a function of $\log_2(N)$ in Fig. 4.17 for different schedulers. First, we observe that the slope of the curve using the MR scheduler for both $Q = 10, 100$ is 1, which validates the $\mathcal{O}(\log(N))$ dependence of the SE as in Lemma 4.3. Similarly, the RR scheduler also scales as $\mathcal{O}(\log_2(N))$, in line with Theorem 4.1. On the other hand, the performance of the PF scheduler as a function of N crucially depends on the relative value of Q with respect to N. For smaller N, the OOB SNR scales with N^2, and as N increases, the OOB SNR scales as N^ϵ, where $\epsilon \leq 2$ (notice this in the decreasing values of slopes.) This happens because, as N increases, Q is not

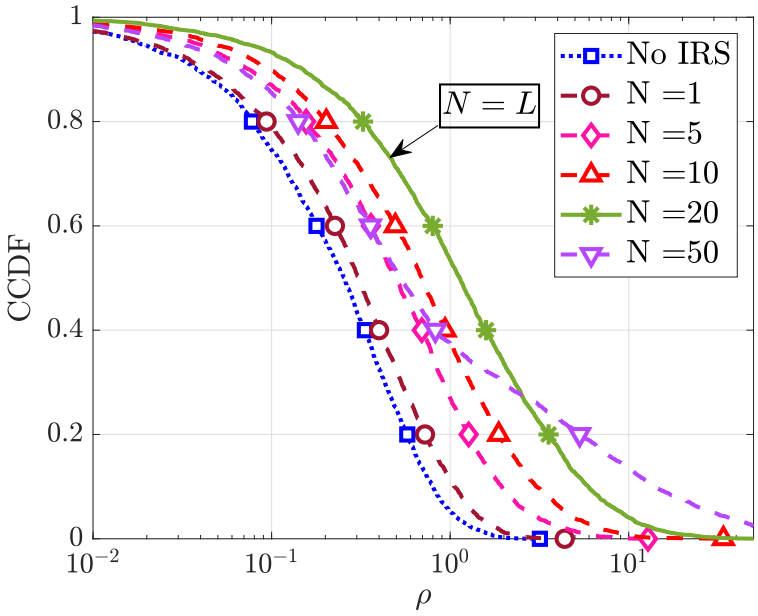

Figure 4.12: CCDF of OOB UE's channel gain $|h_q|^2$ as a function of N in LoS scenarios of the mmWave bands at $C_0\gamma = 150$ dB and $L = 20$.

large enough for the random IRS configuration to be near-optimal for at least one OOB UE at every point in time.

4.7 Conclusions and Future Work

In this chapter, we studied a fundamental issue in an IRS-aided system, namely, the effect of deploying an IRS on the average and instantaneous performance of an OOB operator who has no control over the IRS. Surprisingly, we found that while the IRS optimally serves the in-band UEs, it simultaneously, and at no additional cost, enhances the quality of the channels of the OOB UEs compared to the system without any IRS. This performance enhancement is due to the reception of multiple copies of the signal at the OOB UEs through the IRS. Although this is always true in the sub-6 GHz bands, the degree of enhancement in the mmWave communications is determined by the number of spatial paths in the OOB UE's channel. When the number of paths in the channel is at least the number of resolvable beams at the IRS, the gain is monotonic in the number of IRS elements, similar to sub-6 GHz bands, and is marginal otherwise. Further, we showed

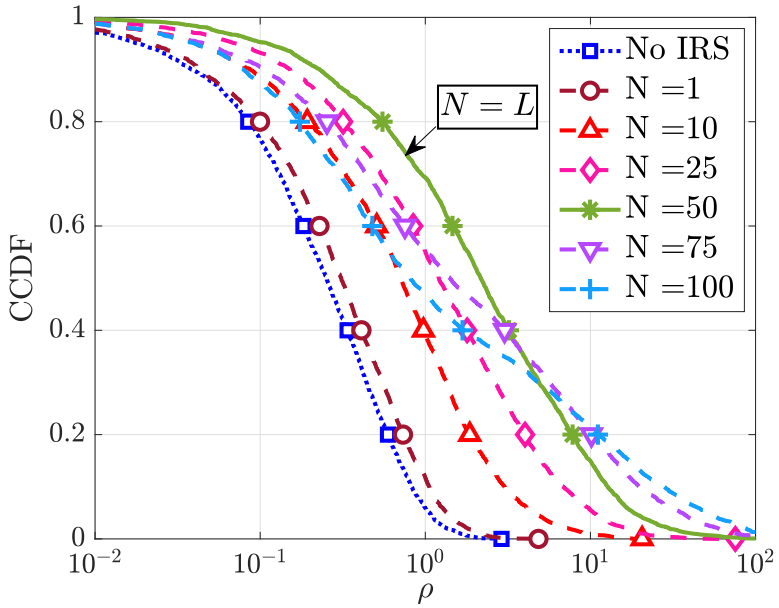

Figure 4.13: CCDF of OOB UE's channel gain $|h_q|^2$ as a function of N in LoS scenarios of the mmWave bands at $C_0\gamma = 150$ dB and $L = 50$.

that the systems where IRS is optimized to all the spatial paths of the in-band UE's channel outperform the ones where IRS is aligned only to the dominant path. This is due to the additional degrees of freedom offered by the IRS in the former, although it incurs additional BS-IRS signaling overhead at the in-band operator to configure the IRS optimally. Therefore, the deployment of an IRS benefits all the other existing network operators, albeit to a lesser extent than the operator that has control over the IRS phase configuration. Further, it is possible to obtain much better benefits at the OOB UEs by using an opportunistic scheduler at the OOB operator.

Future work can include the effect of multiple antennas at the BSs/UEs and study the diversity-multiplexing gain tradeoff at OOB UEs. Other practical considerations, like the non-availability of perfect channel state information, quantized IRS phase shift levels, frequency selectivity of channels, time & frequency offsets, near-field effects, etc., can be accounted for to provide more insights. Another interesting line of study is to analyze the impact of IRSs on the OOB performance in interference-limited scenarios such as multi-cell environments.

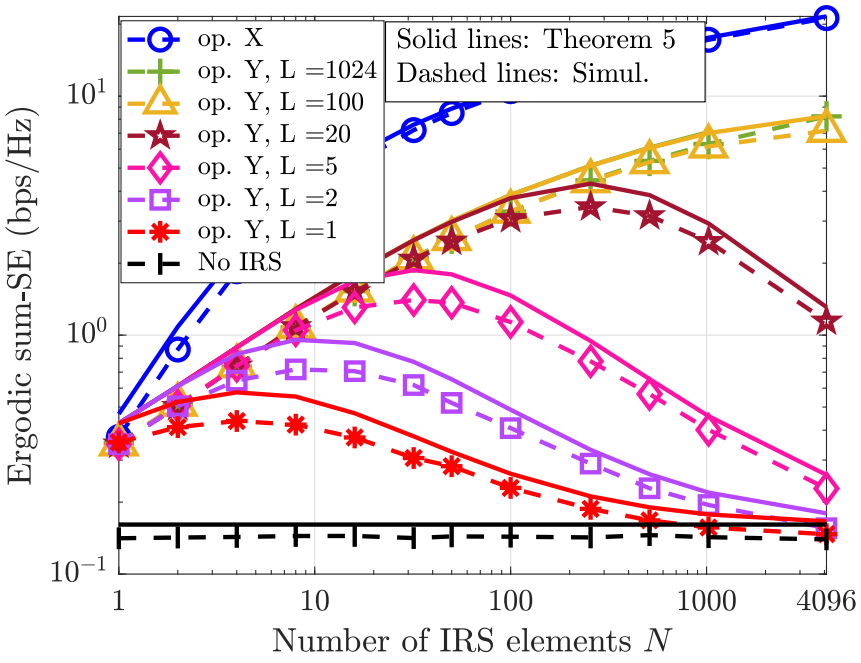

Figure 4.14: Ergodic sum-SE vs. N in (L+)NLoS scenarios. Theorem 4.5 is marked as "Theorem 5" in this plot.

Appendix 4.A Proof of Theorem 4.1

We compute the sum-SEs for both operators one by one below.

4.A.a Ergodic sum-SE of operator X

We first compute $\langle R_k^{(X)} \rangle$ for a given k. By Jensen's inequality, we obtain

$$\langle R_k^{(X)} \rangle \leq \log_2 \left(1 + \mathbb{E} \left[\left| \sum_{n=1}^{N} |f_n^X g_{k,n}| + |h_{d,k}| \right|^2 \right] \frac{P}{\sigma^2} \right). \tag{4.44}$$

We expand the expectation term as follows.

$$\begin{aligned} \left| \sum_{n=1}^{N} |f_n^X g_{k,n}| + |h_{d,k}| \right|^2 &= \sum_{n,m=1}^{N} |f_n^X||g_{k,n}||f_m^X||g_{k,m}| + |h_{d,k}|^2 + 2\sum_{n=1}^{N} |f_n^X||g_{k,n}||h_{d,k}| \\ &= \sum_{n=1}^{N} |f_n^X|^2 |g_{k,n}|^2 + |h_{d,k}|^2 + \sum_{\substack{n,m=1 \\ n \neq m}}^{N} |f_n^X||g_{k,n}||f_m^X||g_{k,m}| + 2\sum_{n=1}^{N} |f_n^X||g_{k,n}||h_{d,k}|. \end{aligned} \tag{4.45}$$

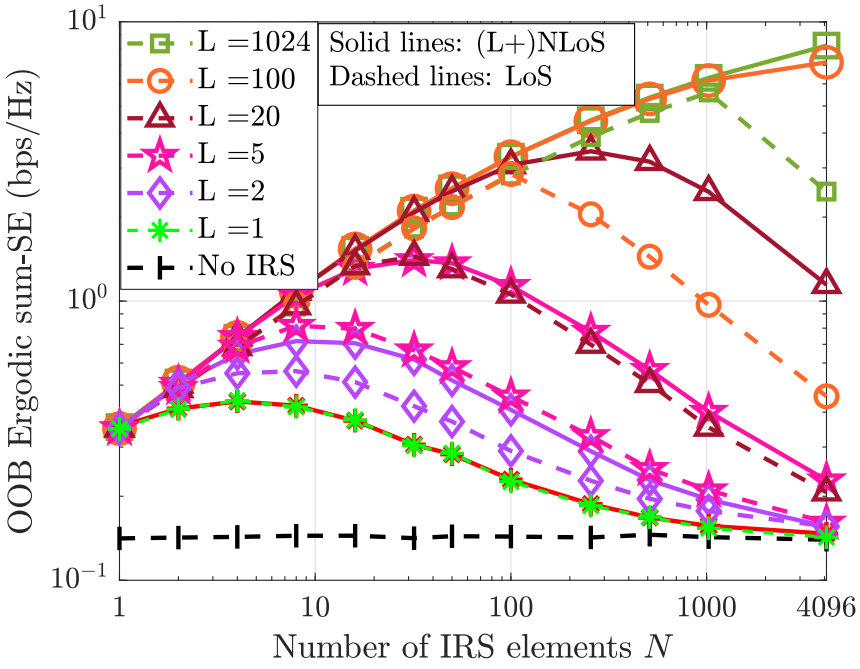

Figure 4.15: Comparison of the sum-SE in LoS and (L+)NLoS scenarios.

Under Rayleigh fading, $\mathbb{E}[|f_n^X|^2] = \beta_{\mathbf{f}^X}, \mathbb{E}[|g_{k,n}|^2] = \beta_{\mathbf{g},k}, \mathbb{E}[|h_{d,k}|^2] = \beta_{d,k}$, $\mathbb{E}[|f_n^X|] = \sqrt{\frac{\pi}{4}\beta_{\mathbf{f}^X}}$, $\mathbb{E}[|g_{k,n}|] = \sqrt{\frac{\pi}{4}\beta_{\mathbf{g},k}}, \mathbb{E}[|h_{d,k}|] = \sqrt{\frac{\pi}{4}\beta_{d,k}}, \forall k = 1,\ldots,K; n = 1,\ldots,N$. Further, all the random variables are independent. Taking the expectation in (4.45), and substituting for these values, we get

$$\mathbb{E}\left[\left|\sum_{n=1}^{N}|f_n^X g_{k,n}|+|h_{d,k}|\right|^2\right] = N^2\left(\frac{\pi^2}{16}\beta_{r,k}\right) + N\left(\beta_{r,k} - \frac{\pi^2}{16}\beta_{r,k} + \frac{\pi^{3/2}}{4}\sqrt{\beta_{d,k}\beta_{r,k}}\right) + \beta_{d,k}, \tag{4.46}$$

where $\beta_{r,k}$ is as defined in the statement of the theorem. Substituting (4.46) in (4.44), and plugging in the resulting expression in (4.14) yields (4.15), as desired.

4.A.b Ergodic sum-SE of operator Y

As above, from Jensen's inequality, we have

$$\langle R_q^{(Y)}\rangle \leq \log_2\left(1 + \mathbb{E}\left[\left|\sum_{n=1}^{N} f_n^Y g_{q,n} + h_{d,q}\right|^2\right]\frac{P}{\sigma^2}\right). \tag{4.47}$$

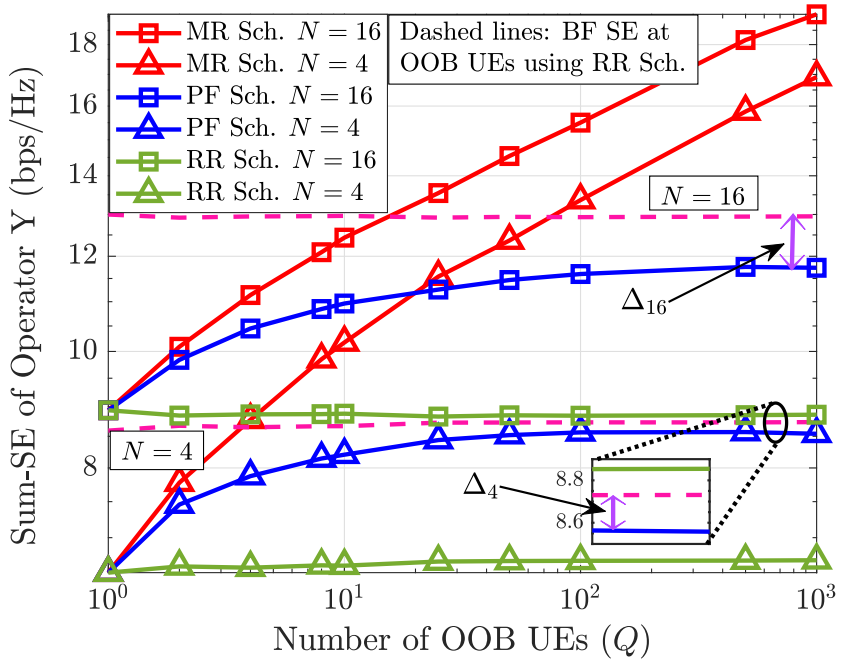

Figure 4.16: OOB SE versus Q for different schedulers.

Proceeding along the same lines, we get

$$\left|\sum_{n=1}^{N} f_n^Y g_{q,n} + h_{d,q}\right|^2 = \sum_{n=1}^{N} |f_n^Y|^2 |g_{q,n}|^2 + |h_{d,q}|^2 + \sum_{\substack{n,m=1 \\ n\neq m}}^{N} f_n^Y g_{q,n} f_m^{Y*} g_{q,m}^* + 2\Re\left(\sum_{n=1}^{N} f_n^Y g_{q,n} h_{d,q}^*\right). \tag{4.48}$$

Taking the expectation and simplifying,

$$\mathbb{E}\left[\left|\sum_{n=1}^{N} f_n^Y g_{q,n} + h_{d,q}\right|^2\right] = N\beta_{r,q} + \beta_{d,k}. \tag{4.49}$$

Substituting (4.49) in (4.47), and plugging in the resulting expression in (4.14) yields (4.16).

Appendix 4.B Proof of Theorem 4.2

We recognize that $\tilde{h}_{1,q} \triangleq |h_{1,q}|^2 \sim \exp(1/(N\beta_{r,q} + \beta_{d,q}))$, and $\tilde{h}_{2,q} \triangleq |h_{2,q}|^2 \sim \exp(1/\beta_{d,q})$. Now, $Z_N^{(Y)}$ is the difference between two exponential random variables. We first show that the correlation coefficient between $\tilde{h}_{1,q}$ and $\tilde{h}_{2,q}$ decays inversely with N. Recall that the correlation coefficient is defined $\rho_{12} \triangleq \mathbb{E}\left[(\tilde{h}_{1,q} - \mathbb{E}[\tilde{h}_{1,q}])(\tilde{h}_{2,q} - \mathbb{E}[\tilde{h}_{2,q}])\right] \Big/ \sigma_1\sigma_2$,

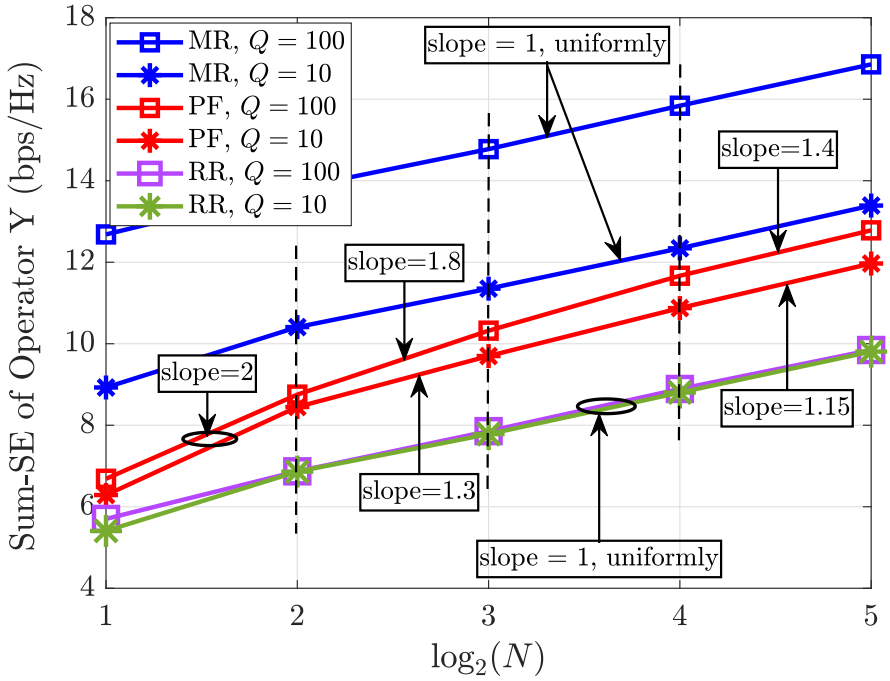

Figure 4.17: OOB SE versus $\log_2(N)$ for different schedulers.

where σ_1^2 and σ_2^2 are the variances of $\tilde{h}_{1,q}$ and $\tilde{h}_{2,q}$, respectively. We can verify that 1) $\mu_1 \triangleq \mathbb{E}[\tilde{h}_{1,q}] = N\beta_{r,q} + \beta_{d,q}$, and $\mu_2 \triangleq \mathbb{E}[\tilde{h}_{2,q}] = \beta_{d,q}$ 2) $\sigma_1^2 = (N\beta_{r,q} + \beta_{d,q})^2$, and $\sigma_2^2 = \beta_{d,q}^2$. Thus, we get $\rho_{12} = \left(\mathbb{E}\left[\tilde{h}_{1,q}\tilde{h}_{2,q}\right] - (N\beta_{r,q} + \beta_{d,q})\,\beta_{d,q}\right) \Big/ (N\beta_{r,q} + \beta_{d,q})\,\beta_{d,q}$. Using (4.18), it is easy to verify that $\mathbb{E}\left[\tilde{h}_{1,q}\tilde{h}_{2,q}\right] = N\beta_{r,q}\beta_{d,q} + 2\beta_{d,q}^2$. After simplification, we have

$$\rho_{12} = \frac{1}{(1 + N\,(\beta_{r,q}/\beta_{d,q}))}, \tag{4.50}$$

which decays inversely with N. We now use a result from [128, Eq. 4.24] which characterizes the distribution of the difference of two dependent and non-identically distributed chi-square random variables, and obtain the CDF of $Z_N^{(Y)}$ as

$$F_{Z_N^{(Y)}}(z) = \begin{cases} \dfrac{8}{\mu_1\mu_2(1-\rho_{12}^2)\gamma\alpha^-} e^{\left(\frac{\alpha^- z}{4}\right)}, & \text{if } z < 0, \\ 1 - \dfrac{8}{\mu_1\mu_2(1-\rho_{12}^2)\gamma\alpha^+} e^{-\left(\frac{\alpha^+ z}{4}\right)}, & \text{if } z \geq 0, \end{cases} \tag{4.51}$$

where

$$\gamma = \frac{2\sqrt{(\mu_2 - \mu_1)^2 + 4\mu_1\mu_2(1-\rho_{12}^2)}}{\mu_1\mu_2(1-\rho_{12}^2)}; \alpha^{\pm} = \gamma \pm \frac{2\,(\mu_2 - \mu_1)}{\mu_1\mu_2(1-\rho_{12}^2)}. \tag{4.52}$$

For large N, using (4.50) to let $\rho_{12} \to 0$ in (4.51), (4.52), and recognizing that $\forall z$, $\bar{F}_{Z_N^{(Y)}}(z) = 1 - F_{Z_N^{(Y)}}(z)$, we obtain

$$\bar{F}_{Z_N^{(Y)}}(z) = \begin{cases} 1 - \dfrac{\mu_2}{\mu_1 + \mu_2} e^{\frac{z}{\mu_2}}, & \text{if } z < 0, \\ \dfrac{\mu_1}{\mu_1 + \mu_2} e^{-\frac{z}{\mu_1}}, & \text{if } z \geq 0, \end{cases} \tag{4.53}$$

Substituting for μ_1 and μ_2 into (4.53) completes the proof. ■

Appendix 4.C Proof of the decay rate of outage probability and SNR offset at in-band UEs

Below, we compute the decay rate of the outage probability and SNR offset for the in-band UEs (as in Theorem 4.2).

4.C.a Outage Probability

Let $X \triangleq \left| |h_d| + \sum_n |f_n||g_n| \right|^2$ be the channel gain at an arbitrary in-band UE (dropping index k). Then, the outage probability is

$$P_{\text{out}}^{\rho} = \Pr(X \leq \rho). \tag{4.54}$$

Since the true distribution of X is complicated due to multiple products and summations, we find an upper bound on P_{out}^{ρ} as

$$X = \left| |h_d| + \sum_n |f_n||g_n| \right|^2 \geq \left| \sum_n |f_n||g_n| \right|^2 \triangleq Y, \quad \text{almost surely.}$$

As a result, we have

$$P_{\text{out}}^{\rho} = \Pr(X \leq \rho) \leq \Pr\left(\left| \sum_n |f_n||g_n| \right|^2 \leq \rho \right). \tag{4.55}$$

Now by Central Limit Theorem (CLT) [129], we have

$$Z \triangleq \sum_n |f_n||g_n| \longrightarrow \mathcal{N}\left(N\frac{\pi}{4}\sqrt{\beta_r}, N\left(1-\frac{\pi^2}{16}\right)\beta_r\right). \tag{4.56}$$

Using (4.56), we can simplify (4.55) as

$$\begin{aligned} P_{\text{out}}^{\rho} &\overset{(a)}{\leq} 1 - Q\left(\frac{\sqrt{\rho}}{c_1\sqrt{N}} - c_2\sqrt{N}\right) - Q\left(\frac{\sqrt{\rho}}{c_1\sqrt{N}} + c_2\sqrt{N}\right) \\ &\overset{(b)}{\approx} 2Q\left(c_2\sqrt{N}\right), \end{aligned} \tag{4.57}$$

where, in (a), $c_1 \triangleq \sqrt{\left(1-\frac{\pi^2}{16}\right)\beta_r}$ and $c_2 \triangleq \frac{\pi}{\sqrt{16-\pi^2}}$, and (b) follows as for fixed ρ, $\frac{\sqrt{\rho}}{c_1\sqrt{N}} \to 0$ for large N. Now, by applying the Chernoff bound to $Q(\cdot)$ in (4.57), we see that $Q(c_2\sqrt{N}) \to 0$ at the rate of $\mathcal{O}(e^{-N})$. Hence, the outage probability in (4.54) also decays at least as fast as $\mathcal{O}(e^{-N})$.

4.C.b CCDF of the SNR offset

Let the channel gain with and without an IRS be $h_1 \triangleq \left||h_d| + \sum_n |f_n||g_n|\right|^2$ and $h_2 \triangleq |h_d|^2$. To compute the CCDF of $O \triangleq h_1 - h_2$, using (4.56), we notice

$$\bar{F}_O(\rho) \triangleq \Pr\left(h_1 - h_2 \geq \rho\right) \geq \Pr\Bigg(\underbrace{|Z|^2 - |h_d|^2}_{\triangleq O'} \geq \rho\Bigg). \tag{4.58}$$

Now, we can simplify the lower bound of (4.58) as

$$\Pr\left(|Z|^2 - |h_d|^2 \leq \rho\right) = \mathbb{E}_Z\left[\Pr\left(|z|^2 - |h_d|^2 \leq \rho | Z = z\right)\right] \tag{4.59}$$

$$= \mathbb{E}_Z\left[\Pr\left(|h_d|^2 \geq |z|^2 - \rho | Z = z\right)\right] \overset{(a)}{=} \mathbb{E}_Z\left[e^{-\left(\frac{|z|^2-\rho}{\beta_d}\right)}\right] \tag{4.60}$$

$$= \sqrt{\frac{8}{N\pi(16-\pi^2)\beta_r}} \int_{-\infty}^{\infty} e^{-\left(\frac{|z|^2-\rho}{\beta_d} + \frac{\left(z - N\frac{\pi}{4}\sqrt{\beta_r}\right)^2}{2N\left(1-\frac{\pi^2}{16}\right)\beta_r}\right)} \mathrm{d}z, \tag{4.61}$$

where in (a), we used the property of the exponentially distributed random variable $|h_d|^2$. To compute the above integral, we define $\alpha \triangleq 2N\left(1-\frac{\pi^2}{16}\right)\beta_r$, $\eta \triangleq N\frac{\pi}{4}\sqrt{\beta_r}$.

Then, by using standard integral solvers, we can show that

$$\Pr\left(|Z|^2-|h_d|^2\geq \rho\right) = 1 - \frac{\sqrt{\beta_d}}{\sqrt{\beta_d+\alpha}} e^{-\left(\frac{\beta_d\eta^2-(\beta_d+\alpha)\rho}{\beta_d^2+\alpha\beta_d}\right)}. \tag{4.62}$$

The above probability can be shown to be proportional to

$$1-(1/\sqrt{N})\times e^{-N}\times e^{\left(\frac{1/N}{1/N}\right)} \sim 1-\mathcal{O}\left(e^{-N}\right). \tag{4.63}$$

Thus, the lower bound grows to 1 exponentially in N, and hence the CCDF of the random variable O also grows to 1 at least as fast as the decay rate of e^{-N} to 0. ■

Appendix 4.D Proof of Theorem 4.3

We derive the SEs of both operators separately below.

4.D.a Ergodic sum-SE of operator X

Let the average SE seen by UE-k be $\langle S_{k,1}^{(X)}\rangle$. Then the ergodic sum-SE of operator X is $\bar{S}_1^{(X)} = \frac{1}{K}\sum_{k=1}^{K}\langle S_{k,1}^{(X)}\rangle$. By Jensen's inequality,

$$\langle S_{k,1}^{(X)}\rangle \leq \log_2\left(1+\mathbb{E}\left[|h_k|^2\right]\frac{P}{\sigma^2}\right). \tag{4.64}$$

We recognize that

$$|h_k|^2 = \left|N\gamma_{X,k}\dot{\mathbf{a}}_N^H(\omega_{X,k}^1)\boldsymbol{\theta}^{\text{opt}} + h_{d,k}\right|^2 \tag{4.65}$$

$$\overset{(a)}{=} \left|h_{d,k} + N^2\frac{h_{d,k}\left|\gamma_{X,k}\right|^2}{|h_{d,k}\gamma_{X,k}|}\times\dot{\mathbf{a}}_N^H(\omega_{X,k}^1)\dot{\mathbf{a}}_N(\omega_{X,k}^1)\right|^2, \tag{4.66}$$

where (a) is due to (4.27). Further, using $\dot{\mathbf{a}}_N^H(\omega_{X,k}^1)\dot{\mathbf{a}}_N(\omega_{X,k}^1) = \frac{1}{N}$, we can compute $\mathbb{E}\left[|h_k|^2\right] = \mathbb{E}\left[||h_{d,k}| + N\left|\gamma_{X,k}\right||^2\right] = \mathbb{E}\left[|h_{d,k}|^2\right] + N^2\mathbb{E}\left[|\gamma_{X,k}|^2\right] + 2N\mathbb{E}\left[|h_{d,k}|\left|\gamma_{X,k}\right|\right]$. Using the results from Sec. 4.2.b, this can be simplified as

$$\mathbb{E}\left[|h_k|^2\right] = N^2\beta_{r,k} + N\left(\frac{\pi^{3/2}}{4}\right)\sqrt{\beta_{r,k}\beta_{d,k}} + \beta_{d,k}. \tag{4.67}$$

Substituting the above in (4.64), and plugging it into the expression for $\bar{S}_1^{(X)}$ yields (4.28).

4.D.b Ergodic sum-SE of operator Y

Recall that the ergodic sum-SE of operator Y is $\bar{S}_1^{(Y)} = \frac{1}{Q}\sum_{q=1}^{Q}\langle S_{q,1}^{(Y)}\rangle$. Then, the channel seen by an arbitrary OOB UE, say UE-q, can be derived in a similar manner as (4.25) and is given by

$$h_q = h_{d,q} + \frac{N}{\sqrt{L}}\sum_{l=1}^{L}\gamma_{l,Y}^{(1)}\gamma_{l,q}^{(2)}\dot{\mathbf{a}}_N^H(\omega_{Y,q}^l)\boldsymbol{\theta}^{\text{opt}}, \tag{4.68}$$

where $\boldsymbol{\theta}^{\text{opt}}$ is given by (4.27), and $\gamma_{l,Y}^{(1)}, \gamma_{l,q}^{(2)}$ denote the channel gains of the paths between BS-IRS, and IRS-UE, respectively, corresponding to the lth cascaded path. Then we have

$$\begin{aligned} h_q &= h_{d,q} + \frac{N^2}{\sqrt{L}}\sum_{l=1}^{L}\gamma_{l,Y}^{(1)}\gamma_{l,q}^{(2)}\frac{h_{d,k}\gamma_{X,k}^*}{|h_{d,k}\gamma_{X,k}|}\dot{\mathbf{a}}_N^H(\omega_{Y,q}^l)\dot{\mathbf{a}}_N(\omega_{X,k}^1) \\ &= h_{d,q} + \frac{N^2}{\sqrt{L}}\sum_{l=1}^{L}\gamma_{l,Y}^{(1)}\gamma_{l,q}^{(2)}\frac{e^{j\angle h_{d,k}}}{e^{j\angle\gamma_{X,k}}}\dot{\mathbf{a}}_N^H(\omega_{Y,q}^l)\dot{\mathbf{a}}_N(\omega_{X,k}^1) \\ &\overset{d}{=} h_{d,q} + \frac{N^2}{\sqrt{L}}\sum_{l=1}^{L}\gamma_{l,Y}^{(1)}\gamma_{l,q}^{(2)}\dot{\mathbf{a}}_N^H(\omega_{Y,q}^l)\dot{\mathbf{a}}_N(\omega_{X,k}^1), \end{aligned} \tag{4.69}$$

where, in the last step, we used the fact that the product term $\gamma_{l,Y}^{(1)}\gamma_{l,q}^{(2)}$ is circularly symmetric. We also have

$$\langle S_{q,1}^{(Y)}\rangle \triangleq \mathbb{E}\left[S_{q,1}^{(Y)}\right] = \mathbb{E}\left[\log_2\left(1+|h_q|^2\frac{P}{\sigma^2}\right)\right]. \tag{4.70}$$

Consider $L < N$. Now, let $\mathcal{E}_1$ be the event that one of the L angles of the OOB channel "matches" with the IRS angle, and $\mathcal{E}_0$ be the event that none of the L angles of the OOB channel match with the IRS angle. Then, we can write (4.70) as

$$\langle S_{q,1}^{(Y)}\rangle \overset{(a)}{=} \sum_{i=0}^{1}\mathbb{E}\left[S_{q,1}^{(Y)}\mathbb{1}_{\{\mathcal{E}_i\}}\right] \overset{(b)}{=} \sum_{i=0}^{1}\mathbb{E}\left[S_{q,1}^{(Y)}\middle|\mathcal{E}_i\right]\mathsf{Pr}(\mathcal{E}_i), \tag{4.71}$$

where $\mathbb{1}_{\{\mathcal{E}_i\}}$ is the indicator for the occurrence of event $\mathcal{E}_i$, (a) is because $\mathcal{E}_0$ and $\mathcal{E}_1$ are mutually exclusive and exhaustive; (b) is due to the law of iterated expectations. Also, from (4.7), and flat-top directivity of the IRS, $\mathsf{Pr}(\mathcal{E}_1) = L/N$, and $\mathsf{Pr}(\mathcal{E}_0) = (1 - L/N)$.

Then from (4.8), and Jensen's inequality, we have

$$\mathbb{E}\left[S_{q,1}^{(Y)}\middle|\mathcal{E}_1\right] \leq \log_2\left(1+\mathbb{E}\left[\left|h_{d,q}+\frac{N}{\sqrt{L}}\gamma_{l^*,Y}^{(1)}\gamma_{l^*,q}^{(2)}\right|^2\right]\frac{P}{\sigma^2}\right), \tag{4.72}$$

$$\text{and,} \qquad \mathbb{E}\left[S_{q,1}^{(Y)}\middle|\mathcal{E}_0\right] \leq \log_2\left(1+\mathbb{E}\left[|h_{d,q}|^2\right]\frac{P}{\sigma^2}\right), \tag{4.73}$$

where $l^* = \arg_l\left\{\dot{\mathbf{a}}_N^H(\omega_{Y,q}^l)\dot{\mathbf{a}}_N(\omega_{X,k}^1) = 1/N\right\}$. We can show that (similar to Sec. 4.A.b), $\mathbb{E}\left[|h_q|^2\middle|\mathcal{E}_1\right] = \left(\frac{N^2}{L}\beta_{r,q}+\beta_{d,q}\right)$, and $\mathbb{E}\left[|h_q|^2\middle|\mathcal{E}_0\right] = \beta_{d,q}$. Collecting all the terms and substituting in (4.70) and using the expression for $\bar{S}_1^{(Y)}$ yields (4.29). Now, when $L \geq N$, since an N-element IRS can steer at most N resolvable beams, some of the paths will be clustered together, and the above analysis holds by replacing L with N. We cover both cases by $\bar{L} = \min\{L, N\}$ in (4.29).

Appendix 4.E Proof of Theorem 4.4

Assume $L < N$. From (4.69), we compute probability $P =$

$$\mathsf{Pr}\left(\left|h_{d,q}+\frac{N^2}{\sqrt{L}}\sum_{l=1}^{L}\gamma_{l,Y}^{(1)}\gamma_{l,q}^{(2)}\dot{\mathbf{a}}_N^H(\omega_{Y,q}^l)\dot{\mathbf{a}}_N(\omega_{X,k}^1)\right|^2 < \rho\right). \tag{4.74}$$

By the total law of probability, we obtain $P = \mathsf{Pr}(|h_q|^2 < \rho|\mathcal{E}_1)\mathsf{Pr}(\mathcal{E}_1)+\mathsf{Pr}(|h_q|^2 < \rho|\mathcal{E}_0)\mathsf{Pr}(\mathcal{E}_0)$, where $\mathcal{E}_0$ and $\mathcal{E}_1$ are as defined in Sec. 4.D.b. Thus, we can simplify P as

$$\mathsf{Pr}\left(\left|h_{d,q}+\frac{N}{\sqrt{L}}\gamma_{l^*,Y}^{(1)}\gamma_{l^*,q}^{(2)}\right|^2 < \rho\right)\mathsf{Pr}(\mathcal{E}_1) + \mathsf{Pr}\left(|h_{d,q}|^2 < \rho\right)\mathsf{Pr}(\mathcal{E}_0). \tag{4.75}$$

Let $\left\{\tilde{\gamma}_{l^*,Y}^{(1)}, \tilde{\gamma}_{l^*,q}^{(2)}\right\} \triangleq \sqrt{\frac{N}{\sqrt{L}}}\left\{\gamma_{l^*,Y}^{(1)}, \gamma_{l^*,q}^{(2)}\right\}$. Then, by [130, Eq. 17],

$$\mathsf{Pr}\left(\left|h_{d,q}+\tilde{\gamma}_{l^*,Y}^{(1)}\tilde{\gamma}_{l^*,q}^{(2)}\right|^2 < \rho\right) = 1-\frac{Le^{\frac{L\beta_{d,q}}{N^2\beta_{r,q}}}}{N^2\beta_{r,q}}\mathcal{I}_0\left(\rho;\beta_{d,q},\frac{N^2}{L}\beta_{r,q}\right). \tag{4.76}$$

Also, $\mathsf{Pr}(|h_{d,q}|^2 < \rho) = 1-e^{-\rho/\beta_{d,q}}$. Collecting these together completes the proof of (4.30) when $L < N$. Similarly, we can prove for $L \geq N$. To obtain (4.31), it suffices to show that

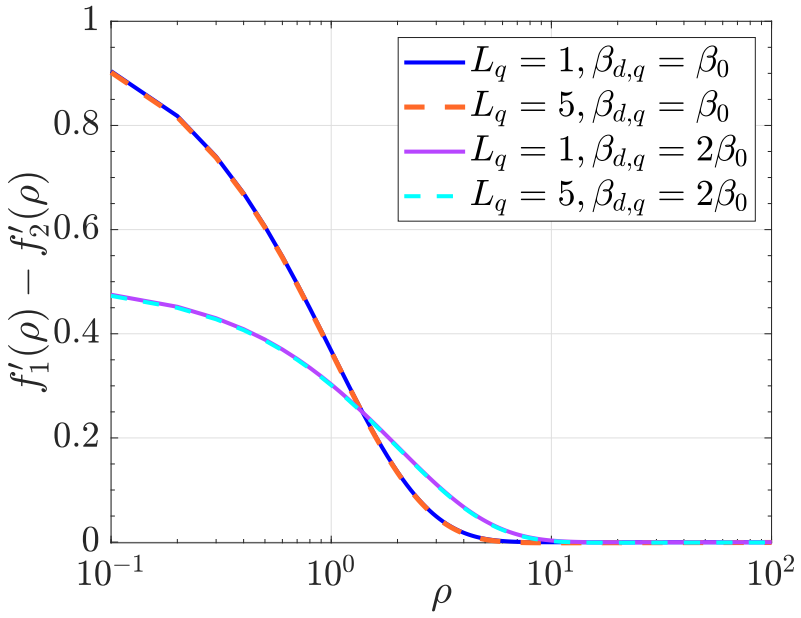

Figure 4.18: Graph of $f'(\rho)$ vs. ρ with $N = 128$.

$$\forall L \lesseqgtr N, \quad \mathsf{Pr}(G_1 > \rho) - \mathsf{Pr}(G_0 > \rho) \geq 0 \overset{(a)}{\iff} \frac{\bar{L}}{N}\left(\frac{\bar{L}e^{\frac{\bar{L}\beta_{d,q}}{N^2\beta_{r,q}}}}{N^2\beta_{r,q}}\mathcal{I}_0\left(\rho; \beta_{d,q}, \frac{N^2}{\bar{L}}\beta_{r,q}\right) - e^{-\rho/\beta_{d,q}}\right) \geq 0, \quad (4.77)$$

where (a) is due to (4.30). From [131], we know that $\mathcal{I}_0(\cdot)$ is related to the generalized upper incomplete Gamma function $\Gamma(\alpha, x; b)$ for appropriate α, x, b, and hence we can simplify

$$\mathcal{I}_0\left(\rho; \beta_{d,q}, \frac{N^2}{\bar{L}}\beta_{r,q}\right) = \frac{N^2\beta_{r,q}}{\bar{L}}\Gamma\left(1, \frac{\bar{L}\beta_{d,q}}{N^2\beta_{r,q}}; \frac{\bar{L}\rho}{N^2\beta_{r,q}}\right). \quad (4.78)$$

Then, it suffices to show that

$$f(\rho) \triangleq \underbrace{e^{\frac{\bar{L}\beta_{d,q}}{N^2\beta_{r,q}}}\Gamma\left(1, \frac{\bar{L}\beta_{d,q}}{N^2\beta_{r,q}}; \frac{\bar{L}\rho}{N^2\beta_{r,q}}\right)}_{\triangleq f_1(\rho)} - \underbrace{e^{-\rho/\beta_{d,q}}}_{\triangleq f_2(\rho)} \geq 0. \quad (4.79)$$

We first prove a few properties of $f(\rho)$. *1)* $f(0) = 0$: Clearly, $f_2(0) = 1$. Now, $f_1(0) = e^{\frac{\bar{L}\beta_{d,q}}{N^2\beta_{r,q}}}\Gamma\left(1, \frac{\bar{L}\beta_{d,q}}{N^2\beta_{r,q}}; 0\right)$. But, $\Gamma(1, x; 0) = \Gamma(1, x)$ where $\Gamma(\alpha, x)$ is the upper incomplete Gamma function. Hence, $f_1(0) = e^{\frac{\bar{L}\beta_{d,q}}{N^2\beta_{r,q}}}\Gamma\left(1, \frac{\bar{L}\beta_{d,q}}{N^2\beta_{r,q}}\right)$. But from [132, Eq. 8.4.5], $\Gamma(1, x) = e^{-x}$. Thus, $f_1(0) = 1$ and hence $f(0) = f_1(0) - f_2(0) = 0$. *2)* $f(\rho)$ *is non-decreasing*:

From [133], $\partial\Gamma(\alpha,x;b)/\partial b = -\Gamma(\alpha-1,x;b)$ and thus, $f_1'(\rho) = -e^{\frac{\bar{L}\beta_{d,q}}{N^2\beta_{r,q}}}\Gamma\left(0, \frac{\bar{L}\beta_{d,q}}{N^2\beta_{r,q}}; \frac{\bar{L}\rho}{N^2\beta_{r,q}}\right)$.

Further, for practical values of the system parameters, $\bar{L}\beta_{d,q}/N^2\beta_{r,q} \leq 1$, and thus we can approximate $f_1'(\rho) \approx -2e^{\frac{\bar{L}\beta_{d,q}}{N^2\beta_{r,q}}} K_0\left(\frac{2}{N}\sqrt{\frac{\bar{L}\rho}{\beta_{r,q}}}\right)$, where $K_0(x)$ is the zeroth-order modified Bessel function of the second kind. Further, $f_2'(\rho) = -\left(1/d\right)e^{-\frac{\rho}{d}}$. Hence, we can show that $f'(\rho) = f_1'(\rho) - f_2'(\rho) \geq 0\ \forall \rho \in \mathbb{R}^+$ (see Fig. 4.18). Finally, since $f(\rho)$ is non-decreasing, $f(\rho) \geq f(0) = 0$. ■

Appendix 4.F Proof of Lemma 4.1

Using (4.34), we simplify $\rho_{\nu,\theta} = N\mathbb{E}\left[\left|\dot{\mathbf{a}}^H(\nu)\boldsymbol{\theta}^{\text{opt}}\right|\right]$ as

$$
\begin{aligned}
&= \mathbb{E}\left[\left|\sum_{n=1}^{N} e^{j\pi(n-1)\nu} \frac{\sum_{l=1}^{L} \gamma_{l,X}^{(1)*}\gamma_{l,k}^{(2)*} e^{-j(n-1)\pi\omega_{X,k}^l}}{\left|\sum_{l=1}^{L} \gamma_{l,X}^{(1)*}\gamma_{l,k}^{(2)*} e^{-j(n-1)\pi\omega_{X,k}^l}\right|}\right|\right] \\
&\overset{(a)}{\geq} \frac{1}{\sqrt{L}}\mathbb{E}\left[\frac{1}{\|\mathbf{h}_c\|_2}\left|\sum_{n=1}^{N} e^{j\pi(n-1)\nu}\sum_{l=1}^{L} \gamma_{l,X}^{(1)*}\gamma_{l,k}^{(2)*} e^{-j(n-1)\pi\omega_{X,k}^l}\right|\right] \\
&\overset{(b)}{=} \frac{1}{\sqrt{L}}\mathbb{E}\left[\frac{1}{\|\mathbf{h}_c\|_2}\left|\sum_{l=1}^{L} \gamma_{l,X}^{(1)*}\gamma_{l,k}^{(2)*}\sum_{n=1}^{N} e^{j\pi(n-1)(\nu-\omega_{X,k}^l)}\right|\right] \\
&= \frac{1}{\sqrt{L}}\mathbb{E}\left[\frac{1}{\|\mathbf{h}_c\|_2}\left|\sum_{l=1}^{L} \gamma_{l,X}^{(1)*}\gamma_{l,k}^{(2)*}\frac{e^{jN\frac{\pi}{2}(\nu-\omega_{X,k}^l)}}{e^{j\frac{\pi}{2}(\nu-\omega_{X,k}^l)}} \times \frac{\sin\left(0.5N\pi(\nu-\omega_{X,k}^l)\right)}{\sin\left(0.5\pi(\nu-\omega_{X,k}^l)\right)}\right|\right],
\end{aligned}
\tag{4.80}
$$

where $\mathbf{h}_c \triangleq [\gamma_{1,X}^{(1)}\gamma_{1,k}^{(2)}, \ldots, \gamma_{L,X}^{(1)}\gamma_{L,k}^{(2)}]^T$. Also, (a) is because $\left|\sum_{l=1}^{L} \gamma_{l,X}^{(1)*}\gamma_{l,k}^{(2)*} e^{-j(n-1)\pi\omega_{X,k}^l}\right| \leq \sqrt{L\sum_{l=1}^{L}|\gamma_{l,X}^{(1)}\gamma_{l,k}^{(2)}|^2}$ (the Cauchy-Schwarz inequality), and (b) is obtained by changing the order of summation. We recognize that

$$
\frac{\sin\left(0.5N\pi(\nu-\omega_{X,k}^l)\right)}{\sin\left(0.5\pi(\nu-\omega_{X,k}^l)\right)} = F_N(\nu-\omega_{X,k}^l),
\tag{4.81}
$$

where $F_N(\cdot)$ is the *Fejér Kernel* given by

$$
F_N(x) = \begin{cases} N + o(N), & \text{if } \ x = 0, \\ o(N), & \text{if } \ x = \pm\frac{k}{N}, k \in \mathbb{N}. \end{cases}
\tag{4.82}
$$

As a consequence, we have

$$F_N(\nu-\omega_{X,k}^l)=\begin{cases}N+o(N), & \text{if } \nu\in\left\{\omega_{X,k}^1,\ldots,\omega_{X,k}^L\right\},\\ o(N), & \text{if } \nu\in\mathbf{\Phi}\setminus\left\{\omega_{X,k}^1,\ldots,\omega_{X,k}^L\right\}.\end{cases} \tag{4.83}$$

Thus, when $\nu\in\mathbf{\Phi}\setminus\left\{\omega_{X,k}^1,\omega_{X,k}^2,\ldots,\omega_{X,k}^L\right\}$, $\rho_{\nu,\theta}\overset{N\to\infty}{\longrightarrow}0$; and when $\nu\in\left\{\omega_{X,k}^1,\omega_{X,k}^2,\ldots,\omega_{X,k}^L\right\}$, we have $\rho_{\nu,\theta}\geq\frac{N}{\sqrt{L}}\times\mathbb{E}\left[\frac{|h_{l^*}|}{\|\mathbf{h}_c\|_2}\right]$, implying $\rho_{\nu,\theta}=\Omega\left(\frac{N}{\sqrt{L}}\right)+o(N)$. ■

Appendix 4.G Proof of Theorem 4.5

We derive the SEs of both operators separately below.

4.G.a Ergodic sum-SE of operator X

As before, we first compute the ergodic SE of UE-k, $\langle S_{k,L}^{(X)}\rangle$, and then evaluate the ergodic sum-SE of operator X. Using (4.32) and (4.34), the ergodic SE of UE-k is bounded by

$$\langle S_{k,L}^{(X)}\rangle\leq\log_2\left(1+\mathbb{E}\left[\left||h_{d,k}|+\frac{1}{\sqrt{L}}\sum_{n=1}^{N}\left|\sum_{l=1}^{L}\gamma_{l,X}^{(1)}\gamma_{l,K}^{(2)}e^{j\pi(n-1)\omega_{X,k}^l}\right|\right|^2\right]\frac{P}{\sigma^2}\right). \tag{4.84}$$

Using the fact that the distribution of $\gamma_{l,X}^{(1)}\gamma_{l,K}^{(2)}$ is circularly symmetric, we can rewrite the inner term as

$$\mathbb{E}\left[\left||h_{d,k}|+\frac{N}{\sqrt{L}}\left|\sum_{l=1}^{L}\gamma_{l,X}^{(1)}\gamma_{l,K}^{(2)}\right|\right|^2\right]=\mathbb{E}\left[|h_{d,k}|^2+\frac{N^2}{L}\left|\sum_{l=1}^{L}\gamma_{l,X}^{(1)}\gamma_{l,K}^{(2)}\right|^2+\frac{2N}{\sqrt{L}}|h_{d,k}|\left|\sum_{l=1}^{L}\gamma_{l,X}^{(1)}\gamma_{l,K}^{(2)}\right|\right]. \tag{4.85}$$

Term I: It is straightforward to see that $\mathbb{E}[|h_{d,k}|^2]=\beta_{d,k}$.

Term II: Finally, we can write

$$\mathbb{E}\left[\left|\sum_{l=1}^{L}\gamma_{l,X}^{(1)}\gamma_{l,K}^{(2)}\right|^2\right]=\mathbb{E}\left[\sum_{l=1}^{L}\left|\gamma_{l,X}^{(1)}\gamma_{l,K}^{(2)}\right|^2\right]+\mathbb{E}\left[\sum_{l,\ell=1;l\neq\ell}^{L}\gamma_{l,X}^{(1)}\gamma_{l,K}^{(2)}\gamma_{\ell,X}^{(1)*}\gamma_{\ell,K}^{(2)*}\right]\overset{(a)}{=}L\beta_{r,k}, \tag{4.86}$$

where (a) is due to the zero-mean and independence of $\left\{\gamma_{l,X}^{(1)}, \gamma_{l,K}^{(2)}\right\}_l$ across the paths.

Term III: We have the following sequence of relations

$$\mathbb{E}\left\{|h_{d,k}|\left|\sum_{l=1}^{L}\gamma_{l,X}^{(1)}\gamma_{l,K}^{(2)}\right|\right\} \overset{(a)}{\leq} \mathbb{E}|h_{d,k}|\sqrt{\mathbb{E}\left[\left|\sum_{l=1}^{L}\gamma_{l,X}^{(1)}\gamma_{l,K}^{(2)}\right|^2\right]} = \frac{1}{2}\sqrt{\pi\beta_{d,k}}\cdot\sqrt{L\beta_{r,k}},$$

where (a) follows by using the independence of $h_{d,k}$ and $\sum_{l=1}^{L}\gamma_{l,X}^{(1)}\gamma_{l,K}^{(2)}$, followed by the Jensen's inequality. Collecting all the terms yields (4.36).

4.G.b Ergodic sum-SE of operator Y

Consider the case $L < N$. As above, the channel seen at the UE-q is

$$h_q = h_{d,q} + \frac{N}{\sqrt{L}}\sum_{l=1}^{L}\gamma_{l,Y}^{(1)}\gamma_{l,q}^{(2)}\dot{\mathbf{a}}_N^H(\omega_{Y,q}^l)\boldsymbol{\theta}, \tag{4.87}$$

where $\boldsymbol{\theta}$ is optimized by operator-X and is given by (4.34). The IRS vector aligns along L directions of $\boldsymbol{\Phi}$, while the OOB UE's channel is oriented along L directions independent of the IRS. We let the random variable X denote the instantaneous SE at UE-q, and Y denotes the number of matching (spatial) paths between the UE-q's channel and the IRS response. Clearly, the possible support of Y is the set of integers from 0 to L. We now compute $\langle S_{q,L}^{(Y)}\rangle = \mathbb{E}[X]$ as

$$\mathbb{E}[X] = \mathbb{E}_Y[\mathbb{E}_X[X|Y]] = \sum_i \mathbb{E}_X[X|Y=i]\mathsf{Pr}(Y=i). \tag{4.88}$$

When $L < N$, we can show that the probability mass function (pmf) of Y is given by

$$\mathsf{Pr}(Y=i) = \frac{\binom{L}{i}\binom{N-L}{L-i}}{\binom{N}{L}}, i = i_0, i_0+1, \ldots, L, \tag{4.89}$$

and 0 otherwise, where $\binom{x}{y}$ is the usual binomial coefficient, and $i_0 = \max\{0, 2L-N\}$. This is because, if $N-L \leq L$, not more than $N-L$ spatial paths of the OOB channel can be misaligned with the IRS, and hence, the support of the above pmf begins at $2L-N$. Next, we compute the term $\mathbb{E}_X[X|Y=i]$, which is the average SE seen by UE-q when

exactly i of the spatial paths are common between the IRS response and scheduled UE-q's channel angles. Then, $\mathbb{E}_X[X|Y=i]$

$$\overset{(a)}{\leq} \log_2\left(1+\mathbb{E}\left[\left|h_{d,q}+\frac{N}{\sqrt{L}}\sum_{l'\in\mathcal{I}_i}\gamma_{Y,q}^{l'}\dot{\mathbf{a}}_N^H(\omega_{Y,q}^{l'})\boldsymbol{\theta}\right|^2\right]\frac{P}{\sigma^2}\right)$$

$$\overset{(b)}{=} \log_2\left(1+\mathbb{E}\left[\left|h_{d,q}+\frac{N}{L}\sum_{l'\in\mathcal{I}_i}\gamma_{Y,q}^{l'}\right|^2\right]\frac{P}{\sigma^2}\right), \tag{4.90}$$

where (a) is due to Jensen's inequality, $\gamma_{Y,q}^{l'} \triangleq \gamma_{l',Y}^{(1)}\gamma_{l',q}^{(2)}$, and $\mathcal{I}_i$ denotes the index set of the common path indices between the IRS and UE-q's channel such that $|\mathcal{I}_i|= i$, and (b) is due to Lemma 4.1. By expanding the square term and using the statistics of the random variables, we can show that the above expectation becomes $\beta_{d,q}+i\frac{N^2}{L^2}\beta_{r,q}$. Plugging this into (4.88) and evaluating the ergodic sum-SE yields (4.37) when $L<N$. Now, for $L\geq N$ (and hence $\bar{L}\triangleq\min\{L,N\}=N$), since the IRS can orient to at most N beams, with probability 1, every channel path of the UE is aligned to one of directions to which the IRS is steered. Thus, we have $\langle S_{q,L}^{(Y)}\rangle$

$$\leq \log_2\left(1+\mathbb{E}\left[\left|h_{d,q}+\sqrt{N}\sum_{l=1}^{N}\gamma_{Y,q}^{l}\dot{\mathbf{a}}_N^H(\omega_{Y,q}^{l})\boldsymbol{\theta}\right|^2\right]\frac{P}{\sigma^2}\right)$$

$$= \log_2\left(1+\mathbb{E}\left[\left|h_{d,q}+\sum_{l=1}^{N}\gamma_{Y,q}^{l}\right|^2\right]\frac{P}{\sigma^2}\right) \tag{4.91}$$

$$= \log_2\left(1+(\beta_{d,q}+N\beta_{r,q})\frac{P}{\sigma^2}\right). \tag{4.92}$$

The proof of (4.37) for $L\geq N$ now easily follows. ■

5 Distributed IRSs Always Benefit Every Mobile Operator

Chapter Highlights

In this chapter, we investigate the impact of multiple distributed intelligent reflecting surfaces (IRSs), which are deployed and optimized by a mobile operator (MO), on the performance of user equipments (UEs) served by other co-existing out-of-band (OOB) MOs that do not control the IRSs. We show that, under round-robin scheduling, in mmWave frequencies, the ergodic sum spectral efficiency (SE) of an OOB MO increases logarithmically in the total number of IRS elements with a pre-log factor that increases with the ratio of the number of OOB paths through the IRS to the number of elements at an IRS. We further show that the maximum achievable SE of the OOB MO scales log-linearly with the total IRS elements, with a pre-log factor of 1. Then, we specify the minimum number of IRSs as a function of the channel parameters and design a distributed IRS system in which an OOB MO almost surely obtains the maximum SE. Finally, we prove that the outage probability at an OOB UE decreases exponentially as the number of IRSs increases, even though they are randomly configured from the OOB UE's viewpoint. The latter is attributed to the fact that multiple distributed IRSs enable *spatial diversity* in the channel at a UE served by an OOB UE. We numerically verify our theory and conclude that distributed IRSs always help every MO, but the MO controlling the IRSs benefits the most.

5.1 Introduction

Intelligent reflecting surfaces (IRSs) have been envisioned to meet the high data requirements for future wireless systems [3, 134, 135]. They are made up of several passive elements that can be independently tuned to reflect signals in desired directions. Further, in a distributed version of it, multiple IRSs are uniformly spread out in the environment, which provides additional diversity benefits to the system. Also, in practice, multiple mobile operators (MOs) coexist in a geographical area and independently serve multiple user equipments (UEs) over non-overlapping frequency bands. Then, it is important to understand how a distributed IRS deployed and optimized by only one of the MOs affects the performance of other out-of-band (OOB) MOs. This aspect is pertinent because an IRS does not have a band-pass filter and reflects every signal that impinges on it over a wide bandwidth. This chapter analyzes the impact of distributed IRSs on other MOs in the mmWave band.

A few works in the literature have shown that distributed IRSs improve multiplexing gains in multiple antenna systems [134, 135]. Similarly, they have been used to reduce link blockages in ultra-reliable and low-latency communication (URLLC) applications [136]. Further, multiple IRSs can be used to improve coverage in cellular systems [5]. Also, distributed IRSs have been leveraged to efficiently mitigate multi-user interference in multi-user scenarios [137]. Finally, these merits can be obtained with minimal channel estimation overheads [138].

The above-mentioned existing works implicitly assume that a single MO controls the IRSs. However, if multiple MOs simultaneously exist and only one of them deploys multiple IRSs to serve its UEs optimally, then the impact of the IRSs on the performance of the OOB MOs (which do not control the IRSs) is unexplored but is an important aspect to be understood in real-world deployment scenarios. Further, BSs of different MOs typically do not cooperate with each other. Hence, existing approaches that jointly optimize the IRS phases by cooperation across BSs cannot be used to solve this problem. Although we studied this aspect in a single IRS case in Chapter 4, which is published in [80], the channel properties in distributed IRSs are different due to multiple independent links offered by

the IRSs. This leads to new results & insights, so it merits an independent study for the multiple IRS scenario.

We consider two MOs, X and Y, operating on non-overlapping mmWave bands. The (in-band) MO X deploys and optimizes multiple distributed IRSs to serve a UE in every time slot. The (OOB) MO Y does not deploy any IRS and is oblivious to MO X's IRSs.[1] Then, our key contributions are:

1. Under round-robin (RR) scheduling, we derive the ergodic sum spectral efficiencies (SE) of the MOs. If N is the total number of IRS elements, we show that the SE of MO X grows as $\mathcal{O}(2\log_2(N))$, and the SE of MO Y scales as $\mathcal{O}(\tau\log_2(N))$, where the pre-log factor $\tau \in [0,1]$ increases with the ratio of the number of OOB paths through the IRS to the number of elements at an IRS. (See Theorem 5.1.)

2. We design a distributed IRS system and specify the minimum number of IRSs for MO Y to *almost surely* achieve the maximum SE (i.e., for $\tau = 1$.) (See Proposition 5.1.)

3. Finally, we show that the outage probability at an arbitrary OOB UE decreases exponentially as the number of IRSs deployed by MO X increases. (See Theorem 5.2.)

Through numerical simulations, we affirm that distributed IRSs enhance the performance of not only the UEs for which it is optimized but also of other OOB UEs at no additional signal processing costs, both instantaneously and on average.

Notation: For general notations used in this chapter, see the section on "General Mathematical Notations" on page ix. For the notations/variables specific to this chapter, please refer to Table 5.1.

5.2 System Model and Problem Statement

We consider a wireless system where two MOs, X and Y, provide services to K and Q UEs on non-overlapping mmWave frequency bands using their base stations: BS-X and BS-Y,

[1]The broad conclusions of this chapter can be shown to hold for any number of OOB MOs and also when every MO has its own set of IRSs.

Variable	Definition	Variable	Definition
S	Number of IRSs	$\gamma_{i,s,p}^{(1)}$	Gain of ith path from BS-p to IRS-s
M	Number of elements at an IRS	$\gamma_{j,s,t}^{(2)}$	Gain of jth path from IRS-s to UE-t
N	Total number of IRS elements	$\gamma_{p,s,t}$	Dominant cascaded path from BS-p to UE-t via IRS-s
K	Number of UEs served by BS-X	$h_{d,k}$	Direct channel from BS-X to UE-k
Q	Number of UEs served by BS-Y	$h_{d,q}$	Direct channel from BS-Y to UE-q
$L_{s,p}^{(1)}$	Number of paths from BS-p to IRS-s	$\mathbf{g}_{s,k}/\mathbf{g}_{s,q}$	Channel from IRS-s to UE-k/q
$L_{s,t}^{(2)}$	Number of paths from IRS-s to UE-t	$\mathbf{f}_s^X/\mathbf{f}_s^Y$	Channel from BS-X/Y to IRS-s
L	No. of cascaded paths via IRS ($L = L_1L_2$)	$\boldsymbol{\theta}_s$ or $\boldsymbol{\Theta}_s$	Phase shift vector/matrix at IRS-s
$\omega_{X,s,k}^1$	Dominant cascaded normalized angle from BS-X to UE-k via IRS-s	$\omega_{Y,s,q}^{\ell}$	Cascaded normalized angle from BS-Y to UE-q via IRS-s in ℓth path
P	Transmit power at the BS	β_x	Path loss in link-x
σ^2	Noise variance at the UE	$\bar{S}_M^{(X)}$ / $\bar{S}_M^{(Y)}$	Achievable ergodic sum-SEs of MOs X / Y
d/λ	Ratio of inter-elemental spacing to the signal wavelength	h_k/h_q	Overall channel from BS-X to UE-k / BS-Y to UE-q

Table 5.1: Commonly encountered variables/notations in chapter 5.

as shown in Fig. 5.1. For simplicity and to isolate the *impact of IRSs* on the system, we consider a single antenna BSs [139]. However, all our results directly extend to multiple antenna BSs. MO X deploys and optimizes $S > 1$ distributed IRSs with M elements each (with a total of $N = SM$ IRS elements) to optimally serve its (in-band) UEs in every time slot. On the other hand, MO Y does not have an IRS and is oblivious to the presence of MO X's IRSs. The downlink signal received at the kth (in-band) UE served by BS-X is[2]

$$y_k = \left(h_{d,k} + \sum_{s=1}^{S} \mathbf{g}_{s,k}^T \boldsymbol{\Theta}_s \mathbf{f}_s^X \right) x_k + n_k, \tag{5.1}$$

where $\{\mathbf{g}_{s,k}, \mathbf{f}_s^X\} \in \mathbb{C}^{M\times 1}$ are the channels from sth IRS to kth UE and BS-X to sth IRS, respectively; the diagonal matrix $\boldsymbol{\Theta}_s$ contains the phase shifts of the elements at sth IRS,

[2]We neglect inter-IRS reflections; they experience higher path loss and contribute to negligible received energy compared to single IRS reflections.

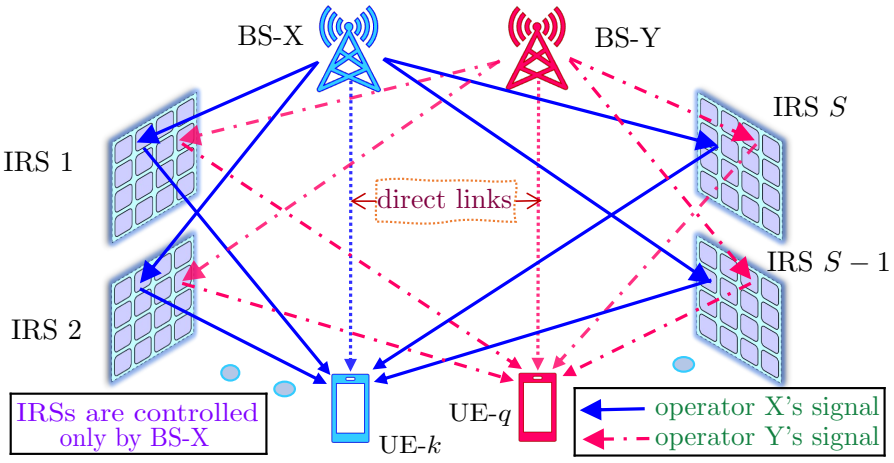

Figure 5.1: Network scenario of a distributed IRS-aided two-operator system.

i.e.,

$$\boldsymbol{\Theta}_s \triangleq \text{diag}\left(\left[e^{j\zeta_{1,s}}, e^{j\zeta_{2,s}}, \ldots, e^{j\zeta_{M,s}}\right]\right) \in \mathbb{C}^{M\times M}, \tag{5.2}$$

where $\zeta_{m,s}$ is the phase shift at mth element of sth IRS, $h_{d,k}$ is the direct channel from BS to UE-k. Also, x_k is UE-k's data symbol with $\mathbb{E}[|x_k|^2] = P$, and n_k is the additive noise with $n_k \sim \mathcal{CN}(0, \sigma^2)$. Similarly, at OOB UE-$q$ served by BS-Y,

$$y_q = \left(h_{d,q} + \sum_{s=1}^{S} \mathbf{g}_{s,q}^T \boldsymbol{\Theta}_s \mathbf{f}_s^Y\right) x_q + n_q. \tag{5.3}$$

We consider the Saleh-Valenzuela channel model [65]:

$$\mathbf{f}_s^p = \sqrt{\frac{M}{L_{s,p}^{(1)}}} \sum_{i=1}^{L_{s,p}^{(1)}} \gamma_{i,s,p}^{(1)} \mathbf{a}_M^*(\phi_{s,p}^i); \text{ and } \mathbf{g}_{s,t} = \sqrt{\frac{M}{L_{s,t}^{(2)}}} \sum_{j=1}^{L_{s,t}^{(2)}} \gamma_{j,s,t}^{(2)} \mathbf{a}_M^*(\psi_{s,t}^j), \tag{5.4}$$

where $p \in \{X, Y\}$, $L_{s,p}^{(1)}$ and $L_{s,t}^{(2)}$ are the number of resolvable spatial paths in the BS-p to sth IRS, and sth IRS to UE-t links, respectively. For notational simplicity, we let $L_{s,X}^{(1)} = L_{s,Y}^{(1)} \triangleq L_1$, and $L_{s,t}^{(2)} = L_2 \; \forall t, s$. Further, $\phi_{s,p}^i$ and $\psi_{s,t}^j$ denote the sines of the angle of arrival of the signal from BS-p at sth IRS in the ith path, and the departure from sth IRS to the tth UE in the jth path, respectively, where sine of an angle (ϕ_χ) is related to the physical angle (χ) by[3] $\phi_\chi = (2d/\lambda)\sin(\chi)$. Here, d and λ represent the IRS inter-element distance

[3]In the sequel, the term "angle" will denote the sine of a physical angle.

and the signal wavelength, respectively. The fading coefficients, $h_{d,t}, \gamma^{(1)}_{i,s,p}$ and $\gamma^{(2)}_{j,s,t}$, are independently sampled from $\mathcal{CN}(0, \beta_{d,t}), \mathcal{CN}(0, \beta_{\mathbf{f}^p})$, and $\mathcal{CN}(0, \beta_{\mathbf{g},t})$, respectively, where β's are the link path losses.[4] The array response vector of a uniform linear array (ULA) based IRS is denoted by $\mathbf{a}_M(\phi)$, with angle ϕ (and $d = \lambda/2$)[5]:

$$\mathbf{a}_M(\phi) = 1/\sqrt{M}\left[1, e^{-j\pi\phi}, \ldots, e^{-j(M-1)\pi\phi}\right]^T. \tag{5.5}$$

Recall that an M-element IRS forms at most M resolvable beams [65, 121]. So, the path angles in (5.4) are drawn independently and uniformly at random from the angle-book, $\mathbf{\Phi} \triangleq \left\{\left(-1 + \frac{2i}{M}\right) | i = 0, \ldots, M-1\right\}$. Further, since only one of the $L \triangleq L_1 L_2$ cascaded paths contains most of the energy, aligning the IRS along this path procures near-optimal benefits at the in-band UEs. So, the overall channels to the in-band UEs can be simplified by their dominant paths [66]. Using (5.4) in (5.1) with $L_1 = L_2 = 1$, the effective channel for UE-k is, h_k

$$= h_{d,k} + M \sum_{s=1}^{S} \gamma^{(1)}_{1,s,X} \gamma^{(2)}_{1,s,k} \mathbf{a}^H_M(\psi^1_{s,k}) \mathbf{\Theta}_s \mathbf{a}^*_M(\phi^1_{s,X}) \tag{5.6}$$

$$\overset{(a)}{=} h_{d,k} + M \sum_{s=1}^{S} \left(\gamma^{(1)}_{1,s,X} \gamma^{(2)}_{1,s,k} \left(\mathbf{a}^H_M(\phi^1_{s,X}) \odot \mathbf{a}^H_M(\psi^1_{s,k})\right)\right) \boldsymbol{\theta}_s$$

$$\overset{(b)}{=} h_{d,k} + M \sum_{s=1}^{S} \gamma_{X,s,k} \dot{\mathbf{a}}^H_M(\omega^1_{X,s,k}) \boldsymbol{\theta}_s, \tag{5.7}$$

where $\boldsymbol{\theta}_s \triangleq \text{diag}(\mathbf{\Theta}_s)$, (a) is due to the properties of Hadamard products. In (b), $\omega^1_{X,s,k} \triangleq \sin^{-1}\left(\sin(\phi^1_{s,X}) + \sin(\psi^1_{s,k})\right)$, $\gamma_{X,s,k} \triangleq \gamma^{(1)}_{1,s,X} \gamma^{(2)}_{1,s,k}$, and $\dot{\mathbf{a}}_M(\cdot)$ is the array vector normalized by M (see (5.5)), i.e., $\dot{\mathbf{a}}_M(\cdot) = \frac{1}{\sqrt{M}} \mathbf{a}_M(\cdot)$. Also, since the IRS is not optimized for the OOB UEs, we retain the channel at an OOB UE-q with all the paths and simplify it as

$$h_q = h_{d,q} + \frac{M}{\sqrt{L}} \sum_{s=1}^{S} \sum_{\ell=1}^{L} \gamma^{\ell}_{Y,s,q} \dot{\mathbf{a}}^H_M(\omega^{\ell}_{Y,s,q}) \boldsymbol{\theta}_s, \tag{5.8}$$

[4] We consider the path losses $\beta_{\mathbf{f}^p}$ and $\beta_{\mathbf{g},t}$ to be independent of the IRS index [126]. In practice, the path losses of these links depend on the exact IRS locations. Optimizing the IRS locations is beyond the scope of this work.

[5] The results in the chapter can be extended to other types of IRS geometries. We consider the ULA geometry for simplicity [55].

where $L \triangleq L_{s,Y}^{(1)} L_{s,q}^{(2)}$, $\{\gamma_{Y,s,q}^{\ell}\}_{\ell=1}^{L} \triangleq \{\gamma_{i,s,Y}^{(1)} \gamma_{j,s,q}^{(2)}\}_{i=1,j=1}^{L_{s,Y}^{(1)}, L_{s,q}^{(2)}}$ $\forall s$.

We can now mathematically state our problem. Suppose the BS-X configures all the S IRSs to maximize the SE at UE-k by solving the joint optimization problem (across the IRSs):

$$\left\{\boldsymbol{\Theta}_s^{\text{opt}}\right\}_{s=1}^{S} = \underset{\{\boldsymbol{\Theta}_s\}_{s=1}^{S}}{\arg\max} \log_2 \left(1 + \left| h_{d,k} + \sum_{s=1}^{S} \mathbf{g}_{s,k}^T \boldsymbol{\Theta}_s \mathbf{f}_s^X \right|^2 \frac{P}{\sigma^2}\right), \tag{P1}$$

subject to $\boldsymbol{\Theta}_s \in \mathbb{C}^{M \times M}$ being diagonal matrices with unit modulus entries. Then, these phases are randomly tuned from an OOB UE's viewpoint. This is because different MOs do not coordinate with each other, and so it is not feasible to configure the IRSs that are jointly optimal to UEs served by both BS-X and BS-Y. In this context, we address the following:

1. What is the effect of the randomly configured IRSs on the ergodic SE of the UE served by the OOB MO Y?

2. What is the best ergodic sum-SE that the OOB MO Y can obtain, and when is it achievable?

3. How does the outage probability of (OOB) UE-q scale with S, M, and the channel parameters?

We answer the above questions in the following sections.

5.3 Ergodic Sum Spectral Efficiency Analysis

We begin by noting that the optimal IRS configuration at the sth IRS, i.e., the solution to (P1), can be obtained as

$$\boldsymbol{\theta}_s^{\text{opt}} = \frac{h_{d,k} \gamma_{X,s,k}^*}{|h_{d,k} \gamma_{X,s,k}|} \times M \dot{\mathbf{a}}_M(\omega_{X,s,k}^1). \tag{5.9}$$

Clearly, $\boldsymbol{\theta}_s^{\text{opt}}$ has nonzero response in the direction of the in-band UE-k's channel via the sth IRS [80, Fig. 3]. However, since the OOB channels through the IRSs are also directional,

with nonzero probability, one or more of the IRSs also align with an OOB UE's channel. Specifically, for single IRS with a flat-top beamforming pattern [122], with probability $\bar{L}/M$ ($\bar{L} \triangleq \min\{L, M\}$), the IRS aligns with the OOB UE, and with probability $1 - \bar{L}/M$, it does not align to the OOB UE, following a Bernoulli distribution [80, Proof of Theorem 3]. Now, with S distributed IRSs, since the beam patterns are independent across IRSs and the channels at the OOB UE via each IRS are independent, the overall beamforming pattern at the OOB UE follows the distribution of the sum of S independent and identically distributed Bernoulli random variables, i.e., the Binomial distribution. In this view, we next characterize the sum-SE of MOs under round-robin (RR) scheduling of UEs.

Theorem 5.1. *Consider a distributed IRS-aided mmWave system consisting of S non-colocated IRSs, each with M elements. Then, if the IRSs are optimized (as per (5.9)) to serve the UEs of MO X in every time slot, the ergodic sum-SEs of MOs X and Y, $\bar{S}_M^{(X)}$ and $\bar{S}_M^{(Y)}$ under RR scheduling, scale as*

$$\bar{S}_M^{(X)} \approx \frac{1}{K}\sum_{k=1}^{K} \log_2\left(1 + \left[N^2\left(\frac{\pi^2}{16} + \eta\left(1 - \frac{\pi^2}{16}\right)\right)\beta_{r,k} + N\frac{\pi^{3/2}}{4}\sqrt{\beta_{d,k}\beta_{r,k}} + \beta_{d,k}\right]\frac{P}{\sigma^2}\right), \tag{5.10}$$

and $\bar{S}_M^{(Y)} \approx$

$$\begin{cases} \dfrac{1}{Q}\displaystyle\sum_{q=1}^{Q}\sum_{\mathfrak{s}=0}^{S} \frac{S!}{(S-\mathfrak{s})!\,\mathfrak{s}!}\left(\frac{L}{M}\right)^{\mathfrak{s}}\left(1 - \frac{L}{M}\right)^{S-\mathfrak{s}} \log_2\left(1 + \left[\frac{\mathfrak{s}M^2}{L}\beta_{r,q} + \beta_{d,q}\right]\frac{P}{\sigma^2}\right), & \text{if } L < M, \\ \dfrac{1}{Q}\displaystyle\sum_{q=1}^{Q} \log_2\left(1 + (\beta_{d,q} + N\beta_{r,q})\frac{P}{\sigma^2}\right), & \text{if } L \geq M, \end{cases} \tag{5.11}$$

respectively, where N is the total number of IRS elements ($N = SM$), and $\eta \triangleq M/N$.

Proof. See Appendix 5.A. ■

We observe from Theorem 5.1 that the ergodic sum-SE of even an OOB MO monotonically grows in N, with the peak scaling of $\mathcal{O}(\log_2(N))$ when $L \geq M$. For $L < M$, as we show in Sec. 5.6, the OOB SE scales as $\mathcal{O}(\tau \log_2(N))$ for $\tau \in [0, 1)$. Here, the exact value of τ depends on how L compares with M. The primary reason for this improvement in the

OOB SE is that the IRSs create more paths that enrich the channel at the OOB UEs. We note that the above results generalize the work of [80], which considers $S = 1$. Further, the SE at the (in-band) MO X still scales as $\mathcal{O}(2\log_2(N))$, similar to single IRS setups. Thus, deploying multiple IRSs in a distributed manner retains optimal benefits at the in-band MO and helps other MOs simultaneously at no significant overhead.

5.4 Design for achieving $\mathcal{O}(\log_2(N))$ growth in OOB SE

From (5.11), it is clear that the OOB SE maximally scales log-linearly in the number of IRS elements and is achieved when the number of paths L is sufficiently large. Specifically, if $L \geq M$, every IRS contributes to the signal at an OOB UE. We leverage this fact to design new specifications for distributed IRS systems in the following result to almost surely procure $\mathcal{O}(\log_2(N))$ growth in the OOB SE for any L, N.

Proposition 5.1. *Consider a system where an MO deploys and controls multiple IRSs in a distributed fashion, using a total of N IRS elements. If the number of IRSs S each with M elements providing L cascaded paths at an OOB UE, satisfy*

$$M \leq M^* \triangleq N^{\delta^*}, \text{ and, } S \geq S^* \triangleq \left\lceil N^{1-\delta^*} \right\rceil, \tag{5.12}$$

where $\delta^* = \min\{1, \log_N L\}$, then almost surely, the OOB SE attains the maximum scaling of $\mathcal{O}(\log_2(N))$ for any N, L.

Proof. If S and M satisfy (5.12), we have $L/M \geq 1$ under any scenario. Thus, almost surely, every IRS contributes to the signal at an OOB UE. So, the overall channel at the OOB UE is (5.22), for which the ergodic SE scales as $\mathcal{O}(\log_2(N))$. ■

Proposition 5.1 says that if the number of paths is $L = N^\delta$ for $0 \leq \delta \leq 1$, then a distributed system designed as per (5.12) gives maximum possible benefits at the OOB MO. In this case, the rate-scaling laws precisely match those derived for the sub-6 GHz bands in the previous chapter. Specifically, when multiple IRSs are deployed in a distributed manner, the channel exhibits rich scattering characteristics, and hence, the properties of

the channel are largely governed by the properties of sub-6 GHz bands of communications. Further, this does not affect the optimal growth of the SE for MO X.

Next, we analyze the instantaneous channel characteristics at an OOB UE due to these arbitrarily configured IRSs.

5.5 Outage Probability Evaluation

We now examine the outage probability of an OOB UE-q as a function of the IRS and channel parameters. The outage probability is $P^{\rho}_{\text{out},q} \triangleq \mathsf{Pr}(|h_q|^2 \leq \rho)$, which from (5.8) becomes

$$P^{\rho}_{\text{out},q} = \mathsf{Pr}\left(\left|h_{d,q} + \frac{M}{\sqrt{L}} \sum_{s=1}^{S} \sum_{\ell=1}^{L} \gamma^{\ell}_{Y,s,q} \dot{\mathbf{a}}^{H}_{M}(\omega^{\ell}_{Y,s,q}) \boldsymbol{\theta}_s \right|^2 \leq \rho\right). \tag{5.13}$$

Intuitively, each IRS provides an independent link at the OOB UE, so multiple IRSs should provide better diversity gains than single or no IRS scenarios. We have the following result.

Theorem 5.2. *The outage probability at an OOB UE-q due to S randomly configured and distributed IRSs, each with M elements and contributing to L paths, is given by*

$$P^{\rho}_{\text{out},q} = \left(1 - e^{-\rho/\beta_{d,q}}\right) \mathrm{P}_0^S, \tag{5.14}$$

where

$$\mathrm{P}_0 = 1 - \frac{\bar{L}}{M}\left(\frac{\bar{L} e^{\frac{\bar{L}\beta_{d,q}}{M^2\beta_{r,q}}}}{M^2\beta_{r,q}} \mathcal{I}_0\left(\rho; \beta_{d,q}, \frac{M^2}{\bar{L}}\beta_{r,q}\right) - e^{-\frac{\rho}{\beta_{d,q}}}\right) - e^{-\frac{\rho}{\beta_{d,q}}},$$

$\bar{L} \triangleq \min\{L, M\}$, *and* $\mathcal{I}_0(x; c_1, c_2) \triangleq \int_{c_1}^{\infty} e^{-\left(\frac{x}{t} + \frac{t}{c_2}\right)} dt$.

Proof. See Appendix 5.B. ∎

Theorem 5.2 clearly shows that the outage probability at an OOB UE decreases exponentially in S, even though the IRSs are randomly configured from UE-q's viewpoint. Thus, a distributed IRS-aided system provides instantaneous benefits even to an OOB

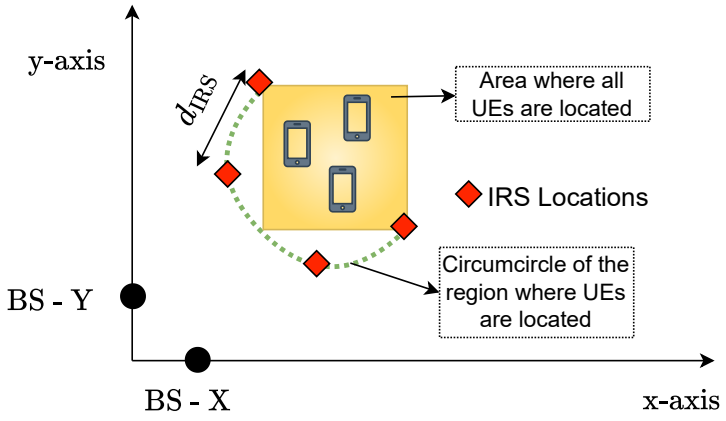

Figure 5.2: System setup for $S = 4$.

MO without incurring optimization costs. We next illustrate our findings via Monte Carlo simulations.

5.6 Numerical Results

We consider that BS-X is located at $(50, 0)$, BS-Y at $(0, 50)$, and the UEs in a rectangular region $\mathcal{R} \triangleq [900, 1100] \times [900, 1100]$. The IRSs are uniformly spaced on a semi-circular part of the circle that circumscribes $\mathcal{R}$, as shown in Fig. 5.2. Note that our results hold true for any other choice of IRS locations and the distance between the IRSs. The path loss is modeled as $\beta = C_0(d_0/d)^\alpha$, where C_0 is the path loss at the reference distance d_0, d is the node distance, and α is the path loss exponent which is $2, 2.2$ and 4.5 in the BS-IRS, IRS-UE, and BS-UE links. Further, BS-X and BS-Y serve $K = 10$ and $Q = 10$ UEs using an RR scheduler over $10,000$ time slots.

In Fig. 5.3, we plot the ergodic sum-SE of both MOs versus the total number of IRS elements, N, for different values of S. We use $C_0\,(P/\sigma^2) = 150$ dB and $L = 2$ [80]. We first observe that the SE of the MO X is invariant to the number of IRSs in the system. Thus, the optimal SE scaling of $\mathcal{O}(2\log_2(N))$ is retained for any S. However, the OOB SE significantly changes with S. For e.g., when $S = 4$, until some point, the OOB SE log-linearly increases in N and then exhibits log-sub-linear growth for larger values of N (in the regime where $L < M$), i.e., the pre-log factor of OOB SE lies in $[0, 1)$. The latter is

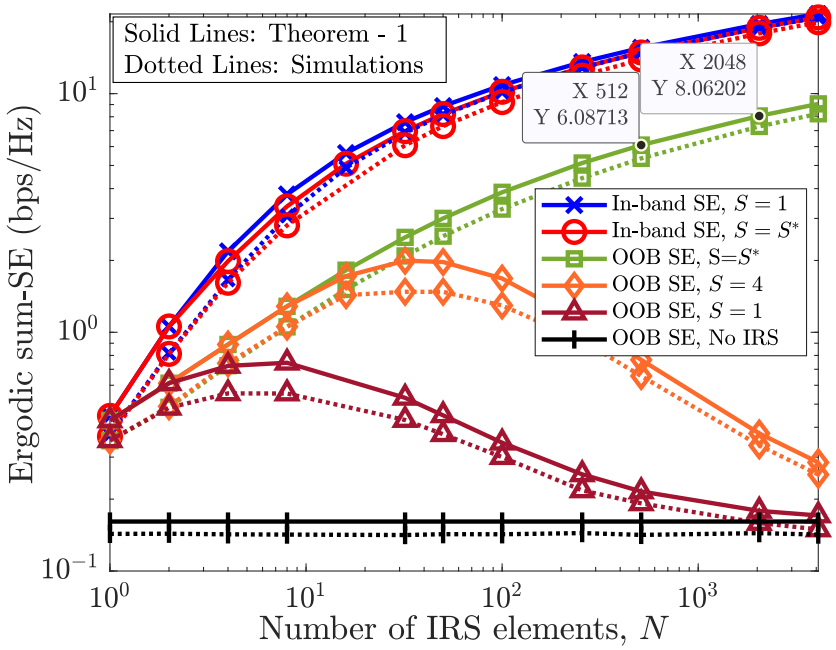

Figure 5.3: Ergodic sum-SE of the MOs X, Y vs. N. Results with $S = 1$ are reported in [80].

because, for large N and fixed small L, unless S is reasonably large, the OOB UE does not benefit much. We then plot the OOB SE for $S = S^*$, where S^* is as per Proposition 5.1. In this case, as indicated in the data marked inside the figure, a $4\times$ increase in N leads to a boost of the SE by 2 bps/Hz. Note that $2 + \log_2(N) = 1 \cdot \log_2((4N))$. In other words, the OOB SE uniformly achieves the (maximum) scaling of $\log_2(N)$ with sufficiently many IRSs. We also compare our results with those in [80], which considers $S = 1$ on the same plot. The OOB SE obtained in distributed IRSs is clearly better than the single IRS case. Also, the simulations match well with Theorem 5.1, illustrating the accuracy of the rate laws and the Bernoulli distribution-based analysis for an OOB MO.

In Fig. 5.4, we illustrate the tightness of Proposition 5.1. Specifically, we plot the SE pre-log factor: $\tau \triangleq \bar{S}_M^{(X)/(Y)}/\log_2(N)$ as a function of S. Each sub-plot represents a system with different L, through $\delta \triangleq \log_N L$ with $N = 128$. The plot shows that the result in Proposition 5.1 is tight because, in all cases, when $S < S^*$, $\tau \in [0, 1)$, i.e., the OOB SE grows only log-sub-linearly in N. Contrarily, for $S \geq S^*$, the OOB-SE scales as $\mathcal{O}(\log_2(N))$ for any N, L. Also, for the in-band UE, $\tau = 2$, in line with Fig. 5.3. Further, since the OOB SE does not depend on N in the absence of IRSs, we have $\tau = 0$.

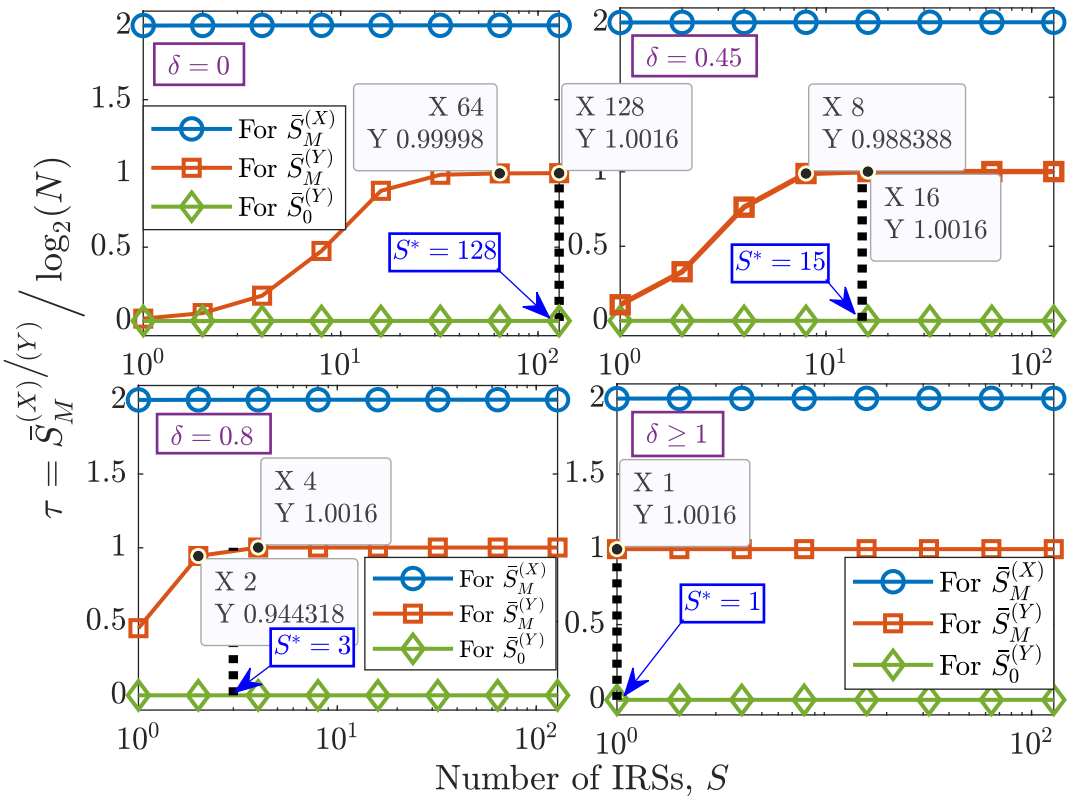

Figure 5.4: Pre-log factor of OOB SE, τ vs. S as a function of δ (or L).

Finally, in Fig. 5.5, we plot the outage probability at an OOB UE (after normalizing the channel path losses) with $\rho = 0.5$ as a function of S for different L through $\delta = \log_N L$, and $N = 512$. For a given δ (or L), the outage probability decreases exponentially in the number of IRSs, in line with Theorem 5.2. Further, for a fixed S, the outage probability decreases with δ as the likelihood that the randomly configured IRSs help the OOB UE increases with the number of paths.

5.7 Conclusions

We studied the impact of distributed IRSs on the performance of an OOB MO that is oblivious to the presence of the IRSs. We showed that the maximum SE of the OOB MO grows log-linearly in the number of IRS elements; we also developed design specifications that almost surely achieve this SE. Finally, we proved that the outage probability at an OOB UE decays exponentially in the number of IRSs, free of cost. Thus, distributed IRSs

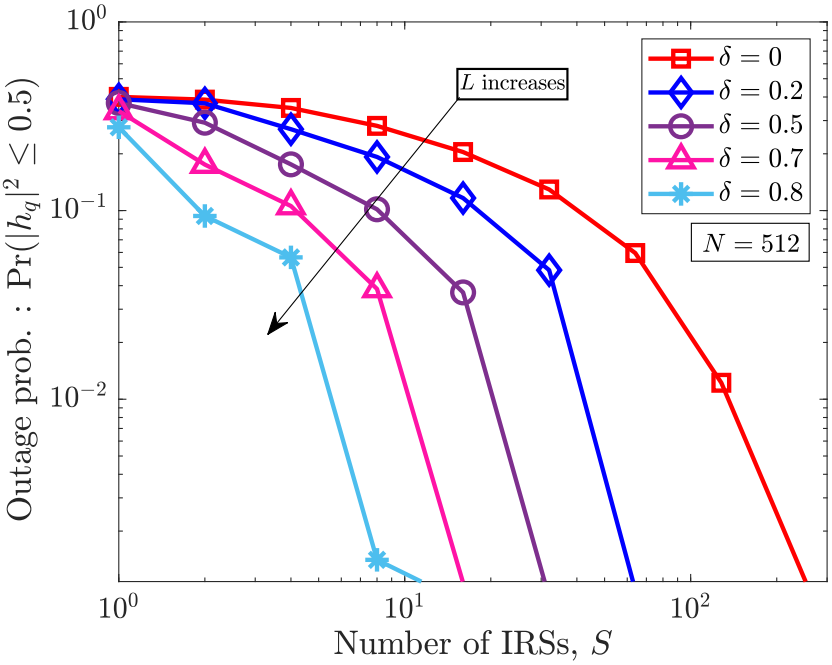

Figure 5.5: Outage probability vs. S at an OOB UE.

help all MOs in the area. Future work includes extending our results to interference-limited scenarios in multi-cell systems.

Appendix 5.A Proof of Theorem 5.1

We prove the theorem for MOs X and Y separately, one by one, below.

5.A.a Ergodic sum-SE of MO-X

Let the ergodic SE at an arbitrary UE served by MO X, say k, be $\langle S_M^{k,X} \rangle$. Then, the ergodic sum-SE of MO X under RR scheduling is $\bar{S}_M^{(X)} = \frac{1}{K} \sum_{k=1}^{K} \langle S_M^{k,X} \rangle$. Computing the exact expression for $\langle S_M^{k,X} \rangle$ leads to intractable forms and is not insightful. So, we apply the Jensen's approximation to $\langle S_M^{k,X} \rangle$ and obtain

$$\langle S_M^{k,X} \rangle = \mathbb{E}\left[\log_2\left(1 + |h_k|^2 \frac{P}{\sigma^2}\right)\right] \approx \log_2\left(1 + \mathbb{E}\left[|h_k|^2\right] \frac{P}{\sigma^2}\right), \tag{5.15}$$

where the expectations are taken with respect to the channels of UE-k. To evaluate $|h_k|^2$, we use (5.9) in (5.7), and obtain the overall channel gain at UE-k as shown below:

$$|h_k|^2 = \left|\,|h_{d,k}| + M\sum_{s=1}^{S}|\gamma_{X,s,k}|\right|^2 = |h_{d,k}|^2 + M^2\left(\sum_{s=1}^{S}|\gamma_{X,s,k}|\right)^2 + 2M|h_{d,k}|\sum_{s=1}^{S}|\gamma_{X,s,k}|. \quad (5.16)$$

Next, we evaluate the expected values of the three terms in (5.16), below:

Term I: It is clear that $\mathbb{E}[|h_{d,k}|^2] = \beta_{d,k}$. Let $\beta_{r,k} \triangleq \beta_{\mathbf{f}^X}\beta_{\mathbf{g},k}$.

Term II: We compute this term as following:

$$\mathbb{E}\left[\left(\sum_{s=1}^{S}|\gamma_{X,s,k}|\right)^2\right] = \mathbb{E}\left[\sum_{\substack{s,p=1\\ s\neq p}}^{S}|\gamma_{X,s,k}||\gamma_{X,p,k}| + \sum_{s=1}^{S}|\gamma_{X,s,k}|^2\right] = S(S-1)\left(\frac{\pi}{4}\sqrt{\beta_{r,k}}\right)^2 + S\beta_{r,k}. \quad (5.17)$$

Collecting and re-arranging the factors, the expected value of $M^2\left(\sum_{s=1}^{S}|\gamma_{X,s,k}|\right)^2$ is $M^2\beta_{r,k}\left[S^2\frac{\pi^2}{16} + S\left(1-\frac{\pi^2}{16}\right)\right]$.

Term III: Finally, we can show $2M\mathbb{E}\left[|h_{d,k}|\sum_{s=1}^{S}|\gamma_{X,s,k}|\right] = MS\frac{\pi^{3/2}}{4}\sqrt{\beta_{r,k}\beta_{d,k}}$, due to independence of $h_{d,k}$ and $\gamma_{X,s,k}$. Summing the above terms and using it in $\bar{S}_M^{(X)}$ yields (5.10).

5.A.b Ergodic sum-SE of MO-Y

Let the ergodic SE at an arbitrary OOB UE, say q, be $\langle S_M^{q,Y}\rangle$. Then, under RR scheduling, the ergodic sum-SE is $\bar{S}_M^{(Y)} = \frac{1}{Q}\sum_{q=1}^{Q}\langle S_M^{q,Y}\rangle$. First, we prove (5.11) for $L < M$. Define the random variable A_{s} to denote whether the sth IRS aligns with the channel to OOB UE-q or not; then $A_{\mathrm{s}} \sim \mathrm{Ber}(L/M)$ for all s. Further, let B count the number of IRSs aligning to the channel of UE-q; then, $B = \sum_{\mathrm{s}=1}^{S} A_{\mathrm{s}}$. So, $B \sim \mathrm{Bin}(S, L/M)$. Now,

$$\langle S_M^{q,Y}\rangle = \mathbb{E}_{|h_q|^2,B}\left[\log_2\left(1+\frac{|h_q|^2P}{\sigma^2}\right)\mathbb{1}_{\{B\in\{0,1,2,\ldots,S\}\}}\right] \quad (5.18)$$

$$\overset{(a)}{=} \sum_{\mathfrak{s}=0}^{S}\mathbb{E}_{|h_q|^2}\left[\log_2\left(1+\frac{|h_q|^2P}{\sigma^2}\right)\middle| B=\mathfrak{s}\right]\mathsf{Pr}(B=\mathfrak{s}) \quad (5.19)$$

$$\overset{(b)}{\approx} \sum_{\mathfrak{s}=0}^{S}\log_2\left(1+\mathbb{E}\left[|h_q|^2\middle|B=\mathfrak{s}\right]\frac{P}{\sigma^2}\right)\mathsf{Pr}(B=\mathfrak{s}), \quad (5.20)$$

where (a) is due to the law of iterated expectations, and (b) is due to Jensen's approximation, which is known to be numerically tight. Now, using the probability mass function of a Binomial distribution, we have $\mathsf{Pr}(B=\mathfrak{s}) = \dfrac{S!}{(S-\mathfrak{s})!\,\mathfrak{s}!}\left(\dfrac{L}{M}\right)^{\mathfrak{s}}\left(1-\dfrac{L}{M}\right)^{S-\mathfrak{s}}$. Further, $\mathbb{E}\left[|h_q|^2\middle|B=\mathfrak{s}\right]$ is the average channel gain at UE-q when the beams from exactly $\mathfrak{s}$ of the IRSs align with one of the L paths to UE-q through these IRSs. Then, the channel gain due to these *contributing* IRSs is computed as (see (5.8))

$$|h_q|^2\Big|\{B=\mathfrak{s}\} = \left|h_{d,q} + \frac{M}{\sqrt{L}}\sum_{s=1}^{\mathfrak{s}}\gamma^{\ell^*}_{Y,s,q}\right|^2, \tag{5.21}$$

where $\gamma^{\ell^*}_{Y,s,q}$ is the channel gain of the cascaded path that aligns with the sth IRS. We can now show that $\mathbb{E}\left[|h_q|^2\middle|B=\mathfrak{s}\right] = (\mathfrak{s}M^2/L)\beta_{r,q} + \beta_{d,q}$, where $\beta_{r,q} \triangleq \beta_{\mathbf{f}^Y}\beta_{\mathbf{g},q}$. Collecting all the terms for (5.20) and plugging into $\bar{S}^{(Y)}_M$ yields (5.11) for $L < M$. Now, for $L \geq M$, the probability term $\bar{L}/M = 1$. So, every IRS almost surely aligns with the OOB UE. Thus, the overall channel gain and its mean are

$$|h_q|^2 = \left|h_{d,q} + \sqrt{M}\sum_{s=1}^{S}\gamma^{\ell^*}_{Y,s,q}\right|^2, \text{ and} \tag{5.22}$$

$N\beta_{r,q} + \beta_{d,q}$, respectively. The proof can now be finished.

Appendix 5.B Proof of Theorem 5.2

Let $\mathcal{E}_s$ denote the event that sth IRS aligns with the OOB UE's channel. Then, $\mathcal{E}_0$ is the event that no IRS aligns with the OOB channel. We can write

$$P^{\rho}_{\text{out},q} \overset{(a)}{=} \mathsf{Pr}\left(|h_q|^2\mathbb{1}_{\{\mathcal{E}_0\cup\mathcal{E}_1\cup\cdots\cup\mathcal{E}_S\}} \leq \rho\right) \tag{5.23}$$

$$= \mathbb{E}_{\mathbb{1}_{\{\mathcal{E}_0\}},\ldots,\mathbb{1}_{\{\mathcal{E}_S\}}}\left[\mathsf{Pr}\left(|h_q|^2 \leq \rho\middle|\mathbb{1}_{\{\mathcal{E}_0\}},\ldots,\mathbb{1}_{\{\mathcal{E}_S\}}\right)\right] \tag{5.24}$$

$$\overset{(b)}{=} \prod_{\mathfrak{s}=0}^{S}\mathbb{E}_{\mathbb{1}_{\{\mathcal{E}_s\}}}\left[\mathsf{Pr}\left(|h_q|^2 \leq \rho\middle|\mathbb{1}_{\{\mathcal{E}_s\}}\right)\right] \tag{5.25}$$

$$\overset{(c)}{=} \mathsf{Pr}(|h_{d,q}|^2 \leq \rho)\left(\mathbb{E}_{\mathbb{1}_{\{\mathcal{E}_1\}}}\left[\mathsf{Pr}\left(|h_q|^2 \leq \rho\middle|\mathbb{1}_{\{\mathcal{E}_1\}}\right)\right]\right)^S, \tag{5.26}$$

where (a) is because $\{\mathcal{E}_{\mathfrak{s}}\}_{\mathfrak{s}=0}^{S}$ is a set of mutually exhaustive events, (b) is because these events are independent, and in (c), the first product term is because under $\mathcal{E}_0$, the channel at UE-q is only due to the direct link from BS-Y, and the second term is because $\{h_q^{\mathfrak{s}}\}_{\mathfrak{s}=1}^{S}$ and $\{\mathbb{1}_{\{\mathcal{E}_{\mathfrak{s}}\}}\}_{\mathfrak{s}=1}^{S}$ are sets of i.i.d. random variables. Here, $h_q^{\mathfrak{s}}$ is the component of h_q via the $\mathfrak{s}$th IRS. We can now evaluate the expectation term in (5.26) as

$$\mathbb{E}_{\mathbb{1}_{\{\mathcal{E}_1\}}}\left[\mathsf{Pr}(|h_q|^2 \leq \rho \middle| \mathbb{1}_{\{\mathcal{E}_1\}})\right] = \left(1-\frac{\bar{L}}{M}\right)\left(\mathsf{Pr}(|h_{d,q}|^2 \leq \rho)\right) + \frac{\bar{L}}{M}\left(\mathsf{Pr}\left(\left|h_{d,q}+\frac{M}{\sqrt{\bar{L}}}\gamma_{Y,1,q}^{\ell^*}\right|^2 \leq \rho\right)\right). \quad (5.27)$$

While it is easy to show that $\mathsf{Pr}(|h_{d,q}|^2 \leq \rho) = 1 - e^{-\rho/\beta_{d,q}}$, the second term in the above can be computed using [80, Appendix C]. Finally, plugging all these values in (5.26) yields (5.14).

6 Low-Complexity Channel Estimation for Distributed IRS-Aided MIMO Exploiting Subspace Properties

Chapter Highlights

In the previous chapter, it was demonstrated that deploying multiple intelligent reflecting surfaces (IRSs) in a distributed manner in the environment enhances performance for all users. However, this also introduces an additional challenge due to an increase in channel estimation overhead due to the presence of more channel links. To address this, in this chapter, we propose a novel method for estimating all cascaded IRS channels in a multiple-IRS-assisted mmWave massive multiple-input multiple-output (MIMO) system. The proposed approach significantly reduces pilot overhead compared to existing methods.

We exploit the inherent structure in mmWave channels to reformulate the channel estimation problem as one of the directions of arrival (DoA) and departure (DoD) estimations in the cascaded channel. In turn, this allows us to use subspace-based methods from array signal processing to develop a *joint estimation of signal parameters via rotational invariance technique (ESPRIT)-multiple signal classification (MUSIC)* algorithm for estimating the DoA at the BS and the DoD from the UE. As described earlier, an attractive feature of the scheme is its low pilot overhead requirement: unlike existing methods, the number of pilot symbols does not scale with the number of IRS elements or the number of antennas at the BS; it only depends on the number of IRSs deployed and the number of antennas at the UE. We compare our method against state-of-the-art methods, and numerically illustrate its superior performance and robustness to the number of IRSs in the system.

6.1 Introduction

Intelligent reflecting surfaces (IRSs) are made of many passive elements that can be tuned to reflect an incoming signal in any desired direction by appropriately adjusting the reflection coefficients of the elements. This can be used to combine the signals coherently reflected from the IRS elements at a desired location, enhancing the throughput/reliability without costing additional bandwidth or transmit power [2,3,69]. However, realizing these benefits is contingent upon accurately estimating the channel state information (CSI) of all the links in the system.

We first briefly discuss existing work on CSI estimation in IRS-aided multi-antenna mmWave systems to set the context of this chapter. A few basic approaches to estimating all the channels (which include the cascaded and direct links) in the system using the principle of least squares are described in [21,26,27]. However, these methods incur very high complexity in terms of the number of pilot transmissions required (the overhead scales linearly with the number of IRS elements in the system.) Furthermore, when multiple non-co-located IRSs are deployed (called distributed IRS in this chapter) to enhance the performance in dense heterogeneous networks [3,140–142], the channel estimation problem becomes even more complex: the pilot overhead is proportional to the total number of elements across all the IRSs [28, 29]. To circumvent these shortcomings, several works aim to exploit the structure in the underlying IRS-aided mmWave wireless channels to reduce the time complexity of the CSI estimation protocol. Specifically, they exploit the fact that the channels exhibit a spatial sparsity structure that arises because there are only a few line-of-sight (LoS) paths that propagate through the environment [30], which in turn makes the BS-IRS and IRS-UE channels low-rank and sparse in the angular domain. Subsequently, they use a sparse signal recovery-based algorithm to estimate the CSI [31–35] under the compressed sensing paradigm. However, to successfully recover the sparse channels under this framework, these algorithms require a certain minimum number of antennas to be deployed at the BS and/or UE. Moreover, the performance guarantees are contingent upon the effective measurement matrix satisfying a restricted isometry property, which is hard to verify because the measurement matrix is not choosable in

practice. Thus, although these approaches incur a low time complexity, they suffer from high system requirements and computational complexity.

One approach to overcome the above-mentioned difficulty in CS-based approaches is to pose the CSI estimation problem as one of direction finding/estimation and solve it using subspace methods. Along this line, an initial study was conducted in [143], where the authors use subspace methods, namely, *estimation of signal parameters via rotational invariance technique (ESPRIT)* [144] and *multiple signal classification (MUSIC)* [145] algorithms, to sequentially estimate the angles in the channel. However, a part of their work assumes the availability of a few *active* IRS elements, which not only drives up the cost of implementation but also requires additional signal processing at the IRS. Moreover, the authors consider a system with a single IRS, i.e., they do not consider the scenario of distributed IRSs. Thus, to the best of our knowledge, no existing work explores subspace-based approaches for low complexity CSI acquisition in distributed IRS-aided mmWave MIMO systems exploiting the spatial structure in the channels.

Our work, different from the existing approaches, considers a scenario of a distributed IRS-aided mmWave massive MIMO (mMIMO) system. We exploit the channel structure to estimate the cascaded CSI using subspace-based methods, namely, ESPRIT and MUSIC, with low pilot overhead. Our specific contributions are as follows:

1. We reformulate the cascaded CSI estimation problem as one of the direction of arrival (DoA) and direction of departure (DoD) estimation in an equivalent channel model. We then develop a cascaded CSI estimation algorithm at the BS (in the uplink mode) for distributed IRS-aided mMIMO systems by exploiting the spatial structure of mmWave channels based on a combination of direction-finding algorithms in the array processing literature. In particular, since the channel model has both DoAs and DoDs coupled, we develop a *joint ESPRIT-MUSIC* algorithm that jointly estimates the DoA at the BS and DoD from the UE, with the estimation being performed at the BS. The DoA is estimated first and is passed as an input to the DoD estimator using an appropriately chosen MUSIC-based cost function. Then, the path gain coefficients are estimated using a low complexity least-squares (LS) method.

We note that, by virtue of joint DoA-DoD estimations, the number of independent variables to be estimated reduces to only the number of DoAs, and the corresponding DoDs are computed using the MUSIC algorithm. As a consequence, the algorithm also ensures that the DoA and corresponding DoD are paired automatically, without any ambiguity pertaining to the cascaded links through the IRSs. This approach is different from the conventional use of ESPRIT and MUSIC, where they are used to estimate the angles separately. To the best of our knowledge, this is the first work that solves the CSI estimation problem in a distributed passive IRS-aided mMIMO scenario using joint subspace-based methods.

2. We show that our approach yields accurate channel estimates with a dramatically reduced pilot overhead compared to conventional methods. This is made possible by the aforementioned reformulation, which reduces the number of parameters to be estimated to depend only on the total number of paths in the system, i.e., on the number of IRSs and the number of antennas at the UE and *not* on the total number of IRS elements and the number of BS antennas, which are generally very large in mmWave mMIMO systems.

3. We compare our method against that in [33], where the sparsity in the angular domain of the mmWave channel is exploited to formulate the problem as a multiple measurement vector (MMV) based sparse recovery problem, which is then solved using simultaneous orthogonal matching pursuit (SOMP). We numerically show that our method significantly outperforms SOMP, especially as the number of IRSs increases.

Thus, subspace-based methods are promising for low-complexity and low-overhead cascaded channel estimation in multiple IRS-assisted mmWave massive MIMO communications. The technique described in this chapter is also applicable to time division duplexed (TDD) communications, where it can aid in acquiring the CSI of the downlink channel by exploiting channel reciprocity.[1] Thus, it can also be useful for IRS-aided downlink

[1]Our proposed channel estimation method works directly in the downlink also, with the estimation being performed at the UE instead of at the BS.

Variable	Definition	Variable	Definition
K	Number of IRSs	$\mathbf{H}$	Overall uplink channel from UE to BS
L_k	Number of elements at IRS-k	$\mathbf{H}_d$	Direct channel from UE to BS
M	Number of antennas at BS	$\mathbf{G}$	Overall UE - BS cascaded channel
N	Number of antennas at UE	$\mathbf{H}_{2,k}$	Channel from UE to IRS-k
N_k	No. of paths from IRS-k to UE	$\mathbf{H}_{1,k}$	Channel from IRS-k to BS
ψ_k	Direction of arrival at BS from IRS-k	$\phi_{i,k}$	Direction of departure at UE to IRS-k in ith path
N_d	No. of paths from UE to BS in direct channel	$\gamma_{i,k}$	Gain of the cascaded channel in the ith path via IRS-k
$\mathbf{\Theta}_k$	Phase shift matrix at IRS-k	T_1, T_2	Number of pilot transmissions in short, long time scales

Table 6.1: Commonly encountered variables/notations in chapter 6.

communications.

Notation: For general notations used in this chapter, see the section on "General Mathematical Notations" on page ix; and $\text{argmax}^{(N)}$ refers to the N dominant argument values. For the notations/variables specific to this chapter, please refer to Table 6.1.

6.2 Channel Model

We consider a communication system comprising an M-antenna BS, K IRSs which are deployed at arbitrary locations in the vicinity of the BS, with the kth IRS equipped with L_k elements, and an N-antenna user equipment (UE), as shown in Fig. 6.1. For ease of presentation, we assume that the antennas at the UE, BS, and the IRS elements are configured as a uniform linear array (ULA) [76]. We index the IRSs by the set $[K] \triangleq \{1, 2, \ldots, K\}$. We consider uplink communication from the UE to the BS and focus on developing low pilot overhead schemes for estimating the cascaded UE-IRS-BS channels at the BS in this distributed IRS-assisted system.

Let the direct path from the UE to the BS be denoted by $\mathbf{H}_d \in \mathbb{C}^{M \times N}$. Let the channels between the UE and the kth IRS be denoted by $\mathbf{H}_{2,k} \in \mathbb{C}^{L_k \times N}$ and that between the kth IRS and the BS be denoted by $\mathbf{H}_{1,k} \in \mathbb{C}^{M \times L_k}$. We denote the reflection coefficient matrix

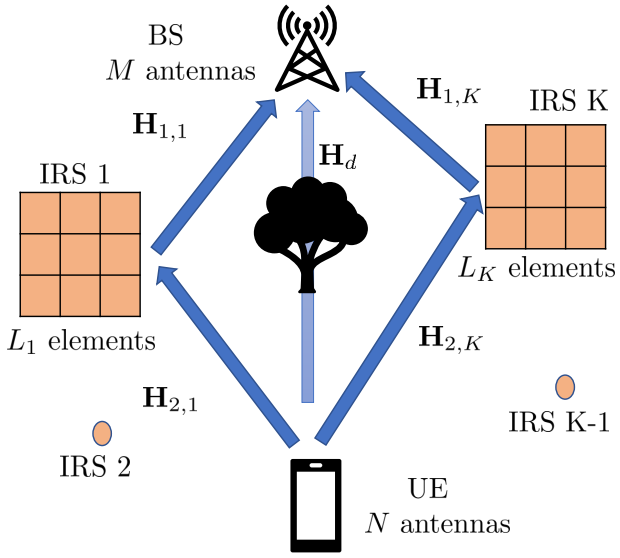

Figure 6.1: An N-antenna UE is transmitting to an M-antenna BS, assisted by K IRSs, with the kth IRS equipped with L_k elements.

at the kth IRS by the diagonal matrix $\mathbf{\Theta}_k \in \mathbb{C}^{L_k \times L_k}$ where the diagonal elements are of the form $\eta_l e^{j\theta_l}$, with $\eta_l \leq 1$. The IRSs are envisioned to establish LoS links between the BS and the IRS and between the IRS and the UE [86]. Hence, in the context of mmWave communication, we consider the Saleh-Valenzuela model [146] to model all the channels. The IRSs are typically deployed at a height and have strong LoS links with the BS. So, we set the number of spatial paths between the BS and IRS to one,[2] similar to [76], but there can exist more than one spatial path between each UE and IRS. Specifically, the links via the kth IRS are modeled as

$$\mathbf{H}_{2,k} = \sum_{i=1}^{N_k} \alpha_{i,k} \mathbf{a}_{L_k}(\omega_{i,k}) \mathbf{a}_N^T(\phi_{i,k}), \quad \forall k \in [K], \tag{6.1}$$

and

$$\mathbf{H}_{1,k} = \beta_k \mathbf{a}_M(\psi_k) \mathbf{a}_{L_k}^T(\nu_k), \quad \forall k \in [K], \tag{6.2}$$

where N_k represents the number of spatial paths between the UE and the kth IRS, $\alpha_{i,k}$ and β_k represent the path gain coefficients of the ith path from the UE to kth IRS and the path

[2]It is straightforward to extend our algorithm to the case with multiple paths between the BS and IRS, so this is not a major limitation of this work.

between the kth IRS and BS, respectively. Here, $\mathbf{a}_X \in \mathbb{C}^{X\times 1}, X \in \{N, M, L_1, L_2, \ldots, L_K\}$ represents the array steering response vector of a ULA (with inter-elemental distance set to half the wavelength) and is given by $\mathbf{a}_X(\theta) = [1, e^{-j\pi\sin(\theta)}, \ldots, e^{-j(X-1)\pi\sin(\theta)}]^T$, and $\omega_{i,k}, \phi_{i,k}, \psi_k, \nu_k$ represent the DoA at the kth IRS from the UE through ith path, the DoD from the UE to the kth IRS in the ith path, the DoA at the BS from the kth IRS and the DoD at the kth IRS to the BS, respectively. Similarly, the direct path between the UE and the BS is modeled as

$$\mathbf{H}_d = \sum_{j=1}^{N_d} \zeta_j \mathbf{a}_M(\chi_j)\mathbf{a}_N^T(\rho_j), \tag{6.3}$$

where N_d represents the number of spatial paths between the UE and BS in the direct path, ζ_j represents the path gain coefficient of jth path between the UE and the BS, χ_j and ρ_j represent the DoA at the BS and DoD from the UE through the jth path, respectively. Thus, the effective uplink channel, denoted by $\mathbf{H} \in \mathbb{C}^{M\times N}$, is given by

$$\mathbf{H} = \mathbf{H}_d + \sum_{k=1}^{K} \mathbf{H}_{1,k}\mathbf{\Theta}_k\mathbf{H}_{2,k} = \mathbf{H}_d + \mathbf{G}. \tag{6.4}$$

We can isolate the cascaded channel links due to the fading components by setting $\mathbf{\Theta}_k = \mathbf{I}_{L_k} \forall k$ in the above. We use this in the next section.

6.3 Cascaded Channel Estimation Design

The received uplink pilot signal at the BS, $\mathbf{y}' \in \mathbb{C}^{M\times 1}$, is given by

$$\mathbf{y}' = \mathbf{H}\mathbf{x} + \mathbf{n}', \tag{6.5}$$

where $\mathbf{x} \in \mathbb{C}^{N\times 1}$ is the pilot symbol vector and $\mathbf{n}'$ is additive noise sampled from $\mathcal{CN}(\mathbf{0}, \sigma^2\mathbf{I}_M)$, where σ^2 denotes the noise variance. We assume that the direct channel is known at the

BS.[3] Hence, we subtract the direct signal to obtain

$$\mathbf{y} = \mathbf{G}\mathbf{x} + \mathbf{n}'. \tag{6.6}$$

The UE transmits $T_1 \geq N$ orthogonal pilot sequences so that the received pilot signal at the BS, $\mathbf{Y} \in \mathbb{C}^{M \times T_1}$, is

$$\mathbf{Y} = \mathbf{G}\mathbf{X} + \mathbf{N}', \tag{6.7}$$

where $\mathbf{X} \in \mathbb{C}^{N \times T_1}$ is a unitary pilot matrix ($\mathbf{X}\mathbf{X}^H = T_1\mathbf{I}_N/N$) and $\mathbf{N}'$ is the associated channel noise matrix. Note that, in order to ensure the orthogonality of the pilot sequences, we need $T_1 \geq N$, and in the sequel, we choose $T_1 = N$. At the BS, we post-multiply $\mathbf{Y}$ by $\mathbf{X}^H$ to get $\mathbf{Z} \in \mathbb{C}^{M \times N}$ as

$$\mathbf{Z} \triangleq \mathbf{Y}\mathbf{X}^H = \mathbf{G} + \mathbf{N}, \tag{6.8}$$

where $\mathbf{N} = \mathbf{N}'\mathbf{X}^H$. Note that the statistics of $\mathbf{N}$ remain the same as $\mathbf{N}'$ since $\mathbf{X}$ is unitary. In what follows, we derive the structure of the effective cascaded channel obtained as a result of (6.1) and (6.2). From (6.4), we have

$$\mathbf{G} = \sum_{k=1}^{K}\sum_{i=1}^{N_k} \alpha_{i,k}\beta_k \mathbf{a}_M(\psi_k) \underbrace{\mathbf{a}_{L_k}^T(\nu_k)\mathbf{\Theta}_k\mathbf{a}_{L_k}(\omega_{i,k})}_{\triangleq \epsilon_{i,k}} \mathbf{a}_N^T(\phi_{i,k}) = \sum_{k=1}^{K}\sum_{i=1}^{N_k} \underbrace{\alpha_{i,k}\beta_k\epsilon_{i,k}}_{\triangleq \gamma_{i,k}^{\text{tot}}} \mathbf{a}_M(\psi_k)\mathbf{a}_N^T(\phi_{i,k}), \tag{6.9}$$

where $\{\gamma_{i,k}^{\text{tot}}\}$ denotes the effective gain coefficient for the ith path through the kth IRS. Thus, when $\mathbf{\Theta}_k = \mathbf{I}_{L_k}$ for $k \in [K]$, $\gamma_{i,k}^{\text{tot}} = \gamma_{i,k}$ where $\gamma_{i,k}$ represents the cascaded channel gain coefficients in the system. We see that the DoA/DoD at the IRS can actually be abstracted out; in fact, only the cascaded channel is required for IRS optimization. Let

$$\widetilde{\mathbf{A}}_M \triangleq [\mathbf{a}_M(\psi_1)\mathbf{1}_{N_1}^T, \ldots, \mathbf{a}_M(\psi_K)\mathbf{1}_{N_K}^T], \tag{6.10}$$

where $\widetilde{\mathbf{A}}_M \in \mathbb{C}^{M \times \sum_{i=1}^{K} N_i}$, and

[3] This can be accomplished, for example, by deactivating all the IRSs and performing the channel estimation at the BS, as described in [23]. Alternatively, in many IRS-assisted scenarios, it is common to assume that the direct path is absent due to blockages [147].

$$\mathbf{A}_N \triangleq [\mathbf{a}_N(\phi_{1,1}), \ldots, \mathbf{a}_N(\phi_{N_1,1}), \ldots, \mathbf{a}_N(\phi_{1,K}), \ldots, \mathbf{a}_N(\phi_{N_K,K})] \in \mathbb{C}^{N \times \sum_{i=1}^{K} N_i}. \quad (6.11)$$

Then, $\mathbf{G}$ in (6.9) can be written as

$$\mathbf{G} = \widetilde{\mathbf{A}}_M \mathbf{\Gamma} \mathbf{A}_N^T, \quad (6.12)$$

where $\mathbf{\Gamma}$ is an $\sum_{i=1}^{K} N_i \times \sum_{i=1}^{K} N_i$ diagonal matrix with $\gamma_{i,k}$ as its diagonal entries. From (6.12), we can write (6.8) as

$$\mathbf{Z} = \widetilde{\mathbf{A}}_M \mathbf{\Gamma} \mathbf{A}_N^T + \mathbf{N}. \quad (6.13)$$

Vectorizing (6.13), we get a *snapshot* of observations

$$\mathbf{z} = \mathbf{A}_{\text{eff}} \boldsymbol{\gamma} + \mathbf{n}, \quad (6.14)$$

where $\mathbf{z} = \text{vec}(\mathbf{Z}), \boldsymbol{\gamma} = \text{diag}(\mathbf{\Gamma}), \mathbf{A}_{\text{eff}} = \mathbf{A}_N \diamond \widetilde{\mathbf{A}}_M \in \mathbb{C}^{MN \times \sum_{i=1}^{K} N_i}$ and $\mathbf{n} = \text{vec}(\mathbf{N})$. Notice that (6.14) is precisely an array signal model for a (virtual) array of MN sensors [148]. Thus, we can view (6.14) as a direction-finding problem to estimate the DoAs and the DoDs (with both the operations being performed at the BS.) Interestingly, our reformulation allows the algorithm to proceed by first estimating the DoAs at the BS and then estimating the DoDs from the UEs using the DoAs obtained in the first step. The two steps can be efficiently performed using subspace-based methods, namely, *ESPRIT* and *MUSIC* algorithms, respectively [144], [145]. We call this algorithm a *joint* ESPRIT-MUSIC algorithm to indicate that the estimation of DoDs from the UEs utilizes the knowledge of DoAs at the BS. This simplifies the complexity of the solution to a simple 1-dimensional grid search for angle estimation, in contrast to employing a brute-force search over a 2-dimensional grid. Thus, we jointly and non-iteratively estimate the angles and reduce the number of variables to be estimated to equal the number of DoAs at the BS.

Remark 6.1 (On the number of antennas at BS and UEs)**.** *To solve for DoAs and DoDs from* (6.14) *using the subspace methods, namely, ESPRIT and MUSIC, we need* $MN \geq (\sum_k N_k) + 1$. *However, this condition can be easily met in practice since* M *is large and* N_k *is small in typical mmWave systems. Hence, the proposed algorithm is robust to the number of IRSs in the system as long as* N_k *is not too large.*

Remark 6.2 (On the number of pilot transmissions)**.** *In solving for DoAs and DoDs using subspace methods, we estimate the data covariance matrix from the array response observations. Suppose T_2 independent snapshots of the form (6.14) are used to compute a sample covariance matrix, which is then used to estimate the DoA and DoDs, with each snapshot obtained using $T_1 = N$ pilot transmissions. Thus, the total number of pilot transmissions required is NT_2. To choose T_2, since the rank of the true covariance matrix is at least $\sum_k N_k$, we require that $T_2 > \sum_k N_k$. In contrast, the number of pilot transmissions required for least squares (LS) channel estimation is at least $MN\sum_k L_k$, and, in practice, $NT_2 \ll MN\sum_k L_k$. Thus, the subspace-based approach entails low pilot overhead that does not scale with the number of IRS elements.*

As mentioned in Remark 6.2, T_2 snapshots are collected to form $\mathbf{Z}' \in \mathbb{C}^{MN\times T_2}$ as $\mathbf{Z}' = [\mathbf{z}_1, \mathbf{z}_2, \ldots, \mathbf{z}_{T_2}]$. To obtain independent snapshots, we enable the IRSs with $T_2 - 1$ random phase configurations in addition to the first snapshot $\mathbf{z}_1$ obtained with $\mathbf{\Theta}_k = \mathbf{I}_{L_k} \forall k \in [K]$.[4] The sample covariance matrix is computed as $\widehat{\mathbf{R}} \triangleq \frac{1}{T_2}\sum_{t=1}^{T_2} \mathbf{z}_t\mathbf{z}_t^H$, and the DoAs at the BS from all the K IRS links are estimated using ESPRIT as outlined in Algorithm 6.1. Next, using the obtained DoA estimates, a joint estimate for the $\sum_k N_k$ DoDs from the UEs is obtained using MUSIC (with a grid size of d), as outlined in Algorithm 6.2.[5] The central idea of *joint ESPRIT-MUSIC* based estimation is as follows. The received uplink signal lies in the subspace spanned by the array steering vectors corresponding to the true DoA(s) at the BS. So, we can use the ESPRIT-based method to identify this subspace, and this step does not depend on the DoDs from the UEs. Subsequently, an estimate of the signal vector that corresponds to the true DoD from the UE is identified as the vector orthogonal to the noise subspace formed using the estimated DoAs at the BS. This is accomplished through steps 4 and 5 in Algorithm 6.2 [145, 148].[6] As a result, we obtain

[4] Any other method which generates independent snapshots of the form (6.14) can be used for selecting the remaining $T_2 - 1$ IRS phase configurations.

[5] Algorithm 6.2 requires the knowledge of N_k. We provide a heuristic method to estimate N_k for every k in Sec. 6.4.

[6] It is known that while ESPRIT is a computationally efficient algorithm, MUSIC is efficient in its performance, i.e., it achieves Cramer Rao Lower Bound (CRLB) [149]. Examining the best choice of subspace methods under various IRS-aided system settings is relegated to future work.

Algorithm 6.1: DoA estimation at the BS using ESPRIT

Input: $\widehat{\mathbf{R}}, M, N, K$

1 Perform the eigenvalue decomposition of $\widehat{\mathbf{R}} = \mathbf{U}\boldsymbol{\Lambda}\mathbf{U}^H$ and obtain $(\boldsymbol{\Lambda}, \mathbf{U})$.

2 Select the K dominant eigenvectors of $\mathbf{U}$ to form a basis for the signal subspace, $\mathbf{U}_S$.

3 Define selection matrices $\mathbf{W}_1 \triangleq [\mathbf{I}_{MN-1} \mid \mathbf{0}_{MN-1}]$ and $\mathbf{W}_2 \triangleq [\mathbf{0}_{MN-1} \mid \mathbf{I}_{MN-1}]$.

4 Compute $\mathbf{U}_{S,1} = \mathbf{W}_1\mathbf{U}_S$ and $\mathbf{U}_{S,2} = \mathbf{W}_2\mathbf{U}_S$.

5 Obtain $\boldsymbol{\Omega} = \mathbf{U}_{\mathbf{S},1}^{\dagger}\mathbf{U}_{\mathbf{S},2}$.

6 Compute the eigen values of $\boldsymbol{\Omega}$ as $\xi_1, \xi_2, \xi_3, \ldots, \xi_K$.

7 Compute $\widehat{\psi}_k = \sin^{-1}\left(-\frac{\arg(\xi_k)}{\pi}\right)$, where $\arg(x) = \tan^{-1}\left(\frac{\Im(x)}{\Re(x)}\right)$, $k = 1, \ldots, K$

Output: $\left\{\widehat{\psi}_k\right\}_{k=1}^{K}$

an estimate of $\mathbf{A}_{\text{eff}}$, denoted by $\widehat{\mathbf{A}}_{\text{eff}}$ and finally, given the DoA and DoD estimates, the channel path gain coefficients $\boldsymbol{\gamma}$ are estimated by the LS method. Since the IRS phase configuration was chosen to be an identity matrix for the first snapshot, we have

$$\widehat{\boldsymbol{\gamma}} = \widehat{\mathbf{A}}_{\text{eff}}^{\dagger}\mathbf{z}_1 = \left(\widehat{\mathbf{A}}_{\text{eff}}^H\widehat{\mathbf{A}}_{\text{eff}}\right)^{-1}\widehat{\mathbf{A}}_{\text{eff}}^H\mathbf{z}_1. \tag{6.15}$$

Thus, $\left[\widehat{\mathbf{A}}_{\text{eff}}, \widehat{\boldsymbol{\gamma}}\right]$ can be used to compute an estimate for the cascaded channel $\mathbf{G}$ in (6.12).

Computational complexity: We assess the computational complexity of Algorithms 6.1 and 6.2 in terms of the order of the number of floating point operations (flops) required. From [150], it is easy to see that the complexity of Algorithm 6.1 scales as $\mathcal{O}(M^3N^3 + M^2N^3T_2)$, while that of Algorithm 6.2 scales as $\mathcal{O}(M^2N^2P + M^2NT_2)$ where $P = \pi/d$ and d is the desired angular resolution. Thus, the complexity is polynomial in the problem parameters.

6.4 Numerical Results

In this section, we evaluate the proposed channel estimation algorithm via Monte Carlo simulations. We set $M = 256$, $N = 2$, $N_1 = 2$ and $N_k = 1$ for $k \in \{2, 3, 4\}$, K up to 4, and $L_i = 512$ for $i \in \{1, 2, 3, 4\}$. Since the proposed scheme requires substantially fewer pilot transmissions than the LS method, and the LS method completely fails at the low

Algorithm 6.2: Estimation of the DoD from the UE using MUSIC

Input: $M, N, K, \{N_k\}_{k=1}^{K}, \left\{\widehat{\psi}_k\right\}_{k=1}^{K}, (\mathbf{\Lambda}, \mathbf{U}), d$

1 Select the $MN - \sum_k N_k$ eigen vectors of $\mathbf{U}$ corresponding to the least $MN - \sum_k N_k$ eigenvalues to form a basis for noise sub-space, $\mathbf{U}_N$.

2 **for** $k = 1$ *to* K **do**

3 **for** $\phi = -\frac{\pi}{2}$ *to* $\frac{\pi}{2}$ *in steps of* d **do**

4 $\mathbf{P}_{\text{spec}}(k, \phi) = \frac{1}{\left\|\left\{[\mathbf{a}_N(\phi) \otimes \mathbf{I}_M]\mathbf{a}_M(\widehat{\psi}_k)\right\}^H \mathbf{U}_N\right\|_2^2}$.

5 $\left\{\widehat{\phi}_{i,k}\right\}_{i=1}^{N_k} = \arg\max_{\phi}^{(N_k)} \ \mathbf{P}_{\text{spec}}(k, \phi)$.

Output: $\left\{\widehat{\phi}_{i,k}\right\}_{i=1,k=1}^{N_k,K}$.

pilot levels, we do not compare the proposed method against the LS method. Instead, we compare its performance with the SOMP approach, which exploits sparsity in mmWave channels [33].

6.4.a Performance With Number of IRSs

In Fig. 6.2, we plot the normalized mean square error (NMSE) in channel estimation versus the SNR for different numbers of IRSs in the system, with $T_1 = N$ and $T_2 = 10$. We see that the NMSE of SOMP degrades with increasing K, i.e., when the number of measurements, MN, remains fixed while the sparsity level increases. This happens because the theory of CS mandates that the number of measurements needs to scale linearly with the sparsity level of the vector to be recovered [151], which is not the case here. On the other hand, the performance of the proposed method is insensitive to increasing K. This is intuitive because an increase in K only increases the number of sources for which the angle estimation is sought, and, as per Remark 6.1, as long as $(\sum_k N_k) + 1 \leq MN$, the algorithm successfully estimates the angles. Thus, the performance of the proposed algorithm is robust to the number of IRSs in the system, in contrast to the performance of SOMP or LS, whose performance degrades with K, even for small values of K.

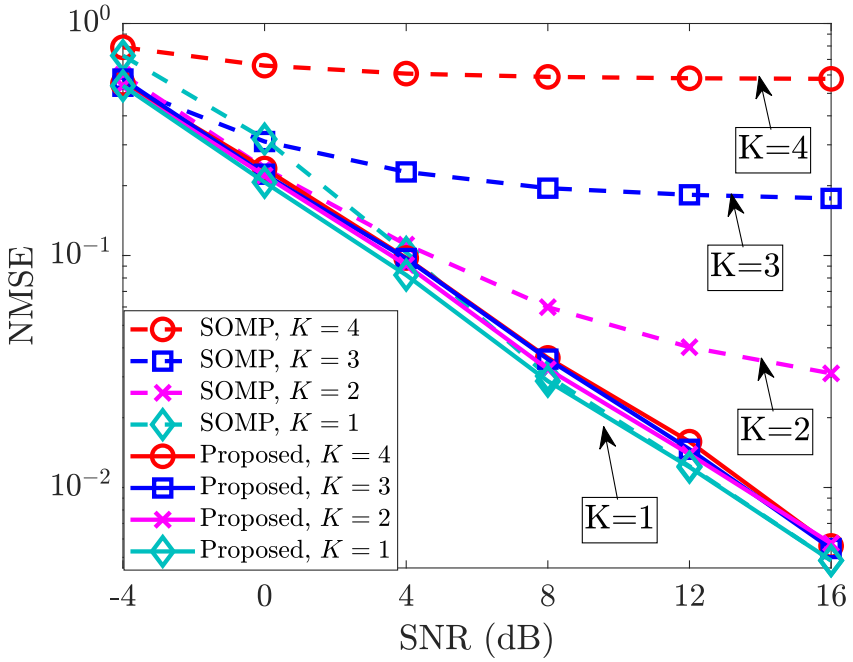

Figure 6.2: NMSE vs SNR for $K = 1, 2, 3, 4$.

6.4.b Performance With Number of Pilot Transmissions

In Fig. 6.3, we plot the NMSE vs. SNR of the proposed approach and SOMP, for varying number of snapshots, and with $K = 2$, $N_1 = 2$ and $N_2 = 1$. Specifically, we consider the regime of $T_2 > \sum_k N_k$ as per Remark 6.2. We first observe that increasing the number of snapshots does not affect the NMSE of SOMP (especially at higher SNRs): this is because increasing T_2 only increases the number of measurement vectors, and success recovery of CS algorithms only loosely depends on the number of measurement vectors, provided the number of measurements is large enough. However, as mentioned earlier, the performance of SOMP can degrade when MN is small or K is large, in which case, the performance of SOMP will be far inferior to that of the proposed method for any number of snapshots. This is because when sparse signal recovery algorithms fail, they typically fail completely. On the other hand, the performance of the proposed algorithm keeps improving with the number of snapshots because the covariance matrix estimate becomes more accurate, leading to better estimation of the DoAs and DoDs. We see that the NMSE stabilizes within as few as 10 snapshots. When $T_2 = 4$ (note that $\sum_k N_k = 3$) or more, the performance improves dramatically with SNR, and the scheme outperforms

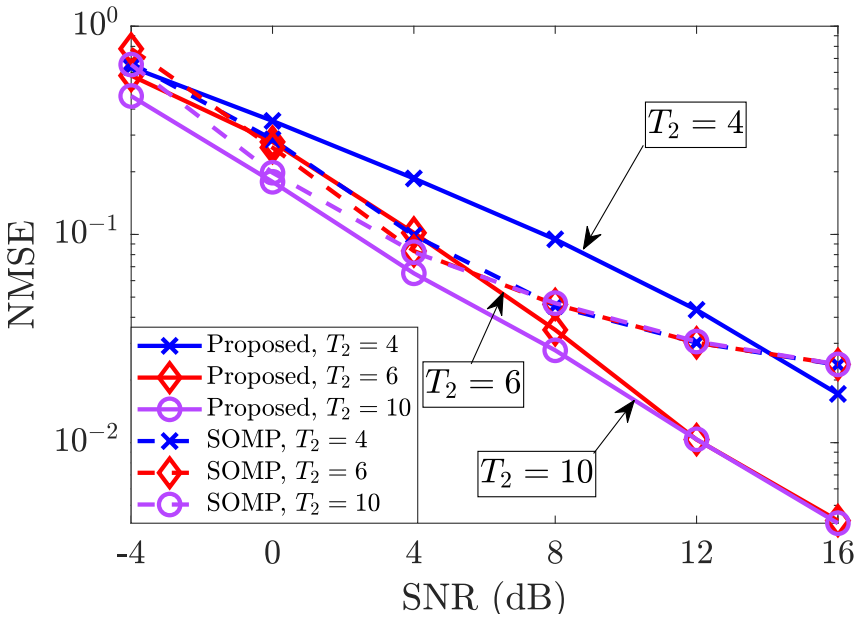

Figure 6.3: NMSE vs SNR for $T_2 = 4, 6, 10$.

SOMP at higher SNRs. These observations are in line with Remark 6.2.

6.4.c Pairing Capability of the Joint Estimator

In Fig. 6.4, we illustrate the pairing capability of the joint ESPRIT-MUSIC based DoA-DoD estimator corresponding to each IRS in the system. In particular, we consider $K = 4$ (with $N_1 = 2, N_2 = N_3 = N_4 = 1$), and the corresponding choice of DoDs ($\{\phi_{i,k}\}$) and DoAs ($\{\psi_k\}$) (in degrees) at the UE and BS, respectively as given in Table 6.2. To show the pairing, we plot the MUSIC spectrum with a particular DoA estimate ψ_k (obtained via ESPRIT) as the input and determine the DoD(s) $\{\phi_{i,k}\}_{i=1}^{N_k}$ from the spectrum. The figure shows that correct pairing between the DoAs and DoDs is accomplished without any ambiguity, which illustrates the utility of our approach of using subspace-based methods for joint estimation of the angles, applied to the scenario of distributed IRS in a mmWave mMIMO system.

6.4.d Heuristic Method To Determine $\sum_k N_k$ and $N_k \ \forall \ k$

As mentioned in the previous section, Algorithm 6.2 requires the knowledge of $N_k \ \forall \ k$. In this subsection, we briefly describe a heuristic approach to estimate N_k based on the

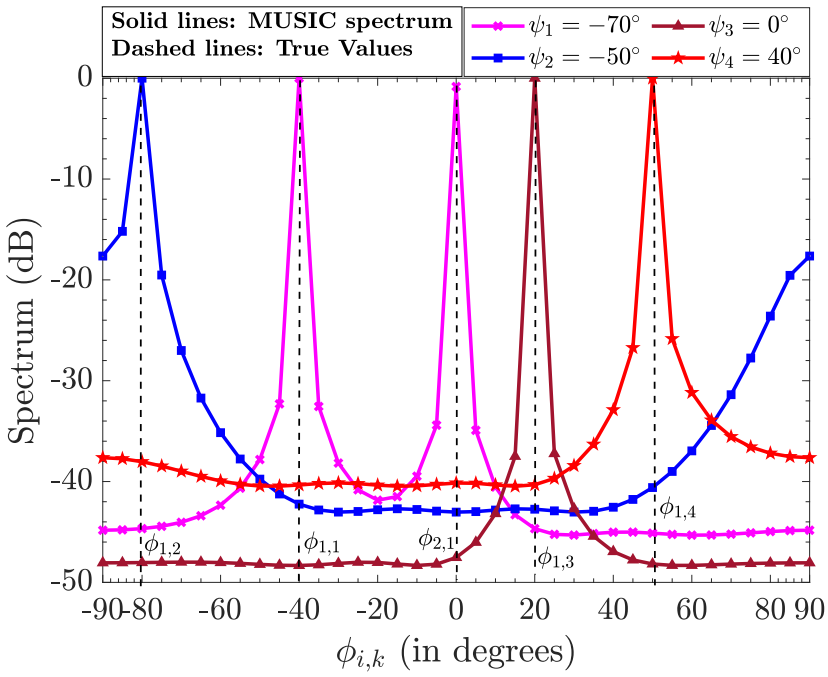

Figure 6.4: MUSIC spectrum at 20 dB SNR for $T_2 = 20$.

Table 6.2: DoD and DoA Parameters for Fig. 6.4.

	Paths indexed by IRSs			
Angles	**IRS-1**	**IRS-2**	**IRS-3**	**IRS-4**
DoDs	$\phi_{1,1} = -40°$, $\phi_{2,1} = 0°$	$\phi_{1,2} = -80°$	$\phi_{1,3} = 20°$	$\phi_{1,4} = 50°$
DoAs	$\psi_1 = -70°$	$\psi_2 = -50°$	$\psi_3 = 0°$	$\psi_4 = 40°$

observed data. Inspired by principal component analysis and the scree plot method [152], we consider the magnitude of the normalized eigen-spectrum of the sample covariance matrix of the received signal and plot it in decreasing order in Fig. 6.5. In this figure, the normalized eigen-spectrums for the cases with 4 IRSs ($N_1 = 2, N_k = 1$ for $k \in \{2, 3, 4\}$) and 2 IRSs ($N_1 = 2, N_2 = 1$) are shown for two different values of SNR. We identify the *transition zone*, which demarcates the end of *dominant* eigenvalues that correspond to all the signal components, and declare the estimate of $\sum_k N_k$ to be the number of such dominant eigenvalues. We also note from Fig. 6.5 that, at both high and low SNR, the transition zone is sufficiently sharp to enable accurate estimates of the number of dominant

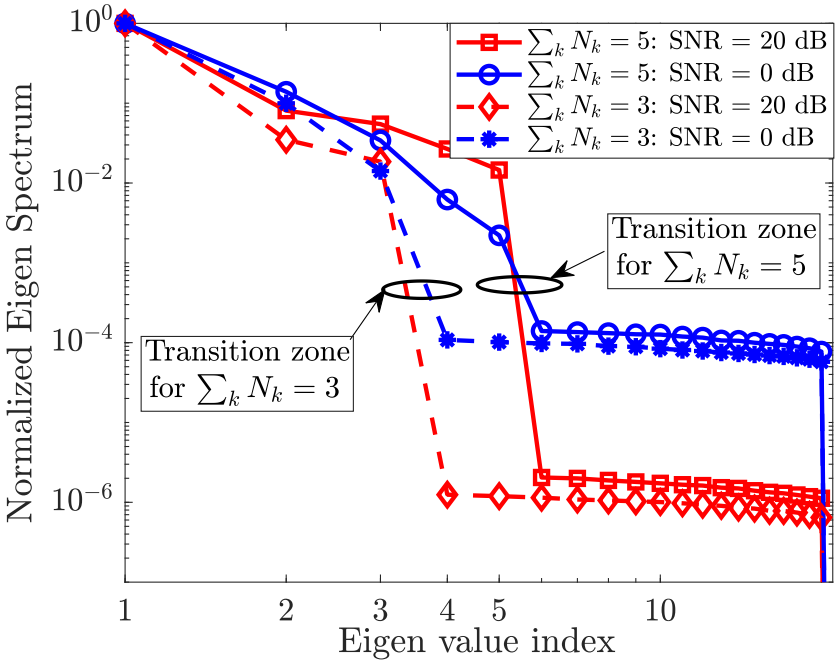

Figure 6.5: Normalized eigen-spectrum for $T_2 = 20$.

eigenvalues.

We use the estimate of $\sum_k N_k$ in step 1 of Algorithm 6.2; then, for every k, we can obtain an estimate of N_k from the MUSIC spectrum in steps 4 and 5, by analyzing the local extremum points (or) by using thresholding methods such as described in [153]. Following this, we can estimate the DODs from the UE as outlined in Algorithm 6.2.

6.5 Conclusions

In this chapter, we presented a novel algorithm for cascaded channel estimation for distributed IRS-aided mmWave mMIMO systems leveraging techniques from the array signal processing literature. We showed that accurate channel estimation is possible with far fewer pilots compared to conventional CSI estimation methods. In particular, the number of pilots needed only scales with the total number of paths between the IRSs and the UE and the number of antennas at the UE, but is independent of the number of elements in the IRS. This is because the proposed technique exploits the structure in the mmWave channels to dramatically reduce the number of parameters to be estimated, followed by

using classical array processing methods to solve the nonlinear estimation problem. We also empirically noted that the proposed estimator offers robust performance as the number of IRSs in the system is increased, compared to the performance of the SOMP-based estimator. Future work can theoretically analyze the performance of this estimator and extend it to non-line-of-sight scenarios.

7 Performance of Multi-IRS-Aided Multiple Operator Systems

Chapter Highlights

This chapter extends the work pursued in Chapter 4, where we consider that each mobile operator (MO) deploys and controls an intelligent reflecting surface (IRS) to serve its own user equipments (UEs), which leads to multiple in-band and out-of-band (OOB) reflections in the system via each IRS. In this context, this chapter addresses the following questions: Can an MO still continue to control its IRS independently of other MOs and IRSs? Is joint optimization of the IRSs deployed by different MOs and inter-MO cooperation needed? To that end, by considering the mmWave bands, we first derive the ergodic sum spectral efficiency (SE) in a 2-MO system for the following schemes:

1. Joint optimization of an overall phase angle of the IRSs with MO cooperation,
2. MO cooperation via time-sharing, and
3. No cooperation between the MOs.

We find that even with no cooperation between the MOs, the performance of a given MO is not degraded by the presence of an OOB MO deploying and independently controlling its own IRS. On the other hand, the SE gain obtained at a given MO using joint optimization and cooperation over the no-cooperation scheme decreases inversely with the number of elements in the IRS deployed by the other MO. We generalize our results to a multiple MO setup and show that the gain in the sum-SE over the no-cooperation case increases at least linearly with the number of OOB MOs. Finally, we numerically verify our findings and conclude that every MO can independently operate and tune its IRS; cooperation via optimizing an overall phase only brings marginal benefits in practice.

7.1 Introduction

Millimeter-wave (mmWave) frequency bands have been incorporated into current wireless standards to enable high data rates by leveraging the availability of large bandwidths [1]. However, a concern with the use of mmWave bands is the high propagation loss, which limits cellular coverage. Intelligent reflecting surfaces (IRSs) have recently been introduced to tackle this issue by providing virtual line-of-sight paths [3]. Further, in real-life scenarios, multiple mobile operators (MOs) using different and non-overlapping frequency bands coexist in a geographical area and provide independent services to different user equipments (UEs) that are subscribed to them. In such a scenario, since an IRS is a passive device and does not contain a bandpass filter, it reflects the signals of every MO in the system. Thus, it remains unclear whether MOs can independently optimize their IRSs for their UEs or if cooperation among MOs is required due to the presence of IRSs. This chapter addresses these issues and offers insights into multiple MO systems aided by IRSs in the mmWave bands.

7.1.a Related Work & Motivation

The IRS literature has seen significant growth in recent years. For instance, [154] and [9] investigate the joint design of active and passive beamforming for sub-6 GHz and mmWave systems, respectively. In [89], the authors propose channel estimation and IRS phase optimization techniques tailored to orthogonal frequency division multiplexing (OFDM)-based systems. The work in [155] explores multiple access schemes in IRS-assisted networks, while [156] demonstrates the performance gains of IRSs over conventional relays. Additionally, [39] highlights the potential of IRSs in enhancing physical-layer security. The study in [157] extends IRS deployment to multi-cell environments, and [158] introduces machine learning-based techniques for optimizing IRS reflection coefficients. A comprehensive review of the applications and benefits of IRSs in mmWave systems can be found in [3, 159, 160].

In [161] and [162], hybrid beamforming architectures were proposed for IRS-aided mmWave systems using instantaneous and statistical channel state information (CSI), respectively.

Following this, [163] and [164] solved for optimal power control coefficients/UE associations and IRS configurations, respectively, to maximize the sum-rate of UEs in multiple-IRS setups. In [65], a beam training problem for IRSs exploiting the channel sparsity was solved, and in [25] and [138], novel CSI estimation techniques were proposed for centralized and distributed IRS setups, respectively. However, all these works implicitly assume the presence of only one MO that deploys and controls the IRS. The problem becomes more challenging when we consider more than one MO in the system. To explain, MOs are typically allotted non-overlapping frequency bands centered at nearby carrier frequencies to provide service to the UEs subscribed to them. So, the MO that deploys and controls the IRS (called the in-band MO) tunes the IRS phase configuration in the frequency band allotted to the MO to best serve its own UEs. However, the IRSs are passive, i.e., they do not contain any active signal processing/RF circuitry such as a band-pass filter to selectively reflect signals whose frequency content lies only within the band allotted to the in-band operator. As a result, any other MO providing service in the same geographical area in a nearby frequency allocation will naturally have its signals reflected off the IRS with an arbitrary phase shift. For example, the n257 band in 5G new radio (NR) operates in the mmWave frequencies and spans 26.5-29.5 GHz, i.e., a bandwidth of 3 GHz [165, Table 5.2-1]. Given that the maximum carrier bandwidth in 5G NR is 400 MHz, the n257 band could be used by at least 7 different service providers/MOs (and more in geographies where the allotted bandwidth to each MO is less than 400 MHz). Then, since these MOs use the same frequency range to provide services to their UEs but use non-overlapping frequency bands, the IRS elements will reflect signals impinging on them from all MOs with similar efficiency.

In this context, [108] studied CSI estimation in IRS-aided multiple MO systems, and [166] experimentally evaluated the performance impact of IRS in the presence of multiple MOs. Further, [109, 110, 167] and [168–172] considered joint optimization of the IRS configurations and allocation of disjoint IRSs/sub-IRSs to different bands/MOs via cooperation. However, most of these works assume that complete CSI for all links is available at all MOs, necessitating extensive inter-MO cooperation. Such cooperation between MOs is

Table 7.1: Summary of literature on IRS-aided multiple MO systems.

	[154]	[9]	[155]	[108]	[166]	[109]	[110]	[167]	[168]	[169]	[170]	[171]	[172]	[80]	[125]	[173]	This work
Frequency band†	S6	M	S6	S6	S6	S6	S6	M	S6	M	S6	M	M	S6, M	M	S6	M
More than one MO?				✓	✓	✓		✓	✓	✓	✓	✓	✓	✓	✓	✓	✓
Multiple UEs per MO?	✓		✓			✓		✓	✓	✓	✓			✓	✓		✓
Multiple access scheme◇	T	—	T, F	—	—	S	—	S	S	S	S	—	—	T	T	—	T
CSI requirement/exchange#	F	F	F	F	P	F	F	F	F	P	P	P	F	P	P	P	P
Multiple IRSs?		✓						✓	✓	✓	✓				✓		✓
Low-complexity solution					✓					✓	✓		✓	✓	✓	✓	✓
MO-cooperative joint optimization schemes						✓	✓	✓									✓
MO-cooperative resource sharing schemes								✓				✓	✓				✓
Closed form performance analysis	✓	✓		✓										✓	✓	✓	✓
Quantifying the effects of OOB IRSs				✓										✓	✓	✓	✓
Quantifying the gains of inter-MO cooperation																	✓

† M: mmWave bands; S6: sub-6 GHz bands

◇ T / F / S: Time / Frequency / Space division multiple access

F: Full CSI required/exchanged; P: Partial CSI required/exchanged

often infeasible in practice. Moreover, the precise benefits of jointly controlling all IRSs in enhancing the overall network performance across multiple MOs remain largely unclear and unquantified. Our prior works in Chapters 4 and 5, which are also published in [80, 125], respectively, quantified the out-of-band performance impact of the IRS when only one MO deploys one or more IRSs, and [173] considered setups where each MO deploys its own IRS in the sub-6 GHz band. Table 7.1 presents a quick comparison of our work against the prior studies on IRS-assisted multiple-MO systems. For the first time in the literature, this chapter explores several aspects of IRS-aided multiple MO systems in mmWaves: quantifying the benefits of inter-MO cooperation and joint optimization, low-complexity algorithmic solutions for such cooperation, and an in-depth performance analysis with closed-form expressions. Notably, these closed-form expressions offer useful insights into the behavior and limits of such systems under various *practical* transmission schemes. Further, we make these contributions without compromising the generality of the system model.

7.1.b Contributions

To set the context, we use the following terminology: the IRSs and UEs controlled/served by an MO of interest are termed *in-band*, and other IRSs/UEs in the system are called *out-of-band (OOB)* with respect to this same MO. We make the following key contributions in this chapter:

1. Considering that 2 MOs, X and Y, control an IRS each, we derive the ergodic sum spectral-efficiency (SE) of the MOs when an overall phase at each IRS is configured as per the following implementation schemes (see Theorem 7.1):

   (a) *Optimization with Time-sharing*: In each time slot, while an MO serves its own UE, the overall phases at the IRSs are optimized for a UE served by either MO-X or MO-Y.

   (b) *Joint-optimization with MO cooperation*: The overall IRS phases are jointly tuned to maximize the weighted sum-SE of UEs scheduled by MOs in every time slot.

   (c) *No MO cooperation*: In this scheme, each MO focuses exclusively on optimizing its IRSs to ensure coherent signal reception at only its own UEs.

2. We show that the IRS controlled by one MO does not degrade the sum-SE of the other MO. We quantify the gain in the sum-SE of the MOs obtained with/without OOB IRS, and with/without cooperation (for time-sharing/joint optimization) as a function of the number of OOB IRS elements (see Theorem 7.2.)

3. We next extend our results to a system with more than 2 MOs, which deploy and control an IRS each. In particular, we derive the ergodic-sum-SE of the MOs for the above-mentioned three schemes (see Theorem 7.3.)

4. Finally, even with more than 2 MOs, we show that the OOB IRSs do not degrade the in-band performance. Further, although joint optimization/time sharing with MO cooperation still offers marginal gains relative to sum-SE when the MOs do not cooperate, the gain increases at least linearly with the number of OOB MOs. (see Theorem 7.4.)

Our results are elegant and insightful in that they readily characterize the ergodic sum-SE of the MOs in IRS-aided mmWave systems as a function of system parameters such as the number of IRS elements, in-band and OOB cascaded channel paths, SNR of operation, etc.

We numerically validate our analytical results and illustrate that joint optimization/cooperation among MOs provides marginal gains compared to when an MO configures its IRS without any cooperation. For instance, with 2-MOs, each with 16-element IRSs, the performance gain in the SE of an MO obtained at 80 dB transmit SNR via joint optimization and cooperation over a no-cooperation policy is about 2%. Also, this improvement monotonically decreases with the number of OOB IRS elements and transmit SNR; for e.g., it is 0.4% and 0.08% for $N = 32, 64$, respectively. As a result, cooperation between MOs to optimize the IRSs may not be needed in IRS-aided mmWave systems with multiple MOs. Each MO can deploy and control its IRS independently, and the IRS of one MO does not degrade the performance of another MO.

Notation: For general notations used in this chapter, see the section on "General Mathematical Notations" on page ix. For the notations/variables specific to this chapter, please refer to Table 7.2.

7.2 System Model and Problem Description

Multiple MOs operating over different and non-overlapping mmWave bands simultaneously exist in a given geographical area and provide services to the UEs subscribed to them. For mathematical brevity, we describe the model for a system with two MOs, say X and Y, but the model directly extends to any number of MOs, as we describe in Sec. 7.5. The MOs X and Y operate over non-overlapping frequency bands, and both use time-division multiple access (TDMA) to serve one of K UEs on a frequency band centered at f_1 and one of Q UEs on a frequency band centered at f_2, respectively, in each time slot. Also, their base stations,[1] BS-X and BS-Y, deploy and control an N_1-element IRS-X and an

[1]For simplicity, we use single antenna BSs in this work, similar to [110, 169]. However, our results can also be extended to multiple antenna cases.

N_2-element IRS-Y, respectively. Due to the high attenuation in the mmWaves, the direct links between the BSs and UEs are blocked [25, 174]. The downlink signal received at UE-k, served by MO-X, is given by

$$y_k = \left(\mathbf{g}_{\mathrm{X}k}^T \boldsymbol{\Theta}_1 \mathbf{f}_{\mathrm{XX}} + \mathbf{g}_{\mathrm{Y}k}^T \boldsymbol{\Theta}_2 \mathbf{f}_{\mathrm{XY}}\right) x_k + n_k, \tag{7.1}$$

where $\mathbf{g}_{\mathrm{X}k} \in \mathbb{C}^{N_1}$ and $\mathbf{g}_{\mathrm{Y}k} \in \mathbb{C}^{N_2}$ are the channels from IRS-X and IRS-Y to UE-k, respectively; $\mathbf{f}_{\mathrm{XX}} \in \mathbb{C}^{N_1}$ and $\mathbf{f}_{\mathrm{XY}} \in \mathbb{C}^{N_2}$ are the channels from BS-X to IRS-X and IRS-Y, respectively, x_k is the information symbol for UE-k with average power constraint $\mathbb{E}[|x_k|^2] \leq P$ and $n_k \sim \mathcal{CN}(0, \sigma^2)$ is the additive noise at UE-k. Similarly, the downlink signal from BS-Y to UE-q, served by MO-Y, can be written as

$$y_q = \left(\mathbf{t}_{\mathrm{X}q}^T \boldsymbol{\Theta}_1 \mathbf{f}_{\mathrm{YX}} + \mathbf{t}_{\mathrm{Y}q}^T \boldsymbol{\Theta}_2 \mathbf{f}_{\mathrm{YY}}\right) x_q + n_q, \tag{7.2}$$

where $\mathbf{t}_{\mathrm{X}q} \in \mathbb{C}^{N_1}$ and $\mathbf{t}_{\mathrm{Y}q} \in \mathbb{C}^{N_2}$ are the channels from IRS-X and IRS-Y to UE-q, respectively, $\mathbf{f}_{\mathrm{YX}} \in \mathbb{C}^{N_1}$ and $\mathbf{f}_{\mathrm{YY}} \in \mathbb{C}^{N_2}$ are the channels from BS-Y to IRS-X and IRS-Y, respectively, x_q is the information symbol for UE-q with power constraint $\mathbb{E}[|x_q|^2] \leq P$ and $n_q \sim \mathcal{CN}(0, \sigma^2)$ is the additive noise at UE-q. In particular, $\mathbf{f}_{ab}$ denotes the channel from BS-a to IRS-b, $\mathbf{g}_{cd}$ denotes the channel from IRS-c to the dth UE served by MO-X, and $\mathbf{t}_{cd}$ denotes the channel from IRS-c to the dth UE served by MO-Y. Finally, $\boldsymbol{\Theta}_1 \in \mathbb{C}^{N_1 \times N_1}$ and $\boldsymbol{\Theta}_2 \in \mathbb{C}^{N_2 \times N_2}$ are diagonal matrices with unit modulus reflection coefficients of IRS-X and IRS-Y, respectively. Figure 7.1 illustrates our system model.

Terminology: Since MO-X configures IRS-X to serve UE-k, we refer to the IRS-X and UE-k as the *in-band* IRS and UE, respectively, from MO-X's viewpoint. Similarly, the IRSs or UEs that are not controlled/served by the BS-X (operating on a different band) are *out-of-band (OOB)* nodes from MO-X's viewpoint. Further, the link from MO-X to UE-k via IRS-X is the in-band channel; the links from MO-X to UE-k via OOB IRSs are OOB channels. These apply to other MOs also.

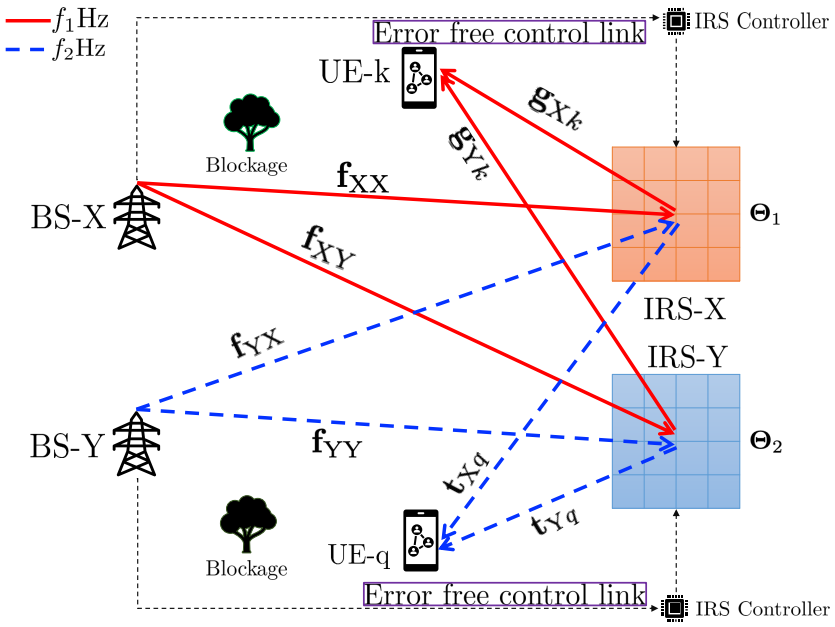

Figure 7.1: System Model of 2-BS & 2-IRS system.

7.2.a Channel Model

We use the standard Saleh-Venezuela (SV) model to describe the channels in the mmWave frequency bands [25, 65]. The channel from BS-Z to IRS-W ($Z, W \in \{\mathrm{X}, \mathrm{Y}\}$) is

$$\mathbf{f}_{ZW} = \sqrt{N_p \Big/ L_Z^{(p)}} \sum\nolimits_{l=1}^{L_Z^{(p)}} \gamma_{l,Z}^{(p)} \mathbf{a}_{N_p}^*(\phi_{l,Z}^{(p)}), \tag{7.3}$$

where $p = 1 \cdot \mathbb{1}_{\{W=\mathrm{X}\}} + 2 \cdot \mathbb{1}_{\{W=\mathrm{Y}\}}$, $L_Z^{(p)}$ is the number of resolvable paths from BS-Z to the IRS-W and $\phi_{l,Z}^{(p)}$ is the sine of the angle of arrival of the lth path from BS-Z to IRS-W. Similarly, the channel from IRS-W to UE-r served by MO-X/MO-Y is given by

$$\mathbf{g}_{Wr} \Big/ \mathbf{t}_{Wr} = \sqrt{N_p \Big/ L_r^{(p)}} \sum\nolimits_{l=1}^{L_r^{(p)}} \gamma_{l,r}^{(p)} \mathbf{a}_{N_p}^*(\psi_{l,r}^{(p)}), \tag{7.4}$$

where $L_r^{(p)}$ is the number of resolvable paths from IRS-W to UE-r, $\psi_{l,r}^{(p)}$ is the sine of angle of departure of lth path from IRS-W to UE-r, and N_p is the number of IRS elements in IRS-W. The sine terms are sampled from an appropriate distribution $\mathcal{P}_{\mathcal{A}}$, which is discussed in the sequel. The fading coefficients, $\gamma_{l,Z}^{(p)}$ and $\gamma_{l,r}^{(p)}$ are independently sampled from $\mathcal{CN}(0, \beta_Z^{(p)})$ and $\mathcal{CN}(0, \beta_r^{(p)})$, respectively, where $\beta_Z^{(p)}$ and $\beta_r^{(p)}$ denote the path loss in

$$h_k = \frac{N_1}{\sqrt{L_{k1}}} \sum_{l=1}^{L_{k1}} \gamma_{l,X}^{(1)} \gamma_{l,k}^{(1)} \mathbf{a}_{N_1}^H(\psi_{l,k}^{(1)}) \boldsymbol{\Theta}_1 \mathbf{a}_{N_1}^*(\phi_{l,X}^{(1)}) + \frac{N_2}{\sqrt{L_{k2}}} \sum_{l=1}^{L_{k2}} \gamma_{l,X}^{(2)} \gamma_{l,k}^{(2)} \mathbf{a}_{N_2}^H(\psi_{l,k}^{(2)}) \boldsymbol{\Theta}_2 \mathbf{a}_{N_2}^*(\phi_{l,X}^{(2)}) \tag{7.6}$$

$$\overset{(a)}{=} \frac{N_1}{\sqrt{L_{k1}}} \sum_{l=1}^{L_{k1}} \gamma_{l,X}^{(1)} \gamma_{l,k}^{(1)} \left(\mathbf{a}_{N_1}^H(\phi_{l,X}^{(1)}) \odot \mathbf{a}_{N_1}^H(\psi_{l,k}^{(1)}) \right) \boldsymbol{\theta}_1 + \frac{N_2}{\sqrt{L_{k2}}} \sum_{l=1}^{L_{k2}} \gamma_{l,X}^{(2)} \gamma_{l,k}^{(2)} \left(\mathbf{a}_{N_2}^H(\phi_{l,X}^{(2)}) \odot \mathbf{a}_{N_2}^H(\psi_{l,k}^{(2)}) \right) \boldsymbol{\theta}_2, \tag{7.7}$$

BS-IRS and IRS-UE links, respectively. Finally, we consider an N-element uniform linear array (ULA) based IRS,[2] similar to [33], with half-wavelength inter-element spacing; its array response vector $\mathbf{a}_N(\psi)$ is

$$\mathbf{a}_N(\psi) = \frac{1}{\sqrt{N}} [1, e^{-j\pi\psi}, \ldots, e^{-j(N-1)\pi\psi}]^T \in \mathbb{C}^N. \tag{7.5}$$

7.2.a.i Cascaded Channel Representation

Substituting the expressions for individual channels given in (7.3), (7.4) into (7.1), the channel at UE-k can be simplified as in (7.6), (7.7) on the top of a page, where $L_{k1} \triangleq L_X^{(1)} L_k^{(1)}$ is the number of resolvable in-band paths from BS-X to UE-k through IRS-X (see Sec. 7.2.a.ii for details on resolvability), $L_{k2} \triangleq L_X^{(2)} L_k^{(2)}$ is the number of resolvable OOB paths from BS-X to UE-k through IRS-Y, $\boldsymbol{\theta}_1 = \text{diag}(\boldsymbol{\Theta}_1) \in \mathbb{C}^{N_1}$, $\boldsymbol{\theta}_2 = \text{diag}(\boldsymbol{\Theta}_2) \in \mathbb{C}^{N_2}$, and (a) is obtained using the properties of the Hadamard product. The first and second terms in (7.6), (7.7) represent the effective channels through the in-band IRS-X and the OOB IRS-Y, respectively. Since the Hadamard product of two array vectors is also an array vector aligned to a different angle, we have

$$h_k = \frac{N_1}{\sqrt{L_{k1}}} \sum_{l=1}^{L_{k1}} \gamma_{l,X}^{(1)} \gamma_{l,k}^{(1)} \dot{\mathbf{a}}_{N_1}^H(\omega_{X,k,l}^{(1)}) \boldsymbol{\theta}_1 + \frac{N_2}{\sqrt{L_{k2}}} \sum_{l=1}^{L_{k2}} \gamma_{l,X}^{(2)} \gamma_{l,k}^{(2)} \dot{\mathbf{a}}_{N_2}^H(\omega_{X,k,l}^{(2)}) \boldsymbol{\theta}_2, \tag{7.8}$$

[2]Similar results as in this chapter can also be easily obtained for other array types such as planar arrays.

where $\omega_{X,k,l}^{(1)} \triangleq \sin_{(p)}^{-1}\Big(\sin(\phi_{l,X}^{(1)})+\sin(\psi_{l,k}^{(1)})\Big)$, and $\omega_{X,k,l}^{(2)} \triangleq \sin_{(p)}^{-1}\Big(\sin(\phi_{l,X}^{(2)})+\sin(\psi_{l,k}^{(2)})\Big)$ denote the cascaded channel at UE-k from MO-X via IRS-X, and IRS-Y, respectively, in the lth path. Here, $\sin_{(p)}^{-1}(x)$ is defined so that $x \in [-1, 1)$, the principal argument of the inverse sine function [33], [80, Eq. 32]. Further, $\dot{\mathbf{a}}_N(\omega) \triangleq \frac{1}{\sqrt{N}}\mathbf{a}_N(\omega)$, with $\mathbf{a}_N(\omega)$ as defined in (7.5). Similarly, the channel at UE-q is

$$h_q = \frac{N_1}{\sqrt{L_{q1}}}\sum_{l=1}^{L_{q1}} \gamma_{l,Y}^{(1)}\gamma_{l,q}^{(1)}\dot{\mathbf{a}}_{N_1}^H(\omega_{Y,q,l}^{(1)})\boldsymbol{\theta}_1 + \frac{N_2}{\sqrt{L_{q2}}}\sum_{l=1}^{L_{q2}} \gamma_{l,Y}^{(2)}\gamma_{l,q}^{(2)}\dot{\mathbf{a}}_{N_2}^H(\omega_{Y,q,l}^{(2)})\boldsymbol{\theta}_2, \tag{7.9}$$

where $L_{q1} \triangleq L_Y^{(1)}L_q^{(1)}$ is the number of resolvable OOB paths from BS-Y to UE-q via IRS-X; $L_{q2} \triangleq L_Y^{(2)}L_q^{(2)}$ is the number of resolvable in-band paths from BS-Y to UE-q via IRS-Y.

7.2.a.ii Angle Distribution

We now explain the distribution of the cascaded angles specified in (7.8), (7.9). Since an N-element ULA can form at most N *resolvable beams* [65, 119], the paths with angular separations smaller than the Rayleigh resolution limit, i.e., $2\pi/N$ radians, are unresolvable and appear as a single path with an appropriate fading coefficient. To that end, we define the set of resolvable beams formed by the IRS as

$$\mathcal{A} \triangleq \{\mathbf{a}_N(\omega), \omega \in \boldsymbol{\Omega}\}\,; \boldsymbol{\Omega} \triangleq \left\{\left(-1+\frac{2i}{N}\right)\middle| i = 0, \ldots, N-1\right\},$$

where $\boldsymbol{\Omega}$ is the *resolvable anglebook* of the IRS. Then, we model its distribution $\mathcal{P}_{\mathcal{A}}$ by a uniform distribution:

$$\mathcal{P}_{\mathcal{A}}(\omega) = (1/|\boldsymbol{\Omega}|)\cdot \mathbb{1}_{\{\omega\in\boldsymbol{\Omega}\}} = (1/N)\cdot \mathbb{1}_{\{\omega\in\boldsymbol{\Omega}\}}. \tag{7.10}$$

Hence, we sample all the cascaded angles, $\{\omega_{X,k,l}^{(1)}\}_l$, $\{\omega_{X,k,l}^{(2)}\}_l$, $\{\omega_{Y,q,l}^{(1)}\}_l$, $\{\omega_{Y,q,l}^{(2)}\}_l$ from $\boldsymbol{\Omega}$ given above, similar to [33]. Furthermore, since IRS-X(Y) forms at most N_1 (N_2) resolvable paths, we have $L_{k1}, L_{q1} \leq N_1$; $L_{k2}, L_{q2} \leq N_2$.

7.2.b Choice of IRS Configurations

Recall that MO-X controls the (in-band) IRS-X to optimally serve its UEs, while BS-X cannot directly control the (OOB) IRS-Y. Similarly, MO-Y controls the (in-band) IRS-Y, and (OOB) IRS-X is not directly controllable by BS-Y. In such a scenario, at any instant in time, one of the cascaded in-band paths (in (7.8) and (7.9)) contains the maximum energy, and aligning the in-band IRSs to that path will procure near-optimal benefits [9]. Without loss of generality, we label the strongest path as the first in-band path. Then, the strongest in-band cascaded path of UE-k is $h_{k,1} \triangleq \frac{N_1}{\sqrt{L_{k1}}}\gamma_{1,X}^{(1)}\gamma_{1,k}^{(1)}\dot{\mathbf{a}}_{N_1}^H(\omega_{X,k,1}^{(1)})\boldsymbol{\theta}_1$. Further, recall that each MO prioritizes optimizing its IRS to align it along the in-band channel at its scheduled UE. In particular, since MO-X controls $\boldsymbol{\theta}_1$, to maximize the the channel gain $|h_{k,1}|^2$, by using Cauchy-Schwartz (CS) inequality, the nth entry of the optimal IRS configuration vector $\boldsymbol{\theta}_1^{\text{opt}}$ is $\theta_{1,n} = e^{j\phi_1}e^{j\left(-\angle\gamma_{1,X}^{(1)}-\angle\gamma_{1,k}^{(1)}-\pi(n-1)\omega_{X,k,1}^{(1)}\right)}$, where ϕ_1 is an overall phase angle applied to IRS-X which still preserves the optimality.[3] Similarly, we can obtain the optimal configuration for IRS-Y that maximizes $|h_{q,1}|^2$. Thus, the optimal IRS phase vectors can be written compactly as [80]

$$\boldsymbol{\theta}_1^{\text{opt}} = \frac{\gamma_{1,X}^{(1)*}\,\gamma_{1,k}^{(1)*}}{\left|\gamma_{1,X}^{(1)}\gamma_{1,k}^{(1)}\right|} \times N_1\dot{\mathbf{a}}_{N_1}(\omega_{X,k,1}^{(1)}) \times e^{j\phi_1}, \tag{7.11}$$

$$\boldsymbol{\theta}_2^{\text{opt}} = \frac{\gamma_{1,Y}^{(2)*}\,\gamma_{1,q}^{(2)*}}{\left|\gamma_{1,Y}^{(2)}\gamma_{1,q}^{(2)}\right|} \times N_2\dot{\mathbf{a}}_{N_2}(\omega_{Y,q,1}^{(2)}) \times e^{j\phi_2}, \tag{7.12}$$

respectively, and the choice of ϕ_1, ϕ_2 will be explained next.

Remark 7.1. *The IRS configurations in (7.11) and (7.12) do not require knowledge of the channel through the OOB IRS and hence are scalable for any number of MOs. Notably, even in the absence of OOB MOs, the in-band IRS associated with the MO will still procure an SNR that scales quadratically in the number of IRS elements. Consequently, the goal of this chapter is to demonstrate the utility of choosing the overall phase shifts ϕ_1 and ϕ_2*

[3] For e.g., it can be chosen to phase-align the channel $h_{k,1}$ with the overall virtual "direct path" formed by the cascaded channel through IRS-Y, i.e., with the phase of the second term in (7.8). We will explain this in the sequel.

Variable	Definition	Variable	Definition
N_1/N_2	Number of elements in IRS-X / IRS-Y	$\gamma_{l,Z}^{(p)}$	Gain of the lth path from BS-Z to IRS-p
M	Total number of MOs	$\gamma_{l,r}^{(p)}$	Gain of the lth path from IRS-p to UE-r
$\boldsymbol{\Theta}_1/\boldsymbol{\Theta}_2$	Phase matrix at IRS-X / IRS-Y	$\beta_{X,k}^{(1)}/\beta_{X,k}^{(2)}$	Path loss in the BS-X to UE-k link via IRS-X / IRS-Y
K	Number of UEs served by BS-X	$\beta_{Y,q}^{(1)}/\beta_{Y,q}^{(2)}$	Path loss in the BS-Y to UE-q link via IRS-X / IRS-Y
Q	Number of UEs served by BS-Y	$\mathbf{f}_{ZW}$	Channel from BS-Z to IRS-W
L_{k1}/L_{k2}	Number of resolvable paths from BS-X to UE-k through IRS-X / IRS-Y	$\mathbf{g}_{Wr}\big/\mathbf{t}_{Wr}$	Channel from IRS-W to UE-r served by MO-X / MO-Y
L_{q1}/L_{q2}	Number of resolvable paths from BS-Y to UE-q through IRS-X / IRS-Y	h_k/h_q	Overall channel from BS-X to UE-k / BS-Y to UE-q
ϕ_1/ϕ_2	Overall phase shift applied at IRS-X / IRS-Y by BS-X / BS-Y	ζ	Fraction of time slots to optimize the IRSs to UE-k served by MO-X
$\omega_{X,k,l}^{(1)}/\omega_{X,k,l}^{(2)}$	Cascaded normalized angle of lth path from BS-X to UE-k via IRS-X / IRS-Y	$\omega_{Y,q,l}^{(1)}/\omega_{Y,q,l}^{(2)}$	Cascaded normalized angle of lth path from BS-Y to UE-q via IRS-X / IRS-Y
P	Transmit power at the BSs	CO	Boolean parameter to indicate whether we allow inter-MO cooperation
σ^2	Noise variance at the UEs	$\langle R_{\mathrm{X}}\rangle/\langle R_{\mathrm{Y}}\rangle$	Achievable ergodic sum-SEs of MOs X / Y

Table 7.2: Commonly encountered variables/notations in chapter 7.

via cooperation rather than cooperatively optimizing the complete IRS phase vectors.

Remark 7.2. *For BS-X and BS-Y to configure IRS-X and IRS-Y to phase values given in (7.11) and (7.12), respectively, both BSs must acquire the knowledge of the respective in-band CSIs at their in-band UEs-k and q, respectively. A straightforward approach to achieve this is via inter-MO cooperation during channel estimation (CE), as follows: when one MO performs in-band CE through its IRS, the OOB IRSs are turned off to prevent inter-MO pilot and IRS contamination [108]. This allows all MOs to configure their IRSs according to (7.11) and (7.12). We note that designing and analyzing the feasibility of practical CE protocols in IRS-aided multiple MO systems remains an open problem. However, since our goal is to characterize the impact of multiple MOs deploying IRSs on each other's achievable data rates, we do not account for these overheads in our analysis.*

7.2.c Problem Statement

In a 2-MO system, as shown in Fig. 7.1, each IRS will reflect the signals transmitted by both the MOs. Then, the SE achieved by UE-k scheduled by MO-X at time slot t is

$$R_k(t) = \log_2\left(1 + \frac{P}{\sigma^2}\left|\mathbf{g}_{\mathrm{X}k}^T\boldsymbol{\Theta}_1(t)\mathbf{f}_{\mathrm{XX}} + \mathbf{g}_{\mathrm{Y}k}^T\boldsymbol{\Theta}_2(t)\mathbf{f}_{\mathrm{XY}}\right|^2\right),$$

and the SE achieved by UE-q scheduled by MO-Y is

$$R_q(t) = \log_2\left(1 + \frac{P}{\sigma^2}\left|\mathbf{t}_{\mathrm{X}q}^T\boldsymbol{\Theta}_1(t)\mathbf{f}_{\mathrm{YX}} + \mathbf{t}_{\mathrm{Y}q}^T\boldsymbol{\Theta}_2(t)\mathbf{f}_{\mathrm{YY}}\right|^2\right),$$

where $\boldsymbol{\Theta}_1(t)$ and $\boldsymbol{\Theta}_2(t)$ are set using $\boldsymbol{\theta}_1^{\mathrm{opt}}$ and $\boldsymbol{\theta}_2^{\mathrm{opt}}$ as given in (7.11) and (7.12), respectively for the UEs scheduled in time slot t. However, note that the choice of overall phase shifts ϕ_1 and ϕ_2 still offers flexibility in terms of being able to combine signals at UEs across both in-band and OOB IRSs. In this context, we consider the following scenarios:

1. *Joint optimization of IRSs with MO cooperation*: Here, the MOs cooperate to jointly tune the overall phase shifts at the IRSs in every time slot t to maximize the weighted sum-SE of the scheduled UEs. Mathematically, the problem is

$$\phi_1{}^{\mathrm{opt}}(t), \phi_2{}^{\mathrm{opt}}(t) = \underset{\phi_1(t),\phi_2(t)}{\arg\max}\, w_k R_k(t) + w_q R_q(t), \tag{P1}$$

   where w_k, w_q are the weights associated with acheivable SEs of UEs k, q of MO-X and Y, respectively.

2. *Optimization of IRSs with time-sharing*: Here, a subset (denoted by $\mathcal{T}_X$) of the time slots are used by MO-X to configure the overall phase shifts of both IRSs to maximize the SE of UE-k, and the remaining time slots (denoted by $\mathcal{T}_Y$) are used by MO-Y to optimize the overall phase shifts at the IRSs for UE-q. Mathematically, in every time slot t,

$$\phi_1{}^{\mathrm{opt}}(t), \phi_2{}^{\mathrm{opt}}(t) = \underset{\phi_1(t),\phi_2(t)}{\arg\max} \sum_{i\in\{X,Y\}} R_i(t)\mathbb{1}_{\{t\in\mathcal{T}_i\}}. \tag{P2}$$

3. *Optimization of IRSs without MO cooperation*: Here, the two MOs optimize only their own IRSs to maximize the SE of their UEs (by ignoring the presence of an IRS deployed

by another MO.) Mathematically, we realize this by setting:

$$\phi_1^{\text{opt}}(t) = \phi_2^{\text{opt}}(t) = 0, \ \forall t. \tag{7.13}$$

Then, we answer the following questions:

- How does the ergodic SE of the MOs scale with the system parameters in all the cases?
- Does the presence of an OOB IRS degrade the performance of a given MO?
- What is the value of cooperation between the MOs in terms of the achievable ergodic SE?
- How do the above answers extend to $M > 2$ MO-systems?

We answer these questions in the following sections.

7.3 Performance Analysis in a 2-MO System

This section analyzes the achievable ergodic sum-SE of the 2-MO system described above. We first make the following observations about the IRS configurations in (7.11) and (7.12):

1. The IRS vectors are directional in nature and point to the angle of the channel to which it is optimized.
2. Although the IRS vector $\boldsymbol{\theta}_1^{\text{opt}}$ aligns to the in-band path at UE-k, it is a random phasor from the UE-q's viewpoint. Similarly, $\boldsymbol{\theta}_2^{\text{opt}}$ is optimal to UE-q's in-band path, and is randomly configured from UE-k's viewpoint.

From these observations, IRS-X aligns with the channel to UE-q with probability $\frac{L_{q1}}{N_1}$ and it does not contribute to the channel at UE-q with probability $1 - \frac{L_{q1}}{N_1}$ [80, Proof of Theorem 3]. Similarly, IRS-Y contributes to the channel at UE-k with probability $\frac{L_{k2}}{N_2}$ and does not align with UE-k with probability $1 - \frac{L_{k2}}{N_2}$. Based on these, four events arise as summarized in Fig. 7.2. Hence, the overall achievable performance in a 2-MO system is determined

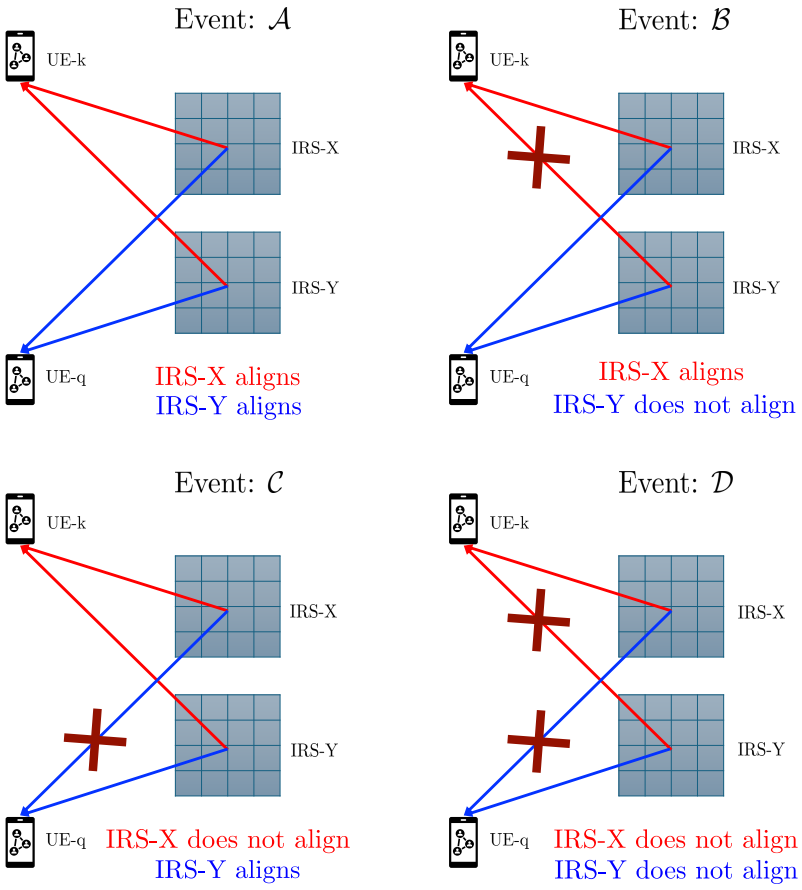

Figure 7.2: Illustration of all possible events in 2-IRS aided 2-MO system.

by the choice of the overall phase shifts, ϕ_1 and ϕ_2, used in these four events.[4] We next analyze the performances of the different schemes listed in Sec. 7.2.c with varying degrees of cooperation between the MOs under these events.

7.3.a Event $\mathcal{A}$: IRS-X and IRS-Y align to UE-q and UE-k, resp.

In this event, both IRS-X and IRS-Y align with one of the angles of the L_{q1} and L_{k2} OOB paths at UEs-q and k, respectively. Now, since the alignment of IRS-X with UE-q's channel is independent of the alignment of IRS-Y with UE-k's channel, the probability of event $\mathcal{A}$ is

$$\Pr(\mathcal{A}) = (L_{q1}/N_1) \times (L_{k2}/N_2). \tag{7.14}$$

[4]These events correspond to the OOB effect of the IRSs; by (7.11) and (7.12), each IRS is always aligned to the in-band UE's channel from its BS.

Now, under event $\mathcal{A}$, there exists indices l_k^* and l_q^* such that

$$\begin{aligned} l_k^* &= \arg_l \left\{ N_2 \dot{\mathbf{a}}_{N_2}^H(\omega_{X,k,l}^{(2)}) \dot{\mathbf{a}}_{N_2}(\omega_{Y,q,1}^{(2)}) = 1 \right\}, \text{ and} \\ l_q^* &= \arg_l \left\{ N_1 \dot{\mathbf{a}}_{N_1}^H(\omega_{Y,q,l}^{(1)}) \dot{\mathbf{a}}_{N_1}(\omega_{X,k,1}^{(1)}) = 1 \right\}, \end{aligned} \tag{7.15}$$

where $\arg_l\{\cdot\}$ returns the index l for which the condition in the braces is satisfied. In other words, the angles of l_k^*th and l_q^*th OOB paths at UE-k and UE-q match with the angles pointed by the phase configurations at IRS-Y and IRS-X, respectively.

Then, using the expressions for IRS vectors in (7.11), and (7.12), we simplify the channels of UE-k, q in (7.8) and (7.9) as

$$h_k = \frac{N_1}{\sqrt{L_{k1}}} \left| \gamma_{1,X}^{(1)} \gamma_{1,k}^{(1)} \right| \times e^{j\phi_1} + \frac{N_2}{\sqrt{L_{k2}}} \left| \gamma_{l_k^*,X}^{(2)} \gamma_{l_k^*,k}^{(2)} \right| \times e^{j(\phi_2+\phi_a)}, \tag{7.16}$$

$$h_q = \frac{N_1}{\sqrt{L_{q1}}} \left| \gamma_{l_q^*,Y}^{(1)} \gamma_{l_q^*,q}^{(1)} \right| \times e^{j(\phi_1+\phi_b)} + \frac{N_2}{\sqrt{L_{q2}}} \left| \gamma_{1,Y}^{(2)} \gamma_{1,q}^{(2)} \right| \times e^{j\phi_2}, \tag{7.17}$$

respectively, where $\phi_a \triangleq \angle\gamma_{l_k^*,X}^{(2)} + \angle\gamma_{l_k^*,k}^{(2)} - \angle\gamma_{1,Y}^{(2)} - \angle\gamma_{1,q}^{(2)}$ and $\phi_b \triangleq \angle\gamma_{l_q^*,Y}^{(1)} + \angle\gamma_{l_q^*,q}^{(1)} - \angle\gamma_{1,X}^{(1)} - \angle\gamma_{1,k}^{(1)}$, denote the phase differences between OOB and in-band paths at IRSs X and Y, respectively. Now, if both the IRSs have to constructively add the received signals at both UEs-k, q, we need

$$\phi_1 = \phi_2 + \phi_a, \tag{7.18}$$

$$\text{(and) } \phi_2 = \phi_1 + \phi_b, \tag{7.19}$$

at IRS X and Y, respectively. However, since $\phi_a, \phi_b \in \mathcal{U}[-\pi, \pi)$ are i.i.d. random variables, (7.18) and (7.19) hold simultaneously with zero probability. That is, almost surely, neither IRS can be optimal for both UEs simultaneously. With this in mind, we analyze the 3 schemes in Sec. 7.2.c.

7.3.a.i Joint-optimization of IRSs with MO cooperation

Here, the MOs jointly optimize the overall phase shifts ϕ_1 and ϕ_2 at the IRSs to maximize the weighted sum-SE of the UEs scheduled by both MOs. We first rewrite (7.16) and (7.17)

as

$$h_k = \alpha e^{j\phi_1} + \gamma e^{j(\phi_2+\phi_a)}, \tag{7.20}$$

$$h_q = \beta e^{j(\phi_1+\phi_b)} + \delta e^{j\phi_2}, \tag{7.21}$$

where, $\alpha \triangleq \frac{N_1}{\sqrt{L_{k1}}}|\gamma^{(1)}_{1,X}\gamma^{(1)}_{1,k}|$, $\gamma \triangleq \frac{N_2}{\sqrt{L_{k2}}}|\gamma^{(2)}_{l^*_k,X}\gamma^{(2)}_{l^*_k,k}|$, $\beta \triangleq \frac{N_1}{\sqrt{L_{q1}}}|\gamma^{(1)}_{l^*_q,Y}\gamma^{(1)}_{l^*_q,q}|$, and $\delta \triangleq \frac{N_2}{\sqrt{L_{q2}}}|\gamma^{(2)}_{1,Y}\gamma^{(2)}_{1,q}|$. Then, ϕ_1 and ϕ_2 are determined as $\phi_1^{\text{opt}}, \phi_2^{\text{opt}} =$

$$\underset{\phi_1,\phi_2}{\arg\max} \quad w_k \log_2\left(1+\frac{P}{\sigma^2}|h_k|^2\right) + w_q \log_2\left(1+\frac{P}{\sigma^2}|h_q|^2\right)$$

where ϕ_1, ϕ_2 are the overall phase shifts set by the BS-X and Y at IRS-X and Y, respectively, w_k and w_q are the weights allotted to the SE achieved by UEs k and q, respectively. Let $\phi \triangleq \phi_2 - \phi_1$, $x \triangleq 1 + \frac{P}{\sigma^2}(\alpha^2+\gamma^2)$, $v \triangleq 2\alpha\gamma$, $y \triangleq 1 + \frac{P}{\sigma^2}(\beta^2+\delta^2)$ and $z \triangleq 2\beta\delta$. Then the above problem is equivalent to ϕ^{opt}

$$= \underset{\phi}{\arg\max}\, f(\phi) = \left((x + v\cos(\phi+\phi_a))^{w_k}(y + z\cos(\phi-\phi_b))^{w_q}\right).$$

Since $f(\phi)$ depends only on the difference $\phi = \phi_2 - \phi_1$, the optimization variables can be reduced to a single variable ϕ. Notably, the solution to this optimization problem inherently accounts for the operating SNR. By the first order condition, $f'(\phi) = 0$, which is

$$f(\phi)\left\{\frac{w_k v\sin(\phi+\phi_a)}{x+v\cos(\phi+\phi_a)} + \frac{w_q z\sin(\phi-\phi_b)}{y+z\cos(\phi-\phi_b)}\right\} = 0. \tag{7.22}$$

Since the roots of (7.22) do not admit a closed-form solution, we employ a low complexity Newton-Raphson's algorithm [175] to solve for ϕ, which is outlined in Algorithm 7.1. Although the Newton-Raphson method entails multiple iterations, we use only a single iteration to reduce complexity. In Sec. 7.6, we numerically show that a single iteration with appropriate initialization yields comparable solutions to high-complexity off-the-shelf optimizers. In particular, we initialize ϕ based on the weights allotted to the MOs: we compute the weighted sum rate with $\phi = -\phi_a$ and $\phi = \phi_b$, and choose the value that yields the higher weighted sum-SE. Finally, with ϕ^{opt} in hand, the ergodic SEs of UEs k

Algorithm 7.1: Newton-Raphson based single iteration method

1 **If** $w_k R_k(\phi_a, 0) + w_q R_q(\phi_a, 0) \geq w_k R_k(0, \phi_b) + w_q R_q(0, \phi_b)$, $\phi_{init} \leftarrow -\phi_a$.

2 **else** $\phi_{init} \leftarrow \phi_b$.

3 Obtain $f'(\phi) \leftarrow -f(\phi)\left\{\frac{w_k v \sin(\phi+\phi_a)}{x+v\cos(\phi+\phi_a)} + \frac{w_q z \sin(\phi-\phi_b)}{y+z\cos(\phi-\phi_b)}\right\}$.

4 Compute the second-derivative, $f''(\phi)$ as follows:

$$f''(\phi) = \frac{(f'(\phi))^2}{f(\phi)} - f(\phi)\left\{\frac{w_k v\{x\cos(\phi+\phi_a)+v\}}{(x+v\cos(\phi+\phi_a))^2} + \frac{w_q z\{y\cos(\phi-\phi_b)+z\}}{(y+z\cos(\phi-\phi_b))^2}\right\}. \tag{7.25}$$

5 Update $\phi^{\text{opt}} \leftarrow \phi_{init} - \frac{f'(\phi)}{f''(\phi)}\Big|_{\phi=\phi_{init}}$

and q are given by

$$\langle R_k|\mathcal{A}\rangle \approx \log_2\left(1 + \frac{P}{\sigma^2}\left|\frac{N_1}{\sqrt{L_{k1}}}\left|\gamma^{(1)}_{1,X}\gamma^{(1)}_{1,k}\right| e^{j\phi_1^{\text{opt}}} + \frac{N_2}{\sqrt{L_{k2}}}\left|\gamma^{(2)}_{l_k^*,X}\gamma^{(2)}_{l_k^*,k}\right| e^{j(\phi_2^{\text{opt}}+\phi_a)}\right|^2\right), \tag{7.23}$$

$$\langle R_q|\mathcal{A}\rangle \approx \log_2\left(1 + \frac{P}{\sigma^2}\left|\frac{N_1}{\sqrt{L_{q1}}}|\gamma^{(1)}_{l_q^*,Y}\gamma^{(1)}_{l_q^*,q}|e^{j(\phi_1^{\text{opt}}+\phi_b)} + \frac{N_2}{\sqrt{L_{q2}}}|\gamma^{(2)}_{1,Y}\gamma^{(2)}_{1,q}|e^{j\phi_2^{\text{opt}}}\right|^2\right). \tag{7.24}$$

7.3.a.ii Optimization of IRSs with time sharing

Here, the MOs optimize the overall phase shifts of the IRSs to the UE scheduled by either MO-X or MO-Y, in a time-shared manner. Now, in the time slots used to optimize ϕ_1 and ϕ_2 to UE-k scheduled by BS-X, from (7.16), we need to choose $\phi_1 = \phi_a$ and $\phi_2 = 0$, respectively. Then, (7.16) and (7.17) simplify to

$$h_k = \left(\frac{N_1}{\sqrt{L_{k1}}}\left|\gamma^{(1)}_{1,X}\gamma^{(1)}_{1,k}\right| + \frac{N_2}{\sqrt{L_{k2}}}\left|\gamma^{(2)}_{l_k^*,X}\gamma^{(2)}_{l_k^*,k}\right|\right) e^{j\phi_a}, \tag{7.26}$$

$$h_q = \frac{N_1}{\sqrt{L_{q1}}}\left|\gamma^{(1)}_{l_q^*,Y}\gamma^{(1)}_{l_q^*,q}\right| e^{j(\phi_a+\phi_b)} + \frac{N_2}{\sqrt{L_{q2}}}\left|\gamma^{(2)}_{1,Y}\gamma^{(2)}_{1,q}\right|. \tag{7.27}$$

We have the following lemma to characterize the in-band SE.

Lemma 7.1. *Let* $\{X_i\}_{i=1}^N$ *be i.i.d random variables such that* $X_i \sim \mathcal{CN}(0,1)$. *If* $M \triangleq \max(|X_1|, |X_2|, \ldots, |X_N|)$, *and* $G \triangleq \max(|X_1|^2, |X_2|^2, \ldots, |X_N|^2)$, *the expected values of*

M, G are

$$\mathbb{E}[M] = f(N) \triangleq N \sum\nolimits_{n=0}^{N-1} \binom{N-1}{n} (-1)^n \frac{1}{(n+1)^{\frac{3}{2}}} \sqrt{\frac{\pi}{4}}, \tag{7.28}$$

and

$$\mathbb{E}[G] = g(N) \triangleq N \sum\nolimits_{n=0}^{N-1} \binom{N-1}{n} (-1)^n \frac{1}{(n+1)^2}, \tag{7.29}$$

respectively.

Proof. Straightforward, hence omitted. ■

Using Lemma 7.1, we can show that $\mathbb{E}\left[|\gamma_{1,X}^{(1)}\gamma_{1,k}^{(1)}|\right] = (f(L_{k1}))^2\sqrt{\beta_{X,k}^{(1)}}$, and $\mathbb{E}\left[|\gamma_{1,X}^{(1)}\gamma_{1,k}^{(1)}|^2\right] = (g(L_{k1}))^2\beta_{X,k}^{(1)}$, where $\beta_{X,k}^{(1)} \triangleq \beta_X^{(1)}\beta_k^{(1)}$ and $\beta_{X,k}^{(2)} \triangleq \beta_X^{(2)}\beta_k^{(2)}$. Similarly, let $\beta_{Y,q}^{(1)} \triangleq \beta_Y^{(1)}\beta_q^{(1)}$ and $\beta_{Y,q}^{(2)} \triangleq \beta_Y^{(2)}\beta_q^{(2)}$. Conditioned on event $\mathcal{A}$, by Jensen's approximation, the ergodic SE of UE-k, q is

$$\langle R_i|\mathcal{A}\rangle \approx \log_2\left(1 + \mathbb{E}[|h_i|^2]P/\sigma^2\right), \quad i \in \{k, q\}, \tag{7.30}$$

where using (7.26), (7.27), we obtain the following:

$$\mathbb{E}[|h_k|^2] = \frac{N_1^2}{L_{k1}}(g(L_{k1}))^2\beta_{X,k}^{(1)} + \frac{N_2^2}{L_{k2}}\beta_{X,k}^{(2)} + \frac{\pi N_1 N_2}{2\sqrt{L_{k1}L_{k2}}}(f(L_{k1}))^2\sqrt{\beta_{X,k}^{(1)}\beta_{X,k}^{(2)}}, \tag{7.31}$$

$$\mathbb{E}\left[|h_q|^2\right] = \frac{N_1^2}{L_{q1}}\beta_{Y,q}^{(1)} + \frac{N_2^2}{L_{q2}}\beta_{Y,q}^{(2)}(g(L_{q2}))^2 + \frac{\pi N_1 N_2}{2\sqrt{L_{q1}L_{q2}}}(f(L_{q2}))^2\sqrt{\beta_{Y,q}^{(1)}\beta_{Y,q}^{(2)}} \times \mathbb{E}[\cos(\phi_a + \phi_b)]. \tag{7.32}$$

Since $\phi_a, \phi_b \sim \mathcal{U}[-\pi, \pi)$, we have $\mathbb{E}[\cos(\phi_a + \phi_b)] = 0$. So,

$$\mathbb{E}\left[|h_q|^2\right] = \frac{N_1^2}{L_{q1}}\beta_{Y,q}^{(1)} + \frac{N_2^2}{L_{q2}}(g(L_{q2}))^2\beta_{Y,q}^{(2)}. \tag{7.33}$$

Using (7.31) and (7.33) in (7.30), the ergodic SEs of UE-k, q when ϕ_1, ϕ_2 are optimized only for UE-k can be obtained as

$$\langle R_k|\mathcal{A}\rangle \approx \log_2\left(1 + \frac{P}{\sigma^2}\left\{\frac{N_1^2}{L_{k1}}(g(L_{k1}))^2\beta_{X,k}^{(1)} + \frac{N_2^2}{L_{k2}}\beta_{X,k}^{(2)} + \left(\frac{\pi N_1 N_2}{2\sqrt{L_{k1}L_{k2}}}\right)(f(L_{k1}))^2\sqrt{\beta_{X,k}^{(1)}\beta_{X,k}^{(2)}}\right\}\right), \tag{7.34}$$

$$\langle R_q|\mathcal{A}\rangle \approx \log_2\left(1 + \frac{P}{\sigma^2}\left\{\frac{N_1^2}{L_{q1}}\beta_{Y,q}^{(1)} + \frac{N_2^2}{L_{q2}}(g(L_{q2}))^2\beta_{Y,q}^{(2)}\right\}\right). \tag{7.35}$$

Similarly, in the time slots used to optimize ϕ_1, ϕ_2 for UE-q, from (7.17), $\phi_1 = 0$ and $\phi_2 = \phi_b$. Then, similar to (7.34) and (7.35), the ergodic SE of UE-k, q is

$$\langle R_k|\mathcal{A}\rangle \approx \log_2\left(1+\frac{P}{\sigma^2}\left\{\frac{N_1^2}{L_{k1}}(g(L_{k1}))^2\beta_{X,k}^{(1)}+\frac{N_2^2}{L_{k2}}\beta_{X,k}^{(2)}\right\}\right), \tag{7.36}$$

$$\langle R_q|\mathcal{A}\rangle \approx \log_2\left(1+\frac{P}{\sigma^2}\left\{\frac{N_1^2}{L_{q1}}\beta_{Y,q}^{(1)}+\frac{N_2^2}{L_{q2}}(g(L_{q2}))^2\beta_{Y,q}^{(2)}+\left(\frac{\pi N_1 N_2}{2\sqrt{L_{q1}L_{q2}}}\right)(f(L_{q2}))^2\sqrt{\beta_{Y,q}^{(1)}\beta_{Y,q}^{(2)}}\right\}\right). \tag{7.37}$$

Therefore, using the expressions in (7.34) to (7.37), under a time-sharing scheme, with a fraction of time-slots, say ζT_c, $\zeta \in (0,1)$ (T_c is the coherence time) used to optimize overall phase shifts of both IRSs to UE-k, and remaining $(1-\zeta)T_c$ slots used to tune the overall phase shifts at both IRSs to serve UE-q, the overall ergodic SEs of the MOs are as

$$\begin{aligned}\langle R_k|\mathcal{A}\rangle_{\text{time-sharing}} \approx{}& (1-\zeta)\log_2\left(1+\frac{P}{\sigma^2}\left\{\frac{N_1^2}{L_{k1}}(g(L_{k1}))^2\beta_{X,k}^{(1)}+\frac{N_2^2}{L_{k2}}\beta_{X,k}^{(2)}\right\}\right)\\ &+\zeta\log_2\left(1+\frac{P}{\sigma^2}\left\{\frac{N_1^2}{L_{k1}}(g(L_{k1}))^2\beta_{X,k}^{(1)}+\frac{N_2^2}{L_{k2}}\beta_{X,k}^{(2)}+\frac{\pi N_1 N_2}{2\sqrt{L_{k1}L_{k2}}}(f(L_{k1}))^2\sqrt{\beta_{X,k}^{(1)}\beta_{X,k}^{(2)}}\right\}\right),\end{aligned} \tag{7.38}$$

$$\begin{aligned}\langle R_q|\mathcal{A}\rangle_{\text{time-sharing}} \approx{}& \zeta\log_2\left(1+\frac{P}{\sigma^2}\left\{\frac{N_1^2}{L_{q1}}\beta_{Y,q}^{(1)}+\frac{N_2^2}{L_{q2}}(g(L_{q2}))^2\beta_{Y,q}^{(2)}\right\}\right)\\ &+(1-\zeta)\log_2\left(1+\frac{P}{\sigma^2}\left\{\frac{N_1^2}{L_{q1}}\beta_{Y,q}^{(1)}+\frac{N_2^2}{L_{q2}}(g(L_{q2}))^2\beta_{Y,q}^{(2)}+\frac{\pi N_1 N_2}{2\sqrt{L_{q1}L_{q2}}}(f(L_{q2}))^2\sqrt{\beta_{Y,q}^{(1)}\beta_{Y,q}^{(2)}}\right\}\right).\end{aligned} \tag{7.39}$$

7.3.a.iii Optimization of IRSs without cooperation

In this case, the MOs optimize their IRSs by only considering the in-band channels at their UEs. So, the overall phase shifts can be set to $\phi_1 = \phi_2 = 0$ as per (7.13). Hence, the ergodic SE at UE-k, q is given by (7.36) and (7.35), respectively. The cross terms (as in (7.34) and (7.37)) do not appear in these expressions as the signals from the IRSs do not add coherently at the UEs.

7.3.b Evt. $\mathcal{B}$: IRS-X aligns to UE-q, IRS-Y does not align to UE-k

Here, one of the L_{q1} OOB paths at UE-q aligns with IRS-X's beam, while none of the L_{k2} OOB paths at UE-k match with IRS-Y's beam. Hence, the probability of event $\mathcal{B}$ is

$$\Pr(\mathcal{B}) = (L_{q1}/N_1) \cdot (1 - (L_{k2}/N_2)) \,. \tag{7.40}$$

There is no need for joint optimization of ϕ_1, ϕ_2 here because only one of the MO's UE gets signals reflected from both IRSs. Then, the channels at UE-k, q are

$$h_k = \frac{N_1}{\sqrt{L_{k1}}} \left| \gamma_{1,X}^{(1)} \gamma_{1,k}^{(1)} \right| \times e^{j\phi_1}, \tag{7.41}$$

$$h_q = \frac{N_1}{\sqrt{L_{q1}}} \left| \gamma_{l_q^*,Y}^{(1)} \gamma_{l_q^*,q}^{(1)} \right| e^{j(\phi_1+\phi_b)} + \frac{N_2}{\sqrt{L_{q2}}} \left| \gamma_{1,Y}^{(2)} \gamma_{1,q}^{(2)} \right| e^{j\phi_2}. \tag{7.42}$$

Since IRS-Y does not contribute to UE-k, the SE achieved by UE-k is only due to IRS-X and is independent of ϕ_1. On the other hand, for coherent addition of in-band and OOB paths to maximize $|h_q|^2$ in (7.42), we need $\phi_2 = \phi_1 + \phi_b$, and we choose the simplest solution for this, namely $\{\phi_1 = 0; \phi_2 = \phi_b\}$ so that BS-X need not apply any additional overall phase. Then,

$$\begin{aligned} h_k &= \frac{N_1}{\sqrt{L_{k1}}} \left| \gamma_{1,X}^{(1)} \gamma_{1,k}^{(1)} \right|, \text{ and} \\ h_q &= \left(\frac{N_1}{\sqrt{L_{q1}}} \left| \gamma_{l_q^*,Y}^{(1)} \gamma_{l_q^*,q}^{(1)} \right| + \frac{N_2}{\sqrt{L_{q2}}} \left| \gamma_{1,Y}^{(2)} \gamma_{1,q}^{(2)} \right| \right) \times e^{j\phi_b}. \end{aligned} \tag{7.43}$$

So, the ergodic SE of UE-k, q when ϕ_1, ϕ_2 are optimized to UE-q in $(1-\zeta)T_c$ time slots can be obtained as

$$\langle R_k | \mathcal{B} \rangle \approx \log_2 \left(1 + \frac{P}{\sigma^2} \left\{ \frac{N_1^2}{L_{k1}} (g(L_{k1}))^2 \beta_{X,k}^{(1)} \right\} \right), \tag{7.44}$$

and (7.39), respectively. Similarly, with no MO cooperation, the SE at UE-k, q are as in (7.44) and (7.35), respectively.

To summarize, when event $\mathcal{B}$ occurs, for 1) joint optimization with MO cooperation, the SEs of UEs k and q are given by (7.44) and (7.37), respectively; for 2) optimization with time-sharing schemes, the SEs of UEs k and q are given by (7.44) and (7.39), respectively.

With 3) no cooperation, the SEs are given by (7.44) and (7.35), respectively.

7.3.c Evt. $\mathcal{C}$: IRS-X does not align to UE-q, IRS-Y aligns to UE-k

This event is the complement of event $\mathcal{B}$ described above, i.e., one of the L_{k2} OOB paths at UE-k aligns with IRS-Y, but none of the L_{q1} OOB paths at UE-q matches with the beam formed by IRS-X. Hence,

$$\Pr(\mathcal{C}) = (1 - (L_{q1}/N_1)) \cdot (L_{k2}/N_2). \tag{7.45}$$

Following the analysis similar to event $\mathcal{B}$, the final expressions for the ergodic SEs of UE-k, q when ϕ_1, ϕ_2 are optimized to UE-k for ζT_c time slots are given in (7.38), and as

$$\langle R_q|\mathcal{C}\rangle \approx \log_2\left(1 + \frac{P}{\sigma^2}\left\{\frac{N_2^2}{L_{q2}}(g(L_{q2}))^2\beta_{Y,q}^{(2)}\right\}\right), \tag{7.46}$$

respectively. Similarly, without MO cooperation, the SEs at UEs k and q are given by (7.36) and (7.46), respectively.

Thus, whenever event $\mathcal{C}$ occurs, for 1) joint optimization with MO cooperation, the SEs of UEs k, q are given by (7.34) and (7.46); for 2) optimization with time-sharing, the SEs of UEs k, q are given by (7.38) and (7.46), respectively. With 3) no cooperation, the SEs are as in (7.36), and (7.46), respectively.

7.3.d Event $\mathcal{D}$: IRS-X, Y do not align to UE-q, k, respectively

In this final event, none of the L_{q1} and L_{k2} OOB paths match with IRS-X and IRS-Y, respectively. The probability of this event is given by

$$\Pr(\mathcal{D}) = (1 - (L_{q1}/N_1)) \cdot (1 - (L_{k2}/N_2)). \tag{7.47}$$

Since none of the IRSs align with an OOB UE, this event completely obviates the need for tuning ϕ_1, ϕ_2. The channel coefficients under this event are

$$h_k = \frac{N_1}{\sqrt{L_{k1}}}\left|\gamma_{1,X}^{(1)}\gamma_{1,k}^{(1)}\right| e^{j\phi_1},\ h_q = \frac{N_2}{\sqrt{L_{q2}}}\left|\gamma_{1,Y}^{(2)}\gamma_{1,q}^{(2)}\right| e^{j\phi_2}, \tag{7.48}$$

respectively, and the ergodic SEs of UE-k, q are given by

$$\langle R_k|\mathcal{D}\rangle = \langle R_k|\mathcal{B}\rangle, \text{ and } \langle R_q|\mathcal{D}\rangle = \langle R_q|\mathcal{C}\rangle, \tag{7.49}$$

where $\langle R_k|\mathcal{B}\rangle$ and $\langle R_q|\mathcal{C}\rangle$ are as per (7.44), (7.46), respectively.

To summarize, whenever event $\mathcal{D}$ occurs, for 1) joint optimization with MO cooperation, 2) optimization with time-sharing, and 3) with no MO schemes cooperation, the SEs of UEs k and q are the same for all 3 schemes as given in (7.49). We now state our main result on the overall ergodic sum-SEs of both the MOs under round-robin (RR) scheduling.

Theorem 7.1. *Under the SV channel model in the mmWave bands, when MOs X & Y control an IRS each to serve their subscribed UEs, the ergodic sum-SE of MOs X and Y under RR scheduling is characterized in the following:*

1. *Optimization of IRSs with time sharing where ζT_c time slots are alloted to MO-X and $(1-\zeta)T_c$ time slots are alloted to MO-Y: $\langle R_X^{\zeta}\rangle_{TS}$, $\langle R_Y^{\zeta}\rangle_{TS}$ as in (7.50) and (7.51), with $\mathsf{CO}=1$:*

$$\begin{aligned}\langle R_X^{\zeta}\rangle_{TS} \approx \frac{1}{K}\sum_{k=1}^{K}\Bigg\{&\left(1-\frac{L_{k2}}{N_2}\right)\log_2\left(1+\frac{P}{\sigma^2}\frac{N_1^2}{L_{k1}}(g(L_{k1}))^2\beta_{X,k}^{(1)}\right)\\ &+(1-\zeta)\frac{L_{k2}}{N_2}\log_2\left(1+\frac{P}{\sigma^2}\left\{\frac{N_1^2}{L_{k1}}(g(L_{k1}))^2\beta_{X,k}^{(1)}+\frac{N_2^2}{L_{k2}}\beta_{X,k}^{(2)}\right\}\right)\\ &+\zeta\frac{L_{k2}}{N_2}\log_2\Bigg(1+\frac{P}{\sigma^2}\Bigg\{\frac{N_1^2}{L_{k1}}(g(L_{k1}))^2\beta_{X,k}^{(1)}+\frac{N_2^2}{L_{k2}}\beta_{X,k}^{(2)}\\ &+\mathbb{1}_{\{\mathsf{CO}=1\}}\frac{\pi N_1N_2(f(L_{k1}))^2\sqrt{\beta_{X,k}^{(1)}\beta_{X,k}^{(2)}}}{2\sqrt{L_{k1}L_{k2}}}\Bigg\}\Bigg)\Bigg\},\end{aligned} \tag{7.50}$$

$$\begin{aligned}\langle R_Y^{\zeta}\rangle_{TS} \approx \frac{1}{Q}\sum_{q=1}^{Q}\Bigg\{&\left(1-\frac{L_{q1}}{N_1}\right)\log_2\left(1+\frac{P}{\sigma^2}\frac{N_2^2}{L_{q2}}(g(L_{q2}))^2\beta_{Y,q}^{(2)}\right)\\ &+\zeta\frac{L_{q1}}{N_1}\log_2\left(1+\frac{P}{\sigma^2}\left\{\frac{N_1^2}{L_{q1}}\beta_{Y,q}^{(1)}+\frac{N_2^2}{L_{q2}}(g(L_{q2}))^2\beta_{Y,q}^{(2)}\right\}\right)\\ &+(1-\zeta)\frac{L_{q1}}{N_1}\log_2\Bigg(1+\frac{P}{\sigma^2}\Bigg\{\frac{N_1^2}{L_{q1}}\beta_{Y,q}^{(1)}+\frac{N_2^2}{L_{q2}}(g(L_{q2}))^2\beta_{Y,q}^{(2)}\\ &+\mathbb{1}_{\{\mathsf{CO}=1\}}\frac{\pi N_1N_2(f(L_{q2}))^2\sqrt{\beta_{Y,q}^{(1)}\beta_{Y,q}^{(2)}}}{2\sqrt{L_{q1}L_{q2}}}\Bigg\}\Bigg)\Bigg\}.\end{aligned} \tag{7.51}$$

2. *Joint-optimization of IRSs with MO cooperation: The ergodic rates for MO-X and MO-Y are given as in (7.52) and (7.53), respectively, where ϕ_1^{opt} and ϕ_2^{opt} are chosen such that $\phi^{\text{opt}} = \phi_2^{\text{opt}} - \phi_1^{\text{opt}}$ is a solution obtained from Algorithm 7.1:*

$$\langle R_X \rangle_{JO} \approx \frac{1}{K}\sum_{k=1}^{K}\left\{\frac{L_{q1}L_{k2}}{N_1N_2}\log_2\left(1+\frac{P}{\sigma^2}\left|\frac{N_1}{\sqrt{L_{k1}}}\left|\gamma_{1,X}^{(1)}\gamma_{1,k}^{(1)}\right|e^{j\phi_1^{\text{opt}}}+\frac{N_2}{\sqrt{L_{k2}}}\left|\gamma_{l_k^*,X}^{(2)}\gamma_{l_k^*,k}^{(2)}\right|e^{j(\phi_2^{\text{opt}}+\phi_a)}\right|^2\right)\right.$$
$$+\left(1-\frac{L_{k2}}{N_2}\right)\log_2\left(1+\frac{P}{\sigma^2}\left\{\frac{N_1^2}{L_{k1}}(g(L_{k1}))^2\beta_{X,k}^{(1)}\right\}\right)$$
$$+\left(1-\frac{L_{q1}}{N_1}\right)\frac{L_{k2}}{N_2}\log_2\left(1+\frac{P}{\sigma^2}\left\{\frac{N_1^2}{L_{k1}}(g(L_{k1}))^2\beta_{X,k}^{(1)}\right.\right.$$
$$\left.\left.\left.+\frac{N_2^2}{L_{k2}}\beta_{X,k}^{(2)}+\left(\frac{\pi N_1N_2(f(L_{k1}))^2\sqrt{\beta_{X,k}^{(1)}\beta_{X,k}^{(2)}}}{2\sqrt{L_{k1}L_{k2}}}\right)\right\}\right)\right\}, \tag{7.52}$$

$$\langle R_Y \rangle_{JO} \approx \frac{1}{Q}\sum_{q=1}^{Q}\left\{\frac{L_{q1}L_{k2}}{N_1N_2}\log_2\left(1+\frac{P}{\sigma^2}\left|\frac{N_1}{\sqrt{L_{q1}}}|\gamma_{l_q^*,Y}^{(1)}\gamma_{l_q^*,q}^{(1)}|e^{j(\phi_1^{\text{opt}}+\phi_b)}+\frac{N_2}{\sqrt{L_{q2}}}|\gamma_{1,Y}^{(2)}\gamma_{1,q}^{(2)}|e^{j\phi_2^{\text{opt}}}\right|^2\right)\right.$$
$$+\left(1-\frac{L_{q1}}{N_1}\right)\log_2\left(1+\frac{P}{\sigma^2}\left\{\frac{N_2^2}{L_{q2}}(g(L_{q2}))^2\beta_{Y,q}^{(2)}\right\}\right)$$
$$+\left(1-\frac{L_{k2}}{N_2}\right)\frac{L_{q1}}{N_1}\log_2\left(1+\frac{P}{\sigma^2}\left\{\frac{N_2^2}{L_{q2}}(g(L_{q2}))^2\beta_{Y,q}^{(2)}\right.\right.$$
$$\left.\left.\left.+\frac{N_1^2}{L_{q1}}\beta_{Y,q}^{(1)}+\left(\frac{\pi N_1N_2(f(L_{q2}))^2\sqrt{\beta_{Y,q}^{(1)}\beta_{Y,q}^{(2)}}}{2\sqrt{L_{q1}L_{q2}}}\right)\right\}\right)\right\}. \tag{7.53}$$

Further, an upper bound on the SEs $\langle R_X \rangle_{JO}$ and $\langle R_Y \rangle_{JO}$ without relying on Algorithm 7.1 can be obtained as $\langle R_X \rangle_{JO} \leq \langle R_X^{\zeta} \rangle_{TS}\big|_{\zeta=1}$ and $\langle R_Y \rangle_{JO} \leq \langle R_Y^{\zeta} \rangle_{TS}\big|_{\zeta=0}$, respectively, where $\langle R_X^{\zeta} \rangle_{TS}$, $\langle R_Y^{\zeta} \rangle_{TS}$ are given as in (7.50) and (7.51), with $\mathsf{CO} = 1$.

3. *Optimization of IRSs without MO cooperation: $\langle R_X \rangle_{NCO}$, $\langle R_Y \rangle_{NCO}$ as given in (7.50) and (7.51) with $\mathsf{CO} = 0$.*

Proof. We only prove (7.50) (and (7.52)), for MO-X; the proof of (7.51) (and (7.53)) is similar. Using the law of total expectation, at a given UE-k, the ergodic SE (for all three schemes) is

$$\langle R_k \rangle = \sum_{i \in \{\mathcal{A},\mathcal{B},\mathcal{C},\mathcal{D}\}} \langle R_k | i \rangle \Pr(i), \tag{7.54}$$

where the probabilities can be found using (7.14), (7.40), (7.45), and (7.47) for events

$\mathcal{A}, \mathcal{B}, \mathcal{C}$, and $\mathcal{D}$, respectively. As a consequence, under RR scheduling, the ergodic sum-SE of MO-X is

$$\langle R_X \rangle = (1/K) \sum_{k=1}^{K} \langle R_k \rangle. \tag{7.55}$$

Next, the scheme-specific ergodic SE is characterized below.

- Optimization of IRSs with time-sharing: In this scheme, $\langle R_k | i \rangle$ can be obtained from (7.38), (7.44), (7.38), and (7.49) for events $\mathcal{A}, \mathcal{B}, \mathcal{C}$, and $\mathcal{D}$, respectively, then using (7.54) and (7.55), the result in (7.50) for MO-X follows.

- Joint-optimization of IRSs with MO cooperation: We obtain the values of $\langle R_k | i \rangle$ by using (7.23), (7.44), (7.34), and (7.49) for events $\mathcal{A}, \mathcal{B}, \mathcal{C}$, and $\mathcal{D}$, respectively. Then, substituting these values into (7.54) and in (7.55) yields the expression in (7.52).

  Further, the ergodic SE obtained at a UE by jointly optimizing the IRSs is, at most, the SE obtained by optimizing the overall phases of both the IRSs to that UE in all time slots when it is scheduled. Thus, the SE with joint optimization is upper bounded by the expressions for the time-sharing scheme given above, but with $\zeta = 1$ and $\zeta = 0$ for MO-X and MO-Y, respectively. This establishes the upper bounds in the Theorem.

- For the no cooperation scheme, $\langle R_k | i \rangle$ can be found from (7.36), (7.44), (7.36), (7.44) for events $\mathcal{A}, \mathcal{B}, \mathcal{C}$, and $\mathcal{D}$, respectively, and using them in (7.54), (7.55), the result follows.

This completes the proof of the theorem. ■

We interpret Theorem 7.1 as follows. At MO-X, in the time-sharing scheme, among the time slots in which the OOB IRS-Y aligns with UE-k (which happens with probability L_{k2}/N_2), for a ζ fraction of the total time slots, the overall phase shifts of both IRSs are optimized to UE-k only and procures an array gain that scales as $\mathcal{O}\left((N_1 + N_2)^2\right)$. For the other $(1 - \zeta)$ fraction of time slots, since the IRSs add the signals coherently at UE-q served by MO-Y, the array gain at UE-k is only due to an incoherent addition of signals from the IRSs, i.e., it scales as $\mathcal{O}(N_1^2 + N_2^2)$. On the other hand, when IRS-Y does not align with UE-k (which happens with probability $1 - L_{k2}/N_2$), the array gain scales

only as $\mathcal{O}\left(N_1^2\right)$. Similarly, under the joint-optimization scheme, whenever IRS-Y aligns with UE-k, but IRS-X does not align with UE-q, i.e., with event $\mathcal{C}$ which happens with probability $(1 - L_{q1}/N_2)L_{k2}/N_2$, the solution for joint optimization boils to that obtained under time-sharing with $\zeta = 1$, which procures a full array gain of $\mathcal{O}\left((N_1 + N_2)^2\right)$. When both the IRSs align with both the UEs, i.e., under event $\mathcal{A}$, due to the non-availability of closed-form expressions for ϕ_1^{opt} and ϕ_2^{opt}, we do not have an explicit SE-scaling law for this event. However, it is expected that the scaling of the array gain in this case lies between $\mathcal{O}\left(N_1^2 + N_2^2\right)$ and $\mathcal{O}\left((N_1 + N_2)^2\right)$. Finally, when IRS-Y does not align with UE-k, the array gain again scales only as $\mathcal{O}(N_1^2)$. We can have similar interpretations at MO-Y as well. Based on the above, we make the following observations:

- The sum-SE of MO-X scales at least as $\mathcal{O}(\log_2(N_1^2))$ in all cases, which is due to the array gain that is obtained in the absence of OOB IRSs. Thus, in general, IRS deployed by one MO *does not degrade* the achievable SE at other MOs.

- When both IRSs align to their respective OOB UEs, the best possible SE of an MO can potentially scale as $\mathcal{O}\left(\log_2(N_1 + N_2)^2\right)$. However, this is not simultaneously achievable at both MOs, as noted in the discussion following (7.19) in Sec. 7.3.a. Further, even if it were possible to satisfy (7.18) and (7.19) simultaneously and achieve a sum-SE of $\mathcal{O}\left(\log_2(N_1 + N_2)^2\right)$ at both MOs, we will next show that the resultant gain in the overall SE is small because of the low-probability nature of both IRSs aligning to OOB UEs.

7.4 Quantifying the Effect of Out-of-Band IRSs

In the previous section, we characterized the ergodic sum-SE of a system with 2 MOs, each optimizing an IRS to serve its UEs. We analyzed three schemes that allow different degrees of cooperation between MOs. However, from a practical viewpoint, it is helpful to explicitly quantify the gain/loss in the ergodic SE with/without OOB IRSs and with-/without cooperation between MOs. To that end, considering one of the MOs, say MO-X, we present the following result.

Theorem 7.2. *Under the SV channel model in the mmWave bands, under RR scheduling, the maximum gain in the ergodic sum-SE of MO-X*

1. *with, versus without, OOB IRS-Y is given by*

$$\triangle\langle R_X\rangle_{OOB} = \frac{1}{K}\sum_{k=1}^{K}\frac{L_{k2}}{N_2}\log_2\left(1+\left\{\frac{\left(\frac{N_2^2}{L_{k2}}\beta_{X,k}^{(2)}+\mathbb{1}_{\{\mathsf{CO}=1\}}\frac{\pi N_1 N_2 (f(L_{k1}))^2\sqrt{\beta_{X,k}^{(1)}\beta_{X,k}^{(2)}}}{2\sqrt{L_{k1}L_{k2}}}\right)}{\left(\frac{\sigma^2}{P}+\frac{N_1^2}{L_{k1}}(g(L_{k1}))^2\beta_{X,k}^{(1)}\right)}\right\}\right). \tag{7.56}$$

2. *with cooperation (i.e., jointly optimize/time-share the IRSs) versus no cooperation between MOs in the presence of the OOB IRS-Y is bounded as*

$$\triangle\langle R_X\rangle_{CO} \leq \frac{1}{K}\sum_{k=1}^{K}\frac{L_{k2}}{N_2}\log_2\Big(1+\Psi(L_{k1})\frac{\pi}{4}\Big), \tag{7.57}$$

where $\Psi(L_{k1}) \triangleq (f(L_{k1}))^2\Big/g(L_{k1})$.

Proof. We prove the two statements separately below.

7.4.a Gain with versus without OOB IRS

To bound the gain in sum-SE obtained by MO-X with and without the OOB IRS, we consider two cases: 1) the OOB IRS is present, and it coherently adds the signals at the UEs of MO-X in all time slots if cooperation is allowed, and 2) the OOB IRS is absent. Let the sum-SE $\langle R_X^{\zeta}\rangle_{\text{TS}}$ given in (7.50) with and without the OOB IRS be denoted by $\langle R_X^{\zeta}\rangle_{\text{W-IRS}}$ and $\langle R_X^{\zeta}\rangle_{\text{WO-IRS}}$, respectively. Then the maximum gain in SE is given by

$$\triangle\langle R_{\text{X}}\rangle_{\text{OOB}} \triangleq \langle R_X^{\zeta}\rangle_{\text{W-IRS}}\Big|_{\zeta=1} - \langle R_X^{\zeta}\rangle_{\text{WO-IRS}}, \tag{7.58}$$

where $\zeta = 1$ captures that the overall phase shifts at both the IRSs are used to coherently add the signals at the UEs served by MO-X in all time slots. Then, substituting for the resulting values in the above equation and noting that the sum-SE without the OOB IRS follows by substituting $N_2 = 0$ in (7.50) and recognizing that the pre-log term L_{k2}/N_2 is unity in the absence of the OOB IRS, we obtain (7.56).

7.4.b Gain with versus without cooperation

We first consider time-sharing. Let the sum-SE at MO-X with and without cooperation be denoted as $\langle R_{\mathrm{X}}\rangle^{\mathrm{TS}}_{\text{W-CO}}$ and $\langle R_{\mathrm{X}}\rangle^{\mathrm{TS}}_{\text{WO-CO}}$, respectively, i.e., from (7.50), $\langle R_{\mathrm{X}}\rangle^{\mathrm{TS}}_{\text{W-CO}} = \langle R^{\zeta}_{\mathrm{X}}\rangle_{\mathrm{TS}}$ with $\mathsf{CO} = 1$, and $\langle R_{\mathrm{X}}\rangle^{\mathrm{TS}}_{\text{WO-CO}} = \langle R^{\zeta}_{\mathrm{X}}\rangle_{\mathrm{TS}}$ with $\mathsf{CO} = 0$. Then, the maximum gain in the sum-SE of MO-X with versus without cooperation is

$$\triangle\langle R_{\mathrm{X}}\rangle_{\mathrm{TS}} \triangleq \langle R_{\mathrm{X}}\rangle^{\mathrm{TS}}_{\text{W-CO}}\Big|_{\zeta=1} - \langle R_{\mathrm{X}}\rangle^{\mathrm{TS}}_{\text{WO-CO}} \tag{7.59}$$

$$= \frac{1}{K}\sum_{k=1}^{K}\frac{L_{k2}}{N_2}\log_2\left(1+\frac{\pi}{2}\cdot\frac{\frac{N_1N_2}{\sqrt{L_{k1}L_{k2}}}(f(L_{k1}))^2\sqrt{\beta^{(1)}_{X,k}\beta^{(2)}_{X,k}}}{\frac{\sigma^2}{P}+\left(\frac{N_1^2}{L_{k1}}(g(L_{k1}))^2\beta^{(1)}_{X,k}+\frac{N_2^2}{L_{k2}}\beta^{(2)}_{X,k}\right)}\right)$$

$$\overset{(b)}{\lessapprox} \frac{1}{K}\sum_{k=1}^{K}\frac{L_{k2}}{N_2}\log_2\left(1+\Psi(L_{k1})\frac{\pi}{4}\right), \tag{7.60}$$

where $\Psi(L_{k1})$ is as defined in the theorem and in (b) we used a high SNR approximation and the fact that $\left((N_1/\sqrt{L_{k1}})g(L_{k1})\sqrt{\beta^{(1)}_{X,k}} - (N_2/\sqrt{L_{k2}})\sqrt{\beta^{(2)}_{X,k}}\right)^2 \geq 0$.

Next, under the joint optimization scheme, let the SE with and without cooperation be $\langle R_{\mathrm{X}}\rangle^{\mathrm{JO}}_{\text{W-CO}}$ and $\langle R_{\mathrm{X}}\rangle^{\mathrm{JO}}_{\text{WO-CO}}$, respectively, i.e., from (7.52), $\langle R_{\mathrm{X}}\rangle^{\mathrm{JO}}_{\text{W-CO}} = \langle R_{\mathrm{X}}\rangle_{\mathrm{JO}}$, and $\langle R_{\mathrm{X}}\rangle^{\mathrm{JO}}_{\text{WO-CO}} = \langle R^{\zeta}_{\mathrm{X}}\rangle_{\mathrm{TS}}$ with $\mathsf{CO} = 0$. Then, the maximum gain in the SE is

$$\triangle\langle R_{\mathrm{X}}\rangle_{\mathrm{JO}} = \langle R_{\mathrm{X}}\rangle^{\mathrm{JO}}_{\text{W-CO}} - \langle R_{\mathrm{X}}\rangle^{\mathrm{JO}}_{\text{WO-CO}} \tag{7.61}$$

$$\overset{(c)}{\leq} \langle R_{\mathrm{X}}\rangle^{\mathrm{TS}}_{\text{W-CO}}\Big|_{\zeta=1} - \langle R_{\mathrm{X}}\rangle^{\mathrm{TS}}_{\text{WO-CO}}, \tag{7.62}$$

where in (c), we use Theorem 7.1 that the SE achieved by jointly optimizing the IRSs is upper bounded by the SE when the IRSs are optimized for the UE served by MO-X in all time slots. Finally, we note that (7.62) can be characterized as given in (7.60). Thus, under both schemes, the gain with versus without cooperation can be unified into a single expression, $\triangle\langle R_X\rangle_{\mathrm{CO}}$, in (7.57). This completes the proof. ■

From (7.56) of Theorem 7.2, we observe that the gain in the sum-SE is strictly non-negative. Thus, the ergodic sum-SE at MO-X can only improve in the presence of an OOB IRS. In particular, we also make the following observations:

- **Gain with OOB IRS at Low-SNR**: In the low SNR regime, since $\frac{\sigma^2}{P} \gg 1$, we have $\frac{\sigma^2}{P} + \frac{N_1^2}{L_{k1}}(g(L_{k1}))^2\beta_{X,k}^{(1)} \approx \frac{\sigma^2}{P}$. Using this in (7.56), and also using $\log_2(1+x) \approx \frac{x}{\ln(2)}$ when $x \ll 1$, we obtain the simplified expression for the gain obtained by an in-band MO due to an OOB-IRS in (7.63), at low-SNR scenarios:

$$\triangle\langle R_{\mathrm{X}}\rangle_{\mathrm{OOB}}^{\text{L-SNR}} \approx \frac{1}{K}\sum_{k=1}^{K}\frac{1}{\ln(2)}\left(N_2\beta_{X,k}^{(2)} + \mathbb{1}_{\{\mathsf{CO}=1\}}\frac{\pi N_1 (f(L_{k1}))^2\sqrt{\beta_{X,k}^{(1)}\beta_{X,k}^{(2)}}}{2}\cdot\sqrt{\frac{L_{k2}}{L_{k1}}}\right)\frac{P}{\sigma^2}. \tag{7.63}$$

  In this case, the gain increases linearly with the number of IRS elements, particularly those of the OOB IRS, and the SNR of operation. This behavior can be attributed to the fact that the OOB IRS enables the reception of additional copies of the signal at the UE (either coherently or incoherently, depending on the level of MO cooperation) whenever the OOB IRS aligns with the UE served by MO-X (an event occurring with probability L_{k2}/N_2). These additional signal paths enhance the *average* received SNR at the in-band UE.

- **Gain with OOB IRS at High-SNR**: Here, since $\frac{\sigma^2}{P} \ll 1$, we have $\frac{\sigma^2}{P}+\frac{N_1^2}{L_{k1}}(g(L_{k1}))^2\beta_{X,k}^{(1)}$ $\approx \frac{N_1^2}{L_{k1}}(g(L_{k1}))^2\beta_{X,k}^{(1)}$. Using this approximation, along with the fact that $\log_2(1+x) \approx \log_2(x)$ when $x \gg 1$, we get the simplified expression for the SE gain in the high-SNR regime as given in (7.64):

$$\triangle\langle R_{\mathrm{X}}\rangle_{\mathrm{OOB}}^{\text{H-SNR}} \approx \frac{1}{K}\sum_{k=1}^{K}\frac{L_{k2}}{N_2}\log_2\left(1+\left(\frac{N_2}{N_1}\right)^2\frac{L_{k1}}{L_{k2}}\cdot\frac{\beta_{X,k}^{(2)}}{(g(L_{k1}))^2\beta_{X,k}^{(1)}} + \mathbb{1}_{\{\mathsf{CO}=1\}}\cdot\frac{\pi N_2}{2N_1}\cdot\frac{(f(L_{k1}))^2\sqrt{\beta_{X,k}^{(2)}L_{k1}}}{(g(L_{k1}))^2\sqrt{\beta_{X,k}^{(1)}L_{k2}}}\right). \tag{7.64}$$

  Contrary to the low-SNR regime, the gain at high SNR exhibits a unimodal behavior with respect to the number of elements at the OOB IRS. This arises because, although a larger OOB IRS can potentially deliver more signal copies when aligned with the in-band UE, the probability of such alignment decreases as the number of elements at the OOB IRS increases. The alignment probability is initially high, allowing the overall SE gain

Table 7.3: Variation of $\Psi(L)$ as a function of L.

L	1	2	5	10	25	40
$\Psi(L)$	0.79	0.87	0.93	0.96	0.97	0.98

to improve with N_2. However, the alignment probability decreases as N_2 increases, and this outweighs the logarithmic increase in the gain. This leads to an overall reduction in the gain, resulting in the observed unimodal trend. Moreover, the gain does not scale significantly with SNR, since the in-band UE already enjoys high SE at high SNR. Thus, only marginal improvements are observed unless the OOB IRS offers substantial additional contribution (which is less likely as N_2 increases.)

- The best SE gain in (7.57) obtained by cooperation is directly proportional to L_{k2}/N_2, but depends weakly on L_{k1} through the $\Psi(L_{k1})$ term, as shown in Table 7.3. However, the gain decreases as the number of OOB IRS elements N_2 increases.

In the next section, we extend our results to a general setting where more than two operators exist and each deploys its own IRS to serve its UEs optimally.

7.5 Performance Analysis with $M > 2$ MOs

We consider that M MOs serve a given geographical area, and their respective BSs: {BS-1, BS-2,..., BS-M} provide services to $\{K_1, K_2, \ldots, K_M\}$ UEs at the same time over non-overlapping bands. Further, UE-k_l denotes the kth UE served by the lth MO. For simplicity, we let the number of elements in each IRS equal N. At any UE served by an in-band MO, due to the presence of $M-1$ OOB IRSs, M different events arise, similar to Sec. 7.3, and we denote them by $\mathcal{E}_0, \ldots, \mathcal{E}_{M-1}$. Specifically, $\mathcal{E}_m$ is the event that exactly m OOB IRSs align with UE-k_1 on one of the OOB paths through them. Further, the event that an OOB IRS phase configuration aligns with an OOB path is independent across the OOB IRSs, so, the number of OOB IRSs, m, that contribute to the channel at any UE follows a binomial distribution, i.e., $m \sim \text{Bin}\left(M-1, \frac{L_{k1}}{N}\right)$. As a consequence, $\Pr(\mathcal{E}_m) = \binom{M-1}{m}\left(\frac{L_{k_1}}{N}\right)^m\left(1-\frac{L_{k_1}}{N}\right)^{(M-1-m)}$, where L_{k_1} is the number of resolvable OOB paths at UE-k_1 via an IRS, and here $L_{k1} \leq N$. Then, similar to (7.16), conditioned on

$\mathcal{E}_m$, the channel from BS-1 to UE-k_1 is given by

$$h_{k_1} = \frac{N}{\sqrt{L_{k_1}}} \left\{ \left| \gamma_{1,\mathrm{B}_1}^{(1)} \gamma_{1,k_1}^{(1)} \right| e^{j\phi_1} + \sum_{i=2}^{m+1} \left| \gamma_{l^*,\mathrm{B}_1}^{(m_i)} \gamma_{l^*,k_1}^{(m_i)} \right| e^{j(\phi_{m_i} + \phi_{m_{i1}})} \right\},$$

where symbols have similar meanings as in Sec. 7.3. For example, $\gamma_{1,\mathrm{B}_1}^{(1)}$ denotes the channel coefficient between the first IRS (superscript) and BS-1 (second subscript) along the first (dominant) path (first subscript); $\gamma_{1,k_1}^{(1)}$ denotes the channel coefficient between the first IRS and the k_1th UE along the first path. Also, $m_i \in \{2, \ldots, M\}$, such that $m_i \neq m_j$ when $i \neq j$, i.e., $\{m_i\}_{i=2}^{m+1}$ denotes the indices of the m OOB IRSs for which some l^*th path aligns with UE-k_1. Further, $\gamma_{l^*,\mathrm{B}_1}^{(m_i)}$ and $\gamma_{l^*,k_1}^{(m_i)}$ denote the coefficients of the channnels from BS-1 to IRS-m_i and IRS-m_i to UE-k_1 that correspond to the l^*th OOB cascaded path via the aligning IRS-m_i which contributes to the recieved signal at UE-k_1. Then, we model $\gamma_{l^*,\mathrm{B}_1}^{(m_i)} \sim \mathcal{CN}(0, \beta_{\mathrm{B}_1})$, $\gamma_{l^*,k_1}^{(m_i)} \sim \mathcal{CN}(0, \beta_{k_1})$, where β_{B_1} and β_{k_1} are the path losses in the BS-1 to IRS-1 and IRS-1 to UE-k_1 links, respectively.[5] Finally, $\phi_{m_{i1}}$ is the phase difference of the matching cascaded OOB path at UE-k_1 via the m_ith IRS and the in-band path, and ϕ_{m_i} is an overall extra phase applied at IRS-m_i. Next, we analyze the ergodic sum-SE of MO-1 for different schemes as discussed in the 2-MO case, which entails varying degrees of cooperation among the MOs.

7.5.a Time-sharing of the IRSs with MO Cooperation

In this scheme, under event $\mathcal{E}_m$, for a ζ_1 fraction of time slots, all the m matching OOB IRSs coherently add the signals at UE-k_1 and in the other $1-\zeta_1$ fraction of slots, UE-k_1 receives an incoherent addition of signals from the OOB IRSs. Then, similar to Sec. 7.3.a, to maximize $|h_{k_1}|^2$ at UE-k_1 in the ζ_1 fraction of slots, we set $\phi_{m_i} = -\phi_{m_{i1}}$, and $\phi_1 = 0$. The overall channel coefficient at UE-k_1 under event $\mathcal{E}_m$ is

$$h_{k_1}^{(\zeta_1)} \overset{d}{=} \frac{N}{\sqrt{L_{k1}}} \left\{ \left| \gamma_{1,\mathrm{B}_1}^{(1)} \gamma_{1,k_1}^{(1)} \right| + \sum_{i=2}^{m+1} \left| \gamma_{l^*,\mathrm{B}_1}^{(m_i)} \gamma_{l^*,k_1}^{(m_i)} \right| \right\}, \tag{7.65}$$

[5] For simplicity of exposition, the path losses are equal across IRSs [126].

and its average gain in (7.66) is obtained as

$$\mathbb{E}\Big[\Big|h_{k_1}^{(\zeta)}\Big|^2\Big] = \frac{N^2}{L_{k_1}}\Bigg\{\mathbb{E}\Bigg[\Big|\gamma_{1,\mathrm{B}_1}^{(1)}\gamma_{1,k_1}^{(1)}\Big|^2 + \sum_{i=2}^{m+1}\Big|\gamma_{l^*,\mathrm{B}_1}^{(m_i)}\gamma_{l^*,k_1}^{(m_i)}\Big|^2 + 2\sum_{i=2}^{m+1}\Big|\gamma_{l^*,\mathrm{B}_1}^{(m_i)}\gamma_{l^*,k_1}^{(m_i)}\gamma_{1,\mathrm{B}_1}^{(1)}\gamma_{1,k_1}^{(1)}\Big| + \sum_{\substack{i,j=2\\ i\neq j}}^{m+1}\Big|\gamma_{l^*,\mathrm{B}_1}^{(m_i)}\gamma_{l^*,k_1}^{(m_i)}\gamma_{l^*,\mathrm{B}_1}^{(m_j)}\gamma_{l^*,k_1}^{(m_j)}\Big|\Bigg]\Bigg\} \tag{7.66}$$

$$= \frac{N^2}{L_{k_1}}\beta_{\mathrm{B}_1,k_1}\Bigg\{(g(L_{k1}))^2 + m\Big(1+\frac{\pi}{2}(f(L_{k1}))^2 + \frac{\pi^2}{8}\frac{(m-1)}{2}\Big)\Bigg\}, \tag{7.67}$$

where $\beta_{\mathrm{B}_1,k_1} \triangleq \beta_{\mathrm{B}_1}\beta_{k_1}$. For other $(1-\zeta_1)$ fraction of slots,

$$h_{k_1}^{(1-\zeta_1)} \triangleq \frac{N}{\sqrt{L_{k_1}}}\Bigg\{\Big|\gamma_{1,\mathrm{B}_1}^{(1)}\gamma_{1,k_1}^{(1)}\Big| + \sum_{i=2}^{m+1}\Big|\gamma_{l^*,\mathrm{B}_1}^{(m_i)}\gamma_{l^*,k_1}^{(m_i)}\Big|e^{j\phi_{m_i1}}\Bigg\}, \tag{7.68}$$

and its average gain can be similarly obtained as

$$\mathbb{E}\Big[\Big|h_{k_1}^{(1-\zeta_1)}\Big|^2\Big] = \frac{N^2}{L_{k_1}}\beta_{\mathrm{B}_1,k_1}\Bigg\{(g(L_{k1}))^2 + m\Bigg\}. \tag{7.69}$$

Then, by using Jensen's approximation, the ergodic sum-SE of MO-X conditioned on event $\mathcal{E}_m$ is given in (7.70):

$$\langle R_{k_1}^{(\zeta_1)}|\mathcal{E}_m\rangle_{\mathrm{TS}} \approx \zeta_1\log_2\Bigg(1+\frac{P}{\sigma^2}\frac{N^2}{L_{k_1}}\beta_{\mathrm{B}_1,k_1}\Bigg\{(g(L_{k1}))^2+m\Big(1+\frac{\pi}{2}(f(L_{k1}))^2+\frac{\pi^2}{8}\frac{(m-1)}{2}\Big)\Bigg\}\Bigg) + (1-\zeta_1)\cdot\log_2\Bigg(1+\frac{P}{\sigma^2}\frac{N^2}{L_{k_1}}\beta_{\mathrm{B}_1,k_1}\Bigg\{(g(L_{k1}))^2+m\Bigg\}\Bigg). \tag{7.70}$$

7.5.b Joint-Optimization of IRSs with MO Cooperation

In the joint optimization scheme, the overall phase angles at the IRSs, i.e., ϕ_{m_i}, are chosen to maximize the weighted sum-SE of all UEs scheduled by every MO in a time slot. In this case, the SE of each MO under different events can be characterized similarly to the previous section. Consequently, the overall sum-SE of any given MO can be obtained similarly to (7.52), and we omit the details for brevity.

7.5.c No cooperation among the MOs

When the MOs do not cooperate, the overall IRS phase-shifts are set as $\{\phi_1, \phi_{m_i}\}_{i=2}^{m+1} = 0$. So, the channel becomes

$$h_{k_1} = \frac{N}{\sqrt{L_{k_1}}}\left\{\left|\gamma_{1,\mathrm{B}_1}^{(1)}\gamma_{1,k_1}^{(1)}\right| + \sum_{i=2}^{m+1}\left|\gamma_{l^*,\mathrm{B}_1}^{(m_i)}\gamma_{l^*,k_1}^{(m_i)}\right| e^{j\phi_{m_i 1}}\right\},$$

for which, we have $\mathbb{E}\Big[|h_{k_1}|^2\Big] = \frac{N^2}{L_{k_1}}\beta_{\mathrm{B}_1,k_1}\Big\{(g(L_{k1}))^2 + m\Big\}$. Then the ergodic SE of MO-1, under event $\mathcal{E}_m$, is

$$\langle R_{k_1}|\mathcal{E}_m\rangle_{\mathrm{NCO}} \approx \log_2\left(1 + \frac{P}{\sigma^2}\frac{N^2}{L_{k1}}\beta_{\mathrm{B}_1,k_1}\Big\{(g(L_{k1}))^2 + m\Big\}\right).$$

We next characterize the overall ergodic sum-SE of a MO (say MO-1) when $M > 2$ MOs coexist, similar to Theorem 7.1.

Theorem 7.3. *Under the SV channel model in the mmWave bands, when $M > 2$ MOs control an IRS each to serve its subscribed UEs, the ergodic sum-SE of MO-1 under RR scheduling is characterized as:*

1. *Optimization of IRSs with time sharing where $\zeta_1 T_c$ time slots alloted to MO-X and $(1-\zeta_1)T_c$ time slots are alloted to other MOs: $\langle R_1^{\zeta_1}\rangle_{TS}$, as given in (7.71) with $\mathsf{CO} = 1$:*

$$\langle R_1^{(\zeta_1)}\rangle_{TS} \approx \frac{1}{K_1}\sum_{k_1=1}^{K_1}\sum_{m=0}^{M-1}\binom{M-1}{m}\left(\frac{L_{k_1}}{N}\right)^m\left(1-\frac{L_{k_1}}{N}\right)^{(M-m-1)}$$
$$\times\left\{\zeta_1\log_2\left(1+\frac{P}{\sigma^2}\frac{N^2}{L_{k_1}}\beta_{B_1,k_1}\left\{(g(L_{k1}))^2 + m + \mathbb{1}_{\{\mathsf{CO}=1\}}\, m\frac{\pi}{2}\left((f(L_{k1}))^2 + \frac{\pi(m-1)}{8}\right)\right\}\right)\right.$$
$$\left.+(1-\zeta_1)\cdot\log_2\left(1+\frac{P}{\sigma^2}\frac{N^2}{L_{k_1}}\beta_{B_1,k_1}\Big\{(g(L_{k1}))^2+m\Big\}\right)\right\}, \tag{7.71}$$

2. *Joint-optimization of IRSs with MO cooperation: The ergodic rate for MO-1 can be obtained similar to (7.52) with $\phi_{m_i}^{\mathrm{opt}}$ determined similar to Algorithm 7.1. Further, an upper bound on the SEs $\langle R_1\rangle_{JO}$ without relying on $\phi_{m_i}^{\mathrm{opt}}$ can be obtained as $\langle R_1\rangle_{JO} \leq \langle R_1^{\zeta_1}\rangle_{TS}\Big|_{\zeta_1=1}$, where $\langle R_X^{\zeta_1}\rangle_{TS}$ is given in (7.71) with $\mathsf{CO} = 1$.*

3. *No MO Cooperation: $\langle R_1\rangle_{NCO}$ as in (7.71) with $\mathsf{CO} = 0$.*

Proof. By the law of total expectation, $\langle R_{k_1} \rangle = \sum_m \langle R_{k_1} | \mathcal{E}_m \rangle \Pr(\mathcal{E}_m)$, and under RR scheduling, we note $\langle R_1 \rangle \triangleq \frac{1}{K_1} \sum_{k_1=1}^{K_1} \langle R_{k_1} \rangle$. Using the values of $\langle R_{k_1} \rangle$ under the three schemes in $\langle R_1 \rangle$ completes the proof. ■

Next, similar to Theorem 2, we can characterize the gain in the sum-SE due to the presence of the OOB IRSs over that in the absence of OOB IRSs and the gain due to cooperation over the no-cooperation case. We illustrate this in the following result, which shows that cooperation offers only a marginal improvement in the sum-SE.

Theorem 7.4. *Under the SV channels in mmWaves and RR scheduling, the maximum gain in the ergodic sum-SE of MO-1*

1. with vs. without OOB IRSs is approximately given by (7.72):

$$\Delta \langle R_1 \rangle_{OOB} \approx \frac{1}{K_1} \sum_{k_1=1}^{K_1} \sum_{m=1}^{M-1} \binom{M-1}{m} \left(\frac{L_{k_1}}{N} \right)^m \left(1 - \frac{L_{k_1}}{N} \right)^{(M-m-1)} \times \log_2 \left(1 + \frac{m + \mathbb{1}_{\{\mathsf{CO}=1\}} m \frac{\pi}{2} \left((f(L_{k1}))^2 + \frac{\pi(m-1)}{8} \right)}{(g(L_{k1}))^2} \right). \quad (7.72)$$

2. with cooperation (i.e., jointly optimize/time-share the IRSs) vs. no cooperation between MOs in the presence of the OOB IRSs is bounded as in (7.73):

$$\triangle \langle R_1 \rangle_{CO} \leq \frac{1}{K_1} \sum_{k_1=1}^{K_1} \sum_{m=1}^{M-1} \binom{M-1}{m} \left(\frac{L_{k_1}}{N} \right)^m \left(1 - \frac{L_{k_1}}{N} \right)^{(M-m-1)} \times \log_2 \left(1 + \frac{\pi \sqrt{m}}{4} \left\{ \Psi(L_{k1}) + \frac{\pi(m-1)}{8 g(L_{k1})} \right\} \right). \quad (7.73)$$

Proof. It is similar to Theorem 7.2. We omit for brevity. ■

Considering the $m = 1$ term in (7.72) and (7.73), and comparing them with (7.64) and (7.57) respectively, we see that the gain in SE due to the presence of M IRSs scales approximately as $M-1$ times the gain in the 2-MO case. This is because there are $M-1$ OOB IRSs that can align with a given UE. In addition, we can obtain further gains in the SE, captured by the summands corresponding to $m = 2$ to $m = M-1$, when $m \geq 2$ OOB

IRSs happen to be aligned to the UE. However, the event that m IRSs align with a UE occurs with exponentially lower probability due to the $(L/N)^m$ term. Thus, the presence of M MOs does not degrade the sum SE of a given operator; in fact, it provides a gain in the sum SE that increases at least linearly with M.

In the next section, we numerically illustrate our findings via Monte Carlo simulations.

7.6 Numerical Results and Discussion

We first illustrate the results for 2 MOs as in Sec. 7.3 and 7.4.

7.6.a 2-MO and 2-IRS System

BS-X and BS-Y are located at $(0, 200)$, and $(200, 0)$ (in meters), and IRS-X and IRS-Y are located at $(0, 0)$ and $(200, 200)$, respectively. All UEs are uniformly located in a rectangular region with diagonally opposite corners $(0, 0)$ and $(200, 200)$. The path loss is modeled as $\beta = C_0 \, (d_0/d)^\alpha$, where $C_0 = -60$ dB is the path loss at the reference distance $d_0 = 1$ m, d is the distance between nodes, and α is the path loss exponent [154]. We use $\alpha = 2$ for both BS-IRS, and the IRS-UE paths [9]. We use RR scheduling to serve $K = Q = 10$ UEs over 1000 time slots by the respective MOs.

In Fig. 7.3, we plot the achievable ergodic sum-SE of MO-X vs. $\log_2 N$ (where $N = N_1 = N_2$), under event $\mathcal{A}$, and study the performance of the three schemes described in Sec. 7.3.a. The SE, when jointly optimal overall IRS phases are used to maximize the equal-weighted sum-SE of UEs scheduled by the MOs using a general high complexity off-the-shelf solver using the `findpeaks` function of MATLAB (curve labeled `Joint optimization solver`) nearly overlaps with that obtained using the low-complexity single-iteration Algorithm 7.1 (curve labeled `Joint optim. with Alg. 1`). This shows that the proposed single-iteration Newton's algorithm is a practically viable solution, offering near-optimal performance with significantly reduced complexity. This effectiveness is largely due to the carefully chosen initialization strategy (given in lines 1–5 of Algorithm 7.1), which provides provable convergence guarantees [175, Theorem 9.1]. Further, the SE using the joint optimization scheme is slightly inferior to the time-sharing

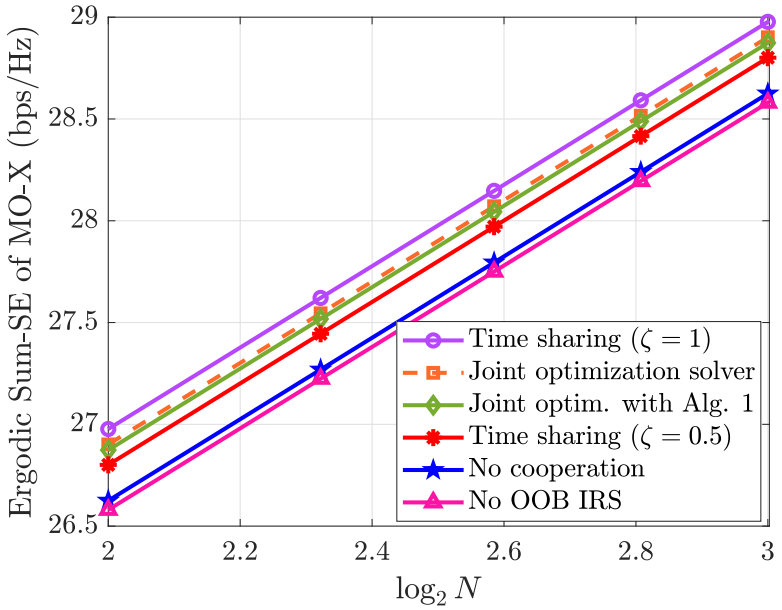

Figure 7.3: Ergodic sum-SE of MO-X vs. $\log_2 N$ conditioned on Event $\mathcal{A}$ at $C_0\gamma = 150$ dB and $L_{k1} = 1, L_{k2} = 10$.

scenario with $\zeta = 1$ (curve labeled `Time sharing` $\zeta = 1$). This is because no UE gets the full array gain of $\mathcal{O}((N_1 + N_2)^2)$ in any time slot under a joint-optimization scheme. The performance obtained by MO-X with time-sharing ($\zeta = 1$) is about 0.5 bps/Hz higher than that obtained without an OOB IRS (curve labeled `No OOB IRS`). This is because, under event $\mathcal{A}$, the OOB IRS approximately doubles the SNR at the UE (thereby improving the SE by 1 bps/Hz) when the UE is closer to the OOB IRS than the in-band IRS. On the other hand, when the UE is closer to the in-band IRS than the OOB IRS, the SNR is nearly the same as that in the absence of the OOB IRS. These two events are equally likely under the simulation setup considered, hence, the average gain in SE through cooperation is about 0.5 bps/Hz. The performance obtained by MO-X with no cooperation nearly matches that obtained in the absence of the OOB IRS (the bottom two curves), because the SNR gain from the OOB IRS under event $\mathcal{A}$ is negligible when the overall phase of the IRS is arbitrary. More importantly, the OOB IRS does not degrade the SE even if the MOs do not cooperate. Finally, the ergodic sum-SE of MO-X is log-quadratic in N in all scenarios, thus, the array gain from IRS-X is always obtained.

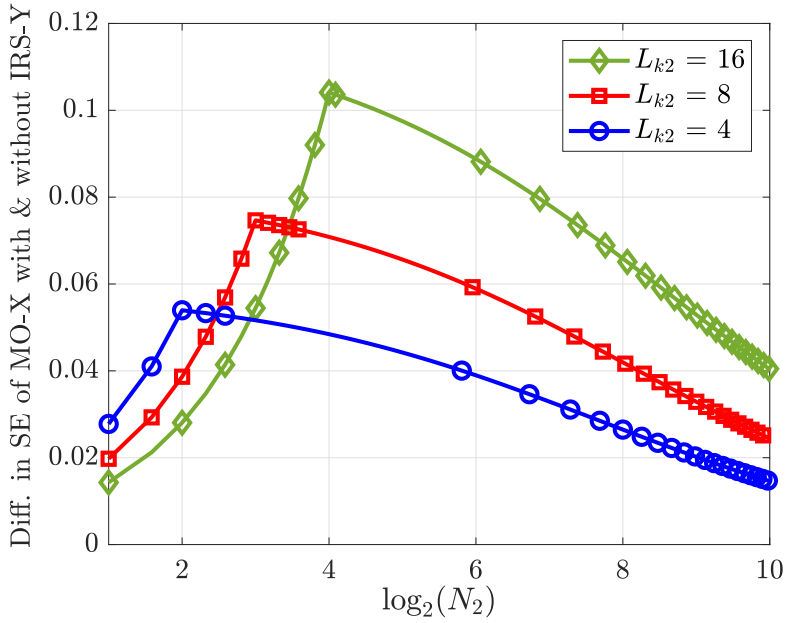

Figure 7.4: Diff. in sum-SE of MO-X with and without OOB IRS vs. $\log_2(N_2)$.

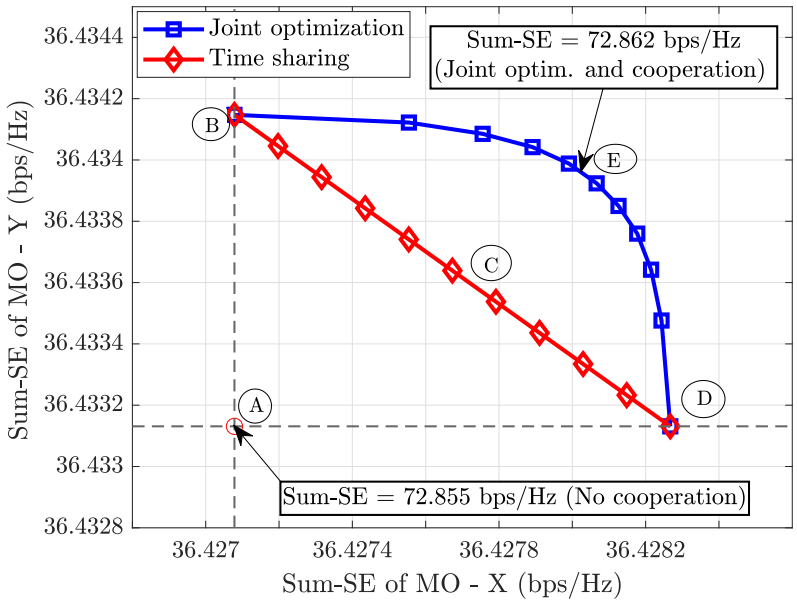

Figure 7.5: Rate Region of the MOs at $L_{k1} = 1, L_{k2} = 5$, $L_{q1} = 8, L_{q2} = 1$.

Next, in Fig. 7.4, for a fixed number of elements at IRS-X (at $N_1 = 64$), we plot the difference between the ergodic sum-SE of MO-X obtained in the presence and absence of the OOB IRS-Y vs. the number of OOB IRS elements (in the log-domain) as a function of the number of OOB paths, L_{k2}. To capture the maximum possible difference, we consider that

whenever IRS-Y aligns to the in-band UE of MO-X, both MOs cooperate and implement the time-sharing scheme with $\zeta = 1$. Then, for a given L_{k2}, we observe that the difference is non-negative, and further, this gain in the SE due to the presence of OOB IRS-Y is an unimodal function in N_2 with the peak occurring at $N_2 = L_{k2}$. This is in line with the theoretical expression given by (7.64) in Theorem 7.2. Intuitively, at smaller values of N_2, with high probability, IRS-Y aligns with the in-band UE of MO-X; so, when N_2 increases, the overall SNR increases for MO-X. However, for larger values of N_2, the probability that the IRS-Y aligns to MO-X's UE becomes small, in turn causing the difference (or) gain in the SE with and without an OOB IRS to decrease. Finally, as L_{k2} increases, the gain increases because the probability of IRS-Y aligning to MO-X increases, further enhancing the channel gain at in-band UEs of MO-X. Thus, an OOB IRS benefits MO-X more when there are many paths via the OOB IRS at the UEs served by MO-X.

In Fig. 7.5, we plot the achievable rate regions of the two MOs (normalized by the bandwidths) for $N_1 = N_2 = 256$ and $C_0\gamma = 150$ dB under two different schemes: 1) time-sharing (corresponding to the curve (B)-(C)-(D) with (B), (C), and (D) obtained at $\zeta = 0, 0.5$, and 1, respectively), and 2) weighted-sum-SE joint optimization given in Algorithm 7.1 (corresponding to the curve (B)-(E)-(D)). The sum-SE obtained via Algorithm 7.1 upper bounds the sum-SE of the time-sharing scheme. This is because, in the former, the IRS overall phases are jointly optimal for scheduled UEs of both the MOs in any time slot. Also, the achievable sum-SE under the joint optimization peaks at the point at (*E*) when $w_1 = w_2 = 0.5$. On the same plot, point (*A*), which denotes the no-cooperation scenario, provides a sum-SE that is smaller than that obtained by cooperation. In any case, the overall gain between the points (*A*) and (*E*) is small due to the sparse scattering of mmWave channels. Therefore, while the presence of the OOB IRS always enhances the ergodic SE achieved by the UEs served by all MOs, the additional gain obtained via optimizing the overall phase of the IRS is marginal.

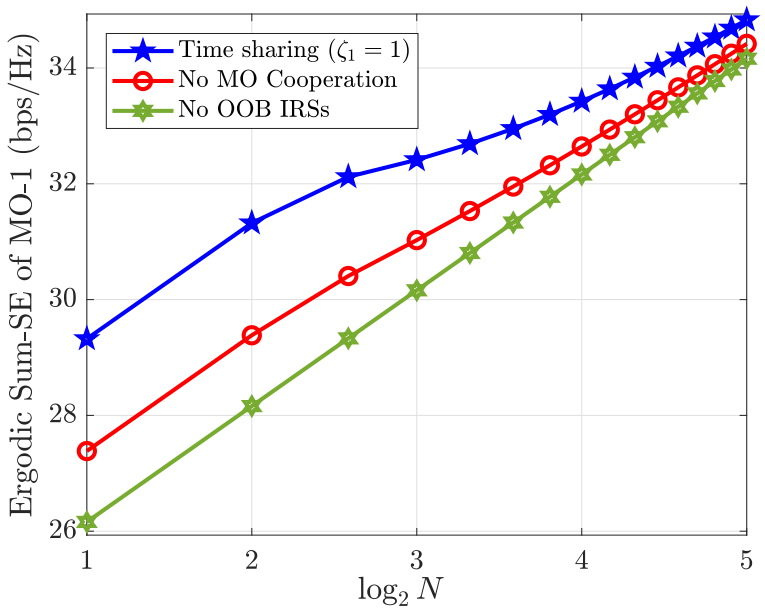

Figure 7.6: Sum-SE of MO-1 vs. $\log_2 N$ with 4-MOs, $C_0\gamma = 150$ dB, $L = 5$.

7.6.b $M > 2$-MO and $M > 2$-IRS System

We next investigate the performance obtained with more than 2 MOs for different schemes with and without cooperation. We consider 4 MOs, with each MO deploying an IRS to serve its UEs optimally. The BSs of MO-$1, 2, 3$, and 4 are located at $(0, 0)$, $(200, 0)$, $(200, 200)$, and $(0, 200)$ (in meters), respectively, and the IRSs are located in a circular region centered at $(100, 100)$ with radius 5 meters. The rest of the settings are the same as considered for the 2-MO case.

In Fig. 7.6, we plot the ergodic sum-SE of MO-1 vs. $\log_2 N$ for $C_0\gamma = 150$ dB, and $L = 5$, where N is the number of IRS elements in each IRS, and investigate the SE performance of MO-1 for three extreme scenarios: a) time-sharing with $\zeta_1 = 1$, b) no MO cooperation scheme, and in 3) absence of all IRSs except IRS-1 which is deployed by MO-1. We observe that the SE of MO-1 in the presence of OOB IRSs strictly outperforms the achievable SE in the absence of OOB IRSs. This is because, besides the in-band IRS, the OOB IRSs contribute to the signal strength at the UE served by MO-1. With cooperation, the performance can be further improved by ensuring the coherent addition of signals arriving at the UE via the contributing IRSs. However, for large N, the probability

that an OOB IRS aligns with a given UE becomes small, and the SE in the presence of OOB IRSs coincides with that obtained in the absence of OOB IRSs. Nonetheless, even with an arbitrary number of MOs, the ergodic SE of an MO does not degrade due to the presence of uncontrollable IRSs deployed by other MOs.

7.7 Conclusions

In this chapter, we addressed an important problem in IRS-aided practical mmWave wireless systems: the effect of IRSs deployed by one MO on the performance of another existing OOB MO, which has an IRS of its own. Starting with the case where 2 MOs each deploy an IRS to serve their UEs optimally, we first examined different scenarios that arise due to the impact of an IRS on the OOB MOs. Subsequently, we derived the ergodic sum-SE of the MOs under three schemes. In the first scheme, the MOs cooperate and jointly optimize an overall phase angle of the IRSs; in the next, the MOs only cooperate by optimizing the overall phase in a time-sharing manner, and in the final scheme, the MOs do not cooperate and function independently. Our key findings were two-fold: 1) even when the MOs do not cooperate, the IRS of one MO does not degrade the sum-SE of another MO, and 2) the best possible gain obtained in the sum-SE by allowing for MO cooperation compared to no cooperation scheme decreases inversely with the number of IRS elements in the OOB MO. The primary reason behind these observations is the spatial sparsity in the mmWave band channels. This avoids degradation due to the OOB IRS and also makes significant enhancement unlikely. We extended our results to a system with more than 2 MOs, and showed that a given MO's performance improves linearly with the number of OOB MOs in the area. Future work could include extending our results to interference-limited scenarios and accounting for multi-user and inter-cell interferences, different duplexing modes, user-mobility with statistical CSI, adopting multi-user scheduling techniques [79,103], etc.

Part III

IRS-Aided Wideband Beamforming: Handling Beam-split Effects

8 Wideband Beamforming in IRS-Aided Communications: Mitigating Beam-Split Effects

Chapter Highlights

This chapter addresses the mitigation of spatial-wideband (SW) and the resulting beam-split (B-SP) effects in intelligent reflecting surface (IRS)-aided wideband systems. The SW effect occurs when the signal delay across the IRS aperture exceeds the system's sampling duration, causing the user equipment's (UE) effective channel to vary with frequency. This leads to the B-SP effect, wherein the IRS cannot coherently beamform at a given UE over the entire bandwidth, reducing array gain and throughput.

We demonstrate that partitioning a single IRS into multiple smaller IRSs and distributing them in the environment can naturally mitigate the SW effect (and hence the B-SP effect) by parallelizing the spatial delays and exploiting angle diversity benefits. By determining the maximum number of IRS elements to limit B-SP effects and analyzing the achievable sum-rate, we demonstrate that our approach ensures a minimum positive rate over the entire bandwidth of operation. However, distributed IRSs may introduce temporal delay spread (TDS) due to multipath propagation and reduce the achievable flat channel gain. To minimize TDS and maintain the full array gain, we show that the optimal placement of the IRSs is on an ellipse with the base station (BS) and UE as the focal points. We subsequently analyze the impact of the optimal IRS placement on TDS and throughput for a UE located within a hotspot served by the IRSs. Finally, we illustrate that distributed IRSs enhance angle diversity, which exponentially reduces the outage probability due to B-SP effects as the number of IRSs increases. Numerical results validate the efficacy and simplicity of our method compared to state-of-the-art solutions.

8.1 Introduction

Intelligent reflecting surfaces (IRS) are envisioned to improve the performance of wireless systems by beamforming signals in desired directions using independently reconfigurable passive phase shifters [2, 69, 176]. One of the key use cases for IRSs is to create a *virtual line-of-sight (LoS) path* to multiple user equipments (UEs) clustered in a hotspot area when the LoS path between the hotspot and a base station (BS) is obstructed. However, the cascaded link via the IRS encounters a multiplicative path loss, and an IRS with a large number of elements has to be used to achieve appreciable benefits [177]. Large arrays cause the signal delay across the aperture to be comparable to or even exceed the sampling duration. This results in *spatial-wideband* (SW) effects [178], which manifests as the beam-squint (B-SQ) and *beam-split* (B-SP) effects in the frequency domain, and severely degrades the array gain and the throughput at a UE. This chapter addresses this problem using distributed IRSs that naturally mitigate the SW and resulting B-SP effects at almost no additional complexity.

8.1.a The Beam-Split: Curse of the Spatial-Wideband Effect

In high-frequency millimeter wave (mmWave) bands with large bandwidths (BW), the channel between two nodes is typically directional because there are only a few significant scatterers. These directions are independent of the operating frequencies as long as the delay spread of the channel is much smaller than the system sampling duration, known as the *narrowband* condition. However, when an IRS with a large number of elements is used, the spatial delay spread across the aperture can easily exceed the sampling period and violate the narrowband condition. This results in the spatial-wideband effect, where even a LoS channel becomes frequency-selective.

In this scenario, the main challenge is that the IRS fails to coherently beamform across the entire BW allotted to a UE in the system. Specifically, when the IRS is configured as a phased array tuned to a specific frequency component within the BW, e.g., the carrier frequency (which is typically the case), the SW effect induces the B-SQ and B-SP effects in the frequency domain, which severely degrades the array gain at other frequencies within

the BW. In the B-SQ effect, the beam formed by the IRS squints at different angles across frequencies, though the angular spread across the BW remains within the main lobe of the beam. In contrast, the B-SP is a more severe form of B-SQ and occurs when the number of IRS elements or allotted BW (or both) further increases. In the B-SP effect, the beam formed by the IRS at the tuned frequency splits into distinct, resolvable beams on other frequencies within the BW. Consequently, the IRS fails to beamform and constructively combine signals at the UE over the full BW, severely degrading the achievable channel gain and spectral efficiency. While the SW effects can be circumvented by reducing the number of IRS elements or the total BW, this also lowers the achievable channel gain and system throughput. Therefore, it is crucial to design efficient methods, preferably with low complexity, to mitigate SW and the resulting B-SP effects in IRS-aided wideband systems.

8.1.b Related Work & Motivation

Most existing studies on IRS-aided systems overlook the B-SP effects resulting from the SW effects and overestimate the achievable benefits of an IRS. Only a few works address the wideband effects; we summarize them below.

In [46, 47], and [48], methods for channel estimation and beam training were developed accounting for the SW effects. Localization of UEs using SW effects was discussed in [49]. Optimization of IRS phases to maximize the sum-rate in orthogonal frequency division multiplexing (OFDM) systems with B-SQ effects was studied in [179]. In [13] and [14], joint optimization of the IRS configuration and BS precoder was explored for multiple-input multiple-output (MIMO) terahertz systems. In [20], the achievable ergodic rate of a MIMO-OFDM system with B-SQ effects was examined, and [180] solved for optimal IRS configuration to maximize the signal-to-interference-plus-noise ratio (SINR) with B-SQ effects. Finally, [50] and [51] used B-SQ effects to enhance the cell coverage and performance of OFDM-based multiple access.

Along the lines of mitigating the SW (and hence the B-SP effects), existing works often use true time-delay (TTD) units at the IRS to compensate for the excess signal delay across the aperture, thereby eliminating the SW effects [52]. In [54], a hardware-efficient design

of TTD-enabled IRS was investigated, and [53] used delay-phase units to eliminate the B-SP effects in both far-field and near-field scenarios. In [55], the TTDs and BS precoder were jointly optimized to maximize the sum-rate of a multi-user system, and [181] used TTDs to design an efficient IRS-aided cell-free wideband MIMO system. Further, in [182], TTD units were proposed as a means to mitigate B-SP effects in holographic RIS-assisted systems. In contrast, [183] utilized TTD units to control the B-SP effect for improving the accuracy of sensing multiple UEs in the network. However, using TTD units at an IRS presents a number of challenges: 1) the number of TTD units increases with the number of IRS elements, requiring more hardware and space; 2) high-resolution TTDs are necessary for precise delay compensation, which increases power consumption, and 3) since the IRS elements continuously receive signals from the BS, apply a delay, and then reflect the signal toward the UE, the overall operation becomes full-duplex in nature. This introduces self-interference (SI) at each IRS element, and to alleviate it, sophisticated SI cancellation techniques are required at each element of the IRS [177], which further complicates the design and hardware requirements. These issues can potentially undermine the hardware cost and energy efficiency benefits of using IRSs. In particular, to the best of our knowledge, no paper in the literature describes the hardware implementation and demonstration of a TTD-enabled IRS. Yet another approach is to virtually partition a single large IRS into multiple sub-IRSs, with each sub-IRS optimized to the channels over distinct frequency bands [184]. Although this provides a flat response across the BW, the achievable array gain scales only with the number of elements at a sub-IRS and not with the total number of IRS elements. Finally, while [185] and [186] suggest that multiple IRSs can reduce the impact of B-SQ, they do not analyze the performance of distributed IRSs accounting for B-SQ or explicitly design a distributed IRS architecture to mitigate these wideband effects.

To address the above issues, in this work, we propose an alternative approach without relying on TTDs and use a distributed IRS design instead of a single large IRS. When properly designed, we show that a distributed IRS can inherently overcome the SW effect

without increasing complexity or sacrificing performance.[1]

8.1.c Contributions & Takeaways

We now list the key contributions of this work.

1. **SW effect reduction:** We mathematically show that a distributed IRS design naturally parallelizes the spatial delays and mitigates the SW effect. (See Sec. 8.3.a.)

2. **Number of IRS elements**: We determine the maximum number of elements at each IRS so that the loss in the array gain due to B-SP is within acceptable limits while retaining the achievable peak gain. (See Theorem 8.1.)

3. **Sum-rate and array gain:** Next, we analyze the impact of the *temporal delay spread* (TDS) caused by multiple paths arriving at the UE through different IRSs. We show that the achievable rate on every subcarrier (SC) scales log-quadratically in the number of elements at each IRS and at least log-linearly in the number of IRSs, thus effectively mitigating deep nulls in the channel response due to the B-SP effect. Further, when the TDS is zero, the sum-rate across all the SCs spanning the BW grows log-quadratically in the total number of IRS elements. (See Theorem 8.2.)

4. **Optimizing the IRS locations:** Having noted that the value of TDS is crucial in determining the achievable flat channel gain, we next focus on optimizing the IRS locations:

   (a) *Single UE:* To minimize the TDS at a single UE, we show that it is optimal to position the IRSs on an ellipse with the locations of BS and UE as its foci. The optimal TDS then becomes zero. (See Theorem 8.3.)

   (b) *Multiple UEs:* With multiple UEs located within a hotspot, we position the IRSs over an ellipse whose foci are given by the location of the BS and the centroid of

[1] Note that B-SQ and B-SP effects can arise in both far-field and near-field scenarios [53]. To illustrate our core idea, this chapter will focus on cases where the BS/UEs are in the far-field of the IRS(s). Extensions to near-field scenarios will be considered for future work.

the distribution of the UE locations. We derive the achievable TDS at an arbitrary location and subsequently characterize a lower bound on the achievable sum-rate using the distributed IRSs. (See Prop. 8.1 and Theorem 8.4.)

5. **Angle diversity gain:** Finally, we reveal that multiple IRSs additionally introduce angle diversity gain due to multiple independent paths seen by the UE. In particular, we show that the probability that the array gain equals the worst-case acceptable value (due to the residual B-SQ) decreases exponentially with the number of IRSs. On the other hand, the outage probability of a centralized IRS for a target SNR close to the peak array gain is bounded away from zero as the number of IRS elements increases. (See Theorem 8.5.)

We numerically validate our results and illustrate the efficacy of our solution in mitigating the SW and the resulting B-SP effects. For instance, when the BW is 400 MHz around $f_c = 30$ GHz, with a total of 1024 IRS elements, if we use a centralized large IRS, only 12.5% of the total BW gets an array gain which is within 3 dB of the peak array gain. On the other hand, if we deploy 8 distributed IRSs, each with 128 elements, the entire 400 MHz BW obtains an array gain that is within the 3 dB margin of the peak array gain (see Fig. 8.6). As a result, the difference in the sum-rate obtained with the distributed IRS and the TTD-enabled IRS (which completely eliminates the B-SP, albeit at a higher complexity) is less than 0.5 bps/Hz (see Fig. 8.7.) Finally, even with finite TDS, distributed IRS still performs far superiorly to the centralized case, with the sum-rate exhibiting log-quadratic growth in the total number of IRS elements. (see Fig. 8.10.) Thus, distributed IRS mitigates B-SP effects and provides the full array gain over the entire BW at almost no added complexity.

Notation: For general notations used in this chapter, see the section on "General Mathematical Notations" on page ix. For the notations/variables specific to this chapter, please refer to Table 8.1.

Variable	Definition	Variable	Definition
S	Number of IRSs	λ	Signal wavelength at carrier frequency
M	Number of elements at an IRS	N_{CP}	Number of samples in the cyclic prefix
N	Total number of IRS elements	ϵ	Tolerable loss factor in array gain due to residual beam-squint
$\eta^{(1)}$, $\eta^{(2)}$, η	Propagation delay in BS-IRS, IRS-UE, cascaded links in centralized case	$\eta_s^{(1)}$, $\eta_s^{(2)}$, η_s	Propagation delay in BS-IRS-s, IRS-s-UE, cascaded links in distributed case
ψ/ω	Direction of arrival/departure at IRS from BS/to UE in centralized case	ψ_s/ω_s	Direction of arrival/departure at IRS -s from BS/to UE in distributed case
ϕ/ϕ_s	Cascaded channel angle via the IRS in centralized/distributed scenarios	$h(t)$	Impulse response of channel at a UE
$\boldsymbol{\theta}, \boldsymbol{\theta}_s$	Phase shift vector at a centralized IRS/ IRS-s in distributed scenario	$H[k]$	Frequecy response of channel at a UE
c	Velocity of light: 3×10^8 m/s	$\Delta\tau^{\text{C}}$/ $\Delta\tau_s^{\text{D}}$	Delay spread in the channel via IRS /IRS-s in centralized/distributed cases
W	Bandwidth of operation	p_k/σ^2	Ratio of transmit power to noise power on subcarrier-k
K	Number of subcarriers in the OFDM	α, γ, β	Complex ch. gains with path loss
f_c, f_k	Carrier frequency, baseband frequency of kth subcarrier	d_0	Radius of the region $\mathcal{R}_u$
d	Inter-elemental spacing at the IRS	$\mathbb{P}_\rho^k$	ρ-outage probability on subcarrier-k

Table 8.1: Commonly encountered variables/notations in chapter 8.

8.2 System Model

8.2.a Channel Impulse Response and Spatial-Wideband Effect

Consider the system depicted in Fig. 8.1(a), where a BS communicates with a UE, and is assisted by an N-element IRS in the mmWave frequency band. For simplicity, and following past work in the area, we assume that the IRS is implemented as a uniform linear array (ULA) with inter-element spacing denoted by d [46,53,55,179]. The baseband impulse response of the channel from the BS to the nth IRS element is given by [54]

$$h_{1,n}(t) = \sqrt{\alpha}\delta\left(t - \eta^{(1)} - (n-1)\frac{d}{c}\sin(\psi)\right) \times e^{-j2\pi f_c \eta^{(1)}} \times e^{-j2\pi f_c (n-1)\frac{d}{c}\sin(\psi)}, \tag{8.1}$$

where α, $\eta^{(1)}$, f_c, and ψ represent the path-loss, propagation delay in the link from BS to a reference element (either the first or last element, depending on whether ψ is positive

or negative) of IRS, the carrier frequency, and the direction of arrival (DoA) of the signal from the BS to the IRS, respectively. Finally, $c = 3 \times 10^8$ m/s denotes the speed of light, and $\delta(t)$ stands for the Dirac-delta function.

Similarly, the baseband impulse response of the channel from the nth IRS element to the UE is

$$h_{2,n}(t) = \sqrt{\gamma}\delta\left(t - \eta^{(2)} + (n-1)\frac{d}{c}\sin(\omega)\right) \times e^{-j2\pi f_c \eta^{(2)}} \times e^{j2\pi f_c (n-1)\frac{d}{c}\sin(\omega)}, \tag{8.2}$$

where γ, $\eta^{(2)}$, and ω denote the path-loss, delay, and direction of departure (DoD) from the IRS to the UE, respectively. Hence, the effective channel from the BS to the UE is[2]

$$\begin{aligned} h(t) &= \sum_{n=1}^{N} \theta_n h_{2,n}(t) \circledast h_{1,n}(t) \\ &= \sum_{n=1}^{N} \theta_n \tilde{h}_1 \tilde{h}_2 \delta\left(t - \eta - (n-1)\frac{d}{c}\left(\sin(\psi) - \sin(\omega)\right)\right) \times e^{-j2\pi f_c (n-1)\frac{d}{c}\sin(\phi)}, \end{aligned} \tag{8.3}$$

where $\tilde{h}_1 \triangleq \sqrt{\alpha} e^{-j2\pi f_c \eta^{(1)}}$, $\tilde{h}_2 \triangleq \sqrt{\gamma} e^{-j2\pi f_c \eta^{(2)}}$, and $\circledast$ stands for the convolution operator. Further, θ_n, $\eta \triangleq \eta^{(1)} + \eta^{(2)}$, and $\phi \triangleq \sin^{-1}_{(p)}\left(\sin(\psi) - \sin(\omega)\right)$ denote the phase shift introduced by the nth IRS element, the total propagation delay, and the effective cascaded angle at the UE, respectively. Also, $\sin^{-1}_{(p)}(x)$ is defined so that $x \in [-1, 1)$, the principal argument of the inverse sine function [33], [80, Eq. 32]. Thus, the *spatial delay spread* of the channel through the IRS is

$$\Delta\tau^{\mathrm{C}} = (N-1)\frac{d}{c}\left|\left(\sin(\psi) - \sin(\omega)\right)\right|. \tag{8.4}$$

When both N and the BW (denoted by W) are large, the *narrowband* condition: $\Delta\tau^{\mathrm{C}} \ll 1/W$, ceases to hold. Then, the spatial delay incurred by the signal while traversing across the IRS aperture becomes comparable to or more than the sampling duration, leading to the spatial-wideband effect [178]. To elaborate, from (8.3), the channel frequency response

[2]The direct path from the BS to UE can be blocked/weak compared to the channel via the IRS, so we do not account for direct path in our model [46].

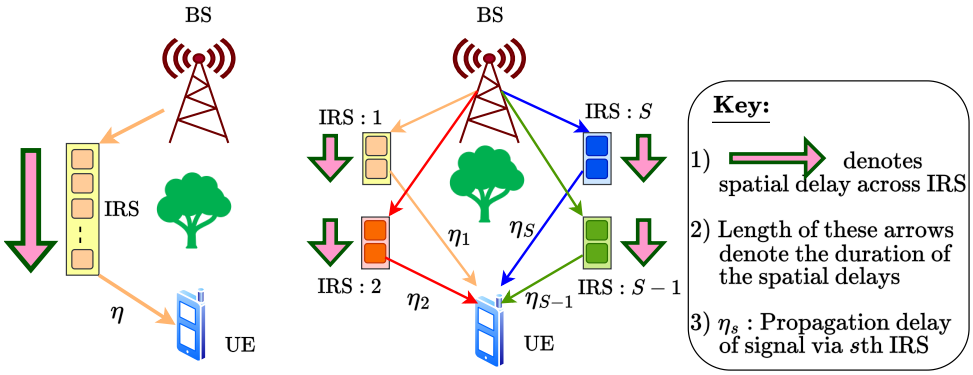

(a) Centralized IRS (b) Distributed IRSs

Figure 8.1: Distributed IRSs reduce spatial delays and mitigate SW & B-SP effects. The TDS is 0 only when the propagation delays are equal: $\eta_1 = \eta_2 \ldots = \eta_S$.

is

$$\begin{aligned} H(f) &\overset{(a)}{=} \tilde{h} \sum_{n=1}^{N} \theta_n e^{-j2\pi(n-1)\frac{d}{c}\{f(\sin(\psi)-\sin(\omega))+f_c\sin(\phi)\}} \\ &\overset{(b)}{=} \tilde{h} \sum_{n=1}^{N} \theta_n e^{-j\pi(n-1)\sin(\phi)\left\{1+\frac{f}{f_c}\right\}} \\ &\overset{(c)}{=} \sqrt{N}\tilde{h}\boldsymbol{\theta}^H \mathbf{a}_N\left(\sin^{-1}_{(p)}\left\{(1+(f/f_c))\sin(\phi)\right\}\right), \end{aligned} \tag{8.5}$$

where, in (a), we absorbed η into receiver timing offset and defined the cascaded channel coefficient as $\tilde{h} \triangleq \tilde{h}_1\tilde{h}_2$; in (b), we set $d = \lambda_c/2$, where λ_c is the carrier wavelength and used the definition of ϕ; in (c), we defined the IRS configuration vector $\boldsymbol{\theta} \triangleq [\theta_1^*, \ldots, \theta_N^*]^T$, where $(\cdot)^*$ stands for complex conjugation and $\mathbf{a}_N(\cdot)$ is the array steering vector given by

$$\mathbf{a}_N(x) \triangleq 1/\sqrt{N}\left[1, e^{-j\pi\sin(x)}, \ldots, e^{-j\pi(N-1)\sin(x)}\right]^T.$$

Therefore, considering an OFDM system with K SCs, the channel on the kth SC is

$$H[k] \triangleq H(f_k) = \sqrt{N}\tilde{h}\boldsymbol{\theta}^H \mathbf{a}_N\left(\sin^{-1}_{(p)}\left\{(1+(f_k/f_c))\sin(\phi)\right\}\right), \tag{8.6}$$

where f_k is the baseband frequency of the kth SC, given by

$$f_k = -\frac{W}{2} + \frac{W}{2K} + (k-1)\frac{W}{K}, \quad k = 1, \ldots, K.$$

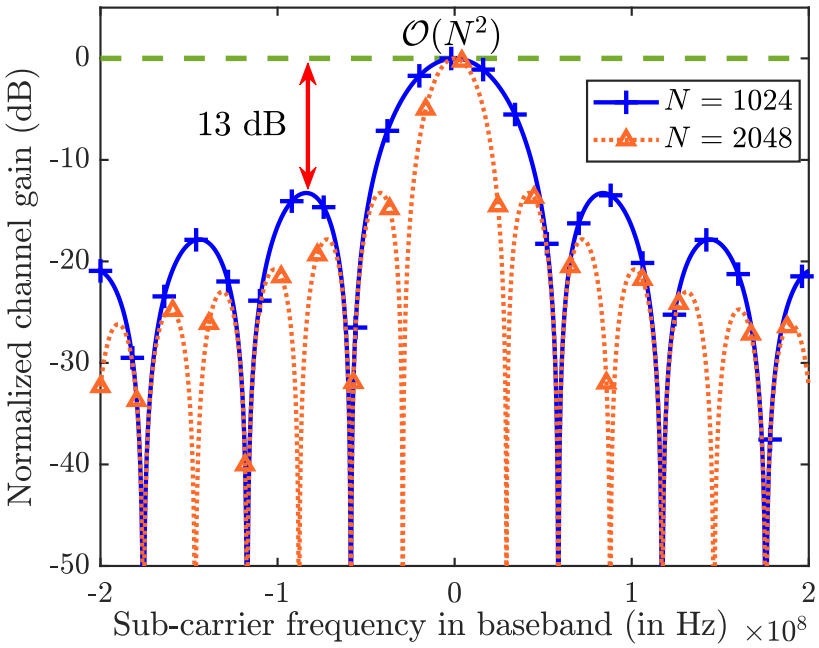

Figure 8.2: B-SP effect at $f_c = 30$ GHz, $W = 400$ MHz, $\phi = 90°$.

8.2.b The Beam-split Effect

Consider the setting where a BS provides service to a UE over a wide bandwidth, W. Then, in the presence of a large IRS, the channel coefficient on the kth SC is given in (8.6). So, the physical angle ϕ of the cascaded channel manifests as

$$\phi_{f_k} = \sin^{-1}_{(p)}\left\{\left(1 + \frac{f_k}{f_c}\right)\sin(\phi)\right\} \tag{8.7}$$

on the kth SC, which equals ϕ only if $f_k = 0$ or $\phi = 0$. Thus, if the frequency-independent phase shifters at the IRS are tuned at the carrier frequency, $f_k = 0$, i.e., $\boldsymbol{\theta} = \mathbf{a}_N(\phi)$, they can only beamform to ϕ over a small BW around $f_k = 0$ [3] (unless $\phi = 0$.) This results in the *beam-split effect*, and it degrades the array gain on SCs for which $f_k \neq 0$. Further, the B-SP effect is more pronounced at a UE whose cascaded angle is $\phi = 90°$. For e.g., in Fig. 8.2, we plot the normalized channel gain, $|H[k]|^2$ vs. the SC frequency, f_k when the IRS is tuned to $f_k = 0$. We see that only a few SCs around $f_k = 0$ achieve the full array gain of N^2, while other SCs face a loss of at least 13 dB. In particular, B-SP reduces the

[3] This holds true even if the IRS is tuned at a different frequency, $f'_k \neq 0$.

array gain to 0, producing deep nulls in the channel gain of SCs at frequencies

$$f_{\text{NULL}} = \frac{2f_c}{N}q, \quad q = \pm 1, \pm 2, \ldots, \pm \left\lfloor \frac{WN}{4f_c} \right\rfloor.$$

Moreover, the B-SP effect is exacerbated when N increases and further reduces the system throughput. In this view, to mitigate the B-SP effect, in this chapter, we propose a distributed IRS design using S non-colocated M-element IRSs with $SM = N$ to limit the degradation in the array gain across all SCs. Specifically, the number of IRS elements, M, can be adjusted to control the B-SP effect, and the number of IRSs, S, can be chosen to obtain an array gain of $\mathcal{O}(N^2)$ over the complete BW. Furthermore, in this case, unless the IRSs are positioned appropriately, the signal from each IRS experiences a different propagation delay and leads to a non-zero *temporal delay spread* (TDS) in the overall channel, as shown in Fig. 8.1(b). Then, we address the following questions.

1. Considering a TDS $= 0$ case, what (S, M) ensures that the worst-case B-SP results in a loss of no more than $(1-\epsilon)^2$ in the channel gain compared to the peak IRS array gain:

$$\{S, M\} : \min_{k \in [K]} |H[k]|^2 \Big|_{\phi_s = 90^\circ} \geq (1-\epsilon)^2 |H[K/2]|^2, \tag{8.8}$$

   where ϕ_s denotes the cascaded angle via IRS-s and $\epsilon \in [0, 1)$ dictates the acceptable loss in array gain relative to the center SC. Here, $\phi_s = 90^\circ$ captures the worst-case B-SP. Note that the condition in (8.8) ensures that the array gain is within a tolerable and residual B-SQ controlled by ϵ.

2. How does the solution perform when multiple IRSs cause a non-zero TDS due to signals from each IRS arriving at the UE at different sampling time instants?

Remark 8.1. *Fundamentally, the B-SP effect arises due to the interplay of using phase shifters and SW effects at the IRS. In particular, phase shifters are effective for compensating the differential delays across the IRS aperture and form a beam only if the narrowband condition, $\Delta\tau \ll 1/W$, is met [63]. However, we enforce the narrowband criterion by limiting the number of IRS elements to retain the low complexity phased array-based IRS*

architectures for beamforming even in wideband systems. Since defining the boundary between narrowband and wideband regimes is hard in the time domain, we resolve this by examining the B-SP effect in the frequency domain and ensuring that the narrowband condition is satisfied.

8.3 Mitigating beam-split Via Distributed IRSs

As discussed, the B-SP effect in the frequency domain arises due to the SW effect caused by the propagation delay across the IRS aperture in the time domain. This can be circumvented if $\Delta\tau^{\mathrm{C}} \ll 1/W$ is satisfied. Given the bandwidth W, this can be ensured by reducing the number of IRS elements. However, this also has the undesirable effect of decreasing the array gain from the IRS and, hence, the throughput. This loss can be avoided by a distributed IRS design, as explained below.

8.3.a Parallelizing the Spatial Delays using Distributed IRSs

The advantage of a distributed design is that it *parallelizes* the spatial delay across the aperture, which otherwise increases *serially* in the number of elements in a large centralized IRS. In particular, partitioning and distributing a single large IRS into multiple non-colocated smaller IRSs reduces the delay across each IRS, i.e., if an N-element IRS is split into S IRSs with M-elements, the delay across the aperture of sth IRS is

$$\Delta\tau_s^{\mathrm{D}} = (M-1)\,(d/c)\,|(\sin(\psi_s) - \sin(\omega_s))| \approx \Delta\tau^{\mathrm{C}}/S, \tag{8.9}$$

where ψ_s and ω_s denote the DoA and DoD at the sth IRS, respectively. Thus, the delay across the aperture of each IRS is reduced approximately by a factor S, as shown in Fig. 8.1(b), decreasing the influence of the SW effect. Further, in Sec. 8.5, we also show that distributed IRSs provide angle diversity gains, making it unlikely for the worst-case B-SP to happen at every IRS, further reducing the impact of the B-SP effect.

8.3.b Number of Elements per IRS

We now determine the number of elements per IRS, M, which parallelizes the spatial delay and guarantees (8.8) for the TDS $= 0$ case, and extend it to the TDS $\neq 0$ case in Corollary 8.1.

Theorem 8.1. *Consider a system with S non-colocated M-element IRSs with a total of N IRS elements (i.e., $SM = N$) with TDS $= 0$. Then, the maximum M for which the array gain due to all IRSs on every SC is at least $(1-\epsilon)^2 N^2$ is*

$$M^* \triangleq \min\left\{\max\left\{\left\lfloor \frac{4\sqrt{6\epsilon}}{\pi}\frac{f_c}{W}\right\rfloor, 1\right\}, N\right\}, \tag{8.10}$$

$\epsilon \in [0,1)$ dictates the tolerable loss in array gain w.r.t. N^2.

Proof. See Appendix 8.A. ■

Therefore, if N is the total number of IRS elements, then deploying at least $S = N/M$ IRSs with M as per Theorem 8.1 will prevent the adverse impact of the B-SP effect.

8.3.c Sum-Rate Analysis: Centralized vs. Distributed IRSs

In this section, we analyze the achievable sum-rate of the distributed design and also analyze the achievable performance when the channel experiences a nonzero TDS.

In general, the signal arriving at the UE through each IRSs could be time-offset relative to the UE's timing, giving rise to a TDS in the signals arriving through the different IRSs. For analytical tractability, we model the propagation delay via the sth IRS as a random variable, $\tilde{\eta}_s \sim \mathcal{U}[0, T_0]$, independent and identically distributed (i.i.d.) across IRSs. Here, T_0 is the maximum TDS that the IRSs can introduce at the UE's location. We now characterize the achievable sum-rate across SCs at a UE under centralized and distributed IRS scenarios.

Theorem 8.2. *In an mmWave-OFDM system with K SCs spanning a BW of W at carrier frequency f_c and a total of N IRS elements, the sum-rate at a UE with channel angle ϕ*

and $\phi_1, \ldots, \phi_S$ *under centralized and distributed IRS setups with* $M = M^*$ *set as per Theorem 8.1 satisfy*

$$\bar{R}_C \approx \frac{1}{K + N_{CP}^C} \sum_{k=1}^{K} \log_2 \left(1 + \frac{p_k \sigma_{\mathrm{h}}^2}{\sigma^2} N^2 \operatorname{sinc}^2 \left(N \frac{f_k}{2f_c} \sin(\phi)\right)\right), \tag{8.11}$$

and

$$\begin{aligned} \bar{R}_D \geq \mathsf{R}_{\min} &\triangleq \frac{1}{K + N_{CP}^D} \sum_{k=1}^{K} \log_2 \Big(1 + \frac{p_k \sigma_{\mathrm{h}}^2}{\sigma^2} M^2 (1-\epsilon)^2 \left[S^2 \operatorname{sinc}^2(f_k T_0)\right. \\ &\qquad \left. + S\left(1 - \operatorname{sinc}^2(f_k T_0)\right)\right]\Big), \qquad (8.12) \\ &\geq \mathsf{R}_{\min}^{L\text{-}bound} \triangleq \frac{1}{K + N_{CP}^D} \sum_{k=1}^{K} \log_2 \left(1 + \frac{p_k \sigma_{\mathrm{h}}^2}{\sigma^2} S M^2 (1-\epsilon)^2\right), \qquad (8.13) \end{aligned}$$

respectively, where $\sigma_{\mathrm{h}}^2 = |\tilde{h}|^2 = |\tilde{h}_1|^2 \approx \ldots \approx |\tilde{h}_S|^2$ *is the channel gain via the IRSs*[4]*,* p_k *and* σ^2 *are the transmit and noise power at the* k*th SC, and* N_{CP}^C, N_{CP}^D *are the cyclic prefix (CP) lengths in the centralized and distributed IRS setups*[5]*, which are respectively*

$$N_{CP}^C = \left\lceil (N-1)\frac{W}{f_c} \right\rceil, \; N_{CP}^D = \left\lceil (M-1)\frac{W}{f_c} + WT_0 \right\rceil, \tag{8.14}$$

where T_0 *is the maximum TDS induced by the IRSs at a UE.*

Proof. See Appendix 8.B. ■

From Theorem 8.2, we observe that, unlike a centralized scenario, which results in zero rates on many SCs, the distributed IRS provides a positive rate that scales at least as much as $\mathcal{O}(\log(SM^2))$ on all SCs, which guarantees a lower bound on the sum-rate given

[4]We consider equal path losses in the paths across all IRSs only for the sake of analysis and to present how the performance scales with the number of IRSs and IRS elements. Our solution is applicable even when path losses are unequal among the cascaded links through each IRS.

[5]The CP in OFDM is used to (a) eliminate inter-symbol interference, and (b) convert the linear convolution with a frequency-selective channel into circular convolution, which diagonalizes the channel in the frequency domain. However, this does not eliminate the SW effect itself. Specifically, large IRS apertures cause significant delay spreads, which result in the B-SP effect with SC-dependent channel variations as shown in Fig. 8.2. The gain on a given SC is still governed by the time-domain channel's impulse response via a Fourier transform. Thus, while CP simplifies OFDM-based signal processing, it does not mitigate the SW-induced B-SP effects inherent to large IRSs.

by $R_{\min}^{\text{L-bound}}$ in (8.13). Hence, distributed IRSs can effectively mitigate the SW and the resulting B-SP effects in the system under any circumstance. We also make the following observations from this theorem:

8.3.c.i Effect of nonzero TDS on the number of IRS elements, M^*

Even in the presence of non-zero TDS in the overall channel at the UE, our design based on Theorem 8.1 ensures that SW effect gets mitigated. We formalize this in the following.

Corollary 8.1. *For a distributed IRS system having a finite TDS, the value of M given by Theorem 8.1 still mitigates the B-SP in the sense of procuring an array gain which is at least a $(1-\epsilon)^2$ factor of the peak array gain obtained on SCs around $f_k = 0$.*

Proof. See Appendix 8.C. ■

Fundamentally, the TDS does not affect the value of M used to mitigate the B-SP effects. This is because by controlling M, we directly tune the tolerable spatial delay at each IRS, which is independent of the presence and location of other IRSs.

8.3.c.ii Channel gain via distributed IRSs

Although the distributed IRSs provide (an almost) flat response over the entire BW, this flat gain can go as low as $\mathcal{O}(SM^2)$. In particular,

(a) From (8.12), the (flat) gain is dictated by M and the convex combination, $S^2\,\text{sinc}^2(f_kT_0)+S(1-\text{sinc}^2(f_kT_0))$:

- If $T_0 \ll 1/W$, then $\text{sinc}(f_kT_0) \approx 1$ on all SCs, ensuring a array gain of $S^2M^2 = N^2$ on all SCs.
- If $T_0 \gtrsim 1/W$, then $\text{sinc}(f_kT_0) \approx 0$ around the band-edge frequencies. Then, an array gain of at least SM^2 is obtained over the BW of the operation.
- If $f_k = 0$, $\text{sinc}(f_kT_0) = 1$ for any T_0, and a full array gain of N^2 is obtained. This is because when the IRS is tuned to the center frequency: $f_k = 0$, for any T_0, there exists a smaller BW around $f_k = 0$, in which the IRS phase shifts can always

compensate for the differential delays across the IRSs, yielding the array gain of N^2.

(b) From the above, the locations of the IRSs are important:

- If the locations of IRSs are such that $T_0 \ll 1/W$, then TDS ≈ 0, and the signals from IRSs can coherently add at the UE, giving $\mathcal{O}(N^2)$ gain on all SCs.
- If the IRSs are positioned such that they introduce a finite TDS, then the IRSs whose propagation delays are within the same sampling interval constructively add the signals at the UE, and the IRSs whose propagation delays fall at different sampling bins incoherently add the signals at the UE. This gives rise to a channel gain fluctuation between $\mathcal{O}(SM^2)$ and $\mathcal{O}(N^2)$.
- Finally, if the IRSs are positioned such that the propagation delays of each IRS fall on distinct sampling bins, giving rise to larger TDS, the signals from different IRSs do not coherently superimpose at the UE, leading to an incoherent channel gain that scales as $\mathcal{O}(SM^2)$.

In summary, a distributed IRS design:

1. overcomes the SW effect in IRS-aided wideband systems *without any deep-nulls* in the channel gain at the UE, and
2. results in an almost flat response whose gain varies as

$$\forall k \in [K] : \mathcal{O}(SM^2) \leq |H[k]|^2 \leq \mathcal{O}(S^2M^2 = N^2),$$

depending on the relative location of IRSs and the TDS.

Remark 8.2 (Choice of ϵ)**.** *The parameter ϵ in Theorems 8.1, 8.2, which captures the tolerable loss in the array gain across SCs, is the designer's choice; a few suggestions are given below.*

1. *The spatial range in the half-power beam width (HPBW) procures most of the array gain of the IRS [187]. So, setting $\epsilon = 1 - \frac{1}{\sqrt{2}}$ ensures that the HPBW of each IRS*

spans full BW at a UE. Then, the signal lies within the HPBW of a virtual array with $N = SM$ elements if the TDS is small.

2. *In the 5G NR setting, all SCs are alloted the same modulation & coding scheme index (MCSI) [188]. Then, an ϵ that maps the spectral efficiencies of all SCs to the same MCSI can be chosen to reap the full achievable throughput.*

Remark 8.3. *Our solution to mitigate the SW effect applies to any IRS geometry. In particular, the aperture length, measuring the farthest distance between two IRS elements, determines the impact of the SW effect. For instance, for a uniform planar array (UPA) based IRS, the number of elements in Theorem 8.1 corresponds to the number of diagonal elements of the UPA. We numerically illustrate the performance of our solution under a UPA configuration in Fig. 8.7.*

Further, when the number of IRSs increases, the number of IRS controllers also increases in the system. On the other hand, one can still use low-pilot overhead channel estimation algorithms with multiple IRSs, as given in [138].

8.3.d Extension to Multiple-Antenna Systems

We now extend our solution to a multi-antenna BS scenario; the approach can be easily adapted to the setup where the UEs are also equipped with multiple antennas. We consider an N_t-element ULA at a BS serving a UE via an N-element IRS over a bandwidth W, as shown in Fig. 8.3. Let $p_m(t)$ denote the precoding filter at the mth BS antenna, and $g_m(t)$ be the cascaded channel between the mth antenna and the UE, for $m \in [N_t]$. Following the same steps as in (8.3), we obtain

$$g_m(t) = \sum_{n=1}^{N} \theta_n \tilde{h}_{1,m} \tilde{h}_2 \delta\left(t - \eta_m - (n-1)\frac{d}{c}\left(\sin(\psi) - \sin(\omega)\right)\right) e^{-j2\pi f_c (n-1)\frac{d}{c}\sin(\phi)}, \quad (8.15)$$

where $\tilde{h}_{1,m} = \sqrt{\alpha} e^{-j2\pi f_c \eta_m^{(1)}}$ with $\eta_m^{(1)}$ being the propagation delay from the mth BS antenna to a reference IRS element, and η_m $(= \eta_m^{(1)} + \eta^{(2)})$ is the total propagation delay from the mth antenna to the UE via the reference element of the IRS. By using the properties of

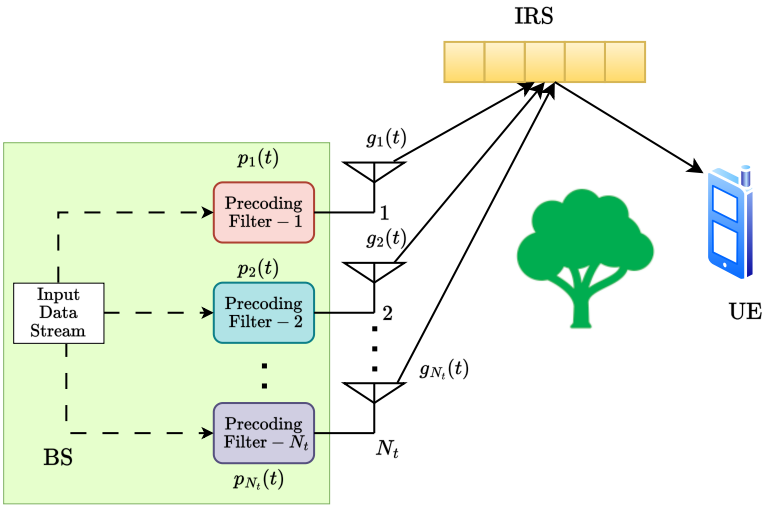

Figure 8.3: System with multiple-antenna BS.

the ULA, we can express $\eta_m^{(1)}$ as

$$\eta_m^{(1)} = \eta^{(1)} + (m-1)\frac{d_{\text{BS}}}{c}\sin(\varrho), \tag{8.16}$$

where $\eta^{(1)}$ is the delay from the reference BS antenna to the reference IRS element, d_{BS} is the inter-antenna spacing at the BS, and ϱ is the DoD of the signal at the BS. Then, we simplify (8.15) and obtain

$$g_m(t) = \sum_{n=1}^{N} \theta_n \tilde{h}_1 \tilde{h}_2 \delta\left(t - \eta - (m-1)\frac{d_{\text{BS}}}{c}\sin(\varrho) - (n-1)\frac{d}{c}\left(\sin(\psi) - \sin(\omega)\right)\right) \times e^{-j2\pi f_c\left((m-1)\frac{d_{\text{BS}}}{c}\sin(\varrho) + (n-1)\frac{d}{c}\sin(\phi)\right)}, \tag{8.17}$$

where η and $\tilde{h}_1$ are defined as given in (8.3). From (8.17), the overall channel experiences a *two-tier* B-SP effect, one originating from the IRS and the other from the BS array—due to SW effects at both ends. However, since the BS is not as constrained by power and hardware limitations, it is practically feasible to equip each antenna with a TTD unit, enabling effective compensation for the SW and the resulting B-SP effect at the BS. Accordingly, the impulse response of the precoding filter at the mth antenna is given

by [53]

$$p_m(t) = e^{j\phi_{m,\mathrm{BS}}}\delta\left(t - \tau_{m,\mathrm{BS}}\right), \tag{8.18}$$

where $\phi_{m,\mathrm{BS}}$ and $\tau_{m,\mathrm{BS}}$ denote the phase and delay applied at the mth antenna. Then, the overall channel is given by

$$h(t) = \sum_{m=1}^{N_t} g_m(t) \circledast p_m(t). \tag{8.19}$$

Substituting $g_m(t)$ and $p_m(t)$ from (8.17) and (8.18) into (8.19), we obtain the overall channel expression as

$$h(t) = \sum_{n=1}^{N} \theta_n \tilde{h}_1 \tilde{h}_2 \sum_{m=1}^{N_t} \delta\left(t - \eta - (m-1)\frac{d_{\mathrm{BS}}}{c}\sin(\varrho) - (n-1)\frac{d}{c}\left(\sin(\psi) - \sin(\omega)\right) - \tau_{m,\mathrm{BS}}\right) \times e^{j\phi_{m,\mathrm{BS}}} \times e^{-j2\pi f_c\left((m-1)\frac{d_{\mathrm{BS}}}{c}\sin(\varrho) + (n-1)\frac{d}{c}\sin(\phi)\right)}. \tag{8.20}$$

To mitigate the B-SP effect, we configure the TTD units as follows:

$$\tau_{m,\mathrm{BS}} = \tau_{0,\mathrm{BS}} - (m-1)\frac{d_{\mathrm{BS}}}{c}\sin(\varphi), \text{ and} \tag{8.21}$$

$$\phi_{m,\mathrm{BS}} = 2\pi f_c (m-1)\frac{d_{\mathrm{BS}}}{c}\sin(\varphi), \tag{8.22}$$

where $\tau_{0,\mathrm{BS}}$ is a common delay applied at all the antenna elements to ensure a causal implementation of the TTDs at the BS array. As a result, the overall channel boils down to

$$h(t) = N_t \sum_{n=1}^{N} \theta_n \tilde{h}_1 \tilde{h}_2 \delta\left(t - \eta - \tau_{0,\mathrm{BS}} - (n-1)\frac{d}{c} \times \left(\sin(\psi) - \sin(\omega)\right)\right) \times e^{-j2\pi f_c (n-1)\frac{d}{c}\sin(\phi)}, \tag{8.23}$$

which is a scaled version of the channel with a single-antenna BS (as in (8.3)), except for an extra timing offset of $\tau_{0,\mathrm{BS}}$, with the scaling factor equal to the number of BS antennas.

Thus, the results we develop in this chapter identically hold for any number of antennas at the BS, without changing the core contributions and the main conclusions of the chapter.

8.4 Optimizing the Locations of Distributed IRSs

From the preceding discussions, we further make the following crucial observations. For a channel with a large TDS,

- The achievable channel gain flattens at $\mathcal{O}(SM^2)$, with a loss of $10\log_{10}(S)$ dB from the maximum gain of $\mathcal{O}(N^2)$,
- The required length of the CP increases linearly with the TDS, increasing the OFDM overheads with many IRSs.

As a consequence, selecting arbitrary locations for the IRSs results in diminished performance compared to the maximum achievable performance (for e.g., the array gain that scales as N^2 on all SCs), despite its benefit in alleviating the SW effect and preventing deep nulls in the channel response. Thus, we now shift our focus to optimizing the placement of the IRSs to minimize the resulting TDS in the system.

Optimizing the locations of IRSs is critically dependent on the positions of the UE and the BS. Further, the BS usually serves multiple non-colocated UEs, especially in densely populated hotspot scenarios where IRSs are used to enhance service quality [104]. In such cases, determining the IRS locations based on a single UE's location may be suboptimal. However, since optimizing the IRS locations with multiple UEs makes the problem intractable, we first focus on optimizing the IRS locations considering a single UE, gain insights, and then analyze the scenario for multiple UEs.

8.4.a Optimizing the Locations of IRSs For a Single User

Let the BS be located at $\mathbf{0} \triangleq [0,0]^T$ on the x-y plane without loss of generality. Let the location of the UE be $\mathbf{p} = [p_1, p_2]^T \in \mathbb{R}^2$, and the location of IRSs be $\mathcal{Q} = \{\mathbf{q}_1, \mathbf{q}_2, \ldots, \mathbf{q}_S\}$, where $\mathbf{q}_s \in \mathbb{R}^2$. Then, define the following:

$$T_{\max}(\mathcal{Q}) = \max_{1\le s\le S} \left(\|\mathbf{q}_s\|_2 + \|\mathbf{p}-\mathbf{q}_s\|_2\right)/c, \tag{8.24}$$

$$T_{\min}(\mathcal{Q}) = \min_{1\le s\le S} \left(\|\mathbf{q}_s\|_2 + \|\mathbf{p}-\mathbf{q}_s\|_2\right)/c, \tag{8.25}$$

the maximum and minimum propagation delays from BS to the UE via the IRSs. The TDS in the BS-UE channel is

$$T_d^{\mathrm{D}}(\mathcal{Q}) \triangleq T_{\max}(\mathcal{Q}) - T_{\min}(\mathcal{Q}).$$

Then, the locations of the IRSs can be found as

$$\mathcal{Q}^* \triangleq \{\mathbf{q}_1^*, \mathbf{q}_2^*, \ldots, \mathbf{q}_S^*\} = \arg \min_{\mathbf{q}_1,\ldots,\mathbf{q}_S} T_d^{\mathrm{D}}(\mathcal{Q}). \tag{P1}$$

We have the following result that solves the problem in (P1).

Theorem 8.3. *When BS and UE are located at points* $\mathbf{0}$ *and* $\mathbf{p}$*, respectively, the optimal locations of IRSs* $(\mathbf{q}_1^*, \ldots, \mathbf{q}_S^*)$ *as the solution to* (P1) *satisfy the equation:*

$$g_{\lambda,\mathbf{p}}(\mathbf{q}) \triangleq \left\| \mathbf{R}_{\omega,\mathbf{p}}^{\lambda} \left(\mathbf{q} - \frac{\mathbf{p}}{2} \right) \right\|_2^2 - 1 = 0, \tag{8.26}$$

where we define $\omega \triangleq \tan^{-1}\left(\dfrac{p_2}{p_1}\right)$*, and*

$$\mathbf{R}_{\omega,\mathbf{p}}^{\lambda} \triangleq \begin{bmatrix} \dfrac{2\cos(\omega)}{\lambda} & \dfrac{2\sin(\omega)}{\lambda} \\ \dfrac{2\sin(\omega)}{\sqrt{\lambda^2 - \|\mathbf{p}\|_2^2}} & -\dfrac{2\cos(\omega)}{\sqrt{\lambda^2 - \|\mathbf{p}\|_2^2}} \end{bmatrix}, \tag{8.27}$$

with $\lambda \in \mathbb{R}_+$ *being a constant satisfying* $\lambda > \|\mathbf{p}\|_2$*. Further, when the points in* $\mathcal{Q}$ *satisfy* (8.26)*, the optimal TDS is* $T_d^{D^*} = 0$*.*

Proof. See Appendix 8.D. ■

From Theorem 8.3, we note that for a point-point system, the geometric locus of all optimal IRS locations belongs to a family of confocal ellipses, with the BS and UE located at their foci. Specifically, we can choose any $\lambda > \|\mathbf{p}\|_2$, as per the required distance between the BS/UE and IRSs, and find S distinct solutions to (8.26); these provide a set of IRS locations that solve (P1). Then, the TDS can be avoided entirely (i.e., $T_0 = 0$ in (8.12)), in turn ensuring the maximum array gain scaling of $\mathcal{O}(N^2)$ on all SCs.

More intuitively, a centralized IRS leads to a non-negligible spatial delay spread in the channel, causing the SW effects. On the other hand, a distributed IRS splits a single

IRS into several non-colocated IRSs with fewer elements each that are placed on the circumference of an ellipse, as described in Theorem 8.3. This ensures that the IRSs do not cause significant spatial or temporal delay spread, resulting in a nearly flat response over the full BW at the peak array gain.

8.4.b Performance with Multiple Users

Note that Theorem 8.3 cannot be used to determine the IRS locations that are jointly optimal to multiple UEs because:

1. Unless the UEs are colocated, the locations given by (8.26) are not optimal to all the UEs, i.e., no single solution exists for IRS locations so that the TDS in the channels at all UEs can simultaneously be minimized to $T_d^{\mathrm{D}^*} = 0$.

2. Even if the optimization problem in (P1) is solved for each scheduled UE, the solutions are not practically realizable because the locations of IRSs are typically fixed once deployed and do not change with time.

To that end, we adopt a reasonable choice of IRS locations that minimize the TDS across all the UEs, as explained next.

We now consider a scenario where the BS serves multiple UEs located in a small square hotspot region, assisted by the distributed IRSs. In this case, a metric of interest is the TDS computed using the propagation delays averaged over the distribution of UE locations within the hotspot area. The expected value of the propagation delay of a path from the BS to UE via an IRS placed at $\mathbf{q}$ is

$$\bar{\tau}(\mathbf{q}) = \mathbb{E}_{\mathbf{p}\sim \mathrm{f}_{\mathbf{p}}} \left[\|\mathbf{q}\|_2 + \|\mathbf{p}-\mathbf{q}\|_2\right]/c,$$

where $\mathbf{p}$ and $\mathrm{f}_{\mathbf{p}}$ denote the UE location and its distribution, respectively. We now make the following observation:

$$\mathbb{E}_{\mathbf{p}\sim \mathrm{f}_{\mathbf{p}}} \left[\|\mathbf{q}\|_2 + \|\mathbf{p}-\mathbf{q}\|_2\right] \approx \|\mathbf{q}\|_2 + \|\mathbb{E}_{\mathbf{p}\sim \mathrm{f}_{\mathbf{p}}} [\mathbf{p}] - \mathbf{q}\|_2, \tag{8.28}$$

where we used the Jensen's approximation over the convex $\|\cdot\|_2$ norm. Note that this

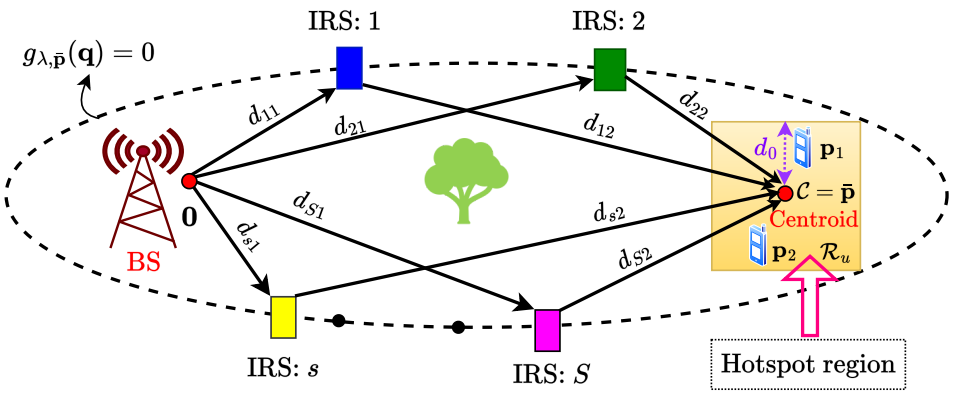

Figure 8.4: Geometric locus of IRS locations in the presence of multiple UEs.

approximation is accurate when the sum-variance of the components of $\mathbf{p}$ is small, e.g., when the UEs are clustered in a hotspot region around a central point, as is the case in typical IRS deployments [104]. Now, using (8.28) yields propagation delays via the IRSs similar to (8.24) and (8.25), except that the UE location, $\mathbf{p}$, is replaced by the centroid of the distribution of the UE locations, $\bar{\mathbf{p}} \triangleq \mathbb{E}_{\mathbf{p}\sim f_{\mathbf{p}}}[\mathbf{p}]$. Thus, Theorem 8.3 can be re-used for multiple UEs also: when multiple UEs are randomly distributed in a hotspot zone, a pragmatic choice of IRS locations is to place them on an ellipse with foci at BS and $\mathcal{C} = \mathbb{E}[\mathbf{p}]$, the *centroid* of the UE distribution, $f_{\mathbf{p}}(\mathbf{p}), \mathbf{p} \in \mathcal{R}_u$, as shown in Fig. 8.4. Then, a natural question is: What is the TDS at a UE arbitrarily located in the hotspot area? We have the following result.

Proposition 8.1. *Consider S distributed IRSs with M elements each, such that the IRSs are positioned at $\mathbf{q}_1, \mathbf{q}_2, \ldots, \mathbf{q}_S$ which lie on ellipse whose focal points are given by the locations of the BS and the centroid, $\bar{\mathbf{p}}$ (i.e., the IRS locations satisfy $g_{\lambda,\bar{\mathbf{p}}}(\mathbf{q}) = 0$ in (8.26), for some λ satisfying $\lambda > \|\bar{\mathbf{p}}\|_2$.) Then the TDS at a UE located within the hotspot at a distance r (in meters) from the centroid, and at an angle φ, measured anticlockwise w.r.t. the major axis of the ellipse, is*

$$\Delta\tau = \frac{2r}{c} \sin\left(\varphi + \frac{\nu_{\bar{S}} + \nu_{\bar{s}}}{2}\right) \sin\left(\frac{\nu_{\bar{s}} - \nu_{\bar{S}}}{2}\right), \tag{8.29}$$

where $\nu_s \triangleq \sin^{-1}\left(\frac{\|\mathbf{q}_s\|_2}{\|\mathbf{q}_s-\bar{\mathbf{p}}\|_2}\sin(\chi_s)\right)$, $c = 3\times 10^8$ *m/s,* $\bar{S} \triangleq \arg\max_{1\le s\le S} r\cos(\nu_s+\varphi)$, $\bar{s} \triangleq \arg\min_{1\le s\le S} r\cos(\nu_s+\varphi)$, *and* $\chi_s \triangleq \tan^{-1}\left(\frac{[\mathbf{q}_s]_2}{[\mathbf{q}_s]_1}\right) - \tan^{-1}\left(\frac{[\bar{\mathbf{p}}]_2}{[\bar{\mathbf{p}}]_1}\right)$.

Proof. See Appendix 8.E. ■

From Proposition 8.1, we see that the TDS at an arbitrary UE scales at most linearly with the distance between the UE and the centroid within the hotspot zone. In particular, if the UE is located in a square hotspot zone with side length $2d_0$, the maximum TDS experienced at a UE is $\Delta\tau = \frac{2\sqrt{2}d_0}{c}$ and is obtained when the UE is located at a corner of the hotspot region and $\varphi + (\nu_{\bar{S}} + \nu_{\bar{s}})/2 = \nu_{\bar{s}} - \nu_{\bar{S}} = \pi/2$. The minimum TDS is 0 and is obtained when the UE is at the centroid ($r = 0$) or $\varphi + (\nu_{\bar{S}} + \nu_{\bar{s}})/2$ is an integer multiple of π. In the sequel, for a given deployment of the IRSs, we model the TDS as a random variable $\Delta\tau \overset{\text{i.i.d.}}{\sim} \mathcal{U}[0, 2\sqrt{2}d_0/c]$ across UEs. Then, similar to Theorem 8.2, we characterize the average sum-rate obtained under a time-division multiple access (TDMA) of UEs over the hotspot region in the following result.

Theorem 8.4. *Consider an mmWave OFDM system with K SCs where a BS serves UEs within a hotspot zone of radius d_0 using S distributed IRSs as shown in Fig. 8.4, each with $M = M^*$ elements as in Theorem 8.1. When the IRSs are placed on an ellipse whose focal points are given by the locations of BS and the centroid of the hotspot zone, the average achievable sum-rate, $\bar{R}_D^{\text{opt}}$, within the hotspot region obeys*

$$\bar{R}_D^{\text{opt}} \ge \mathsf{R}_{\min}^{\text{opt}} \triangleq \frac{1}{K+N_{CP}^D}\sum_{k=1}^{K}\log_2\left(1+\frac{p_k\sigma_{\text{h}}^2}{\sigma^2}M^2(1-\epsilon)^2 \times\left[S^2\,\text{sinc}^2\left(\frac{2\sqrt{2}d_0 f_k}{c}\right)+S\left\{1-\text{sinc}^2\left(\frac{2\sqrt{2}d_0 f_k}{c}\right)\right\}\right]\right),$$

where the parameters N_{CP}^D, p_k, σ^2, σ_{h}^2 and ϵ are the same as defined in the statement of Theorem 8.2.

Proof. For a hotspot zone shaped in the form of a square with semi-side length d_0, the farthest distance a UE can be located from the centroid is $\sqrt{2}d_0$. Then, using Proposition 8.1, the proof follows by setting $T_0 = 2\sqrt{2}d_0/c$ in Theorem 8.2. ■

Theorem 8.4 explicitly characterizes a lower bound on the achievable sum-rate as a function of the parameters of the hotspot region, unlike the characterization in Theorem 8.2, which is for some value of the maximum TDS, T_0, introduced by the IRSs. Also, Theorem 8.2 characterizes the rate at a given UE location when the IRSs are deployed such that the TDS at the UE is $\mathcal{U}[0, T_0]$. To obtain Theorem 8.4, we deploy the IRSs on an ellipse and consider a UE deployed in a small hotspot region such that the TDS across the UE locations is $\mathcal{U}[0, 2\sqrt{2}d_0/c]$. In particular, for smaller hotspot sizes, $\text{sinc}^2(2\sqrt{2}d_0 f_k/c) \approx 1 - 8\pi^2 d_0^2 f_k^2/3c^2$. As a result, the channel gain on each SC scales as $S^2 - 8\pi^2 d_0^2 f_k^2 \left(S + S^2\right)/3c^2$. Thus, for a fixed M, S, the array gain at any UE within the hotspot and not located at its centroid deviates away from the full array gain of S^2M^2 at no more than a rate of $\mathcal{O}(d_0^2)$ when the IRSs are placed on the circumference of an ellipse as shown in Fig. 8.4. Further, an array gain of at least SM^2 is obtained on all SCs, in line with the preceding discussions.

Remark 8.4. *Note that the elliptical deployment scenario as considered in this chapter serves only as a representative use case to explicitly quantify the reduction in array gain due to finite TDS, and does not affect the generality of the central idea pursued in this chapter. Also, as explained earlier, this setup, where the IRSs serve a dense hotspot of UEs, is a well-recognized use case to reap the benefits of the IRS in the literature [104, 189]. In this view, even when UEs are arbitrarily located, our results still hold in the sense that the radius of the hotspot can be appropriately scaled by the maximum UE-IRS distance.*

8.5 Distributed IRSs Enable Angle Diversity

Thus far, we have discussed the advantages of a distributed design in mitigating the SW effects by parallelizing the spatial delays. Yet another useful characteristic of a distributed implementation is the diversity benefits that multiple IRSs can bring into the system [125]. In light of this, we now demonstrate a different flavor of how distributed IRSs can aid in mitigating the SW effects. Specifically, in the following, we evaluate the ρ-outage

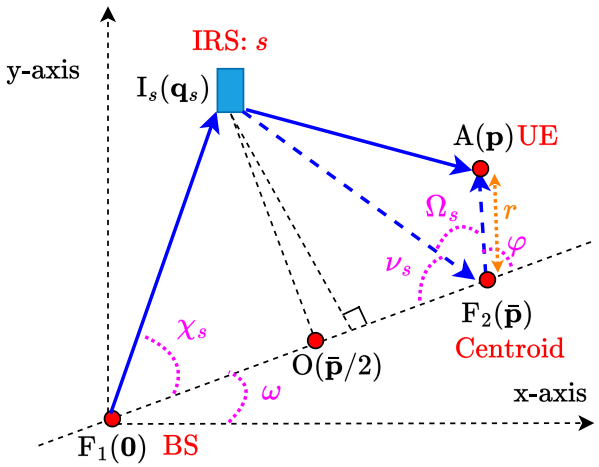

Figure 8.5: Computing the TDS at an arbitrary UE.

probability on SC-k, $k = 1, \ldots, K$, defined as

$$\mathbb{P}_\rho^k \triangleq \mathsf{Pr}\left(\left\{\phi_1, \ldots, \phi_S : |H[k]|^2 \leq \rho\right\}\right), \tag{8.30}$$

where $H[k]$ is UE's channel on SC-k. Our result shows that as long as the target channel gain is below an upper bound ρ_D^k, the outage probability decreases exponentially with the number of IRSs deployed. On the other hand, the outage probability of a centralized IRS is bounded away from zero regardless of the value of N, the number of IRS elements.

Theorem 8.5. *Let the IRSs be tuned to match the cascaded channel angle on the carrier frequency, i.e., at $f_k = 0$. Then, on SC-k, the ρ-outage probability*

1. *of an M-element S-distributed IRSs obeys*

$$\mathbb{P}_\rho^k \leq e^{-2S\left(\left\{1-\frac{\sqrt{\rho}}{SM\xi\sigma_{\mathrm{h}}^{min}}\right\}\frac{24f_c^2}{\pi^2M^2f_k^2}-\mu_X^{max}\right)^2}, \rho \in (0, \rho_D^k), \tag{8.31}$$

where $\rho_D^k \triangleq M^2S^2\xi^2(\sigma_{\mathrm{h}}^{min})^2\left(1-\mu_X^{max}\frac{\pi^2M^2f_k^2}{24f_c^2}\right)$, $\mu_X^{max} \triangleq \max\limits_{s\in[S]}\left\{\frac{1}{2}-\frac{\sin\left(2\phi_s^{(2)}\right)-\sin\left(2\phi_s^{(1)}\right)}{4\left(\phi_s^{(2)}-\phi_s^{(1)}\right)}\right\}$ and $[\phi_s^{(1)}, \phi_s^{(2)}]$ denotes the cascaded angular range of the area as seen by the sth IRS, $\sigma_{\mathrm{h}}^{min} \triangleq \min_s|\tilde{h}_s|$, and $\xi \in (0, 1)$ is a constant.

2. of an N-element centralized IRS obeys

$$\mathbb{P}_{\rho}^{k} \geq 1 - \frac{1}{\phi_0}\left\{\sin^{-1}\left(\frac{2f_c\sigma_{\mathrm{h}}}{\pi f_k\sqrt{\rho}}\right)\right\}, \text{ for } \rho \geq \frac{4f_c^2\sigma_{\mathrm{h}}^2}{\pi^2 f_k^2 c_0^2}, \tag{8.32}$$

where $[-\phi_0, \phi_0] \subseteq [-\pi/2, \pi/2]$ is the cascaded angular range of the area as seen by the IRS, and $c_0 = \sin(\phi_0)$.[6]

Proof. See Appendix 8.F. ■

Thus, with high probability, while a centralized IRS severely degrades the achievable array gain due to the SW effect, a distributed IRS prevents the adverse impact of the B-SP effect. The exponential fall of $\mathbb{P}_{\rho}^{k}$ in S with distributed IRSs is due to the *angle* diversity provided by multiple IRSs, i.e., each IRS provides a path at the UE whose cascaded angle is independent of other IRSs. This advantage is in addition to parallelizing the spatial delays across the IRSs.

The upper bound on the target array gain, ρ_D^k, is the product of $M^2S^2\xi^2(\sigma_{\mathrm{h}}^{\min})^2$, the maximum array gain obtainable from S IRSs with M elements each, and $(1 - (\mu_X^{\max}\pi^2M^2f_k^2/24f_c^2))$, which captures the unavoidable loss in array gain due to the spatial delay spread incurred by an M-element IRS. The value of the 2nd term depends on the angular range $[\phi_s^{(1)}, \phi_s^{(2)}]$ seen by the IRSs. If the interval is narrow and concentrated about 0, then this term is nearly 1. Also, as $\mu_X^{\max}$ decreases, the outage probability in (8.31) decreases and ρ_D^k increases, allowing for better channel gains from the system. On the other hand, in the centralized scenario, as N increases, the SW effect kicks in, and the outage probability in (8.32) at any f_k other than the central SC remains bounded away from zero for all $\rho = \mathcal{O}(N^2)$. Notably, as the angular range widens, the outage probability becomes high even at moderate target SNR.

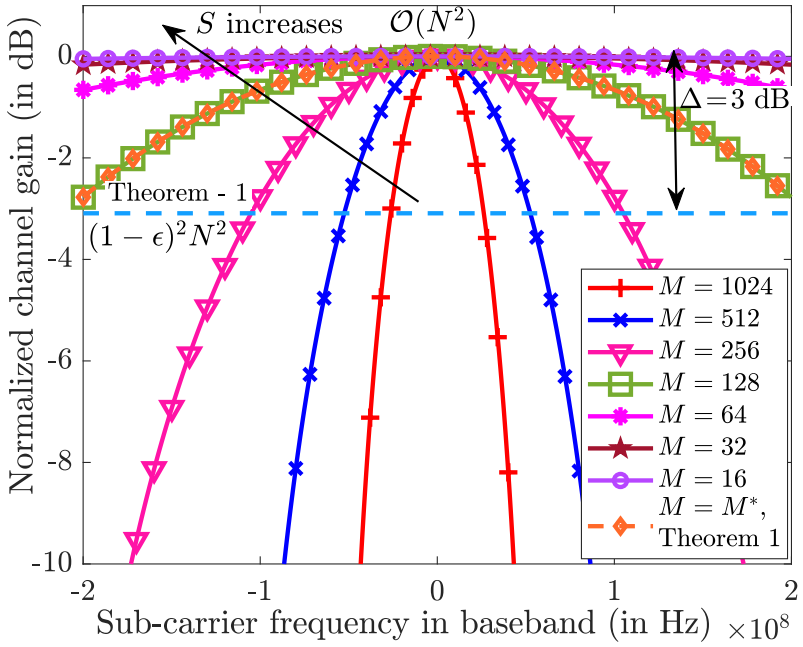

Figure 8.6: Mitigating B-SP effects via distributed IRSs for $N = 1024$.

8.6 Numerical Results and Discussions

We now illustrate our findings through Monte Carlo simulations. Unless mentioned otherwise, the BS is positioned at the origin $\mathbf{0}$, while the UE can be located within a rectangular hotspot region $\mathcal{R}_u$ with diagonally opposite corners specified by $[90, 30]^T$ and $[110, 50]^T$. The multiple IRSs are located on an ellipse with $\lambda = 140$. The path loss for each link is modeled as $\mathsf{PL} = C_0(d_{\text{ref}}/d)^\chi$, where $C_0 = -50$ dB is the reference path loss measured at $d_{\text{ref}} = 1$ meter, d is the link distance, and χ is the path-loss exponent, set equal to 2 for both BS-IRS and IRS-UE links. We consider an OFDM system with $W = 400$ MHz, $K = 2000$ SCs, and $f_c = 30$ GHz, assisted by an IRS with $N = 1024$ elements [80,121,190]. Further, we consider a *transmit* SNR of $P/\sigma^2 = 130$ dB.

[6]We consider a symmetrical angular range for ease of presentation. The approach easily extends to any arbitrary angular interval.

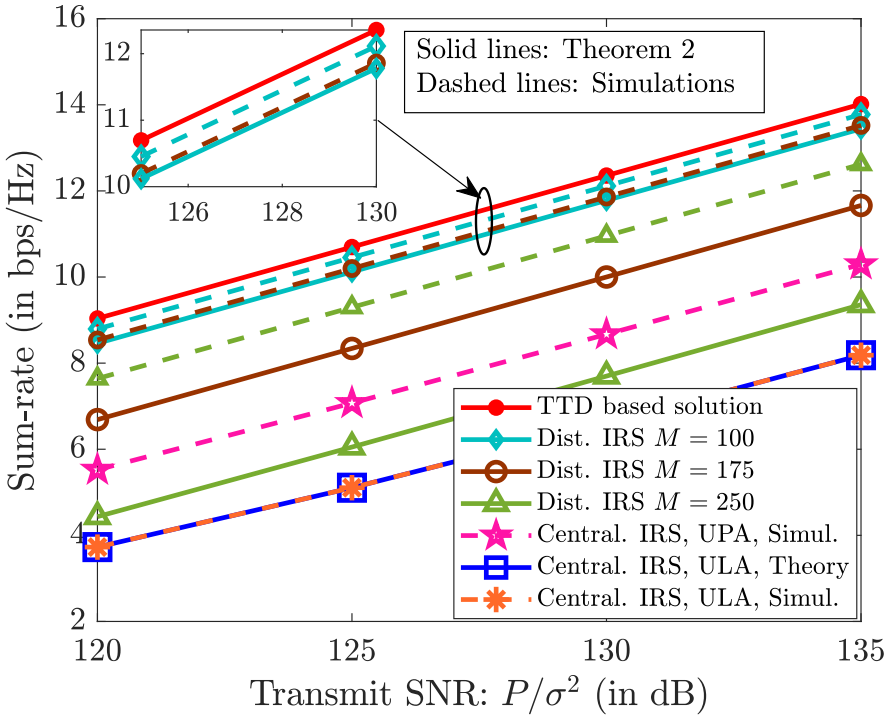

Figure 8.7: Sum-rate vs. Transmit SNR.

8.6.a Results for Zero Temporal Delay Spread: $T_0 = 0$

Channel gain

For the zero TDS scenario, we consider that the UE is located at $\bar{\mathbf{p}} = \mathbb{E}_{\mathbf{p}\sim \mathrm{f}_{\mathbf{p}}}[\mathbf{p}]$, the centroid of the distribution of UE locations within the region $\mathcal{R}_u$. In this case, since the IRSs are positioned as per Theorem 8.3, the signals via the paths from all the IRSs arrive at the UE simultaneously, leading to zero TDS. In Fig. 8.6, we plot the channel gain (normalized by the path loss) at the UE vs. the baseband SC frequency for different values of M, the number of elements at each IRS. Each curve corresponds to the system with $S = N/M$ IRSs, where the IRSs are positioned on the ellipse such that $\phi_s = 90^\circ \ \forall s$, capturing the worst-case B-SP effect. First, for $M = 1024, S = 1$, which denotes the centralized IRS case, the channel obtains the full array gain of N^2 only at $f_k = 0$ (i.e., at f_c) and decays by several dB on SCs away from $f_k = 0$, illustrating the B-SP effect. When $M < N$, i.e., $S > 1$, the channel gain becomes flatter across the BW and eventually achieves the full-array gain of N^2 on all SCs, illustrating the mitigation of the B-SP effect using multiple

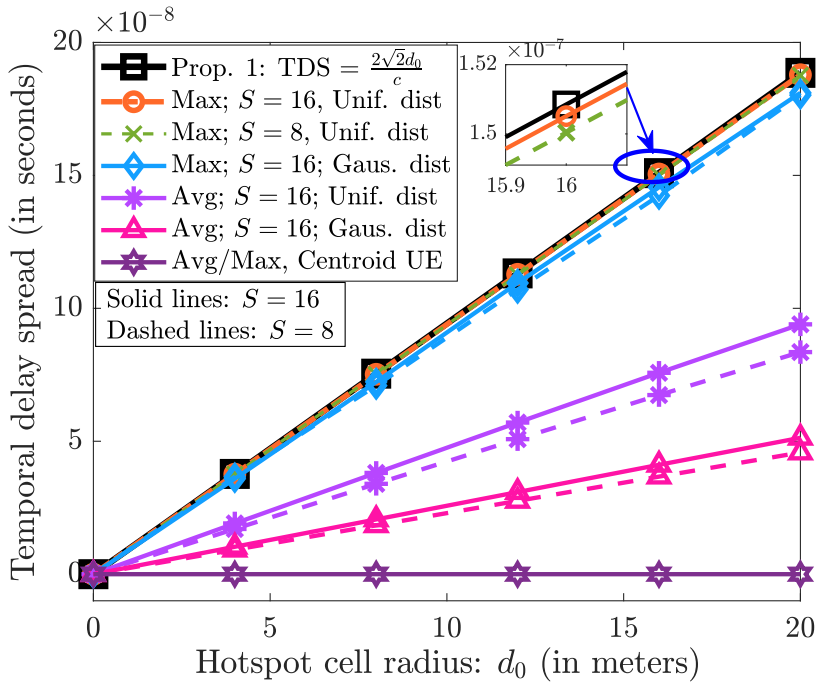

Figure 8.8: TDS vs. d_0 for different number of IRSs, S.

distributed IRSs. We also validate Theorem 8.1 (marked as "Theorem 1" on the plot) for $\epsilon \approx 0.3$, which ensures that the channel gain on all SCs is within the HPBW of the IRS beam (note the 3 dB mark.) Using (8.10), $\epsilon = 0.3$, we get $M = 128$, and we plot the channel gain for this system and benchmark it with the theoretical gain of $(1-\epsilon)^2 N^2$. The gain is clearly above the benchmark on all SCs, in line with Theorem 8.1.

8.6.a.i Sum-rate

Next, in Fig. 8.7, we plot the achievable sum-rate vs. the transmit SNR P/σ^2 for the distributed system and contrast it with the centralized IRS setup, under uniform transmit power allocation across the SCs. We consider systems with $M = 100, 175, 250$, which correspond to channel gains that are at least 66%, 20%, and 2% of the peak array gain of N^2 over the entire BW. The sum-rate of the distributed setup is better than the centralized version, and this gets more pronounced as M decreases. The reasons for this are twofold:

1. The B-SP effect reduces in the distributed setup due to the smaller aperture delays and angle diversity effects (Sec. 8.3.a and Sec. 8.5.) So, the per-SC rate and the overall sum-rate increase as S (M) increases (decreases.)

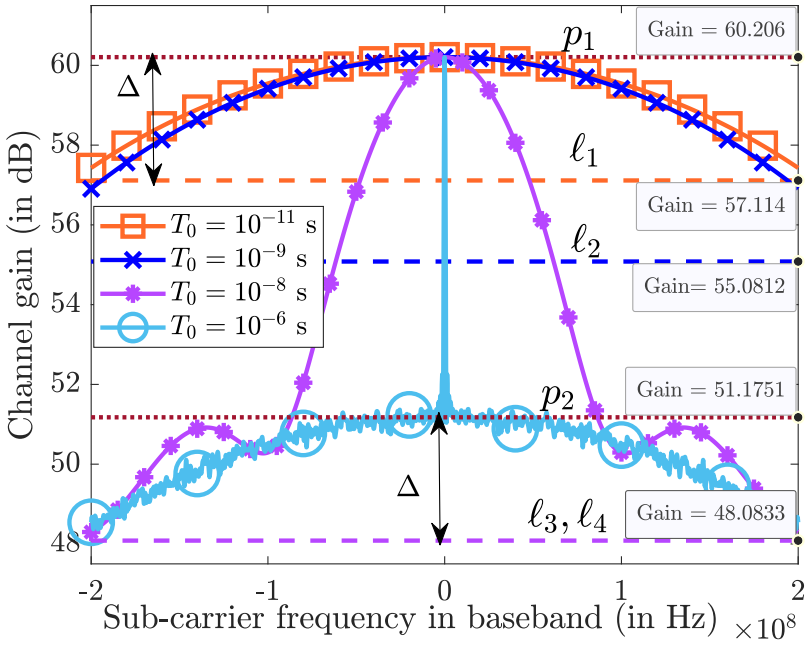

Figure 8.9: Mitigating B-SP effects with finite TDS for $\Delta = 3$ dB.

2. The CP overheads are larger in the centralized case compared to the distributed case. This is due to parallelizing aperture delays, resulting in a smaller channel delay spread in the latter. Thus, the centralized IRS suffers a further loss in the achievable sum-rate.

The plot also confirms that the scaling law derived in Theorem 8.2 indeed lower-bounds the achievable rate for the distributed IRS scenario. Further, we compare the performance of the distributed IRS solution against the existing approach of using TTDs as described in [52–55, 181]. TTDs apply an additional delay at each IRS element and counteract the signal delay across the IRS, thereby eliminating the SW and the resulting B-SP effects. However, this comes at the cost of additional complexities: 1) the number of TTDs scales with N, requiring more hardware & space; 2) high-resolution TTDs are needed for precise delay compensation, which consumes power, and 3) a sophisticated full duplex capability at the IRS to simultaneously receive, delay and reflect signals toward the UE, all of which defeats the energy-efficient nature of IRSs. From Fig. 8.7, the distributed IRS achieves the same performance as that obtained using TTDs without any extra complexity. Finally, we demonstrate that our approach achieves better performance than an $N/4 \times 4$ UPA in place of the ULA. Although a UPA-based IRS outperforms its ULA counterpart with the

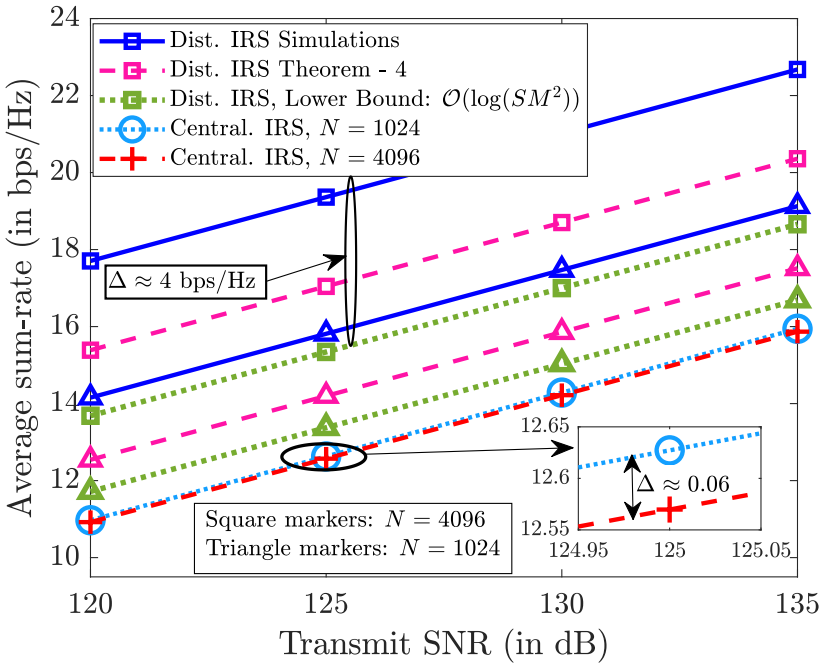

Figure 8.10: Sum-rate vs. Transmit SNR with non-zero TDS.

same N owing to the reduced impact of the B-SP effect in the former [185], it does not fully eliminate the B-SP effect. In contrast, our approach is IRS geometry agnostic and effectively mitigates the B-SP effect to deliver superior performance.

8.6.b Results for Non-zero Temporal Delay Spread: $T_0 > 0$

We now analyze how distributed IRSs can alleviate the B-SP effect even when the IRSs introduce non-zero TDS in the channel at the UE located at an arbitrary location within the hotspot zone $\mathcal{R}_u$ of radius d_0, as illustrated in Fig. 8.4.

8.6.b.i Amount of TDS

We first assess the amount of TDS experienced by a UE located away from the centroid. In Fig. 8.8, we plot TDS versus d_0 for different S, the number of IRSs, considering two distributions for the UE locations: 1) a uniform distribution within $\mathcal{R}_u$, and 2) a 2-dimensional truncated Gaussian distribution with mean $\bar{\mathbf{p}}$ and standard deviation $\sigma_U = d_0/3$, with its support being $\mathcal{S}_U \triangleq \{\mathbf{p} \in \mathbb{R}^2 : \|\mathbf{p} - \bar{\mathbf{p}}\|_\infty \leq d_0\}$. We observe that both the average TDS and the maximum TDS increase as d_0 increases. This is because the IRS placements are

optimized to achieve zero TDS only at the centroid of the location distribution within $\mathcal{R}_u$, and the TDS increases as we move away from the centroid (see Proposition 8.1). Furthermore, since the truncated Gaussian distribution is more concentrated around the centroid than the uniform distribution, the TDS in the former is smaller than that in the latter, but both are well upper-bounded by the maximum TDS predicted by Proposition 8.1 (marked as "Prop. 1" on the plot.)

8.6.b.ii Channel gain

In Fig. 8.9, considering the worst-case B-SP effect, we plot the channel gain vs. the SC frequency for different values of T_0. The sampling time is $T_s = 1/W = 2.5 \times 10^{-9}$ seconds. We also plot the following equations:

$$
\begin{aligned}
p_1 : g_1(f_k) &= N^2; f_k \in [-W/2, W/2]. \\
\ell_1 : g_2(f_k) &= (1-\epsilon)^2 M^2 \left[S^2 h^2(10^{-11}) + S\left(1 - h^2(10^{-11})\right)\right] \\
\ell_2 : g_3(f_k) &= (1-\epsilon)^2 M^2 \left[S^2 h^2(10^{-9}) + S\left(1 - h^2(10^{-9})\right)\right] \\
p_2 : g_4(f_k) &= SM^2; f_k \in [-W/2, W/2]. \\
\ell_3 : g_5(f_k) &= (1-\epsilon)^2 M^2 \left[S^2 h^2(10^{-8}) + S\left(1 - h^2(10^{-8})\right)\right] \\
\ell_4 : g_6(f_k) &= (1-\epsilon)^2 M^2 \left[S^2 h^2(10^{-6}) + S\left(1 - h^2(10^{-6})\right)\right]
\end{aligned}
$$

where $h^2(t) \triangleq \text{sinc}^2(Wt/2)$. The lines $\ell_1, \ell_2, \ell_3, \ell_4$ represent the minimum channel gains in non-zero TDS scenarios, unlike the zero gains that occur from the B-SP effect. As long as $T_0 < T_s$ (i.e., when the paths from all IRSs arrive within the same sampling interval), the IRS phase configurations can compensate for differential delays across the IRSs, and provide a full array gain of $S^2M^2 = N^2$ on all SCs, with only a minor loss due to permissible B-SQ (in this case, it is set to 3 dB.) However, when $T_0 \geq T_s$ and as T_0 increases, the array gain over the SCs decreases and flattens below N^2, as described in Theorem 8.4. For large T_0 (e.g., 10^{-5} s), the channel gain flattens at around approximately $\mathcal{O}(SM^2)$, with a 3 dB residual B-SQ loss. This is because, in this case, the gain at the UE is obtained only due to the incoherent superposition of signals from the IRSs. However, at the SC where $f_k = 0$, since the IRSs' phase shifts can fully compensate for any differential path

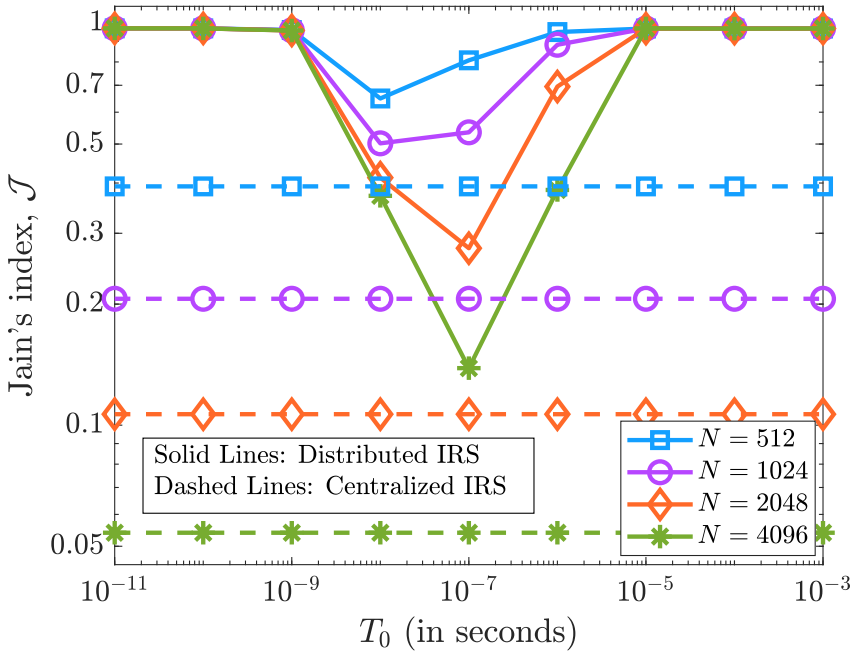

Figure 8.11: Jain's index, $\mathcal{J}$ across SCs for $K = 2000$.

delay, the channel gain still scales as N^2. Thus, the distributed IRS effectively mitigates the B-SP effect and ensures a flat response across the BW, even after accounting for the nonzero TDS.

8.6.b.iii Average sum-rate

In Fig. 8.10, we evaluate the average sum-rate of the distributed IRS system, designed for $\epsilon \approx 0.3$, by plotting it against the transmit SNR, P/σ^2, for $N = 1024$ and 4096. The results are averaged over multiple UE locations within a hotspot defined by $\bar{\mathbf{p}} = [80, 80]^T$, $d_0 = 12$ meters, and the IRSs placed on an ellipse with $\lambda = 160$. For $N = 1024$, the distributed IRS significantly outperforms the centralized IRS, even after accounting for the nonzero TDS in the former setup. Further, the curve obtained based on Theorem 8.4 (labeled "Theorem 4" on the plot) lower-bounds the empirical sum-rate, confirming the accuracy of our analysis. Additionally, we show the worst-case lower bound on the rate that scales as $\mathcal{O}(\log(SM^2))$ on the plot. The gap between the achievable sum-rate and this lower bound is high, showing that our solution can perform much better than the incoherent gain of $\mathcal{O}(\log(SM^2))$ on all SCs. Finally, when the number of IRS elements

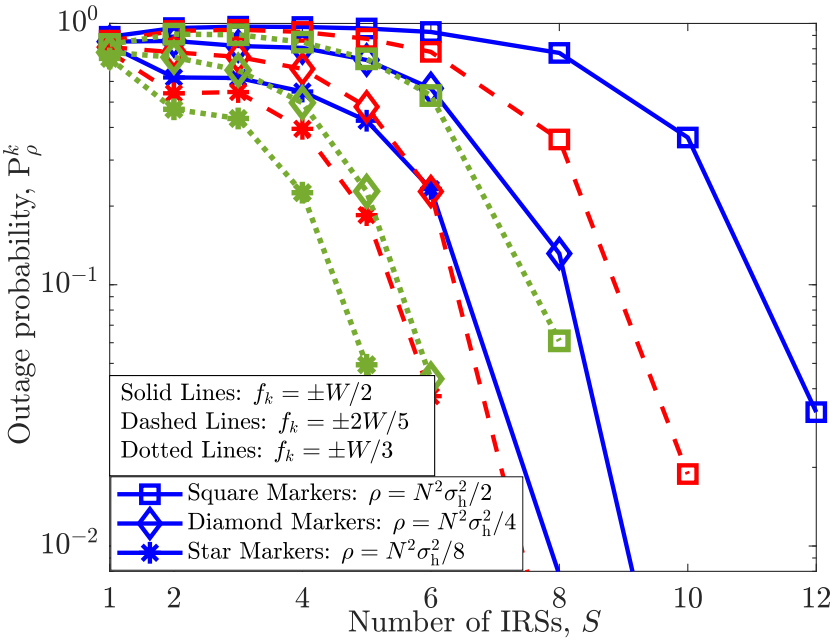

Figure 8.12: B-SP induced outage probability versus S.

quadruples from $N = 1024$ to $N = 4096$, the rate improves by 4 bps/Hz, demonstrating that our method achieves the full array gain of $\mathcal{O}(N^2)$ (since $\log_2((4N)^2) = 4 + \log_2(N^2)$). In contrast, the sum-rate using centralized IRS marginally reduces due to the B-SP effect.

8.6.b.iv Jain's index

Next, in Figure 8.11, we demonstrate the flatness in the channel gain across SCs by plotting the Jain's index as a function of T_0. The Jain's index is calculated using the channel gains on different SCs as

$$\mathcal{J} \triangleq \frac{\left(\sum_{k=1}^{K} |H[k]|^2\right)^2}{K \sum_{k=1}^{K} |H[k]|^4}.$$

We can show that $\frac{1}{K} \leq \mathcal{J} \leq 1$, with $\mathcal{J} = 1$ achieved when the channel gains are equal on all SCs. In Fig. 8.11, we depict Jain's index for both the centralized and distributed IRS setups for different values of N. For any given N, the index $\mathcal{J}$ for a distributed IRS is approximately 1 for small T_0, then decreases below 1 for moderate T_0, and returns to 1 for large T_0. This behavior can be explained as follows. For small T_0, the channel

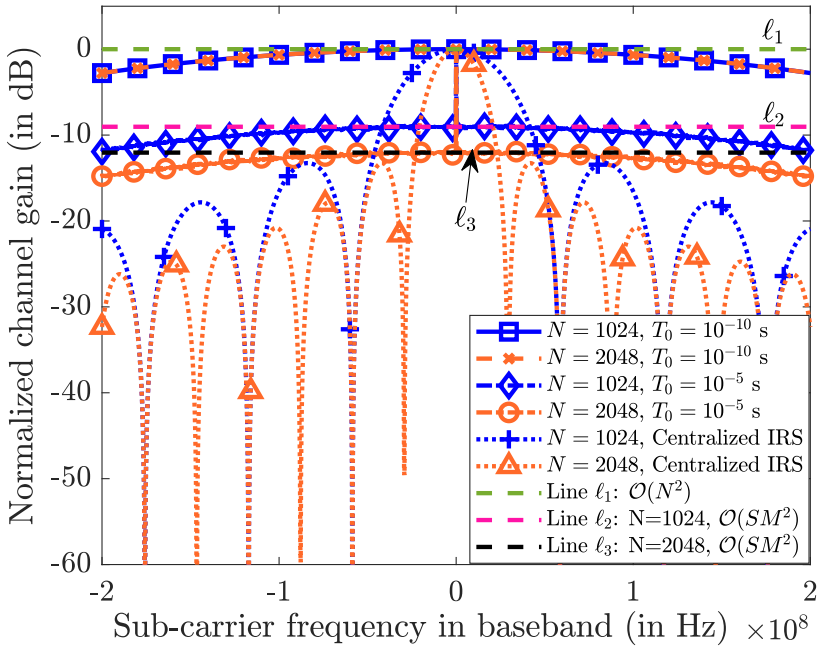

Figure 8.13: Channel gains in centralized vs. distributed IRSs.

gain uniformly scales as $\mathcal{O}(N^2)$ on all SCs within the HPBW of the main lobe, yielding $\mathcal{J} \approx 1$. As T_0 increases, the channel gain fluctuates between $\mathcal{O}(SM^2)$ and $\mathcal{O}(S^2M^2)$ across different SCs as illustrated in Fig. 8.9, causing $\mathcal{J}$ to drop below 1. When T_0 becomes high, $\mathcal{J}$ increases again to 1 because the channel exhibits an almost flat response within 3 dB of the peak gain of $\mathcal{O}(SM^2)$ due to the incoherent addition of signals from the IRSs. Since S increases with N (M remains constant since we design the system for $\epsilon \approx 0.3$), the gap between SM^2 and S^2M^2 increases as N increases, leading to larger fluctuations in the channel gain at moderate T_0. This results in a lower Jain's index $\mathcal{J}$ for intermediate T_0 as N increases. Importantly, the Jain's index obtained using a distributed IRS is much higher than in the corresponding centralized IRS scenario, showing that the distributed IRS can effectively flatten the channel frequency response even after accounting for the nonzero TDS.

8.6.c Diversity Benefits of Distributed IRSs

We next showcase how distributed IRSs can also leverage diversity benefits to further mitigate the B-SP effects in Fig. 8.12. To this end, we simulate the B-SP induced outage

probability $\mathbb{P}_{\rho}^{k}$ as a function of S for various UE location realizations. The plot clearly shows that $\mathbb{P}_{\rho}^{k}$ decreases exponentially with the number of IRSs, in line with Theorem 8.5. Multiple IRSs provide independent paths with different channel angles, and the resulting angle diversity makes it unlikely that all IRSs experience the worst-case spatial delay spread. Further, $\mathbb{P}_{\rho}^{k}$ decreases as ρ decreases, in line with the inferences from Theorem 8.5. Note that $\rho = N^2\sigma_{\mathrm{h}}^2/2^{\ell}$ corresponds to an allowed loss of 3ℓ dB relative to the peak array gain of N^2. Thus, larger degradation in the array gain due to the B-SP is less likely to happen with distributed IRSs. Similarly, since the B-SP effects are less pronounced near the center SC, $\mathbb{P}_{\rho}^{k}$ reduces as $|f_k|$ is near 0, in line with Theorem 8.5. Thus, distributed IRSs also provide instantaneous benefits to minimize the SW and the resulting B-SP effects.

8.6.d Array Gain Using Distributed vs. Centralized IRS

Finally, in Fig. 8.13, we summarize a big picture of the solution by comparing the channel gain obtained using a distributed IRS with the conventional centralized IRS. Distributed IRSs can completely combat the B-SP effect and provide a significantly better array gain on all SCs. Although the channel gain with distributed IRSs concentrates about $\mathcal{O}(SM^2)$ when the TDS is arbitrarily large and is less than $\mathcal{O}(N^2)$, this still avoids deep nulls, ensuring that the IRS can focus on the desired UE on all SCs. Even the reduced gain with distributed IRSs due to large TDS is much better than the array gain using a centralized IRS on all SCs other than the center SC. Thus, the distributed IRSs effectively mitigate the SW effect (and hence the B-SP) and outperform the centralized IRS at almost no additional complexity.

8.7 Conclusions

We tackled the issue of SW and the resulting B-SP effects in IRS-aided wideband systems by identifying that the SW effect primarily stems from the linear increase of spatial delay spread across the IRS aperture. In this view, we proposed a distributed IRS design that *a*) parallelizes spatial delay and *b*) utilizes angle diversity, collectively mitigating the SW and B-SP effects. In particular, we detailed how to determine the number of elements

at each IRS, the number of IRSs, and the placement of the IRSs that can eliminate the SW effects while procuring the optimal array gain over the entire BW for a given total number of IRS elements. Our solution provides uniformly positive benefits over the full BW at any UE with no significant complexity compared to existing methods. Potential future work includes extending the solutions to account for near-field effects and mobility scenarios. Another interesting direction is to extend the setup for serving multiple UEs in a multiplexed manner using distributed IRSs in the presence of B-SP effects, and to rigorously compare and contrast this approach with schemes that serve only a single UE.

Appendix 8.A Proof of Theorem 8.1

We begin the proof by noting that similar to (8.6), the channel at the UE on SC-k due to S IRSs can be written as

$$H[k] = \sum_{s=1}^{S} \sqrt{M}\tilde{h}_s \boldsymbol{\theta}_s^H \mathbf{a}_M\left(\phi_{f_k,s}\right) e^{-j2\pi f_k(\eta_s-\tau_0)}, \tag{8.33}$$

where $\tilde{h}_s, \eta_s, \tau_0$ denote the cascaded channel coefficient via the sth IRS, the propagation delay via the sth IRS, and receiver timing offset, respectively; $\boldsymbol{\theta}_s \in \mathbb{C}^M$ is the phase shift vector at the sth IRS, and $\phi_{f_k,s}$ is the cascaded angle at the UE via the sth IRS on SC-k as given in (8.7) with ϕ_s being the physical angle via the sth IRS. Since we consider that the TDS is 0, $(\eta_s - \tau_0)W \ll 1$ holds, and hence, we drop the exponential term in (8.33). Then, by tuning $\boldsymbol{\theta}_s$, $s = 1, \ldots, S$ to the center SC at $f_k = 0$, and by invoking the Cauchy-Schwarz (CS) inequality, we obtain the optimal phase configurations:

$$\boldsymbol{\theta}_s = \sqrt{M} e^{j\angle \tilde{h}_s} \mathbf{a}_M(\phi_s), \ \forall s = 1, \ldots, S. \tag{8.34}$$

Substituting (8.34) in (8.33), we have

$$|H[k]|^2 = \left| M \sum_{s=1}^{S} |\tilde{h}_s| \mathbf{a}_M^H(\phi_s) \mathbf{a}_M\left(\phi_{f_k,s}\right) \right|^2, \tag{8.35}$$

Now, when $M > 1$, to account for the worst-case B-SP effect, we use $\phi_s = 90°$ as in (8.8) and simplify the channel gain as $|H[k]|^2=$

$$\left|\sum_{s=1}^{S}|\tilde{h}_s|\frac{1-e^{-j\pi M\frac{f_k}{f_c}}}{1-e^{-j\pi\frac{f_k}{f_c}}}\right|^2 \overset{(a)}{=} M^2\,\mathrm{sinc}^2\left(M\frac{f_k}{2f_c}\right)\left|\sum_{s=1}^{S}|\tilde{h}_s|\right|^2, \tag{8.36}$$

where, in (a), we use $\sin(x) \approx x$ for $x = \pi f_k/(2f_c) \ll 1$, and $\mathrm{sinc}(x) \triangleq \sin(\pi x)/\pi x$. Clearly, at $f_k = 0$, the response in (8.36) is maximum and decreases as $f_k \to \pm W/2$. Now using (8.36), the condition in (8.8) becomes

$$\min\left\{\mathrm{sinc}^2\left(M\frac{f_k}{2f_c}\right), k = 1, 2, \ldots, K\right\} \geq (1-\epsilon)^2\,. \tag{8.37}$$

A necessary condition for (8.37) to hold is not to have a null response across the entire BW. Since $\mathrm{sinc}^2(x) = 0$ when $x \in \mathbb{Z}$, the set of integers, from (8.37) we need to satisfy

$$MW/4f_c \leq 1 \implies M \leq M_1^* \triangleq \lfloor 4f_c/W \rfloor\,. \tag{8.38}$$

This ensures that the channel response across the BW lies within the main lobe width of the beam formed by the IRS at the center SC. Now, since $\mathrm{sinc}^2(x)$ is a decreasing function for $x \in [0, 1]$, a sufficient condition for (8.37) is

$$\begin{gathered}|H[0]|^2 = |H[K]|^2 \geq (1-\epsilon)^2|H[K/2]|^2, \text{ i.e.,}\\ \mathrm{sinc}^2\left(\pm\frac{MW}{4f_c}\right) \geq (1-\epsilon)^2 \overset{(b)}{\implies} M \leq M_2^* \triangleq \left\lfloor \frac{4\sqrt{6\epsilon}}{\pi}\frac{f_c}{W}\right\rfloor,\end{gathered} \tag{8.39}$$

where in (b), we used the 1st order Taylor's approximation: $\mathrm{sinc}(x) \approx 1 - \pi^2x^2/6$, which is tight in the region of design interest. Now, from (8.38), and (8.39), we get

$$M \leq M^* \triangleq \min\{M_1^*, M_2^*\} = M_2^*, \tag{8.40}$$

where the last step follows because for $\epsilon \in [0, 1)$, $M_2^* \leq M_1^*$. Finally, since $1 \leq M \leq N$, we modify (8.40) as

$$M \leq M_{\text{mod}}^* \triangleq \min\{\max\{M_2^*, 1\}, N\},$$

yielding the desired result in (8.10).

Appendix 8.B Proof of Theorem 8.2

In an OFDM system with K SCs, the sum-rate is

$$\bar{R} \triangleq \mathbb{E}_{H[k]}\left[\frac{1}{K+N_{\mathrm{CP}}}\sum_{k=1}^{K}\log_2\left(1+\frac{p_k}{\sigma^2}|H[k]|^2\right)\right]$$
$$\overset{(a)}{\approx} \frac{1}{K+N_{\mathrm{CP}}}\sum_{k=1}^{K}\log_2\left(1+\frac{p_k}{\sigma^2}\mathbb{E}\left[|H[k]|^2\right]\right), \tag{8.41}$$

where in (a), we used the Jensen's approximation. We next compute $\mathbb{E}\left[|H[k]|^2\right]$ for centralized & distributed IRSs below:

Centralized scenario: The channel gain for a centralized scenario can be found using (8.36) with $M = N$, $S = 1$. Then,

$$\mathbb{E}\left[|H[k]|^2\right] = N^2\,\mathrm{sinc}^2\left(N\frac{f_k}{2f_c}\sin(\phi)\right)\underbrace{\mathbb{E}[|\tilde{h}|^2]}_{=\sigma_{\mathrm{h}}^2}, \tag{8.42}$$

and substituting the above into (8.41) yields (8.11).

Distributed scenario: Let $\tilde{\eta}_s \triangleq \eta_s - \tau_0$ be the propagation delay of the path via the sth IRS w.r.t the timing offset at the UE. Since $(\eta_s - \tau_0)W \ll 1$ may not hold always in general, from (8.33), the channel gain at a UE on SC-k is given by

$$|H[k]|^2 = \left|M\sum_{s=1}^{S}|\tilde{h}_s|\mathbf{a}_M^H(\phi_s)\mathbf{a}_M\left(\phi_{f_k,s}\right)e^{-j2\pi f_k\tilde{\eta}_s}\right|^2.$$

Similar to (8.36), the expected channel gain is $\mathbb{E}\left[|H[k]|^2\right]$

$$= \mathbb{E}\left[\left|\sum_{s=1}^{S}|\tilde{h}_s|\frac{1-e^{-j\pi M\frac{f_k}{f_c}\sin(\phi_s)}}{1-e^{-j\pi\frac{f_k}{f_c}\sin(\phi_s)}}e^{-j2\pi f_k\tilde{\eta}_s}\right|^2\right] \tag{8.43}$$

$$\overset{(b)}{\geq} M^2 \operatorname{sinc}^2\left(M\frac{f_k}{2f_c}\right)\mathbb{E}\left[\left|\sum_{s=1}^{S}|\tilde{h}_s|e^{-j2\pi f_k\tilde{\eta}_s}\right|^2\right], \tag{8.44}$$

where in (b), we applied the result from Theorem 8.1. We now simplify the above expectation term as

$$\mathbb{E}\left[\left|\sum_{s=1}^{S}|\tilde{h}_s|e^{-j2\pi f_k\tilde{\eta}_s}\right|^2\right] = \sum_{s=1}^{S}|\tilde{h}_s|^2 + \sum_{\substack{s=1\\ s\neq s'}}^{S}\sum_{s'=1}^{S}|\tilde{h}_s||\tilde{h}_{s'}|\mathbb{E}\left[e^{-j2\pi f_k\tilde{\eta}_s}\right]\mathbb{E}\left[e^{j2\pi f_k\tilde{\eta}_{s'}}\right]. \tag{8.45}$$

Now we compute $\mathbb{E}\left[e^{j2\pi f_k\tilde{\eta}_s}\right]$ as shown below.

$$\begin{aligned}\mathbb{E}\left[e^{j2\pi f_k\tilde{\eta}_s}\right] = \frac{1}{T_0}\int_0^{T_0} e^{j2\pi f_k\eta}\mathrm{d}\eta = \frac{1}{T_0}\frac{e^{j2\pi f_k\eta}}{j2\pi f_k}\bigg|_0^{T_0} = \frac{1}{T_0}\frac{e^{j\pi f_kT_0}\left(e^{j\pi f_kT_0}-e^{-j\pi f_kT_0}\right)}{j2\pi f_k}\\ = e^{j\pi f_kT_0}\cdot\frac{\sin\left(\pi f_kT_0\right)}{\pi f_kT_0} = e^{j\pi f_kT_0}\operatorname{sinc}\left(f_kT_0\right).\end{aligned} \tag{8.46}$$

Similarly, we can show that

$$\mathbb{E}\left[e^{-j2\pi f_k\tilde{\eta}_s}\right] = e^{-j\pi f_kT_0}\operatorname{sinc}\left(f_kT_0\right). \tag{8.47}$$

Using (8.46) and (8.47) in (8.45), we get

$$\begin{aligned}\mathbb{E}\left[\left|\sum_{s=1}^{S}|\tilde{h}_s|e^{-j2\pi f_k\tilde{\eta}_s}\right|^2\right] &= S\sigma_{\mathrm{h}}^2 + S(S-1)\sigma_{\mathrm{h}}^2\operatorname{sinc}^2\left(f_kT_0\right)\\ &= \sigma_{\mathrm{h}}^2\left(S^2\operatorname{sinc}^2(f_kT_0) + S(1-\operatorname{sinc}^2(f_kT_0))\right).\end{aligned}$$

Now, using the above in (8.44), we obtain

$$\mathbb{E}\left[|H[k]|^2\right] \geq (1-\epsilon)^2M^2\sigma_{\mathrm{h}}^2\left(S^2\operatorname{sinc}^2(f_kT_0) + S(1-\operatorname{sinc}^2(f_kT_0))\right). \tag{8.48}$$

Substituting (8.48) in (8.41) and by the monotonicity of $\log(\cdot)$, (8.12) follows. We get (8.13) by lower bounding the convex combination: $S^2\operatorname{sinc}^2(f_kT_0)+S(1-\operatorname{sinc}^2(f_kT_0)) \geq S$.

Next, note that the CP lengths should exceed the channel delay spread. The delay spread, τ under centralized and distributed IRSs are $\Delta\tau^{\mathrm{C}}$ from (8.4), and $\max_{s\in[S]}\left\{\Delta\tau_s^{\mathrm{D}}+\tilde{\eta}_s\right\}$ from (8.9), respectively. In particular, the CP length in the distributed IRS case should

account for the residual spatial delay spread and the temporal delay spread introduced by the multiple IRSs. Then, using these expressions in the length of discrete-time channel taps: $N_{\mathrm{CP}} = \lceil W\tau \rceil$, we get

$$N_{\mathrm{CP}}^{\mathrm{C}} = \left\lceil (N-1)\frac{W}{2f_c}\Delta S^{\mathrm{C}} \right\rceil, \quad \text{and}$$
$$N_{\mathrm{CP}}^{\mathrm{D}} = \left\lceil \max_{1\le s\le S} \left\{ (M-1)\frac{W}{2f_c}\Delta S_s^{\mathrm{D}} + W\tilde{\eta}_s \right\} \right\rceil,$$

respectively, where $\Delta S^{\mathrm{C}} \triangleq |\sin(\psi) - \sin(\omega)|$, $\Delta S_s^{\mathrm{D}} \triangleq |\sin(\psi_s) - \sin(\omega_s)|$. Now, to satisfy the CP requirements at any UE, we upper bound the delays and set $\Delta S^{\mathrm{C}} = \Delta S^{\mathrm{D}} = 2$, and $\tilde{\eta}_s = T_0$. Then the desired CP lengths in (8.14) follow.

Appendix 8.C Proof of Corollary 8.1

When the TDS is non-negligible, we set $\phi_1 = \phi_2 = \ldots \phi_S = 90°$ in (8.43) to capture the worst case B-SP and obtain the simplified channel gain on SC-k as

$$|H[k]|^2 = M^2 \operatorname{sinc}^2\left(M\frac{f_k}{2f_c}\right)\left|\sum_{s=1}^{S}|\tilde{h}_s|e^{-j2\pi f_k\tilde{\eta}_s}\right|^2. \tag{8.49}$$

Next, using (8.49), the condition in (8.8) can be simplified as

$$\operatorname{sinc}^2\left(M\frac{f_k}{2f_c}\right) \ge (1-\epsilon)^2\left|\sum_{s=1}^{S}|\tilde{h}_s|\right|^2 \Big/ \left|\sum_{s=1}^{S}|\tilde{h}_s|e^{-j2\pi f_k\tilde{\eta}_s}\right|^2$$
$$\overset{(a)}{\ge} (1-\epsilon)^2\frac{\left|\sum_{s=1}^{S}|\tilde{h}_s|\right|^2}{S\sum_{s=1}^{S}|\tilde{h}_s|^2} \overset{(b)}{=} (1-\epsilon)^2\left\|\tilde{\mathbf{h}}\right\|_1^2 \Big/ S\left\|\tilde{\mathbf{h}}\right\|_2^2, \tag{8.50}$$

where (a) follows by the CS inequality, and in (b), we define $\tilde{\mathbf{h}} \triangleq [|\tilde{h}_1|, \ldots, |\tilde{h}_S|]^T$. Since $\|\tilde{\mathbf{h}}\|_1 \le \sqrt{S}\|\tilde{\mathbf{h}}\|_2$ [191], a sufficient condition for (8.50) becomes that given in (8.37), and hence rest of the proof follows similar to TDS = 0 case.

Appendix 8.D Proof of Theorem 8.3

By their definitions, we note that $T_{\max}(\mathcal{Q}) \geq T_{\min}(\mathcal{Q}) \geq 0$ for all $\mathcal{Q} \subset \mathbb{R}^2_S \triangleq \underbrace{\mathbb{R}^2 \times \ldots \times \mathbb{R}^2}_{S \text{ times}}$. In other words, $T_d^{\mathrm{D}*} = 0$ is the global minimum of the problem: $\min_{\mathcal{Q} \subset \mathbb{R}^2_S} T_d^{\mathrm{D}}(\mathcal{Q})$, and is achieved by a $\mathcal{Q}^*$ for which $T_{\max}(\mathcal{Q}^*) = T_{\min}(\mathcal{Q}^*)$. Thus, the possible global optimal set of IRS locations, $\mathcal{Q}^*$, should be such that $\|\mathbf{q}_s\|_2 + \|\mathbf{p} - \mathbf{q}_s\|_2 = \lambda$ for all $s \in [S]$ and λ is some constant. In other words, the sum-distance of the IRS from the BS and UE should be constant across the IRS locations. Now, using [192, Page 2], it can be shown that an ellipse with the focal points coinciding with the locations of BS and UE satisfies this property. Hence, the IRS locations should lie on an ellipse constructed with the BS and UE as foci. Particularly, the equation of the ellipse is

$$\frac{\left((q_1 - q_{10})\cos(\omega) + (q_2 - q_{20})\sin(\omega)\right)^2}{a^2} + \frac{\left((q_1 - q_{10})\sin(\omega) - (q_2 - q_{20})\cos(\omega)\right)^2}{b^2} = 1, \tag{8.51}$$

where $\mathbf{q} = [q_1, q_2]^T$ is a candidate IRS location, $\mathbf{q}_0 = [q_{10}, q_{20}]^T$ is the center of the ellipse, ω is the angle made by the major axis of ellipse with the x-axis, a and b are lengths of the semi-major axis and semi-minor axis, respectively. Now, with focal points given by $\mathbf{0}$ and $\mathbf{p}$, the centre of the ellipse is $\mathbf{q}_0 = \mathbf{p}/2$. Similarly, using the properties of the ellipse, we can show $a = \lambda/2$, $b = \sqrt{\lambda^2 - \|\mathbf{p}\|_2^2}\big/2$,[7] and $\omega = \tan^{-1}(p_2/p_1)$, with $\mathbf{p} = [p_1, p_2]^T$. Using these values in (8.51) and compactly representing it through (8.26) completes the proof.

Appendix 8.E Proof of Proposition 8.1

To measure the TDS at an arbitrary UE located at (say) $\mathrm{A}(\mathbf{p})$, we first compute the total propagation delay of the signal from the BS to A via the sth IRS. For convenience, we label the locations of the BS, IRS-s, and centroid by F_1, I_s, F_2, respectively, as shown in Fig. 8.5. For the triangle $\mathrm{I}_s\mathrm{AF}_2$, we apply the cosine rule [193, Sec. 12.7] to obtain

$$\mathsf{d}(\mathrm{I}_s, \mathrm{A})^2 = \mathsf{d}(\mathrm{I}_s, \mathrm{F}_2)^2 + \mathsf{d}(\mathrm{F}_2, \mathrm{A})^2 - 2\mathsf{d}(\mathrm{I}_s, \mathrm{F}_2) \cdot \mathsf{d}(\mathrm{F}_2, \mathrm{A})\cos(\Omega_s), \tag{8.52}$$

[7] Note that, by applying the triangle inequality property to the triangle formed by BS, UE, and an IRS, it holds that $\lambda > \|\mathbf{p}\|_2$.

where $\mathsf{d}(\mathrm{A},\mathrm{B})$ measures the distance between points A and B, and Ω_s is the angle between the lines $\mathrm{I}_s\mathrm{F}_2$ and AF_2. Using (8.52), we make the following simplifications:

$$\begin{aligned}\mathsf{d}(\mathrm{I}_s,\mathrm{A}) &= \sqrt{\mathsf{d}(\mathrm{I}_s,\mathrm{F}_2)^2 + r^2 - 2r\cdot\mathsf{d}(\mathrm{I}_s,\mathrm{F}_2)\cos(\Omega_s)} \\ &= \sqrt{\mathsf{d}(\mathrm{I}_s,\mathrm{F}_2)^2\left(1+\frac{r^2}{\mathsf{d}(\mathrm{I}_s,\mathrm{F}_2)^2} - 2\frac{r}{\mathsf{d}(\mathrm{I}_s,\mathrm{F}_2)}\cos(\Omega_s)\right)} \\ &\overset{(a)}{=} \mathsf{d}(\mathrm{I}_s,\mathrm{F}_2)\left(1-\frac{r}{\mathsf{d}(\mathrm{I}_s,\mathrm{F}_2)}\cos(\Omega_s)+\mathcal{O}\left(\frac{r^2}{\mathsf{d}(\mathrm{I}_s,\mathrm{F}_2)^2}\right)\right) \\ &\overset{(b)}{\approx} \mathsf{d}(\mathrm{I}_s,\mathrm{F}_2) - r\cos(\Omega_s) \overset{(c)}{=} \mathsf{d}(\mathrm{I}_s,\mathrm{F}_2) + r\cos(\nu_s+\varphi),\end{aligned}$$

where in (a), we used Taylor's expansion: $\sqrt{1+x} = 1 + x/2 + \mathcal{O}(x^2)$; in (b), we neglected higher order terms because the UEs are clustered in a hotspot, i.e., $r \ll \mathsf{d}(\mathrm{I}_s,\mathrm{F}_2)$; and in (c), we used the fact $\varphi + \Omega_s + \nu_s = \pi$ and $\cos(\pi-\theta) = -\cos(\theta)$. As a result, the total propagation delay in the channel at the UE from BS via the sth IRS can be written as $\tau_s^{\mathrm{A}} =$

$$\frac{\mathsf{d}(\mathrm{F}_1,\mathrm{I}_s)+\mathsf{d}(\mathrm{I}_s,\mathrm{A})}{c} \approx \frac{\mathsf{d}(\mathrm{F}_1,\mathrm{I}_s)+\mathsf{d}(\mathrm{I}_s,\mathrm{F}_2)+r\cos(\nu_s+\varphi)}{c}.$$

Then, the TDS at the UE is given by $\Delta\tau^{\mathrm{A}} =$

$$\max_{1\le s\le S}\tau_s^{\mathrm{A}} - \min_{1\le s\le S}\tau_s^{\mathrm{A}} = \frac{r}{c}\left(\cos(\nu_{\bar{S}}+\varphi)-\cos(\nu_{\bar{s}}+\varphi)\right), \tag{8.53}$$

where we used the constant sum-distance property of the ellipse stated in Theorem 8.3, i.e., $\mathsf{d}(\mathrm{F}_1,\mathrm{I}_s)+\mathsf{d}(\mathrm{I}_s,\mathrm{F}_2) = \lambda\ \forall s$, and the definition of $\bar{S}$, $\bar{s}$ as in the statement of the Proposition. Using the trigonometric identity of the difference between two cosines in (8.53), (8.29) follows. Finally, using the sine rule [193, Sec. 12.7] in triangle $\mathrm{F}_1\mathrm{I}_s\mathrm{F}_2$, we get $\nu_s \triangleq \sin^{-1}\left(\{\|\mathbf{q}_s\|_2/\|\mathbf{q}_s-\bar{\mathbf{p}}\|_2\}\sin(\chi_s)\right)$, where χ_s can be determined as $\chi_s = \tan^{-1}([\mathbf{q}_s]_2/[\mathbf{q}_s]_1) - \omega$ (see Fig. 8.5.) Collecting all these terms into (8.53) completes the proof.

Appendix 8.F Proof of Theorem 8.5

Distributed IRS: Using (8.35), the ρ-outage probability in (8.30) is simplified as:

$$\mathbb{P}_{\rho}^{k} \overset{(a)}{=} \mathsf{Pr}\left\{ \left(\sum_{s=1}^{S} |\tilde{h}_s| \cos(\zeta_{s,k}) \operatorname{sinc}\left(\frac{M f_k}{2 f_c} \sin(\phi_s) \right) \right)^2 + \left(\sum_{s=1}^{S} |\tilde{h}_s| \sin(\zeta_{s,k}) \operatorname{sinc}\left(\frac{M f_k}{2 f_c} \sin(\phi_s) \right) \right)^2 \leq \rho / M^2 \right\}$$
$$\leq \mathsf{Pr}\left\{ \left(\sum_{s=1}^{S} |\tilde{h}_s| \cos(\zeta_{s,k}) \operatorname{sinc}\left(\frac{M f_k}{2 f_c} \sin(\phi_s) \right) \right)^2 \leq \rho / M^2 \right\},$$

where in (a), $\zeta_{s,k} \triangleq \pi(M-1) f_k \sin(\phi_s)/2 f_c$. By design, $\zeta_{s,k} \ll \pi/2$, so that $\cos(\zeta_{s,k}) > \xi > 0$, for $s \in [S]$ and some constant ξ. Using the definition of $\sigma_{\mathrm{h}}^{\min}$, we upper bound the above as

$$\mathbb{P}_{\rho}^{k} \leq \mathsf{Pr}\left(\sum_{s=1}^{S} \operatorname{sinc}\left(\frac{M f_k}{2 f_c} \sin(\phi_s) \right) \leq \sqrt{\rho} \Big/ M \xi \sigma_{\mathrm{h}}^{\min} \right). \tag{8.54}$$

Now, by using the 1st order Taylor's series, $\operatorname{sinc}(x) \geq 1 - \pi^2 x^2/6$; so, we can further upper bound (8.54) as

$$\mathbb{P}_{\rho}^{k} \leq \mathsf{Pr}\left(\sum_{s=1}^{S} \left\{ 1 - \frac{\pi^2 M^2 f_k^2}{24 f_c^2} \sin^2(\phi_s) \right\} \leq \sqrt{\rho} \Big/ M \xi \sigma_{\mathrm{h}}^{\min} \right)$$
$$= \mathsf{Pr}\left(\sum_{s=1}^{S} \sin^2(\phi_s) \geq \left\{ S - \frac{\sqrt{\rho}}{M \xi \sigma_{\mathrm{h}}^{\min}} \right\} \frac{24 f_c^2}{\pi^2 M^2 f_k^2} \right). \tag{8.55}$$

For $s = 1, \ldots, S$, $\phi_s \sim \mathcal{U}[\phi_s^{(1)}, \phi_s^{(2)}]$ are independent across IRSs, so that $X_s \triangleq \sin^2(\phi_s)$ are also independent random variables with mean $\mu_{X_s} \triangleq \mathbb{E}[\sin^2(\phi_s)]$ given by

$$\mu_{X_s} = \frac{1}{\phi_s^{(2)} - \phi_s^{(1)}} \int_{\phi_s^{(1)}}^{\phi_s^{(2)}} \sin^2(\phi) \mathrm{d}\phi = \frac{1}{2} - \frac{\sin\left(2\phi_s^{(2)}\right) - \sin\left(2\phi_s^{(1)}\right)}{4\left(\phi_s^{(2)} - \phi_s^{(1)}\right)}.$$

Let $\mu_X \triangleq \sum_{s=1}^{S} \mu_{X_s}$. Then, we simplify (8.55) as:

$$\mathbb{P}_{\rho}^{k} \leq \mathsf{Pr}\left(\sum_{s=1}^{S}(X_s - \mu_{X_s}) \geq \left\{S - \frac{\sqrt{\rho}}{M\xi\sigma_{\mathrm{h}}^{\min}}\right\}\frac{24f_c^2}{\pi^2 M^2 f_k^2} - \mu_X\right) \tag{8.56}$$

$$\overset{(b)}{\leq} \mathsf{Pr}\left(\sum_{s=1}^{S}(X_s - \mu_{X_s}) \geq \left\{S - \frac{\sqrt{\rho}}{M\xi\sigma_{\mathrm{h}}^{\min}}\right\}\frac{24f_c^2}{\pi^2 M^2 f_k^2} - S\mu_X^{\max}\right) \tag{8.57}$$

$$\overset{(c)}{\leq} e^{-2S\left(\left\{1-\frac{\sqrt{\rho}}{SM\xi\sigma_{\mathrm{h}}^{\min}}\right\}\frac{24f_c^2}{\pi^2M^2f_k^2}-\mu_X^{\max}\right)^2},$$

where in (b), we upper bounded the probability by lower bounding the tail in (8.56) using $\mu_X^{\max} \triangleq \max_{s\in[S]} \mu_{X_s}$; in (c), since $\rho \in (\rho_{\mathrm{D}}^{k}, 1)$, the tail value in (8.57) is positive, and we used the Hoeffding's inequality for bounded random variables [194], i.e., $0 \leq X_s \leq 1\ \forall s \in [S]$. This completes the proof of (8.31).

Centralized IRS: Consider the complementary probability

$$\bar{\mathbb{P}}_{\rho}^{k} \triangleq \mathsf{Pr}\left(\left\{\phi : |H[k]|^2 \geq \rho\right\}\right). \tag{8.58}$$

Upon simplifying (8.58) similar to the above, we get

$$\bar{\mathbb{P}}_{\rho}^{k} = \mathsf{Pr}\left(\mathrm{sinc}\left(\frac{Nf_k\sin(\phi)}{2f_c}\right) \geq \frac{\sqrt{\rho}}{N\sigma_{\mathrm{h}}}\right) \tag{8.59}$$

$$\overset{(d)}{\leq} \mathsf{Pr}\left(|\sin(\phi)| \leq \frac{2f_c\sigma_{\mathrm{h}}}{\pi f_k\sqrt{\rho}}\right) \overset{(e)}{=} \frac{1}{\phi_0}\sin^{-1}\left(\frac{2f_c\sigma_{\mathrm{h}}}{\pi f_k\sqrt{\rho}}\right),$$

where in (d), we used $\mathrm{sinc}(x) \leq 1/\pi|x|$, and this upper bounds the probability in (8.59); and in (e), for the values of ρ as in the statement of the theorem, with $\phi \sim \mathcal{U}[-\phi_0, \phi_0]$, we used the cumulative distribution function of $Y \triangleq |\sin(\phi)|$ given by

$$F_Y(\kappa) = \frac{1}{\phi_0}\int_0^{\kappa}\frac{1}{\sqrt{1-y^2}}\mathrm{d}y, \text{ if } \kappa \in (0, c_0),$$

with $\kappa = 2f_c\sigma_{\mathrm{h}}\big/\pi f_k\sqrt{\rho}$. Computing the complementary probability completes the proof of (8.32) and the theorem.

9 Wideband Beamforming in IRS-Aided Communications: Exploiting Beam-Split Effects via Opportunistic OFDMA

Chapter Highlights

In wideband systems operating at mmWave frequencies, intelligent reflecting surfaces (IRSs) equipped with many passive elements can compensate for channel propagation losses. Then, as mentioned in Chapter 8, a phenomenon known as the beam-split (B-SP) occurs in which the phase shifters at the IRS elements fail to beamform at a desired user equipment (UE) over the total allotted bandwidth (BW). While B-SP is commonly regarded as a performance-limiting impairment, in this chapter, we take an optimistic viewpoint and exploit the B-SP to improve system performance using orthogonal frequency division multiple access (OFDMA). We first show that, under the B-SP effect, the IRS inherently exhibits a *multi-directional beamforming* behavior, directing its energy toward different spatial angles at different frequency components. Capitalizing on this property, we then propose an opportunistic OFDMA scheme wherein the IRS phase shifts are randomly configured, and multiple UEs are *opportunistically* scheduled over different subcarriers (SCs) using a max-rate scheduling policy. We rigorously prove that, when the number of UEs is large, the B-SP can almost surely procure the optimal array gain on all SCs (possibly at different UEs). Subsequently, we characterize a sufficient condition on the number of UEs to witness near-optimal gains in practical systems. Finally, we show that the proposed OFDMA scheme enjoys multi-user diversity benefits, yielding further throughput enhancements beyond that obtained via optimal beamforming. Numerical simulations reveal that the OFDMA scheme outperforms the existing IRS-aided wideband beamforming solutions at low cost and complexity.

9.1 Introduction

Intelligent reflecting surfaces (IRSs) are envisioned to enhance the throughput of next-generation wireless systems [2, 176]. An IRS comprises numerous passive elements that apply controllable phase shifts to manipulate the wireless channel between nodes. By appropriately configuring these phase angles, the IRS can coherently combine the signal copies at the receiver (e.g., a user equipment (UE)), thereby improving the signal-to-noise ratio (SNR) and throughput. In high-frequency bands such as millimeter waves (mmWaves), where the propagation losses are severe, IRSs can help to enhance the channel quality [174, 195]. However, a large number of IRS elements is typically required to overcome the multiplicative path loss experienced in the cascaded base station (BS)-IRS-UE channel. In such cases, signal delay as it propagates across the IRS aperture may become comparable or even exceed the sampling duration, leading to the *spatial-wideband* (SW) effect, and, consequently, the *beam-split* (B-SP) effect in the frequency domain [178]. This chapter rigorously analyzes how the B-SP effect alters the directional response of an IRS and proposes an opportunistic orthogonal frequency division multiple access (OFDMA) scheme that exploits the B-SP to enhance system performance.

9.1.a Challenges, Importance and Novelty

A key objective of the next-generation wireless systems is to deliver enhanced mobile broadband (eMBB) connectivity to all devices, and one way to facilitate this is to perform communications in high-frequency bands like mmWave, where abundant spectrum is available, which can enhance the data rates [196]. However, mmWave signals suffer from severe propagation losses, which degrade the SNR and limit the coverage. To address this, IRSs have been proposed to create *virtual line-of-sight* (LoS) links between the BS and UE, thereby improving the signal strength [9]. As explained before, an IRS consists of numerous passive elements with individually tunable phase shifts that allow for constructive combining of the signals at the UE, in turn providing a beamforming/array gain. A large number of IRS elements is typically used to provide sufficient beamforming gain to compensate for the high path losses [140]. However, when a wide bandwidth (BW) is used

in conjunction with a large IRS array, the signal propagation delay across the IRS aperture can become comparable to or exceed the sampling period, even under LoS settings. This violates the narrowband condition and leads to a multi-tap channel in the time domain, and causes the *beam-split* (B-SP) effect, where the IRS fails to focus its beam at a given UE over the entire BW, thereby degrading the array gain and throughput [52, 54, 178].

Addressing the B-SP effect at the IRS is generally challenging because phase shifters can only approximate delays under narrowband conditions, where beamforming by controlling the phases is effective [63]. In wideband regimes, this approximation breaks down, making it difficult for an IRS to coherently beamform across the entire bandwidth. This reduction in array gain is a fundamental consequence of the fact that IRSs use phase shifters for beamforming. Thus, it is important and non-trivial to mitigate the B-SP effect for two main reasons: (a) the B-SP effect undermines the core advantage of using an IRS for enhancing the throughput in mmWave bands, and (b) existing solutions for mitigating B-SP in conventional antenna arrays cannot be directly applied to an IRS due to the passive nature and associated hardware & power constraints at the IRS.

As explained in the sequel, most prior work treats the B-SP effect as detrimental and advocates solutions to suppress it. In our work, we adopt a novel perspective wherein we propose a new scheme that exploits the B-SP effect, while still limiting the loss of array gain and improving the system performance.

9.1.b Related Work

First, most of the existing work on IRS-aided mmWave systems ignores B-SP-induced impairments (e.g., [9, 174, 195]), and hence overestimates the performance of IRS-aided wideband systems. This literature survey focuses on chapters discussing wideband effects in IRS-aided systems.

Considering beam-squint (B-SQ), a milder form of the B-SP effect, channel estimation and beam training methods were proposed in [46, 47], while [49] explored UE localization. IRS phase optimization to maximize sum-rate in OFDM systems was considered in [179],

and joint design of IRS and BS precoding for multiple-input multiple-output (MIMO) terahertz systems was studied in [13,14]. The ergodic rate performance of MIMO-OFDM under B-SQ was analyzed in [20], signal-to-interference-plus-noise ratio (SINR) maximizing IRS configurations were derived in [180], and in [51], phase shifts are optimized to adjust the beam widths of the IRS in an OFDMA framework. Along the lines of mitigating the SW effect, existing works often use true time-delay (TTD) units at the IRS to compensate for the excess signal delay across the aperture, thereby eliminating the SW effects [52]. In [54], the design of TTD-enabled IRS was investigated, [53] considered the use of delay-phase units to eliminate the B-SP effects in both far-field and near-field scenarios, and in [55], the TTDs and BS precoder were jointly optimized to maximize the sum-rate of a multi-user system. However, using TTD units at an IRS 1) increases the number of TTD units and demands more hardware and space; 2) increases the power consumption due to necessity for precise delay compensation, and 3) requires a self-interference cancellation mechanism due to the full-duplex nature of the IRS elements that have to continuously receive signals from the BS, apply a delay, and then reflect the signal toward the UE [177]. In particular, to the best of our knowledge, no chapter in the literature describes the hardware implementation and demonstration of a TTD-enabled IRS. Finally, in our prior work [197], also described in Chapter 8, we show that instead of a TTD-based IRS, appropriately splitting a large IRS into multiple distributed IRSs and placing them at carefully chosen locations can naturally mitigate the B-SP effects without compromising on the performance and has low complexity. However, this approach targets scheduling a single UE across the entire BW, and the effectiveness of it to mitigate the B-SP critically depends on the placement of IRSs relative to the BS and UE locations. Hence, this solution is well suited for scenarios where a single UE or a cluster of UEs, such as those in a small, dense hotspot; it is less effective when the UEs may be arbitrarily located.

In contrast with the above approaches, which aim to mitigate the B-SP effect, this chapter explores an opportunistic OFDMA scheme that takes an optimistic view of the B-SP effect and leverages it to enhance system performance through randomly configured IRS phase shifts. Although [16, 198] address problems related to IRS-assisted OFDMA, they focus

on sub-6 GHz bands where B-SP effects are not significant.

9.1.c Contributions of this chapter

By revisiting the modeling of a large IRS-aided mmWave wideband system from first principles, we first demonstrate the emergence of the B-SP effect at a given UE and how it degrades the array gain at the UE across the BW allocated to it. We then argue that, by the *law of conservation of energy*, the IRS must redirect energy towards other spatial directions on frequencies where the IRS fails to coherently reflect towards the intended UE. Motivated by this observation, we make the following key contributions in this chapter.

1. **Directional response**: We first show that an IRS configured to reflect in a specific direction at one frequency also exhibits directionality at other angles on different frequency components. We derive a closed-form expression that illustrates this directional response of the IRS (see Lemma 9.1.)

2. **Multi-directional beamforming**: Using the derived directional response of the IRS, we identify the sub-BW over which the IRS beamforms in a fixed direction while maintaining the array gain within the half-power beamwidth. Subsequently, we show that the B-SP effect enables the IRS to simultaneously beamform toward multiple resolvable directions over non-overlapping sub-bands within the total system BW (see Lemma 9.2 and Theorem 9.1.)

3. **Exploiting B-SP via opportunistic OFDMA**: Leveraging the multi-directional response of IRS under the B-SP effect, we show that when there are a large number of UEs and the IRS phases are randomly sampled from an appropriate distribution, on every subcarrier (SC), at least one UE will almost surely procure the full array gain from the IRS (see Theorem 9.2.)

4. **Scaling of number of UEs**: We next determine a sufficient number of UEs to obtain near-optimal beamforming gain across the entire BW with high probability; we show that the number of UEs scales linearly in the number of resolvable beams formed by the IRS (see Proposition 9.1.)

5. **Rate-scaling law**: Finally, considering an opportunistic OFDMA framework which employs a max-rate scheduler, we derive the system throughput, and show that it not only exploits the B-SP effect and delivers full array gain on every SC but also harnesses multi-user diversity benefits over the BW to further enhance performance. (see Theorem 9.3.)

Through extensive numerical simulations, we validate that the proposed scheme effectively exploits the B-SP effect to achieve full beamforming gain across all SCs, thereby significantly improving overall throughput. For example, we show that with just 20 UEs, in a system with 1024 element IRS operating over a BW of 400 MHz centered at 30 GHz, the proposed opportunistic OFDMA with randomized IRS configuration outperforms the conventional round-robin (RR) scheduling-based scheme, where the entire BW is allocated to a single UE with the IRS optimized for it. Thus, an opportunistic OFDMA framework, even with randomly configured IRS phase coefficients, can effectively mitigate the adverse impact of the B-SP effect from a network-level perspective while requiring low time and computational complexities.

9.2 System Model and Problem Statement

We consider a downlink wideband mmWave system where a BS equipped with N_t antennas serves K UEs. The system uses OFDM modulation with N SCs spanning a total BW of W centered at a carrier frequency f_c, and is assisted by an M-element IRS to enhance the throughput of the system. We consider that the antenna array at the BS and the IRS are implemented as a uniform linear array (ULA) with inter-element spacing d_{BS}, and d_{IRS}, respectively.[1] For simplicity of exposition, we consider a single antenna at the UEs, and the approach directly extends to multiple antenna UEs also. Further, due to the sparse scattering of signals at mmWave frequencies, we model the channel between the nodes with line-of-sight (LoS) components, as described next.

[1]The ideas pursued in this chapter can be directly applied to other types of array geometries at the BS/IRS. For example, in Remark 9.2, we discuss how the results of this chapter extend to a planar array-based geometry.

9.2.a Channel Model

In the downlink mode of the communication, the baseband impulse response of the channel from the n'th antenna at BS to the mth IRS element can be written as [46]

$$g_{n',m}(t) = \alpha_{n',m} e^{-j2\pi f_c \tau^{\mathsf{BI}}_{n',m}} \delta(t - \tau^{\mathsf{BI}}_{n',m}), \tag{9.1}$$

where $\delta(t)$ is the Dirac-delta function, $\alpha_{n',m}$ corresponds to the large scale channel parameter (accounting for the path loss) from the n'th antenna at the BS to mth element of the IRS, and $\tau^{\mathsf{BI}}_{n',m}$ is the delay in the channel from n'th BS antenna to mth IRS element. Similarly, the impulse response of the channel in the baseband domain from the mth IRS element to UE-k is given by

$$u_{m,k}(t) = \beta_{m,k} e^{-j2\pi f_c \tau^{\mathsf{IU}}_{m,k}} \delta(t - \tau^{\mathsf{IU}}_{m,k}), \tag{9.2}$$

where $\beta_{m,k}$ and $\tau^{\mathsf{IU}}_{m,k}$ denote the large-scale parameter and delay in the channel from the mth IRS element to UE-k.

Thus, the impulse response of the overall channel from the n'th BS antenna to UE-k via the IRS can be written as[2]

$$h_{n'}(t) = \sum\nolimits_{m=1}^{M} \theta_m g_{n',m}(t) \circledast u_{m,k}(t) \tag{9.3}$$

$$= \sum\nolimits_{m=1}^{M} \theta_m \alpha_{n',m} \beta_{m,k} \delta\left(t - \tau^{\mathsf{BI}}_{n',m} - \tau^{\mathsf{IU}}_{m,k}\right) e^{-j2\pi f_c \left(\tau^{\mathsf{BI}}_{n',m} + \tau^{\mathsf{IU}}_{m,k}\right)}, \tag{9.4}$$

where $\circledast$ denotes the linear convolution operator, and θ_m is the reflection coefficient tuned at the mth IRS element modeled as $\theta_m = \zeta_m e^{j\vartheta_m}$, where ζ_m and ϑ_m denote the amplitude and phase of the reflection coefficient at mth IRS element. For simplicity, we consider that $\zeta_m = 1 \; \forall m \in [M] \triangleq \{1, \ldots, M\}$.

Using the properties of the ULA geometry, the channel delays via the IRS relative to a

[2] We neglect the direct path between the BS and the UEs due to the high attenuation losses faced by the mmWave signals [31], [80, Sec. IV.A].

$$h_{n'}(t) = \sum_{m=1}^{M} \theta_m \alpha_{n',m} \beta_{m,k} \delta \left(t - \tau_{n'}^{\mathsf{BI_0}} - \eta_k^{\mathsf{I_0U}} - \frac{d_{\mathrm{IRS}}}{c}(m-1)\left(\sin(\psi) - \sin(\omega_k)\right) \right) \times e^{-j2\pi f_c (\tau_{n'}^{\mathsf{BI_0}} + \eta_k^{\mathsf{I_0U}})} e^{-j2\pi f_c \frac{d_{\mathrm{IRS}}}{c}(m-1)(\sin(\psi)-\sin(\omega_k))}. \quad (9.7)$$

reference IRS element can be expressed as:

$$\tau_{n',m}^{\mathsf{BI}} = \tau_{n'}^{\mathsf{BI_0}} + \frac{d_{\mathrm{IRS}}}{c}(m-1)\sin(\psi), \quad (9.5)$$

$$\tau_{m,k}^{\mathsf{IU}} = \eta_k^{\mathsf{I_0U}} - \frac{d_{\mathrm{IRS}}}{c}(m-1)\sin(\omega_k), \quad (9.6)$$

where $\tau_{n'}^{\mathsf{BI_0}}, \eta_k^{\mathsf{I_0U}}$ are the signal propagation delays from n'th BS antenna to reference IRS element, and reference IRS element to UE-k, respectively; $c = 3 \times 10^8$ m/s denotes the speed of light; ψ and ω_k represent the direction of arrival (DoA) from the BS and departure (DoD) towards UE-k, respectively, at the IRS. Now, using (9.5) and (9.6) in (9.4), the channel to UE-k from the n'th BS antenna can be simplified as given in (9.7) at the top of the next page.

Similarly, we express the delay from n'th BS antenna as

$$\tau_{n'}^{\mathsf{BI_0}} = \eta^{\mathsf{BI_0}} + (n'-1)\frac{d_{\mathrm{BS}}}{c}\sin(\chi), \quad (9.8)$$

where $\eta^{\mathsf{BI_0}}$ is the propagation delay from the reference BS antenna to the reference IRS element, and χ is the DoD at the BS towards the IRS. Let $\eta_k \triangleq \eta^{\mathsf{BI_0}} + \eta_k^{\mathsf{I_0U}}$ denote the overall propagation delay from the reference antenna at the BS to UE-k via the reference element of the IRS. Further, since the large-scale path loss is nearly the same across the BS/IRS array, we let $\alpha_{n',m} \approx \alpha$, and $\beta_{m,k} \approx \beta_k \ \ \forall n' \in [N_t], m \in [M]$ [46].

Let $p_{n'}(t)$ denote the response of the transmit precoding filter used at the n'th BS antenna. Then, the effective channel at UE-k is given by

$$h(t) = \sum_{n'=1}^{N_t} h_{n'}(t) \circledast p_{n'}(t). \quad (9.9)$$

Now, using (9.7) in (9.9) and simplifying, the final form of $h(t)$ can be obtained as given

$$h(t) = \sum_{n'=1}^{N_t} \sum_{m=1}^{M} \theta_m \bar{\alpha} \bar{\beta}_k \delta \left(t - \eta_k - \frac{d_{\text{BS}}}{c}(n'-1)\sin(\chi) - \frac{d_{\text{IRS}}}{c}(m-1)\left(\sin(\psi) - \sin(\omega_k)\right) \right) \circledast p_{n'}(t) \times e^{-j2\pi f_c \left(\frac{d_{\text{BS}}}{c}(n'-1)\sin(\chi) + \frac{d_{\text{IRS}}}{c}(m-1)(\sin(\psi)-\sin(\omega_k)) \right)}, \quad (9.10)$$

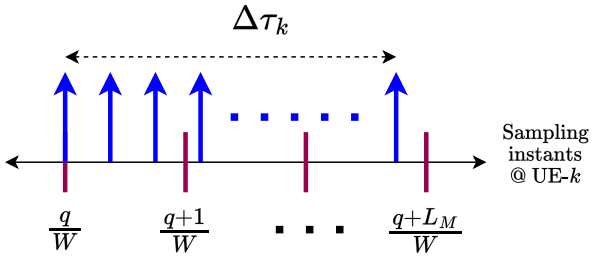

Figure 9.1: Illustration of SWE when the SDS $\Delta\tau_k$ spans L_M taps.

in (9.10) on the next page, where $\bar{\alpha} \triangleq \alpha e^{-j2\pi f_c \eta^{\mathsf{BI}_0}}$ and $\bar{\beta}_k \triangleq \beta_k e^{-j2\pi f_c \eta_k^{\mathsf{I}_0\mathsf{U}}}$ denote the complex channel gain in the BS-IRS and IRS-UE links, respectively.

9.2.b Spatial-Wideband Effect

The expression for the channel given in (9.10) corresponds to a multipath scenario where every BS antenna and each IRS element act as a scatterer and provide a copy of the transmitted signal at the UE. Thus, the *spatial delay spread* (SDS) induced by the channel at UE-k, denoted by $\Delta\tau_k$, is

$$\Delta\tau_k = \frac{d_{\text{BS}}}{c}(N_t - 1)\sin(\chi) + \frac{d_{\text{IRS}}}{c}(M-1)\left(\sin(\psi) - \sin(\omega_k)\right). \quad (9.11)$$

Clearly, the SDS in the channel at UE-k depends on the DoD at the BS, DoA, and DoD at the IRS: If $\sin(\psi) - \sin(\omega_k) = 0$, and $\chi = 0$, the SDS is 0, and if $\sin(\psi) - \sin(\omega_k) = 2$ and $\chi = 90°$, the SDS takes the maximum value given by $\Delta\tau_{k,\max} = (N_t - 1)\frac{d_{\text{BS}}}{c} + 2(M-1)\frac{d_{\text{IRS}}}{c}$. However, when the SDS becomes comparable to or exceeds $T_s = 1/W$, the narrowband condition is violated and the channel becomes frequency-selective, resulting in the spatial-wideband effect (SWE) [178]. The SWE occurs when the delay incurred by the signal while propagating across the aperture of the BS or IRS becomes comparable to the

sampling duration of the signal, and gives rise to a frequency-selective multi-tap channel (see Figure 9.1). Note that the SWE arises even with pure LoS paths in the channel. Hence, different from conventional multipath links due to multiple distributed scatterers, the frequency-selective properties under the SWE result in a different phenomenon called the beam-split effect, as described next.

9.2.c The Beam-Split Effect

Owing to the frequency selectivity induced by the SWE, OFDM becomes a natural choice for the transmission of data signals. To this end, applying a Fourier transform to (9.10), the frequency response of the channel to UE-k on a baseband frequency f (with $|f| \leq W/2$) can be obtained as

$$H_k(f) = \bar{\alpha}\bar{\beta}_k e^{-j2\pi f \eta_k} \sum_{n'=1}^{N_t} e^{-j2\pi(f+f_c)(n'-1)\frac{d_{\mathrm{BS}}}{c}\sin(\chi)} P_{n'}(f) \times \sum_{m=1}^{M} e^{-j2\pi(f+f_c)(m-1)\frac{d_{\mathrm{IRS}}}{c}(\sin(\psi)-\sin(\omega_k))} e^{j\vartheta_m}, \quad (9.12)$$

where the symbols are as defined previously and $P_{n'}(f)$ is the frequency response of the filter $p_{n'}(t)$. Since our goal is to enhance the throughput, maximizing the channel gain in (9.12) is desirable. In this view, by using the Cauchy-Schwarz inequality, we can obtain $|H_k(f)|^2 \leq |U_k(f)|^2$, where

$$|U_k(f)|^2 \triangleq \left|\bar{\alpha}\bar{\beta}_k N_t\right|^2 \left| \sum_{m=1}^{M} e^{-j2\pi(f+f_c)(m-1)\frac{d_{\mathrm{IRS}}}{c}\sin(\phi_k)} e^{j\vartheta_m} \right|^2, \quad (9.13)$$

with $\phi_k \triangleq \sin^{-1}_{(p)}(\sin(\psi) - \sin(\omega_k))$ being the cascaded channel angle at UE-k via the IRS, and $\sin^{-1}_{(p)}(x)$ is defined such that x lies in the principal argument of the inverse sine function, $[-1, 1)$ [33], [80, Eq. 32]. Note that, for any k, we can achieve the upper bound $|U_k(f)|^2$ in (9.13) when

$$P_{n'}(f) = e^{j2\pi(f+f_c)(n'-1)\frac{d_{\mathrm{BS}}}{c}\sin(\chi)}, \quad (9.14)$$

which corresponds to the transmit filter response given by

$$p_{n'}(t) = \delta\left(t + (n'-1)\frac{d_{\text{BS}}}{c}\sin(\chi)\right) e^{j2\pi f_c(n'-1)\frac{d_{\text{BS}}}{c}\sin(\chi)}. \tag{9.15}$$

Interestingly, the transmit filter achieving the upper bound is independent of the UE being served, so that the full-beamforming gain from the BS array can be obtained using a single UE-independent precoding configuration (of course, the array gain achieved does depend on the UE index). We refer the reader to Remark 9.1 at the end of this section for further details on the implementation of the transmit filter in (9.15).

Suppose we tune the IRS phase to maximize the channel gain at the centre frequency, $f = 0$, that is, we set

$$\vartheta_m = j2\pi f_c(m-1)\frac{d_{\text{IRS}}}{c}\sin(\phi_k). \tag{9.16}$$

Then, with $P_{n'}(f)$ chosen as per (9.14), the overall channel gain on a baseband frequency f with $M > 1$ can be simplified as

$$\begin{aligned}|H_k(f)|^2 &= \left|\bar{\alpha}\bar{\beta}_k N_t\right|^2 \left|\sum\nolimits_{m=1}^{M} e^{-j2\pi f(m-1)\frac{d_{\text{IRS}}}{c}\sin(\phi_k)}\right|^2 \\ &\overset{(a)}{=} \left|\gamma_k^{\mathsf{C}}\right|^2 M^2 \operatorname{sinc}^2\left(\frac{Mf}{2f_c}\sin(\phi_k)\right),\end{aligned} \tag{9.17}$$

where in (a), we defined $\gamma_k^{\mathsf{C}} \triangleq \bar{\alpha}\bar{\beta}_k N_t$ and the fact that $\sin(x) \approx x$, when $x = \pi f d_{\text{IRS}}\sin(\phi_k)/c \ll 1$; $\operatorname{sinc}(x) \triangleq \frac{\sin(\pi x)}{\pi x}$, and we set $d_{\text{IRS}} = \lambda_c/2$, where λ_c is the carrier wavelength. From (9.17), we see that, unless $f = 0$ or $\phi_k = 0$, the UE experiences a reduced array gain relative to the maximum value of M^2 at other frequency components within the BW; this is known as the *beam-split (B-SP) effect.*

More generally, if we configure the IRS coefficients to form a beam at UE-k on the nth SC of the OFDM system, $n \in [N]$, the overall channel gain at UE-k on frequency f is

$$|H_k(f)|^2 \approx M^2\left|\gamma_k^{\mathsf{C}}\right|^2 \operatorname{sinc}^2\left(\frac{M(f_n - f)}{f_c}\sin(\phi_k)\right), \tag{9.18}$$

where $f_n = \frac{nW}{N} - \frac{W}{2} - \frac{W}{2N}$ is the baseband frequency of nth SC. We pictorially illustrate the adverse impact of the B-SP effect in Fig. 9.2. When the BW, or the number of IRS

Variable	Definition	Variable	Definition
M	Number of elements at an IRS	$h_k(t)$	Impulse response of channel at UE-k
K	Total number of UEs	$H_k(f)$, $H(k,t,f)$	Frequency response of channel at UE-k Channel at UE-k in time slot t on frequency f
N	Number of subcarriers in OFDM	N_t	Number of antennas at the BS
$\tau_{m,k}^{\mathsf{IU}}$, $\tau_{n',m}^{\mathsf{BI}}$, $\tau_{n'}^{\mathsf{BI}_0}$	Delay from mth IRS element to UE-k; n'th BS antenna to mth IRS element; n'th BS antenna to reference IRS element	$\eta_k^{\mathsf{I}_0\mathsf{U}}$, η^{BI_0}, η_k	Delay from reference (ref.) IRS elmnt. to UE-k; Ref. BS antenna to ref. IRS element; Ref. BS antenna tto UE-k via ref. IRS element
$p_n(t)$, $P_n(f)$	Impulse/Frequency response of precoding filter at nth BS antenna	$\bar{\alpha}$, $\bar{\beta}_k$	Complex ch. gains of BS-IRS, IRS-UE-k links
$\phi_k, \varphi_k^{\mathsf{C}}$	Cascaded channel angle at UE-k in physical and normalized domain	$\rho_1, \rho_{2,k}$	Path loss of BS-IRS, IRS-UE-k links
χ, ω_k, ψ	Angle of departure from BS-IRS; IRS to UE-k; angle of arrival at IRS from BS	P/σ^2	Ratio of total transmit power to noise power on a subcarrier
$\boldsymbol{\theta}, \vartheta_m$	Phase shift vector at the IRS, phase applied at the mth IRS element	f_c, f_n	Carrier frequency, baseband frequency of nth subcarrier
c	Velocity of light: 3×10^8 m/s	W	Bandwidth of operation
$d_{\text{BS}}, d_{\text{IRS}}$	Inter-elemental spacing at BS/IRS	λ	Signal wavelength at carrier frequency

Table 9.1: Commonly encountered variables/notations in chapter 9.

elements, or both, become large, the resulting degradation in array gain due to the B-SP effect becomes a major limitation in the deployment of IRSs for wideband communication systems.

9.2.d Problem Statement

From the above discussion, it is evident that the B-SP effect prevents a single UE from achieving the full array gain of M^2 over the entire signal BW. Although the B-SP effect can be mitigated by reducing the number of IRS elements M or the BW W, it has the undesirable consequence of decreasing the overall system throughput. On the other hand, intuitively, if the IRS does not form a beam in a single direction on all SCs, by the *law of conservation of energy*, the reflected energy must necessarily be radiated in different directions across the SCs. In effect, the IRS forms beams pointing towards different UEs in the system across the SCs. Motivated by this, we propose to employ an OFDMA scheme, where different UEs are scheduled across the SCs, thereby *exploiting the B-SP effect*. Specifically, we answer the following:

1. How does the directional response of the IRS vary across the BW under the B-SP

effect when IRS configurations are tuned to reflect in a specific direction at a given frequency?[3]

2. Under the B-SP effect, develop and analyze an OFDMA scheme that schedules different UEs on distinct SCs by formulating and solving the following scheduling problem:

   Maximize the system throughput obtained over T time slots w.r.t. all schedulers $\mathsf{SCH}(n,t)$, where $\mathsf{SCH} : [N] \times [T] \to [K]$ maps the SC index n and time slot t to UE index k:

$$\max_{\mathsf{SCH}(n,t)} \frac{1}{T} \sum_{t=1}^{T} \sum_{n=1}^{N} \frac{W}{N} \log_2 \left(1 + \frac{P}{N_t N \sigma^2} |H(\mathsf{SCH}(n,t), t, f_n)|^2 \right), \tag{P0}$$

   where P is the total transmit power, which is divided equally across the N SCs, σ^2 is the noise variance per SC, and $H(k,t,f)$ is the channel to UE-k at time (slot) t and on frequency f. The factor N_t accounts for the power normalization since the BS is equipped with N_t antennas.

We address these aspects in Secs. 9.3 and 9.4, respectively.

Remark 9.1 (Using true-time delay units at the BS and IRS)**.** *From* (9.15)*, we note that each BS antenna applies a timing advance via a TTD unit, which introduces a frequency-dependent phase shift, followed by a frequency-independent phase. While a TTD-enabled array is feasible at the BS, equipping each IRS element with a TTD unit to counteract the SW effect significantly increases hardware complexity and power consumption due to the need for high-precision delays and the requirement of a self-interference cancellation mechanism to handle the full-duplex operation, as explained in Sec. 9.1.b. These practical limitations restrict the applicability of TTDs at the IRS.*

Remark 9.2 (Extension to other geometry)**.** *The B-SP effect arises regardless of the array geometry employed at the BS or IRS. However, its severity is governed by the number of*

[3]We note that B-SQ and B-SP effects can arise in both far-field and near-field scenarios [53]. For the sake of illustrating our core idea, in this chapter, we focus on the case where the BS/UEs are in the far-field of the IRS(s). Extension to near-field scenarios is relegated to future work.

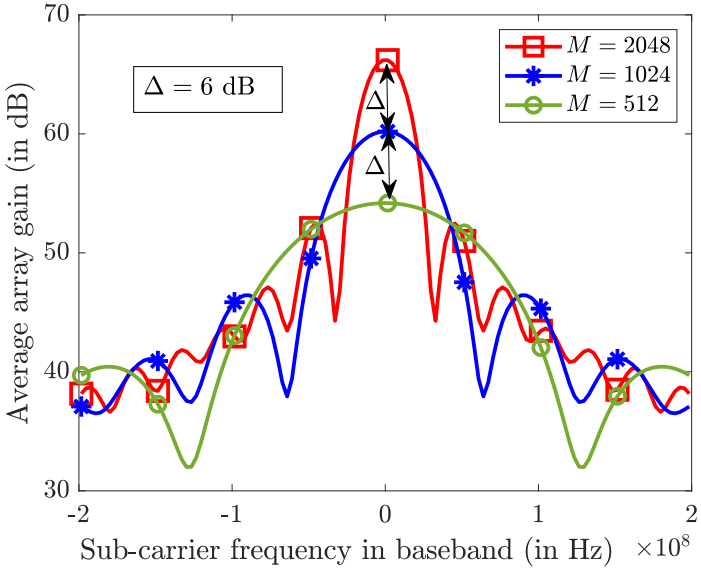

Figure 9.2: Average array gain vs. SC frequency when IRS is optimized to $f_n = 0$ for different number of IRS elements, M, with $W = 400$ MHz. Although the gain at $f_n = 0$ increases with M, the gain on other SCs degrades as M increases due to the B-SP effect.

elements across the array aperture. For example, in planar arrays, elements along the diagonal contribute to the B-SP effects. Accordingly, our proposed ideas and methods generalize to arbitrary array geometries by appropriately scaling the number of elements across the aperture of the array geometry.

Notation: For general notations used in this chapter, see the section on "General Mathematical Notations" on page ix. For the notations/variables specific to this chapter, please refer to Table 9.1.

9.3 Beam-split Enables Multi-Directional Beamforming at the IRS

To accurately characterize the frequency-selective properties of the channel at a UE under the B-SP effect, we first rewrite (9.13) for $d_{\text{IRS}} = \lambda_c/2$ compactly as follows:

$$|H_k(f)|^2 = |\gamma_k^{\mathsf{C}}|^2 \left| \boldsymbol{\theta}^H \mathbf{a}_M \left(\sin_{(p)}^{-1} \left\{ \left(1 + \frac{f}{f_c} \right) \sin(\phi_k) \right\} \right) \right|^2, \tag{9.19}$$

where $\boldsymbol{\theta} \triangleq \left[e^{-j\vartheta_1}, e^{-j\vartheta_2}, \ldots, e^{-j\vartheta_M}\right]^T$ is the IRS configuration vector (with conjugate phases introduced for notational compactness), and $\mathbf{a}_M(x)$ is the array steering response vector of an M-element ULA oriented at the angle x given by

$$\mathbf{a}_M(x) \triangleq \left[1, e^{-j\pi \sin(x)}, \ldots, e^{-j(M-1)\pi \sin(x)}\right]^T. \tag{9.20}$$

9.3.a Directional Response of the IRS under B-SP effect

In Lemma 9.1 below, we determine the directional response of the IRS on the frequencies across the BW of operation when the IRS is tuned to a given frequency within the BW.

Lemma 9.1. *Let $f_0, \tilde{f}_0 \in [-W/2, W/2]$ be two frequency components within the BW of operation in the baseband domain. If the IRS is configured to reflect in a cascaded spatial direction of ϕ at frequency f_0, then, on frequency $\tilde{f}_0$, the IRS reflects at a cascaded angle $\tilde{\phi}$ given by*

$$\tilde{\phi} = \sin^{-1}_{(p)}\left\{\left(\frac{f_0 + f_c}{\tilde{f}_0 + f_c}\right)\sin(\phi)\right\}. \tag{9.21}$$

Proof. See Appendix 9.A. ■

Lemma 9.1 reinforces the fact that under the influence of the B-SP effect, the IRS can no longer focus towards the desired UE located in a given cascaded angle over the entire BW of operation unless $\phi = 0$. However, as alluded to in Sec. 9.2.d, by the law of conservation of energy, the IRS has to necessarily form a beam in a different direction on frequencies other than the frequency to which the IRS is tuned, and the above lemma formally captures this aspect.

9.3.b Frequency Response of the IRS under B-SP effect

We note that Lemma (9.1) characterizes the directional response of an IRS, specifying the direction at which the IRS beamforms on a given frequency when it is actually tuned to reflect in a chosen direction on a different frequency. However, if the angular shift across two different frequencies exceeds the *Rayleigh resolution limit* of an array [63], the IRS effectively beamforms in multiple resolvable directions over the system bandwidth. In this view, we have the following result.

Lemma 9.2. *In an M-element IRS-aided wideband system with BW equal to W, the half-power beam width (HPBW) of the beam formed by the IRS towards the cascaded angle of ϕ on frequency f spans only a sub-band whose BW is given by*

$$W_\phi = \min\left\{\frac{4}{\pi}\sqrt{6\left(1-\frac{1}{\sqrt{2}}\right)}\cdot\frac{f_c}{M\sin(\phi)}, W\right\}. \tag{9.22}$$

Proof. See Appendix 9.B. ■

We now make the following remarks based on Lemma 9.2:

1. The BW W_ϕ corresponding to the HPBW of the beam formed by the IRS in direction ϕ is independent of the tuned frequency f_0. This indicates that the IRS exhibits a multi-directional response when it is tuned to any frequency within this BW. However, W_ϕ varies with ϕ because the impact of the B-SP depends on ϕ, as characterized in (9.17).

2. Even if the entire BW W is allotted to a single UE located at a physical angle of ϕ, the IRS provides the beamforming gain to this UE only over an effective BW given by (9.22).

9.3.c The Multi-directional Beamforming

Based on the preceding discussions, when the IRS is tuned to reflect in direction ϕ_1 at a particular frequency, Lemma 9.1 characterizes its response across spatial directions, while Lemma 9.2 captures its response as a function of different frequency components within the BW. We now combine both these results and provide the main result of this section, which establishes the *multi-directional beamforming* property of the IRS under the B-SP effect.

Theorem 9.1. *Consider an M-element IRS-aided wideband system operating over a bandwidth of W around the carrier frequency f_c. Let $f_L \triangleq f_c - W/2$ denote the lower-edge frequency component of the band, and suppose the IRS is tuned to align with a cascaded angle ϕ_1 on the 1st sub-band, whose center frequency is*

$$f_1' \triangleq f_L + \frac{W_{\phi_1}}{2} = f_L + \frac{2}{\pi}\sqrt{6\left(1-\frac{1}{\sqrt{2}}\right)}\cdot\frac{f_c}{M\sin(\phi_1)}. \tag{9.23}$$

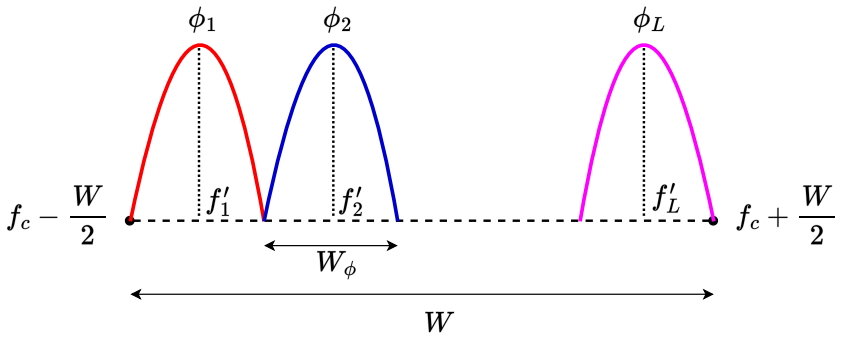

Figure 9.3: Illustration of multi-directional beamforming with B-SP effect.

Now construct the set $\Phi_{\phi_1} \triangleq \{\phi_1, \ldots, \phi_{L_{\phi_1}}\}$ *as follows:*

$$\phi_\ell = \sin^{-1}_{(p)} \left\{ \left(\frac{f_1' + f_c}{f_\ell' + f_c} \right) \sin(\phi_1) \right\}, \quad \ell = 2, \ldots, L_{\phi_1}, \tag{9.24}$$

where the frequencies $\{f_\ell'\}_\ell$ *are given by*

$$f_\ell' = f_1' + (\ell - 1)\sqrt{6\left(1 - \frac{1}{\sqrt{2}}\right)} \frac{4f_c}{M\pi \sin(\phi_1)}, \tag{9.25}$$

for $\ell = 2, \ldots, L_{\phi_1}$ *and* L_{ϕ_1} *is given by*

$$L_{\phi_1} \triangleq \left\lceil \frac{MW \sin(\phi_1)}{1.7 f_c} \right\rceil. \tag{9.26}$$

Then, Φ_{ϕ_1} *constitutes a set of* resolvable angles, *i.e.,* $|\sin(\phi_i) - \sin(\phi_j)| \geq \mathcal{O}\left(\frac{1}{M}\right)$ *for* $i \neq j$, $i, j = 1, 2, \ldots, L_{\phi_1}$, *and such that the normalized correlation response of the IRS on the* ℓ*th sub-band obeys*

$$\rho_{\ell,\ell'} \triangleq \frac{1}{M^2} \left| \mathbf{a}_M^H(\phi_\ell) \mathbf{a}_M(\phi_{\ell'}) \right|^2 = \begin{cases} 1, & \text{if } \phi_{\ell'} = \phi_\ell, \\ \kappa, & \text{if } \phi_{\ell'} \neq \phi_\ell, \end{cases} \tag{9.27}$$

$\forall \ell' \in [L]$, *where* κ *is a small number s.t.* $\kappa \to 0$ *as* $M \to \infty$. *Consequently,* L_{ϕ_1} *in* (9.26) *is the number of resolvable beams formed by the IRS when it is tuned to reflect in direction* ϕ_1.

Proof. See Appendix 9.C. ■

From Theorem 9.1, we note that the number of beams formed by the IRS, L_ϕ, depends on the ratio MW/f_c, which is the term that controls the impact of the B-SP effect in (9.17). Clearly, when B-SP is not negligible, $MW/f_c > 1$, and the number of beams formed increases linearly with this ratio. Similarly, when the B-SP effect is negligible, i.e., $MW/f_c \ll 1$, (9.26) yields $L_\phi = 1$, which is consistent with the existing studies on IRS-aided mmWave systems where the IRS is envisioned to beamform at a given UE over the full BW [9, 174, 195]. To illustrate Theorem 9.2 in a practical case, consider a 5G NR compliant IRS-aided mmWave system with $M = 1024$, $W = 400$ MHz, $\phi = 90°$, and $f_c = 30$ GHz. Then, using (9.26), we get $L_\phi \approx 8$; which means the IRS can beamform up to 8 resolvable directions at the same time; each covering a BW equal to $400/8 = 50$ MHz and spanning the HPBW of a beam. Theorem 9.1 is pictorially illustrated in Fig. 9.3.

Capitalizing on the *multi-directional beamforming*, we next propose the *opportunistic OFDMA scheme* that exploits the B-SP effect of the IRS to maximize the system throughput.

9.4 Exploiting Beam Split Via Opportunistic OFDMA

Since the B-SP effect causes a degradation in the achievable array gain over the BW if a single UE were to be scheduled over the entire BW, we propose to adopt an OFDMA framework wherein we schedule multiple UEs on different SCs. This fits naturally into the constraints imposed by the B-SP effect since no single UE is typically allotted the full BW. This motivates us to exploit the B-SP effect and enhance the throughput via an opportunistic OFDMA scheme.

To this end, we first solve for the optimal scheduler $\mathsf{SCH}(\cdot)$ in (P0) and then analyze the effectiveness of OFDMA in exploiting the B-SP effect to enhance the system performance.

9.4.a The Opportunistic OFDMA for Exploiting the Beam-Split

From (P0), we note that the scheduler $\mathsf{SCH}(n,t)$ is decoupled across all N SCs and T time slots; thus it can equivalently posed as solving NT independent optimization problems with the solution to $\mathsf{SCH}(n,t)$ depending on only the nth SC and tth time slot. Then, invoking

the monotonicity property of the $\log(\cdot)$ function, the optimal scheduler that solves (P0) is one that maximizes the channel gain on each SC in every slot, i.e.,

$$\forall n \in [N], t \in [T],\ \mathsf{SCH}^{\text{opt}}(n,t) = \underset{k\in[K]}{\arg\max}\ |H(k,t,f_n)|^2, \tag{9.28}$$

and scheduler which implements (9.28) is referred to as the max-rate scheduler in the rest of this chapter. We call the overall scheme *opportunistic OFDMA* because the system opportunistically schedules different UEs across the system BW and time to maximize the aggregate throughput, for a given IRS configuration (or sequence of configurations over time). However, note that different IRS configurations can lead to different scheduling outcomes and throughputs. Hence, we propose to randomly configure the IRS from a distribution that is aware of the channel model in every time slot [103]. Now, since the UEs can be located anywhere at random in the system, we model the sine of the cascaded angle at different UEs as a uniform random variable: $\varphi_k^{\mathsf{C}} \triangleq \sin(\phi_k) \overset{d}{=} \tilde{\varphi}^{\mathsf{C}} \overset{\text{i.i.d.}}{\sim} \mathcal{U}[-1,1]$, where $\overset{d}{=}$ stands for "equal in distribution" [80]. Then, using [103, Sec. III.C], the random IRS configurations are sampled independently across slots as

$$\phi_m(t) = \pi(m-1)a(t),\ a(t) \overset{\text{i.i.d.}}{\sim} \mathcal{U}[-1,1],\ t \in [T]. \tag{9.29}$$

Further, in [199], it has been shown that randomly sampling the IRS phase angles as per (9.29) is throughput-optimal in a narrowband setting. We use the above random configuration in the wideband setting also, mainly because it is simple to implement (no coordination with the BS is required), and, as we will see, it offers superlative performance.

Now, to illustrate how the B-SP effect can be exploited, using (9.29) in (9.19), we deduce that the channel gain at the kth UE on the nth SC at time slot t is given by

$$|H(k,t,f_n)|^2 = M^2\left|\gamma_k^{\mathsf{C}}\right|^2 \text{sinc}^2\left(M\left(a(t) - \varphi_k^{\mathsf{C}}\left(1+\frac{f_n}{f_c}\right)\right)\right). \tag{9.30}$$

Then, for a given $a(t)$ at slot $t \in [T]$, on every SC $n \in [N]$, if there exists at least one UE $k^*(t,n) \in [K]$ such that

$$a(t) - \varphi_{k^*(t,n)}^{\mathsf{C}}\left(1+\frac{f_n}{f_c}\right) \approx 0, \tag{9.31}$$

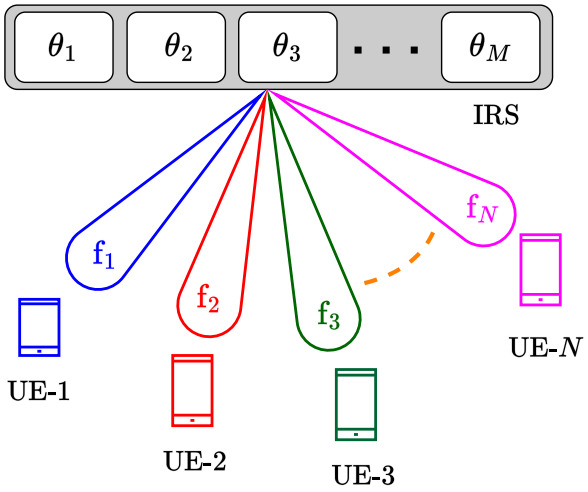

Figure 9.4: Illustration of opportunistic OFDMA by exploiting the B-SP. Different colors indicate different frequency sub-bands.

we can nearly achieve the maximum array gain of M^2 for every $t \in [T]$ and $n \in [N]$ by scheduling UE $k^*(t,n)$. This way, in mmWave bands with large bandwidth, each SC can obtain the optimal array gain of M^2 in every time slot by exploiting multi-user diversity. This is illustrated in Fig. 9.4. In Sec. 9.4.b, we formally show that under the B-SP effect and with a large number of UEs, at least one UE almost surely achieves the full array gain on every SC and time slot. Subsequently, we use this to analyze the achievable throughput of the above-described opportunistic OFDMA scheme in Sec. 9.4.d.

9.4.b Eliminating B-SP via Multi-user Diversity Almost Surely

To facilitate further analysis, we define the *normalized array gain*, $G_M(k,t,n)$, acheived by UE-k on SC-n in slot t via an M-element IRS whose configurations are randomly chosen according to (9.29) as

$$G_M(k,t,n) \triangleq \frac{|H(k,t,f_n)|^2}{M^2\left|\gamma_k^{\mathsf{C}}\right|^2} \in [0,1], \tag{9.32}$$

with $G_M(k,t,n) = 1$ implying that a full-array gain is obtained. We then have the following theorem.

Theorem 9.2. *In an M-element IRS-aided wideband system with N subcarriers and K UEs, when we tune the IRS using randomized configurations sampled as per (9.29), the*

normalized array gain defined in (9.32) *satisfies*

$$\lim_{K\to\infty} \mathsf{Pr}\left(\bigcap_{n=1}^{N}\bigcup_{k=1}^{K}\left\{\varphi_k^{\mathsf{C}} \in [-1,1] : G_M(k,t,n)=1\right\}\right) = 1. \tag{9.33}$$

As a result, the IRS almost surely provides the full array gain of M^2 *(possibly at different UEs) over the entire BW, i.e.,*

$$\mathsf{Pr}\left(\left\{\lim_{K\to\infty} \forall t\in[T], \forall n\in[N], \exists\ k^*(t,n)\in[K] : |H(k^*,t,f_n)|^2 = \left|\gamma_{k^*}^{\mathsf{C}}\right|^2 M^2\right\}\right) = 1, \tag{9.34}$$

where $k^*(t,n)$ *denotes UE selected at slot* t *and SC* n*.*

Proof. See Appendix 9.D. ■

Theorem 9.2 shows that the B-SP effect at the IRS can be positively leveraged to obtain the full-array gain at multiple UEs. In hindsight, the result can be attributed to the *multi-directional beamforming* capability of the IRS under the B-SP effect, as described in Theorem 9.1, which enables the IRS to form beams across a range of spatial directions.

9.4.c How Many UEs are Sufficient in Practice?

In the previous section, we theoretically proved hat we can obtain *full array gain* from the IRS as $K\to\infty$. A related question of practical interest is: *Under what scaling of the number of UEs does the near-beamforming condition hold with high probability?* We answer this next.

Proposition 9.1. *Let* $\epsilon,\delta\in(0,1)$ *be small positive constants. Consider an IRS-aided wideband system with* M *reflecting elements,* N *subcarriers spanning a total bandwidth of* W*, and a carrier frequency of* f_c*. If the number of UEs,* K*, satisfies*

$$K \geq K^* \triangleq -\frac{\ln\left(\frac{N}{\delta}\right)}{\ln\left(1-\frac{\sqrt{3\epsilon}}{\pi M\left(1+(W/2f_c)\right)}\right)}, \tag{9.35}$$

then, with probability at least $1-\delta$*, there exists at least one UE on every subcarrier that achieves an array gain of* $(1-\epsilon)M^2$*.*

Proof. See Appendix 9.E. ■

Based on Proposition 9.1, to effectively exploit the B-SP effect and obtain full array gain over the BW, the minimum number of UEs, K^*, scales as follows:

1. As δ decreases, we target a higher probability of success. For this, the number of UEs scales as $\mathcal{O}(\ln(1/\delta))$. In particular, as $\delta \to 0$, $K^* \to \infty$, consistent with Theorem 9.2.

2. Reducing ϵ corresponds to a lower tolerance for degradation in the achievable array gain of M^2. This, in turn, requires K^* to scale roughly as $\mathcal{O}(1/\sqrt{\epsilon})$ so that at least one UE aligns closely with the IRS beam direction. This is again consistent with Theorem 9.2. (see also [127, Prop. 1].)

3. As either M (the number of IRS elements) or W (system BW) increases, the B-SP effect becomes more pronounced, leading to a larger number of IRS-formed beams, in accordance with Theorem 9.1. Consequently, more UEs are needed so that at least one can be scheduled corresponding to every distinct beam formed by the IRS.

   In fact, when $MW/2f_c \ll 1$, we can approximate $-\ln(1-x) \approx x$ in the denominator of (9.35), and observe that $K^* \sim \Omega\left(MW \Big/ f_c\right) \sim \Omega(L_{90^\circ})$, where L_{90° is the number of resolvable beams formed by the IRS as given in (9.26) with $\phi = 90^\circ$. This is because the system requires at least as many UEs as the maximum number of resolvable beams that can be formed by the IRS via the B-SP effect.

We note that the requirement on the number of UEs in our design aligns well with current wireless system practices and does not represent an additional requirement specific to our study. Notably, one of the key wireless use-cases is massive machine-type communications (MMTC), which is envisioned to support 10^6 users per km^2 [77].[4]

9.4.d Acheivable Throughput

Having established that the B-SP effect enables full array gain at different UEs across the BW, we now derive the achievable throughput under the opportunistic OFDMA scheme

[4]For example, in a small cell of radius 100 m and a user activity rate of 10%, there will be a few hundred active UEs at a given time; roughly the scale of the number of UEs we consider in this work.

described in Sec. 9.4.a when $\bar{\alpha}$ is modeled as a deterministic channel with $|\bar{\alpha}|^2 = \rho_1$ [199], while $\bar{\beta}_k \sim \mathcal{CN}(0, \rho_{2,k})$ represents a Rayleigh fading channel. Here, ρ_1 and $\rho_{2,k}$ denote the respective path losses. For analytical tractability, we assume that all UEs experience identical path loss, similar to [75].

Theorem 9.3. *The system throughput of an OFDMA scheme in a randomly configured IRS (as per (9.29)) aided wideband system using a max-rate scheduler (as per (9.28)) and equal power allocation across all SCs satisfies*

$$\lim_{K\to\infty} \left(R^{(K)} - \mathcal{O}\left\{ W \log_2 \left(1 + \frac{\rho P}{N\sigma^2} N_t M^2 \ln K \right) \right\} \right) = 0,$$

where $\rho \triangleq \rho_1\rho_2$ is the cascaded path loss across the UEs, and other symbols are as defined earlier.

Proof. See Appendix 9.F. ■

Theorem 9.3 confirms that a channel gain of $\mathcal{O}(M^2)$ can indeed be obtained on all SCs by exploiting the B-SP effects at the IRS. Further, in the presence of channel fading, we can get an additional SNR boost by a factor of $\ln K$, which is the benefit of multi-user diversity, similar to that derived in [103, Theorem 4] for sub-6 GHz systems on top of the array gain from the BS antennas that scales linearly in N_t.

Remark 9.3. *In our proposed scheme, to implement the opportunistic scheduler, the BS should know the index of the UE with the best channel gain on each SC. This can be obtained using efficient, low-complexity feedback schemes on an SC-by-SC basis. For e.g., the timer-feedback mechanism in [82] uses a single pilot, and on every SC, the UE with the best channel quality feeds back to the BS much earlier than other UEs. Thus, the proposed scheme reaps optimal IRS gains without requiring channel estimation or phase optimization algorithms, making it attractive for implementing and performing wideband communications using an IRS.*

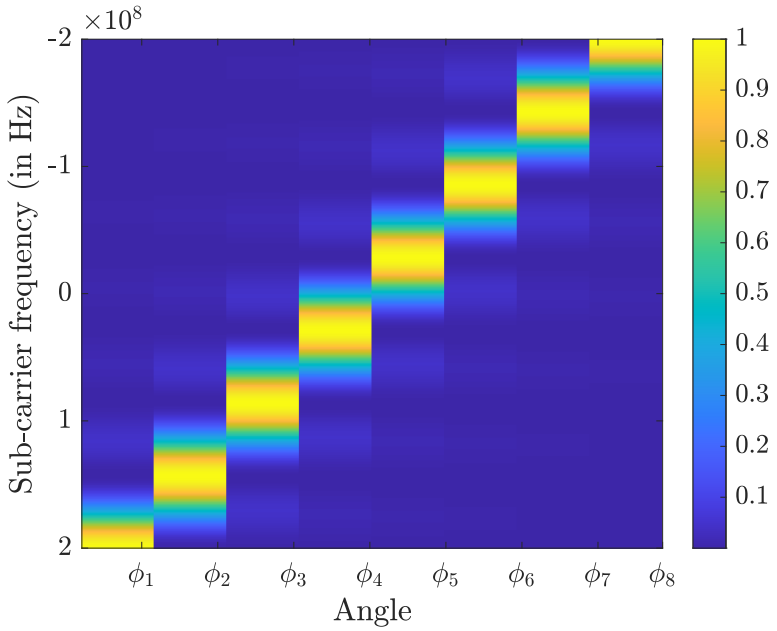

Figure 9.5: Heat map of the normalized array gain as a function of angle & frequency at $\phi = 90°$.

9.5 Numerical Results

We numerically illustrate the throughput enhancement obtained by exploiting the B-SP effect via OFDMA using Monte Carlo simulations. The OFDM framework spans a bandwidth of $W = 400$ MHz at an mmWave carrier frequency of $f_c = 30$ GHz using $N = 1024$ SCs. The BS is located at $(0, 0)$ and an $M = 1024$ element IRS is located at $(100, 100)$ (meters). The UEs are uniformly distributed around the IRS such that the cascaded angles span the interval $(50°, 90°)$. The BS uses a total transmit power of $P = 40$ dBm, and the receiver noise power is $\sigma^2 = -120$ dBm. The path loss is modeled as $\mathsf{PL} = C_0 \left(d_0/d_{\text{link}}\right)^{\mu_{\text{link}}}$, where $C_0 = -60$ dB is the path loss at the reference distance of $d_0 = 1$ m, d_{link} is the link distance, and μ_{link} denotes the path loss exponent, set to 2 and 2.2 in the BS-IRS and IRS-UE links, respectively [46, 106].

9.5.a Multi-Directional Property of the IRS under B-SP Effect

We first illustrate the multi-directional beamforming property of the IRS given in Theorem 9.1 under the B-SP effect.

In Fig. 9.5, we present a heatmap of the normalized array gain as a function of angle

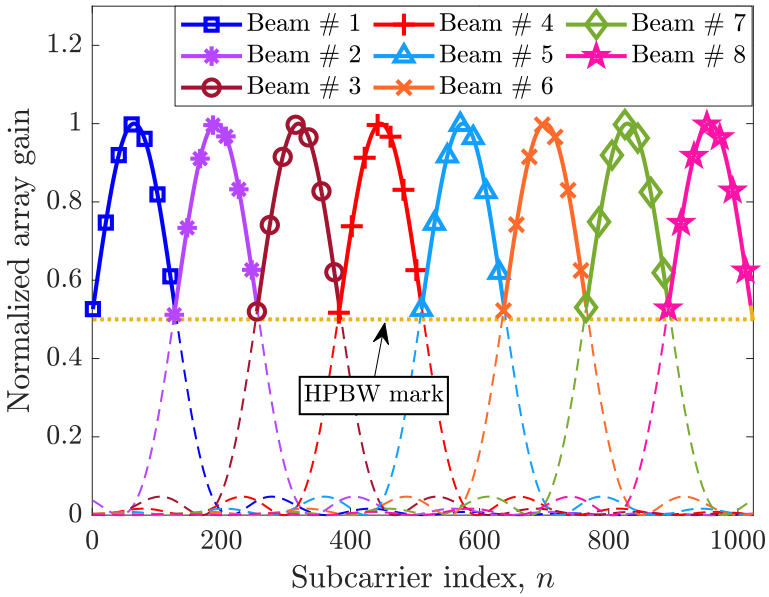

Figure 9.6: Envelope of the normalized array gain vs. SC frequency at $\phi = 90°$.

and subcarrier frequency in the baseband domain. The values along the x-axis represent the angles specified in Theorem 9.1. From the heatmap, we observe that the IRS indeed reflects its energy in different directions as we sweep across the BW.

In Fig. 9.6, we plot the normalized gain of the IRS as a function of SC frequency when it is configured to reflect toward $\phi = 90°$ at the center frequency, $f_n = 0$. Each curve, labeled Beam #1 to #8, represents the IRS response in a specific direction, corresponding to the angles derived in Lemma 9.1 for $f_n = 0$, $\phi = 90°$, and $\tilde{f}_0$ set to $\{f'_\ell\}_{\ell=1}^{L_\phi}$ determined using (9.25) from Theorem 9.1. The figure shows that the IRS achieves full array gain in different *resolvable* directions (i.e., the angles which do not lie within the HPBW of the beam formed on other angles) over distinct frequency bands centered around the frequencies given by (9.25), thereby confirming that the IRS exhibits multi-directional beamforming simultaneously across multiple contiguous and non-overlapping sub-bands. Furthermore, the number of resolvable beams formed across the system BW is 8 in this figure, which matches the theoretical value derived in Theorem 9.1.

In Fig. 9.7 and Fig. 9.8, we repeat the previous experiment with the IRS now configured to reflect toward $\phi = 50°$ at the center frequency $f_n = 0$. Similar to the earlier case, we observe that the IRS provides beamforming gain in multiple directions across different

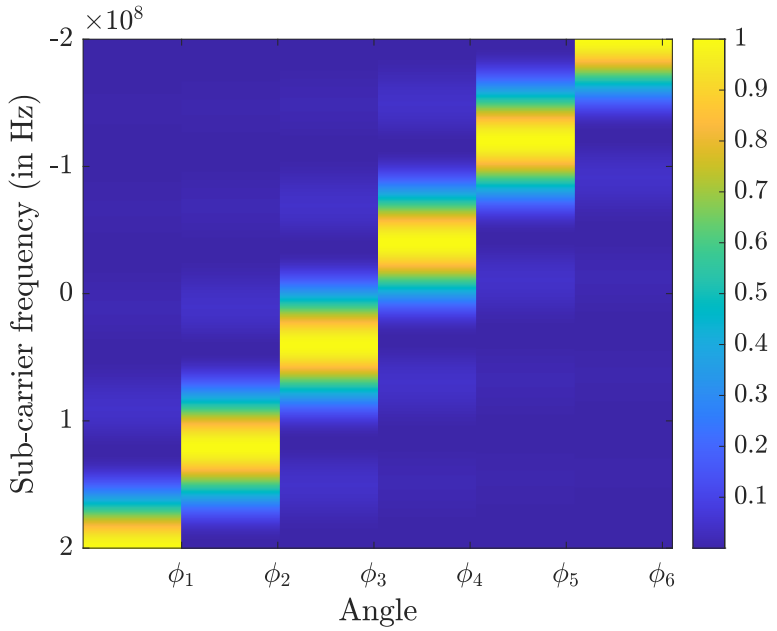

Figure 9.7: Heat map of the normalized array gain as a function of angle & frequency at $\phi = 50°$.

SCs, showing its ability to form several resolvable beams over the BW. However, unlike Fig. 9.5 and Fig. 9.6, the number of beams formed across the system bandwidth is smaller for $\phi = 50°$ compared to $\phi = 90°$. This reduction arises because, as the reflection angle moves away from 90°, the signal experiences a relatively smaller SDS through the IRS, as described in (9.11). Consequently, the SWE and the resulting B-SP phenomenon become less pronounced. According to Theorem 9.1, a weaker B-SP leads to fewer resolvable beams. Thus, this experiment highlights that both the beamforming capability of the IRS and the number of beams it can form depend on the angle at which it is configured to reflect at $f_n = 0$.

9.5.b Performance of Opportunistic OFDMA under B-SP Effect

Leveraging the multi-directional beamforming capability of the IRS, we now turn our attention to demonstrating the performance of the proposed opportunistic OFDMA scheme.

Figure 9.9 illustrates the normalized array gain averaged over the UEs vs. the baseband SC frequency for three scenarios:

1. A single UE is scheduled in each time slot across the full BW using RR scheduling,

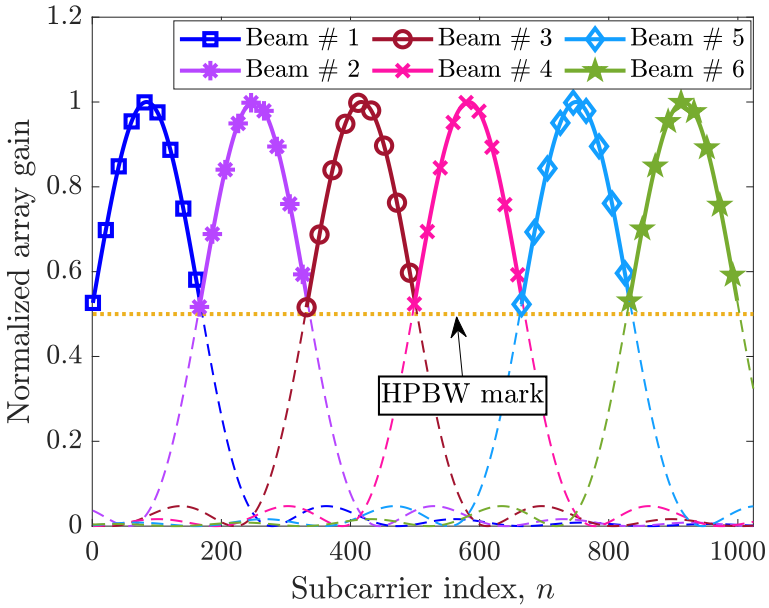

Figure 9.8: Envelope of the normalized array gain vs. SC frequency at $\phi = 50°$.

where the IRS is optimized for the scheduled UE at $f_n = 0$ in every slot.

2. The IRS is randomly configured according to (9.29), and UEs are served via OFDMA using a max-rate scheduler, assuming no channel fading (i.e., γ_k^{C} is deterministic.)

3. The IRS is again randomly configured as per (9.29), but UEs are scheduled using the max-rate scheduler while accounting for random channel fading.

In the RR case (with the curve marked as "`Round-robin SU-OFDM...`"), the array gain peaks at $\mathcal{O}(M^2)$ only at $f_n = 0$, and significantly deteriorates at other subcarriers due to the B-SP effect. This clearly demonstrates how a phase-shifter is not sufficient to beamform a wideband signal. In contrast, when multiple UEs are multiplexed via OFDMA, the average channel gain observed at the BS becomes more uniform across the BW. Notably, in the absence of fading, the gain remains flat at its peak value of $\mathcal{O}(M^2)$, highlighting the advantage of leveraging B-SP through OFDMA. When channel fading is included, the average gain increases further owing to multi-user diversity and clearly outperforms even the peak gain achieved with RR scheduling. Finally, we also benchmark our scheme against the widely adopted approach that employs TTD units at the IRS to mitigate the

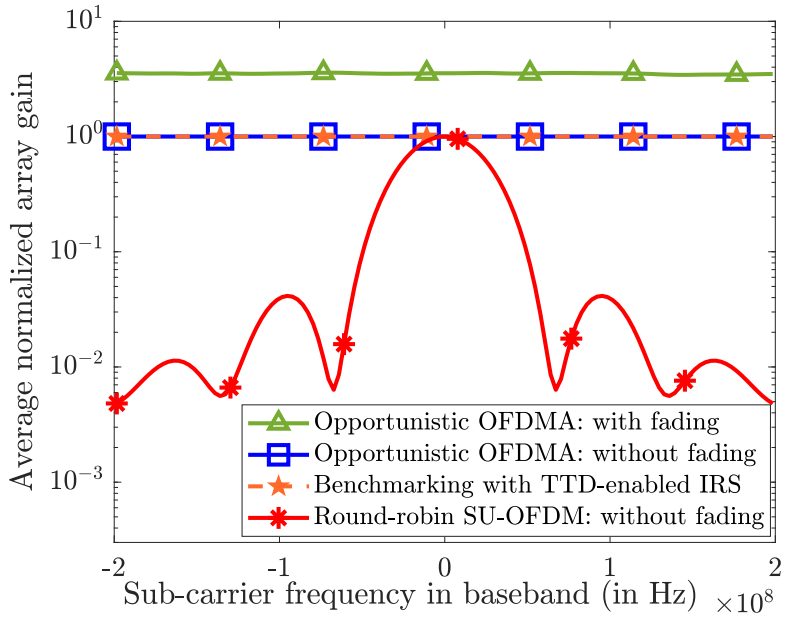

Figure 9.9: Avg. normalized array gain with $K = 1000$, $M = 1024$.

B-SP effect, as discussed in Sec. 9.1.b. The results show that the proposed method not only outperforms the TTD-based scheme but also offers significant advantages in terms of implementation. Specifically, the proposed scheme retains the use of a more practical phased-array-based IRS and circumvents the three major sources of complexity associated with TTD-based IRSs, as detailed in Sec. 9.1.b. This validates that our approach is a low-complexity yet effective solution for harnessing the benefits of IRSs even in wideband beamforming scenarios.

Next, in Fig. 9.10, we evaluate the system throughput as a function of the number of UEs, K, for the three scenarios outlined in the previous paragraph. In the RR case, the rate falls short of the ideal scaling $\mathcal{O}(\log_2(M^2))$ due to the B-SP effect and remains constant with increasing K, since RR scheduling does not exploit multi-user diversity. In contrast, with a max-rate scheduler, the rate increases with K because it *opportunistically* schedules the UEs with better channel conditions. In the absence of channel fading, the throughput exceeds that achieved under RR scheduling with as few as 20 UEs and gradually converges to the optimal rate scaling of $\mathcal{O}(\log_2(M^2))$ for larger values of K (in fact, just $K = 200$ UEs are sufficient), in line with Theorem 9.2. When channel fading is present, multi-user diversity yields an additional gain, improving the rate to $\mathcal{O}(\log_2(M^2 \ln K))$, as predicted by

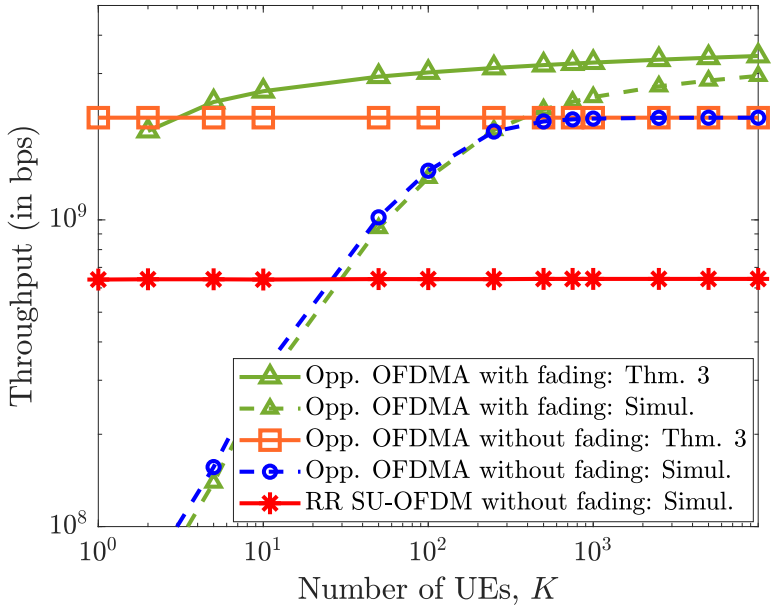

Figure 9.10: Throughput vs. No. of UEs, K, for $M = 1024$.

Theorem 9.3. These results demonstrate that by leveraging the B-SP effect and employing opportunistic scheduling across the SCs with multiple UEs, the proposed scheme achieves near-optimal performance on all SCs simultaneously.

Finally, in Fig. 9.11, we evaluate the effectiveness of the proposed scheme by plotting the system throughput versus the number of IRS elements (on a log-scale) for the three scenarios. For small M, all curves exhibit a slope of $2W$, indicating that the full array gain of M^2 is realized across all SCs spanning a BW of W. However, as M increases, the B-SP effect becomes significant, causing the slope of the RR scheduler curve to fall below $2W$. In contrast, the slope remains close to $2W$ for the max-rate scheduling scenarios, confirming that the full array gain from the IRS is retained across all SCs by exploiting the B-SP effect via opportunistic scheduling. The vertical offsets between the curves with and without fading reflect the additional rate gains from multi-user diversity in the presence of fading, which scale as $\mathcal{O}(\log \ln K)$.

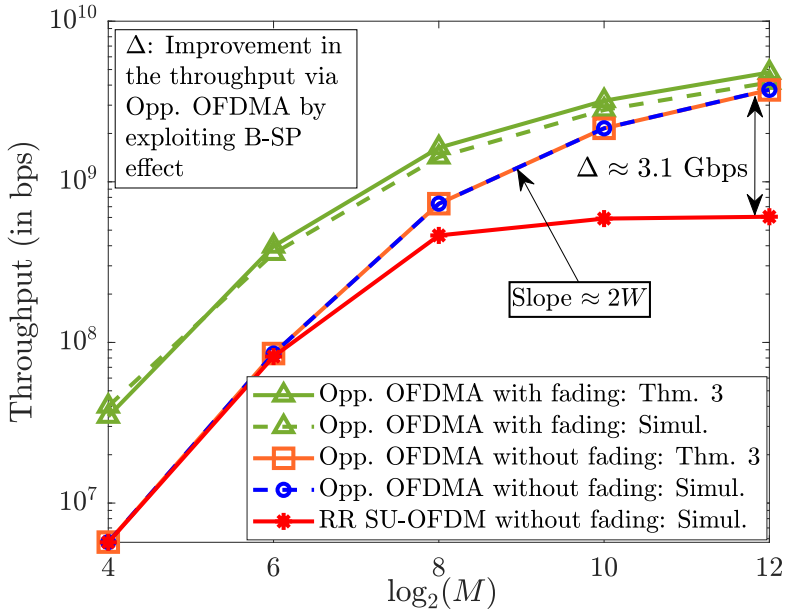

Figure 9.11: Throughput vs. No. of IRS elements, M, for $K = 5000$.

9.6 Conclusions

In this chapter, we demonstrated that the B-SP effect, which is typically considered a limitation in IRS-aided wideband systems, can instead be harnessed to enhance the system performance. We first established that, under the B-SP effect, the IRS exhibits a multi-directional beamforming property, which enables the IRS to focus its reflected energy toward different spatial directions on different SCs. Exploiting this property of the B-SP effect, we showed that by employing an OFDMA framework with a max-rate scheduling policy, it is possible to almost surely achieve the full array gain of the IRS on all SCs, provided a sufficiently large number of UEs are present in the system. We then derived the corresponding rate scaling laws and proved that the proposed scheme not only achieves the optimal beamforming gain over the entire BW, but also benefits from multi-user diversity, leading to further performance enhancements. Future directions can include integrating fairness-aware UE scheduling and addressing quality-of-service constraints like guaranteed rate requirements, etc.

Appendix 9.A Proof of Lemma 9.1

From (9.19), dropping the index k for simplicity, and using the Cauchy-Schwarz inequality, the IRS phase configuration that maximizes $|H(f)|^2$ and reflects the transmitted signal in a cascaded angle of ϕ on frequency f_0 is given by

$$\boldsymbol{\theta}^{\text{opt}} = \mathbf{a}_M \left(\sin_{(p)}^{-1} \left\{ \left(1 + \frac{f_0}{f_c} \right) \sin(\phi) \right\} \right). \tag{9.36}$$

To determine the directional response of the IRS vector in (9.36) on another frequency $\tilde{f}_0$, we first evaluate the beam-scanning function, which is defined as follows.

$$g(\nu) \triangleq \left| \boldsymbol{\theta}^{\text{opt}\,H} \mathbf{a}_M \left(\sin_{(p)}^{-1} \left\{ \left(1 + \frac{\tilde{f}_0}{f_c} \right) \sin(\nu) \right\} \right) \right|^2 \tag{9.37}$$

$$= \left| \sum_{m=1}^{M} e^{j\pi(m-1)\left\{ \left(1+\frac{f_0}{f_c}\right) \sin(\phi) - \left(1+\frac{\tilde{f}_0}{f_c}\right) \sin(\nu) \right\}} \right|^2 \tag{9.38}$$

$$= \frac{\sin^2 \left(\frac{\pi M}{2} \left\{ \left(1 + \frac{f_0}{f_c} \right) \sin(\phi) - \left(1 + \frac{\tilde{f}_0}{f_c} \right) \sin(\nu) \right\} \right)}{\sin^2 \left(\frac{\pi}{2} \left\{ \left(1 + \frac{f_0}{f_c} \right) \sin(\phi) - \left(1 + \frac{\tilde{f}_0}{f_c} \right) \sin(\nu) \right\} \right)} \tag{9.39}$$

$$\overset{(a)}{\approx} M^2 \mathbb{F}_M^2 \left(\left(1 + \frac{f_0}{f_c} \right) \sin(\phi) - \left(1 + \frac{\tilde{f}_0}{f_c} \right) \sin(\nu) \right), \tag{9.40}$$

where in (a), $\mathbb{F}_M(x)$ is the Fejér Kernel [200], which satisfies

$$\mathbb{F}_M(x) = \begin{cases} 1 + o(M), & \text{if } x = 0, \\ 0, & \text{if } x \in \mathbb{Z} \backslash \{0\}, \\ o(M), & \text{if } x \in \mathbb{R} \backslash \mathbb{Z}. \end{cases} \tag{9.41}$$

Thus, to evaluate the angle at which the IRS vector has the largest response on frequency $\tilde{f}_0$, we set the argument of $\mathbb{F}_M(x)$ in (9.40) to 0, which upon simplification along with letting $\nu = \tilde{\phi}$ yields the desired result in (9.21).

Appendix 9.B Proof of Lemma 9.2

When the IRS is set to align with the channel at a UE whose cascaded angle is ϕ on frequency f_0, the corresponding IRS configuration vector is given by (9.36). Then, the normalized IRS response on another frequency band centered at $\tilde{f}_0$ in the direction of ϕ can be evaluated as

$$\rho(\tilde{f}_0) \triangleq \frac{1}{M^2}\left|\boldsymbol{\theta}^{\text{opt}\,H}\mathbf{a}_M\left(\sin^{-1}_{(p)}\left\{\left(1+\frac{\tilde{f}_0}{f_c}\right)\sin(\phi)\right\}\right)\right|^2. \tag{9.42}$$

By simplifying (9.42) similar to the proof of Lemma 9.1, we get

$$\rho(\tilde{f}_0) = \left(\frac{\sin\left\{\frac{\pi M}{2}\left(\frac{f_0-\tilde{f}_0}{f_c}\right)\sin(\phi)\right\}}{M\sin\left\{\frac{\pi}{2}\left(\frac{f_0-\tilde{f}_0}{f_c}\right)\sin(\phi)\right\}}\right)^2, \tag{9.43}$$

which achieves the maximum when $f_0 = \tilde{f}_0$ or $\phi = 0$. Now, the frequency points corresponding to the HPBW of the beam formed by the IRS towards ϕ at f_0 can be obtained by setting $\rho(\tilde{f}_0) = 0.5$. Further, by using $|f_0 - \tilde{f}_0|/f_c \ll 1$ and $\sin(x) \approx x$ for $x \ll \pi$, from (9.43), we obtain a simplified relation for determining the sub-BW covering the HPBW of the beam as:

$$\text{sinc}\left(\frac{M\sin(\phi)}{2}\left(\frac{f_0-\tilde{f}_0}{f_c}\right)\right)^2 \geq \frac{1}{2}. \tag{9.44}$$

Using the 1st order Taylor's approximation: $\text{sinc}(x) \approx 1-\frac{\pi^2x^2}{6}$, which is tight in the regime of our interest, (9.44) simplifies to

$$\left|f_0-\tilde{f}_0\right| \leq \Delta f_\phi \triangleq \frac{2}{\pi}\sqrt{6\left(1-\frac{1}{\sqrt{2}}\right)}\cdot\frac{f_c}{M\sin(\phi)}, \tag{9.45}$$

From (9.45), we deduce that on a frequency component $\tilde{f}_0$ which is away from f_0 by a factor of least Δf_ϕ, the IRS gain response in the direction of ϕ drops below the peak gain by at least a factor of $1/2$. Therefore, (9.45) characterizes the *effective one-sided bandwidth* for which appreciable array gain (corresponding to the HPBW) can be obtained from the

IRS in the direction of ϕ. Since $\tilde{f}_0$ can lie on either side of the frequency component f_0, (9.22) can be obtained by setting $W_\phi = 2\Delta f_\phi$ and noting that W_ϕ cannot exceed W.

Appendix 9.C Proof of Theorem 9.1

We first note that the frequencies $\{f'_\ell\}_{\ell=1}^{L_{\phi_1}}$ form an arithmetic progression with a common difference precisely equal to W_{ϕ_1}, as characterized in Lemma 9.2. According to Lemma 9.1, the angles $\{\phi_\ell\}_{\ell=1}^{L_{\phi_1}}$ defined in (9.24) correspond to the directions in which the IRS forms beams at frequencies f'_ℓ, for $\ell = 2, \ldots, L_{\phi_1}$, when the IRS is actually configured to reflect toward the direction ϕ_1 at frequency f'_1.

Now, since W_{ϕ_1} quantifies the effective sub-BW over which the HPBW of the beam formed by the IRS extends, a frequency separation of at least W_{ϕ_1} between adjacent f'_ℓ ensures that the corresponding beam directions ϕ_ℓ are sufficiently separated in the angular domain, i.e., by $\mathcal{O}(1/M)$, which marks the Rayleigh resolution limit of the array. Consequently, these directions become *resolvable* by the IRS, and hence satisfy the resolvability condition given in (9.27).

Finally, the total number of resolvable beams formed by the IRS across the entire bandwidth when it is tuned to reflect toward ϕ_1 at $f = f'_1$ can be obtained by taking the ratio of the total bandwidth W to the effective sub-BW W_{ϕ_1} associated with the HPBW of a single beam. That is,

$$N_{\text{res}} = \frac{W}{W_{\phi_1}} = \frac{\pi}{4}\left(\sqrt{6\left(1 - \frac{1}{\sqrt{2}}\right)}\right)^{-1} \cdot \frac{MW\sin(\phi_1)}{f_c}, \tag{9.46}$$

which, upon simplification and rounding up to the next largest integer, denoted by L_{ϕ_1}, gives the expression in (9.26).

Appendix 9.D Proof of Theorem 9.2

To prove (9.33), by using the continuity of probability, it suffices to show that

$$\mathsf{Pr}\left(\lim_{K\to\infty}\bigcap_{n=1}^{N}\bigcup_{k=1}^{K}\left\{\varphi_k^{\mathsf{C}}\in[-1,1]:G_M(k,t,n)=1\right\}\right)=1, \tag{9.47}$$

which means to establish that as $K\to\infty$, the event $\mathcal{A}_K\triangleq\bigcap_{n=1}^{N}\bigcup_{k=1}^{K}\left\{\varphi_k^{\mathsf{C}}\in[-1,1]:G_M(k,t,n)=1\right\}$ occurs almost surely.

Now, by involking a result from [201, Sec 7.2, Lemma 10(a)], a necessary and sufficient condition for (9.47) to hold true can be rewritten as: $\forall\epsilon>0$,

$$\mathsf{Pr}\left(\lim_{K\to\infty}\sup\bigcup_{n=1}^{N}\bigcap_{k=1}^{K}\left\{\varphi_k^{\mathsf{C}}:|G_M(k,t,n)-1|>\epsilon\right\}\right)=0. \tag{9.48}$$

Define the event $\mathcal{A}_K^{\epsilon}\triangleq\bigcap_{n=1}^{N}\bigcup_{k=1}^{K}\left\{\varphi_k^{\mathsf{C}}:|G_M(k,t,n)-1|\leq\epsilon\right\}$, and the probability of its complementary event is computed as

$$\begin{aligned}\mathsf{Pr}\left((\mathcal{A}_K^{\epsilon})^c\right)&=\mathsf{Pr}\left(\bigcup_{n=1}^{N}\bigcap_{k=1}^{K}\left\{\varphi_k^{\mathsf{C}}:|G_M(k,t,n)-1|>\epsilon\right\}\right)\\&\overset{(a)}{\leq}\sum_{n=1}^{N}\mathsf{Pr}\left(\bigcap_{k=1}^{K}\left\{\varphi_k^{\mathsf{C}}:|G_M(k,t,n)-1|>\epsilon\right\}\right)\\&\overset{(b)}{=}\sum_{n=1}^{N}\prod_{k=1}^{K}\mathsf{Pr}\left(\left\{\varphi_k^{\mathsf{C}}:|G_M(k,t,n)-1|>\epsilon\right\}\right),\end{aligned} \tag{9.49}$$

where in (a), we used the union-bound over the events associated with all the N-SCs, and in (b), we used the fact that the events $\mathcal{A}_K^{\epsilon,k,n}\triangleq\left\{\varphi_k^{\mathsf{C}}:|G_M(k,t,n)-1|\leq\epsilon\right\}$ (and their complements) are independent across $k\in[K]$. In the sequel, we characterize the probability of $\mathcal{B}_K^{\epsilon,k,n}\triangleq\left(\mathcal{A}_K^{\epsilon,k,n}\right)^c$, the complementary event of $\mathcal{A}_K^{\epsilon,k,n}$. To this end, note that

$$\mathcal{B}_K^{\epsilon,k,n}\overset{(c)}{=}\left\{\varphi_k^{\mathsf{C}}:\mathrm{sinc}^2\left(M\left(a(t)-\left(1+\frac{f_n}{f_c}\right)\varphi_k^{\mathsf{C}}\right)\right)\leq 1-\epsilon\right\}$$

$$\overset{(d)}{=} \left\{ \varphi_k^{\mathsf{C}} \in [-1,1] : \left| a(t) - \left(1 + \frac{f_n}{f_c}\right) \varphi_k^{\mathsf{C}} \right| \geq \frac{\sqrt{3\epsilon}}{\pi M} \right\}$$

$$= \left\{ \varphi_k^{\mathsf{C}} \in [-1,1] : \varphi_k^{\mathsf{C}} \notin \left(a(t) \pm \frac{\sqrt{3\epsilon}}{\pi M} \right) \Big/ \left(1 + \frac{f_n}{f_c}\right) \right\}, \tag{9.50}$$

where in (c), we used the expressions in (9.32) followed by (9.30), and in (d), we used the Taylor's approximation: $\text{sinc}^2(x) \approx 1 - \pi^2 x^2/3$, which is tight under the regime of interest to us. Now, since $\varphi_k^{\mathsf{C}} \sim \mathcal{U}[-1,1]$, we can show that

$$\mathsf{Pr}\left(\mathcal{B}_K^{\epsilon,k,n}\right) = 1 - \frac{\sqrt{3\epsilon}}{\pi M \left(1 + \frac{f_n}{f_c}\right)} \overset{(e)}{\leq} 1 - \frac{\sqrt{3\epsilon}}{\pi M \left(1 + \frac{W}{2f_c}\right)}, \tag{9.51}$$

where we noted that $|f_n| \leq W/2,\ n \in [N]$. Using (9.51) in (9.49), we obtain

$$\mathsf{Pr}\left((\mathcal{A}_K^{\epsilon})^c\right) \leq N \left(1 - \frac{\sqrt{3\epsilon}}{\pi M \left(1 + \frac{W}{2f_c}\right)}\right)^K. \tag{9.52}$$

Now, consider the infinite sum:

$$P_\infty^{\epsilon} \triangleq \sum_{K=1}^{\infty} \mathsf{Pr}\left((\mathcal{A}_K^{\epsilon})^c\right) \overset{(e)}{\leq} N \sum_{K=1}^{\infty} \left(1 - \frac{\sqrt{3\epsilon}}{\pi M \left(1 + \frac{W}{2f_c}\right)}\right)^K$$

$$\overset{(g)}{=} P_\infty^{\epsilon,\mathrm{U}} \triangleq \frac{\pi N M \left(1 + \frac{W}{2f_c}\right)}{\sqrt{3\epsilon}}, \tag{9.53}$$

where in (e), we used (9.52), and in (g), we used the formula of an infinite geometric series. Now since we have $\forall \epsilon > 0,\ 0 \leq P_\infty^{\epsilon} \leq P_\infty^{\epsilon,\mathrm{U}} < \infty$, by using Borel-Cantelli Lemma [201, Sec 7.3, Theorem 10(a)], we deduce that

$$\forall \epsilon > 0, \quad \mathsf{Pr}\left(\lim_{K\to\infty} \sup \left(\mathcal{A}_K^{\epsilon}\right)^c\right) = 0, \tag{9.54}$$

which proves the statement in (9.48). Consequently, we have

$$\mathsf{Pr}\left(\lim_{K\to\infty} \mathcal{A}_K\right) = \mathsf{Pr}\left(\lim_{K\to\infty} \bigcap_{n=1}^{N} \bigcup_{k=1}^{K} \left\{ \varphi_k^{\mathsf{C}} : G_M(k,t,n) = 1 \right\}\right) = 1, \tag{9.55}$$

which completes the proof of (9.33). Note that this holds for all time slots $t \in [T]$. Finally,

using the sequential definition of the almost sure convergence of random variables in (9.47), the result in (9.34) follows. Importantly, (9.34) rigorously shows that, in every slot and SC, despite exhibiting a B-SP, the IRS will provide a full-array gain to at least one UE when the number of UEs is large. This completes the proof.

Appendix 9.E Proof of Proposition 9.1

We first define the "$(1-\epsilon)M^2$ *success event*":

$$\mathcal{E}_{k,n}^{\epsilon} \triangleq \left\{\varphi_k^{\mathsf{C}} \in [-1,1] : G_M(k,t,n) \geq 1-\epsilon\right\}, \tag{9.56}$$

that denotes the event that the array gain on SC-n at UE-k is at least $(1-\epsilon)M^2$ at some time t. Since the success of the overall scheme is determined by obtaining a near-optimal array gain for at least one UE, we define the *overall probability of* $(1-\epsilon)M^2$ *success event* as

$$P_{\text{succ}}^{\epsilon} \triangleq \mathsf{Pr}\left(\bigcap_{n=1}^{N}\bigcup_{k=1}^{K}\mathcal{E}_{k,n}^{\epsilon}\right). \tag{9.57}$$

Note that the above probability is exactly the probability of the event, $\mathcal{A}_K^{\epsilon}$ defined after (9.48) in the proof of Theorem 9.2. Thus, by directly using the expression given in (9.52), we get

$$P_{\text{succ}}^{\epsilon} \geq 1 - N\left(1 - \frac{\sqrt{3\epsilon}}{\pi M\left(1+\frac{W}{2f_c}\right)}\right)^{K}. \tag{9.58}$$

Finally, by substituting for $P_{\text{succ}}^{\epsilon} = 1-\delta$, and upon rearranging the terms above, we obtain the desired expression in (9.35).

Appendix 9.F Proof of Theorem 9.3

Note that the throughput under equal power allocation across all SCs (from (P0)) with a max-rate scheduler is

$$R_{\text{MR}} \triangleq \frac{1}{T}\sum_{t=1}^{T}\sum_{n=1}^{N}\frac{W}{N}\log_2\left(1+\frac{P}{N_t N\sigma^2}\max_{k\in[K]}|H(k,t,f_n)|^2\right). \tag{9.59}$$

Now, considering that the channels are jointly stationary and ergodic and using Jensen's approximation over the $\log_2(\cdot)$ function, we simplify (9.59) as $R_{\text{MR}} \approx$

$$R^{(K)} \triangleq \sum_{n=1}^{N} \frac{W}{N} \log_2 \left(1 + \frac{P}{N_t N \sigma^2} \mathbb{E}\left[\max_{k\in[K]} |H(k,t,f_n)|^2\right]\right). \tag{9.60}$$

To characterize the expectation in (9.60), using (9.30), we can show that $|H(k,t,f_n)|^2 =$

$$M^2 N_t^2 \rho_1 \rho_2 \left|\tilde{\gamma}_k^{\mathsf{C}}\right|^2 \operatorname{sinc}^2\left(M\left(a(t) - \varphi_k^{\mathsf{C}}\left(1 + \frac{f_n}{f_c}\right)\right)\right), \tag{9.61}$$

with $\gamma_k^{\mathsf{C}} \triangleq \sqrt{\rho_1 \rho_2} N_t \tilde{\gamma}_k^{\mathsf{C}}$, where $\tilde{\gamma}_k^{\mathsf{C}} \overset{\text{i.i.d.}}{\sim} \mathcal{CN}(0,1)$ and $\rho_2 = \rho_{2,k}\, \forall\, k$ under the equal path loss assumption. From Theorem 9.2, as $K \to \infty$, we know that on every SC, at least one UE will be in near-beamforming configuration. Then, the maximum of the terms given in (9.61) is the maximum over the channel gains among those UEs for whom the IRS phases are in near-beamforming configurations (i.e., for those UEs for whom $|H(k,t,f_n)|^2 = M^2 N_t^2 \rho_1 \rho_2 \left|\tilde{\gamma}_k^{\mathsf{C}}\right|^2$). Thus, we have

$$\mathbb{E}\left[\max_{k\in[K]} |H(k,t,f_n)|^2\right] \approx M^2 N_t^2 \rho_1 \rho_2 \mathbb{E}\left[\max_{k\in[K]} \left|\tilde{\gamma}_k^{\mathsf{C}}\right|^2\right] + \mathcal{O}(1). \tag{9.62}$$

Now, to characterize the expected value of the order statistic in (9.62), we first recognize that $\left|\tilde{\gamma}_k^{\mathsf{C}}\right|^2$ is an exponential random variable with mean 1, and then by using results from extreme value theory [103, Lemma 3], we can show that, for large K, $\max_{k\in[K]} \left|\tilde{\gamma}_k^{\mathsf{C}}\right|^2$ grows as l_K, where $F(l_K) = 1 - \frac{1}{K}$ with $F(z) = 1 - e^{-z}$, which is the cumulative distribution function of a unit mean exponential random variable. Then, using the value of $l_K = \ln K$ in (9.62), and substituting the resulting expression in (9.60), we can show that the throughput scales as

$$R^{(K)} \lesssim W \log_2 \left(1 + \frac{\rho P}{N\sigma^2} N_t M^2 \ln K\right), \tag{9.63}$$

which is restated in the statement of the theorem.

10 Wideband Beamforming in IRS-Aided Communications: Optimization for Sub-6 GHz Bands

Chapter Highlights

Exploiting the benefits of intelligent reflecting surfaces (IRSs) requires optimizing the discrete reflection coefficients of the IRS elements, which crucially depend on the availability of accurate channel state information (CSI) of all links in the system. Further, in wideband systems employing orthogonal frequency division multiplexing (OFDM), a given IRS configuration cannot be simultaneously optimal for all the subcarriers, and hence, the phase optimization is not straightforward.

In this final technical chapter of the thesis, we propose a novel IRS phase configuration scheme in OFDM systems by first leveraging the sparsity of the channel in the angular domain to estimate the CSI using a simultaneous orthogonal matching pursuit (SOMP) algorithm, which incurs low-pilot overheads and then devising a novel and computationally efficient binary IRS phase configuration algorithm using majorization-minimization (MM). The key highlight of this technique is that it directly optimizes the sum-rate across the OFDM subcarriers at a given UE, as opposed to the existing sub-optimal approaches to maximize an upper bound on the sum-rate. The proposed MM approach addresses the original problem by reformulating it into a sequence of sub-problems derived using a series of matrix inequalities, each of which can be efficiently solved in closed form. Simulation results illustrate the efficacy of the approach in comparison with the state-of-the-art.

10.1 Introduction

The use of intelligent reflecting surfaces (IRSs) for enhancing the throughput and coverage of wireless communications is a topic of intense research [2, 69]. IRSs are made of passive meta-material elements, and by optimizing the reflection coefficient at every IRS element, we can improve the data rate, especially in mmWave bands. However, this requires accurate knowledge of the channel state information (CSI) of all the links in the system, which is resource-intensive and computationally expensive to acquire. For example, least squares (LS) channel estimation [202] incurs a pilot overhead that grows linearly with the number of IRS elements. Moreover, optimizing the IRS configuration for OFDM-based wideband communications is challenging because the discrete-valued reflection coefficients need to be chosen to maximize the sum rate across all subcarriers. In this direction, a few IRS phase optimization methods in an OFDM framework have been developed [202, 203]; but due to the underlying complicated objective function, they optimize an upper bound on the sum rate, potentially making the solution suboptimal. Further, using LS-based channel estimation makes the overall procedure complex in terms of both time and computations.

In this work, we propose a powerful and elegant solution for optimizing the IRS reflection coefficients (or phase angles) that directly maximizes the sum rate in single-input single-output (SISO)-OFDM systems and a low pilot overhead CSI estimation procedure that exploits the underlying joint row-sparsity in the channel. For ease of exposition, we consider the IRS phases to be sampled from a binary set $\{-1, +1\}$, but we briefly discuss the extension to the case of arbitrary discrete phase angles in Remark 10.2.

The specific contributions of this chapter are as follows. We first develop a low pilot overhead channel estimation algorithm by leveraging the sparsity in the OFDM channel induced by the IRS. To elaborate, the cascaded BS-IRS and IRS-UE channels are sparse in the angular domain and further exhibit joint row sparsity across the OFDM subcarriers. We exploit this to estimate the CSI using the simultaneous orthogonal matching pursuit (SOMP) algorithm [204]. Next, we propose a novel and computationally efficient binary

phase optimization procedure for IRS-assisted OFDM systems using the majorization-minimization (MM) [67] and directly optimize the sum rate. The key novelty of using an MM-based approach is finding a lower bound on the non-convex sum rate that is tight at the current iterate and amenable to optimization via closed-form solutions. We develop such bounds using a series of matrix inequalities and eventually provide a closed-form solution to the inner optimization problem.

We empirically evaluate the performance of the IRS configuration algorithm in Sec. 10.4 and compare it with existing approaches. The results show that using SOMP for channel estimation reduces the pilot overhead by 96% while achieving a lower normalized mean squared error (NMSE) compared to the LS estimate. Also, by directly optimizing the sum rate, our binary IRS phase optimization algorithm offers 10% better sum rate, on average, compared to the method in [203], where the authors optimize an upper bound on the sum rate, with the computational complexity of two methods being similar. Also, the proposed method achieves the same average sum rate as [203] with a reduction in SNR by $\approx 21.5\%$, illustrating that it is a promising approach to IRS phase configuration.

Notation: For general notations used in this chapter, see the section on "General Mathematical Notations" on page ix. For the notations/variables specific to this chapter, please refer to Table 10.1.

10.2 System Model

We consider a wideband OFDM communication link between a single antenna base station (BS) and a single antenna user equipment (UE) in a wireless environment equipped with an N-element IRS, as in [70]. Let $x[n]$ denote the baseband signal transmitted by the BS in the discrete-time domain. The downlink signal $y[n]$ received at the UE is given by

$$y[n] = \sum_{\ell=0}^{M-1} h_{\boldsymbol{\theta}}[\ell] x[n-\ell] + w[n], \tag{10.1}$$

Variable	Definition	Variable	Definition
N	Number of IRS elements	L_d	Total number of direct paths
M	No. of taps in the time-domain channel	L_a	No. of paths from BS to IRS
$\boldsymbol{\theta}$	IRS phase shift vector	L_b	No. of paths from IRS to UE
K	Number of OFDM sub-carriers	β_x	Path loss in link-x
$\mathbf{v}_\ell$	Cascaded channel vector in ℓth tap	ϕ_{ℓ_1}	Direction of arrival in ℓ_1th path from BS to IRS
$h_d[\ell]$	Direct channel in the ℓth tap	ϕ_{ℓ_2}	Direction of departure in ℓ_2th path at the IRS to UE
$h_{\boldsymbol{\theta}}[\ell]$	Overall channel in ℓth tap parameterized by $\boldsymbol{\theta}$	P	Total transmit power at BS
B	Bandwidth of the signal	N_0	Noise power spectral density
η	Propagation delay of 1st path	$\tilde{\mathbf{h}}_k$	Composite channel on subcarrier-k
$\tau_{d,\ell}$	Delay of ℓth direct path	ω_{ℓ_1,ℓ_2}	Angle of the cascaded path corr. to ℓ_1th path from BS to IRS, and ℓ_2th path from IRS to UE in mth tap
τ_{r,ℓ_1,ℓ_2}	Delay in the cascaded path corresponding to the ℓ_1th path from BS to IRS and ℓ_2th path from IRS to UE	γ_{m,ℓ_1,ℓ_2}	Cascaded channel gain corresponding to ℓ_1th path from BS to IRS, and ℓ_2th path from IRS to UE in mth tap

Table 10.1: Commonly encountered variables/notations in chapter 10. **Note**: All variables with a bar on top of them denote the frequency-domain representations of the time-domain expressions.

where $\{h_{\boldsymbol{\theta}}[\ell]\}_{\ell=0}^{M-1}$ is the M-tap time-domain impulse response of the channel, which depends on the fading coefficients and the IRS phase configuration $\boldsymbol{\theta}$, and $w[n] \sim \mathcal{CN}(0, N_0)$ is the independent and identically distributed (i.i.d.) AWGN. In an OFDM setup with K subcarriers ($M < K$), denoting the K-point discrete Fourier transform (DFT) of the received signal after removing the cyclic prefix, the impulse response of the channel, the transmitted signal, and noise by $\bar{\mathbf{y}}$, $\bar{\mathbf{h}}_{\boldsymbol{\theta}}$, $\bar{\mathbf{x}}$, and $\bar{\mathbf{w}}$, respectively, all $K \times 1$ complex vectors, we can rewrite (10.1) in the frequency domain as

$$\bar{\mathbf{y}} = \bar{\mathbf{h}}_{\boldsymbol{\theta}} \odot \bar{\mathbf{x}} + \bar{\mathbf{w}}. \tag{10.2}$$

We model the ℓth tap of the time-domain channel in (10.1) as

$$h_{\boldsymbol{\theta}}[\ell] = h_d[\ell] + \mathbf{v}_\ell^T \boldsymbol{\theta}, \tag{10.3}$$

where $h_d[\ell]$ is the ℓth tap in the direct path (not involving the IRS), $\mathbf{v}_\ell \in \mathbb{C}^N$ is the

cascaded channel vector[1] in the ℓth tap via each of the N elements, and $\boldsymbol{\theta}$ denotes the IRS phase configuration, i.e., the reflection coefficients programmed in the N IRS elements, with entries in $\{-1, +1\}$. Consequently,

$$\bar{\mathbf{h}}_\theta = \mathbf{F} \begin{bmatrix} h_d[0] + \mathbf{v}_0^T \boldsymbol{\theta} \\ \vdots \\ h_d[M-1] + \mathbf{v}_{M-1}^T \boldsymbol{\theta} \end{bmatrix} = \underbrace{\mathbf{F}\mathbf{h}_d}_{\triangleq \bar{\mathbf{h}}_d} + \underbrace{\mathbf{F}\mathbf{V}^T \boldsymbol{\theta}}_{\triangleq \bar{\mathbf{V}}^T \boldsymbol{\theta}}, \tag{10.4}$$

where $\mathbf{h}_d = [h_d[0], \ldots, h_d[M-1]]^T$, $\mathbf{V} = [\mathbf{v}_0, \ldots, \mathbf{v}_{M-1}] \in \mathbb{C}^{N \times M}$, $\mathbf{F}$ is a matrix containing the first M columns of the $K \times K$ DFT matrix. Now, we model the direct path as

$$\mathbf{h}_d = \sum_{\ell=1}^{L_d} \beta_{d,\ell} \begin{bmatrix} \text{sinc}(0 + B(\eta - \tau_{d,\ell})) \\ \vdots \\ \text{sinc}(M - 1 + B(\eta - \tau_{d,\ell})) \end{bmatrix}, \tag{10.5}$$

where L_d is the number of propagation paths, $\beta_{d,\ell}$ is the path gain of the ℓth path, and B, η, and $\tau_{d,\ell}$ denote the system bandwidth, common delay applied at the receiver for time synchronization, and the propagation delay in the ℓth direct path. Furthermore, since IRSs are envisaged to be installed at tall locations, we consider line-of-sight communications between BS and IRS and between IRS and the UE, as in [86]. Thus, the cascaded channel is given as

$$\mathbf{V} = \sum_{\ell_1=1}^{L_a} \sum_{\ell_2=1}^{L_b} \beta_{r,\ell_1,\ell_2} (\mathbf{a}(\phi_{\ell_1}) \odot \mathbf{a}(\varphi_{\ell_2})) \times \begin{bmatrix} \text{sinc}(0 + B(\eta - \tau_{r,\ell_1,\ell_2})) \\ \vdots \\ \text{sinc}(M - 1 + B(\eta - \tau_{r,\ell_1,\ell_2})) \end{bmatrix}^T, \tag{10.6}$$

where L_a and L_b are the number of paths from the BS to the IRS and from the IRS to the UE, respectively. β_{r,ℓ_1,ℓ_2} and τ_{r,ℓ_1,ℓ_2} represent the path gain and propagation delay associated with the cascaded ℓ_1-ℓ_2th path. Further, ϕ_{ℓ_1} and φ_{ℓ_2} represent the direction of arrival (DoA) and the direction of departure (DoD) at the IRS, respectively. Here, $\mathbf{a}$ represents the array steering response vector of the IRS. We consider the IRS arranged as

[1]The cascaded channel is the linear convolution of the BS-IRS and IRS-UE channels in the time domain (Hadamard product in the frequency domain.)

a uniform linear array (ULA) [86], whence

$$\mathbf{a}(\psi) = \left[1, e^{-j\frac{2\pi d}{\lambda}\sin(\psi)}, \ldots, e^{-j(N-1)\frac{2\pi d}{\lambda}\sin(\psi)}\right]^T, \tag{10.7}$$

where d is the inter-elemental spacing and λ is the wavelength.

10.3 Proposed IRS Configuration Approach

10.3.a Channel Estimation

We perform channel estimation in two stages. In the first stage, the direct path $\mathbf{h}_d$ is estimated using two pilot symbols. In the second stage, the cascaded channel $\mathbf{V}$ is estimated by exploiting the sparsity in the angular domain.

10.3.a.i Stage I: Direct channel estimation

In this step, the BS transmits a pilot signal to the UE with the IRS phase configuration set to $\mathbf{1}_N$ during the first transmission and $-\mathbf{1}_N$ in the second transmission. As a consequence,

$$\bar{\mathbf{y}}_1 = \mathbf{F}\left(\mathbf{h}_d + \mathbf{V}^T\mathbf{1}_N\right) \odot \bar{\mathbf{x}} + \bar{\mathbf{w}}_1, \tag{10.8}$$

$$\bar{\mathbf{y}}_2 = \mathbf{F}\left(\mathbf{h}_d - \mathbf{V}^T\mathbf{1}_N\right) \odot \bar{\mathbf{x}} + \bar{\mathbf{w}}_2, \tag{10.9}$$

where the subscripts 1 and 2 denote the pilot transmission indices. The maximum likelihood (ML) estimate of the direct path in the frequency domain ($\bar{\mathbf{h}}_d$), denoted by $\hat{\bar{\mathbf{h}}}_d$, is

$$\hat{\bar{\mathbf{h}}}_d = ((\bar{\mathbf{y}}_1 + \bar{\mathbf{y}}_2)/2) \oslash \bar{\mathbf{x}}. \tag{10.10}$$

10.3.a.ii Stage II: Cascaded channel estimation

In this stage, the component due to the direct path is removed from the received pilot signals prior to the cascaded channel estimation. Specifically, for Q pilot transmissions,

$$\bar{\mathbf{Y}} = \left(\bar{\mathbf{H}}_d + \mathbf{F}\mathbf{V}^T\mathbf{\Theta}\right) \odot \bar{\mathbf{X}} + \bar{\mathbf{W}}, \tag{10.11}$$

where $\bar{\mathbf{Y}} \in \mathbb{C}^{K\times Q}$ is the received OFDM signal, $\bar{\mathbf{H}}_d = \bar{\mathbf{h}}_d \otimes \mathbf{1}_Q^T$, $\boldsymbol{\Theta} \in \{-1,+1\}^{N\times Q}$ is the IRS phase configuration matrix, $\bar{\mathbf{X}}$ is the pilot symbol matrix, and $\bar{\mathbf{W}}$ is the noise matrix at the receiver. After matched filtering and removing the contribution from the direct path, we get

$$\bar{\mathbf{Z}} = \mathbf{F}\mathbf{V}^T\boldsymbol{\Theta} + \bar{\mathbf{N}}, \tag{10.12}$$

where $\bar{\mathbf{Z}} \triangleq (\bar{\mathbf{Y}} \oslash \bar{\mathbf{X}}) - (\hat{\bar{\mathbf{h}}}_d \otimes \mathbf{1}_Q^T)$, and $\bar{\mathbf{N}}$ is the residual noise matrix. To exploit the sparsity in the angular domain of the cascaded channel, we first decompose the channel $\mathbf{V}$ as given below. Let $\tilde{\mathbf{a}}(\omega_{\ell_1,\ell_2}) \triangleq \mathbf{a}(\phi_{\ell_1}) \odot \mathbf{a}(\varphi_{\ell_2})$ and $\gamma_{m,\ell_1,\ell_2} \triangleq \beta_{r,\ell_1,\ell_2}\ \mathrm{sinc}(m + B(\eta - \tau_{r,\ell_1,\ell_2}))$. From (10.6), we have

$$\mathbf{V} = \left[\sum_{\ell_1=1}^{L_a}\sum_{\ell_2=1}^{L_b} \gamma_{1,\ell_1,\ell_2}\tilde{\mathbf{a}}(\omega_{\ell_1,\ell_2}), \cdots, \sum_{\ell_1=1}^{L_a}\sum_{\ell_2=1}^{L_b} \gamma_{M,\ell_1,\ell_2}\tilde{\mathbf{a}}(\omega_{\ell_1,\ell_2})\right],$$

which can be compactly written as $\mathbf{V} = \tilde{\mathbf{A}}\boldsymbol{\Gamma}$, where $\tilde{\mathbf{A}} \in \mathbb{C}^{N\times L_aL_b}$ collects the steering vectors corresponding to the L_aL_b paths, and $\boldsymbol{\Gamma} \in \mathbb{C}^{L_aL_b\times M}$ contains the path gains associated with the L_aL_b paths. Since the path gains, delays, and DoA/DoDs are unknown, we first sparsify $\boldsymbol{\Gamma}$, denoted by $\tilde{\boldsymbol{\Gamma}}_t \in \mathbb{C}^{d\times M}$, using a dictionary matrix $\mathbf{D}_{\tilde{\mathbf{A}}} \triangleq [\tilde{\mathbf{a}}(\omega_1), \tilde{\mathbf{a}}(\omega_2), \ldots, \tilde{\mathbf{a}}(\omega_d)] \in \mathbb{C}^{N\times d}$. Here, $d \gg L_aL_b$ depends on the resolution required for estimating the DoA/DoD. As a result, from (10.4), we have $\bar{\mathbf{V}} = \mathbf{D}_{\tilde{\mathbf{A}}}\tilde{\boldsymbol{\Gamma}}$ where $\tilde{\boldsymbol{\Gamma}} \in \mathbb{C}^{d\times K}$ is a jointly row L_aL_b-sparse matrix with row support $\mathcal{S}$ s.t. $\mathcal{S} \subseteq [d]$. Note that $\mathcal{S}$ depends on the true DoA/DoDs, and the values of $\tilde{\boldsymbol{\Gamma}}$ depend on $\tilde{\boldsymbol{\Gamma}}_t$. From (10.4) and (10.12),

$$\mathbf{Y}_{\text{sens}} \triangleq \bar{\mathbf{Z}}^T = \underbrace{\boldsymbol{\Theta}^T\mathbf{D}_{\tilde{\mathbf{A}}}}_{\triangleq\mathbf{A}_{\text{sens}}}\tilde{\boldsymbol{\Gamma}} + \underbrace{\bar{\mathbf{N}}^T}_{\triangleq\mathbf{N}_{\text{sens}}}.$$

To estimate $\bar{\mathbf{V}}$, consider the compressed sensing problem:

$$\begin{aligned} \min_{\tilde{\boldsymbol{\Gamma}}} \quad & \sum_{j=1}^{d} \mathbb{1}\left\{\left\|[\tilde{\boldsymbol{\Gamma}}]_{j,:}\right\|_0 = K\right\}, \\ \text{s.t.} \quad & \mathbf{Y}_{\text{sens}} = \mathbf{A}_{\text{sens}}\tilde{\boldsymbol{\Gamma}} + \mathbf{N}_{\text{sens}}. \end{aligned} \tag{P0}$$

Algorithm 10.1: SOMP for cascaded channel estimation

Input: $\mathbf{Y} = \mathbf{Y}_{\text{sens}}, \mathbf{A} = \mathbf{A}_{\text{sens}}, \epsilon =$ error tolerance.

Initialize: $\mathcal{S}^{(0)} = \emptyset$, $\tilde{\mathbf{\Gamma}}^{(0)} = \mathbf{O}_{d\times K}$, $n = 0$.

while $\|\mathbf{Y} - \mathbf{A}\tilde{\mathbf{\Gamma}}^{(n)}\|_F^2 \geq \epsilon$ **do**

  $j_{n+1} = \underset{j\in[d]\setminus S^{(n)}}{arg\,max}\{\|[\mathbf{A}^H(\mathbf{Y} - \mathbf{A}\tilde{\mathbf{\Gamma}}^{(n)})]_{j,:}\|_2^2\}$,

  $\mathcal{S}^{(n+1)} \leftarrow \mathcal{S}^{(n)} \cup \{j_{n+1}\}$,

  $\tilde{\mathbf{\Gamma}}^{n+1} = \left([\mathbf{A}]_{:,\mathcal{S}^{(n+1)}}\right)^{\dagger}\mathbf{Y}$,

  $n \leftarrow n + 1$,

Let $\mathcal{S}^{\text{fin}} \triangleq \mathcal{S}^{(n)}$, $\mathbf{A}^{\text{fin}} \triangleq [\mathbf{A}]_{:,\mathcal{S}^{\text{fin}}}$, $\tilde{\mathbf{\Gamma}}^{\text{fin}} \triangleq (\mathbf{A}^{\text{fin}})^{\dagger}\mathbf{Y}$.

Output: $\mathcal{S}^{\text{fin}}, \tilde{\mathbf{\Gamma}}^{\text{fin}}$.

In the sequel, we use the simultaneous orthogonal matching pursuit (SOMP) algorithm [204] to solve (P0), which first estimates the row support of $\tilde{\mathbf{\Gamma}}$ followed by its entries (see Algorithm 1.) Let $\mathcal{S}^{\text{fin}}$ and $\tilde{\mathbf{\Gamma}}^{\text{fin}}$ be the estimated row support and the path gains, respectively. Then, the cascaded channel estimate is

$$\hat{\tilde{\mathbf{V}}} = [\mathbf{D}_{\tilde{\mathbf{A}}}]_{:,\mathcal{S}^{\text{fin}}}\tilde{\mathbf{\Gamma}}^{\text{fin}}. \tag{10.13}$$

10.3.b Phase Optimization

As described earlier, we consider the sum rate across subcarriers as the metric, which we seek to maximize by choosing the IRS phase configuration, $\boldsymbol{\theta}$, with entries $\in \{-1, +1\}$. For a given configuration, with equal power allocation and perfect CSI at the receiver, the sum rate over the subcarriers in (10.2) is

$$R = \frac{B}{K+M-1}\sum_{k=0}^{K-1}\log_2\left(1 + \frac{P|\bar{\mathbf{h}}_\theta[k]|^2}{BN_0}\right) \text{ bit/s}, \tag{10.14}$$

where P is transmit power and N_0 is the noise power spectral density. We also define the transmit SNR, $\rho \triangleq \frac{P}{BN_0}$. For the kth subcarrier ($k = 0, 1, \ldots, K-1$), we have

$$\bar{\mathbf{h}}_\theta[k] = \sum_{j=1}^{N}\theta_j\bar{\mathbf{v}}_k[j] + \bar{\mathbf{h}}_d[k] = \tilde{\boldsymbol{\theta}}^H\tilde{\mathbf{h}}_k, \tag{10.15}$$

where $\tilde{\mathbf{h}}_k = [\bar{h}_d[k], \bar{\mathbf{v}}_k^T]^T \in \mathbb{C}^{(N+1)\times 1}$, and $\tilde{\boldsymbol{\theta}} = [1, \boldsymbol{\theta}^T]^T$. Letting $\mathbf{h}_k \triangleq \sqrt{\rho}\tilde{\mathbf{h}}_k$, we formulate the following problem:

$$\begin{aligned} \max_{\tilde{\boldsymbol{\theta}}} \quad & R = \frac{B}{K+M-1} \underbrace{\sum_{k=0}^{K-1} \log_2\left(1 + \tilde{\boldsymbol{\theta}}^H \mathbf{h}_k \mathbf{h}_k^H \tilde{\boldsymbol{\theta}}\right)}_{\triangleq R^{(K)}}, \\ \text{s.t.} \quad & \tilde{\boldsymbol{\theta}} \in \{-1, +1\}^{N+1}, \ \tilde{\boldsymbol{\theta}}[1] = 1. \end{aligned} \tag{P1}$$

We solve this optimization problem using the majorization-minimization (MM) method [67]. In what follows, we make a sequence of simplifications to (P1) and eventually formulate an equivalent problem (see (P3)) which can be solved computationally easily. We now use the following lemma.

Lemma 10.1. *([205, Lemma 4]) Let* $\mathbf{P}$ *and* $\mathbf{Q}$ *be two* $S \times S$ *Hermitian matrices such that* $\mathbf{Q} \succeq \mathbf{P}$. *Then, for any* $\mathbf{x}_0 \in \mathbb{C}^S$, *the quadratic function* $\mathbf{x}^H\mathbf{P}\mathbf{x}$ *is majorized by* $\mathbf{x}^H\mathbf{Q}\mathbf{x} + 2\Re\left(\mathbf{x}^H\left(\mathbf{P}-\mathbf{Q}\right)\mathbf{x}_0\right) + \mathbf{x}_0^H\left(\mathbf{Q}-\mathbf{P}\right)\mathbf{x}_0$ *at* $\mathbf{x}_0$.

Lemma 10.1 implies that, for matrices $\mathbf{P}$ and $\mathbf{Q}$ that satisfy the assertion in the lemma, $\forall \mathbf{x} \in \mathbb{C}^{S\times 1}$, $\mathbf{x}^H\mathbf{P}\mathbf{x} \leq \mathbf{x}^H\mathbf{Q}\mathbf{x} + 2\Re(\mathbf{x}^H(\mathbf{P}-\mathbf{Q})\mathbf{x}^{(i)}) + \mathbf{x}^{(i)H}\left(\mathbf{Q}-\mathbf{P}\right)\mathbf{x}^{(i)}$, with equality at $\mathbf{x} = \mathbf{x}^{(i)}$. Let $\mathbf{P} = \mathbf{O}_{(N+1)}$, $\mathbf{Q} = \mathbf{h}_k\mathbf{h}_k^H$ and $\mathbf{x} = \tilde{\boldsymbol{\theta}}$. Note that $\mathbf{Q} \succeq \mathbf{P}$. Then, from (P1), we get

$$R^{(K)} \geq \sum_{k=0}^{K-1} \log_2\left(1 + 2\Re(\tilde{\boldsymbol{\theta}}^H\mathbf{h}_k\mathbf{h}_k^H\tilde{\boldsymbol{\theta}}^{(i)})\tilde{\boldsymbol{\theta}}^{(i)H}\mathbf{h}_k\mathbf{h}_k^H\tilde{\boldsymbol{\theta}}^{(i)}\right), \tag{10.16}$$

for all $\tilde{\boldsymbol{\theta}} \in \mathbb{C}^{(N+1)\times 1}$ with equality at $\tilde{\boldsymbol{\theta}} = \tilde{\boldsymbol{\theta}}^{(i)}$, where i is the iteration index of the algorithm. Let $C_k^{(i)} \triangleq 1 - \tilde{\boldsymbol{\theta}}^{(i)H}\mathbf{h}_k\mathbf{h}_k^H\tilde{\boldsymbol{\theta}}^{(i)}$ and $\check{\mathbf{h}}_k^{(i)} \triangleq \mathbf{h}_k\mathbf{h}_k^H\tilde{\boldsymbol{\theta}}^{(i)}$. The above equation simplifies to

$$R^{(K)} \geq \sum_{k=0}^{K-1} \log_2\left(C_k^{(i)} + 2\Re(\tilde{\boldsymbol{\theta}}^H\check{\mathbf{h}}_k^{(i)})\right). \tag{10.17}$$

We now use the following lemma.

Lemma 10.2. *([206, Lemma 1]) For* $\mathbf{Z}, \mathbf{Y} \succeq 0$, *the function* $f(\mathbf{Z},\mathbf{Y}) \triangleq \log|(\mathbf{Z}^{-1}\mathbf{Y})|$ *can be lower bounded as* $f(\mathbf{Z},\mathbf{Y}) \geq -\left\{\log|\mathbf{Z}^{(i)}| + \mathrm{tr}((\mathbf{Z}^{(i)})^{-1}\mathbf{Z} - \mathbf{I}_K) + \log|(\mathbf{Y}^{(i)})^{-1}| + \mathrm{tr}(\mathbf{Y}^{(i)}\mathbf{Y}^{-1} - \mathbf{I}_K)\right\}$, *with equality at* $\mathbf{Z} = \mathbf{Z}^{(i)}; \mathbf{Y} = \mathbf{Y}^{(i)}$.

Let $\mathbf{Y} \triangleq \text{diag}(\{C_k^{(i)} + 2\Re(\tilde{\boldsymbol{\theta}}^H \check{\mathbf{h}}_k^{(i)})\}_{k=0}^{K-1})$, $\mathbf{Z} \triangleq \mathbf{I}_K$, and $\mathbf{Y}^{(i)} = \mathbf{Y}\,|_{\tilde{\boldsymbol{\theta}}=\tilde{\boldsymbol{\theta}}^{(i)}}$. By Lemma 10.2, we can majorize (10.17) as

$$R^{(K)} \geq -\sum_{k=0}^{K-1} \frac{C_k^{(i)} + 2\Re(\tilde{\boldsymbol{\theta}}^{(i)H} \check{\mathbf{h}}_k^{(i)})}{C_k^{(i)} + 2\Re(\tilde{\boldsymbol{\theta}}^H \check{\mathbf{h}}_k^{(i)})} + \xi,$$

where ξ represents terms which are irrelevant for optimization of $\tilde{\boldsymbol{\theta}}$. Hence, by the MM technique, problem (P1) simplifies to

$$\begin{aligned} \min_{\tilde{\boldsymbol{\theta}}} \quad & \sum_{k=0}^{K-1} f_k(\tilde{\boldsymbol{\theta}}), \\ \text{s.t.} \quad & \tilde{\boldsymbol{\theta}} \in \{-1, +1\}^{N+1}\,,\, \tilde{\boldsymbol{\theta}}[1] = 1, \end{aligned} \tag{P2}$$

for some $\tilde{\boldsymbol{\theta}}^{(i)}$, where $f_k(\tilde{\boldsymbol{\theta}}) \triangleq (C_k^{(i)} + \tilde{\boldsymbol{\theta}}^{(i)T} \mathbf{g}_k^{(i)})/(C_k^{(i)} + \tilde{\boldsymbol{\theta}}^T \mathbf{g}_k^{(i)})$, with and $\mathbf{g}_k^{(i)} \triangleq 2\Re(\check{\mathbf{h}}_k^{(i)})$ and the terms independent of $\tilde{\boldsymbol{\theta}}$ are ignored. We now consider the following optimization problem, which we will use to solve for $\tilde{\boldsymbol{\theta}}$ in (P2).

$$\begin{aligned} \max_{\tilde{\boldsymbol{\theta}}} \quad & \sum_{k=0}^{K-1} \tilde{\boldsymbol{\theta}}^T \mathbf{q}_k^{(i)}, \\ \text{s.t.} \quad & \tilde{\boldsymbol{\theta}} \in \{-1, +1\}^{N+1}\,,\, \tilde{\boldsymbol{\theta}}[1] = 1, \end{aligned} \tag{P3}$$

where, for some $\tilde{\boldsymbol{\theta}}^{(i)}$, $\mathbf{q}_k^{(i)}$ is defined as follows.

$$\mathbf{q}_k^{(i)} \triangleq \frac{\mathbf{g}_k^{(i)}}{C_k^{(i)} + \tilde{\boldsymbol{\theta}}^{(i)T} \mathbf{g}_k^{(i)}} + \mathbb{1}\left\{C_k^{(i)} \geq \|\mathbf{g}_k^{(i)}\|_1\right\} \frac{2\,\tilde{\boldsymbol{\theta}}^{(i)} \|\mathbf{g}_k^{(i)}\|_2^2 \left(C_k^{(i)} + \|\mathbf{g}_k^{(i)}\|_1\right)}{\left(C_k^{(i)} - \|\mathbf{g}_k^{(i)}\|_1\right)^3}. \tag{10.18}$$

Lemma 10.3. *The variable $\tilde{\boldsymbol{\theta}}$ that solves (P3) also solves (P2).*

Proof. See Appendix 10.A. ■

Thus, in a given MM-based iteration, the solution to (P3) is

$$\tilde{\boldsymbol{\theta}}^{(i+1)} = \text{sgn}((\mathbf{q}_{\text{sum}}^{(i)}[1])^* \mathbf{q}_{\text{sum}}^{(i)}), \tag{10.19}$$

where $\mathbf{q}_{\text{sum}}^{(i)} = \sum_{k=0}^{K-1} \mathbf{q}_k^{(i)}$. In summary, we first converted the problem (P1) which is logarithmic in $\tilde{\boldsymbol{\theta}}$ and hence not amenable for optimization, into an equivalent problem (P2) which is polynomial in $\tilde{\boldsymbol{\theta}}$. Finally, we simplified it to (P3) which is linear in $\tilde{\boldsymbol{\theta}}$, and whose solution can be computed easily using (10.19). Thus, the complete procedure is as follows: For every UE,

1. Compute the frequency domain channel estimate of the direct and cascaded channels between the BS and the UE as per (10.10) and (10.13), respectively.

2. Randomly initialize a phase configuration vector and iteratively compute (10.19) until the rate converges, e.g., until the normalized change in the rate obtained in successive iterates falls below a threshold δ, say 0.001.

Remark 10.1. *Since the algorithm for phase optimization is based on the MM principle, convergence to a stationary point of the rate is guaranteed from any initialization [67].*

Remark 10.2. *If the IRS phase angles are drawn from a discrete set $\mathcal{T}$ containing more than two levels, following a similar approach, equation (10.19) modifies to*

$$\tilde{\boldsymbol{\theta}}^{(i+1)} = round(\mathbf{q}_{gen}^{(i)}/(\mathbf{q}_{gen}^{(i)}[1])), \tag{10.20}$$

where $round(x)$ outputs the nearest element in $\mathcal{T}$ to x with $\tilde{\boldsymbol{\theta}}^{(i+1)}[1] = 1 \ \forall i$, and $\mathbf{q}_{gen}^{(i)}$ is

$$\mathbf{q}_{gen}^{(i)} \triangleq \sum_{k=0}^{K-1} \left(\frac{2\Re(\check{\mathbf{h}}_k^{(i)})}{C_k^{(i)} + 2\Re\left(\tilde{\boldsymbol{\theta}}^{(i)H}\check{\mathbf{h}}_k^{(i)}\right)} + \mathbb{1}\left\{C_k^{(i)} \geq 2\|\Re(\check{\mathbf{h}}_k^{(i)})\|_1\right\} \frac{8\,\tilde{\boldsymbol{\theta}}^{(i)}\|\Re(\check{\mathbf{h}}_k^{(i)})\|_2^2\left(C_k^{(i)} + 2\|\check{\mathbf{h}}_k^{(i)}\|_2^2\right)}{\left(C_k^{(i)} - 2\|\Re(\check{\mathbf{h}}_k^{(i)})\|_1\right)^3} \right). \tag{10.21}$$

10.4 Numerical Results

In this section, we evaluate the performance of the algorithms presented in this chapter and compare them against existing methods in the literature. A single antenna BS is located at $(0, 0)$ (in meters), the IRS is at $(0, 50)$ with $N = 256$, and single antenna

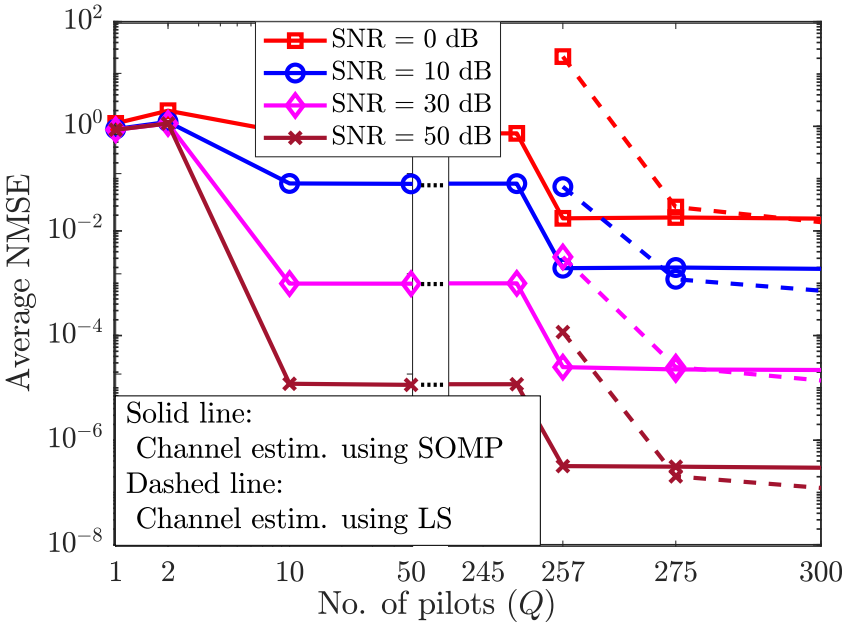

Figure 10.1: Average NMSE as a function of the number of pilots.

UEs are uniformly distributed in the rectangular region with diagonally opposite corners $(-50, 100)$ and $(50, 150)$. The path losses are computed as $\beta = 1/d^{\alpha}$ where d is the distance, and α is the path loss exponent. We use $\alpha = 1.2, 2.4$ and 3.2 in the BS-IRS, IRS-UE, and BS-UE (direct) links, respectively. For simplicity, we set $L_a = 1, L_b = 1$, and $L_d = 10$ for all the UEs. Further, we consider a BS with transmit SNR, $\rho = 65$ dB. We consider a system with $M = 10, K = 16$ with the total number of UEs set to 20, and all share the same total bandwidth, $B = 10$ MHz. Then, in the absence of the IRS, a UE closest to the BS witnesses an average SNR of ≈ 9 dB, while it is ≈ -5 dB for a UE at the farthest point.

In Fig. 10.1, we plot the average normalized mean square error (NMSE) of SOMP-based channel estimation, which exploits sparsity in the angular domain of the channel. We use NMSE (rather than MSE) in order to compare the performances of the channel estimation algorithms in a manner that is independent of parameter scales. At each SNR value, the NMSE is averaged across all the UEs and is plotted as a function of the number of pilot transmissions Q. We also plot the performance of LS-based channel estimation on the same figure. LS estimation requires $Q \geq N + 1 = 257$, while the

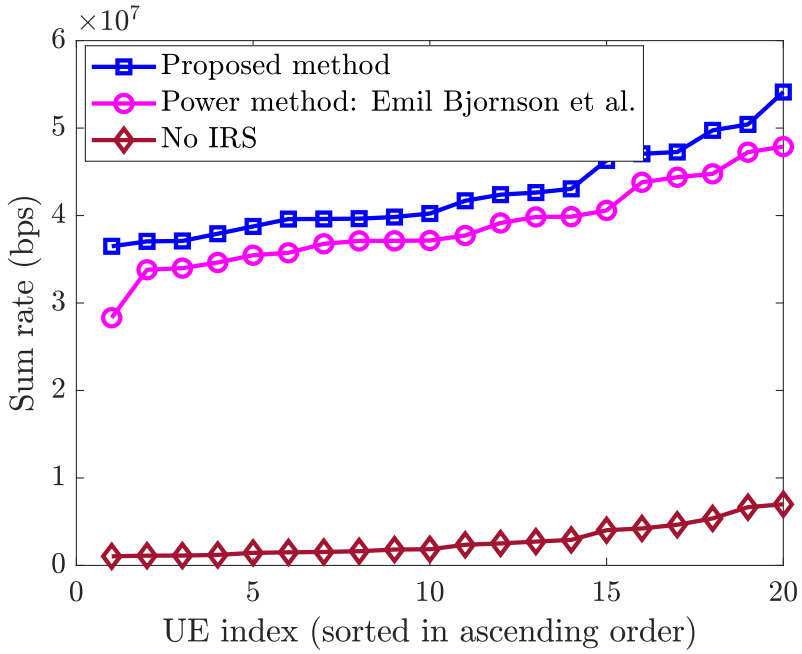

Figure 10.2: Sum rate as a function of UE index. Results are compared against method in [203].

SOMP estimator performs nearly as well with as few as 10 pilots, representing a saving of 96% of the pilot overhead. In fact, even with $N+1$ pilot transmissions, the NMSE obtained with SOMP is still lower than the LS counterpart. Also, the computational complexity of SOMP is much smaller than LS estimation. From [207], SOMP requires $\mathcal{O}(dQKL_aL_b + QK(L_aL_b)^2 + Q(L_aL_b)^3 + (L_aL_b)^4)$ flops in the worst case using naive implementation methods, while LS incurs $\mathcal{O}((N+1)^3+K(N+1)^2)$ flops. Since $L_aL_b \ll d$, the complexity of SOMP is dominated by $\mathcal{O}(dQKL_aL_b) \ll \mathcal{O}((N+1)^3+K(N+1)^2)$ when N is large compared to other system parameters.

Next, in Fig. 10.2, we study the performance boost obtained by optimizing the IRS with binary phase configurations ($\{-1,+1\}$) in an OFDM system and compare it against the non-IRS aided counterpart. We also compare the performance against the solution reported in [203], which uses the classical power method to compute the eigenvalues and eigenvectors of matrices and optimizes the IRS. However, this approach optimizes Jensen's inequality-based upper bound on the sum rate instead of directly optimizing (10.14), leading to a suboptimal solution. On average, the proposed method yields 10% better rate than the power method and 191% better rate than that obtained without an IRS. In

terms of the SNR, the MM-based method developed in this chapter achieves the same rate as in [203] at $\approx 21.5\%$ lower SNR (not illustrated in the plot for brevity.) Furthermore, while the power-based approach took ≈ 4 average iterations per UE for convergence, the proposed method took ≈ 6 average iterations for convergence. Thus, the MM method exhibits superior performance with approximately the same time complexity.

10.5 Conclusions

We developed a new algorithm for IRS phase configuration in OFDM systems. We exploited the joint row sparsity in the IRS-aided links to estimate the channel using the SOMP algorithm with low pilot overhead. Our IRS phase optimization procedure uses matrix inequalities that enable the use of majorization-minimization to obtain an elegant and computationally efficient iterative solution. We empirically showed that sparsity-based channel estimation combined with MM-based phase optimization outperforms the state-of-the-art.

Appendix 10.A Proof of the Lemma 10.3

Recall that the multivariate Taylor series expansion is

$$f(\mathbf{y}) = (\mathbf{x}) + (\mathbf{y}-\mathbf{x})^T \bigtriangledown f(\mathbf{x}) + \frac{1}{2}((\mathbf{y}-\mathbf{x})^T \bigtriangledown^2 f(\boldsymbol{\zeta})(\mathbf{y}-\mathbf{x})),$$

for $\boldsymbol{\zeta} = \alpha\mathbf{x} + (1-\alpha)\mathbf{y}$ with $\alpha \in [0,1]$. We let $\mathbf{x} = \tilde{\boldsymbol{\theta}}^{(i)}$, $\mathbf{y} = \tilde{\boldsymbol{\theta}}$, and $f(\cdot) = \sum_k f_k(\cdot)$. For our problem, $\bigtriangledown f_k\left(\tilde{\boldsymbol{\theta}}^{(i)}\right) = \dfrac{-\mathbf{g}_k^{(i)}}{C_k^{(i)} + \tilde{\boldsymbol{\theta}}^{(i)T}\mathbf{g}_k^{(i)}}$ and $\bigtriangledown^2 f_k\left(\boldsymbol{\zeta}\right) = \dfrac{\mathbf{g}_k^{(i)}\mathbf{g}_k^{(i)T}\left(C_k^{(i)} + \tilde{\boldsymbol{\theta}}^{(i)T}\mathbf{g}_k^{(i)}\right)}{\left(C_k^{(i)} + \boldsymbol{\zeta}^T\mathbf{g}_k^{(i)}\right)^3}$. Since $\mathbf{g}_k^{(i)}\mathbf{g}_k^{(i)T}$ is a rank-1 matrix, we have $\|\mathbf{g}_k^{(i)}\|_2^2\mathbf{I} \succeq \mathbf{g}_k^{(i)}\mathbf{g}_k^{(i)T}$. So, the third term in the Taylor expansion can be bounded as

$$\sum_{k=0}^{K-1}\left(\tilde{\boldsymbol{\theta}} - \tilde{\boldsymbol{\theta}}^{(i)}\right)^T \frac{C_k^{(i)} + \tilde{\boldsymbol{\theta}}^{(i)T}\mathbf{g}_k^{(i)}}{\left(C_k^{(i)} + \boldsymbol{\zeta}^T\mathbf{g}_k^{(i)}\right)^3}\mathbf{g}_k^{(i)}\mathbf{g}_k^{(i)T}\left(\tilde{\boldsymbol{\theta}} - \tilde{\boldsymbol{\theta}}^{(i)}\right)$$

$$\leq \sum_{k=0}^{K-1} \mathbb{1}\left\{C_k^{(i)} \geq \|\mathbf{g}_k^{(i)}\|_1\right\} \left(\tilde{\boldsymbol{\theta}} - \tilde{\boldsymbol{\theta}}^{(i)}\right)^T \frac{C_k^{(i)} + \tilde{\boldsymbol{\theta}}^{(i)T}\mathbf{g}_k^{(i)}}{\left(C_k^{(i)} - \|\mathbf{g}_k^{(i)}\|_1\right)^3} \times \|\mathbf{g}_k^{(i)}\|_2^2 \left(\tilde{\boldsymbol{\theta}} - \tilde{\boldsymbol{\theta}}^{(i)}\right), \quad (10.22)$$

and note that equality is satisfied at the current iterate, i.e., $\tilde{\boldsymbol{\theta}} = \tilde{\boldsymbol{\theta}}^{(i)}$. We obtain the right hand side using the fact that $\boldsymbol{\zeta}^T \mathbf{g}_k^{(i)} \leq \|\mathbf{g}_k^{(i)}\|_1$, as the entries of $\boldsymbol{\zeta} \in [-1, 1]$. The last term in the above can be simplified as $(\tilde{\boldsymbol{\theta}} - \tilde{\boldsymbol{\theta}}^{(i)})^T(\tilde{\boldsymbol{\theta}} - \tilde{\boldsymbol{\theta}}^{(i)}) = 2(N+1) - 2\tilde{\boldsymbol{\theta}}^T\tilde{\boldsymbol{\theta}}^{(i)}$.

Finally, collecting terms that are important for the optimization of $\tilde{\boldsymbol{\theta}}$, (P2) boils down to (P3). ■

11 | Conclusion

This thesis has, on the whole, focused on (a) intelligent reflecting surface (IRS)-assisted opportunistic communications, (b) performance of IRS-assisted wireless systems with multiple operators, and (c) IRS-assisted wideband beamforming. On *opportunistic communications*, the major contribution was the development of a low-complexity scheme to procure optimal benefits from the IRS but without explicitly optimizing the IRS, by harnessing the multi-user diversity benefits. With *multiple operators*, we found that an IRS deployed by one mobile operator positively aids the other out-of-band (OOB) mobile operator (MO) free of cost. Finally, on *wideband beamforming*, we devised low-complexity techniques to enable a phased-array based IRS architecture to beamform a wideband signal by efficiently handling the beam-split and frequency-selective effects that arise in the mmWave and sub-6 GHz bands, respectively. Importantly, this thesis elucidates how a randomly configured IRS can extract its benefits with very low complexity and overhead.

In the following, we recapitulate our key findings in these three aspects of IRS-aided wireless systems as they were developed across the chapters.

11.1 Summary of the Thesis

In Chapter 2, we investigated IRS-assisted opportunistic communication (OC) schemes to leverage and enhance multi-user diversity gains in both narrowband and wideband channels within the sub-6 GHz spectrum. These schemes eliminate the need for explicit channel estimation and computationally intensive phase optimization, requiring minimal or no signaling between the base station (BS) and the IRS. We began by showing that in narrowband i.i.d. channels, an OC scheme with a randomly configured IRS can approach

the performance of an optimized IRS as the number of user equipments (UEs) increases. The key idea here is that with many UEs whose channels are independent across UEs, a randomly chosen IRS configuration will be nearly-optimal to at least one UE in the system, and opportunistically scheduling such a UE yields optimal benefits. However, achieving this requires the number of UEs to grow exponentially with the number of IRS elements, which can limit the practical applicability of the approach. To alleviate this, we developed two alternative approaches: one leveraging additional reflection diversity, and the other exploiting the underlying channel structure in IRS-assisted systems. The latter approach, in particular, enables substantial performance gains even with large IRS arrays, without requiring a very large number of UEs. We then extended the OC scheme to wideband orthogonal frequency division multiplexing (OFDM) systems and analyzed the performance of two variants: single-user (SU)-OFDM and OFDMA. Overall, our results show that IRS-assisted OC schemes can deliver significant performance improvements over conventional designs, while maintaining low overhead and complexity. Next, in Chapter 3, we extended our analysis to spatially correlated IRS channels. We first derived the optimal sampling distribution for IRS phase configurations and showed that, under this distribution, the number of UEs required scales exponentially only with the rank of the IRS channel covariance matrix, rather than with the number of IRS elements. In summary, we demonstrated that it is possible to realize near-optimal beamforming gains with a moderate number of users and minimal computational or signaling overhead, without explicit IRS phase optimization.

In Chapter 4, we explored another scenario where randomly configured IRS phases can benefit practical multi-operator wireless networks. We began by analyzing a two-operator system where only one MO deploys and controls an IRS. Due to its passive nature and lack of band-pass filtering, the IRS also reflects signals from the OOB MO, imparting random phase shifts to its channel. Interestingly, we demonstrated that the IRS still improves OOB performance by enabling the reception of multiple signal copies at the OOB UE. Specifically, in the sub-6 GHz band, the IRS enhances the rich-scattering environment, while in the mmWave regime, it establishes a virtual line-of-sight (LoS) path with nonzero

probability. Next, in Chapter 5, we showed that multiple distributed IRSs can further improve the OOB performance without affecting the performance of the in-band MO, which controls the IRS. This improvement is primarily due to spatial diversity and multiplexing gains. Also, to ensure a low complexity implementation of a multiple IRS setup, Chapter 6 introduced a novel channel estimation algorithm that leverages the subspace structures to ensure that the pilot overhead is smaller compared to the number of channel parameters in the system. Finally, in Chapter 7, we generalized the setup to scenarios involving more than two MOs, each with its own IRS. Our analysis revealed that the benefits of inter-operator cooperation during data transmission are limited, suggesting that each MO can operate effectively and independently while still benefiting from its IRS.

In the final part of the thesis, we investigated the challenges of wideband beamforming using IRSs. In Chapter 8, we first established that while wideband signals propagate over frequency-selective channels, IRS phase shifters exhibit a frequency-flat response, limiting their ability to beamform across the entire bandwidth. This issue is especially pronounced in the mmWave band, where large IRS apertures violate the narrowband assumption, leading to a spatial-wideband (SW) effect and the resulting beam-split (B-SP) phenomenon. When the IRS is configured for a specific frequency component, the array gain deteriorates at other frequencies, thereby reducing the overall throughput. To address this, we developed two low-complexity solutions. The first, presented in Chapter 8, employs a distributed IRS architecture that mitigates the B-SP effect by parallelizing spatial delays and leveraging angle diversity. We derived the maximum permissible number of elements per IRS to ensure a minimum array gain across the entire bandwidth. Additionally, we analyzed the temporal delay spread (TDS) caused by asynchronous signal arrivals from different IRSs and showed that while TDS introduces performance loss, it still enables a uniform array gain across frequencies, unlike the frequency-dependent degradation seen with B-SP. We also formulated an optimization problem to determine the optimal IRS placement that minimizes TDS over a given UE distribution. In contrast, the second approach in Chapter 9 exploits the B-SP effect itself. Using the principle of energy conservation, we showed that the IRS inherently forms different beams at different frequencies.

Capitalizing on this behavior, we developed an opportunistic OFDMA scheme wherein IRS phase configurations are randomly generated and UEs are opportunistically scheduled over sub-bands. On each sub-band, the IRS will likely favor at least one UE; selecting that UE for data transmission captures the full array gain from a system-level perspective. Finally, in Chapter 10, we considered the sub-6 GHz regime, where frequency selectivity arises from rich multipath scattering. Here, we focused on jointly optimizing the IRS configuration to maximize the OFDM system's sum-rate. The optimization was tackled using a majorization-minimization framework that reformulated the problem into a sequence of analytically solvable sub-problems, each admitting a closed-form solution.

In summary, this thesis explored low-complexity strategies across three key aspects of IRS-assisted wireless systems. Additionally, a comprehensive performance analysis was conducted under diverse channel conditions, including narrowband and wideband regimes, sub-6 GHz and mmWave frequencies, centralized and distributed IRS architectures, and both optimized and random IRS phase configurations.

As with most research, there is always room for further studies and improvement. We catalog a few promising directions below.

11.2 Future Work

1. **Randomly configured IRSs with user mobility and strict latency**: An interesting direction for extending opportunistic scheduling schemes is to incorporate user mobility. When user movement causes significant temporal variations in channel statistics, it becomes essential to adaptively update the sampling distribution of the IRS phase configurations. Designing efficient schemes that can preserve the performance benefits of IRSs while maintaining low complexity in such dynamic scenarios remains a key challenge. Another promising direction is to extend the framework to scenarios where UEs are subject to stringent latency requirements, in which case a straightforward application of opportunistic scheduling may no longer be adequate.

2. **Out-of-band performance in interference-limited scenarios**: This thesis focused on analyzing OOB performance in noise-limited systems. In practical deployments, the coverage area could be divided into multiple cells, each equipped with a BS and one or more IRSs deployed by an MO. In such settings, with a smaller frequency reuse factor, the system experiences multi-cell interference. Also, simultaneous data transmission to multiple UEs by a multi-antenna BS adds multi-user interference even within a single cell. Thus, studying the OOB performance of IRS-aided systems in interference-limited scenarios is a good direction for future research.

3. **Machine learning for programming of IRS phase configurations:** As discussed in Sec 1.2.a, a key challenge in integrating IRSs into practical systems is the significant time and computational overhead required to configure them in real-time. One potential solution to reduce these overheads is to use machine learning (ML) methods that, based on observed measurements, can directly predict the optimal IRS configuration. This approach can avoid explicit channel estimation and phase optimization, thereby simplifying real-time implementation.

4. **Low-complexity beam management in IRS-aided systems**: A major challenge in high-frequency bands like mmWave is establishing beam connectivity between nodes before data transmission begins. The associated overhead of this grows rapidly, as the number of possible beam combinations increases exponentially with the number of devices involved in closing the BS-to-UE transmission loop, which is exacerbated by the presence of IRSs. Thus, designing low-complexity beam management schemes for IRS-aided systems is a promising direction for future research.

5. **Multiplexing capabilities of spatial-wideband effects**: As shown in Chapter 9, a single IRS configuration can effectively serve multiple UEs across different frequency components. This suggests that the SW effect introduces additional degrees of freedom, which may be exploited to enhance the multiplexing gains in multiple antenna systems. A formal mathematical characterization of this intuition could yield insights into the capabilities of large IRS-aided wideband systems.

Bibliography

[1] S. Parkvall, E. Dahlman, A. Furuskar, and M. Frenne, "NR: The new 5G radio access technology," *IEEE Communications Standards Magazine*, vol. 1, no. 4, pp. 24–30, Dec. 2017. [Cited on pages: 1 and 178.]

[2] E. Basar, M. Di Renzo, J. De Rosny, M. Debbah, M.-S. Alouini, and R. Zhang, "Wireless communications through reconfigurable intelligent surfaces," *IEEE Access*, vol. 7, pp. 116 753–116 773, 2019. [Cited on pages: 4, 6, 33, 95, 105, 161, 219, 265, and 302.]

[3] Q. Wu, S. Zhang, B. Zheng, C. You, and R. Zhang, "Intelligent reflecting surface-aided wireless communications: A tutorial," *IEEE Trans. Commun.*, vol. 69, no. 5, pp. 3313–3351, May 2021. [Cited on pages: 7, 34, 95, 105, 144, 161, and 178.]

[4] F. Guidi, A. Guerra, and A. Zanella, "Performance analysis of randomly distributed reconfigurable intelligent surfaces with different phase profiles," *IEEE Trans. Wireless Commun.*, vol. 23, no. 5, pp. 4643–4657, May 2024. [Cited on pages: 7 and 95.]

[5] X. Shi, N. Deng, N. Zhao, and D. Niyato, "Coverage enhancement in millimeter-wave cellular networks via distributed IRSs," *IEEE Trans. Commun.*, vol. 71, no. 2, pp. 1153–1167, Feb. 2023. [Cited on pages: 7, 8, 95, and 144.]

[6] X. Pang, W. Mei, N. Zhao, and R. Zhang, "Cellular sensing via cooperative intelligent reflecting surfaces," *IEEE Trans. Veh. Technol.*, vol. 72, no. 11, pp. 15 086–15 091, Nov. 2023. [Cited on pages: 7, 95, and 100.]

[7] C. Zhao, X. Pang *et al.*, "Energy efficiency optimization of IRS-assisted UAV networks based on statistical channels," *IEEE Wireless Commun. Lett.*, vol. 12, no. 8, pp. 1419–1423, Aug. 2023. [Cited on pages: 7, 95, and 100.]

[8] X. Pang, W. Mei, N. Zhao, and R. Zhang, "Intelligent reflecting surface assisted interference mitigation for cellular-connected UAV," *IEEE Wireless Commun. Lett.*, vol. 11, no. 8, pp. 1708–1712, Aug. 2022. [Cited on pages: 7, 95, and 100.]

[9] P. Wang *et al.*, "Intelligent reflecting surface-assisted millimeter wave communications: Joint active and passive precoding design," *IEEE Trans. Veh. Technol.*, vol. 69, no. 12, pp. 14 960–14 973, Dec. 2020. [Cited on pages: 7, 19, 33, 96, 110, 178, 180, 187, 211, 265, 266, and 281.]

[10] Q. Wu and R. Zhang, "Intelligent reflecting surface enhanced wireless network: Joint active and passive beamforming design," in *Proc. IEEE Global Commun. Conf.*, 2018, pp. 1–6. [Cited on pages: 7, 33, and 59.]

[11] C. Huang, A. Zappone, G. C. Alexandropoulos, M. Debbah, and C. Yuen, "Reconfigurable intelligent surfaces for energy efficiency in wireless communication," *IEEE Trans. Wireless Commun.*, vol. 18, no. 8, pp. 4157–4170, 2019. [Cited on pages: 7 and 33.]

[12] H. Guo, Y.-C. Liang, J. Chen, and E. G. Larsson, "Weighted sum-rate maximization for intelligent reflecting surface enhanced wireless networks," in *Proc. IEEE Global Commun. Conf.*, 2019, pp. 1–6. [Cited on pages: 7 and 33.]

[13] Y. Jiang *et al.*, "Beamforming design for RIS-aided THz wideband communication systems," in *Proc. IEEE 24th Int. Workshop Signal Process. Adv. Wireless Commun. (SPAWC)*, Sep. 2023, pp. 296–300. [Cited on pages: 7, 220, and 267.]

[14] J. Wu and B. Shim, "Frequency-dependent beamforming for RIS-assisted wideband terahertz systems," in *2023 IEEE 97th Vehicular Technology Conference (VTC2023-Spring)*, Jun. 2023, pp. 1–6. [Cited on pages: 7, 220, and 267.]

[15] Y. Yang, B. Zheng, S. Zhang, and R. Zhang, "Intelligent reflecting surface meets OFDM: Protocol design and rate maximization," *IEEE Trans. Commun.*, vol. 68, no. 7, pp. 4522–4535, 2020. [Cited on pages: 7, 33, and 52.]

[16] B. Zheng, C. You, and R. Zhang, "Intelligent reflecting surface assisted multi-user OFDMA: Channel estimation and training design," *IEEE Trans. Wireless Commun.*, vol. 19, no. 12, pp. 8315–8329, 2020. [Cited on pages: 7, 33, 53, and 267.]

[17] Y. Lin, S. Jin, M. Matthaiou, and X. You, "Channel estimation and user localization for IRS-assisted MIMO-OFDM systems," *IEEE Trans. Wireless Commun.*, pp. 1–1, 2021. [Cited on pages: 7 and 33.]

[18] H. Li, W. Cai, Y. Liu, M. Li, Q. Liu, and Q. Wu, "Intelligent reflecting surface enhanced wideband MIMO-OFDM communications: From practical model to reflection optimization," *IEEE Trans. Commun.*, vol. 69, no. 7, pp. 4807–4820, 2021. [Cited on pages: 7 and 33.]

[19] H. Li, R. Liu, M. Liy, Q. Liu, and X. Li, "IRS-enhanced wideband MU-MISO-OFDM communication systems," in *Proc. IEEE Wireless Commun. Netw. Conf.*, 2020, pp. 1–6. [Cited on pages: 7 and 33.]

[20] R. Li *et al.*, "Ergodic achievable rate maximization of RIS-assisted millimeter-wave MIMO-OFDM communication systems," *IEEE Trans. Wireless Commun.*, vol. 22, no. 3, pp. 2171–2184, Mar. 2023. [Cited on pages: 7, 220, and 267.]

[21] D. Mishra and H. Johansson, "Channel estimation and low-complexity beamforming design for passive intelligent surface assisted MISO wireless energy transfer," in *Proc. IEEE Int. Conf. Acoust. Speech Signal Process.*, 2019, pp. 4659–4663. [Cited on pages: 8, 34, and 161.]

[22] Q.-U.-A. Nadeem, H. Alwazani, A. Kammoun, A. Chaaban, M. Debbah, and M.-S. Alouini, "Intelligent reflecting surface-assisted multi-user MISO communication: Channel estimation and beamforming design," *IEEE Open J. Commun. Soc.*, vol. 1, pp. 661–680, 2020. [Cited on pages: 8 and 34.]

[23] X. Wei, D. Shen, and L. Dai, "Channel estimation for RIS assisted wireless communications–part I: Fundamentals, solutions, and future opportunities," *IEEE Commun. Lett.*, vol. 25, no. 5, pp. 1398–1402, 2021. [Cited on pages: 8, 34, 50, and 167.]

[24] ——, "Channel estimation for RIS assisted wireless communications–part II: An improved solution based on double-structured sparsity," *IEEE Commun. Lett.*, vol. 25, no. 5, pp. 1403–1407, 2021. [Cited on pages: 8 and 34.]

[25] T. Lin, X. Yu, Y. Zhu, and R. Schober, "Channel estimation for IRS-assisted millimeter-wave MIMO systems: Sparsity-inspired approaches," *IEEE Trans. Commun.*, vol. 70, no. 6, pp. 4078–4092, Jun. 2022. [Cited on pages: 8, 34, 179, 183, and 184.]

[26] B. Zheng, C. You, and R. Zhang, "Uplink channel estimation for double-IRS assisted multi-user MIMO," in *Proc. IEEE Int. Conf. Commun.*, 2021, pp. 1–6. [Cited on pages: 8 and 161.]

[27] J.-M. Kang, "Intelligent reflecting surface: Joint optimal training sequence and refection pattern," *IEEE Commun. Lett.*, vol. 24, no. 8, pp. 1784–1788, 2020. [Cited on pages: 8 and 161.]

[28] K. B. d. A. Benício, B. Sokal, and A. L. F. de Almeida, "Channel estimation and performance evaluation of multi-IRS aided MIMO communication system," in *Proc. Workshop Commun. Netw. Power Syst. (WCNPS)*, 2021, pp. 1–6. [Cited on pages: 8 and 161.]

[29] H. Alwazani and A. Chaaban, "Channel estimation for distributed intelligent reflecting surfaces assisted multi-user MISO systems," in *2020 IEEE Globecom Workshops (GC Wkshps)*. IEEE, 2020, pp. 1–6. [Cited on pages: 8 and 161.]

[30] X. Wang, L. Kong, F. Kong, F. Qiu, M. Xia, S. Arnon, and G. Chen, "Millimeter wave communication: A comprehensive survey," *IEEE Commun. Surveys Tuts.*, vol. 20, no. 3, pp. 1616–1653, 2018. [Cited on pages: 8 and 161.]

[31] Z. Wan, Z. Gao, and M.-S. Alouini, "Broadband channel estimation for intelligent reflecting surface aided mmwave massive MIMO systems," in *Proc. IEEE Int. Conf. Commun.*, 2020, pp. 1–6. [Cited on pages: 8, 161, and 270.]

[32] J. He, M. Leinonen, H. Wymeersch, and M. Juntti, "Channel estimation for RIS-aided mmwave MIMO systems," in *Proc. IEEE Global Commun. Conf.*, 2020, pp. 1–6. [Cited on pages: 8 and 161.]

[33] J. Chen *et al.*, "Channel estimation for reconfigurable intelligent surface aided multi-user mmwave MIMO systems," *IEEE Trans. Wireless Commun.*, vol. 22, no. 10, pp. 6853–6869, Oct. 2023. [Cited on pages: 8, 22, 102, 103, 111, 161, 163, 171, 185, 186, 225, and 273.]

[34] C. Jia, J. Cheng, H. Gao, and W. Xu, "High-resolution channel estimation for intelligent reflecting surface-assisted mmwave communications," in *Proc. IEEE 31st Annu. Int. Symp. Pers., Indoor Mobile Radio Commun. (PIMRC)*, 2020, pp. 1–6. [Cited on pages: 8 and 161.]

[35] K. Ardah, S. Gherekhloo, A. L. F. de Almeida, and M. Haardt, "TRICE: A channel estimation framework for RIS-aided millimeter-wave MIMO systems," *IEEE Signal Process. Lett.*, vol. 28, pp. 513–517, 2021. [Cited on pages: 8 and 161.]

[36] H. Ibrahim, H. Tabassum, and U. T. Nguyen, "Exact coverage analysis of intelligent reflecting surfaces with nakagami-M channels," *IEEE Trans. Veh. Technol.*, vol. 70, no. 1, pp. 1072–1076, Jan. 2021. [Cited on pages: 8 and 95.]

[37] T. Shafique, H. Tabassum, and E. Hossain, "Stochastic geometry analysis of IRS-assisted downlink cellular networks," *IEEE Trans. Commun.*, vol. 70, no. 2, pp. 1442–1456, Feb. 2022. [Cited on pages: 8 and 95.]

[38] T. Jiang and W. Yu, "Interference nulling using reconfigurable intelligent surface," *IEEE J. Sel. Areas Commun.*, vol. 40, no. 5, pp. 1392–1406, May 2022. [Cited on page: 8.]

[39] M. Cui, G. Zhang, and R. Zhang, "Secure wireless communication via intelligent reflecting surface," *IEEE Wireless Commun. Lett.*, vol. 8, no. 5, pp. 1410–1414, Oct. 2019. [Cited on pages: 8 and 178.]

[40] S. P. Chepuri, N. Shlezinger, F. Liu, G. C. Alexandropoulos, S. Buzzi, and Y. C. Eldar, "Integrated sensing and communications with reconfigurable intelligent surfaces: From signal modeling to processing," *IEEE Signal Process. Mag.*, vol. 40, no. 6, pp. 41–62, Sep. 2023. [Cited on page: 8.]

[41] S. Ren *et al.*, "Configuring intelligent reflecting surface with performance guarantees: Blind beamforming," *IEEE Trans. Wireless Commun.*, vol. 22, no. 5, pp. 3355–3370, May 2023. [Cited on pages: 8, 75, and 95.]

[42] A. Nicolaides *et al.*, "Outage and DMT analysis of partition-based schemes for RIS-aided MIMO fading channels," *IEEE J. Sel. Areas Commun.*, vol. 41, no. 8, pp. 2336–2349, Aug. 2023. [Cited on pages: 8 and 95.]

[43] C. Psomas and I. Krikidis, "Low-complexity random rotation-based schemes for intelligent reflecting surfaces," *IEEE Trans. Wireless Commun.*, vol. 20, no. 8, pp. 5212–5225, Aug. 2021. [Cited on pages: 8, 69, 95, and 108.]

[44] Q. Tao, S. Zhang, C. Zhong, and R. Zhang, "Intelligent reflecting surface aided multicasting with random passive beamforming," *IEEE Wireless Commun. Lett.*, vol. 10, no. 1, pp. 92–96, Jan. 2021. [Cited on pages: 8 and 95.]

[45] K.-W. Huang, H.-M. Wang, and L. Yang, "Smart jamming using reconfigurable intelligent surface: Asymptotic analysis and optimization," *IEEE Trans. Wireless Commun.*, vol. 23, no. 1, pp. 637–651, Jan. 2024. [Cited on pages: 8 and 95.]

[46] S. Ma, W. Shen, J. An, and L. Hanzo, "Wideband channel estimation for IRS-aided systems in the face of beam squint," *IEEE Trans. Wireless Commun.*, vol. 20, no. 10, pp. 6240–6253, Oct. 2021. [Cited on pages: 8, 220, 224, 225, 266, 270, 271, and 287.]

[47] A. Abdallah *et al.*, "Deep-learning based channel estimation for RIS-aided mmwave systems with beam squint," in *Proc. IEEE Int. Conf. Commun.*, May 2022, pp. 1269–1275. [Cited on pages: 8, 220, and 266.]

[48] Y. Chen, J. Tan, M. Hao, R. MacKenzie, and L. Dai, "Accurate beam training for RIS-assisted wideband terahertz communication," *IEEE Trans. Commun.*, vol. 71, no. 12, pp. 7425–7440, Dec. 2023. [Cited on pages: 8 and 220.]

[49] K. Keykhosravi *et al.*, "RIS-enabled SISO localization under user mobility and spatial-wideband effects," *IEEE J. Sel. Topics Signal Process.*, vol. 16, no. 5, pp. 1125–1140, Aug. 2022. [Cited on pages: 8, 220, and 266.]

[50] X. Lin *et al.*, "Beamforming on reconfigurable intelligent surface: A codebook design for spatial coverage with beam squint effect," in *Proc. IEEE Int. Conf. Commun. Workshops*, May 2023, pp. 1130–1135. [Cited on pages: 8 and 220.]

[51] Y. Kawamoto *et al.*, "Simultaneous multiple connections and increased frequency efficiency using beam squint approach for IRS-based communication," *IEEE Trans. Veh. Technol.*, vol. 73, no. 11, pp. 17 073–17 082, Nov. 2024. [Cited on pages: 8, 220, and 267.]

[52] H. Sun, S. Zhang, J. Ma, and O. A. Dobre, "Time-delay unit based beam squint mitigation for RIS-aided communications," *IEEE Commun. Lett.*, vol. 26, no. 9, pp. 2220–2224, Sep. 2022. [Cited on pages: 8, 220, 248, 266, and 267.]

[53] W. Hao *et al.*, "The far-/near-field beam squint and solutions for THz intelligent reflecting surface communications," *IEEE Trans. Veh. Technol.*, vol. 72, no. 8, pp. 10 107–10 118, Aug. 2023. [Cited on pages: 8, 221, 222, 224, 236, 248, 267, and 276.]

[54] R. Su *et al.*, "Wideband precoding for RIS-aided THz communications," *IEEE Trans. Commun.*, vol. 71, no. 6, pp. 3592–3604, Jun. 2023. [Cited on pages: 8, 220, 224, 248, 266, and 267.]

[55] F. Zhao *et al.*, "Joint beamforming optimization for IRS-aided THz communication with time delays," *IEEE Wireless Commun. Lett.*, vol. 13, no. 1, pp. 49–53, Jan. 2024. [Cited on pages: 8, 148, 221, 224, 248, and 267.]

[56] Z. Chu, Z. Zhu, F. Zhou, M. Zhang, and N. Al-Dhahir, "Intelligent reflecting surface assisted wireless powered sensor networks for internet of things," *IEEE Trans. Commun.*, vol. 69, no. 7, pp. 4877–4889, July 2021. [Cited on page: 8.]

[57] "Group report, ETSI GR RIS 001, reconfigurable intelligent surfaces (RIS): Use-cases, deployment scenarios and requirements, v1.1.1 rel 14," 2023. [Cited on page: 8.]

[58] TSDSI, "Technical specification, TSDSI, methods and interface design for RIS-assisted communication systems", TSDSI STD 5003 V1.0.0.,," Aug. 2024. [Online]. Available: https://tsdsi.in/published-standards/ [Cited on page: 8.]

[59] A. K. Shrivastava, S. Kumar, K. Sahu, B. Sonwani, D. Sharma, D. S. Srivastava, N. Garg, A. A. Kherani, V. Bhatia, S. Mukherjee, S. Mukhopadhyay, P. Das, R. Mahapatra, D. Das, and B. Lall, "TSDSI standards driven implementation of smart radio environment," in *2023 IEEE International Conference on Advanced Networks and Telecommunications Systems (ANTS)*, Dec. 2023, pp. 497–502. [Cited on page: 8.]

[60] Z. Wang, L. Liu, and S. Cui, "Channel estimation for intelligent reflecting surface assisted multiuser communications: Framework, algorithms, and analysis," *IEEE Trans. Wireless Commun.*, vol. 19, no. 10, pp. 6607–6620, Oct. 2020. [Cited on page: 9.]

[61] D. J. Love, R. W. Heath, V. K. N. Lau, D. Gesbert, B. D. Rao, and M. Andrews, "An overview of limited feedback in wireless communication systems," *IEEE J. Sel. Areas Commun.*, vol. 26, no. 8, pp. 1341–1365, Oct. 2008. [Cited on page: 9.]

[62] C. Bockelmann, N. Pratas, H. Nikopour, K. Au, T. Svensson, C. Stefanovic,

P. Popovski, and A. Dekorsy, "Massive machine-type communications in 5G: physical and MAC-layer solutions," *IEEE Commun. Mag.*, vol. 54, no. 9, pp. 59–65, Sep. 2016. [Cited on page: 11.]

[63] H. L. Van Trees, *Optimum array processing: Part IV of detection, estimation, and modulation theory.* John Wiley & Sons, 2002. [Cited on pages: 14, 228, 266, and 278.]

[64] "3GPP TS 38.101-1, 5G NR: UE radio transmission and reception; Part 1: Range 1 standalone, v 15.2.0 rel 15." [Cited on pages: 19, 35, and 96.]

[65] P. Wang, J. Fang, W. Zhang, and H. Li, "Fast beam training and alignment for IRS-assisted millimeter wave/terahertz systems," *IEEE Trans. Wireless Commun.*, vol. 21, no. 4, pp. 2710–2724, Apr. 2022. [Cited on pages: 19, 96, 103, 110, 147, 148, 179, 184, and 186.]

[66] J. Wang, W. Tang, S. Jin, C.-K. Wen, X. Li, and X. Hou, "Hierarchical codebook-based beam training for RIS-assisted mmwave communication systems," *IEEE Trans. Commun.*, vol. 71, no. 6, pp. 3650–3662, Jun. 2023. [Cited on pages: 19, 96, 110, and 148.]

[67] D. R. Hunter and K. Lange, "A tutorial on MM algorithms," *The American Statistician*, vol. 58, no. 1, pp. 30–37, 2004. [Cited on pages: 26, 303, 309, and 311.]

[68] M. Di Renzo, M. Debbah, D.-T. Phan-Huy, A. Zappone, M.-S. Alouini, C. Yuen, V. Sciancalepore, G. C. Alexandropoulos, J. Hoydis, H. Gacanin *et al.*, "Smart radio environments empowered by reconfigurable AI meta-surfaces: An idea whose time has come," *EURASIP J. Wireless Commun. Netw .*, vol. 2019, no. 1, pp. 1–20, 2019. [Cited on pages: 33 and 75.]

[69] Q. Wu and R. Zhang, "Towards smart and reconfigurable environment: Intelligent reflecting surface aided wireless network," *IEEE Commun. Mag.*, vol. 58, no. 1, pp. 106–112, 2020. [Cited on pages: 33, 34, 161, 219, and 302.]

[70] E. Björnson, H. Wymeersch, B. Matthiesen, P. Popovski, L. Sanguinetti, and E. de Carvalho, "Reconfigurable intelligent surfaces: A signal processing perspective with wireless applications," *arXiv preprint arXiv:2102.00742*, 2021. [Cited on pages: 33 and 303.]

[71] P. Viswanath *et al.*, "Opportunistic beamforming using dumb antennas," *IEEE Trans. Inf. Theory*, vol. 48, no. 6, pp. 1277–1294, Jun. 2002. [Cited on pages: xix, 33, 34, 36, 38, 41, 46, 50, 51, 59, 60, 70, 79, 80, 117, and 118.]

[72] J. Zhao, "A survey of intelligent reflecting surfaces (IRSs): Towards 6G wireless communication networks," *arXiv preprint arXiv:1907.04789*, 2019. [Cited on page: 34.]

[73] Q. Wu and R. Zhang, "Beamforming optimization for wireless network aided by intelligent reflecting surface with discrete phase shifts," *IEEE Trans. Commun.*, vol. 68, no. 3, pp. 1838–1851, 2020. [Cited on page: 34.]

[74] Z. Yang, P. Xu, G. Chen, Y. Wu, and Z. Ding, "Performance analysis of IRS-assisted NOMA networks with randomly deployed users," *IEEE Syst. J.*, pp. 1–12, 2022. [Cited on page: 34.]

[75] Q.-U.-A. Nadeem, A. Zappone, and A. Chaaban, "Intelligent reflecting surface enabled random rotations scheme for the MISO broadcast channel," *IEEE Trans. Wireless Commun.*, vol. 20, no. 8, pp. 5226–5242, Aug. 2021. [Cited on pages: 34, 46, 49, 77, 95, and 286.]

[76] Q.-U.-A. Nadeem, A. Chaaban, and M. Debbah, "Opportunistic beamforming using an intelligent reflecting surface without instantaneous CSI," *IEEE Wireless Commun. Lett.*, vol. 10, no. 1, pp. 146–150, Jan. 2021. [Cited on pages: xix, 34, 35, 36, 43, 44, 46, 53, 59, 75, 81, 84, 86, 95, 117, 164, and 165.]

[77] N. H. Mahmood *et al.*, "Machine type communications: key drivers and enablers towards the 6G era," *EURASIP J. Wirel. Commun. Netw.*, vol. 2021, no. 1, p. 134, 2021. [Cited on pages: 34 and 285.]

[78] M. Sharif and B. Hassibi, "On the capacity of MIMO broadcast channels with partial side information," *IEEE Trans. Inf. Theory*, vol. 51, no. 2, pp. 506–522, 2005. [Cited on page: 34.]

[79] A. Asadi and V. Mancuso, "A survey on opportunistic scheduling in wireless communications," *IEEE Commun. Surveys Tuts.*, vol. 15, no. 4, pp. 1671–1688, 2013. [Cited on pages: 34, 37, and 216.]

[80] L. Yashvanth and C. R. Murthy, "On the impact of an IRS on the out-of-band performance in sub-6 GHz and mmwave frequencies," *IEEE Trans. Commun.*, vol. 72, no. 12, pp. 7417–7434, Dec. 2024. [Cited on pages: xx, 35, 144, 149, 150, 151, 153, 154, 159, 180, 186, 187, 190, 225, 245, 270, 273, and 282.]

[81] A. T. Suresh, N. B. Mehta, and V. Shah, "On optimal timer-based distributed selection for rate-adaptive multi-user diversity systems," in *Natl. Conf. Commun. (NCC)*. IEEE, 2010, pp. 1–5. [Cited on pages: 38, 41, and 58.]

[82] V. Shah, N. B. Mehta, and R. Yim, "Optimal timer based selection schemes," *IEEE Trans. Commun.*, vol. 58, no. 6, pp. 1814–1823, 2010. [Cited on pages: 38, 41, 58, 82, and 286.]

[83] M. Kafesaki, N. Shen, S. Tzortzakis, and C. Soukoulis, "Optically switchable and tunable terahertz metamaterials through photoconductivity," *Journal of Optics*, vol. 14, no. 11, p. 114008, 2012. [Cited on page: 45.]

[84] P. Jung, S. Butz, M. Marthaler, M. Fistul, J. Leppäkangas, V. Koshelets, and A. Ustinov, "Multistability and switching in a superconducting metamaterial," *Nature Communications*, vol. 5, no. 1, pp. 1–6, 2014. [Cited on page: 45.]

[85] E. Dahlman, S. Parkvall, and J. Skold, *5G NR: The next generation wireless access technology*. Academic Press, 2020. [Cited on page: 45.]

[86] G. Tian and R. Song, "Cooperative beamforming for a double-IRS-assisted wireless communication system," *Eurasip J. Adv. Signal Process.*, vol. 2021, no. 1, pp. 1–10, 2021. [Cited on pages: 48, 49, 165, 305, and 306.]

[87] V. Raghavan, J. Cezanne, S. Subramanian, A. Sampath, and O. Koymen, "Beamforming tradeoffs for initial UE discovery in millimeter-wave MIMO systems," *IEEE J. Sel. Topics Signal Process.*, vol. 10, no. 3, pp. 543–559, 2016. [Cited on page: 51.]

[88] "3GPP TR 38.912, 5G: Study on NR access technology, v 14.0 rel 14." [Cited on page: 52.]

[89] B. Zheng and R. Zhang, "Intelligent reflecting surface-enhanced OFDM: Channel estimation and reflection optimization," *IEEE Wireless Commun. Lett.*, vol. 9, no. 4, pp. 518–522, 2020. [Cited on pages: 52 and 178.]

[90] K. D. Katsanos, N. Shlezinger, M. F. Imani, and G. C. Alexandropoulos, "Wideband multi-user MIMO communications with frequency selective RISs: Element response modeling and sum-rate maximization," in *2022 IEEE International Conference on Communications Workshops (ICC Workshops)*, 2022, pp. 151–156. [Cited on page: 52.]

[91] D. Tse and P. Viswanath, *Fundamentals of wireless communication*. Cambridge university press, 2005. [Cited on page: 53.]

[92] S. Kalyani and R. M. Karthik, "The asymptotic distribution of maxima of independent and identically distributed sums of correlated or non-identical gamma random variables and its applications," *IEEE Trans. Commun.*, vol. 60, no. 9, pp. 2747–2758, 2012. [Cited on page: 55.]

[93] H. Exton, *Multiple hypergeometric functions and applications*. Ellis Horwood, 1976. [Cited on page: 55.]

[94] O. Eidous and S. Al-Salman, "One-term approximation for normal distribution function," *Mathematics and Statistics*, vol. 4, no. 1, pp. 15–18, 2016. [Cited on page: 56.]

[95] A. C. Berry, "The accuracy of the gaussian approximation to the sum of independent variates," *Trans. American Mathematical Society*, vol. 49, no. 1, pp. 122–136, 1941. [Cited on page: 57.]

[96] A. Lozano and N. Jindal, "Optimum pilot overhead in wireless communication: A unified treatment of continuous and block-fading channels," in *2010 European Wireless Conference (EW)*. IEEE, 2010, pp. 725–732. [Cited on page: 59.]

[97] E. Björnson, "Optimizing a binary intelligent reflecting surface for OFDM communications under mutual coupling," *arXiv preprint arXiv:2106.04280*, 2021. [Cited on page: 64.]

[98] K. Najim, E. Ikonen, and A.-K. Daoud, *Stochastic processes: estimation, optimisation and analysis*. Elsevier, 2004. [Cited on page: 64.]

[99] P. Billingsley, *Probability and Measure. 3rd Wiley*, 1995. [Cited on page: 71.]

[100] B. C. Arnold, N. Balakrishnan, and H. N. Nagaraja, *A first course in order statistics*. SIAM, 2008. [Cited on page: 72.]

[101] R. Wang, Z. Wang, L. Liu, S. Zhang, and S. Jin, "Reducing channel estimation and feedback overhead in IRS-aided downlink system: A quantize-then-estimate approach," *IEEE Trans. Wireless Commun.*, vol. 24, no. 2, pp. 1325–1338, Feb. 2025. [Cited on page: 75.]

[102] V. Jamali, G. C. Alexandropoulos, R. Schober, and H. V. Poor, "Low-to-zero-overhead IRS reconfiguration: Decoupling illumination and channel estimation," *IEEE Commun. Lett.*, vol. 26, no. 4, pp. 932–936, Apr. 2022. [Cited on page: 75.]

[103] L. Yashvanth and C. R. Murthy, "Performance analysis of intelligent reflecting surface assisted opportunistic communications," *IEEE Trans. Signal Process.*, vol. 71, pp. 2056–2070, 2023. [Cited on pages: xix, 75, 78, 84, 95, 105, 108, 117, 119, 216, 282, 286, and 300.]

[104] K. Yoshikawa *et al.*, "User and passive beam scheduling scheme for liquid crystal IRS-assisted mmwave communications," in *Proc. European Conf. on Antennas and Propagation (EuCAP)*, Mar. 2024, pp. 1–5. [Cited on pages: 81, 237, 240, and 242.]

[105] J. Nam, A. Adhikary, J.-Y. Ahn, and G. Caire, "Joint spatial division and multiplexing: Opportunistic beamforming, user grouping and simplified downlink scheduling," *IEEE J. Sel. Topics Signal Process.*, vol. 8, no. 5, pp. 876–890, Oct. 2014. [Cited on page: 81.]

[106] "3GPP Rep. TR 38.901 V16.1.0: Study on channel model for frequencies from 0.5 to 100 GHz," *3GPP, Sophia Antipolis, France*, Dec. 2019. [Cited on pages: 85 and 287.]

[107] O. Roy and M. Vetterli, "The effective rank: A measure of effective dimensionality," in *Proc. 15th Eur. Signal Process. Conf.*, Sep. 2007, pp. 606–610. [Cited on page: 86.]

[108] D. Gürgünoğlu, E. Björnson, and G. Fodor, "Combating inter-operator pilot contamination in reconfigurable intelligent surfaces assisted multi-operator networks," *IEEE Trans. Commun.*, vol. 72, no. 9, pp. 5884–5895, Sep. 2024. [Cited on pages: 96, 179, 180, and 188.]

[109] W. Cai, R. Liu, M. Li, Y. Liu, Q. Wu, and Q. Liu, "IRS-assisted multicell multiband systems: Practical reflection model and joint beamforming design," *IEEE Trans. Commun.*, vol. 70, no. 6, pp. 3897–3911, Jun. 2022. [Cited on pages: 96, 179, and 180.]

[110] W. Cai, H. Li, M. Li, and Q. Liu, "Practical modeling and beamforming for intelligent reflecting surface aided wideband systems," *IEEE Commun. Lett.*, vol. 24, no. 7, pp. 1568–1571, Jul. 2020. [Cited on pages: 96, 179, 180, and 182.]

[111] A. Khaleel and E. Basar, "Phase shift-free passive beamforming for reconfigurable intelligent surfaces," *IEEE Trans. Commun.*, vol. 70, no. 10, pp. 6966–6976, Oct. 2022. [Cited on pages: 100 and 101.]

[112] Y. Liu, L. Zhang, and M. A. Imran, "Multi-user beamforming and transmission based on intelligent reflecting surface," *IEEE Trans. Wireless Commun.*, vol. 21, no. 9, pp. 7329–7342, Sep. 2022. [Cited on page: 100.]

[113] A. Nasri, A. H. A. Bafghi, and M. Nasiri-Kenari, "Wireless localization in the presence of intelligent reflecting surface," *IEEE Wireless Commun. Lett.*, vol. 11, no. 7, pp. 1315–1319, Jul. 2022. [Cited on page: 100.]

[114] O. E. Ayach, S. Rajagopal, S. Abu-Surra, Z. Pi, and R. W. Heath, "Spatially sparse precoding in millimeter wave MIMO systems," *IEEE Trans. Wireless Commun.*, vol. 13, no. 3, pp. 1499–1513, Mar. 2014. [Cited on pages: 101 and 103.]

[115] S. J. Lee, "IRS element grouping with element-wise reflection coefficients," *IEEE Wireless Commun. Lett.*, vol. 13, no. 1, pp. 168–172, Jan. 2024. [Cited on pages: 102 and 103.]

[116] Y. Liu, L. Zhang, F. Gao, and M. A. Imran, "Intelligent reflecting surface networks with multiorder-reflection effect: System modeling and critical bounds," *IEEE Trans. Commun.*, vol. 70, no. 10, pp. 6992–7005, Oct. 2022. [Cited on pages: 102 and 103.]

[117] S. Ghiasvand, A. Nasri, A. H. A. Bafghi, and M. Nasiri-Kenari, "MISO wireless localization in the presence of reconfigurable intelligent surface," *arXiv preprint arXiv:2208.09546*, 2022. [Cited on pages: 102 and 103.]

[118] C. D. Meyer, *Matrix Analysis and Applied Linear Algebra*. USA: Society for Industrial and Applied Mathematics, 2000. [Cited on page: 103.]

[119] Z. Xiao, T. He, P. Xia, and X.-G. Xia, "Hierarchical codebook design for beamforming training in millimeter-wave communication," *IEEE Trans. Wireless Commun.*, vol. 15, no. 5, pp. 3380–3392, May 2016. [Cited on pages: 103 and 186.]

[120] A. M. Sayeed and V. Raghavan, "Maximizing MIMO capacity in sparse multipath with reconfigurable antenna arrays," *IEEE J. Sel. Topics Signal Process.*, vol. 1, no. 1, pp. 156–166, Jun. 2007. [Cited on page: 103.]

[121] C. You, B. Zheng, and R. Zhang, "Fast beam training for IRS-assisted multiuser communications," *IEEE Wireless Commun. Lett.*, vol. 9, no. 11, pp. 1845–1849, Nov. 2020. [Cited on pages: 103, 148, and 245.]

[122] S. Singh *et al.*, "Interference analysis for highly directional 60-GHz mesh networks: The case for rethinking medium access control," *IEEE/ACM Trans. Netw.*, vol. 19, no. 5, pp. 1513–1527, Oct. 2011. [Cited on pages: 103 and 150.]

[123] A.-A. A. Boulogeorgos and A. Alexiou, "Ergodic capacity analysis of reconfigurable intelligent surface assisted wireless systems," in *2020 IEEE 3rd 5G World Forum (5GWF)*, 2020, pp. 395–400. [Cited on page: 106.]

[124] S. M. Ross, *Introduction to probability models*. Academic press, 2014. [Cited on page: 109.]

[125] L. Yashvanth and C. R. Murthy, "Distributed IRSs always benefit every mobile operator," *IEEE Wireless Commun. Lett.*, vol. 13, no. 11, pp. 2975–2979, Nov. 2024. [Cited on pages: 113, 180, and 242.]

[126] L. Bai, T. Li, Z. Xiao, and J. Choi, "Performance analysis for SDMA mmwave systems: Using an approximate closed-form solution of downlink sum-rate," *IEEE Access*, vol. 5, pp. 15 641–15 649, 2017. [Cited on pages: 114, 148, and 207.]

[127] L. Yashvanth *et al.*, "Comparative study of IRS assisted opportunistic communications over i.i.d. and LoS channels," in *Proc. IEEE Int. Conf. Acoust. Speech Signal Process. (ICASSP)*, Jun. 2023, pp. 1–5. [Cited on pages: 118, 119, 126, and 285.]

[128] M. K. Simon, *Probability distributions involving Gaussian random variables: A handbook for engineers and scientists*. Springer, 2002. [Cited on page: 132.]

[129] Q. Tao, J. Wang, and C. Zhong, "Performance analysis of intelligent reflecting surface aided communication systems," *IEEE Commun. Lett.*, vol. 24, no. 11, pp. 2464–2468, Nov. 2020. [Cited on page: 134.]

[130] S. Guruacharya, B. K. Chalise, and B. Himed, "On the product of complex gaussians with applications to radar," *IEEE Signal Process. Lett.*, vol. 26, no. 10, pp. 1536–1540, Oct. 2019. [Cited on page: 137.]

[131] F. E. Harris, "Incomplete bessel, generalized incomplete gamma, or leaky aquifer functions," *J. Comput. Appl. Math.*, vol. 215, no. 1, pp. 260–269, 2008. [Cited on page: 138.]

[132] F. W. Olver, D. W. Lozier, R. F. Boisvert, and C. W. Clark, *NIST handbook of mathematical functions*. Cambridge university press, 2010. [Cited on page: 138.]

[133] M. Chaudhry *et al.*, "Generalized incomplete gamma functions with applications," *J. Comput. Appl. Math.*, vol. 55, no. 1, pp. 99–124, 1994. [Cited on page: 139.]

[134] J. Choi, G. Kwon, and H. Park, "Multiple intelligent reflecting surfaces for capacity maximization in LOS MIMO systems," *IEEE Wireless Commun. Lett.*, vol. 10, no. 8, pp. 1727–1731, Aug. 2021. [Cited on page: 144.]

[135] Z. Chen *et al.*, "IRS-aided joint spatial division and multiplexing for mmwave multiuser MISO systems," *IEEE Trans. Wireless Commun.*, vol. 22, no. 11, pp. 7789–7804, Nov. 2023. [Cited on page: 144.]

[136] Y. Zhang, S. R. Khosravirad, X. Chu, and M. A. Uusitalo, "On the IRS deployment in smart factories considering blockage effects: Collocated or distributed?" *IEEE Trans. Wireless Commun.*, pp. 1–1, 2024. [Cited on page: 144.]

[137] X. Peng, X. Hu, and C. Zhong, "Distributed intelligent reflecting surfaces-aided communication system: Analysis and design," *IEEE Trans. Green Commun. Netw.*, vol. 6, no. 4, pp. 1932–1944, Dec. 2022. [Cited on page: 144.]

[138] L. Yashvanth and C. R. Murthy, "Cascaded channel estimation for distributed IRS aided mmwave massive MIMO systems," in *Proc. IEEE Glob. Commun. Conf.*, Dec. 2022, pp. 717–723. [Cited on pages: 144, 179, and 234.]

[139] Y. Zhao *et al.*, "Cooperative reflection and synchronization design for distributed multiple-RIS communications," *IEEE J. Sel. Topics Signal Process.*, vol. 16, no. 5, pp. 980–994, Aug. 2022. [Cited on page: 146.]

[140] W. Mei *et al.*, "Intelligent reflecting surface-aided wireless networks: From single-reflection to multi reflection design and optimization," *Proceedings of the IEEE*, vol. 110, no. 9, pp. 1380–1400, Sep. 2022. [Cited on pages: 161 and 265.]

[141] W. Mei and R. Zhang, "Cooperative beam routing for multi-IRS aided communication," *IEEE Wireless Commun. Lett.*, vol. 10, no. 2, pp. 426–430, 2021. [Cited on page: 161.]

[142] ——, "Multi-beam multi-hop routing for intelligent reflecting surfaces aided massive MIMO," *IEEE Trans. Wireless Commun.*, vol. 21, no. 3, pp. 1897–1912, 2022. [Cited on page: 161.]

[143] X. Hu, R. Zhang, and C. Zhong, "Semi-passive elements assisted channel estimation for intelligent reflecting surface-aided communications," *IEEE Trans. Wireless Commun.*, vol. 21, no. 2, pp. 1132–1142, 2022. [Cited on page: 162.]

[144] R. Roy and T. Kailath, "ESPRIT-estimation of signal parameters via rotational invariance techniques," *IEEE Trans. Acoust., Speech, Signal Process.*, vol. 37, no. 7, pp. 984–995, 1989. [Cited on pages: 162 and 168.]

[145] R. Schmidt, "Multiple emitter location and signal parameter estimation," *IEEE Trans. Antennas Propag.*, vol. 34, no. 3, pp. 276–280, 1986. [Cited on pages: 162, 168, and 169.]

[146] I. A. Hemadeh, K. Satyanarayana, M. El-Hajjar, and L. Hanzo, "Millimeter-wave communications: Physical channel models, design considerations, antenna constructions, and link-budget," *IEEE Commun. Surveys Tuts.*, vol. 20, no. 2, pp. 870–913, 2018. [Cited on page: 165.]

[147] A. Papazafeiropoulos, P. Kourtessis, S. Chatzinotas, and J. M. Senior, "Coverage probability of double-IRS assisted communication systems," *IEEE Wireless Commun. Lett.*, vol. 11, no. 1, pp. 96–100, 2022. [Cited on page: 167.]

[148] S. Haykin and K. R. Liu, *Handbook on array processing and sensor networks*. John Wiley & Sons, 2010. [Cited on pages: 168 and 169.]

[149] B. D. Rao and K. Hari, "Analysis of subspace-based direction of arrival estimation methods," *Sadhana*, vol. 16, no. 3, pp. 183–194, 1991. [Cited on page: 169.]

[150] C. Stoeckle, J. Munir, A. Mezghani, and J. A. Nossek, "DoA estimation performance and computational complexity of subspace- and compressed sensing-based methods," in *WSA 2015; 19th International ITG Workshop on Smart Antennas*, 2015, pp. 1–6. [Cited on page: 170.]

[151] S. Foucart and H. Rauhut, *A Mathematical Introduction to Compressive Sensing*. Applied and Numerical Harmonic Analysis. Birkhäuser., 2013. [Cited on page: 171.]

[152] M. Zhu and A. Ghodsi, "Automatic dimensionality selection from the scree plot via the use of profile likelihood," *Comput. Stat. Data Anal.*, vol. 51, no. 2, pp. 918–930, nov 2006. [Online]. Available: https://doi.org/10.1016/j.csda.2005.09.010 [Cited on page: 174.]

[153] Z. Gong, L. Wu, Z. Zhang, J. Dang, B. Zhu, H. Jiang, and G. Y. Li, "Joint TOA and DOA estimation with CFO compensation using large-scale array," *IEEE Trans. Signal Process.*, vol. 69, pp. 4204–4218, 2021. [Cited on page: 175.]

[154] Q. Wu and R. Zhang, "Intelligent reflecting surface enhanced wireless network via joint active and passive beamforming," *IEEE Trans. Wireless Commun.*, vol. 18, no. 11, pp. 5394–5409, Nov. 2019. [Cited on pages: 178, 180, and 211.]

[155] X. Mu *et al.*, "Joint deployment and multiple access design for intelligent reflecting surface assisted networks," *IEEE Trans. Wireless Commun.*, vol. 20, no. 10, pp. 6648–6664, Oct. 2021. [Cited on pages: 178 and 180.]

[156] E. Björnson, Ö. Özdogan, and E. G. Larsson, "Intelligent reflecting surface versus decode-and-forward: How large surfaces are needed to beat relaying?" *IEEE Wireless Commun. Lett.*, vol. 9, no. 2, pp. 244–248, Feb. 2020. [Cited on page: 178.]

[157] C. Pan *et al.*, "Multicell MIMO communications relying on intelligent reflecting surfaces," *IEEE Trans. Wireless Commun.*, vol. 19, no. 8, pp. 5218–5233, Aug. 2020. [Cited on page: 178.]

[158] T. Jiang, H. V. Cheng, and W. Yu, "Learning to reflect and to beamform for intelligent reflecting surface with implicit channel estimation," *IEEE J. Sel. Areas Commun.*, vol. 39, no. 7, pp. 1931–1945, Jul. 2021. [Cited on page: 178.]

[159] Y. Liu, X. Liu, X. Mu, T. Hou, J. Xu, M. Di Renzo, and N. Al-Dhahir, "Reconfigurable intelligent surfaces: Principles and opportunities," *IEEE Commun. Surveys Tuts.*, vol. 23, no. 3, pp. 1546–1577, 2021. [Cited on page: 178.]

[160] S. Gong *et al.*, "Toward smart wireless communications via intelligent reflecting surfaces: A contemporary survey," *IEEE Commun. Surveys Tuts.*, vol. 22, no. 4, pp. 2283–2314, 4th Quarter 2020. [Cited on page: 178.]

[161] X. Liu *et al.*, "Hybrid beamforming and intelligent reflecting surface design for mmwave MIMO systems," in *Proc. IEEE 8th Int. Conf. Comput. Commun. (ICCC)*, 2022, pp. 882–887. [Cited on page: 178.]

[162] F. Yang *et al.*, "Intelligent reflecting surface-assisted mmWave communication exploiting statistical CSI," in *Proc. IEEE ICC*, 2020. [Cited on page: 178.]

[163] D. Zhao *et al.*, "Joint power allocation and user association optimization for IRS-assisted mmwave systems," *IEEE Trans. Wireless Commun.*, vol. 21, no. 1, pp. 577–590, Jan. 2022. [Cited on page: 179.]

[164] Y. Song *et al.*, "Weighted sum-rate maximization in multi-IRS-aided multi-cell mmwave communication systems for suppressing ICI," *IEEE Trans. Veh. Technol.*, vol. 72, no. 8, pp. 10 234–10 250, Aug. 2023. [Cited on page: 179.]

[165] "3GPP TS 38.101-2 version, 5G: User equipment radio transmission and reception, part 2: Range standalone, v 18.5.0 rel 18." [Cited on page: 179.]

[166] M. Lodro *et al.*, "Experimental evaluation of multi-operator RIS-assisted links in indoor environment," *arXiv preprint arXiv:2206.07788*, 2022. [Cited on pages: 179 and 180.]

[167] X. Lin *et al.*, "Resource allocation for RIS-aided mmwave system with cooperative and non-cooperative base stations," *IEEE Trans. Veh. Technol.*, pp. 1–12, 2024. [Cited on pages: 179 and 180.]

[168] H. Zhang *et al.*, "A hierarchical DRL approach for resource optimization in multi-RIS multi-operator networks," *arXiv preprint arXiv:2410.12320*, 2024. [Cited on pages: 179 and 180.]

[169] S. Schwarz, "Gambling on reconfigurable intelligent surfaces," *IEEE Commun. Lett.*, vol. 28, no. 4, pp. 957–961, Apr. 2024. [Cited on pages: 179, 180, and 182.]

[170] W. Cai *et al.*, "Non-cooperative resource management for intelligent reflecting surface aided networks," *IEEE Trans. Veh. Technol.*, vol. 72, no. 3, pp. 4058–4062, Mar. 2023. [Cited on pages: 179 and 180.]

[171] Y. Zhao *et al.*, "Network coexistence analysis of RIS-assisted wireless communications," *IEEE Access*, vol. 10, pp. 63 442–63 454, 2022. [Cited on pages: 179 and 180.]

[172] J. Angjo *et al.*, "Side effects of IRS: On the need for coordination in 6G multi-operator IRS-assisted networks," in *2023 IEEE Globecom Workshops (GC Wkshps)*, Dec. 2023, pp. 1380–1385. [Cited on pages: 179 and 180.]

[173] N. I. Miridakis *et al.*, "Impact of inter-operator interference via reconfigurable intelligent surfaces," *IEEE Wireless Commun. Lett.*, vol. 13, no. 9, pp. 2536–2540, Sep. 2024. [Cited on page: 180.]

[174] Y. Cao, T. Lv, and W. Ni, "Intelligent reflecting surface aided multi-user mmwave communications for coverage enhancement," in *Proc. IEEE 31st Annu. Int. Symp. Pers., Indoor Mobile Radio Commun.*, Aug. 2020, pp. 1–6. [Cited on pages: 183, 265, 266, and 281.]

[175] E. K. Chong and S. H. Żak, *An introduction to optimization*. John Wiley & Sons, 2013, vol. 75. [Cited on pages: 193 and 211.]

[176] E. Björnson *et al.*, "Reconfigurable intelligent surfaces: A signal processing perspective with wireless applications," *IEEE Signal Process. Mag.*, vol. 39, no. 2, pp. 135–158, Mar. 2022. [Cited on pages: 219 and 265.]

[177] Z. Zhang, L. Dai, X. Chen, C. Liu, F. Yang, R. Schober, and H. V. Poor, "Active RIS vs. passive RIS: Which will prevail in 6G?" *IEEE Trans. Commun.*, vol. 71, no. 3, pp. 1707–1725, Mar. 2023. [Cited on pages: 219, 221, and 267.]

[178] B. Wang, F. Gao, S. Jin, H. Lin, and G. Y. Li, "Spatial- and frequency-wideband effects in millimeter-wave massive MIMO systems," *IEEE Trans. Signal Process.*, vol. 66, no. 13, pp. 3393–3406, Jul. 2018. [Cited on pages: 219, 225, 265, 266, and 272.]

[179] Y. Chen, D. Chen, and T. Jiang, "Beam-squint mitigating in reconfigurable intelligent surface aided wideband mmwave communications," in *Proc. IEEE Wireless Commun. Netw. Conf.*, Mar. 2021, pp. 1–6. [Cited on pages: 220, 224, and 266.]

[180] H. Ozen and G. M. Guvensen, "A robust quantized beam-squint and interference aware statistical beamforming for RIS-aided massive MIMO," in *Proc. IEEE Int. Conf. Commun.*, May 2023, pp. 1307–1312. [Cited on pages: 220 and 267.]

[181] X. Su *et al.*, "Joint precoding for RIS-assisted wideband THz cell-free massive MIMO systems," *arXiv preprint arXiv:2405.07830*, 2024. [Cited on pages: 221 and 248.]

[182] J. Li *et al.*, "Holographic RIS-aided wideband communication with beam-squint mitigation," *IEEE Trans. Commun.*, pp. 1–1, 2024. [Cited on page: 221.]

[183] ——, "User sensing in RIS-aided wideband mmwave system with beam-squint and beam-split," *IEEE Trans. Commun.*, vol. 73, no. 2, pp. 1304–1319, Feb. 2025. [Cited on page: 221.]

[184] F. Gao, B. Wang, C. Xing, J. An, and G. Y. Li, "Wideband beamforming for hybrid massive MIMO terahertz communications," *IEEE J. Sel. Areas Commun.*, vol. 39, no. 6, pp. 1725–1740, Jun. 2021. [Cited on page: 221.]

[185] W. Yan *et al.*, "Beamforming analysis and design for wideband THz reconfigurable intelligent surface communications," *IEEE J. Sel. Areas Commun.*, vol. 41, no. 8, pp. 2306–2320, Aug. 2023. [Cited on pages: 221 and 249.]

[186] G. Sun *et al.*, "Beamforming design for the distributed RISs-aided THz communications with double-layer true time delays," *IEEE Trans. Veh. Technol.*, vol. 73, no. 3, pp. 3886–3900, Mar. 2024. [Cited on page: 221.]

[187] H. Han *et al.*, "On half-power beamwidth of intelligent reflecting surface," *IEEE Commun. Lett.*, vol. 25, no. 4, pp. 1333–1337, Apr. 2021. [Cited on page: 233.]

[188] F. J. Martín-Vega, J. C. Ruiz-Sicilia, M. C. Aguayo, and G. Gómez, "Emerging tools for link adaptation on 5G NR and beyond: Challenges and opportunities," *IEEE Access*, vol. 9, pp. 126 976–126 987, 2021. [Cited on page: 234.]

[189] P. Zivuku, A. B. M. Adam, K. Ntontin, S. Kisseleff, V. N. Ha, S. Chatzinotas, and B. Ottersten, "Geographical fairness in multi-RIS-assisted networks in smart cities: A robust design," *IEEE Trans. Commun.*, vol. 73, no. 8, pp. 6622–6638, Aug. 2025. [Cited on page: 242.]

[190] Z. Xing *et al.*, "Location information assisted beamforming design for reconfigurable intelligent surface aided communication systems," *IEEE Trans. Wireless Commun.*, vol. 22, no. 11, pp. 7676–7695, Nov. 2023. [Cited on page: 245.]

[191] R. A. Horn and C. R. Johnson, *Matrix analysis*. Cambridge university press, 2012. [Cited on page: 259.]

[192] D. Hilbert and S. Cohn-Vossen, *Geometry and the Imagination*. American Mathematical Soc., 2021, vol. 87. [Cited on page: 260.]

[193] J. Bird, *Engineering Mathematics*. CRC Press, 2017. [Online]. Available: https://books.google.co.in/books?id=bAcqDwAAQBAJ [Cited on pages: 260 and 261.]

[194] M. J. Wainwright, *High-dimensional statistics: A non-asymptotic viewpoint*. Cambridge university press, 2019, vol. 48. [Cited on page: 263.]

[195] M. Nemati *et al.*, "RIS-assisted coverage enhancement in millimeter-wave cellular networks," *IEEE Access*, vol. 8, pp. 188 (171–185), 2020. [Cited on pages: 265, 266, and 281.]

[196] X. Ye *et al.*, "Joint codebook selection and MCS adaptation for mmwave eMBB services based on deep reinforcement learning," *IEEE Internet of Things Journal*, vol. 11, no. 19, pp. 31 545–31 560, Oct. 2024. [Cited on page: 265.]

[197] L. Yashvanth, C. R. Murthy, and B. D. Rao, "Mitigating spatial-wideband and beam-split effects via distributed IRSs: Design and analysis," *IEEE Trans. Signal Process.*, pp. 1–16, 2025. [Cited on page: 267.]

[198] Y. Yang, S. Zhang, and R. Zhang, "IRS-enhanced OFDMA: Joint resource allocation and passive beamforming optimization," *IEEE Wireless Commun. Lett.*, vol. 9, no. 6, pp. 760–764, Jun. 2020. [Cited on page: 267.]

[199] L. Yashvanth, C. R. Murthy, and B. D. Rao, "Spatial correlation-aware opportunistic beamforming in IRS-aided multi-user systems," *IEEE Wireless Commun. Lett.*, pp. 1–1, 2025. [Cited on pages: 282 and 286.]

[200] G. Lee, Y. Sung, and J. Seo, "Randomly-directional beamforming in millimeter-wave multiuser MISO downlink," *IEEE Trans. Wireless Commun.*, vol. 15, no. 2, pp. 1086–1100, Feb. 2016. [Cited on page: 294.]

[201] G. Grimmett and D. Stirzaker, *Probability and random processes*, 3rd ed. Oxford university press, 2001. [Cited on pages: 297 and 298.]

[202] B. Zheng and R. Zhang, "Intelligent reflecting surface-enhanced OFDM: Channel estimation and reflection optimization," *IEEE Wireless Commun. Lett.*, vol. 9, no. 4, pp. 518–522, 2020. [Cited on page: 302.]

[203] E. Björnson, "Configuring an intelligent reflecting surface for wireless communications," *arXiv preprint arXiv:2106.03497*, 2021. [Cited on pages: xxii, 302, 303, 313, and 314.]

[204] A. Majumdar, *Compressed sensing for engineers*. CRC Press, 2018. [Cited on pages: 302 and 308.]

[205] R. Ramu Naidu and C. R. Murthy, "Construction of unimodular tight frames for compressed sensing using majorization-minimization," *Signal Processing*, vol. 172, p. 107516, 2020. [Cited on page: 309.]

[206] S. S. Thoota, P. Babu, and C. R. Murthy, "Codebook-based precoding and power allocation for MU-MIMO systems for sum rate maximization," *IEEE Trans. Commun.*, vol. 67, no. 12, pp. 8290–8302, 2019. [Cited on page: 309.]

[207] B. L. Sturm and M. G. Christensen, "Comparison of orthogonal matching pursuit implementations," in *Proc. IEEE 20th Eur. Signal Process. Conf. (EUSIPCO)*, Aug 2012, pp. 220–224. [Cited on page: 313.]